DISSERTATION / DOCTORAL THESIS

Titel der Dissertation / Title of the Doctoral Thesis

3D Modelling of a Triassic Ammonoid Mass Occurrence (Taurus, Turkey) - Ammonoid mass mortality during the Carnian Crisis (Carnian Pluvial Episode)

verfasst von / submitted by

Susanne Mayrhofer, Bakk. MSc

angestrebter akademischer Grad / in partial fulfilment of the requirements for the degree of

Doktorin der Naturwissenschaften (Dr.rer.nat.)

Wien, 2016 / Vienna 2016

Studienkennzahl lt. Studienblatt / degree programme code as it appears on the student record sheet:	A 791 426
Dissertationsgebiet lt. Studienblatt/ field of study as it appears on the student record sheet:	Erdwissenschaften
Betreut von / Supervisor:	Ao. Prof. Dr. Leopold Krystyn

für meine Eltern

Brigitte & Johann Mayrhofer

CONTENTS

ACKNOWLEDGEMENTS 11

ABSTRACT 13

ZUSAMMENFASSUNG 17

ENCOMPASSED PUBLICATIONS 21

CHAPTER I: INTRODUCTION 23

1.1. Introduction to the study area **24**
1.2. The Carnian Pluvial Episode (CPE) **26**
1.3. Methodology **27**
1.3.1. Facies analyses **27**
1.3.2. Geophysical measurements (Susceptibility & Gamma ray) **28**
1.3.3. Triassic Ammonoid biostratigraphy **29**
1.3.4. 3D-visualisation (computed tomography vs. serial grinding) **30**
1.3.5. Orientation measurements and taphonomic analyses **30**
1.4. References **33**

CHAPTER II: ***A delayed carbonate factory breakdown during the Tethyan-wide Carnian Pluvial Episode along the Cimmerian terranes (Taurus, Turkey)***

Abstract **41**
2.1. Introduction **42**
2.2. Geography and geological setting **44**
2.3. Stratigraphic log and biostratigraphy **47**
2.4. Materials and methods **48**
2.5. Facies description **48**
2.6. Facies interpretation **60**
2.7. Discussion **64**
2.8. Conclusions **66**
2.9. Acknowledgments **67**
2.10. References **68**

CHAPTER III: ***Susceptibility and radiometry data used for stratigraphic correlations: case study on Upper Triassic beds in Turkey***

Abstract **77**
3.1. Introduction **78**

3.2. Geography and Geology **80**
3.3. The facies changes at Aşağiyaylabel (AS I and AS IV) and Karapinar (KA I–II & IV) **82**
3.3.1. Aşağiyaylabel I (AS I) **82**
3.3.2. Aşağiyaylabel IV (AS IV) **82**
3.3.3. Karapinar I (KA I) **83**
3.3.4. Karapinar II (KA II) **83**
3.3.5. Karapinar IV (KA IV) **83**
3.4. Methodology **88**
3.5. Results of MS & radiometry measurements **89**
3.5.1. General trends in MS in comparison with the $CaCo_3$ content **89**
3.5.2. The radiometry measurements **93**
3.5.3. Radiometry and MS data correlation: time-series analysis **96**
3.6. MS and radiometry data used for the correlation of time-equivalent sequences **98**
3.7. Conclusions **103**
3.8. Acknowledgements **104**
3.9. References **105**

CHAPTER IV: ***A new ammonoid fauna from the Carnian (Upper Triassic) Kasimlar Formation of the Taurus Mountains (Anatolia, Turkey)***

Abstract **115**
4.1. Introduction **116**
4.2. Geological Setting **118**
4.3. Materials and Methods **120**
4.3.1. Statistical methods **121**
4.3.2. Abbreviations **121**
4.4. Systematic Palaeontology **122**
***Kasimlarceltites* gen. nov** **122**
***Kasimlarceltites krystyni* sp. nov.** **128**
Spirogmoceras Silberling, 1956 **135**
Spirogmoceras cf. *shastense* (Smith, 1904) **136**
Sandlingites Mojsisovics, 1893 **138**
Sandlingites cf. *pilari* Diener, 1917 **138**
Klipsteinia Mojsisovics, 1882 **140**
***Klipsteinia disciformis* sp. nov.** **140**
Neoprotrachyceras Krystyn, 1978 **145**
Neoprotrachyceras attila (Mojsisovics, 1893) **145**
Neoprotrachyceras baconicum (Mojsisovics, 1870) **147**
Sirenites Mojsisovics, 1893 **149**

Sirenites senticosus (Dittmar, 1866) **150**
Anasirenites Mojsisovics, 1893 **153**
***Anasirenites crassicrenulatus* sp. nov.** **154**
Paratropites Mojsisovics, 1893 **157**
Paratropites cf. *hoetzendorfii* Diener, 1917 **158**
Trachysagenites Mojsisovics, 1893 **160**
Trachysagenites cf. *beckei* Diener, 1921 **161**
Proarcestes Mojsisovics, 1893 **162**
Proarcestes sp. **163**
Megaphyllites Mojsisovics, 1879 **163**
Megaphyllites jarbas (Münster, 1841) **164**
Simonyceras Wiedmann, 1970 **167**
Simonyceras simonyi (Hauer, 1847) **167**
4.5. Biostratigraphy ***170***
4.6. Taphonomy of the ammonoid fauna ***172***
4.7. Discussion ***174***
4.7.1. Faunal composition, stratigraphy and facies change within the section at Aşağiyaylabel ***174***
4.7.2. The ammonoid fauna from Aşağiyaylabel in the Tethyan Realm ***177***
4.7.3. Implications for the marine Upper Triassic Mediterranean-Himalayan-Andean Realm ***178***
4.8. Conclusions ***181***
4.9. Acknowledgments ***183***
4.10. Data archiving statement ***183***
4.11. References ***184***

CHAPTER V: ***Computed reconstruction of spatial ammonoid-shell orientation captured from digitized grinding and landmark data***

Abstract ***199***
5.1. Introduction ***200***
5.1.1. Mass occurrences and their internal orientation as key to paleoenvironments ***200***
5.1.2. Serial-grinding as possible alternative to computed tomography ***201***
5.2. Paleontological material ***202***
5.3. Methods ***203***
5.3.1. Serial grinding and digitization ***203***
5.3.2. 3D-visualization ***204***

5.3.3. Orientation measurements **206**

5.4. Spatial orientation as key to the paleoenvironment **213**

5.4.1. Geographical alignment of the aperture **213**

5.4.2. Revised aperture direction **215**

5.4.3. Dip and dip direction of the linear A:B **216**

5.4.4. Dip and azimuth of the plane A-B-C **216**

5.5. Discussion **218**

5.6. Conclusions **220**

5.7. Acknowledgments **221**

5.8. Appendix. Supplementary material **221**

5.9. References **222**

CHAPTER VI: ***Taphonomy and palaeoecology of Late Triassic (Carnian) Ammonoid concentrations from the Taurus Mountains, Turkey***

Abstract **229**

6.1. Introduction **230**

6.2. Geographical and geological Setting **231**

6.3. Material and methods **233**

6.3.1. Statistical methods for analysing the orientation **235**

6.3.2. Rose diagrams **235**

6.3.3. Stereographic plots **235**

6.4. Results **237**

6.4.1. Geometry and internal structure **237**

6.4.2. Lithology and microfacies of the host sediment **237**

6.4.3. Taxonomic composition **238**

6.4.4. Number of ammonoids and gastropods **238**

6.4.5. 3D-arrangement of ammonoid shells **239**

6.4.6. 3D-arrangement of gastropod shells **239**

6.4.7. Shell morphology **241**

6.4.8. Size, shape and sorting **241**

6.4.9. Biofabric **241**

6.4.10. Sedimentary infilling 242
6.4.11. Encrustation, abrasion and bioerosion 242
6.4.12. Mode of preservation and fragmentation 243
6.4.13. Genetic classification 243
6.5. Discussion 247
6.5.1. Transport mechanisms deduced from spatial fossil orientation 248
6.5.2. Genetic classification of the Kasimlarceltites mass occurrence 250
6.5.3. The Kasimlarceltites mass accumulation as a fossil-Lagerstätte 251
6.5.4. Ecology and primary habitat of Kasimlarceltites 252
6.6. Conclusions 254
6.7. Acknowledgements 256
6.8. References 257

CHAPTER VII: ***Taphonomic implications from Upper Triassic mass flow deposits: 2-dimensional reconstructions of an ammonoid mass occurrence (Carnian, Taurus Mountains, Turkey)***

Abstract 265
7.1. Introduction 266
7.2. Geographical setting 268
7.3. Geological setting 269
7.4. Lithology and facies 271
7.5. Material and fossil assemblage 275
7.6. Biostratigraphy 277
7.7. The Kasimlarceltites mass occurrence 278
7.7.1. The Aşağiyaylabel (Kartoz) area 278
7.7.2. The Karapınar (Yukarıyalabel) area 279
7.8. The Kasimlarceltites mass occurrence as an abundance zone 282
7.9. Biostratinomy and taphonomy 283
7.9.1. Ammonoid shell alignment 288
7.9.2. Size groups in Kasimlarceltites 292
7.10. Discussion 298

7.10.1. The Kasimlarceltites mass occurrence as an abundance zone **298**

7.10.2. Biostratinomy and taphonomy **300**

7.10.3. Ammonoid shell alignment **303**

7.10.4. Size groups in Kasimlarceltites **306**

7.11. Conclusions **307**

7.12. Acknowledgments **311**

7.13. References **312**

CHAPTER VIII: SYNOPSIS– *Stratigraphic and palaeoenvironmental conclusions about the Carnian sediments around Aşağiyaylabel and Karapinar (Taurus Mountains, Turkey) in a Tethyan wide context* 325

8.1. A delayed climatic facies change in the Taurus Mountains of Turkey **326**

8.2. Facies change supported by geophysical measurements (MS- and radiometry data) **327**

8.3. The Lower- to Upper Carnian ammonoid fauna at Aşağiyaylabel **328**

8.4. The Kasimlarceltites mass occurrence used as proxy for the environmental conditions during Early Carnian Time **329**

8.5. Summary **331**

8.6. References **333**

APPENDICES

Appendix I - Supplementary Tables for Chapter IV **337**

Appendix II - Supplementary Figures (SF) for Chapter V **346**

Acknowledgements

I warmly thank Alexander Lukeneder, who gave me the opportunity for conducting my investigations within a financially supported project (FWF-P 22109-B17). I am deeply grateful for this financial support, his scientific expertise and supervision, but also for his emotional encouragement.

Sincere thanks go to Leopold Krystyn, who was an encouraging supervisor to me. He gave me enough liberty for evolving my own scientific ideas, but assisted me with his scientific expertise and discussions whenever needed.

I am highly grateful to my co-authors Mathias Harzhauser, Yeşim İslamoğlu, Richard Lein and Gerhard W. Weber, for their guidance with fruitful discussions, constructive comments and critical reviews.

For further constructive comments I would like to thank all the reviewers of the encompassed articles, Marco Balini, Rainer Brandner, Eva Chorvátová, Susan M. Kidwell, Christian Klug, Robert Marschallinger, Jozef Michalík, Federico Olóriz and Michael Wagreich, but also the editors Anne-Christine Da Silva, Peter Doyle, Franz Fürsich, Jessica Pollitt, Julia Sigwart, Andrew Smith, Simo Spassov and Svend Stouge, as well as some anonymous reviewers.

A series of colleagues contributed to this work with different kind of help. I highly appreciate this help and support, and therefore I would like to thank Martin Dockner, Anton Englert, Ulrike Exner, Ursula Göhlich, Thomas Hofmann, Andrzej Kaim, Michael Klein, Andreas Kroh, Oleg Mandic, Martin Maslo, Martin Mayrhofer, Thomas Neubauer, Simon Schneider, Alice Schumacher, Michael Schwaiger, Philipp Strauss, Franz Topka, Marteen Vorn, Eckert Wallbrecher and Julia Wöger.

Further thanks go to my colleagues from the Department for Exhibition & Education (NHMW), especially to Sabine Rubik, for their encouraging support and for providing me flexible time for finishing my thesis.

Finally, I am deeply grateful to my family and friends for all of their encouraging support, help and appreciation over the last years.

ABSTRACT

The present thesis combines 5 peer reviewed articles and one submitted article, published in the course of a project funded by the Austrian Science Fund (P 22109-B17). The project focused on palaeozoologic, lithologic, cyclo- and magnetostratigraphic investigations of Upper Triassic (Carnian) sediments deposited within the Taurus Platform-Units of south-western Turkey. The main aim of this thesis was to trace the genesis and history of the 234 million-years-old *Kasimlarceltites* ammonoid mass occurrence, which is a marker-zone (*Kasimlarceltites* acme zone) represented by several limestone-layers within the Carnian Kasımlar Formation, developed during the early drowning phase of a shallow water platform. The acme zone shows an extension of at least least 5 km^2 in the surroundings of Aşağiyaylabel and represents an important archive for a Late Triassic ecosystem.

The Aşağiyaylabel sequence within the Taurus Mountains of Turkey constitutes an Upper Triassic key section concerning environmental changes during late Early- to early Late Carnian time. One main finding within this section, which represents a deepening sequence from platform carbonates over pelagic- and marly limestones into shales, was the occurrence of the Julian / Tuvalian substage boundary (= Lower- / Upper Carnian boundary) within the Kasımlar Formation. A further important result, based on sedimentological and palaeontological analyses, is a much later onset of the so called Carnian Pluvial Episode (CPE), which has previously been associated with dramatic climate changes throughout the Tethys region. Although the sediments of the Aşağiyaylabel sequence were deposited during the time when the CPE took place, they represent an unexpected, pure carbonate depositional system (chapter II). The onset of the CPE within the western Tethys occurred about 2 million years earlier (= one ammonoid zone) what hints to a diachrony of this event throughout the Tethys, which may occurred earlier at higher palaeolatitudes and later in equatorial areas.

The detected Julian / Tuvalian boundary strata are recognisable by a positive shift in MS- and radiometry values and are traceable along an area of at least 5 km^2. The MS- and radiometry-data at Aşağiyaylabel are the first data from Lower- to Upper Carnian sediments and reliably reflect lithological changes (chapter III). They display an amplified terrigenous input into the marine sediment system, triggered by climatic changes. The boundary from the Kartoz- to the Kasımlar Formation, which represents a change from shallow-water to deeper-water carbonates, shows another, smaller positive shift in the MS-data.

The Aşağiyaylabel sequence is of high taxonomic and biostratigraphic value, as the possibility for investigating a continuous Lower- to Upper Carnian ammonoid record is quite rare. This substantiates the significance of Upper Triassic faunas within the Taurus Mountains and facilitates the correlation with faunal assemblages from other regions in the Tethyan Realm (chapter IV). Concerning biostratigraphic investigations, the sediments of the studied Kasımlar Formation are interpreted as Julian 2 to Tuvalian 1, what represents a detailed proof of the Julian / Tuvalian boundary in this section. Among the stratigraphic significance of those ammonoid faunas, which were deposited during the CPE, some so far unknown Lower Carnian (Julian 2) ammonoid species respectively one new genus from the Kasımlar Formation were described. The newly described genus and species *Kasimlarceltites krystyni* gen. et sp. nov. represents the main faunal element and is found abundantly (*Kasimlarceltites* mass occurrence). Additional new forms within the Lower Carnian Carbonate member (Units A–B) of the Kasımlar Formation, are *Klipsteinia disciformis* sp. nov. and *Anasirenites crassicrenulatus* sp. nov.

A novel three-dimensional reconstruction method, which combines classical orientation analysis with modern 3D-visualisation techniques, was developed for investigating the spatial shell orientation of the *Kasimlarceltites* mass occurrence (chapter V). Dip, dip-direction, and aperture direction of the longitudinal axis of the ammonoids and gastropods as well as dip and azimuth of an imaginary sagittal-plane through each ammonoid were used to determine a statistical NNW/SSE shell orientation from more than 3,000 segmented ammonoids and 200 segmented gastropods. Upon these numbers an estimation of nearly 775 million ammonoids and 50 million gastropods was extrapolated from the segmented and counted individuals for an extension of at least 5 km^2 of the investigated *Kasimlarceltites* limestone bed.

Within chapter VI the newly described method was interpreted in combination with taphonomical and sedimentological results, investigated from samples of additional sections where the *Kasimlarceltites* acme zone was represented (Aşağiyaylabel: AS IV, Karapinar: KA I, II & IV). Furthermore, 2-dimensional orientation measurements from the same localities were constituted within chapter VII. Both methods, 3D- as well as 2D-analyses, show similar results and enable the reconstruction of the history of the mass occurrence and the interpretation of its underlying transport mechanisms. The taphonomic comparisons point to a two-phased genetic history of this mass occurrence which may have started with the formation of the deposit due to episodic anoxic conditions and/or tectonically induced methane degassing. As no traces of bioerosion or encrustation were found and furthermore a significant alignment of the ammonoids was tested, a basinward transport in a diluted sediment, most probably triggered by debris flows, turbidity currents or gravity flows, is assumed. This transport finally led to the secondary deposition as concentration-Lagerstätte sensu Seilacher. The ammonoid shells therefore reflect an allochthonous community, formed by biogenic and sedimentological concentration mechanisms.

Finally, the present thesis contributes to the understanding of the environmental conditions during the Carnian Pluvial Episode within the Tethyan realm. Different classical methods were used in combination with modern as well as with newly established methods. Results were interpreted within a comprehensive context, for contributing to a more detailed insight into the environmental conditions which occurred during the Early to Late Carnian time.

ZUSAMMENFASSUNG

Die folgende Dissertation beinhaltet 5 wissenschaftliche Publikationen und ein eingereichtes Manuskript, welche im Zuge eines vom Österreichischen Forschungsfond (FWF) geförderten Projektes erstellt wurden. Ziel des Projektes (P 22109-B17) war die paläozoologische, paläobiogeo-, litho-, zyklo- und magnetostratigraphische Untersuchung obertriassischer (karnischer) Sedimente im zentralen Taurus Gebirge der südwestlichen Türkei. Der Hauptfokus der Dissertation lag dabei in der Entschlüsselung der Entstehungsgeschichte eines karnischen Ammonoideen-Massenvorkommens (*Kasimlarceltites* Schichten bzw. *Kasimlarceltites* acme zone), welches vor ca. 234 Millionen Jahren innerhalb einiger weniger Kalkgesteinsschichten abgelagert wurde. Die *Kasimlarceltites* acme zone repräsentiert, mit einer Ausdehnung von mehr als 5 km^2, einen Leithorizont innerhalb der Umgebung von Aşağiyaylabel, dessen Untersuchung Einblicke in ein spättriassisches Ökosystem liefern kann.

Der Aufschluss Aşağiyaylabel, im Taurus Gebirges südlich der Stadt Isparta gelegen, stellt eine Schlüssel-Sequenz in Bezug auf Umweltveränderungen am Übergang vom frühen zum späten Karn (Obertrias) dar. Seine Abfolge reicht von Plattformkarbonaten über pelagische und mergelige Kalke bis hin zu Schiefersedimenten. Die Bedeutung dieses Aufschlusses wird durch den Nachweis der Julium / Tuvalium Unterstufengrenze (= Unter- / Oberkarn Grenze) innerhalb der Kasımlar Formation deutlich. Ein wichtiges Ergebnis, gestützt durch sedimentologische und paläontologische Untersuchungen (Kapitel II), ist das Ausbleiben bzw. deutlich spätere Einsetzen der "Carnian Pluvial Episode (CPE)" im Untersuchungsgebiet, welche bislang als zeitgleiche dramatische Klimaveränderung innerhalb der Tethys betrachtet wurde. Im Gegensatz dazu zeigen die Analysen der Sedimentschichten in Aşağiyaylabel innerhalb der CPE ein unerwartetes rein karbonatisches Ablagerungssystem. Die „CPE“ setzt somit in der westlichen Tethys um eine Ammonoideen-Zone (das entspricht ca. 2 Millionen Jahre) später ein, und findet daher innerhalb der Tethys zeitversetzt statt, deutlich früher in höheren Breiten, und später in äquatorialen Breiten.

Die Julium / Tuvalium Grenze konnte mithilfe von geophysikalischen Methoden wie Magnetische Suszeptibilität (MS) und Gamma-ray über eine Distanz von mindestens 5 km^2 korreliert werden, wobei es sich um die ersten geophysikalischen Untersuchungen an unter- / oberkarnischen Sedimenten handelt (Kapitel III). Ein deutlicher Anstieg der radiometrischen Daten sowie der MS-Werte geht mit dem lithologischen Wechsel an der Julium / Tuvalium Grenze einher und spiegelt somit eine direkte Funktion des verstärkten terrigenen Eintrages

in das marine Sedimentsystem wider, welcher höchstwahrscheinlich durch Klima-schwankungen ausgelöst wurde. So konnte beispielsweise ein zusätzlicher leichter Anstieg der MS-Werte am Übergang von den Flachwasser Karbonaten der Kartoz Formation zu den tiefermarineren Karbonaten an der Basis der Kasımlar Formation festgestellt werden.

Neben den Ergebnissen der erwähnten Fazies Untersuchungen und der geophysikalischen Messungen geben die Schichten in Aşağiyaylabel erstmals die Möglichkeit eine Ammonoideen-Fauna über die Unter- / Oberkarn Grenze zu untersuchen (Kapitel IV), was die Bedeutung obertriassischer Faunen innerhalb des Taurus Gebirges heraushebt, und die Korrelation mit Faunen anderer Regionen des tethyalen Raumes erleichtert. Aufgrund der biostratigraphischen Relevanz bestimmter, innerhalb dieser Arbeit beschriebener, Ammonoideen Arten konnte das Alter der untersuchten Abschnitte der Kasımlar Formation als Julium 2 bis Tuvalium 1 eingestuft werden, was eine exakte Festlegung der Julium / Tuvalium Grenze im Profil ermöglicht. Neben den stratigraphischen Erkenntnissen wurden außerdem einige, bislang unbekannte unterkarnische (Julium 2) Ammmonoideen Arten, bzw. eine Ammonoideen Gattung aus der Kasımlar Formation beschrieben. *Kasimlarceltites krystyni* gen. et sp. nov. repräsentiert aufgrund seines Massenvorkommens das am häufigsten auftretende Faunenelement der Lokalität Aşağiyaylabel. *Kasimlarceltites krystyni* gen. et sp. nov. stellt aber nicht das einzige neu beschriebene Faunenelement dar. Auch *Klipsteinia disciformis* sp. nov. und *Anasirenites crassicrenulatus* sp. nov. konnten innerhalb des unterkarnischen karbonatischen Schichtgliedes (Einheit A–B) der Kasımlar Formation entdeckt und neu beschrieben werden.

Um die Entstehung des bereits erwähnten *Kasimlarceltites*-Massenvorkommens besser verstehen zu können, wurde die räumliche Orientierung der Schalenreste innerhalb der Kalkbänke untersucht. Zu diesem Zweck wurde eine neue Methodik zur dreidimensionalen Rekonstruktion interner Strukturen fossiler Massenvorkommen sowie zur Auswertung der Orientierung einzelner Schalenreste im Sediment entwickelt (Kapitel V). Fallwinkel, Fallrichtung und Ausrichtung der Apertur der Längsachse sowie Fallwinkel und Azimut einer imaginären sagittalen Fläche durch jeden Ammoniten wurden zur räumlichen Orientierung eingemessen, wobei eine statistische NNW/SSO Orientierung der Schalenreste von mehr als 3.000 segmentierten Ammonoideen und 200 segmentierten Gastropoden ausgewertet werden konnte. Hochgerechnet auf eine Ausdehnung von 5 km^2 würde das eine Anzahl von fast 775 Millionen Ammonoideen und 50 Millionen Gastropoden ergeben.

Die Ergebnisse der Orientierungsmessungen wurden in Kapitel VI in Zusammenhang mit taphonomischen und sedimentologischen Ergebnissen von Proben weiterer Lokalitäten der *Kasimlarceltites* acme zone (Aşağiyaylabel: AS IV, Karapinar: KA I, II & IV) interpretiert. Zusätzliche zweidimensionale Orientierungsmessungen derselben Lokalitäten werden innerhalb des Kapitels VII beschrieben. Beide Methoden (3D- und 2D-Orientierungsanalysen) zeigen ähnliche Ergebnisse, welche eine Rekonstruktion der Entstehung des Massenvorkommens sowie eine Interpretation dessen Transportmechanismen ermöglichen. Die taphonomischen Untersuchungen lassen auf eine zweiphasige Entstehungsgeschichte dieses Massenvorkommen schließen: Eine primäre Ablagerung aufgrund episodischer anoxischer Bedingungen oder tektonisch induzierter Freisetzung von Methangas, scheint am wahrscheinlichsten. Aufgrund des Fehlens von Bioerosion beziehungsweise Inkrustation kann ein langes Freiliegen der Schalenreste ausgeschlossen werden. Die signifikante Einregelung der Schalenreste lässt auf einen Weitertransport durch fließenden Sedimenttransport, beispielsweise durch Schuttströme, Trübeströme oder Gravitationsströme in Richtung Becken schließen. Der sekundäre Transport führte schlussendlich zu einer Konzentrationslagerstätte sensu Seilacher. Das *Kasimlarceltites* Massenvorkommen stellt daher eine allochthone Ablagerung, basierend auf sedimentologischen Konzentrationsmechanismen dar.

Diese Dissertation trägt zum Verständnis der Umgebungsverhältnisse innerhalb der frühen bis späten karnischen Zeit und deren klimatischen Ereignisse bei, welche durch die „Carnian Pluvial Episode“ innerhalb der Tethys ausgelöst wurden. Verschiedene klassische Methoden sind im Zusammenhang mit modernen sowie neu entwickelten Methoden zur Anwendung gekommen. Die Ergebnisse wurden in einem übergeordneten Zusammenhang betrachtet und interpretiert, um detailliertere Einsichten in die Umweltbedingungen der frühen bis späten karnischen Zeit zu erhalten.

ENCOMPASSED PUBLICATIONS

***Please note that during the composition of this thesis, my name changed from **LUKENEDER S.** to **MAYRHOFER S**.

Chapter II: **LUKENEDER S.***, LUKENEDER A., HARZHAUSER M., ISLAMOGLU Y., KRYSTYN L., LEIN R. 2012. A delayed carbonate factory breakdown during the Tethyan-wide Carnian Pluvial Episode along the Cimmerian terranes (Taurus, Turkey). *Facies*, **58**, 279–296.

Chapter III: **MAYRHOFER S.**, LUKENEDER A. 2015. Susceptibility and radiometry data used for stratigraphic correlations: case study on Upper Triassic beds in Turkey. *In:* DA SILVA A. C., WHALEN M. T., HLADIL J., CHADIMOVA L., CHEN D., SPASSOV S., BOULVAIN F. & DEVLEESCHOUWER X. (eds). Magnetic Susceptibility Application: A Window onto Ancient Environments and Climatic Variations. *Geological Society, London, Special Publications*, **414**, 257–275. http://dx.doi.org/10.1144/SP414.10

Chapter IV: **LUKENEDER S.***, LUKENEDER A. 2014. A new ammonoid fauna from the Carnian (Upper Triassic) Kasimlar Formation of the Taurus Mountains (Anatolia, Turkey). *Palaeontology*, **57 (2)**, 357–396.

Chapter V: **LUKENEDER S.***, LUKENEDER A., WEBER GW. 2014. Computed reconstruction of spatial ammonoid-shell orientation captured from digitized grinding and landmark data. *Computers & Geosciences*, **64**, 104–114.

Chapter VI: **MAYRHOFER S.**, LUKENEDER A., KRYSTYN L. accepted 2016. Taphonomy and palaeoecology of ammonoid shell beds from the Taurus Mountains, Turkey. *Lethaia*.

Chapter VII: LUKENEDER A., **MAYRHOFER S.** 2014. Taphonomic implications from Upper Triassic mass flow deposits: 2-dimensional reconstructions of an ammonoid mass occurrence (Carnian, Taurus Mountains, Turkey). *Geologica Carpathica*, **65/5**, 339–364.

Within the first 5 articles (chapters II–VI) the doctoral candidate made the evaluations, analyses and interpretations of the data as well as wrote the manuscripts. Within chapter VII, the doctoral candidate provided data and partly contributed in writing the manuscript.

CHAPTER I,

INTRODUCTION

The centrepiece of the following thesis is represented by the *Kasimlarceltites* mass occurrence, which is enclosed in the lower part of the Kasımlar Formation within the surroundings of the localities Aşağiyaylabel and Karapınar (at least 5 km^2), located within the Taurus Mountains of southwest Turkey, about 90 km northeast of Antalya. This mass occurrence is of special interest as it was deposited during a time at which Tethyan-wide a climatic crisis occurred. The triggers for this crisis, the Carnian Crisis, are still under discussion and a series of unsolved questions already exists. New insights to the palaeoecological conditions and the ancient environment were expected by the biostratigraphic, taxonomic and taphonomic investigations of the *Kasimlarceltites* mass occurrence, which is part of a most complete stratigraphic sequence from a Lower Carnian carbonate platform (Kartoz Fm.), over marls-bearing limestones (Kasımlar Fm., Lower member), up to shaley sediments of the Upper Carnian (Kasımlar Fm., Upper member).

The results of this thesis were achieved in the course of an FWF-Project (P22109-B17) leaded and initiated by Alexander Lukeneder in 2009. His initial idea for investigating the *Kasimlarceltites* mass occurrence arose from the fact that a larger amount of samples from this mass occurrence already existed within the collection of the Natural History Museum Vienna and the University of Vienna. This material was taken from the main section AS I during previous field trips and excursions organised by Leopold Krystyn in collaboration with Alexander Lukeneder, Mathias Harzhauser, Andreas Gindl, Franz Topka and Philipp Strauss.

The idea was to investigate the taphonomic conditions of the *Kasimlarceltites* mass occurrence by applying modern 3D-visualisation techniques in combination with well-known classical geological methods for getting new insights into the ancient palaeoenvironment and into the scenario which happened when this mass occurrence was deposited and the Carnian Crisis occurred.

As main scientific collaborator within this project, my responsibility was to investigate the already known succession Aşağiyaylabel I (AS I) as well as to search for surrounding localities, AS II–IV and Karapinar I–III (KA I–III), for a better understanding of the lateral extension of this mass occurrence – within a first step by means of facies analysis, ammonoid taxonomy, and geophysical measurements. For further taphonomic orientation analyses, it was needed to develop an adaptive 3D-visualisation technique for investigating the *Kasimlarceltites* mass occurrence.

1.1. Introduction to the study area

The investigated beds represent Lower- to Upper Carnian sediments deposited in the region around Aşağiyaylabel (former Kartoz region), located within the Taurus Mountains of Anatolia (Turkey).

The sediments which crop out in the Taurus Mountains of Turkey generally were formed between the Late Paleozoic (Permian) and the Mesozoic, when the continents Gondwana and Laurasia were combined to the supercontinent Pangea. The Taurus Mountains, together with the Anatolian Mountains, once represented the ancient northern margin of Gondwana. Different from the mostly metamorphosed sediments of the Anatolids are those of the Taurid Mountains, which are usually unmetamorphosed (Robertson *et al.* 2013) though affected by a slight thermal overprint too.

During the Triassic, several oceanic basins were opened, when continental fragments split off from Gondwana and drifted northward towards Eurasia, thereby building the Cimmerian Terranes (Fig. 1.1; Muttoni *et al.* 2009; Robertson *et al.* 2013). Due to this northward drift, the Palaeotethys Ocean (north to the Cimmerian Terranes) underwent subduction and was closed, while the Neotethys (south to the Cimmerian Terranes) was formed at the eastern margin of Gondwana (Sengör 1979; Dercourt *et al.* 1993; Van der Voo 1993; Besse *et al.* 1998; Metcalfe 2006; Muttoni *et al.* 2004; Ruban *et al.* 2007; Muttoni *et al.* 2009). During Carnian time, the Anatolian System (Taurus Mountains, Turkey) has been a part of the Cimmerian Terranes. Not only Turkey, but also todays Iran, Afghanistan, Tibet and Malaysia, were part of these microplates. At this time, the Palaeotethys, north of the Cimmerian Terranes, was still open to the east (Muttoni *et al.* 2009; Fig. 1.1). The shelf areas of the western part of these terranes have been the depositional environment of the sediments found at the investigated sections Aşağiyaylabel and Karapınar within the Taurus Mountains of Turkey.

The Triassic sediments found within the investigated region around Aşağiyaylabel are part of the Anamas-Akseki Autochthonous, and represent a major element within the Taurus Platform Units between the Antalya Suture in the south and the Izmir-Ankara Suture in the north (south of the Isparta Angle; Robertson 1993; Senel 1997; Andrew and Robertson 2002;

Robertson *et al.* 2003). They form the highest summits but also the deepest valleys and play an important role by the formation of the landscape morphology within this region (Dumont 1976). These transgressive sediments of the Kartoz- and Kasımlar Formation are deposited discordant above diverse Palaeozoic rocks (Dumont 1976).

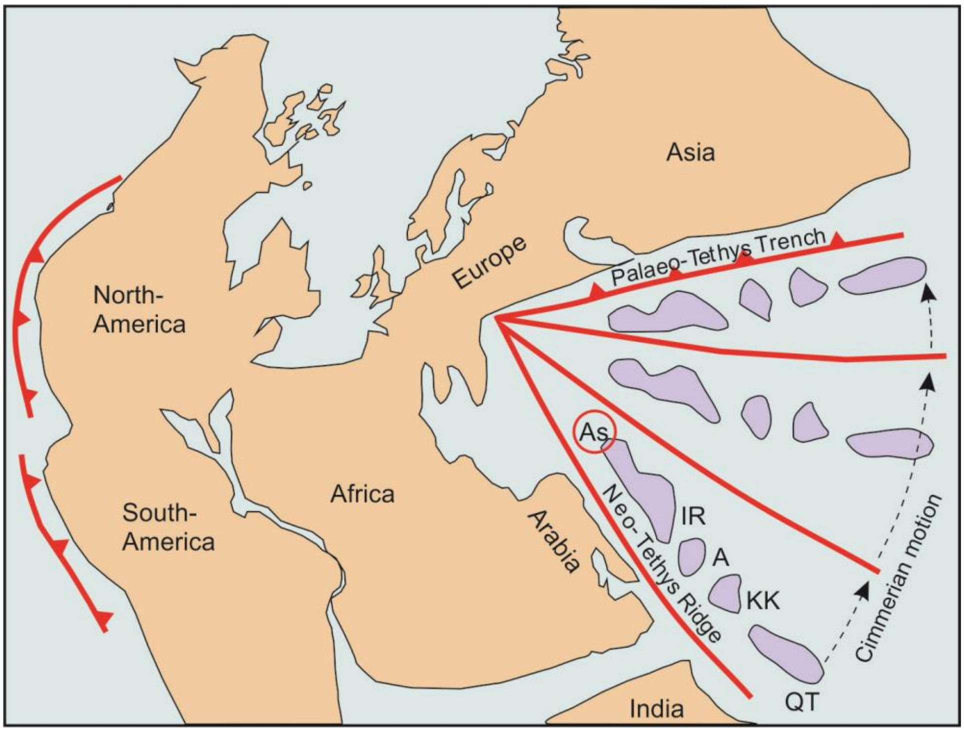

Fig. 1.1. Palaeogeographic motion of the Cimmerian Terranes during the Permian and Triassic. As = Aşağiyaylabel in Turkey, IR = Iran, A = Afghanistan, KK = Karakorma in northern Pakistan, QT = Qiangtang in North-Tibet. Reconstruction slightly modified after Muttoni *et al.* 2009

The Triassic sediments deposited below the Kasımlar Formation are characterized by huge differences in thickness, becoming thicker from southwest to northeast. Beside the Kartoz-series within the region around Aşağiyaylabel and Karapınar, there are two more areas yielding sediments stratigraphically older than the Kasımlar Formation: The Kasımlar region with the Bahçeevleri- and the Haciilyas Formation, as well as the Dipoyraz Dağ with the Muslu-, the Kara Göl- and the Dipoyraz Formation. While the sediments of the Kasımlar region show a thickness of only 100 to 200 m, their time equivalents in the Dipoyraz Dağ (with an altitude between 2000 to 3000 m) reach more than 1000 m (Dumont 1976). Within the region around Aşağiyaylabel and Karapınar, the Kartoz Formation forms characteristic hills and summits with a thickness of about 150 m, deposited unconformably above the Carboniferous Gök-Dağ-series (Dumont 1976). The Kartoz Formation is called after the old name Kartoz (=Asaği-Kartoz) for the little village Aşağiyaylabel where the sediments of this formation were described for the first time.

Dumont (1976) was one of the first who investigated Upper Triassic sediments in the southern Taurus region, with a focus on the Kartoz Formation. Further investigations about the geology of southwestern Turkey were done by Özgül and Arpat (1973), Dumont and Kerey (1975), Monod (1977), Poisson (1977), Gutnic *et al.* (1979), Robertson (1993, 2000), Senel (1997) and Robertson *et al.* (2003). Gindl (2000) had a more detailed look to the Kasımlar Formation, especially to the *Kasimlarceltites* mass occurrence, which he originally named the *Orthoceltites* mass occurrence. Although Gindl recognised within his master thesis (Gindl 2000) that the ammonoid species, which dominates the mass occurrence within the Kasımlar Formation, must represent a new species, he did not realise that it also represents a new genus. Within the taxonomic part of this study (Lukeneder and Lukeneder 2014, Chapter IV) the species *Orthoceltites* n. sp.1 of Gindl (2000) is now classified as "*Kasimlarceltites krystyni"* gen. et sp. nov.

1.2. The Carnian Pluvial Episode (CPE)

Hallam (1996) as well as Hallam and Wignal (1997) noted, that there are four intra-Triassic extinction events of global relevance between the end-Permian and the Jurassic / Triassic extinction event, one of them the "mid-Carnian event". Beside the "mid-Carnian event", they described the Smithian / Spathian-, the Carnian / Norian- and the Norian / Rhaetian boundary events (Hornung 2008). Already Hornung (2008) mentioned that the Triassic period became one of the most studied time slices regarding the documentation and interpretation of biotic crisis (Hornung 2008; Hallam 1996; Erwin *et al.* 2002).

The "mid-Carnian event" took place during the time slice at which the sediments in the surrounding of Aşağiyaylabel and Karapınar were deposited. Therefore the investigated sections are of global significance. The "mid-Carnian event" (Hallam 1996) has reached publicity in form of a series of different names, for example, the "Carnian Crisis" (Hornung 2008), the "Reingraben turning point" (Schlager and Schöllnberger 1974), the "Carnian Pluvial Event" (Simms and Ruffel 1989) or the "Carnian Pluvial Episode" (Lukeneder *et al.* 2012).

This event is represented by a nearly synchronous carbonate platform demise within the Tethyan realm in late Early Carnian time (Julian 1/IIc; Hornung and Brandner 2005; Hornung *et al.* 2005). Nevertheless, this thesis shows that this synchronity is not true for every locality. Within the surroundings of Aşağiyaylabel, the demise starts at the end of the Julian II, exactly at the Julian / Tuvalian boundary (Chapter II), and is therefore synchronous to the demise in the Lagonegro Basin (southern Apennines, Italy), where it is represented by a succession of green shales and radiolarites (Rigo *et al.* 2007). This time shift of the climatic turnover at Aşağiyaylabel is an important result of this thesis.

The trigger mechanisms for the CPE are not definitely solved. Enhanced humidification (Simms and Ruffell 1989; Hornung *et al*. 2007a, b), global warming and monsoonal phases are proposed reasons for the climatic turnover. The rifting of Pangea might be a possible reason for the global warming and as a follow-up result for the humidification of the climate. Dal Corso *et al.* (2012) set the humidification in context with the eruption of the flood basalt province of Wrangellia.

1.3. Methodology

Within this thesis, selected outcrops around the key section of Aşağiyaylabel (AS I) were investigated by different kind of methods. Beside classical facies- and biostratigraphic analyses (chapter II & IV), a range of new approaches, for example geophysical measurements (chapter III) or modern visualisation techniques (chapter V–VI), were used to deduce taphonomic information (chapter VI–VII) about the environment in which the upper Lower- to lower Upper Carnian sediments of Aşağiyaylabel and surroundings were deposited.

1.3.1. Facies analyses

Within chapter II of this thesis a detailed facies analysis and palaeodepth reconstruction was achieved by sedimentological and palaeontological analyses for which the SMF Types of Flügel were used, and therefrom the ancient environment around Aşağiyaylabel interpreted. The classification of sediments concerning their microfacies is used since the forties of the 19^{th} Century (Flügel 1978). One of the first microfacies analysis was done by Pia (1933) and by Sander (1936). Flügel (1972) summarized microfacies criteria and defined Standard Microfacies Types (SMF Types), which were expanded and more strictly defined by Wilson (1975) and are already used within today's research studies as classical standard analysis method for interpreting the ancient environment from the sediments which have been deposited. 24 SMF Types were defined by Wilson (1975) on the basis of grain types and frequency, matrix types, depositional fabrics, fossils and depositional texture types, for using them as supplementary criteria for interpreting the major facies belts zones of an idealised rimmed carbonate shelf (Flügel 2004). Although this method is quite old, it is one of the basic, well-used standard methods for interpreting sedimentary deposits for their depositional environment. Modern techniques like for example geophysical measurements or 3D-visualisation techniques are in most cases interpretable only in combination with basic analyses like facies interpretation or biostratigraphic classification.

1.3.2. Geophysical measurements (Susceptibility & Gamma ray)

At least since Robinson (1990), geophysical measurements (e.g. Susceptibility- or gamma ray logging) are standard methods used in geology for detecting properties of magnetic rocks as there exists a close correlation between magnetic susceptibility (MS)- resp. gamma ray signatures and the marine environment (Ellwood *et al.* 2000; Zhang *et al.* 2000; Racki *et al.* 2002; Da Silva and Boulvain 2006; Babek *et al.* 2010). Magnetic susceptibility is measured for detecting the induced magnetisation which arises at minerals when brought into a low-strength magnetic field (Kodama 2012). Erosion and weathering are the main factors affecting the MS-signature, which are in most cases caused by climatic (Crick *et al.* 2001, 2002) or sea level changes, whether triggered by regression or transgression (Crick *et al.* 1997; Ellwood *et al.* 1999). The gamma ray method measures natural radioactivity, arising from a rock sample. While lower levels are generally measured at sedimentary rocks, higher radiations arise from igneous rocks like granite, but also from shales and phosphate rocks (Tzortzis *et al.* 2003).

Susceptibility- and gamma ray measurements are in most cases done with highly sensitive laboratory machines for detecting specific properties of magnetic rocks (e.g. Hladil *et al.* 2006). Within chapter III, MS- as well as the radiometry measurements were conducted directly in the field, with hand held instruments (GF Instruments: a low-level SM-30 MS meter and a scintillation gamma radiometer, bearing a 51 × 51 mm NaI detector), which do not support such high sensitive measurements as provided by the laboratory devices. Furthermore the radiometry measurements were done without conducting spectral results like potassium (K), uranium (U) or thorium (Th), as such detailed information are not supported by hand held instruments. Within this study, the MS- and radiometry measurements thus were not used for interpreting detailed numerical results, but for interpreting the trend-line of the data measured. MS- and radiometry data from hand held instruments are easy to sample and can represent stable trend lines which might support results achieved from different methods. These methods can be applied as an additional correlation tool, which may prove or question hypothesis taken by different methods as for example facies-, biostratigraphic- or isotopic analyses. The MS- and radiometry data determined from the sections at Aşağiyaylabel (sections I & IV) and Karapinar (sections I–II & IV) well confirm the results achieved through biostratigraphy and facies analysis (chapter II & IV). The lithological boundary between the shallow-water carbonates of the Kartoz Formation and the deeper-water carbonates of the Kasımlar Formation, as well as the lithological change from the carbonate to the shale member of the Kasımlar Fm. (Lower- / Upper Carnian boundary) are well represented by the MS- trend-line but also detectable by the gamma ray data (chapter III).

1.3.3. Triassic Ammonoid biostratigraphy

After the end-Permian mass extinction, two ammonoid families, the otoceratids and the xenodiscids survived, from which the most wide-spread ammonoids during the Triassic, the ceratitids, evolved (Lucas 2010). During the time slice between the Permian / Triassic- and the End Triassic extinction event, the ammonoids underwent enormous radiation and crises, what lead to highly diverse, short living, and widespread species, which reflect perfect requirements for using them as biostratigraphic tools (Balini *et al.* 2010).

Three orders, 80 families, 700 genera and about 5,000 species of Triassic ammonoids can be divided into two large morphogroups, the “trachyostraca” and the “leiostraca”. Most ammonoid families belong to the “trachyostraca”, which is a group of highly ornamented and short-ranging forms used for defining biostratigraphic stages, substages and zones. The “leiostraca” otherwise show smooth shells and relatively long-ranging forms (Balini *et al.* 2010).

Due to the high radiation, ammonoids form, beside conodonts, the main Triassic biostratigraphic markers since the first chronostratigraphic timescale ever has been published by Mojsisovics, Waagen and Diener 1895 (Mojsisovics *et al.* 1895). Tozer (1984) established a review on global Triassic standards compiled from successions of the Alps and Canada (Hornung 2008). Although the Triassic timescale was revised and re-organised several times during the last two centuries, most of the originally defined stages, substages (Mojsisovics *et al.* 1895) and zones are still used today. For example the Cordevolian substage (= *Trachyceras aon* zone), the Julian substage (= *Trachyceras aonoides* zone*)* and the Tuvalian substage (= *Tropites subbullatus* zone*;* Balini *et al.* 2010). Currently two of the 7 stages and all the 15 substages are still based on ammonoid biostratigraphy (Balini *et al.* 2010), with them also the Carnian substages, which were established by Mojsisovics (1874) and Mojsisovics *et al.* (1895). Within the alpine-mediterranean Early Carnian, Krystyn (1978) proposed a revised ammonoid zonation and substage division in which the Cordevolian is eliminated and therefore a single Julian substage established (Krystyn 1978; Hornung 2008; Lucas 2010).

Although ammonoids still provide the base for many substages as well as for two stages of the chronostratigraphic Triassic timescale, they became more and more replaced mostly by conodont stratigraphy, which shows the advantage that their occurrence is not as limited as the occurrence of macrofossils. For example, the four stages Induan, Olenekian, Anisian and Rhaetian are already defined by conodont data (Balini *et al.* 2010). However, the ammonoid biostratigraphy has the advantage of two centuries of research and therefore relies on data from a relatively stable taxonomy, in contrast to the comparably young and therefore more unstable conodont taxonomy (Lucas 2010).

Within this thesis, ammonoids were used for biostratigraphic correlation of the sediments deposited at Aşağiyaylabel and surroundings. Within section AS I one genus (*Kasimlarceltites* gen. nov.) and three species (*Kasimlarceltites krystyni*, *Klipsteinia disciformis* and *Anasirenites crassicrenulatus*) were newly introduced. The Lower- to Upper Carnian boundary was proven by the occurrence of *Anasirenites crassicrenulatus* immediately below and *Spirogmoceras* cf. *shastense* above the boundary between the Carbonate- and the Marlstone member. The section AS I therefore represents one of the rare opportunities for investigating the Lower- to Upper Carnian ammonoid faunal change (Chapter IV).

1.3.4. 3D-visualisation (computed tomography vs. serial grinding)

Since Sollas (1903) used the method of serial grinding for visualising fossil bones of Therapsida and Lysorophia (Camp and Hanna 1937), 3D-visualisation was applied for a wide range of palaeontological studies (e.g., VanderHoof 1931; Simpson 1933; Koslowski 1932; Stensiö 1927; Fourie 1974; Conroy and Vannier 1984; Ketcham and Carlson 2001; Marschallinger 2001; Marschallinger *et al.* 2011; Dockner 2006; Sutton 2008; Garwood *et al.* 2010; Briguglio *et al*. 2011; Kruta *et al.* 2011; Lukeneder 2012). Although in recent years, computed tomography has replaced the method of serial grinding in most studies, there are still samples were computed tomography does not work, for example when the density contrast of the fossils and the embedding sediment is too low. In such cases one has to access to the well-tried method of serial grinding. This is what the study in chapter V shows well. As the density contrast of the ammonoids is nearly the same as for the limestone beds where they have been deposited (2.6–2.8 g/cm^3), computed tomography turned out to be unsuccessful. Therefore the method of serial grinding was used to digitise the ammonoids from a 150 × 45 × 140 mm^3 reference block which was taken from the *Kasimlarceltites* mass occurrence (bed AS 6) of the section Aşağiyaylabel I. 70 slices with a distance of 2 mm were grinded, scanned and therefrom the ammonoids virtually segmented. By using the software package Amira, the ammonoids could be segmented relatively fast and easily from the 2D-slices, using sophisticated segmentation algorithms. The combination of this relatively new approach with already established taphonomic, but also geological orientation methods, made it possible to get insights into the genesis of the *Kasimlarceltites* mass occurrence, and with them to detect some information about the depositional environment during the Carnian time.

1.3.5. Orientation measurements and taphonomic analyses

One of the main questions within this thesis was to decipher the genesis of the *Kasimlarceltites* mass occurrence, and its relation with the Carnian Crisis. The study within chapter V–VII focuses on the taphonomic results of the *Kasimlarceltites* mass occurrences, found within the area around Aşağiyaylabel and Karapinar.

Nearly every kind of trace on an arbitrary fossil can be an evidence for a special process which affected this fossil between its death and its burial, and might therefore be a hint to its depositional environment (Martin 1999). This can be a broken shell which gleans back to an attack by a crayfish, encrustation on some kind of shells or hardground which refer to a long exposure time, or the similar alignment of fossils (e.g. turritellid gastropods, belemnites or ammonoids) which indicate some currents or transport mechanisms influencing the fossils before final deposition (Martin 1999). Many taphonomic processes are thinkable for tracing back a fossils' history.

Therefore the orientations of the ammonoids within the *Kasimlarceltites* mass occurrence have been of special interest for reconstructing their post mortem transport history. In contrast to most studies which focus on the orientation of the fossils from the surfaces of shell beds, the main question of this study was to determine the internal orientation of the ammonoids within the sediment layer. Therefore the method which is used by geologists for defining the orientation of geological lineations and planes, was adapted for the ammonoids and gastropods deposited at AS I bed 6 (Chapter V).

If imagine a sagittal plane through the ammonoids resp. a lineation through the ammonoids or the gastropods, the orientation of these lineations and planes can be analysed in the same way as geological lineations and planes, by using stereographic plots. Stereographic plots are used for the graphical analysis of three dimensional directional data in a two-dimensional way. The spatial orientation of lineations or planes can be described by dip (= angle of fall) and dip direction of the lineation resp. dip and azimuth of the plane. One of the main advantages for using stereographic plots is that only one point shows the three-dimensional orientation of one lineation resp. plane. Therefore a high quantity of data can be plotted within one diagram. The results of nearly 3,000 segmented and measured ammonoids and more than 200 gastropods show a SSE/NNW resp. NNW/SSE alignment of the shells, hinting to a post mortem transport. The method which was developed for the *Kasimlarceltites* mass occurrence can furthermore be easily adapted for the orientation analyses of other fossil mass occurrences.

A series of studies are published to bring a structure within this wide field of traces which can be interpreted in different ways for investigating the original environment respectively the processes which led to their deposition. The research group around Seilacher for example developed a fossil-Lagerstätten concept which divided fossil-Lagerstätten into conservation and concentration deposits (Seilacher 1990). Kidwell *et al.* (1986), on the other hand, established a descriptive nomenclature, including terms like taxonomic composition, bioclastic packing, geometry and internal structure for identifying the genesis of fossil shell concentrations (Martin 1999). Fürsich (1995) included the descriptive parameters “biofabric”, “geometry” and “complexity” for describing shell concentrations.

For interpreting the *Kasimlarceltites* mass occurrence, Kidwell´s approach in combination with Seilacher’s classification was used, with a special focus on the orientation of the ammonoids. Although there are no traces of burrows or encrustation, what means that the exposure time must have been very short, the orientation of the ammonoid-shells might hint to an allochthonous, transported shell concentration. A fast burial must have led to a primary deposition, most probably caused by short anoxic events (Chapter VI). Reworking and transport by gravity or turbidity flows led in a second step to the present concentration-Lagerstätte type sensu Seilacher (1990) indicating the investigated shell orientation toward SSE/NNW resp. NNW/SSE.

1.4. References

ANDREW T. and ROBERTSON A. 2002. The Beyşehir-Hoyran-Hadim nappes: genesis and emplacement of Mesozoic marginal and oceanic unit of the northern Neotethys in southern Turkey. *Journal of the Geological Society of London*, **159**, 529–543.

BABEK O., KALVODA J., ARETZ M., COSSEY P.J., DE VUYST F.X., HERBIG H.G. and SEVASTROPULO G. 2010. The correlation potential of magnetic susceptibility and outcrop gamma-ray logs at Tournaisian-Viséan boundary sections in Western Europe. *In*: DA SILVA A.C. and BOULVAIN F. (eds). Magnetic Susceptibility, Correlations and Palaeozoic Environments. *Geologica Belgica, Brussels*, **13**, 291–308.

BALINI M., LUCAS S.G., JENKS J.F. and SPIELMANN J.A. 2010. Triassic ammonoid biostratigraphy: an overview. 221–262. *In*: LUCAS S.G. (ed.). The Triassic timescale. *Geological Society of London, Special Publication*, **334**, 1–514.

BESSE J., TORCQ F., GALLET Y., RICOU L.E, KRYSTYN L. and SAIDI A. 1998. Late Permian to Late Triassic palaeomagnetic data from Iran: Constraints on the migration of the Iranian block through the Tethyan Ocean and initial destruction of Pangaea. *Geophysical Journal International*, **135/1**, 77–92.

BRIGUGLIO A., METCHER B. and HOHENEGGER J. 2011. Growth rate biometric quantification by x-ray microtomography on larger benthic foraminifera: three-dimensional measurements push nummulitids onto the fourth dimension. *Turkish Journal of Earth Sciences*, **20**, 683–699.

CAMP C.L. and HANNA G.D. 1937. Methods in Paleontology. University of California Press, Berkley, pp. 53–55.

CONROY G.C. and VANNIER M.W. 1984. Noninvasive three-dimensional computer imaging of matrix-filled fossil skulls by high-resolution computed tomography. *Science,* **226**, 456–458.

CRICK R.E., ELLWOOD B.B., EL HASSANI A., FEIST R. and HLADIL J. 1997. Magnetosusceptibility event and cyclostratigraphy (MSEC) of the Eifelian-Givetian GSSP and associated boundary sequences in North Africa and Europe. *Episodes*, **20**, 167–175.

CRICK R.E., ELLWOOD B.B., HLADIL J., EL HASSANI A., HROUDA F. and CHLUPAC I. 2001. Magnetostratigraphy susceptibility of the Pridoli-Lochkovian GSSP (Klonk, Czech Republic) and a coeval sequence in Anti-Atlas Morocco. *Palaeogeography, Palaeoclimatology,* Palaeoecology, **167**, 73–100.

CRICK R.E., DRECSEN R., EL HASSANI A., ELLWOOD B.B., FEIST R., GIRARD C., OVER D.J. and SCHINDLER E. 2002. Magnetostratigraphy susceptibility of the Frasnian/Famennian boundary. *Palaeogeography, Palaeoclimatology, Palaeoecology*, **181**, 67–90.

DAL CORSO J., MIETTO P., NEWTON R.J., PANCOST R.D., PRETO N., ROGHI G. and WIGNALL P.B. 2012. Discovery of a major negative $d^{13}C$ spike in the Carnian (Late Triassic) linked to the eruption of Wrangellia flood basalts. *Geology*, **40**, 79–82.

DA SILVA A.C. and BOULVAIN F. 2006. Upper Devonian carbonate platform correlations and sea level variations recorded in magnetic susceptibility. *Palaeogeography, Palaeoclimatology, Palaeoecology*, **240**, 373–388.

DERCOURT J., RICOU L.E. and VRIELYNCK B. 1993. Atlas Tethys, Palaeoenvironmental Maps. Gauthier-Villars, Paris, 307 p.

DOCKNER M. 2006. Comparison of *Crocuta crocuta* and *Crocuta crocuta spelaea* through computer tomography (Unpublished Diploma thesis). University of Vienna, Vienna, 68 pp.

DUMONT J.F. 1976. Etudes géologiques dans les Taurides Occidentales: Les formations paléozoiques et mésozoiques de la coupole de Karacahisar (Province d´Isparta, Turquie). Dissertation, University of South Paris, p. 213.

DUMONT J.F. and KEREY E. 1975. The Kirkavak Fault. *Bulletin of the Geological Society of Turkey*, **18**, 59–62.

ELLWOOD B.B., CRICK R.E. and EL HASSANI A. 1999. The magnetosusceptibility event and cyclostratigraphy (MSEC) method used in geological correlation of Devonian rocks from Anti-Atlas Morocco. *American Association of Petroleum Geologists Bulletin*, **83**, 1119–1134.

ELLWOOD B.B., CRICK R.E., EL HASSANI A., BENOIST S.L. and YOUNG R.H. 2000. Magnetosusceptibility event and cyclostratigraphy method applied to marine rocks: detrital input v. carbonate productivity. *Geology*, **25**, 1135–1138.

ERWIN D.H., BOWRING S.A. and YUGAN, J. 2002. End-Permian mass extinctions: A review. *In*: KOEBERL C. and MACLEOD, K.G. (eds) Catastrophic Events and Extinctions; Impacts and Beyond. *Geological Society of America Special Paper*, **356**, 363–383.

FLÜGEL E. 1972. Mikrofazielle Untersuchungen in der alpinen Trias: Methoden und Probleme. *Mitteilungen der Gesellschaft der Geologie- und Bergbaustudenten*, **21**, 9–64.

FLÜGEL E. 1978. Mikrofazielle Untersuchungsmethoden von Kalken. Springer-Verlag, Berlin, Heidelberg, New York, 454 p.

FLÜGEL E. 2004. Microfacies of carbonate rocks. Springer, Berlin, p 976.

FOURIE S. 1974. The cranial morphology of *Thrinaxodon liorhinus* Seeley. *Annals of the South African Museum*, **65**, 337–400.

FÜRSICH F.T. 1995. Shell concentrations. *Eclogae Geologicae Helvetiae*, **88/3**, 643–655.

GARWOOD R.G., IMRAN A.R. and SUTTON M.D. 2010. From clergymen to computers – the advent of virtual palaeontology. *Geology Today*, **26(3)**, 96–100.

GINDL A. 2000. Paläoökologie triassischer Ammonitenfaunen des Taurusgebirges (Türkei). Unpublished Diploma thesis, University of Vienna, pp. 80.

GUTNIC M., MONOD O., POISSON A. and DUMONT J.F. 1979. Géologie des Taurides Occidentales (Turquie). *Mémoires de la Société géologique de France*, **137**, 1–112.

HALLAM A. 1996. Major Bio-Events in the Triassic and Jurassic. *In*: Walliser, O.H. (ed.) Global Events and Event-Stratigraphy, Springer, 332 p.

HALLAM A. and WIGNALL P.B. 1997. Mass extinctions and their aftermath. Oxford University Press, Oxford, pp. 330.

HORNUNG T. 2008. The Carnian Crisis in the Tethys Realm. Multistratigraphic Studies and Palaeoclimate Constraints, VDM Verlag Dr. Müller, 235 p.

HORNUNG T. and BRANDNER R. 2005. Biochronostratigraphy of the Reingraben Turnover (Hallstatt Facies Belt): local black shale events controlled by regional tectonics, climatic change and plate tectonics. *Facies,* **51**, 475–494.

HORNUNG T., BRANDNER R. and KRYSTYN L. 2005. Carnian black shale events triggered by Cimmerian-Eurasian collision? Abstract Book/CD, EGU-Meeting April 2005, Vienna.

HORNUNG T., SPATZENEGGER A. and JOACHIMSKY M.M. 2007a. Multistratigraphy of condensed ammonite beds of the Rappoltstein (Berchtesgaden, Southern Germany): unravelling palaeo-environmental conditions on 'Hallstatt deep swells' during the Reingraben Event (late Lower Carnian). *Facies*, **53**, 267–292.

HORNUNG T., BRANDNER R., KRYSTYN L., JOACHIMSKY M.M. and KEIM L. 2007b. Multistratigraphic constraints on the NW Tethyan ''Carnian Crisis''. *New Museum of Natural History and Science Bulletins*, **4**, 59–67.

HLADIL J., GERSL M., STRNAD L., FRANA J., LANGROVA A. and SPISIAK J. 2006. Stratigraphic variation of complex impurities in platform limestones and possible significance of atmospheric dust: a study with emphasis on gamma-ray spectrometry and magnetic susceptibility outcrop logging (Eifelian-Frasnian, Moravia, Czech Republic). *International Journal of Earth Sciences (Geologische Rundschau)*, **95**, 703–723.

KETCHAM R.A. and CARLSON W.D. 2001. Acquisition, optimization and interpretation of X-ray computed tomographic imagery: applications to the geosciences. *Computers and Geosciences*, **27**, 381–400.

KIDWELL S.M., FÜRSICH F.T. and AIGNER T. 1986. Conceptual framework for the analysis and classification of fossil concentrations. *Palaios*, **1**, 228–238.

KODAMA K.P. 2012. Paleomagnetism of Sedimentary Rocks. Process and Interpretation. Wiley-Blackwell, Chichester, UK.

KOSLOWSKI R., 1932. Sur un procédé simple et précis d´effectuer les coupes sérielles des fossiles. *Paläontologische Zeitschrift*, **13**, 316–318.

KRUTA I., LANDMAN N., ROUGET I., CECCA F. and TAFFOREAU P. 2011. The role of ammonites in the Mesozoic Marine Food Web revealed by Jaw Preservation. *Science*, **331/ 6013**, 70–72.

KRYSTYN L. 1978. Eine neue Zonengliederung im alpin-mediterranen Unterkarn. Schriftenreihe der Erdwissenschaftlichen Kommissionen. *Österreichische Akademie der Wissenschaften*, **4**, 37–75.

LUCAS S.G. 2010. The Triassic chronostratigraphic scale: history and status. 17–39. *In*: LUCAS S.G. (ed.). The Triassic timescale. *Geological Society, Special Publication*, **334**, 514 pp.

LUKENEDER S., LUKENEDER A., HARZHAUSER M., ISLAMOGLU Y., KRYSTYN L. and LEIN R. 2012. A delayed carbonate factory breakdown during the Tethyan-wide Carnian pluvial episode along the Cimmerian terranes (Taurus, Turkey). *Facies*, **58**, 279–296.

LUKENEDER A. 2012. Computed 3D visualization of an extinct cephalopod using computer tomographs. *Computers and Geosciences*, **45**, 68–74.

LUKENEDER S. and LUKENEDER A. 2014. A new Ammonoid Fauna from the Carnian (Upper Triassic) Kasımlar Formation of the Taurus Mountains (Anatolia, Turkey). *Palaeontology*, **57/2**, 357–396. Open Access. Doi: 10.1111/pala.12070.

MARSCHALLINGER R. 2001. Three-dimensional reconstruction and visualization of geological materials with IDL – examples and source code. *Computers and Geosciences*, **27**, 419–426.

MARSCHALLINGER R., HOFMANN P., DAXNER-HÖCK G. and KETCHAM R.A. 2011. Solid modeling of fossil small mammal teeth. *Computers and Geosciences*, **37**, 1364–1371.

MARTIN R.E. 1999. Taphonomy. A Process Approach, Cambridge University Press, Cambridge, 1–26.

METCALFE I. 2006. Palaeozoic and Mesozoic tectonic evolution and palaeogeography of East Asian crustal fragments: The Korean Peninsula in context. *Gondwana Research*, **9**, 24–46.

MOJSISOVICS E. 1874. Faunengebiete und Faciesgebilde der Trias-Periode in den Ost-Alpen. *Jahrbuch der Geologischen Reichsanstalt Wien*, **24**, 81–134.

MOJSISOVICS E., WAAGEN W. and DIENER C. 1895. Entwurf einer Gliederung der pelagischen Sedimente des Trias-Systems. *Sitzungsberichte der Kaiserlichen Akademie der Wissenschaften der Mathematisch-Naturwissenschaftlichen Klasse*, 54, 487–490.

MONOD O. 1977. Recherches géologiques dans le Taurus Occidental au sud de Beyşehir (Turquie). Dissertation, University of South Paris, p 442.

MUTTONI G., KENT D.V., GARZANTI E., BRACK P., ABRAHAMSEN N. and GAETANI M. 2004. Erratum to "Early Permian Pangea 'B' to Late Permian Pangea 'A'". [Earth and Planetary Science Letters, v. 215, no. 3, p. 379-394]. *Earth and Planetary Science Letters*, **218/3**, 539–540.

MUTTONI G., GAETANI M., KENT D.V., SCIUNNACH D., ANGIOLINI L., BERRA F., GARZANTI E., MATTEI M. and ZANCHI A. 2009. Opening of the Neo-Tethys Ocean and the Pangea B to Pangea A transformation during the Permian. *GeoArabia*, **14/4**, 17–48.

ÖZGÜL N. and ARPAT E. 1973. Structural units of Taurus orogenic belt and their continuation in the neighbouring regions. *Bulletin of the Geological Society of Greece*, **10**, 156–164.

PIA J. 1933. Die rezenten Kalksteine. *Mineralogische und Petrographische Mitteilungen, Neue Folge.* ***Ergänzungsband***, Leipzig, 420 p.

POISSON A. 1977. Recherches géologiques dans le Taurus Occidental (Turquie). Dissertation, University of South Paris, p 759.

RACKI G., RACKA M., MATYJA H. and DEVLEESCHOUWER X. 2002. The Frasnian/Famennian boundary interval in the South Polish-Moravian shelf basins: integrated event-stratigraphical approach. *Palaeogeography, Palaeoclimatology, Palaeoecology*, **181**, 251–297.

RIGO M., PRETO N., ROGHI G. and TATEO F. 2007. A rise in the carbonate compensation depth of western Tethys in the Carian (Late Triassic): Deep-water evidence for the Carnian Pluvial Event. *Palaeogeography, Palaeoclimatology, Palaeoecology*, **246**, 188–2095.

ROBERTSON A.H.F. 1993. Mesozoic-Tertiary sedimentary and tectonic evolution of Neotethyan carbonate platforms, margins and small ocean basins in the Antalya Complex, southwest Turkey. *Special Publications of the International Association of Sedimentologists*, **20**, 415–465.

ROBERTSON A.H.F. 2000. Mesozoic-Tertiary tectonic-sedimentary evolution of a south Tethyan Oceanic Basin and its margins in southern Turkey. *Geological Society of London Special Publications*, **173**, 97–138.

ROBERTSON A.H.F., POISSON A. and AKINCI Ö. 2003. Developments in research concerning Mesozoic- Tertiary Tethys and neotectonics in the Isparta Angle, SW Turkey. *Geological Journal*, **38**, 195–234.

ROBERTSON A.H.F., PARLAK E. and ÜNLÜGENÇ U.C. 2013. Editorial Introduction to 'Geological Development of Anatolia and the Easternmost Mediterranean Region'. *In:* ROBERTSON A.H.F., PARLAK E. and ÜNLÜGENÇ U.C. (eds). *Geological Development of Anatolia and the Easternmost Mediterranean Region. Geological Soceity Special Publication*, **372**, 1–7.

ROBINSON S.G. 1990. Applications for whole core magnetic susceptibility measurements of deep-sea sediments. Leg 115 results. *Proceedings of the Ocean Drilling Program, Scientific Results*, **115**, 737–771.

RUBAN D.A., AL-HUSSEINI M.I. and IWASAKI Y. 2007. Review of Middle East Paleozoic plate tectonics. *GeoArabia*, **12/3**, 35–56.

SANDER B. 1936. Beiträge zur Kenntnis der Anlagerungsgefüge (Rythmische Kalke und Dolomite aus der Trias). *Tschermarks Mineralogische und Petrographische Mitteilungen*, **48**, 27–139.

SCHLAGER W. and SCHÖLLNBERGER W. 1974. Das Prinzip stratigraphischer Wenden in der Schichtfolge der Nördlichen Kalkalpen. *Mitteilungen der Geologischen Gesellschaft Wien*, **66/67**, 165–193.

SEILACHER A. 1990. Taphonomy of Fossil-Lagerstätten: Overview. *In*: BRIGGS D.E.G. and CROWTHER P.R. (eds). Paleobiology: a synthesis. Blackwell Scientific, Oxford, 266–270.

SENGÖR A.M.C. 1979. Mid-Mesozoic closure of Permo-Triassic Tethys and its implications. *Nature*, **279**, 590–593.

SENEL M. 1997. Türkiye Jeoloji Haritalari, Nr. 4, Isparta Paftasi, Jeoloji Etütleri Dairesi, Ankara, 23 pp.

SIMMS M.J. and RUFFEL A.H. 1989. Synchroneity of climate change and extinctions in the Late Triassic. *Geology*, **17**, 265–268.

SIMPSON G.G. 1933. A simplified serial sectioning technique for the study of fossils. *American Museum Novitates*, **634**, 1–6.

SOLLAS W.J. 1903. A method for investigation of fossils by serial sections. *Philosophical Transactions of the Royal Society*, **B196**, 259–265.

STENSIÖ E.A. 1927. The Downtonian and Devonian Vertebrates of Spitsbergen, Pt.I. Familiy Cephalaspidae. *Skrifter Om Svalbard Og Nordishavet*, **12**, 1–391.

SUTTON M.D. 2008. Tomographic techniques for the study of exceptionally preserved fossils. *Proceedings of the Royal Society*, **B275**, 1587–1593.

TOZER E.T. 1984. The Trias and its ammonoids: the evolution of a time scale. *Geological Survey of Canada Miscellaneous Report*, **35**, 1–171.

TZORTZIS M., TSERTOS H., CHRISTOFIDES S. and CHRISTODOULIDES G. 2003. Gamma-ray measurements of naturally occurring radioactive samples from Cyprus characteristic geological rocks. *Radiation Measurements*, **37**, 221–229.

VAN DER VOO R. 1993. Paleomagnetism of the Atlantic, Tethys and Iapetus Oceans. Cambridge University Press, Cambridge, 411 p.

VANDERHOOF V.L. 1931. *Borophagus littoralis* from the Marine Tertiary of California. *University of California Publications, Bulletin Department of Geological Science*, **vol. 21**, 15–24.

WILSON J.L. 1975. Carbonate facies in geologic history. Springer, Berlin, p 471.

ZHANG S., WANG X. and ZHU H. 2000. Magnetic susceptibility variations of carbonates controlled by sea level changes. Examples in Devonian to Carboniferous strata in southern Guizhou Province, China. *Science in China D, Earth Sciences*, **43**, 266–276.

CHAPTER II,

PUBLISHED 2012 IN FACIES 58: 279–296

A DELAYED CARBONATE FACTORY BREAKDOWN DURING THE TETHYAN WIDE CARNIAN PLUVIAL EPISODE ALONG THE CIMMERIAN TERRANES (TAURUS, TURKEY)

Susanne Lukeneder[a], Alexander Lukeneder[a], Mathias Harzhauser[a], Yeşim İslamoğlu[b], Leopold Krystyn[c], Richard Lein[d]

[a] Museum of Natural History Vienna, Vienna, Austria

[b] MTA - Mine Research Department, Ankara, Turkey

[c] Department of Palaeontology, University of Vienna, Vienna, Austria

[d] Department of Geodynamics and Sedimentology, University of Vienna, Vienna, Austria

Abstract

This paper presents a detailed facies analysis and paleo-depth reconstruction of a latest Early Carnian platform drowning-sequence from the Anatolian terrane (Turkey, Taurus Mountains). A total of eight sedimentary microfacies zones were recorded. An open platform margin passes through a deeper shelf margin setting into a basinal environment influenced by more open-marine conditions. The analysis demonstrates an unexpected, pure carbonate depositional system through the so-called Carnian Pluvial Episode (CPE), which has previously been associated with dramatic climate changes throughout the Tethys region. One main finding, based on sedimentological and paleontological analyses, is a much later drowning of the carbonate platforms in Turkey than in other places. The termination of the Kartoz platform postdates the onset of the CPE in the western Tethys by one ammonite zone, corresponding to about 2 million years. The distinctly earlier demise of (north)western Tethyan carbonate platforms and reefs points to a diachrony of this event throughout the Tethys. The decline of carbonate productivity clearly occurs earlier at higher paleolatitudes and later in equatorial areas. Interpreting the CPE as the result of a global or at least Tethys-wide climatic event is therefore highly ambiguous. The described facies changes at Aşağiyaylabel probably mirror different coupling effects and, only minimally, the Tethyan-wide climate changes during the Carnian Pluvial Episode.

Keywords: Facies change, Carnian Pluvial Episode, Late Triassic, Tethys realm, Taurus Mountains, Turkey.

2.1. Introduction

In Europe, the platform and reef demise during the Early Carnian is known as the Carnian Crisis or the Carnian Pluvial Episode (Simms and Ruffell 1989). According to Kozur and Bachmann (2010), this was a longer and multi-phased process rather than a single event. We therefore prefer the original term Carnian Pluvial Episode (CPE) (Simms and Ruffell 1989) instead of ‘‘Middle Carnian Pluvial Event’’ (Hornung and Brandner 2005), which corresponds to the MCWI (= Middle Carnian Wet Intermezzo) of Kozur and Bachmann (2010). This episode is characterized by abundant siliciclastics transported by large rivers from the Baltic Craton towards the northwestern branch of the Tethys. This resulted in a collapse of the reef and carbonate platform systems and an accumulation of siliciclastic material in basinal areas and on the shelves (Tollmann 1976; Aigner and Bachmann 1992; Hornung and Brandner 2005). This involved an almost complete breakdown of reef ecosystems, combined with an abrupt decline of carbonate production (e.g., Riedel 1991; Rüffer and Zamparelli 1997; Flügel and Senowbari-Daryan 2001; Keim *et al.* 2001). The sudden increase in siliciclastic input (Reingraben Event) explains the breakdown of the carbonate factory (Hornung and Brandner 2005). The ‘‘mid-Carnian Event’’ (after Hallam 1996; Hallam and Wignall 1997) is one of the five main extinction events in the Triassic with global relevance. Palynological investigations by Hochuli and Frank (2000) date the siliciclastic interval of the Cluozza Member (Eastern Swiss Alps) as Lower Carnian (Julian) and indicate humid conditions caused by a major transgressive phase. Gianolla *et al.* (1998) correlated the flooding event of the first Carnian sequence with the Ladinian/Carnian boundary (Gianolla *et al.* 1998; Hochuli and Frank 2000). These humid environmental conditions during the latest Julian and earliest Tuvalian were documented by palynological investigations in the Carnian of the Cave del Predil area (Julian Alps, NE Italy) (Roghi 2004). The ‘‘mid-Carnian Event’’ is the nominal equivalent of the so-called ‘‘Reingraben turning point’’ of Schlager and Schöllnberger (1974), reflected in biofacies, lithofacies, and in evolutionary events mirrored in all facies belts of the entire NW Tethyan continental margin (Hornung and Brandner 2005).

The studied sequence at Aşağiyaylabel starts with shallow-water limestones of the Kartoz Formation, with thick-shelled bivalves and corals. This phase ends with a corroded and iron oxide-stained dissolution surface, pointing to subaerial exposure. The Kartoz Formation is drowned and disconformably overlain by deeper-water, hemipelagic, black limestones of the Kasımlar Formation with a thin level of ammonite floatstones (*Orthoceltites* beds) at the base. This is followed by a thick slump breccia containing up to meter-sized patch reef blocks together with comparably small ammonite coquinas and filament limestone components. The Early to Late Carnian boundary is marked by a change to grey limy marlstones, with rare ammonite- and pelagic-bivalve-bearing layers passing upwards into a thick pile of sterile dark shale with thin silty and rare siliciclastic interbeds. Microfacies analysis shows the Carnian depositional system at Aşağiyaylabel to be an intra-shelf platform environment grading upwards into deeper zones influenced by pelagic conditions.

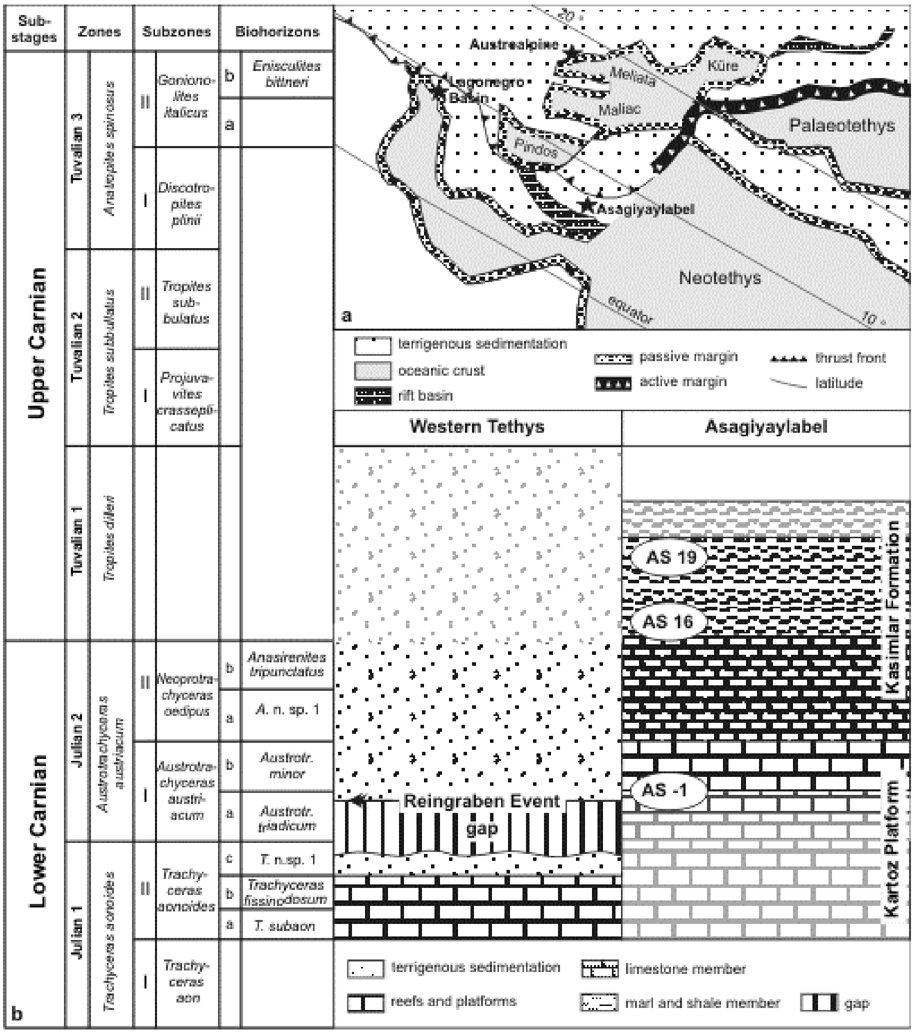

Fig. 2.1. a, Paleogeographic position of the Taurus and Anatolian terranes during the Upper Triassic (after Stampfli *et al.* 2002) with marked position of Aşağiyaylabel, the Lagonegro Basin, and the Austroalpine region. The paleolatitude is based on Moix *et al.* (2008), but contrasts with Muttoni *et al.* (2004). **b,** Late Triassic time-scale accompanied by depositional areas of the western Tethys and the lithological sequence from Aşağiyaylabel.

The main topic at Aşağiyaylabel was originally to determine the environmental conditions and the original paleodepth of the Carnian ammonite mass-occurrence. However, a delayed carbonate productivity crisis at Aşağiyaylabel versus in western Tethys sections casts doubt on the Carnian event hypothesis and sparked the present facies study.

The CPE is dated to the upper *Trachyceras aonoides* and the entire *Austrotrachyceras austriacum* ammonite zones (Fig. 2.1b) with a duration of ca. 3.5 m.y. according to Gradstein *et al.* (2004) and Ogg *et al.* (2008) (based on the involved ammonite zones). This is distinctly longer than the 1 m.y. duration assumed by Hornung *et al.* (2007a, b). Platform drowning and change to argillaceous sedimentation, however, occurred much later in Aşağiyaylabel, i.e., close to or at the top of the *Austriacum* Zone. The main cause of the CPE is still under discussion (Kozur 1989; Simms and Ruffell 1989; Simms *et al.* 1995; Keim *et al.* 2001; Hornung and Brandner 2005; Rigo *et al.* 2007). Global warming, combined with enhanced humidification during the Early Carnian, probably triggered a climate change during that time interval (Hornung *et al.* 2006, 2007a, b; Hornung 2008).

2.2. Geography and geological setting

The Aşağiyaylabel section is located in southwest Turkey, about 90 km northeast of Antalya and approximately 70 km southeast of Isparta (Fig. 2.2). Aşağiyaylabel is accessible from the two major cities of the region, Eğirdir and Beyşehir, located 50 km and 40 km away, respectively. The locality adjoins the small village Aşağiyaylabel (1,000 m above sea-level) on the northern slope of an east to west trending ridge between 1,050 m and 1,100 m at N 37.551389° and E 31.304444°. The former name of Aşağiyaylabel was Kartoz, after which the Kartoz Formation was named (Dumont 1976; Gindl 2000). Geologically, the area is located on the Anamas Dağ carbonate platform or Anamas-Akseki Autochthonous. The Anamas Dağ is part of the so-called Taurus-Platform-Units between the Antalya Suture in the south and the Izmir-Ankara Suture in the north, south of the Isparta Angle (Robertson 1993; Senel 1997; Andrew and Robertson 2002; Robertson *et al.* 2003). The Anamas-Akseki Autochthonous (= Karacahisar-Autochthonous) includes Middle to Late Triassic limestones, marlstones and shales of up to 500 m thickness (Gindl 2000). The geology of southwestern Turkey and the Anamas Dağ carbonate platform has been extensively investigated by Özgül and Arpat (1973), Dumont and Kerey (1975), Monod (1977), Poisson (1977), Gutnic *et al.* (1979), Robertson (1993, 2000), Senel (1997), and Robertson *et al.* (2003).

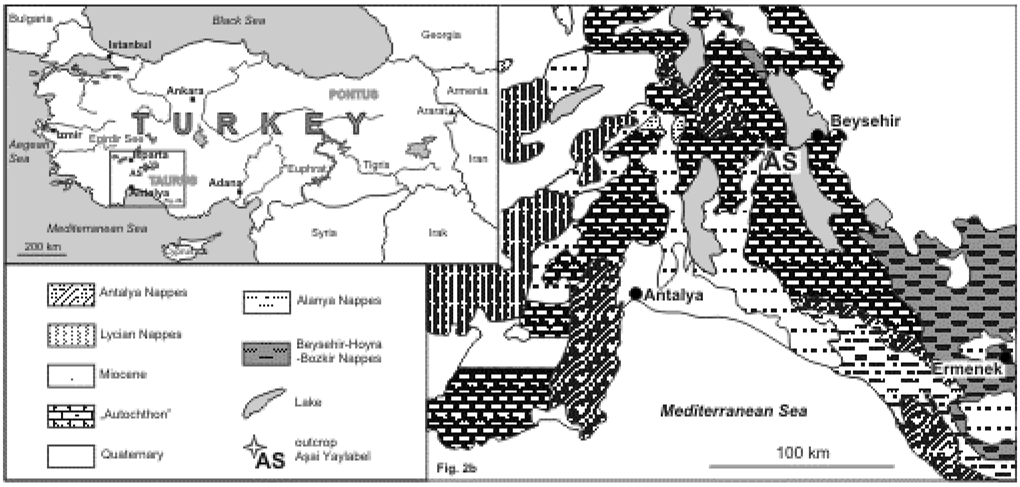

Fig. 2.2. Geography and geology of the investigated area with indicated position of the section Aşağiyaylabel in the Taurus Mountains (Anatolia, Turkey). Tectonic map modified after Gallet *et al.* (2007).

The paleogeographic domain of the Anatolian System (Taurus Mountains, Turkey) was characterized during Triassic times by microplates located in the middle of the western Tethys Ocean. The investigated sequence was deposited in an intra-shelf basin of equatorial paleolatitudes at the western end of the ‘‘Cimmerian terranes’’ or ‘‘Cimmerian blocks’’ (Şengör *et al.* 1984; Dercourt *et al.* 1993, 2000; Gindl 2000; Scotese *et al.* 1989; Scotese 1998, 2001; Stampfli and Borel 2002; Stampfli *et al.* 2002) (Fig. 2.1a). This area was located between the ‘‘old’’ Paleotethys in the north and the Neotethys in the south during the Late Triassic (Carnian, 228–216.5 Ma; Gindl 2000; Gradstein *et al.* 2004). While the Paleotethys Ocean underwent subduction along the southern margin of Eurasia, the young Neotethys Ocean (southern branch of Neotethys, sensu Şengör and Yilmaz 1981) was widened between the African continent and the Cimmerian terranes, which consisted of Turkey, Iran, Afghanistan, Tibet, and Malaysia (Golonka 2004). In the north of these Cimmerian terranes, the Izmir-Ankara Ocean (northern branch of the Neotethys, sensu Şengör and Yilmaz 1981) and the ‘‘old’’ Paleotethys were still open to the east (Tekin *et al.* 2002; Golonka 2004; Tekin and Göncüoğlu 2007; Göncüoğlu *et al.* 2010).

The Triassic sequence of Aşağiyaylabel starts with an angular unconformity above Carboniferous rocks (Dumont 1976; Gindl 2000). The main formations are the Middle to Late Triassic Kartoz Formation (Early Carnian) and the Kasımlar Formation (latest Early Carnian to Late Carnian). The Kartoz Formation consists of shallow water platform carbonates with thick-shelled bivalves (megalodonts) and corals. In contrast, the overlying Kasımlar Formation starts disconformly (e.g., hiatus) with an 8-m-thick pile of deeper-water limestones; this passes via another 12 m of marlstones into shales (Fig. 2.3). The section is dated based on conodonts, ammonites, and halobiids; their detailed age assignment follows Krystyn *et al.* (2002) and Gallet *et al.* (2007). The strata dip approx. 45° towards northeast.

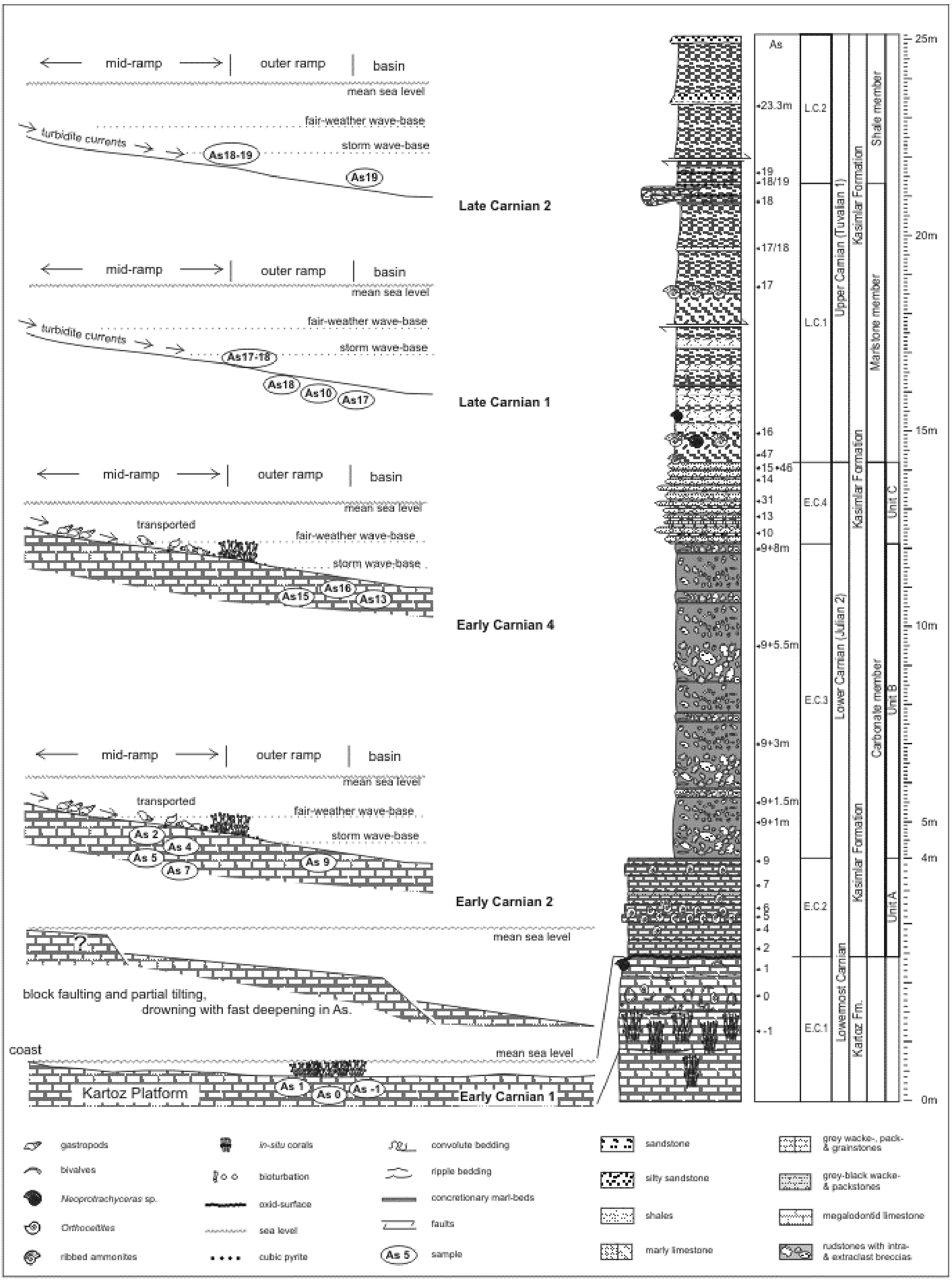

Fig. 2.3. Log of the section Aşağiyaylabel with indicated stratigraphy, sample positions (As 1–As 19) and speculative depositional sections (not to scale) from the Kartoz Formation (Early Carnian 1) and the Kasımlar Formation (Early Carnian 2–Late Carnian; e.g., Julian–Tuvalian). Please note that the scale changes at 4 m. Indicated depositional areas of the facies types As 1 to As 23.3 m correspond to log and stratigraphy to the right. Topography and suggested position of facies types modified after Flügel (2004).

2.3. Stratigraphic log and biostratigraphy

The section at Aşağiyaylabel comprises about 50 m of essentially calcareous beds passing into marlstones (in part marly limestones) and shaly beds with considerable siliciclastic input at the top. The lowermost part (0–2.4 m; As -1, As 0, As 1; Figs. 2.3, 2.4a) is represented by the Kartoz Formation, a Late Triassic (earliest Carnian, Julian 2) light-grey, shallow-water carbonate succession. It comprises corals and thick-shelled bivalves. *Neoprotrachyceras* sp., found in the upper part of bed As 1, dates the upper part of the Formation as Julian 2 (*A. austriacum* Zone). The top of As 1 ends with a corroded and iron-oxide-stained dissolution surface; a hiatus between the top of As 1 and the overlying Kasımlar Formation cannot be excluded.

The overlying Kasımlar Formation (2.4–25 m; As 2 to As 19; Figs. 2.3, 2.4b–h) can be divided into three ‘‘members’’: a carbonate member, a marlstone member, and a shale member. The carbonate member starts with dark-grey to black, thin-bedded limestones containing ammonite-rich beds with a nearly monospecific assemblage of *Orthoceltites* (As 2 to As 9; Fig. 2.4b) and very rare *Sirenites* sp. represented by floatstones of latest Early Carnian age (Julian 2/II). Towards the top thick slump breccias follow; they contain up to meter-sized patch-reef blocks together with small ammonite coquinas and filament-limestone components (4.1–12.1 m; Fig. 2.4c). The overlying well-bedded (cm–dm thick) peloidal filament-wackestone (12.1–14.2 m; As 10 to As 15, respectively As 46) with Early Carnian conodonts (*Gladigondolella tethydis* and *Metapolygnathus*) and an ammonite fauna dominated by the genera *Neoprotrachyceras* and *Anasirenites* are of latest Early Carnian age (*Anasirenites* level of Julian 2/IIb). The bioturbated matrix (Figs. 2.3, 2.4d) contains juvenile halobiid bivalves, sponge spicules, radiolaria, peloids, and planktic crinoids (= *Osteocrinus* sp.). The argillaceous part of the section starts with the following marlstone member. It consists of bioturbated, mostly peloidal filament-packstones, with thin halobiid pavements, gastropods, and ammonites in specific layers (As 47; As 16; As 17; Fig. 2.3). Between 19.5 m and 21.1 m, thin layers of silty sandstone and arkoses are present (As 17/18, As 18; Fig. 2.4g). Ammonites (*Pleurotropites*, *Spirogmoceras*) from As 16 and 17 date the basal part as earliest Late Carnian. At approximately 21.3 m (Fig. 2.4h), the marlstone member is replaced by the shale member, a thicker sequence of mm-thick, laminated black shales that are rare in biogenic components except for some thin halobiid layers.
Overall, the studied succession represents the latest Early Carnian (Julian 2) to earliest Late Carnian (Tuvalian 1) time interval with an exactly dated Early to Late Carnian boundary.

2.4. Materials and methods

A detailed stratigraphic section of the Early to Late Carnian interval was measured and described. Fifty-four thin-sections, collected in 2007 and 2010, of 17 layers were made and used for petrographic studies. The corresponding bed numbers are indicated by the abbreviation As (for Aşağiyaylabel) and the associated bed number (e.g., As 1 = sample from bed 1). Facies were analyzed using a dissecting microscope (Zeiss Discovery V20) with attached digital camera (AxioCam MRc5). Detailed petrographic analyses were done using a petrographic polarization microscope from Leica (Leica DDM4500P) and a digital camera (Leica DFC4420). Sectioning and photographing were done at the Natural History Museum Vienna and the University of Vienna (Department of Petrography).

2.5. Facies description

For a detailed facies description see Table 2.1.

Kartoz Formation

Coral-bafflestone (Fig. 2.3: 0.0–2.4 m; As -1 to As 1). This facies is characterized by a dense abundance of in situ corals (Fig. 2.5a) within the first 70 cm, trapped by a cortoid grainstone matrix (Fig. 2.5b). In addition to in situ corals, thick-shelled in situ bivalves and coquinas with convex down oriented bivalves are common. Weathering-resistant structures (top of calcite-filled corals) are present at the top of the layers. This section represents an open platform. (Figs. 2.3, 2.4a, 2.5a, b; Table 2.1).

Kasımlar Formation

The Kasımlar Formation is composed of the following lithological members and units:

– Carbonate member (units A, B, and C),
– Marlstone member, and
– Shale member

Carbonate member: unit A

The Kasımlar Formation starts with bioclastic pelagic wackestones (Fig. 2.3: 2.4–4.0 m; As 2 to As 9), which were deposited in a deep shelf margin or mid-ramp position (Flügel 2004). The faunal spectrum mirrors two different source areas of the bioclastic input: thin-shelled bivalves (halobiids), which are most common, represent the autochthonous component (deeper shelf margin), whereas the original habitat of the benthic foraminifera (lagenids), the thick-shelled bivalves (megalodontids), and the large, low-spired gastropods was situated on a fore slope or on a shallowmarine ramp. Tilted geopetal fills of gastropods and ammonites (*Orthoceltites* sp.), together with clasts of eroded semilithified sedimentary layers (‘‘plasticlasts’’), prove episodic erosion, downward transport, and re-sedimentation. Bioturbation has mostly obliterated the original arrangement of autochthonous fine-grained sediments (together with thin-shelled bivalves and radiolaria) alternating with coarser grained tempestitic layers. When the original layering is preserved, bedding planes are strongly affected by stylolites (As 4). Common authigenic pyrite (often as well-developed crystals) in different levels of the section (As 4) is probably of synsedimentary origin. However, the high abundance of halobiid bivalves and the dark-colored sediment could point to temporary dysaerobic conditions of the bottom waters and/or the pore-fluids of the unconsolidated sediments (Flügel 2004; McRoberts 2000, 2010). Reddish brown dolomitic spots (As 4) are interpreted as diagenetic overprint during a later emersion phase under arid or semi-arid conditions (Al-Hashimi and Hemingway 1973) (Figs. 2.3, 2.4b, 2.5c–g; Table 2.1).

Carbonate member: unit B

Mass flow deposits with Cipit-boulders (Fig. 2.3: 4.0–12.1m; As 9+x to As9+8m).

These probably tectonically induced gravity-flow deposits demonstrate an important turning point in the basin forming process, which started with down-faulting and block-tilting, accompanied by a steepening of the adjacent slope (Figs. 2.3, 2.4c, 2.5h, 2.6a–f; Table 2.1).

Carbonate member: unit C

Pelagic wackestone/packstone with bioclasts (Fig. 2.3: 12.1–14.2 m; As 10 to As 15).

This part of the section is characterized by a remarkable increase of the proportion of allodapic sediments (As 15). Tempestitic layers with platform-derived material (thick-shelled foraminifera together with rare dasycladacean algae and sponges) alternate with pure mudstones of the background sedimentation, which contain abundant authigenic euhedral pyrite crystals. The ‘‘clotted fabric’’ of the fine-grained ‘‘groundmass’’ (Flügel 1982, p. 119) hints that this matrix was probably originated via decomposition of former peloidal grain-/packstones. The texture of the sediment, which alternates with the allodapic layers, has been strongly affected by pressure solution. Small-sized radiolaria starting at the base of the section (As 10) prove a basinal environment (FZ1, Flügel 1982: tab. 43). The radiolaria are mostly calcified (mould preservation); the original mineralogy and porous wall structure is preserved only in areas that underwent early diagenetic silicification. The presence of thick-shelled bivalves indicates temporary shallowing (Figs. 2.3, 2.4d–e, 2.6g–h, 2.7a; Table 2.1).

Marlstone member

Marlstones with calcareous intercalations (14.2–21.3 m; As 16 to As 18).

The lower segment of this section features a shallowing upward tendency. The sequence starts with partly bioturbated bioclastic wackestones and pelsparitic packstones, followed by shales with a 1.1-m-thick intercalation of carbonates (As 17; bioclastic wackestone) with thick-shelled bivalves. A small (10 cm) arkosic sandstone layer (As 17/18) with echinoid and bryozoan fragments is present at the top of the sequence. Crystals of authigenic pyrite are common in different layers of the succession (Figs. 2.3, 2.4f, 2.7b–f; Table 2.1).

Shale member

Shales with limestone intercalations (21.3–25? m; As 19).

In the sequence at the top, which is exposed above the marlstone member, shales (Fig. 2.4g–h) with episodic intercalations of thin-bedded carbonates dominate. Samples of two of these intercalated carbonate layers (As 18, As 19) are composed of strongly bioturbated peloidal packstone with thin-shelled bivalves, rare radiolaria, and echinoid fragments (Figs. 2.3, 2.4g–h, 2.7g–h; Table 2.1).

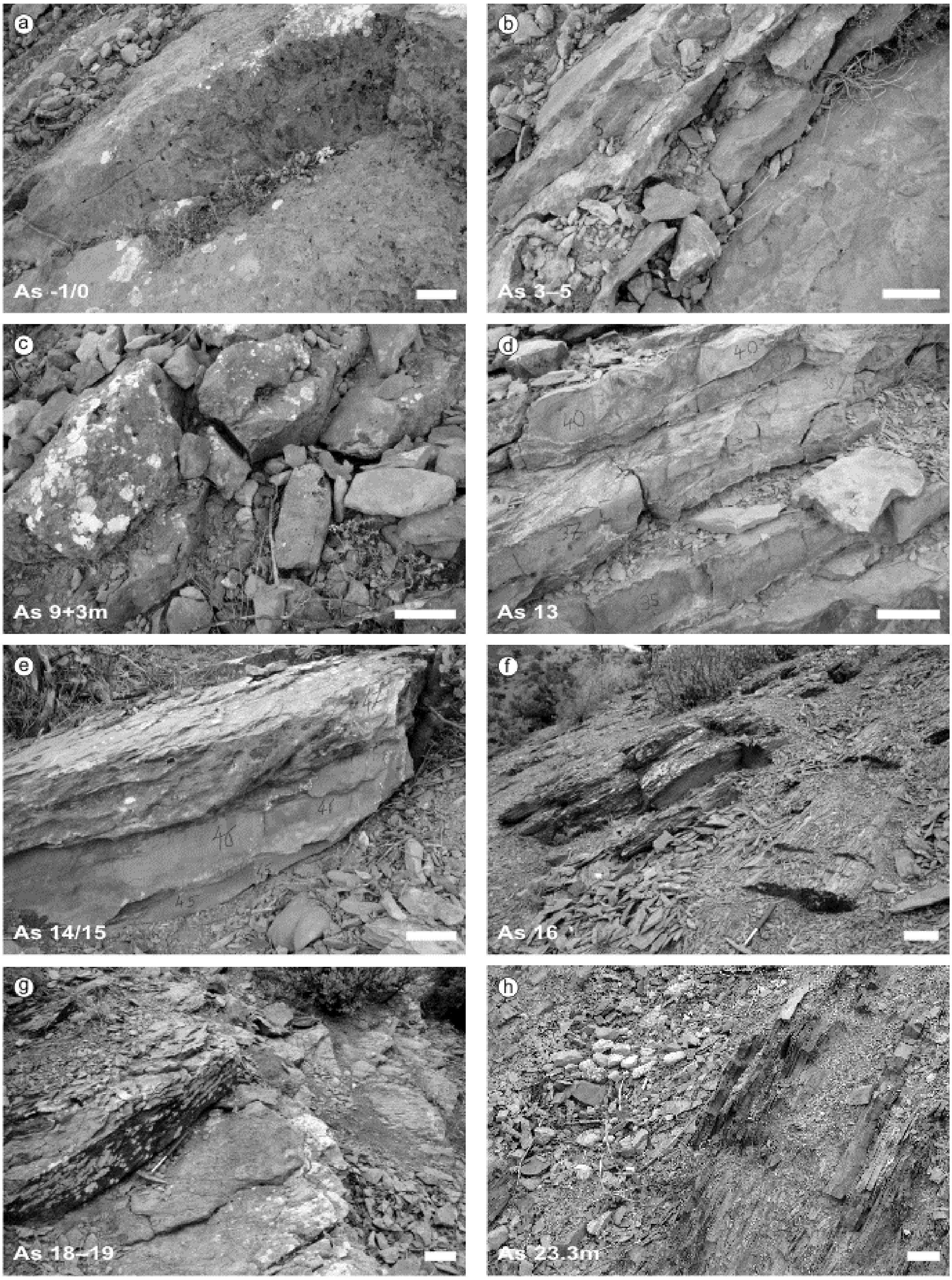

Fig. 2.4. Detailed views of the section at Aşağiyaylabel. Kartoz Formation: **a,** As -1 to As 0, bioclastic bafflestones with abundant in situ corals (thick whitish structure); Kasımlar Formation: **b,** As 3 to As 5, bioclastic floatstones with abundant ammonites (*Orthoceltites*) and halobiid shells accompanied by rare gastropods. **c,** As 9+3 m, thick-bedded debris flow deposits with intra- and extraclast breccias, comprising Cipit boulders, up to meter-sized patch reef blocks, small ammonite coquinas and filament components. **d,** As 13, wavy bedded peloidal filament-packstones, with bioturbated matrix, intercalated by residual sediments containing halobiid bivalves, sponge spicules, radiolaria, and planktic crinoids. **e,** As 14 to As 15, transition from Julian limestones (As 14) to Tuvalian (As 15) peloidal pack- to grainstones at the top with sponge spicules, crinoids, and thin-shelled bivalves (halobiids). **f,** As 16, fine bioclastic wackestones with strongly bioturbated matrix comprising abundant ammonites (e.g., *Neoprotrachyceras*). **g,** As 18/19, slip breccia, siliciclastic breccias and ''floating'' blocks (up to 40 cm in diameter). **h,** As 23.3 m, hundreds of meters composed of shales with intercalated siltstones. Detailed description of beds and facies in text. All scale bars 10 cm.

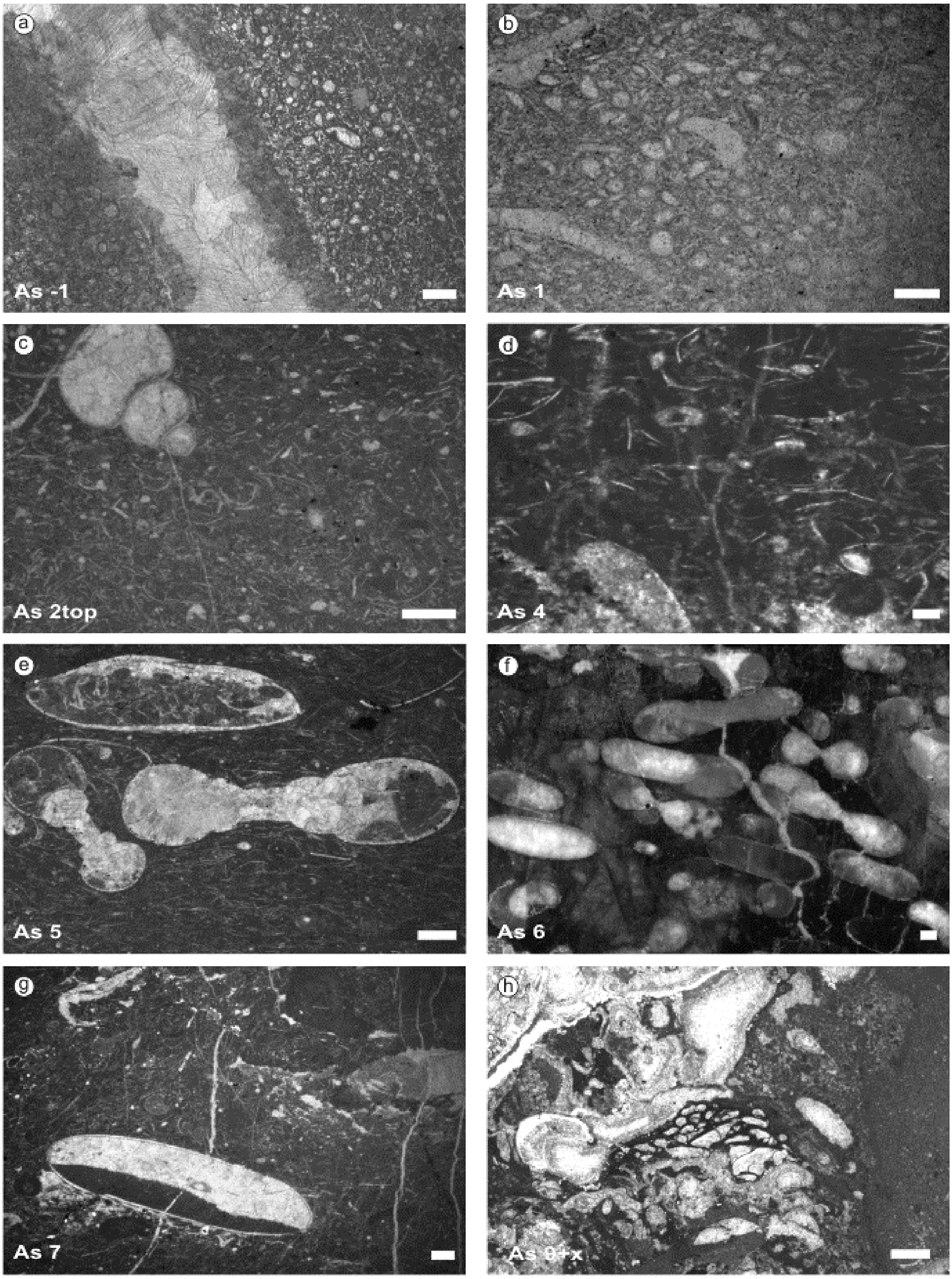

Fig. 2.5. Thin-section photographs of facies As -1 to As 9+x. Kartoz Formation: **a,** As -1, bioclastic bafflestone with abundant in situ corals trapped by cortoid grainstone matrix. Calcitic in situ coral (thick whitish structure). **b,** As 1, bioclastic grainstone with abundant grains encrusted by cyanobacteria together with common megalodontid bivalves and echinoderm fragments. Kasımlar Formation: **c,** As 2top, bioturbated gastropod-bivalve floatstone with micritic peloidal matrix containing thin-shelled halobiid bivalves. **d,** As 4, ammonite-gastropod floatstone with micritic peloidal matrix containing abundant thin-shelled halobiid bivalves. **e,** As 5, bioclastic floatstone with abundant ammonites (*Orthoceltites*) and halobiid shells accompanied by rare gastropods. Ammonites and gastropods filled with coarse sparry calcite floating in micritic matrix. **f,** As 6, ammonite or *Orthocletites* packstone; densely packed and parallel arranged, well-preserved ammonite (*Orthoceltites* sp.) shells forming a coquina. **g,** As 7, bioclastic floatstone with thin-shelled bivalves (halobiids), gastropods (*Omphaloptycha*-like), abundant ammonites (*Orthoceltites*) filled with coarse sparry calcite, and numerous echinoderm fragments. **h,** As 9+x, characteristic sponge-accentuated Cipit facies, rare in corals. All scale bars 1 mm.

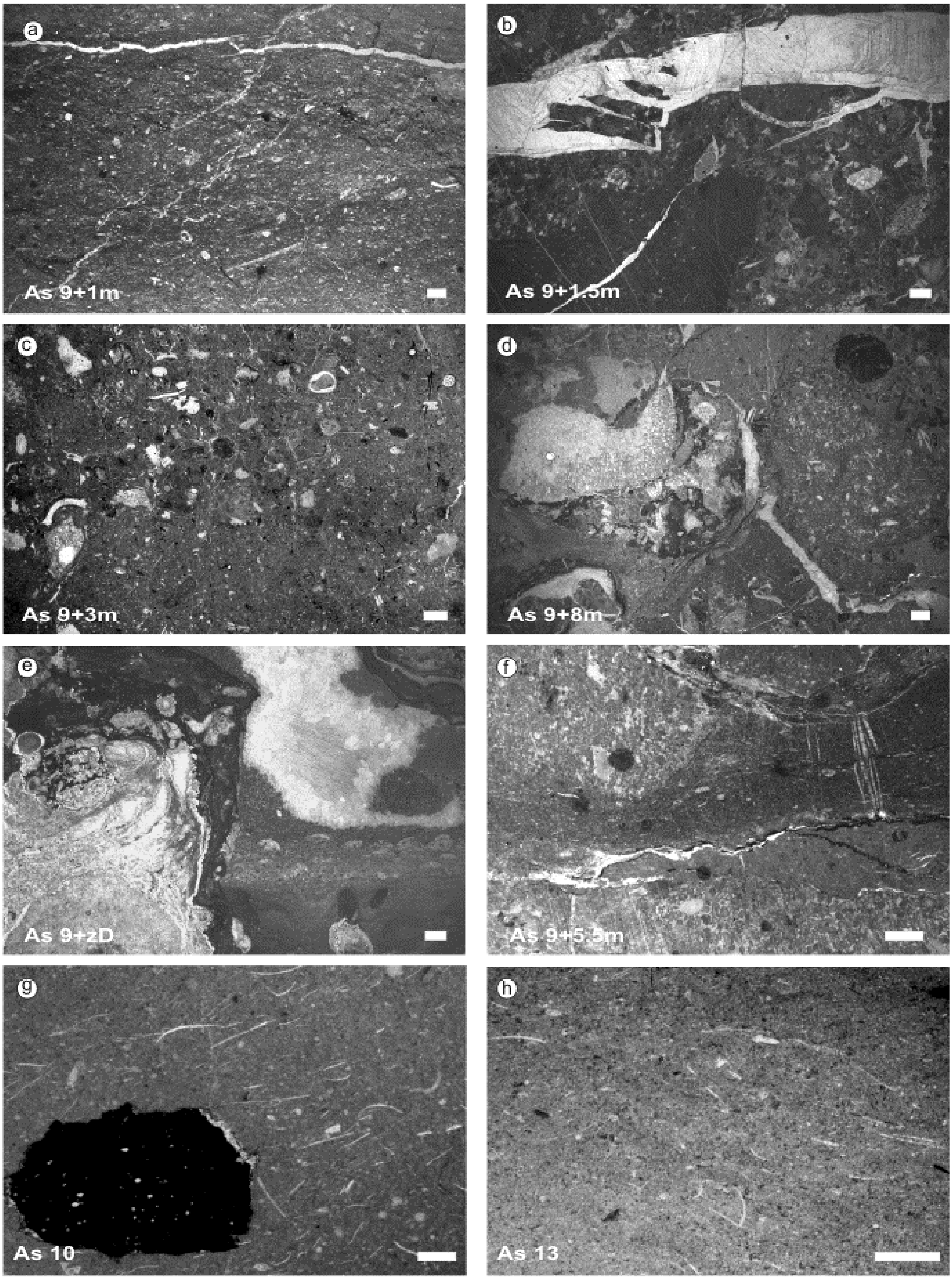

Fig. 2.6. Thin-section photographs of different facies components of debris flow deposits (carbonate member unit B) and pelagic packstones of the carbonate member unit C. **a,** As 9+1 m, component containing material from the deeper ramp. **b,** As 9+1.5 m, component representing pelagic facies. **c,** As 9+3 m, component composed of material derived from shallow water. **d,** As 9+8 m, component containing reef-building organisms (e.g., chaetetid sponge). **e.** As 9+zD, component containing different generations of chaetetids and well-preserved internal sedimentation. **f,** As 9+5.5 m, component representing sedimentation structures indicating plastic deformation of semi-lithified sediment: an excellent example for absorption from the bedrock. **g,** As 10, pelagic packstone with bioclasts, matrix consisting of small peloids (perhaps fecal pellets of halobiid bivalves) with filaments (halobiids), sponge spicules, and radiolaria. **h,** As 13, pelagic packstone with bioclasts, bioturbated matrix with bioturbation containing halobiid bivalves, sponge spicules, radiolaria, peloids, planktic crinoids (=*Osteocrinus* sp.?). Detailed description of thin-sections in text. All scale bars 1 mm.

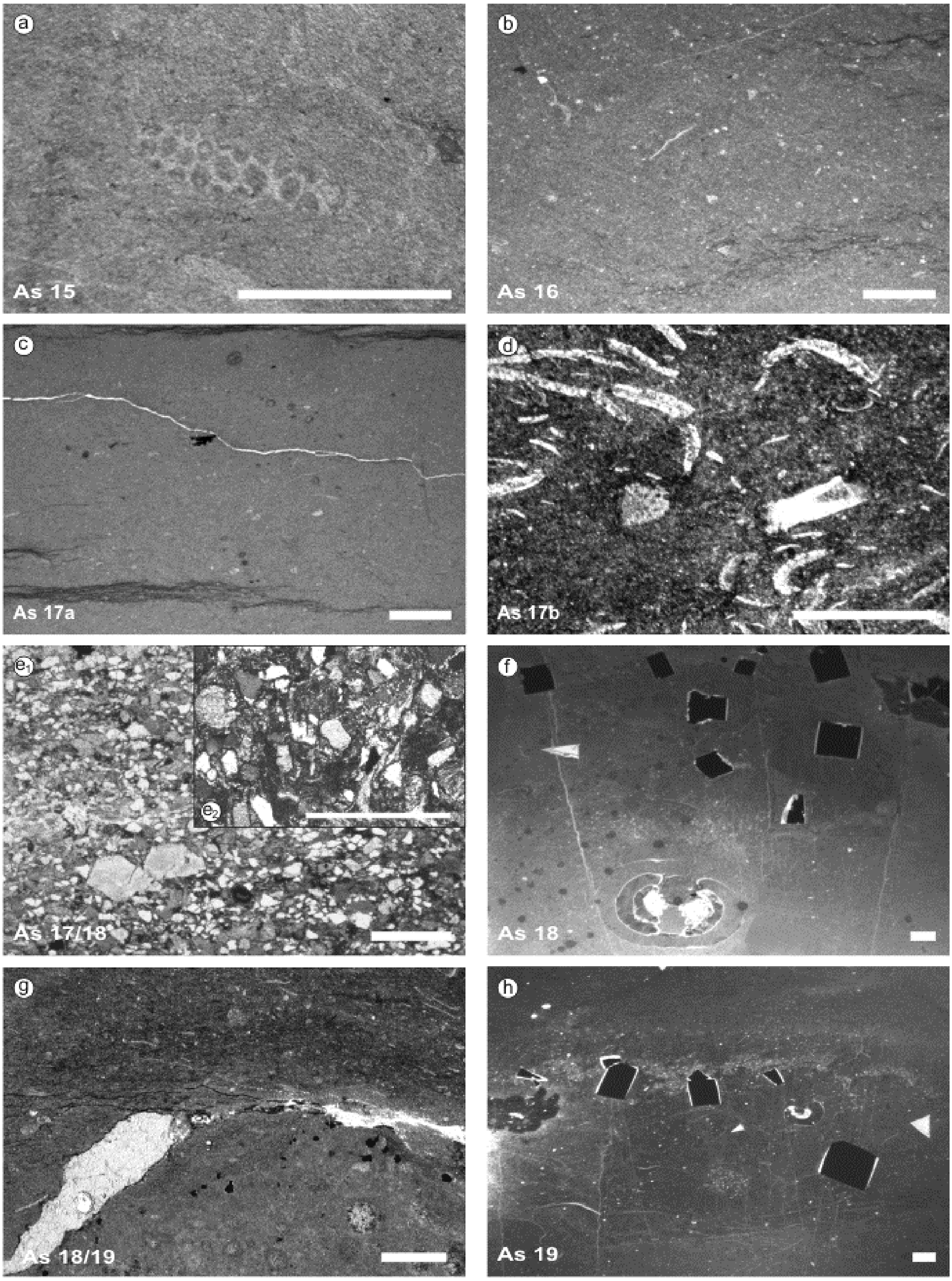
a
As 15
b
As 16
c
As 17a
d
As 17b
e1
e2
As 17/18
f
As 18
g
As 18/19
h
As 19

← **Fig. 2.7.** Thin-section photographs of facies As 15 to As 19. Kasımlar Formation: **a,** As 15, pelagic peloidal pack- to grainstone with biogenic components of dasycladacean green algae, sponge spicules, crinoids, thin- and thick-shelled bivalves (halobiids), miliolid foraminifera, and bryozoans. **b,** As 16, strongly bioturbated, fine bioclastic wackestone with biogenic components such as thin- and thick-shelled bivalves, fragments of echinoids, peloids, radiolaria, foraminifera, and sponge spicules. **c,** As 17a, bivalve wacke- and floatstone containing rare biogenic components such as thin-shelled bivalves (halobiids), foraminifera, and radiolaria. **d,** As 17b, bivalve wacke- and floatstone with abundant bivalve shells (encrusted by fibrous cementation) floating within a micritic peloidal matrix with foraminifera and radiolaria. **e_1,** As 17/18, arkose composed of poorly rounded components, mostly re-sedimented lithoclasts containing biogenic components such as fragments of echinoids and bryozoans, plagioclase, quartz grains, and rare glauconite, cemented by a carbonate matrix. **e_2,** As 17/18, same sample as e_1, shown under a petrographic polarization microscope. **f,** As 18, strongly compacted, bioturbated peloidal packstone with abundant thin-shelled bivalves (halobiids), radiolaria, echinoid fragments, and sponge spicules, with signs of bioturbation, stylolithic structures, and large pyrite crystals (1–3 mm) coated by calcite cement. **g,** Slip breccia, (= same horizon as As 18/19) containing different reworked components and framboidal pyrites. **h,** As 19, argillaceous, bioturbated peloidal packstone with abundant thin-shelled bivalves (halobiids), rare ammonites, radiolaria, echinoid-fragments, and sponge spicules, with signs of bioturbation, stylolithic structures, and abundant large pyrite crystals (1–3 mm) coated by calcite cement. Detailed description of thin-sections in text. All scale bars 1 mm.

Table 2.1. Detailed facies description of investigated thin-sections.

Lithostratigraphic Unit	Level (m)	Biogenic and abiogenic content	Microfacies-zone	see Fig.
Kartoz Fm. Carb. member Sample: As -1, As 0, As 1 Age: Early Carnian	0–2.4	biogenic: in situ corals, bivalves (e.g. megalodonts), crinoids, ammonoids; abiogenic: lithoclasts;	Coral-bafflestone; RMF 12 (SMF 7, FZ 5) Depositional area (Flügel 2004): Open platform	2.3, 2.4a, 2.5a–b
Kasımlar Fm. Carb. member (Unit A) Sample: As 2 Age: Early Carnian	2.4–2.7	biogenic: radiolarians, uniserial lagenid foraminifera, thin- (halobiid) and thick-shelled bivalves, gastropods (*Omphaloptycha*-like), ammonoids partly filled with micritic sediment; fragments of echinoderms, rare ostracods; abiogenic: plasticlasts;	Bioclastic, pelagic wackestone / gastropod/bivalve floatstone within an autochthonous micritic peloidal matrix; SMF 8 Depositional area (Flügel 2004): Deep shelf margin	2.3, 2.5c
Kasımlar Fm. Carb. member (Unit A) Sample: As 4 Age: Early Carnian	2.7–3.0	biogenic: various amounts of thin-shelled bivalves, ammonoids, gastropods (*Omphaloptycha*-like), echinoderms (crinoid-ossicles), biotubation; abiogenic: authigenic pyrite;	Bioclastic, pelagic wackestone / ammonoid floatstone; SMF 8 Depositional area (Flügel 2004): Deep shelf margin	2.3, 2.4b, 2.5d
Kasımlar Fm. Carb. member (Unit A) Sample: As 5 Age: Early Carnian	3.0–3.1	biogenic: thin- and thick-shelled bivalves, ammonoids, echinoderms; abiogenic: plasticlasts;	Bioclastic pelagic wackestone / floatstone with pelsparitic matrix; SMF 8 Depositional area (Flügel 2004): Deep shelf margin	2.3, 2.4b, 2.5e
Kasımlar Fm. Carb. member (Unit A) Sample: As 6 Age: Early Carnian	3.1–3.4	biogenic: ammonoids (to 90 %), halobiid bivalves cover the ammonoid coquina, sponges, gastropods;	Ammonoid or *Orthoceltites* packstone; SMF 12 Depositional area (Flügel 2004): Slope to basinal environment	2.3, 2.5f

Table 2.1. Continued.

Lithostratigraphic Unit	Level (m)	Biogenic and abiogenic content	Microfacies-zone	see Fig.
Kasımlar Fm. Carb. member (Unit A) Sample: As 7 Age: Early Carnian	3.4–3.7	biogenic: thin-shelled bivalves, gastropods (*Omphaloptycha*-like), ammonoids, echinoderms; abiogenic: plasticlasts;	Bioclastic pelagic wackestone / floatstone; SMF 8 Depositional area (Flügel 2004): Deep shelf margin	2.3, 2.5g
Kasımlar Fm. Carb. member (Unit B) Sample: As 9+x to As 9+8m Age: Early Carnian (Julian 2)	4.1–12.1	biogenic: reef building organisms (primarily chaetetids, rare corals), foraminifera, gastropods, bivalves, ammonoids; abiogenic: Cipit boulders, breccias composed of components from different environments: platform or shallow-water facies (patch reef blocks), deeper ramp facies, and pelagic basin facies;	Debris flow deposits, containing up to meter-sized patch reef blocks, Cipit boulders, small ammonoid coquina, and filaments; RMF – Depositional area (Flügel 2004): Slope	2.3, 2.4c, 2.5h, 2.6a–f
Kasımlar Fm. Carb. member (Unit C) Sample: As 10 Age: Early Carnian (Julian 2)	12.3–12.5	biogenic: filaments, peloids, small sized calcitized radiolarians;	Pelagic packstone, with less bioclastic input than As 9; texture consists of small peloids (possibly faecal pellets); RMF 1–3 (FZ1) Depositional area (Flügel 2004): Basinal environment	2.3, 2.6g
Kasımlar Fm. Carb. member (Unit C) Sample: As 13 Age: Early Carnian (Julian 2)	12.7–13.0	biogenic: halobiid bivalves, sponge spicules, radiolarians, peloids, planktic crinoids (*Osteocrinus* sp.);	Pelagic peloidal filament-packstone with bioclasts, similar to As 10; RMF 1–3 Depositional area (Flügel 2004): Basinal environment	2.3, 2.4d, 2.6h
Kasımlar Fm. Carb. member (Unit C) Sample: As 15 Age: Early Carnian (Julian 2)	13.9–14.2	biogenic: thin- and thick-shelled bivalves, echinoderm fragments, miliolid foraminifera, sponges, bryozoans;	Pelagic wackestone (matrix: peloidal pack- to grainstone) with intercalations of fine-grained allodapic layers; RMF 4 Depositional area (Flügel 2004): Outer ramp – basinal environment	2.3, 2.4e, 2.7a

Table 2.1. Continued.

Lithostratigraphic Unit	Level (m)	Biogenic and abiogenic content	Microfacies-zone	see Fig.
Kasımlar Fm. Marlstone member Sample: As 16 Age: Late Carnian (Tuvalian 1)	at 14.9	biogenic: rare, thin- and thick-shelled bivalves, fragments of echinoderms, peloids, radiolarians, foraminifera, sponge spicule; abiogenic: pyrite crystals of authigenic origin;	Mudstone and strongly bioturbated bioclastic wackestone with pelsparitic matrix; RMF 2–3 Depositional area (Flügel 2004): Outer ramp – basinal environment	2.3, 2.4f, 2.7b
Kasımlar Fm. Marlstone member Sample: As 17a Age: Late Carnian (Tuvalian 1)	at 18.6	biogenic: rare fossil debris;	Bioclastic wackestone; Background sedimentation to As 17b, containing rare fossil debris; RMF 5 Depositional area (Flügel 2004): Basinal environment	2.3, 2.7c
Kasımlar Fm. Marlstone member Sample: As 17b Age: Late Carnian (Tuvalian 1)	at 18.6	biogenic: bivalves encrusted by fibrous cement, foraminifera, radiolarians;	Bioclastic wackestone, bivalve shell bed within a micritic peloidal matrix; RMF 5 Depositional area (Flügel 2004): Basinal environment	2.3, 2.7d
Kasımlar Fm. Marlstone member Sample: As 17/18 Age: Late Carnian (Tuvalian 1)	19.6–19.7	biogenic: fragments of echinoids, bryozoans; abiogenic: resedimented lithoclasts, poorly rounded plagioclase, some quartz, rare glauconite grains;	Coarse-grained, siliciclastic grainstone (arcosic), cemented by a carbonate matrix; RMF – Depositional area (Flügel 2004): Event bed deposited within a basinal environment	2.3, 2.7e_{1-2}
Kasımlar Fm. Marlstone member Sample: As 18 Age: Late Carnian (Tuvalian 1)	20.8–20.9	biogenic: abundant thin-shelled bivalves, radiolarians, echinoid fragments, sponges;	Strongly compacted, bioturbated peloidal packstone; RMF 2 Depositional area (Flügel 2004): Outer ramp – basin	2.3, 2.7f

Table 2.1. Continued.

Lithostratigraphic Unit	Level (m)	Biogenic and abiogenic content	Microfacies-zone	see Fig.
Kasımlar Fm. Shale member Sample: As 18/19 Age: Late Carnian (Tuvalian 1)	21.3–21.4	biogenic: thick-shelled bivalves; abiogenic: cavities filled with debris and bordered with oncolithic crusts;	Siliciclastic breccias and “floating” blocks (up to 40 cm in diameter); RMF 15 Depositional area (Flügel 2004): Mid Ramp	2.3, 2.4g, 2.7g
Kasımlar Fm. Shale Member Sample: As 19 Age: Late Carnian (Tuvalian 1)	21.4–21.7	biogenic: thin-shelled bivalves, foraminifera, ammonoids, echinoderms, bioturbation;	Argillaceous burrowed peloidal packstone; RMF 2–3 Depositional area (Flügel 2004): Outer ramp to basin	2.3, 2.4g, 2.7h

Table 2.1. Detailed facies description of investigated thin-sections. **RMF 1**, Calcisiltite and mudstone with peloids, very fine skeletal debris, sponge spicules, sometimes finely laminated. **RMF 2**, Argillaceous burrowed mudstone and wackestone; rare agglutinated foraminifera, ostracods, echinoderms. **RMF 3**, Burrowed bioclastic wackestone and packestone with diverse, common to abundant fossils (bivalves, brachiopods, echinoderms) and peloids. Skeletal grains not worn; whole fossil preservation common. **RMF 4,** Peloidal wackestone and packstone. **RMF 5**, Pelagic mudstone with planktonic microfossils and open-marine nektonic fossils (e.g., ammonites). **SMF 7**, Organic boundstone, platform-margin ‘‘reef’’. **SMF 8**, Whole fossil wackestone/floatstone. **SMF 12**, Limestone with shell concentration. **FZ 2**, Deep shelf. **FZ 5**, Platform-margin reefs. **FZ1**, **FZ3**, **FZ 4,** are missing at Aşağiyaylabel. The nomenclature of ramp- and standard microfacies types (RMF/SMF) as well as facies zones (FZ) is adopted from Dunham (1962), Flügel (1972), and Wilson (1975). Carbonate classification follows the nomenclature of Dunham (1962) and Folk (1959, 1962). Eight microfacies types (Figs. 2.5, 2.6, 2.7) were detected. For the detailed position of the different facies, see Figs. 2.3 and 2.4.

2.6. Facies interpretation

The deepening sequence at Aşağiyaylabel: from the Kartoz Formation to the Kasımlar Formation

Kartoz Formation

The Kartoz Formation is represented by sediments of an open platform, mainly composed of well-sorted cortoid grainstones with rare bioclasts (As -1, As 0, and As 1; Fig. 2.5a, b). A 2.4-m thick layer of a coral bafflestone is intercalated near the top of this sequence. Microscopic vertical fissures extending a few meters below the top of the Kartoz Fm. are partly filled with vadose silt, pointing to at least one episodic period of emersion (Fig. 2.4a). Remaining open spaces were filled in a second phase (see below). The transgressive pulse of the coral carpet layer probably reflects small-scale sea-level fluctuations. A hardground at the top of the Kartoz Formation indicates a period of non-sedimentation during which pelagic sediment sealed the open karst fissures. This points to a rapid drowning of the shallow-water platform. The boundary between the Kartoz Formation and the overlying Kasımlar Formation is characterized by a sharp change in lithology and facies, probably reflecting a hiatus.

Kasımlar Formation

Carbonate member

The Kasımlar Formation starts at 2.4 m with black, 1.5-m-thick limestones marked by densely packed ammonites (*Orthoceltites*) within a micritic matrix. The faunal spectrum (As 2, 4, 5, 6 and 7; Fig. 2.5c–g) suggests two different source areas of the bioclastic input: thin-shelled bivalves (halobiids), which are the most abundant faunal element, are autochthonous, whereas the original habitat of the thick-shelled bivalves and large, low-spired gastropods was situated on a fore slope or on a shallow-marine ramp. Tilted geopetal fills of gastropods, together with clasts of eroded semi-lithified sedimentary layers (‘‘plasticlasts’’), indicate episodic erosion, downward transport, and re-sedimentation. Generally, the assumed original arrangement of autochthonous fine grained sediments alternating with coarser-grained tempestitic layers is obliterated by bioturbation. Where the original bedding is preserved, tops of the beds are strongly affected by pressure solution (As 4). The gastropods are similar to *Omphaloptycha* (Andrzej Kaim, pers. comm.). The tilted geopetal fills of the ammonite and gastropod shells within As 5 (Fig. 2.5e) indicate their lithification within another facies and subsequent transport to the final depositional area. The breccia-like bioclastic floatstones (As 2 to As 9; Fig. 2.5c–g) may be interpreted as distal equivalents of the following 8 m of rudstones with intra and extraclast breccias (Fig. 2.3). The genesis of these mass flow breccias seems to be similar to that of the Cipit boulders (Fig. 2.5h) first described by Richthofen (1860); see also Fürsich and Wendt (1977). Cipit boulders are meter- to tens-of-meters sized isolated blocks embedded in calciturbiditic, volcaniclastic, marly, or argillaceous basinal sediments (Richthofen 1860). The debris flow components of a deeper ramp (Fig. 2.6a) are positioned next to components of pelagic facies (Fig. 2.6b) as well as next to shallow-water material (Fig. 2.6c) and components composed of reefbuilding organisms (Fig. 2.6d). Different generations of chaetetids and well-preserved internal sedimentation are visible (Fig. 2.6e). Similar breccias have been described by Keim and Brandner (2001) and interpreted as indicating extensional synsedimentary tectonics, which leads to scarps, block-tilting, graben structures, and finally to breccia deposition. Sediments and biogenic components of platform margins have thereby been embedded within basinal sediments as gravity displaced carbonate boulders (Brandner *et al.* 1991). Sedimentary structures (Fig. 2.6f) indicate a still plastic or semi-lithified sediment, which underwent further plastic deformation; this sediment originated by the absorption of material from the bedrock during the gravity displacement of the Cipit-like boulders. The tectonically induced gravity-flow deposits are evidence of an important turning point in the basin-forming process, which started with down-faulting, local synsedimentary tectonics, and block-tilting, probably accompanied by a steepening of the adjacent slope. This most likely involved a different geometry of the basin margin as well as another carbonate productivity zone shortly after deposition of the Cipit-like breccias. Through seismic activity, tilting, and down-faulting, a formation of highs in the current basin may be assumed.

This phase ended abruptly and gave way to a deeper-water autochthonous succession of bedded limestones, indicating a basinal environment within the next two meters (As 10, As 46top; Fig. 2.6g), rich in radiolaria and sponge spicules. This part of the section, however, is characterized by a clear increase in allodapic sediments (As 15, As 31; Fig. 2.7a). Productive carbonate platform relicts are indicated by a characteristic, well-preserved (not corroded and/or fragmented) biogenic content (shallow-water and reef-building-organisms: Dasycladacea, chaetetids, calcareous sponges, gastropods) and layers of shallow-water-derived material. There are no indications that the shallow-water material represents reworked Kartoz Platform material, nor is there evidence for a strong subaerial alteration. We therefore interpret this material as having been transported from a contemporaneous marginal area into the basin. The fine-grained texture (As 10 and As 13; Fig. 2.6g–h) consists of small pellets, most probably derived from halobiid bivalves. The recognized global major appearance of osteocrinoids within Ladinian to Carnian strata (Kristan-Tollmann 1970) agrees with occurrences of *Osteorcinus* within sample As 13 of Aşağiyaylabel. At the top of As 46, a layer of thin-shelled pelagic bivalves was detected. The same facies is represented within As 47. Although thin-shelled pelagic bivalves characterize this facies, many other calcitic biogenes (e.g., echinoderms, thick-shelled foraminifera together with rare dasycladacean algae and sponges) are also present. The parallel arrangement of the bivalves indicates current control. Tempestitic layers with platform-derived material alternate with pure mudstones of the background sedimentation (As 15); these mudstones contain abundant euhedral pyrite crystals of authigenic origin. The ‘‘clotted fabric’’ of the fine-grained ‘‘groundmass’’ (Flügel 1982, p. 119) hints that the observed matrix probably originated via decomposition of former peloidal grain-/packstone. The texture of the sediment, which alternates with the allodapic layers, is strongly affected by pressure solution. The radiolaria skeletons are mostly calcified. Thick-shelled bivalves indicate a temporary shallowing.

Marlstone member

The Upper Carnian (Tuvalian 1) is represented by calcareous marls to subordinate marlstones alternating between sediments poor in fossils, except for distinct layers rich in halobiid shells and ammonites (As 47 to As 18/19; Fig. 2.7b–g; Fig. 2.7a–h). The lower part of this interval shows a shallowing-upward tendency. The sequence starts with partly bioturbated bioclastic wackestones and pelsparitic packstones, followed by calcareous marls. The macro-invertebrate fauna of the Tuvalian 1 unit is sparse, except for one *Pleurotropites* layer (As 17; Fig. 2.3) and some halobiid coquinas (*Halobia*, As 18 to As 19; Fig. 2.3, 2.7f, h). Such coquinas occur in deep-water, oxygen-deficient settings as well as in ‘‘pelagic’’ or ‘‘filamentous’’ limestones, which represent fully oxygenated marine settings (e.g., Hallstatt facies; McRoberts *et al.* 2008; McRoberts 2000, 2010). Crystals of authigenic pyrite are common in several layers of the succession (As 16, As 18; Fig. 2.3, 2.7b, f). Thin-section As 17 represents a bioclastic wackestone with thick-shelled bivalves (Fig. 2.7c–d). A small (10 cm) arkosic sandstone layer with echinoid and bryozoan fragments occurs near the top of the sequence (As 17/18; Fig. 2.7e).

Shale member

This member consists of shales with rare, thin carbonate interbeds. One sample of these (As 19; Fig. 2.7h) is composed of strongly bioturbated peloidal packstone with thin-shelled bivalves, rare radiolarians, and echinoid fragments. Apart from the mentioned sandstone layer, another coarse-grained bed occurs at approximately 21 m (As 18/19; Figs. 2.4g, 2.7g); it is composed of an intraformational slump breccia. Subangular boulders are embedded in a brownish-yellow, fine-grained limestone matrix whose color originates from oxidation of pyrite. The light colored angular breccia components are apparently derived from a shallow-water margin of the Kasımlar Basin. Nonetheless, as no such contemporaneous facies exists in the basin, we interpret this breccia to represent reworked material from the Kartoz Formation.

2.7. Discussion

Aşağiyaylabel and the Carnian Pluvial Episode

As noted by Hallam (1996) and Hornung (2008), the CPE was marked by a major facies change from a carbonate-dominated to an argillaceous-dominated sedimentary regime. This phase was also characterized by a major decrease in marine and epicontinental faunas, as seen in many marine invertebrate groups and terrestrial elements such as tetrapods (Hallam 1996; Hornung 2008). The most affected faunas were shallow-water inhabitants (reef builders) of the Tethyan-wide reefs and platforms. This Tethys-wide demise of reef systems and carbonate platforms is dated to the late Julian 1 (Hornung and Brandner 2005; Hornung *et al.* 2006, 2007a, b). Multistratigraphic studies concluded that this demise was synchronous throughout the Tethys area within the *Metapolygnathus carnicus* conodont range zone and the late *T. aonoides* ammonite zone (Hornung 2008). In contrast to the western Tethys, where the turnover occurred within the Early Carnian, in the Taurus Mountains (Aşağiyaylabel) the sedimentation remains carbonate dominated and becomes terrigenous only at the base of the Late Carnian; this corresponds to the boundary between the limestone and the marlstone member of the Kasımlar Formation. These two members are therefore, despite their facial identity, younger than the Early Carnian Alpine Reingraben Shales (Hornung and Brandner 2005) or *Halobia* Shales of northern Turkey (Yurttas-Özdemir 1973) and the Rama Fm. of the Indian Himalaya, respectively (Hornung *et al.* 2006, 2007a, b). Only in the Lagonegro Basin in the southern Apennines (southern Italy) does an interval of green shales and radiolarites (lacking carbonate deposits) correspond in time to the turnover at Aşağiyaylabel. It is interpreted there as a shallowing of the carbonate compensation depth and again as a result of the CPE (Rigo *et al.* 2007).

The mechanism triggering the CPE is still under debate. Generally accepted is that global warming (caused by the rifting of Pangea) enhanced humidification, triggering climate change during the Early Carnian (Hornung *et al.* 2006, 2007a, b; Hornung 2008). Strong humidification by enhanced monsoonal phases led to increased freshwater runoff and enhanced nutrification of the Tethyan Ocean (Simms and Ruffell 1989; Hornung *et al.* 2007a, b), destroying reefs and platforms and reducing nektonic biodiversity. Within the studied section, an outstanding feature is the abrupt facies change but increased carbonate productivity during the Early Carnian (Julian 2). As we have no evidence for terrestrial input during this time interval, the poor nutrient availability probably led to an increased carbonate accumulation rate (Hallock and Schlager 1986). Such a negative correlation between nutrient supply and carbonate productivity suggests poor paleocirculation (De Boer *et al.* 2006). An important result of the present study is the distinctly time-delayed facies change from a carbonate to an argillaceous sedimentation in Aşağiyaylabel. While most sequences of the western Tethys show a turnover within the Early Carnian, the succession in Turkey and the deposits of the Lagonegro Basin are clearly at the Julian–Tuvalian boundary, at least 2 Ma later. Interestingly, this turnover coincides with an extinction event affecting many pelagic taxa of ammonites and conodonts (Krystyn 1983, 1991; Rigo *et al.* 2007; Hornung *et al.* 2007a, b). According to Stampfli *et al.* (2002) and Moix *et al.* (2008), the paleolatitude of Turkey (about 7° N; Fig. 2.1a) and the Lagonegro Basin (about 8–9° N, Fig. 2.1a) was closer to the equator than the South- and Austroalpine segments (about 17° N) of the northern Tethys or the Himalaya (at least 30° S). Muttoni *et al.* (2004) provide an analogous reconstruction, although with a 10° northward shift. We therefore assume that higher latitudes could play an important role by causing an earlier sedimentary turnover. Facies changes at Aşağiyaylabel mirror a coupling effect of lower paleogeographic latitudes (Krystyn 1983, 1991; Rigo *et al.* 2007; Hornung *et al.* 2007a, b) accompanied by Tethyan-wide climate changes during the CPE.

2.8. Conclusions

The studied outcrop at Aşağiyaylabel represents a late Triassic drowning succession marked, like most Tethyan Carnian sequences, by a facies change from carbonates (carbonate platform, patch reefs, hemipelagic limestones) to argillaceous sediments (marlstones, shales). The base of the succession is characterized by a sudden drowning of a carbonate platform followed directly by deeper-water limestones. Synsedimentary tectonics probably triggered the drowning of the Kartoz platform, which led to downfaulting and tilting of the platform and to a new basin geometry along a deeper ramp setting. The fine-grained autochthonous microfacies of the deeper-water limestones suggests a low-energy bottom environment with episodic, current-induced input of coarser-grained tempestitic layers, now obliterated by bioturbation. The pelagic filament (halobiid bivalve) facies is mixed with allochthonous biogenic material (e.g., thick-shelled bivalves, gastropods; also plasticlasts) from the fore-slope or shallow-marine ramp. This points to different source areas of the bioclasts. Synsedimentary unrest is recorded by punctuated redeposition of shallow-water material of reefal and interior ramp origin in the form of breccias and detrital interbeds. These components help to reconstruct the original zonation and differentiation within the ramp; they indicate continuation of reef-favourable conditions until the end of the Early Carnian, when another major sedimentary change led to siliciclastic-dominated sedimentation. The change at the beginning of the Late Carnian to marly and later on to shaly sedimentation is interpreted to reflect climate change due to more humid conditions.

We consider the main litho-change from carbonates to siliciclastic sediments, which at Aşağiyaylabel took place at least 2 Ma later than along the northwestern Tethyan margin, as a similar but diachronous expression of the common late Early Carnian carbonate and reef demise episode. Aşağiyaylabel shares this late turnover to siliciclastic sedimentation with the Lagonegro Basin (Southern Apennines), both of which are ascribed to equatorial Triassic paleolatitudes (approximately 9° N). This leads us to conclude that humidity-driven siliciclastic sedimentation of the so-called Carnian Pluvial Episode probably started earlier at higher paleolatitudes (Alps approximately 17-25° N, Himalaya 30° S) than in equator-near successions. Additional investigations are needed to clarify the time-shift of the major sedimentary change (approx. 2 my) at Aşağiyaylabel. Here, the sedimentary changes are apparently linked more to different coupling effects and a subsequent climate change than to a single climatic event.

2.9. Acknowledgments

This study was funded by project P 22109-B17 of the Austrian Science Fund (FWF). The authors highly appreciate the help and support from the Turkish Geological Survey (MTA) and are thankful for the digging permission within the investigated area. We thank Helga Zeitlhofer (University of Vienna) for help with polarization microscope analysis. Crinoids were determined by Andreas Kroh (Natural History Museum Vienna) and gastropods by Andrzej Kaim (Instytut Paleobiologii PAN, Warsaw, Poland). Franz Topka (Natural History Museum Vienna) assisted in sampling and preparing the ammonite specimens. Anton Englert (Natural History Museum Vienna) prepared the thin-sections. We kindly acknowledge Rainer Brander and an anonymous reviewer for their comments, which greatly improved the quality of this manuscript. We are also extremely grateful to the editor of FACIES, Franz T. Fürsich, for his encouragement and helpful comments.

2.10. References

AIGNER T. and BACHMANN G.H. 1992. Sequence stratigraphic framework of the German Triassic. *Sedimentary Geology*, **80**, 115–135.

AL-HASHIMI W.S. and HEMINGWAY J.E. 1973. Recent dedolomitization and the origin of the rusty crusts of Northumberland. *Journal of Sedimentary Petrology*, **43**, 82–91.

ANDREW T. and ROBERTSON A. 2002. The Beyşehir-Hoyran-Hadim nappes: genesis and emplacement of Mesozoic marginal and oceanic units of the northern Neotethys in southern Turkey. *Journal of the Geolocical Society of London,* **159**, 529–543.

BRANDNER R., FLÜGEL E. and SENOWBARI-DARYAN B. 1991. Microfacies of carbonate slope boulders: indicator of the source area (Middle Triassic: Mahlknecht Cliff, Western Dolomites). *Facies,* **25**, 279–296.

DE BOER PL., HARTING M., MUELLER A. and VAN DER ZWAN K.L. 2006. Distinction between black shales formed in high-productivity and in stagnant-basin settings (abstr.). *American Geophysical Union Fall Meeting,* **2006**, #PP41B-1198.

DERCOURT J., RICOU L.E. and VRIELYNCK B. 1993. Atlas Tethys palaeoenvironmental maps. Gaulthier-Villars, Paris, pp. 307.

DERCOURT J., GAETANI M., VRIELYNCK B., BARRIER E., BIJU-DUVAL B., BRUNET M.F., CADET J.P., CRASQUIN S. and SANDULESCU M. (eds) 2000. Atlas Peri-Tethys – Palaeogeographical maps. Commission of the Geological Map of the World, Paris, pp. 269.

DUMONT J.F. 1976. Etudes géologiques dans les Taurides Occidentales: Les formations paléozoiques et mésozoiques de la coupole de Karacahisar (Province d'Isparta, Turquie). Dissertation, University of South Paris, pp. 213.

DUMONT J. F. and KEREY E. 1975. The Kirkavak Fault. *Bulletin of the Geological Society of Turkey*, **18**, 59–62.

DUNHAM R.J. 1962. Classification of carbonate rocks according to their depositional texture. *In*: Ham W.E. (ed.). Classification of carbonate rocks – a symposium. *Memoir - American Association of Petroleum Geologists*, **1**, 108–121

FLÜGEL E. 1972. Mikrofazielle Untersuchungen in der alpinen Trias: Methoden und Probleme. *Mitteilungen der Gesellschaft der Geologie- und Bergbaustudenten*, **21**, 9–64.

FLÜGEL E. 1982. Microfacies analysis of limestones. Springer, Berlin, pp. 633.

FLÜGEL E. 2004. Microfacies of carbonate rocks. Springer, Berlin, pp. 976.

FLÜGEL E. and SENOWBARI-DARYAN B. 2001. Triassic reefs of the Tethys. *In*: Stanley G.D. JR. (ed.). The history and sedimentology of ancient reef systems. Kluwer Academic/Plenum Publisher, New York, 217–249.

FOLK R.L. 1959. Practical petrographic classification of limestones. Bulletin - *American Association of Petroleum Geologists*, **43**, 1–38.

FOLK R.L. 1962. Spectral subdivision of limestone types. *In*: Ham W.E. (ed.). Classification of carbonate rocks – a symposium. *Memoir - American Association of Petroleum Geologists*, **1**, 62–84.

FÜRSICH F.T. and WENDT J. 1977. Biostratinomy and palaeoecology of the Cassian formation (Triassic) of the Southern Alps. *Palaeogeography Palaeoclimatology Palaeoecology*, **22**, 257–323.

GALLET Y., KRYSTYN L., MARCOUX J. and BESSE J. 2007. New constraints on the End-Triassic (Upper Norian–Rhaetian) magnetostratigraphy. *Earth and Planetary Science Letters*, **255**, 458–470

GIANOLLA P., RAGAZZI R. and ROGHI G. 1998. Upper Triassic amber from the Dolomites (northern Italy) a paleoclimatic indicator? *Rivista Italiana di Paleontologia e Stratigraphy*, **104**, 381–390.

GINDL A. 2000. Paläoökologie triassischer Ammonitenfaunen des Taurusgebirges (Türkei). Unpublished Diploma thesis, University of Vienna, pp. 80.

GOLONKA J. 2004. Plate tectonic evolution of the southern margin of Eurasia in the Mesozoic and Cenozoic. *Tectonophysics,* **381**, 235–273.

GÖNCÜOGLU C.M., SAYIT K. and TEKIN U.K. 2010. Oceanization of the northern Neotethys: geochemical evidence from ophiolitic melange basalts within the Izmir–Ankara suture belt, NW Turkey. *Lithos,* **116**, 175–187.

GRADSTEIN F.M., OGG J.G. and SMITH A.G. 2004. A geologic time scale 2004. Cambridge University Press, Cambridge, pp. 589.

GUTNIC M., MONOD O., POISSON A. and DUMONT J.F. 1979. Géologie des Taurides Occidentales (Turquie). *Mémoires de la Société géologique de France*, **137**, 1–112.

HALLAM A. 1996. Major bio-events in the Triassic and Jurassic. *In*: WALLISER O.H. (ed.). Global events and event-stratigraphy. Springer, Berlin, 265–283.

HALLAM A. and WIGNALL P.B. 1997. Mass extinctions and their aftermath. Oxford University Press, Oxford, pp. 330.

HALLOCK P. and SCHLAGER W. 1986. Nutrient excess and the demise of coral reefs and carbonate platforms. *Palaios,* **1**, 389–398.

HOCHULI A. and FRANK S.M. 2000. Palynology (dinoflagellate cysts, sporepollen) and stratigraphy of the Lower Carnian Raibl Group in the Eastern Swiss Alps. *Eclogae Geologicae Helvetiae*, **93**, 429–443.

HORNUNG T. 2008. A Tethys-wide mid-Carnian (Upper Triassic) carbonate productivity crisis: evidence for the Alpine Reingraben Event from Spiti (Indian Himalaya ?). *In*: Hornung T. (ed.). The Carnian Crisis in the Tethys Realm. Multistratigraphic studies and palaeoclimate constraints. VDM Verlag Dr. Müller, Saarbrücken, pp. 237.

HORNUNG T. and BRANDNER R. 2005. Biochronostratigraphy of the Reingraben Turnover (Hallstatt Facies Belt): local black shale events controlled by regional tectonics, climatic change and plate tectonics. *Facies,* **51**, 475–494.

HORNUNG T., KRYSTYN L. and BRANDNER R. 2006. A Tethys-wide mid Carnian (Upper Triassic) carbonate productivity decline: evidence for the Alpine Reingraben Event from Spiti (Indian Himalaya). *Journal of Asian Earth Sciences*, **30**, 285–302.

HORNUNG T., SPATZENEGGER A. and JOACHIMSKY M.M. 2007a. Multistratigraphy of condensed ammonite beds of the Rappoltstein (Berchtesgaden, Southern Germany): unravelling palaeo-environmental conditions on 'Hallstatt deep swells' during the Reingraben Event (late Lower Carnian). *Facies*, **53**, 267–292.

HORNUNG T., BRANDNER R., KRYSTYN L., JOACHIMSKY M.M. and KEIM L. 2007b. Multistratigraphic constraints on the NW Tethyan ''Carnian Crisis''. *New Museum of Natural History and Science Bulletins*, **4**, 59–67.

KEIM L. and BRANDNER R. 2001. Facies interfingering and synsedimentary tectonics on late Ladinian – early Carnian carbonate platforms (Dolomites, Italy). *Journal of Earth Sciences (Geologische Rundschau)*, **90**, 813–830.

KEIM L., BRANDNER R., KRYSTYN L. and METTE W. 2001. Termination of carbonate slope progradation: an example from the Carnian of the Dolomites, northern Italy. *Sedimentary Geology*, **143**, 303–323.

KOZUR H.W. 1989. Significance of events in conodont evolution for the Permian and Triassic stratigraphy. *Courier Forschungsinstitut Senckenberg*, **117**, 385–408.

KOZUR H.W. and BACHMANN G.H. 2010. The middle Carnian Wet Intermezzo of the Stuttgart Formation (Schilfsandstein), Germanic Basin. *Palaeogeography Palaeoclimatology Palaeoecology*, **290**, 107–119.

KRISTAN-TOLLMANN E. 1970. Die *Osteocrinus*-fazies, ein Leithorizont von Schwebcrinoiden im Oberladin: Unterkarn der Tethys. *Erdöl und Kohle*, **23**, 781–789.

KRYSTYN L. 1983. Das Epidaurus-Profil (Griechenland): ein Beitrag zur Conodonten Standardzonierung des tethyalen Ladin und Unterkarn. *Schriftenreihe der Erdwissenschaftlichen Kommission der Österreichischen Akademie der Wissenschaften*, **5**, 231–258.

KRYSTYN L. 1991. Die Fossillagerstätten der alpinen Trias. Exkursionsführer, pp. 23–78

KRYSTYN L., GALLET Y., BESSE J. and MARCOUX J. 2002. Integrated Upper Carnian to Lower Norian biochronology and implications for the Upper Triassic magnetic polarity time scale. *Earth and Planetary Science Letters*, **203**, 343–351.

MCROBERTS C.A. 2000. A primitive *Halobia* (Bivalvia: Halobioidea) from the Triassic of northeast British Columbia. *Journal of Paleontology*, **74**, 599–603.

MCROBERTS C.A. 2010. Biochronology of Triassic bivalves. *In*: Lucas S.G. (ed.). The Triassic timescale. *Geological Society of London Special Publications*, **334**, 201–219

MCROBERTS C.A., KRYSTYN L. and SHEA A. 2008. Rhaetian (Late Triassic) *Monotis* (Bivalvia: Pectinoida) from the eastern Northern Calcareous Alps (Austria) and the end-Norian crisis in pelagic faunas. *Palaeontology*, **51**, 721–735.

MOIX P., BECCALETTO L., KOZUR H.W., HOCHARD C., ROSSELET F. and STAMPFLI G. 2008. A new classification of the Turkish terranes and sutures and its implication for the paleotectonic history of the region. *Tectonophysics*, **451**, 7–39.

MONOD O. 1977. Recherches géologiques dans le Taurus Occidental au sud de Beyşehir (Turquie). Dissertation, University of South Paris, pp. 442.

MUTTONI G., KENT D., OLSEN P.E., STEFANO P.D., LOWRIE W., BERNASCONI S.M. and HERNÁNDEZ F.M. 2004. Tethyan magnetostratigraphy from Pizzo Mondello (Sicily) and correlation to the Late Triassic Newark astrochronological polarity time scale. *Geological Society of American Bulletin*, **116**, 1043–1058.

OGG J.G., OGG G. and GRADSTEIN F.M. 2008. The concise geologic time scale. Cambridge University Press, Cambridge, pp. 177.

ÖZGÜL N. and ARPAT E. 1973. Structural units of Taurus orogenic belt and their continuation in the neighbouring regions. *Bulletin of the Geological Society of Greece*, **10**, 156–164.

POISSON A. 1977. Recherches géologiques dans les Taurides occidentals (Turquie). Dissertation, University of South Paris, pp. 759.

RICHTHOFEN F.V. 1860. Geognostische Beschreibung der Umgebung von Predazzo, Sanct Cassian und der Seisser Alpe in Süd Tyrol. Justus Perthes Verlag, Gotha, pp. 327.

RIEDEL P. 1991. Korallen in der Trias der Tethys: Stratigraphische Reichweiten, Diversitätsmuster, Entwicklungstrends und Bedeutung als Rifforganismen. *Mitteilungen der Gesellschaft der Geologie- und Bergbaustudenten*, **37**, 97–118.

RIGO M., PRETO N., ROGHI G. and TATEO F. 2007. A rise in the carbonate compensation depth of western Tethys in the Carnian (Late Triassic): deep-water evidence for the Carnian Pluvial Event. *Palaeogeography Palaeoclimatology Palaeoecology*, **246**, 188–205.

ROBERTSON A.H.F. 1993. Mesozoic-Tertiary sedimentary and tectonic evolution of Neotethyan carbonate platforms, margins and small ocean basins in the Antalya Complex, southwest Turkey. *Special Publications of the International Association of Sedimentologists*, **20**, 415–465.

ROBERTSON A.H.F. 2000. Mesozoic-Tertiary tectonic-sedimentary evolution of a south Tethyan Oceanic Basin and its margins in southern Turkey. *Geological Society of London Special Publications*, **173**, 97–138.

ROBERTSON A.H.F., POISSON A. and AKINCI Ö. 2003. Developments in research concerning Mesozoic- Tertiary Tethys and neotectonics in the Isparta Angle, SW Turkey. *Geological Journal*, **38**, 195–234.

ROGHI G. 2004. Palynological investigations in the Carnian of the Cave del Predi area (Julian Alps, NE Italy). *Review of Palaeobotany Palynology*, **132**, 1–35.

RÜFFER T. and ZAMPARELLI V. 1997. Facies and biota of Anisian to Carnian carbonate platforms in the Northern Calcareous Alps (Tyrol and Bavaria). *Facies*, **37**, 115–136

SCHLAGER W. and SCHÖLLNBERGER W. 1974. Das Prinzip stratigraphischer Wenden in der Schichtfolge der Nördlichen Kalkalpen. *Mitteilungen der Geologischen Gesellschaft in Wien*, **66**(**67**), 165–193.

SCOTESE C.R. 1998. Quicktime computer animations. PALEOMAP Project, Department of Geology. University of Texas at Arlington, Arlington.

SCOTESE C.R. 2001. Paleomap Project, http://www.scotese.com/ (July 2001).

SCOTESE C.R., GAHAGAN L.M. and LARSON R.L. 1989. Plate tectonic reconstructions of the Cretaceous and Cenozoic ocean basins. *In*: SCOTESE C.R., SAGER W.W. (eds). Mesozoic and Cenozoic plate reconstructions. Elsevier, Amsterdam, 27–48.

SENEL M. 1997. Türkiye Jeoloji Haritalari, Nr. 4, Isparta Paftasi, Jeoloji Etütleri Dairesi, Ankara**.**

ŞENGÖR A.M.C. and YILMAZ Y. 1981. Tethyan evolution of Turkey: A plate tectonic approach. *Tectonophysics*, **75**, 181–241.

ŞENGÖR A.M.C., YILMAZ Y. and SUNGURLU O. 1984. Tectonics of the Mediterranean Cimmerids: nature and evolution of the western termination of Paleo-Tethys. *Geological Society of London Special Publications*, **17**, 77–112.

SIMMS M.J. and RUFFELL A.H. 1989. Synchronicity of climate change and extinctions in the Late Triassic. *Geology*, **17**, 265–268.

SIMMS M.J., RUFFELL A.H. and JOHNSON A.L.A. 1995. Biotic and climatic changes in the Carnian (Triassic) of Europe and adjacent areas. *In*: Fraser N.C., Sues H.D. (eds). In the shadow of the dinosaurs. Early Mesozoic tetrapods. Cambridge University Press, Cambridge, 352–365.

STAMPFLI G.M. and BOREL G.D. 2002. A plate tectonic model for the Paleozoic and Mesozoic constrained by dynamic plate boundaries and restored synthetic oceanic isochrons. *Earth and Planetary Science Letters*, **196**, 17–33.

STAMPFLI G.M., BOREL G.D., MARCHANT R. and MOSAR J. 2002. Western Alps geological constraints on western Tethyan reconstructions. *Journal of Virtual Explorer*, **8**, 77–106.

TEKIN U.K. and GÖNCÜOĞLU C. 2007. Discovery of the oldest (Upper Ladinian to Middle Carnian) radiolarian assemblages from the Bornova Flysch zone in Western Turkey: implications for the evolution of the Neotethyan Izmir–Ankara Ocean. *Ofioliti,* **32**, 131–150.

TEKIN U.K., GÖNCÜOĞLU C. and TURHAN N. 2002. First evidence of Late Carnian radiolarians from the Izmir–Ankara suture complex, central Sakarya, Turkey: implications for the opening age of the Izmir–Ankara branch of Neo-Tethys. *Geobios*, **35**, 127–135.

TOLLMANN A. 1976. Analyse des klassischen nordalpinen Mesozoikums: Stratigraphie, Fauna und Fazies der Nördlichen Kalkalpen. Monographie der Nördlichen Kalkalpen 2. Franz Deuticke, Wien, pp. 580.

WILSON J.L. 1975. Carbonate facies in geologic history. Springer, Berlin, pp. 471.

YURTTAŞ-ÖZDEMIR Ü. 1973. Über den Schieferton mit *Halobia* der Halbinsel Kocaeli. *Bulletin of the Mineral Research and Exploration Institute of Turkey (Foreign Edition)*, **80**, 43–49.

CHAPTER III,

PUBLISHED 2015 IN GEOLOGICAL SOCIETY, LONDON, SPECIAL PUBLICATIONS 414: 257–275

SUSCEPTIBILITY AND RADIOMETRY DATA USED FOR STRATIGRAPHIC CORRELATIONS: CASE STUDY ON UPPER TRIASSIC BEDS IN TURKEY

Susanne Mayrhofer [a], Alexander Lukeneder [a]

[a] Geological-Palaeontological Department, Natural History Museum Vienna, Burgring 7, 1010 Vienna, Austria

Abstract

A Julian/Tuvalian (= Lower/Upper Carnian) substage boundary within the Kasımlar Formation, recently detected at Aşağiyaylabel (Taurus Mountains, Turkey) by facies analyses and biostratigraphic ammonoid investigations, was additionally detected by magnetic susceptibility (MS) and radiometry data. The Aşağiyaylabel sequence, a key section concerning environmental changes during Early to Late Carnian time, represents a deepening sequence from platform carbonates to pelagic limestones and marls. The Julian/Tuvalian boundary strata can be correlated over wide areas due to a positive shift in MS values from 11–105 × 10^{-6} SI (range AS I, KA IV) at the Lower Carnian sediments to 62–458 × 10^{-6} SI (range AS I, KA IV) at the Upper Carnian sediments as well as in radiometry values from 21.35–83.27 nGy h^{-1} (range AS I, KA IV) at the Lower Carnian sediments to 38.43–130.24 nGy h^{-1} (range AS I, KA IV) at the Upper Carnian sediments. A second, smaller positive shift in MS occurs at the transition from shallow-water carbonates of the Kartoz Formation (211 to 71 × 10^{-6} SI; range AS I–KA II) into deeper-water carbonates from the base of the Kasımlar Formation (3–108 × 10^{-6} SI; range AS I–KA II). This study presents the first MS and radiometry data from Lower to Upper Carnian sediments. They reliably reflect lithological changes and display a direct function of enhanced terrigenous input into marine sediment systems, most probably caused by variations in climatic conditions.

3.1. Introduction

The section AS I at Aşağiyaylabel (Taurus Mountains, Turkey), located within the Taurus Platform Units, comprises an Early to Late Carnian platform deepening sequence. It yields an ammonoid mass occurrence (‘*Kasimlarceltites* acme zone’), deposited during the Early Carnian time (Upper Triassic), which is described from the whole Tethyan realm as an episode which saw the demise of reef and carbonate platforms (Tollmann 1976; Simms and Ruffell 1989; Riedel 1991; Aigner and Bachmann 1992; Hallam 1996; Hallam and Wignall 1997; Rüffer and Zamparelli 1997; Flügel and Senowbari-Daryan 2001; Keim *et al.* 2001; Hornung and Brandner 2005; Kozur and Bachmann 2010; Lukeneder *et al.* 2012).

The sudden deepening at AS I was apparently triggered by synsedimentary tectonics, which led to a new basin geometry along a deeper ramp setting, due to down-faulting and tilting of the platform (Lukeneder *et al.* 2012). Accordingly, the depositional environment at the northern Tethyan passive margin changed from a mid ramp over an outer ramp into a basinal position. Shallow-water carbonates from the Kartoz Formation were replaced by deeper-water limestones and marlstones of the Kasımlar Formation. A low-energy, bottom environment was interpreted based on the autochthonous fine-grained deeper-water limestones. Allochthonous biogenic material, for example, thick-shelled bivalves, gastropods and plasticlasts within the pelagic limestones, indicate episodic input of thin (several millimetres-thick) coarse-grained sediment layers from different source areas (proved by the microfacies; see Table 3.1) of the foreslope or shallow marine ramp (Lukeneder *et al.* 2012). The general deepening of the carbonate ramp at AS I is demonstrated by both the ammonoid biostratigraphy (Lukeneder and Lukeneder 2014) and the facies analysis (Lukeneder *et al.* 2012).

The Julian/Tuvalian boundary (= Lower/Upper Carnian boundary) is also clearly observable at AS I, as demonstrated by detailed facies analyses and ammonoid-biostratigraphic investigations (Lukeneder *et al.* 2012, Lukeneder and Lukeneder 2014). Correlatable sections in the vicinity of AS I represent similar sediment sequences, with somewhat different thickness. Due to the similarities in lithological units (e.g. shallow-water limestones, ammonoid beds, Julian/Tuvalian boundary) the distinct sections can be well correlated. These interpretations, based on facies and biostratigraphy, are strengthened by the magnetic susceptibility (MS) and radiometry values as exemplified in the present paper.

MS is explained as the induced magnetization which arises at minerals within a certain rock sample, brought into a low-strength magnetic field (Kodama 2012). It is one of numerous methods for detecting the properties of magnetic rocks. Such features are important in certain environments (Jovane *et al.* 2013). Since Robinson (1990), MS has become a standard technique for logging sediment cores. A number of additional authors have described a close relationship between the MS signature and the facies of marine environments (Devleeschouwer 1999; Ellwood *et al.* 2000; Zhang *et al.* 2000; Racki *et al.* 2002; Da Silva and Boulvain 2006; Babek *et al.* 2010; Lukeneder *et al.* 2010). This relationship is the result of erosion and weathering, caused by sea-level changes (regression/transgression; Crick *et al.* 1997; Ellwood *et al.* 1999) or by climatic changes (Crick *et al.* 2001, 2002). Whilst most studies concentrate on climate-driven cyclostratigraphic aspects (magnetosusceptibility event and cyclostratigraphy (MSEC); e.g. Crick *et al.* 1997; Ellwood *et al.* 2001, 2013a, 2013b; Whalen and Day 2010), regional events, caused by tempestites or storm events, can be also important for correlation and interpretation at a local scale. Furthermore, many studies measure MS by detailed rock sampling and subsequent highly sensitive laboratory measurements (e.g. Hladil *et al.* 2006).

In contrast to such highly sensitive measurements, the present study represents an ‘averaging’ method (Hladil *et al.* 2006) of MS and radiometry measurements. It compares the MS and radiometry data of the Upper Triassic section AS I from Aşağiyaylabel from the Taurus Mountains of Turkey (Anatolia) with four time-equivalent sections near Aşağiyaylabel (AS IV) and Karapinar (KA I–II & IV). The MS and radiometry values or peaks depict mineralogical and sedimentological variations. These variations can be directly used for straightforward correlations of time-equivalent sequences on a regional scale. MS and radiometry results should be interpreted with caution as trend-data. Nonetheless, the characteristic peaks at the Julian/Tuvalian boundary as well as at the lithological boundary between the shallow-water carbonates (Kartoz Formation) and deeper-water carbonates (Kasımlar Formation) help to localize these particular sequences at surrounding localities. These peaks form the basis of the detailed facies and biostratigraphic investigations undertaken in this study.

3.2. Geography and Geology

Aşağiyaylabel and its surrounding sections are located in southern Turkey (Anatolia) about 90 km NE of Antalya and about 70 km SE of Isparta (Fig. 3.1a, b). The main section (AS I) crops out at the northern slope of an east–west-trending ridge, adjacent to the small village of Aşağiyaylabel (1050–1100 m above sea level, N 37.551389° E 31.304444°). The second section (AS IV) is quite close, 0.5 km NW of AS I (N 37.55479° E 31.30048°; Fig. 3.1c). The village Karapinar (Fig. 3.1b) is about 2.8 km N–NW of Aşağiyaylabel, with its three sections KA I (N 37.57692° E 31.29125°), KA II (N 37.57629° E 31.29205°) and KA IV (N 37.57629° E 31.29205°; Fig. 3.1d). Geologically, both localities – Aşağiyaylabel and Karapinar – belong to the Taurus Platform Units, located within the Anamas Dağ, south of the Izmir-Ankara Suture and north of the Antalya Suture (Robertson 1993; Senel 1997; Andrew and Robertson 2002; Robertson *et al.* 2003; Lukeneder *et al.* 2012). The Anamas Dağ, or Anamas-Akseki Autochthonous, bears a Middle to Upper Triassic sequence of limestones, marlstones and shales that is up to 200 m thick (Gindl 2000). This sequence has already been investigated by Özgül and Arpat (1973), Dumont and Kerey (1975), Monod (1977), Poisson (1977), Gutnic *et al.* (1979), Robertson (1993, 2000), Senel (1997), and Robertson *et al.* (2003). During the Late Triassic, the Anatolian System and therefore the investigated sequences were part of microplates known as 'Cimmerian terranes' within the western Tethyan Ocean, located between the northern Palaeotethys and the southern Neotethys (Şengör *et al*. 1984; Scotese *et al.* 1989; Dercourt *et al.* 1993, 2000; Scotese 1998, 2001; Gindl 2000; Stampfli and Borel 2002; Stampfli *et al.* 2002; Gradstein *et al.* 2004). The subsequent subduction of the Palaeotethys under South Eurasia led to an extension of the Neotethys between Africa and the Cimmerian terranes. The sediments of today's Turkey were deposited on the western parts of the Cimmerian terranes.

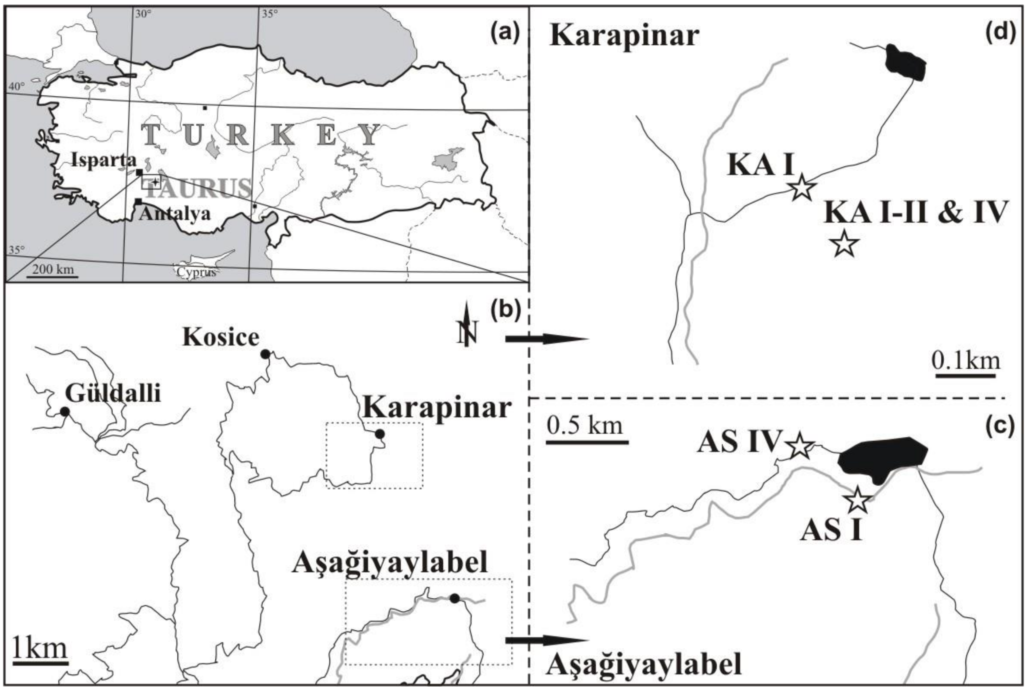

Fig. 3.1. a–b, Geography of the sections at (**c**) Aşağiyaylabel (AS I, AS IV) and (**d**) Karapinar (KA I–II & IV) in the Taurus Mountains (Anatolia, Turkey).

3.3. The facies changes at Aşağiyaylabel (AS I and AS IV) and Karapinar (KA I–II & IV)

3.3.1. Aşağiyaylabel I (AS I)

The main section at Aşağiyaylabel (AS I) consists of the Kartoz Formation and the Kasımlar Formation, embracing the Lower and Upper Carnian. The Kartoz Formation is only marginally represented by the lowermost 1.7 m of the log; this reflects a shallow palaeowater environment (massive limestone-bearing in situ reefs, megalodont bivalves, gastropods, sponges). The Kasımlar Formation, in turn, is represented by at least 33 m, bearing the Carbonate member (Julian 2), the Marlstone member and the Shale member (Tuvalian 1; Lukeneder *et al.* 2012, Lukeneder and Lukeneder 2014; Fig. 3.2). Based on its different facies description, the Carbonate member is subdivided into Carbonate member A (well-bedded dark-grey limestones yielding *Kasimlarceltites krystyni* in masses), B (Cipit-like boulders = mixed carbonate blocks embedded within reworked material) and C (well-bedded dark-grey limestones bearing millimetre-thick spherical bioturbations). The overlying Marlstone member consists of ochre, marly limestones which fade at the top into tectonically laminated shales (Fig. 3.2). The whole 33 m of the Kasımlar log represents a maximum time interval of 1.89–5.5 Ma (Ogg 2012; Lukeneder and Lukeneder 2014). This big difference in absolute values reflects an extreme divergence of two different chronostratigraphic models used for the absolute durations of the Upper Triassic (Ogg 2012). Whilst one model suggests a longer duration of Tuvalian time, the other suggests a longer Rhaetian duration. The deposits of the section AS I show an inclination of c. 50° towards NE. The whole facies description of AS I (Lukeneder *et al.* 2012) is summarized in Table 3.1.

3.3.2. Aşağiyaylabel IV (AS IV)

The sequence starts with 14.5 m of massive shallow-water limestone (equivalent to the Kartoz Formation at AS I), yielding coral debris, sponges and bivalves (articulated and disarticulated). This is followed by 4 m of dark-grey, bedded ammonoid limestones (equivalent to Unit A at AS I; Fig. 3.2), bearing abundant *K. krystyni*. Event beds, which bear masses of *K. krystyni*, alternate with beds exhibiting only rare specimens of *K. krystyni*. The bedded limestones are overlain by 5.2 m of reworked material (equivalent to Unit B of AS I with Cipit boulders) and are sealed by a calcite layer; this may indicate tectonic faulting of undefined dimension. This is tectonically overlain by 3 m of carbonate reef-limestones yielding crinoid debris, and is topped by 0.5 m of coral limestone bearing coral debris, sponges and articulated bivalves (Figs 3.2–3.4, Table 3.1).

3.3.3. Karapinar I (KA I)

The section Karapinar I (KA I) has one of the shortest but most characteristic sequences, represented by only 0.5 m of shallow water limestones followed by a 5.5 m-thick bedded *Kasimlarceltites*-limestone sequence (Fig. 3.2). The shallow-water limestone and deeper-water limestone layers are tectonically overturned. The lithological transition from the shallow-water carbonates of the Kartoz Formation into the ammonoid beds (*K. krystyni* mass occurrence) of the lowermost Kasımlar Formation is the main feature within the transitional part in all known sections (Figs 3.2–3.4, Table 3.1).

3.3.4. Karapinar II (KA II)

KA II, situated close to KA I (100 m SE), yields a very similar sediment sequence. The main difference is the extent of the ammonoid beds with their mass occurrence of *K. krystyni*. Shallow-water carbonates (which are equivalent to the Kartoz Formation of AS I) are replaced after 2 m by 17 m of black ammonoid beds (*K. krystyni* mass occurrence), equivalent to the *Kasimlarceltites* beds at the lowermost part of the Kasımlar Formation at AS I. This section seems to be more complete at the lower part of the Kasımlar Formation, causing an increased thickness of the ammonoid beds in comparison with AS I, AS IV and KA I. The top is formed by 2 m of dolomitized limestone. The shallow-water limestone and deeper-water limestone layers are characterized by a tectonically inverse stratification (Figs 3.2–3.4, Table 3.1).

3.3.5. Karapinar IV (KA IV)

The section KA IV, about 100 m to the north of KA II, represents the shortest, but probably the most important, sequence. It comprises the Lower Carnian (Julian) to Upper Carnian (Tuvalian) facies change with its typical boundary strata, ranging from marly limestones into marlstones. The section is equivalent to the corresponding part at the main section at Aşağiyaylabel (AS I), where the Carbonate member (Unit C, Julian 2) is followed by the Tuvalian Marlstone member above. The abrupt change from the 1 m-thick dark-grey carbonate sequence to ochre marlstones is obvious and is a clear marker level in that area (Fig. 3.2). Two metres of marlstones are directly visible, but an unknown thickness of marlstones is covered by erosional sediments (Figs 3.2, 3.4, Table 3.1).

Facies	Bed Thickness & Geometry					Biogenic Components	Rock-Classification
	AS I	AS IV	KA I	KA II	KA IV		
In situ corals	70 cm massive light-grey limestone	> 1.8 m massive light-grey limestone				*in situ* corals, crinoids and rare ammonoids	Coral bafflestone
Shallow-water limestone	50 cm thick light-grey massive limestone	50–200 cm thick light-grey massive limestone	60 cm massive light-grey limestone bearing breccias	200 cm thick light-grey massive limestone		Abundant grains encrusted by cyanobacteria together with common megalodontid bivalves and echinoderm fragments	Bioclastic grainstone
Cipit-like boulders	8.1 m mixed carbonate blocks embedded within reworked material	8.1 m mixed carbonate blocks embedded within reworked material				Up to metre-sized patch reef blocks, Cipit boulders, small ammonoid-coquina and filaments	Debris flow deposits
Bedded limestones with *Kasimlarceltites*	5–30 cm thick dark-grey limestone beds with wavy surface, stylolithic structures and calcite cleavages	5–45 cm thick dark-grey limestone beds with wavy surface	2–14 cm thick bedded dark-grey limestone beds with wavy surface	12–20 cm thick dark-grey limestone beds with wavy surface and calcite cleavage		Pelsparitic matrix	Pelagic wackestone/ ammonoid-floatstone
Bedded limestones with spherical bioturbation	4–60 cm thick bedded dark-grey limestone beds bearing spherical bioturbation and calcite cleavage				3–12 cm thick bedded dark-grey limestone beds bearing spherical bioturbation and yellowish residual crusts	Intercalations of fine-grained allodapic layers	Peloidal pack- to grainstone
Marly limestones	Tectonically fissile mm-cm laminated yellowish-grey marly limestones				tectonically fissile, mm-cm laminated yellowish-grey marly limestones		Bioclastic wackestone
Shales	Tectonically fissile (in the field of decimetre) brownish shales					Thin shelled bivalves, foraminifera, ammonoids, echinoderms and bioturbaton	Argillaceous borrowed peloidal packstone

Table 3.1. Facies description of the different lithologies from Aşağiyaylabel (AS) and Karapinar (KA).

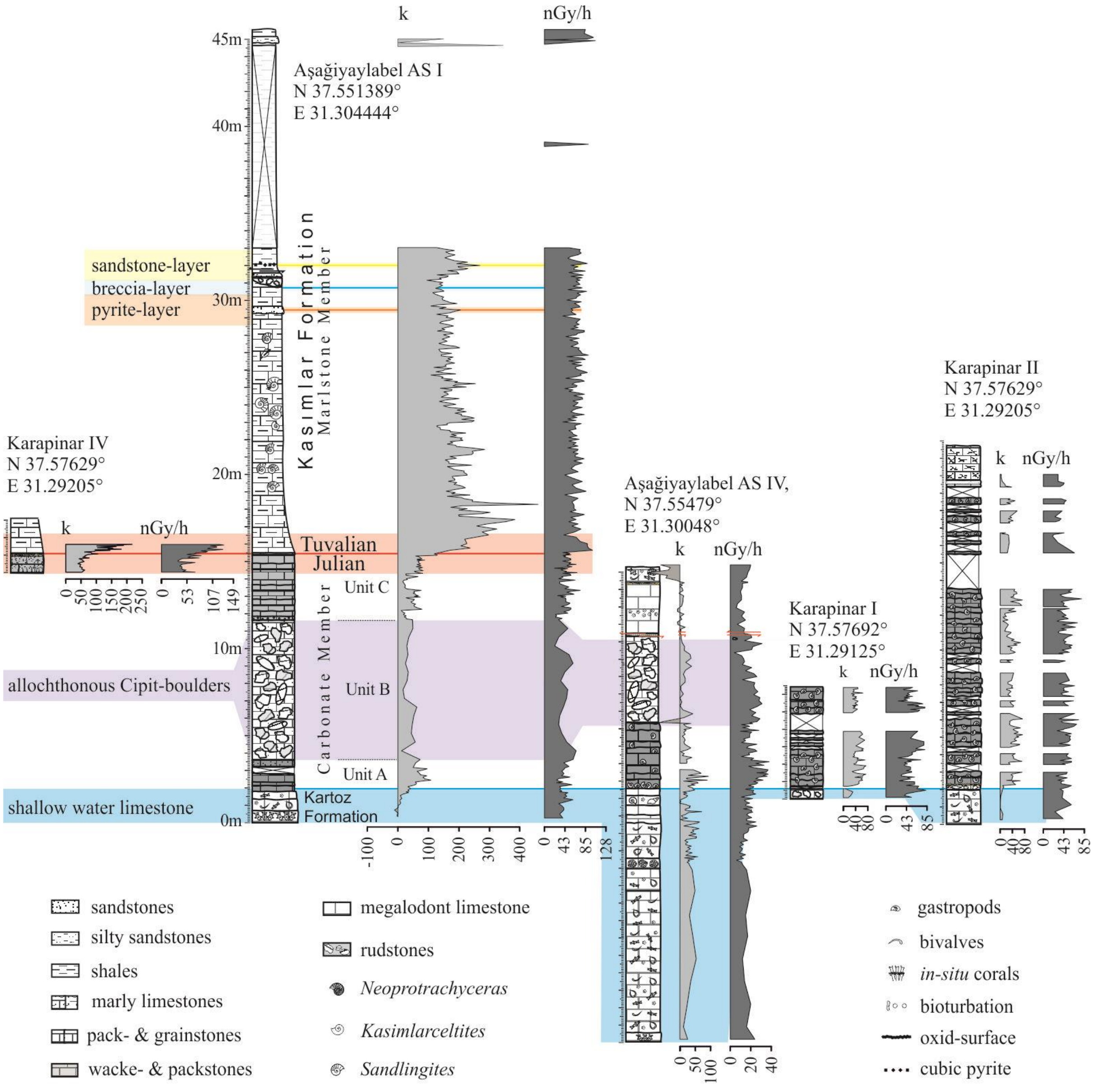

Fig. 3.2. Correlated logs of the sections AS I, AS IV and KA I–II & IV with corresponding magnetic susceptibility (MS: *k*) and radioactivity curves (nGy h^{-1}). *k*, value of volume MS in the natural state; nGy h^{-1}, dose rate.

Fig. 3.3. Detailed views of the shallow-water carbonates from the Kartoz Formation of the sections of Aşağiyaylabel (AS I, AS IV) and Karapinar (KA I, KA II). **a–b**, Platform carbonates with *in situ* corals from sections (**a**) AS I and (**b**) AS IV. **c–f**, Shallow-water reef-debris limestones from (**c**) KA I, (**d**) KA II, (**e**) AS I and (**f**) AS IV. **g**, Transition from shallow-water carbonates from the Kartoz Formation into well-bedded *Kasimlarceltites* beds at the base of the Kasımlar Formation (Carbonate member) at ASI.

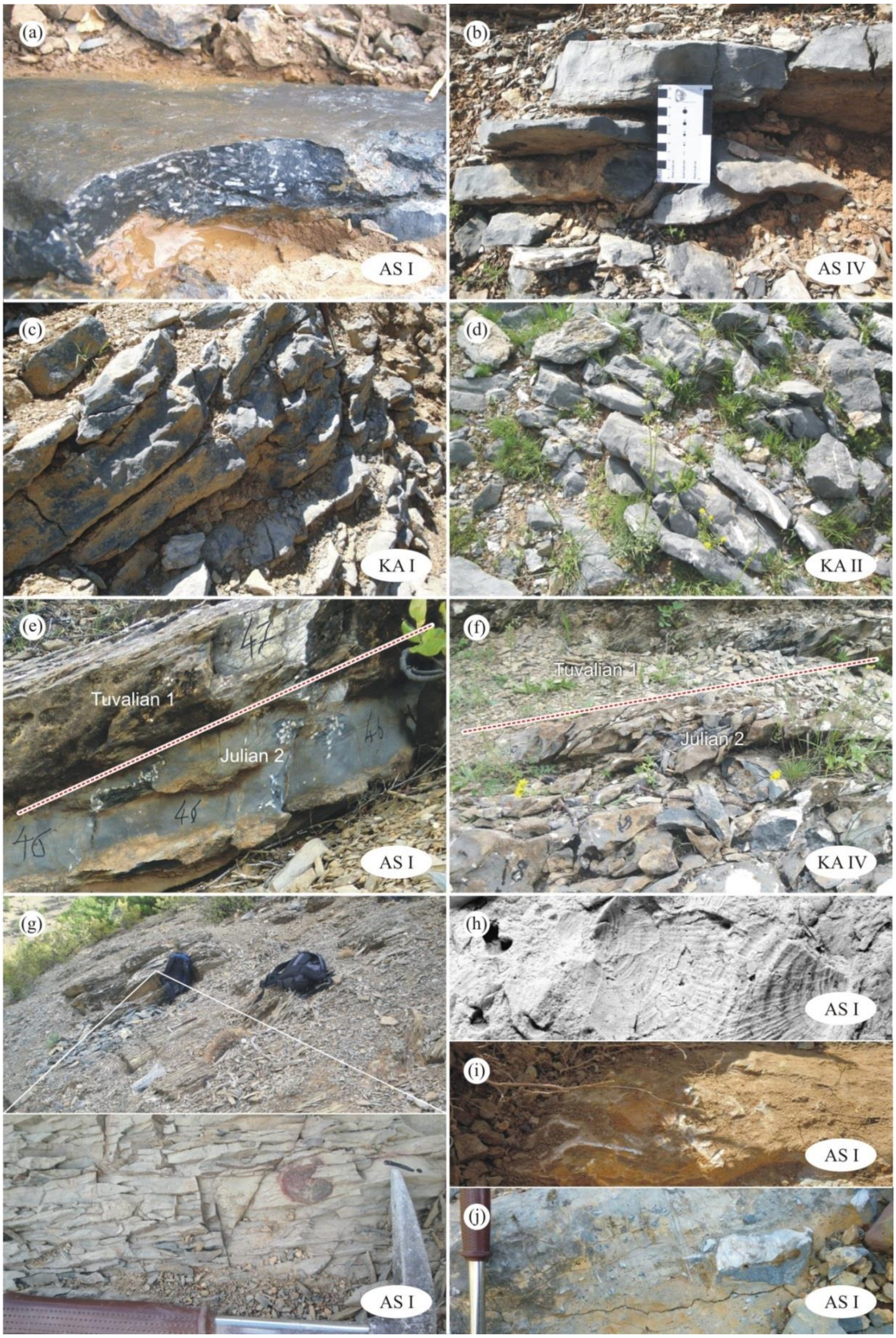

Fig. 3.4. Detailed views of the deeper-water carbonates (Units A, B, C) and the calcareous marls to marlstones of the Marlstone member from the Kasımlar Formation of the Aşağiyaylabel (AS I, AS IV) and Karapinar (KA I–II & IV) sections. **a–d**, Well-bedded *Kasimlarceltites* beds at the base of the Kasımlar Formation (Carbonate member, Unit A) at the sections (**a**) AS I, (**b**) AS IV, (**c**) KA I and (**d**) KA II. **e–f**, Julian/Tuvalian boundary (Lower/Upper Carnian boundary) at the carbonate/marl transitional intervals at the sections (**e**) AS I and (**f**) KA IV within the Kasımlar Formations at the top of Unit C, below the Marlstone member. **g**, Characteristic marls of the Marlstone member (AS I) within the Kasımlar Formation bearing the abundant Tuvalian ammonoid *Paratropites* cf. *hoetzendorfii*. **h**, Layer with accumulation of the bivalve *Halobia* and pyrite cubes within the Marlstone member from AS I. **i**, Sandstone layer of the Marlstone member, AS I. **j**, Breccia layer with shallow-water components within the Marlstone member, AS I.

3.4. Methodology

Magnetic Susceptibility (MS) was measured directly in the field with a hand-held, highly sensitive (1×10^{-7}, measured in SI units; results are indicated throughout as 'value $\times 10^{-6}$ SI'), low-level SM-30 MS meter (GF Instruments) bearing a 50-mm pick-up coil. Bed-by-bed measurements were conducted at distinct beds (e.g. Carbonate member Units A and C). This approach was replaced by a measuring interval between 5 and 50 cm where distinct beds were missing (e.g. Carbonate member Unit C and Marlstone member); 186 measurements of MS were performed in sediments of the Kartoz and Kasımlar Formations at AS I; 171 at AS IV; 85 at KA I; 156 at KA II; and 38 at KA IV. Each single bed was measured at least three times and the average calculated. To prevent measurement errors due to the sensitivity of the hand-held instruments (uneven terrain and therefore variable distance between coil and rock surface), a fresh smooth surface was prepared for each single point measured.

The radiometry was also conducted directly in the field using a hand-held scintillation gamma radiometer (GF Instruments), bearing a 51×51 mm (6 in^3) NaI (Tl) detector. Measurements were taken with an acquisition time of 1 s and a sampling interval between 5 and 50 cm through the whole log. We applied this method as an additional correlation tool and therefore concentrated on the dose rate (nGy h^{-1}) without testing the spectral results (K, U or Th): such detailed information is not supported by the instruments used. The resulting values were transposed to curves (using Microsoft Excel) and correlated with the log (Fig. 3.2). Furthermore we tested the correlation between the MS and radiometry signal for each sequence. The measurements were carried out during several field trips from October 2010 to October 2012 by the Natural History Museum Vienna (NHMV). In contrast to most studies, which focus on cyclostratigraphic results and therefore use highly sensitive laboratory measurements along with high resolution measuring intervals, this study focused only on the MS and radiometry trends in order to correlate different logs of a regional area. Accordingly, data were measured directly in the field at the main locality (AS I) as well as at additional surrounding sites (AS IV, KA I–II & IV) with a maximum measuring interval of 50 cm. Samples did not receive any special preceding preparation; 152 radiometry measurements were performed in sediments of the Kartoz and Kasımlar Formations at AS I; 155 at AS IV; 81 at KA I; 132 at KA II; and 33 at KA IV. Data were subsequently compared with facies analyses and biostratigraphic data of AS I (Lukeneder *et al.* 2012; Lukeneder and Lukeneder 2014) as well as with sections from nearby localities (AS IV, KA I–II & IV).

3.5. Results of MS & radiometry measurements

3.5.1. General trends in MS in comparison with the $CaCO_3$ content

A general increase in the MS values from shallow-water platform limestones over bedded limestones up to the marlstones is evident within all five sections and logs at Aşağiyaylabel and Karapinar (Fig. 3.2, Table 3.2). The most drastic difference can be recognized within both logs from AS I and KA IV in the median values between the bedded limestones (58 × 10^{-6} SI and 56 × 10^{-6} SI for AS I and KA IV, respectively) and the marlstones (171 × 10^{-6} SI and 142 × 10^{-6} SI for AS I and KA IV, respectively). This corresponds to the Julian/Tuvalian boundary (i.e. Lower/Upper Carnian boundary). At this boundary the $CaCO_3$ content at AS I decreases from about 70% at the Julian Carbonate member to 60% and lower at the Tuvalian Marlstone member. The same trend is present at KA IV: the $CaCO_3$ content decreases from 55% at the Julian Carbonate member to 30% from the Tuvalian Marlstone member onward. Although their MS range overlaps (11 to 105 × 10^{-6} SI v. 62 to 458 × 10^{-6} SI), a general increasing trend is clearly recognizable (Table 3.2). The trends and positive shift in the MS curves can be precisely detected within the logs of AS and KA (Fig. 3.2).

Shallow-water carbonates: Kartoz Formation

The shallow-water carbonates of the Kartoz Formation are generally related to diamagnetic substances (Dearing 1999) and therefore show, as expected, negative MS values. The shallow-water platform carbonates, which partly bear *in situ* corals (Figs 3.2 & 3.3a–d), show very similar MS values as well as similar $CaCO_3$ contents (92.9–95.8%). Hence a differentiation based on MS signals or $CaCO_3$ content is not possible in these shallow-water carbonates from the Kartoz Formation. Nevertheless, the lowest MS values are clearly much lower within carbonate deposits having *in situ* corals (minimum -11 × 10^{-6} SI) than within deposits of shallow-water limestones without *in situ* corals (minimum -3 × 10^{-6} SI). Furthermore a generally higher trend of MS values is observable at the shallow-water limestones without *in situ* corals (-11 to 49 × 10^{-6} SI v. -3 to 71 × 10^{-6} SI).

Kasimlarceltites limestones: Kasımlar Formation (Carbonate member Unit A)

Well-bedded *Kasimlarceltites* limestones occur in almost every log, except for KA IV due to its different stratigraphic position (Figs 3.2 & 3.4a–d). The MS values of these black ammonoid beds range between 3 and 93 × 10^{-6} SI at AS IV, between 33 and 108 × 10^{-6} SI at AS I, between 16 and 74 × 10^{-6} SI at KA I, and between 4 and 72 × 10^{-6} SI at KA II. Their values are generally slightly higher than those of the shallow-water limestone deposits (-11 to 71 × 10^{-6} SI; Table 3.2). While their median values are not always higher than the median values of the shallow-water limestones, their maxima are higher by far within all sections (108 × 10^{-6} v. 36 × 10^{-6} SI at AS I; 93 × 10^{-6} v. 71 × 10^{-6} SI at AS IV; 74 × 10^{-6} v. 31 × 10^{-6} SI at KA I; 72 × 10^{-6} v. 11 × 10^{-6} SI at KA II; Fig. 3.2, Table 3.2). The carbonate content in all sections (average 90.6%) is significantly lower than in the shallow-water carbonates (94.1%). This decrease corresponds well to the increase in terrigenous material.

Cipit-like boulders: Kasımlar Formation (Carbonate member Unit B)

An interval with Cipit-like boulders (these being metre- to tens-of-metre-sized isolated blocks embedded in different kinds of sediments; see Richthofen (1860) and Lukeneder *et al.* (2012)) was detected in the Carbonate member (Unit B, Kasımlar Formation) within both sections of Aşağiyaylabel (AS I and AS IV; Fig. 3.2). Cipit-like boulders represent a mixture of allochthonous material from different source areas (e.g. shallow-water environments and deeper deposits), making it impossible to distinguish such sediments from the sediments of the shallow-water limestone sequence (Kartoz Formation) using MS data. Although the MS values show a broad overlap with those of the bedded limestones, the maxima and medians are much lower (maximum 62 × 10^{-6} SI at AS I; median 35 × 10^{-6} SI at AS I resp. 12 × 10^{-6} SI at AS IV) than in the well-bedded limestones (maximum 108 × 10^{-6} SI at AS I; median 61 × 10^{-6} SI at AS I resp. 24 × 10^{-6} SI at AS IV). Additionally, Cipit beds appear with considerably lower values than the marly limestones (equivalent to the Marlstone member; 1 to 62 × 10^{-6} SI v. 62 to 458 × 10^{-6} SI). Nevertheless, the average $CaCO_3$ content at the Cipit-like boulders at AS I (87.9%) is slightly lower than at the shallow-water limestones (average 94.1%) and the *Kasimlarceltites* beds (average 90.6%; Fig. 3.2, Table 3.2).

Well-bedded limestones with spherical precipitations: Kasımlar Formation (Carbonate member Unit C)

Dark-grey to black, well-bedded limestones of the Carbonate member Unit C comprising spherical millimetre- to centimetre-sized precipitations (without *Kasimlarceltites*) occur only at the sequences AS I and KA IV (Fig. 3.4e, f). Unit C is located directly below the Julian/Tuvalian boundary. The MS values, with a median value of 58×10^{-6} SI (at AS I) resp. of 56×10^{-6} SI (at KA IV), are almost identical to those of the bedded limestones bearing *Kasimlarceltites* in Unit A of AS I (median: 61×10^{-6} SI). Nevertheless, the average $CaCO_3$ contents are, in contrast to those at the *Kasimlarceltites* limestones (Unit A), significantly lower: 80.5% at AS I and 86.4% at KA IV (v. 94.1% at AS I; Fig. 3.2, Table 3.2).

Marly limestones: Kasımlar Formation (Marlstone member)

As described above, the MS values of the calcareous marls and marlstones (Marlstone member at AS I and KA IV; Figs 3.2 & 3.4g, Table 3.2) are significantly higher than those from the carbonates of the Kartoz Formation and the underlying Carbonate member of the Kasımlar Formation. The MS data show higher maxima (458×10^{-6} SI at AS I resp. 217×10^{-6} SI at KA IV), and also higher median values (171×10^{-6} SI at AS I resp. 142×10^{-6} SI at KA IV). This increase starts exactly at the Julian/Tuvalian boundary (Fig. 3.2, Table 3.2). A drop in carbonate content (average 26.77% at KA IV and 30.6% at AS I) goes hand in hand with this major positive shift in MS values.

Sandstone layer, breccia layer, pyrite layer: Kasımlar Formation (Marlstone member)

Due to the higher content of paramagnetic minerals such as pyrite (FeS_2) within the pyrite layer or glauconite ($(K, NA) (Fe^{3+}, Al, Mg)_2 ((Si, Al)_4 O_{10}) (OH)_2$) within the sandstone layer, described by Lukeneder *et al.* (2012), some peaks are probably related to lithologically identified pyrite concentrations (200×10^{-6} SI) or sandstone layers (136×10^{-6} SI; Figs 3.2 & 3.4h–i, Table 3.2). The distinct sandstone layer, breccia layer and pyrite layer are detected exclusively within the Marlstone member at the AS I section (Fig. 3.2). We therefore assume that the range of peaks in the MS curve at the Marlstone member can be assigned to such characteristic event beds or layers and are indicative for marginal breccias, glauconite or pyrite layers, which are hardly detectable without geophysical measurements (Figs 3.2 & 3.4h–j).

MS measurements at Aşağiyaylabel and Karapinar generally reflect the influence of a terrigenous input. Higher susceptibility values argue for an increased entry of terrigenous material, additionally reflected by a decrease in the carbonate content.

Facies		AS I	AS IV	KA I	KA II	KA IV	AS - KA
Shallow-water limestones with *in situ* corals	Range Median	-11–2 -5	11–49 35	- -	- -	- -	-11–49
Shallow-water limestones	Range Median	-3–36 9	-1–71 26	6–31 22	0–11 7	- -	-3–71
Cipit-like boulders	Range Median	12–62 35	1–42 12	- -	- -	- -	1–62
Well bedded limestones with *Kasimlarceltites*	Range Median	33–108 61	3–93 24	16–74 43	4–72 36	- -	3–108
Well bedded limestones with spherical percipitations	Range Median	11–96 58	- -	- -	- -	40–105 56	11–105
Calcareous marls to marlstones	Range Median	94–458 171	- -	- -	- -	62–217 142	62–458
Top Julian 2	-	96	-	-	-	84	
Bottom Tuvalian 1	-	119	-	-	-	83	
Sandstone layer	-	136	-	-	-	-	
Breccia layer	-	120	-	-	-	-	
Pyrite layer	-	200	-	-	-	-	

Table 3.2. Magnetic susceptibility values (*k*) of the sections from Aşağiyaylabel (AS I, AS IV) and Karapinar (KA I, KA II, KA IV), measured in SI units: values need to be multiplied by 10^{-6}.

3.5.2. The radiometry measurements

The radiometry variation of a studied section reflects the presence of detrital clays, feldspars, heavy minerals and other minerals arriving by riverine, aeolian or other inputs (Serra *et al.* 1980; Serra 1984; Rider 1990). Higher radiometry may reflect higher clay content. Measurements of radiometry response (nGy h^{-1}) are a powerful tool for interpreting lithological changes within an outcrop (Lukeneder *et al.* 2010).

The radiometry values confirm the increasing trend and positive shift already described by the MS values at the Julian/Tuvalian boundary at AS I and KA IV (Fig. 3.2, Table 3.3). Shallow-water limestones (Kartoz Formation) and well-bedded ammonoid limestones (Kasımlar Formation, Carbonate member, Unit A) are not well distinguishable by the radiometry data (Fig. 3.2, Table 3.3). A significant increase is recognizable again at the Lower/Upper Carnian boundary beds (Julian 2/Tuvalian 1) at AS I and KA IV. The positive shift in radiometry values marks the change from well-bedded carbonates of the Carbonate member (Unit C) to the calcareous marls and marlstones of the Marlstone member, both within the Kasımlar Formation (Fig. 3.2).

Kartoz Formation and Kasımlar Formation with Carbonate member (Unit A-C)

The whole sequences of the Kartoz Formation (shallow-water limestones partly with *in situ* corals) and the Carbonate member of the Kasımlar Formation (well-bedded ammonoid limestones Unit A, Cipit interval Unit B, well-bedded limestones Unit C) are hardly distinguishable from each other by means of their radiometry values (Figs 3.2 & 3.3g, Table 3.3). Their general radiometry ranges are very similar, except for the maximum values of the layers comprising *in situ* corals at AS I (40.57 nGy h^{-1}) and AS IV (51.24 nGy h^{-1}). These radiometry values are slightly lower than the maxima of the shallow-water limestones (59.78 nGy h^{-1} at AS I, 55.51 nGy h^{-1} at AS IV, 83.27 nGy h^{-1} at KA I, and 57.65 nGy h^{-1} at KA II). They are also lower than the maximum at the interval (Unit B) with Cipit-like boulders (66.19 nGy h^{-1} at AS I and AS IV) and the maxima at the bedded limestones with spherical precipitation (Unit C) (74.73 nGy h^{-1} at AS I and 83.27 nGy h^{-1} at KA IV).

Calcareous marls and marlstones: Kasımlar Formation (Marlstone member)

The radiometry values of the calcareous marls and marlstones are generally higher than in all underlying sediment deposits (e.g. Kartoz Formation and Carbonate member of the Kasımlar Formation; Fig. 3.4g, Table 3.3). The positive shift in radiometry values is most distinct at section KA IV (Fig. 3.2), where the values of the Carbonate member range between 34.16 and 83.27 nGy h^{-1} (median 51.24 nGy h^{-1}). The values of the calcareous marls and marlstones lie between 83.27 and 130.24 nGy h^{-1} (median 106.75 nGy h^{-1}). Although the difference is not as significant at section AS I, and ranges overlap (21.35–74.73 nGy h^{-1} in limestones of Unit C compared to 38.43–100.35 nGy h^{-1} in calcareous marls and marlstones), an increase of the radiometry values is clearly recognizable. This is especially evident when comparing the median radiometry values, which is lower (44.84 nGy h^{-1}) in the carbonate parts than in the more marly parts of section AS I (66.19 nGy h^{-1}).

Sandstone layer, breccia layer, pyrite layer: Kasımlar Formation (Marlstone member)

Sandstone layer, breccia layer, pyrite layer: Kasımlar Formation (Marlstone member). The MS peaks from the Marlstone member within the AS I section, already mentioned within the MS-result chapter above, are just as recognizable within the radiometry values. These are related to thin event layers, for example, sandstone layers (55.51 nGy h^{-1} at AS I; Fig. 3.4i), breccia layers (79 nGy h^{-1} at AS I; with shallow-water components; Fig. 3.4j, Table 3.3) or pyrite layers (68.32 nGy h^{-1}; with pyrite and goethite). These peaks, however, are less significant than the MS values.

Facies		AS I	AS IV	KA I	KA II	KA IV	AS – KA
Shallow-water limestones with *in situ* corals	Range Median	32.03–40.57 38.43	25.62–51.24 34.16				25.62–51.24
Shallow-water limestones	Range Median	29.89–59.78 40.57	12.81–55.51 34.16	38.43–83.27 56.58	23.49–57.65 40.57		12.81–83.27
Cipit-like boulders	Range Median	23.49–66.19 42.7	8.54–66.19 46.97				8.54–66.19
Well-bedded limestones with *Kasimlarceltites*	Range Median	25.62–57.65 33.09	21.35–81.13 46.97	25.62–81.13 51.24	17.08–79 44.84		17.08–81.13
Well bedded limestones with spherical percipitations	Range Median	21.35–74.73 44.84				34.16–83.27 51.24	21.35–83.27
Calcareous marls to marlstones	Range Median	38.43–100.35 66.19				83.27–130.24 106.75	38.43–130.24
Top Julian 2		55.51				70.46	
Bottom Tuvalian 1		44.84				91.81	
Sandstone layer		55.51					
Breccia layer		79					
Pyrite layer		68.32					

Table 3.3. Radiometry values (nGy h^{-1}) of the section from Aşağiyaylabel (AS I, AS IV) and Karapinar (KA I–II & IV).

3.5.3. Radiometry and MS data correlation: time-series analysis

For comparing the MS and radiometry curves (Fig. 3.5), we only used data from beds at which both measurements were available. The time alignment of both signals (MS and radiometry) was tested by using cross correlation of two time series with the correlation coefficient r (Davis 1986; Hammer and Harper 2006). Cross correlation is used for optimal alignment of two series (Hammer *et al.* 2008). To do this, one time series is kept in a fixed position, whilst the second time series is slid past, and for each position, the correlation coefficient (r) computed (Fig. 3.5, black line). The correlation coefficient (r; black line) is then plotted as a function of alignment position (Hammer and Harper 2006). The horizontal axis (x) represents the displacement of the radiometry data with respect to the MS data, whilst the vertical axis (y) shows the correlation of both time series for a given displacement. Therefore, the position with the highest correlation coefficient indicates optimal adjustment. Significance is shown by plotting the p-values (Fig. 3.5; grey line). Correlation coefficients (r; black line), which show higher values than the corresponding p-values (grey line), indicate a significant correlation. For a more detailed description of time-series analyses see Hammer and Harper (2006) and Hammer *et al.* (2008).

The results (Fig. 3.5) clearly reveal that both curves of the section AS I and KA IV correlate significantly. A significant peak positive correlation occurs at AS I in the region of two samples delay of the MS signal with respect to the radiometry signal (see Fig. 3.5). This is in contrast to the sections AS IV and KA I–II, where no significant correlation between the two signals was observed. Moreover, certain sequences of AS I do not show positive correlations between the MS and radiometry signals. Examples are the *Kasimlarceltites* beds, or from the top of the Marlstone member onward, where the homogeneous marlstone beds start to alternate with sandstone, breccia and pyrite layers; this might affect the MS signal more significantly than the radiometry signal.

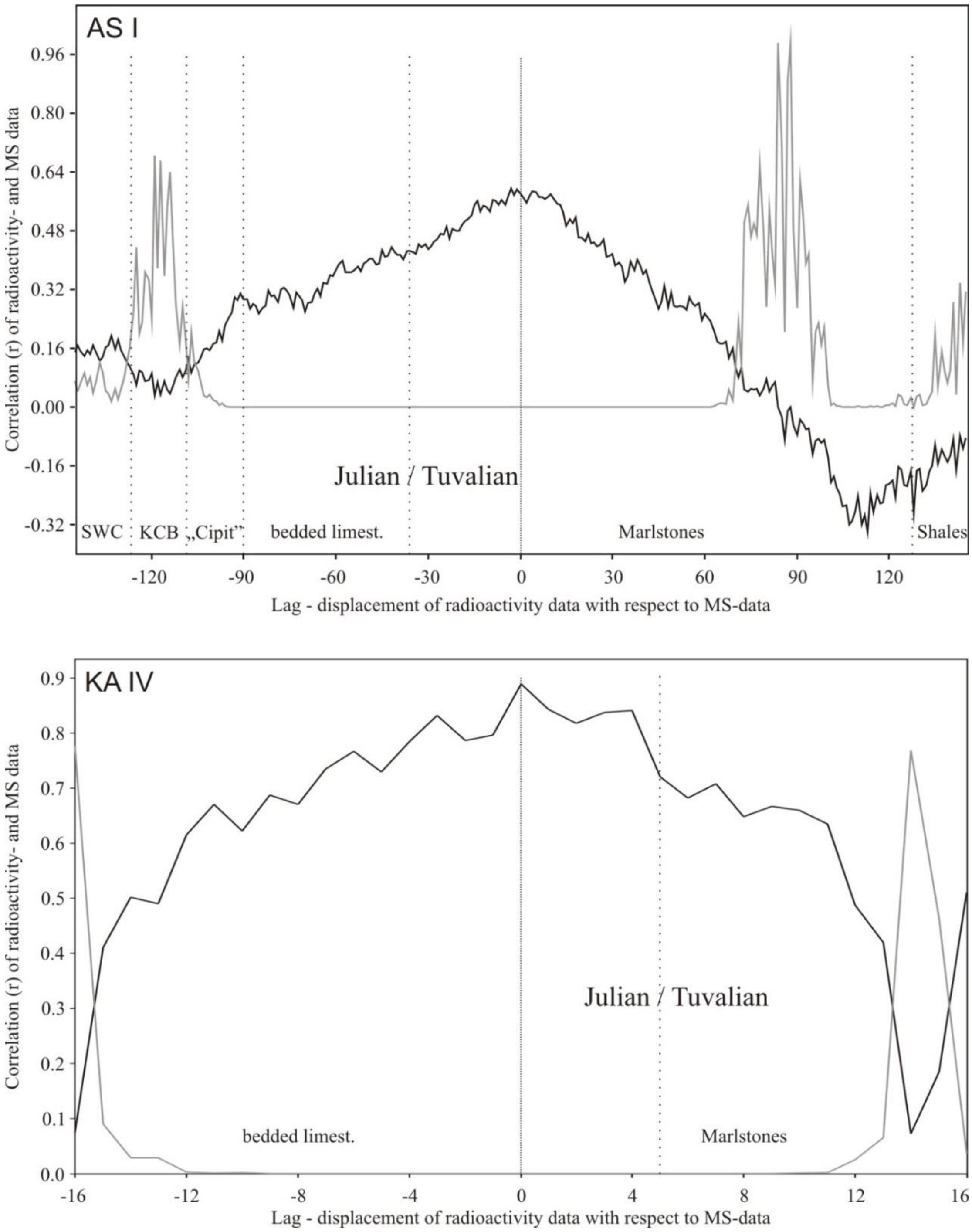

Fig. 3.5. Cross correlation of magnetic susceptibility values v. radiometry values from the sequence AS I and KA IV. Black line represents the correlation coefficient r, whilst the grey line represents the significance in p-values. SWC, Shallow water carbonates; KCB, *Kasimlarceltites* beds.

3.6. MS and radiometry data used for the correlation of time-equivalent sequences

The investigated MS and radiometry data from the area around Aşağiyaylabel and Karapinar are the first to have been measured from Lower to Upper Carnian carbonate sequences. At section AS I, the Julian/Tuvalian boundary could be fixed by ammonoid biostratigraphy (Lukeneder and Lukeneder 2014) and facies analyses (Lukeneder *et al.* 2012).

In the present study, the characteristic lithological change exactly at the Julian/Tuvalian boundary from well-bedded limestones (Unit C) into calcareous marls and marlstones (i.e. Marlstone member at AS I and KA IV) is demonstrated by a distinct MS increase from 58 × 10^{-6} SI at AS I resp. 56 × 10^{-6} SI at KA IV to 171 × 10^{-6} SI at AS I resp. 142 × 10^{-6} SI at KA IV. A similar increase in radiometry values is observed from 44.84 nGy h^{-1} at AS I resp. 51.24 nGy h^{-1} at KA IV to 66.19 nGy h^{-1} at AS I resp. 106.75 nGy h^{-1} at KA IV (Figs 3.2 & 3.5, Tables 3.2 & 3.3). MS and radiometry signals from section AS I were then compared with those from additional sections at Aşağiyaylabel (AS IV) and Karapinar (KA I–II & IV). The intention was to localize a specific part of the sequence at these sections, namely that part which possibly also bears an equivalent of the Julian/Tuvalian boundary. The opportunity to detect such important and characteristic biostratigraphic and lithological boundaries by geophysical measurements (e.g. MS and radiometry) is an additional, preliminary tool for correlation in the field. The measurements can be supported by subsequent measurements in laboratories (e.g. Kappabridge, Karl-Franzens-University, Graz), and ultimately proved by palaeontological and geological investigations. The MS studies, conducted here with hand-held instruments, can also easily be used to find characteristic features in sequences as sequence-boundaries, marked by lithological changes, even at sections where no macrofossil markers are detected in the field.

Sections AS IV and KA I–II lack this characteristic boundary. Section KA IV, however, which shows a similar lithological change from well-bedded calcareous limestones to marly limestones, shows an MS (up to 217 × 10^{-6} SI) and radiometry peak (up to 130.24 nGy h^{-1}) comparable to that found at the Julian/Tuvalian boundary at AS I (Fig. 3.5, Tables 3.2 & 3.3).

Radiometry and MS values studied by a time series analysis show that in both cases (at sections AS I and KA IV) the curves are mostly significantly positively correlated (Fig. 3.5). Accordingly, the primary signal seems to be preserved (except for some parts discussed below).

Both signals show an abrupt increase at the Julian/Tuvalian boundary, which can be interpreted as an increased influx of detrital minerals into the system. The preceding demise of the carbonate platform and the decrease of the $CaCO_3$ content from the Julian to the Tuvalian sediments clearly reflect this siliciclastic entry. This entry probably affected fluviatile systems due to the more humid conditions, which are described in several studies dealing with the carbonate platform demise during Carnian time (Lukeneder *et al.* 2012). The possible trigger mechanisms for this extraordinary ecological incision are still under discussion and therefore the subject of a series of studies. One potential reason is an uplift of extended areas (e.g. the Fennoscandian High of the Cimmerian orogeny), which could have been a trigger for a monsoonal climate (Hornung and Brandner 2005; Preto *et al.* 2010). The resulting new landmasses could have been the source areas for the increased terrigenous input into the northwestern part of the Tethyan Sea. This influx might have led to the well-known carbonate platform demise within the Tethyan realm (Tollmann 1976; Aigner and Bachmann 1992; Hornung and Brandner 2005; Preto *et al.* 2010). Another plausible scenario is magmatic or volcanic activities (e.g. the volcanic series of the Wrangellia terrane or Eastern Mediterranean alkaline volcanics), which could have influenced oceanic circulation, resulting in global climate change (Hornung *et al.* 2007; Preto *et al.* 2010). Robinson (1973) and Parrish (1993) suggest that the wet climate during Carnian time might have been the peak of the monsoonal character that already existed during the transition from the Permian to the Triassic, and therefore can be traced back to the maximum aggregation of the landmasses at that time (Preto *et al.* 2010). The result was a hot and dry climate within the continent interior, alternating wet and dry seasons at the coast of eastern Laurasia and Gondwana (Parrish and Peterson 1988; Dubiel *et al.* 1991; Mutti and Weissert 1995), and a generally wet climate at higher latitudes (Robinson 1973; Preto *et al.* 2010). Furthermore, a sea-level drop, followed by submarine clathrate destabilization and methane degassing (Hornung 2008), are also part of a large compendium of discussed scenarios along with dramatic sea-level rise (Arche and López-Gómez 2014), sediments representing anoxic events beneath siliciclastic sediments (Jerz 1966; Schuler 1968; Hagemeister 1988) and rapid variations in seawater chemistry.

Although the radiometry and MS signals generally correlate positively in both sequences (AS I and KA IV) at which the Julian/Tuvalian boundary was detected, certain intervals of AS I do not support this general correlation trend. This for instance is the case of the well-bedded limestones bearing *K. krystyni*, the top of the Marlstone member, as well as the whole Shale member of AS I, which might be caused, to some extent, by diagenetic overprint. The stylolitic structures (Table 3.1) observed within these beds would support this hypothesis. Nonetheless, the MS signals between these *Kasimlarceltites* beds of the different localities are rather similar (61 × 10^{-6} SI at AS I; 24 × 10^{-6} SI at AS IV; 43 × 10^{-6} SI at KA I; 36 × 10^{-6} SI at KA II), perhaps reflecting a similar diagenetic history of those beds.

These characteristic MS and radiometric peaks at the Julian/Tuvalian boundary can be used as additional stratigraphic correlation tools. Moreover, the other lithological parts (below and above) at AS I also show values similar to those of the surrounding sequences. Although the primary signals might be diagenetically overprinted (because the MS and radiometry signals do not show significant correlation), some comparisons between similar lithologies are possible and are therefore discussed: Whilst at both AS I and KA II the carbonate platform sediments are represented by only 1.8-m-thick and 2.3-m-thick coral-limestones, respectively, the carbonate platform sediments at section AS IV is 14.5 m thick (Fig. 3.2). KA IV lacks the carbonate platform sediments, due to its higher stratigraphic position (Julian/Tuvalian boundary). The corresponding MS values of the shallow-water limestone deposits (AS I, AS IV, KA I, KA II; Fig. 3.2) are very low to negative (-11 to 71 × 10^{-6} SI), as already estimated and expected for the diamagnetic mineral calcite (Algeo *et al.* 2007a). Ellwood and Ledbetter (1977) have already mentioned that MS values are inversely proportional to the $CaCO_3$ content of unconsolidated marine sediments. This fits well with the picture and data shown from Aşağiyaylabel and Karapinar: low MS values, from -11 to 71 × 10^{-6} SI, occur in shallow-water carbonates (Kartoz Formation), higher values, from 3 to 108 × 10^{-6} SI, are found in well-bedded limestones (Carbonate member, Kasımlar Formation), and much higher values, from 62 to 458 × 10^{-6} SI, occur in calcareous marls and marlstones (e.g. Tuvalian Marlstone member, Kasımlar Formation).

Algeo *et al.* (2007b) have described atypical positive instead of negative correlations between MS values and carbonate beds from the Permo- Triassic Guryul Ravine section in Kashmir (India). This Indian section should appear as diamagnetic due to its high calcite content (Algeo *et al.* 2007b). Algeo *et al.* (2007b) explained this positive correlation with the theory that the carbonate fossil concentrations might be produced by winnowing, yielding incorporated paramagnetic heavy minerals which potentially cause the higher MS signal (Ellwood *et al.* 2000; Algeo *et al.* 2007b). The Indian example shows that MS values should always be used cautiously and interpreted solely in combination with facies analyses and different available proxies.

In contrast to the shallow-water carbonates with almost pure limestones, the overlying dark-grey, well-bedded limestones, which bear masses of *K. krystyni*, occur in nearly every section (Unit A at AS I, AS IV, KA I, KA II). Nonetheless, they differ in thickness: whereas at the main section (AS I) the shell beds are condensed and reduced to only 1 m, AS IV bears c. 4 m, KA I .4 m, and KA II c. 17 m. The MS values increase slightly with the onset of the *Kasimlarceltites* limestones, observable at all sections (AS I, AS IV, KA I, KA II) where such beds are detectable. This positive trend indicates the beginning of the demise due to the onset of the siliciclastic runoff. The allochthonous intervals with Cipit-like boulders in Unit B (Carbonate member, Kasımlar Formation) of the sections AS I and AS IV reflect lower MS values due to the shallower carbonate source areas (shallow platform).

The sudden demise of the carbonate platform at the main section AS I, represented by the shift from shallow-water limestones bearing *in situ* corals over shallow-water limestones to bedded limestones and calcareous marls and marlstones, is interpreted as being caused by an increased input of siliciclastic material from the hinterland, triggered by more humid conditions (Lukeneder *et al.* 2012). Due to similar deposits and the similar MS and radiometry trend of the correlated sequences (AS IV, KA I, KA II), the local deepening can be interpreted at least as a regional event that affected a recent area of at least 2.8 km diameter (Aşağiyaylabel to Karapinar).

As mentioned above, we used the MS and radiometry results with caution and interpreted them solely as a trend. This is because we measured them directly in the field without highly sensitive laboratory methods and without special preceding sample preparation. Nonetheless, specific trends and shifts in MS and radiometry values can be detected and are used in combination with other analyses (e.g. geochemistry, facies changes, biostratigraphy). This interdisciplinary approach was particularly successful with regard to the characteristic peaks at the Julian/Tuvalian boundary. Additional distinct peaks along the MS curve, detected within the Marlstone member (AS I), are significant and are well correlated to a single sandstone layer, as well as to a distinct pyrite layer. Although pyrite is a paramagnetic mineral and generally shows low positive susceptibility values, the above-mentioned pyrite layer appears with values of 200×10^{-6} SI. Therefore it is remarkable that such high susceptibility values can be associated with pyrite. Nonetheless, other minerals exhibit stronger paramagnetism than pyrite, such as biotites or certain iron silicates (Dunlop and Özdemir 1997). Moreover, this could hint at partly oxidized pyrite which is probably associated with some magnetite or maghemite, and might be caused by the formation of magnetite or goethite (Lazaroff 1997). Such high values therefore indicate the occurrence of a range of distinct and thin event layers as sandstone and pyrite layers (e.g. AS I, top of marlstone beds). These are lithologically hardly observable in the field but easily detectable by geophysical measurements (e.g. hand-held MS). This shows that MS data and radiometry measurements, along with a trendline and shift interpretation undertaken by comparing and proving already-analysed lithological parameters, are valid methods for a better understanding of stratigraphic and palaeontological datasets. Geophysical measurements, although performed in the field by hand-held instruments, can hint at characteristic parts or layers within sections that are different and yet can be correlated. They can serve as a preliminary tool for subsequent stratigraphic investigations. MS and radiometry data are thus significant proxies for the amount of siliciclastic input, which in turn might reflect some climatic conditions.

3.7. Conclusions

This study presents the first magnetic susceptibility (MS) and radiometry signature of Lower to Upper Carnian sediments. The results from the MS and radiometry logs of the sections are therefore only comparable among themselves (AS I, AS IV and KA I–II & IV). The investigated section comprises the important Julian/Tuvalian substage boundary (=Lower/Upper Carnian boundary) within the Kasımlar Formation, recently detected at Aşağiyaylabel (Taurus Mountains, Turkey). The data are interpreted solely as a trend. Nonetheless, an indicative shift of the MS values (11 to 105 × 10^{-6} SI up to 62 to 458 × 10^{-6} SI) and an increase of the radiometry values (21.35–83.27 nGy h^{-1} up to 38.43–130.24 nGy h^{-1}) perfectly reflect the Julian/Tuvalian (Lower/Upper Carnian) boundary at the sections AS I and KA IV (Fig. 3.2, Tables 3.2 & 3.3). The Julian/Tuvalian boundary is of special interest due to its key position at the beginning of the Carnian Crisis within this area. The boundary is characterized by the change from a carbonate system into a marl-dominated system, triggered by severe climate change during Lower to Upper Carnian time. The Julian/Tuvalian boundary was already indicated by biostratigraphic investigations and facies analyses (Lukeneder *et al.* 2012; Lukeneder and Lukeneder 2014), strengthened herein by the MS and radiometry data from several sections. A second, smaller positive shift in MS and radiometry values is observed at Aşağiyaylabel and Karapinar at the transition from shallow-water carbonates of the Kartoz Formation to deeper-water carbonates from the base of the Kasımlar Formation at its ammonoid beds (AS I, AS IV, KA I, KA II). The latter shift is typical for a transition from pure carbonates to more marly limestones. This seems to have been caused by an increasing amount of siliciclastic material, which accumulated within the northwestern Tethyan shelves and basins due to the onset of increased river runoff, probably triggered by humid conditions. The situation is prolonged and more pronounced at the Julian/Tuvalian boundary when the Carnian Crisis (=Carnian Pluvial Event) started at the western end of the Cimmerian Terranes, as postulated by numerous studies (e.g. Tollmann 1976; Simms and Ruffell 1989; Aigner and Bachmann 1992; Hornung and Brandner 2005; Kozur and Bachmann 2010; Lukeneder *et al.* 2012). This more humid climate phase, with increased terrigenous and siliciclastic input, occurs somewhat later in the Taurus Mountains than in other sections of various European areas (Lukeneder *et al.* 2012).

This study shows that MS and radiometry data, used with caution and in combination with facies analyses and biostratigraphic investigations, constitute a robust tool to detect lithological changes by quantitative trendlines. Additionally, very thin and distinct layers in the otherwise-uniform marls can be detected by the MS measurements. Such event beds are formed by brief but high input of siliciclastic material such as breccia, pyrite accumulation and sandstones. This trendline method, performed by hand-held MS and radiometry instruments, is straightforward, fast, inexpensive and nondestructive. We therefore suggest applying these geophysical methods as additional tools for comparing geological sections and logs. These geophysical approaches (using MS and radiometry devices) are more sensitive than biostratigraphic methods or facies analyses, making them useful tools to detect possible sequences for which more detailed biostratigraphic investigations should be conducted. They are also suitable for comparing logs at which proper biostratigraphic markers are not preserved. More exact data call for the additional use of laboratory equipment (e.g. Kappabridge, Karl-Franzens-University, Graz). This approach supports common facies analyses and palaeontological studies with quantitative data, enhancing the interpretation of past environmental conditions.

3.8. Acknowledgements

The study is part of project P 22109-B17, funded by the Austrian Science Fund (FWF). It was supported by the Turkish Geological Survey (MTA), which was responsible for approving digging permission within the area investigated. The authors appreciate the suggestions and comments of two anonymous reviewers which improved the quality of the manuscript. We thank the volume editor Simo Spassov (Royal Meteorological Institute of Belgium) for his positive advice. The authors thank Oleg Mandic (Natural History Museum Vienna) for useful comments concerning the MS and radiometry analyses, as well as Anton Englert and Franz Topka (both at the Natural History Museum Vienna) for sampling assistance and thin-section preparation.

3.9. References

AIGNER T. and BACHMANN, G. H. 1992. Sequence stratigraphic framework of the German Triassic. *Sedimentary Geology*, **80**, 115–135.

ALGEO T.J., ELLWOOD B., NGUYEN T.K.T., ROWE H. and MAYNARD J.B. 2007a. The Permian-Triassic boundary at Nhi Tao, Vietnam: evidence for recurrent influx of sulfidic watermasses to a shallow-marine carbonate platform. *Palaeogeography, Palaeoclimatology, Palaeoecology*, **252**, 304–327.

ALGEO T.J., HANNIGAN R., ROWE H., BROOKFIELD M., BAUD A., KRYSTYN L. and ELLWOOD B.B. 2007b. Sequencing events across the Permian-Triassic boundary, Guryul Ravine (Kashmir, India). *Palaeogeography, Palaeoclimatology, Palaeoecology*, **252**, 328–346.

ANDREW T. and ROBERTSON A. 2002. The Beyşehir-Hoyran-Hadim nappes: genesis and emplacement of Mesozoic marginal and oceanic units of the northern Neotethys in southern Turkey. *Journal of the Geological Society*, London, **159**, 529–543.

ARCHE A. and LÓPEZ-GÓMEZ J. 2014. The Carnian Pluvial Event in Western Europe: new data from Iberia and correlation with the Western Neotethys and Eastern North America – NW Africa regions. *Earth Science Reviews*, **128**, 196–231.

BABEK O., KALVODA J., ARETZ M., COSSEY P.J., DE VUYST F.X., HERBIG H.G. and SEVASTROPULO G. 2010. The correlation potential of magnetic susceptibility and outcrop gamma-ray logs at Tournaisian-Viséan boundary sections in Western Europe. *In*: DA SILVA A.C. and BOULVAIN F. (eds). Magnetic Susceptibility, Correlations and Palaeozoic Environments. *Geologica Belgica, Brussels*, **13**, 291–308.

CRICK R.E., ELLWOOD B.B., EL HASSANI A., FEIST R. and HLADIL J. 1997. Magnetosusceptibility event and cyclostratigraphy (MSEC) of the Eifelian-Givetian GSSP and associated boundary sequences in North Africa and Europe. *Episodes*, **20**, 167–175.

CRICK R.E., ELLWOOD B.B., HLADIL J., EL HASSANI A., HROUDA F. and CHLUPAC I. 2001. Magnetostratigraphy susceptibility of the Pridoli-Lochkovian GSSP (Klonk, Czech Republic) and a coeval sequence in Anti-Atlas Morocco. *Palaeogeography, Palaeoclimatology, Palaeoecology*, **167**, 73–100.

CRICK R.E., DRECSEN R., EL HASSANI A., ELLWOOD B.B., FEIST R., GIRARD C., OVER D.J. and SCHINDLER E. 2002. Magnetostratigraphy susceptibility of the Frasnian/Famennian boundary. *Palaeogeography, Palaeoclimatology, Palaeoecology*, **181**, 67–90.

DA SILVA A.C. and BOULVAIN F. 2006. Upper Devonian carbonate platform correlations and sea level variations recorded in magnetic susceptibility. *Palaeogeography, Palaeoclimatology, Palaeoecology*, **240**, 373–388.

DAVIS J. C. 1986. Statistics and Data Analysis in Geology. John Wiley, Chichester, UK.

DEARING J.A. 1999. Chapter 4. Magnetic Susceptibility. *In*: WALDE J., OLDFIELD F. and SMITH J. (eds). Environmental Magnetism: A Practical Guide. Technical Guide, No. 6. Quaternary Research Association, London, 35–62.

DERCOURT J., RICOU L.E. and VRIELYNCK B. 1993. Atlas Tethys Palaeoenvironmental Maps. Gaulthier-Villars, Paris.

DERCOURT J., GAETANI M. VRIELYNCK B., BARRIER E. BIJU-DUVAL B., BRUNET M.F., CADET J.P., CRASQUIN S. and SANDULESCU M. 2000. Atlas Peri-Tethys—Palaeogeographical Maps. Commission of the Geological Map of the World, Paris.

DEVLEESCHOUWER X. 1999. La transition Frasnien-Famennien (Dévonien Supérieur) en Europe: Sédimentologie, stratigraphie séquentielle et susceptibilité magnétique. PhD thesis, Université Libre de Bruxelles, Bruxelles, Belgium (in French).

DUBIEL R.F., PARRISH J.T., PARRISH J.M. and GOOD S.C. 1991. The Pangean megamonsoon – evidence from the Upper Triassic Chinle Formation, Colorado Plateau. *Palaios*, **6**, 347–370.

DUMONT J.F. and KEREY E. 1975. Kırkavak Fayı [The Kırkavak Fault]. *Türkiye Jeoloji Kurumu Bülteni [Bulletin of the Geological Society of Turkey]*, **18**, 59–62.

DUNLOP J.D. and ÖZDEMIR Ö. 1997. Rock Magnetism, Fundamentals and Frontiers. Cambridge University Press, Cambridge.

ELLWOOD B.B. and LEDBETTER M.T. 1977. Antarctic bottom water fluctuation in the Vema Channel: effects of velocity changes on particle alignment and size. *Earth and Planetary Science Letters*, **35**, 189–198.

ELLWOOD B.B., CRICK R.E. and EL HASSANI A. 1999. The magnetosusceptibility event and cyclostratigraphy (MSEC) method used in geological correlation of Devonian rocks from Anti-Atlas Morocco. *American Association of Petroleum Geologists Bulletin*, **83**, 1119–1134.

ELLWOOD B.B., CRICK R.E., EL HASSANI A., BENOIST S.L. and YOUNG R.H. 2000. Magnetosusceptibility event and cyclostratigraphy method applied to marine rocks: detrital input v. carbonate productivity. *Geology*, **25**, 1135–1138.

ELLWOOD B.B., CRICK R.E., GARCIA-ALCALDE FERNANDEZ J.L., SOTO F.M., TRUYÓLS-MASSONI M., EL HASSANI A. and KOVAS E.J. 2001. Global correlation using magnetic susceptibility data from Lower Devonian rocks. *Geology*, **29**, 583–586.

ELLWOOD B.B., BRETT C.E., TOMKIN J.H. and MACDONALD W. D. 2013a. Visual identification and quantification of Milankovitch climate cycles in outcrop: an example from the Upper Ordovician Kope Formation, Northern Kentucky. *In*: JOVANE L., HERRERO-BERVERA E., HINNOV L.A. and HOUSEN B.A. (eds). Magnetic Methods and the Timing of Geological Processes. *Geological Society, London, Special Publications*, **373**, 341–353.

ELLWOOD B.B., LAMBERT L.L., TOMKIN J.H., BELL G.L., NESTELL M.K., NESTELL G. P. and WARDLAW B.R. 2013b. Magnetostratigraphy susceptibility for the Guadalupian series GSSPs (Middle Permian) in Guadalupe Mountains National Park and adjacent areas in West Texas. *In*: JOVANE L., HERRERO-BERVERA E., HINNOV L.A. and HOUSEN B.A. (eds). Magnetic Methods and the Timing of Geological Processes. *Geological Society, London, Special Publications*, **373**, 375–94.

FLÜGEL E. and SENOWBARI-DARYAN B. 2001. Triassic reefs of the Tethys. *In*: STANLEY G.D., JR. (ed.). The History and Sedimentology of Ancient Reef Systems. Kluwer Academic/Plenum Publisher, New York, 217–249.

GINDL A. 2000. Paläoökologie triassischer Ammonitenfaunen des Taurusgebirges (Türkei). Unpublished Diploma thesis, University of Vienna.

GRADSTEIN F.M., OGG J.G. and SMITH A.G. 2004. A Geologic Time Scale 2004. Cambridge University Press, Cambridge.

GUTNIC M., MONOD O., POISSON A. and DUMONT J.F. 1979. Géologie des Taurides Occidentales (Turquie). *Mémoire Societe Géologique de France*, **137**, 1–112.

HAGEMEISTER A. 1988. Zyklische Sedimentation auf einer stabilen Karbonatplattform: Die Raibler Schichten (Karn) des Drauzuges/ Kärnten (Österreich). *Facies*, **18**, 83–122.

HALLAM A. 1996. Major bio-events in the Triassic and Jurassic. *In*: WALLISER O.H. (ed.). Global Events and Event-Stratigraphy. Springer, Berlin, 265–283.

HALLAM A. and WIGNALL P.B. 1997. Mass Extinctions and Their Aftermath. Oxford University Press, Oxford. HAMMER Ø. and HARPER A.T. 2006. Paleontological Data Analysis. Blackwell Publishing, Oxford, UK.

HAMMER Ø., HARPER A.T. and RYAN P.D. 2008. PAST, Paleontological statistics. Version 1.87b, http://folk. uio.no/ohammer/past

HLADIL J., GERSL M., STRNAD L., FRANA J., LANGROVA A. and SPISIAK J. 2006. Stratigraphic variation of complex impurities in platform limestones and possible significance of atmospheric dust: a study with emphasis on gamma-ray spectrometry and magnetic susceptibility outcrop logging (Eifelian-Frasnian, Moravia, Czech Republic). *International Journal of Earth Sciences (Geologische Rundschau)*, **95**, 703–723.

HORNUNG T. 2008. The Carnian Crisis in the Tethys Realm. Multistratigraphic Studies and Palaeoclimate Constraints. VDM Verlag Dr. Müller, Saarbrücken, 1–235.

HORNUNG T. and BRANDNER R. 2005. Biochronostratigraphy of the Reingraben Turnover (Hallstatt Facies Belt): local black shale events controlled by regional tectonics, climatic change and plate tectonics. *Facies*, **51**, 475–494.

HORNUNG T., BRANDNER R., KRYSTYN L., JOACHIMSKI M. and KEIM L. 2007. Multistratigraphic constraints on the NW Tethyan 'Carnian crisis'. *In*: LUCAS S.G. and SPIELMANN J.A. (eds). The Global Triassic. *New Mexico Museum of Natural History and Science Bulletin, Albuquerque, New Mexico*, **41**, 59–67.

JERZ H. 1966. Untersuchungen über Stoffbestand, Bildungsbedingungen und Paläogeographie der Raibler Schichten zwischen Lech und Inn (Nördliche Kalkalpen). *Geologia Bavarica*, **56**, 1–99.

JOVANE L., HINNOV L., HOUSEN B. A. and HERRERO-BARVERA E. 2013. Magnetic methods and the timing of geological processes. *In*: JOVANE L., HERRERO-BERVERA E., HINNOV L.A. and HOUSEN B.A. (eds). Magnetic Methods and the Timing of Geological Processes. *Geological Society of London, Special Publications*, **373**, 1–12.

KEIM L., BRANDNER R., KRYSTYN L. and METTE W. 2001. Termination of carbonate slope progradation: an example from the Carnian of the Dolomites, northern Italy. *Sedimentary Geology*, **143**, 303–323.

KODAMA K.P. 2012. Paleomagnetism of Sedimentary Rocks. Process and Interpretation. Wiley-Blackwell, Chichester, UK.

KOZUR H. W. and BACHMANN G.H. 2010. The middle Carnian Wet Intermezzo of the Stuttgart Formation (Schilfsandstein), Germanic Basin. *Palaeogeography, Palaeoclimatology, Palaeoecology*, **290**, 107–119.

LAZAROFF N. 1997. Mineral leaching, iron precipitation, and the sulfate requirement for chemolithotrophic iron oxidation. *In*: Wise D. L. (ed.). Global Environmental Biotechnology. Springer-Verlag, Netherlands, 61–75.

LUKENEDER S. and LUKENEDER A. 2014. A new ammonoid fauna from the Carnian (Upper Triassic) Kasımlar Formation of the Taurus Mountains (Anatolia, Turkey). *Palaeontology*, **57**, 357–396, http://dx.doi.org/10.1111/pala.12070.

LUKENEDER A., HALÁSOVÁ E., KROH A., MAYRHOFER S., PRUNER P., REHÁKOVÁ D., SCHNABL P., SPROVIERI M. and WAGREICH M. 2010. High resolution stratigraphy of the Jurassic-Cretaceous boundary interval in the Gresten Klippenbelt (Austria). *Geologica Carpathica*, **5**, 365–381.

LUKENEDER S., LUKENEDER A., HARZHAUSER M., ISLAMOGLU Y., KRYSTYN L. and LEIN R. 2012. A delayed carbonate factory breakdown during the Tethyan-wide Carnian Pluvial Episode along the Cimmerian terranes (Taurus, Turkey). *Facies*, **58**, 279–296.

MONOD O. 1977. Recherches géologiques dans le Taurus Occidental au sud de Beyşehir (Turquie). PhD thesis, University of South Paris.

MUTTI M. and WEISSERT H. 1995. Triassic monsoonal climate and its signature in Ladinian-Carnian carbonate platforms (Southern Alps, Italy). *Journal of Sedimentary Research*, **B65**, 357–367.

OGG J.G. 2012. Chapter 25. Triassic. *In*: GRADSTEIN F.M., OGG J.G., SCHMITZ M.D. and OGG G.M. (eds). The Geological Time Scale. Elsevier, Amsterdam, 681–730.

ÖZGÜL N. and ARPAT E. 1973. Structural units of Taurus orogenic belt and their continuation in the neighbouring regions. *Geological Society of Greece Bulletin*, **10**, 156–164.

PARRISH J.T. 1993. Climate of the supercontinent Pangea. *Journal of Geology*, **101**, 215–233.

PARRISH J. T. and PETERSON F. 1988. Wind directions predicted from global circulation models and wind directions determined from eolian sandstones of the western United States – a comparison. *Sedimentary Geology*, **56**, 261–282.

POISSON A. 1977. Recherches géologiques dans les Taurides occidentals (Turquie). PhD thesis, University of South Paris.

PRETO N., KUSTATSCHER E. and WIGNALL P.B. 2010. Triassic climates – State of the art and perspectives. *Palaeogeography, Palaeoclimatology, Palaeoecology*, **290**, 1–10.

RACKI G., RACKA M., MATYJA H. and DEVLEESCHOUWER X. 2002. The Frasnian/Famennian boundary interval in the South Polish-Moravian shelf basins: integrated event-stratigraphical approach. *Palaeogeography, Palaeoclimatology, Palaeoecology*, **181**, 251–297.

RICHTHOFEN F.V. 1860. Geognostische Beschreibung der Umgebung von Predazzo, Sanct Cassian und der Seisser Alpe in Süd Tyrol. Justus Perthes Verlag, Gotha.

RIDER H. 1990. Gamma-ray log shape used as a facies indicator: critical analysis of an oversimplified methodology. *In*: HURST A., LOVELL M.A. and MORTON A.C. (eds). Geological Applications of Wireline Logs. *Geological Society, London, Special Publications*, **48**, 27–37.

RIEDEL P. 1991. Korallen in der Trias der Tethys: Stratigraphische Reichweiten, Diversitätsmuster, Entwicklungstrends und Bedeutung als Rifforganismen. *Mitteilungen der Gesellschaft der Geologie- und Bergbaustudenten*, **37**, 97–118.

ROBERTSON A.H.F. 1993. Mesozoic-Tertiary sedimentary and tectonic evolution of Neotethyan carbonate platforms, margins and small ocean basins in the Antalya Complex, southwest Turkey. *International Association of Sedimentologists, Special Publications*, **20**, 415–465.

ROBERTSON A.H.F. 2000. Mesozoic-Tertiary tectonic-sedimentary evolution of a south Tethyan Oceanic Basin and its margins in southern Turkey. *In*: BOZKURT E., WINCHESTER J.A. and PIPER J.D.A. (eds). Tectonics and Magmatism in Turkey and the Surrounding Area. *Geological Society of London, Special Publications*, **173**, 97–138.

ROBERTSON A.H.F., POISSON, A. and AKINCI Ö. 2003. Developments in research concerning Mesozoic-Tertiary Tethys and neotectonics in the Isparta Angle, SW Turkey. *Geological Journal*, **38**, 195–234.

ROBINSON S.G. 1973. Paleoclimatology and continental drift. *In*: Tarling D.H. and Runcorn S.K. (eds). Implications of Continental Drift to the Earth Sciences. Academia Press, London, 449–476.

ROBINSON S.G. 1990. Applications for whole core magnetic susceptibility measurements of deep-sea sediments. Leg 115 results. *Proceedings of the Ocean Drilling Program, Scientific Results*, **115**, 737–771.

RÜFFER T. and ZAMPARELLI V. 1997. Facies and biota of Anisian to Carnian carbonate platforms in the Northern Calcareous Alps (Tyrol and Bavaria). *Facies*, **37**, 115–136.

SCHULER G. 1968. Lithofazielle, sedimentologische u. paläogeographische Untersuchungen in den Raibler Schichten zwischen Inn und Saalach (Nördliche Kalkalpen). *Erlanger Geologische Abhandlungen*, **71**, 1–60.

SCOTESE C.R. 1998. Quicktime Computer Animations. PALEOMAP Project, Department of Geology. University of Texas at Arlington, Arlington.

SCOTESE C. R. 2001. Paleomap Project, http://www. scotese.com/

SCOTESE C.R., GAHAGAN L.M. and LARSON R.L. 1989. Plate tectonic reconstructions of the Cretaceous and Cenozoic ocean basins. *In*: SCOTESE C.R. and SAGER W.W. (eds). Mesozoic and Cenozoic Plate Reconstructions. Elsevier, Amsterdam, 27–48.

SENEL M. 1997. Geological map of Turkey. Nr. 4, Isparta Paftasi. Department of Geology, Ankara, 1–23.

ŞENGÖR A.M.C., YILMAZ Y. and SUNGURLU O. 1984. Tectonics of the Mediterranean Cimmerids: nature and evolution of the western termination of Palaeo-Tethys. *In*: DIXON J.E. and ROBERTSON A.H.F. (eds). The Geological Evolution of the Eastern Mediterranean. *Geological Society, London, Special Publications*, **17**, 77–112.

SERRA O. 1984. Fundamentals of Well-Log Interpretation (Vol. 1): The Acquisition of Logging Data. *Developments in Petroleum Science*, **15A**, Elsevier, Amsterdam.

SERRA O., BALDWIN J. and QUIREIN J. 1980. Theory, interpretation and practical applications of natural gamma ray spectroscopy. *Society of Petrophysicists and Well Log Analysts (SPWLA), 21st Annual Logging Symposium, 8th–11th July, Lafaette, Louisiana*, **27**, Q1–Q30.

SIMMS M.J. and RUFFELL A.H. 1989. Synchronicity of climate change and extinctions in the Late Triassic. *Geology*, **17**, 265–268.

STAMPFLI G.M. and BOREL G.D. 2002. A plate tectonic model for the Paleozoic and Mesozoic constrained by dynamic plate boundaries and restored synthetic oceanic isochrons. *Earth and Planetary Science Letters*, **196**, 17–33.

STAMPFLI G.M., BOREL G.D., MARCHANT R. and MOSAR J. 2002. Western Alps geological constraints on western Tethyan reconstructions. *Journal of the Virtual Explorer*, **8**, 77–106.

TOLLMANN A. 1976. Analyse des klassischen nordalpinen Mesozoikums: Stratigraphie, Fauna und Fazies der Nördlichen Kalkalpen. Monographie der Nördlichen Kalkalpen 2. Franz Deuticke, Wien.

WHALEN M.T. and DAY J.E. 2010. Cross-basin variations in magnetic susceptibility influenced by changing sea level, paleogeography, and paleoclimate: Upper Devonian, Western Canada sedimentary basin. *Journal of Sedimentary Research*, **80**, 1109–1127.

ZHANG S., WANG X. and ZHU H. 2000. Magnetic susceptibility variations of carbonates controlled by sea level changes. Examples in Devonian to Carboniferous strata in southern Guizhou Province, China. *Science in China D, Earth Sciences*, **43**, 266–276.

CHAPTER IV,

PUBLISHED 2014 IN PALAEONTOLOGY 57/2: 357–396

A NEW AMMONOID FAUNA FROM THE CARNIAN (UPPER TRIASSIC) KASIMLAR FORMATION OF THE TAURUS MOUNTAINS (ANATOLIA, TURKEY)

Susanne Lukeneder[a], Alexander Lukeneder[a]

[a] Geological and Palaeontological Department, Natural History Museum of Vienna, Burgring 7, 1010, Vienna, Austria

Abstract

We describe a new ammonoid fauna from the Taurus Mountains of southern Turkey. The Carnian ammonoid fauna from Aşağiyaylabel is presented for the first time. Ammonoids were obtained from limestone to marl beds of an approximately 35-m-thick section, which presents the rare opportunity to investigate ammonoid faunas across the Lower – Upper Carnian boundary. Intense sampling near the village of Aşağiyaylabel led to the recognition of a new Lower Carnian (Julian 2) to Upper Carnian (Tuvalian 1) ammonoid fauna from the Kasimlar Formation. The genus *Kasimlarceltites* gen. nov. is reported for the first time from the Taurus Mountains, which represents the main faunal element and occurs as huge mass occurrence (n » 1 million). *Kasimlarceltites krystyni* gen. et sp. nov., *Klipsteinia disciformis* sp. nov. and *Anasirenites crassicrenulatus* sp. nov. occur within the Lower Carnian Carbonate member (Units A–B) of the Kasimlar Formation from the Taurus Platform Units. Ammonoids described from the marls of the Tuvalian Marlstone member were deposited during a major, Tethyan-wide climate crisis – the so-called Carnian crisis – characterized by a demise of carbonate platforms. Based on the biostratigraphic relevance of certain ammonoid taxa described herein, the age of the analysed parts of the Kasimlar Formation is Julian 2 to Tuvalian 1. The discovery of the new ammonoid assemblages from Aşağiyaylabel substantiates the significance of Upper Triassic faunas within the Taurus Mountains and facilitates the correlation with faunal assemblages from other regions in the Tethyan Realm. The ammonoid fauna and facies indicate a general deepening from open-platform margins, over deeper shelf settings down to an open marine-influenced basinal environment. The tentative habitat for *Kasimlarceltites* gen. nov. is a shallow platform environment to upper mid-ramp.

Keywords: palaeobiogeography, biostratigraphy, Julian, Tuvalian, Tethyan Realm.

4.1. Introduction

Upper Triassic sediments, especially from the Carnian stage, form a major element within the Taurus Mountains. The area around Aşağiyaylabel has already been investigated by Özgül and Arpat (1973), Dumont and Kerey (1975), Monod (1977), Poisson (1977), Gutnic *et al.* (1979), Robertson (1993, 2000), Senel (1997), Gindl (2000), Robertson *et al.* (2003) and Lukeneder *et al.* (2012).

The Carnian section at Aşağiyaylabel displays a lithological change from pure carbonatic to more siliciclastic sedimentation (Lukeneder *et al.* 2012). The facies change occurs exactly at the Lower – Upper Carnian boundary (e.g. Julian – Tuvalian boundary) and represents the beginning of the so-called Carnian pluvial episode at the section at Aşağiyaylabel. Facies interpretations change from open-platform margin conditions, through deeper shelf margin conditions, to finally open marine-influenced basinal conditions (Lukeneder *et al.* 2012).
The Carnian pluvial episode (Simms and Ruffell 1989; Breda *et al.* 2009; Lukeneder *et al.* 2012) occurs at least Tethyan-wide with a huge platform and reef demise.

Due to more humid conditions, an enormous siliciclastic run-off from the Baltic craton was accumulated at the north-western branch of the Tethys (Tollmann 1976; Aigner and Bachmann 1992; Hornung and Brandner 2005). This led to a collapse of the reef ecosystems and carbonate platforms (Hornung and Brandner 2005). During this time, the sediments around Aşağiyaylabel were deposited within an intrashelf area on the western end of the Cimmerian System (Gindl 2000; Stampfli and Borel 2002; Lukeneder *et al.* 2012). Sedimentological and palaeontological investigations show a delayed carbonate factory breakdown during the Carnian pluvial episode for the carbonate platforms in Turkey (Lukeneder *et al.* 2012). The fact that the Carnian pluvial episode started one ammonoid zone (= about two my) earlier along the north-western Tethyan margin, in contrast to Aşağiyaylabel, indicates a diachrony within the Tethys (Lukeneder *et al.* 2012).

The section at Aşağiyaylabel is therefore a key section for detailed investigations of an ammonoid fauna that has been affected by this major environmental change. The worldwide distribution of pelagic ammonoids during the Triassic makes them suitable as a biostratigraphical and palaeogeographical tool (Krystyn 1973). The zonation of stages and substages assumed by Mojsisovics (1869, 1870, 1873–1902, 1879, 1882, 1893, 1896) resulted in a detailed, ammonoid-based Triassic biostratigraphy. This was accepted and is still used by the scientific ammonoid community (Diener 1906, 1917, 1921, 1923; Spath 1934; Krystyn 1973; Tozer 1981, 1984; Lucas 2010). Detailed work on comparable Upper Triassic ammonoid faunas from the Tethyan Realm has been performed by Krystyn and Schlager (1971), Tozer (1971, 1981, 1984, 1994), Krystyn (1973, 1978, 1980, 1982), Tatzreiter (1980, 1982), Balini and Jenks (2007), and Balini *et al.* (2007).

The Global Boundary Stratotype Section and Point for the base of the Carnian stage, and therefore for the Julian substage, has recently been defined by the lowest occurrence of *Daxatina canadensis* (Mietto *et al.* 2007a, b; Balini *et al.* 2010). The further ammonoid zonation of the Carnian stage is based on a major faunal change at the Julian – Tuvalian boundary. Whilst the Julian substage is dominated by the Trachyceratinae (especially *Trachyceras* and *Austrotrachyceras*) and Sirenitinae (e.g. *Sirenites*), the base of the Tuvalian is marked by a crisis related to these groups. In the Tuvalian, Trachyceratinae are represented solely by their final descendant *Trachysagenites*. In contrast to the decline of the Trachyceratinae, mainly the Tropitidae (e.g. *Tropites*, *Paratropites*) and to a lesser extent the Arpaditinae underwent a radiation from the base of the Tuvalian onward and are therefore characteristic faunal elements of the Tuvalian substage (Balini *et al.* 2010). The Carnian ammonoid zonation of Krystyn (1978), which is mostly used by south European workers, is divided into five zones and nine additional subzones. This zonation is well correlated with the British Columbian zonation, reviewed by Tozer (1994), which yields six biozones. It is based, amongst others, on the worldwide occurrence of *Tropites dilleri* (Balini *et al.* 2010). Whilst the Tuvalian 1 is represented in both ammonoid zonations by the *Tropites dilleri* Zone, the Tuvalian 2 is represented by the Tethyan *Tropites subbullatus* Zone as well as by Tozer's *Tropites welleri* Zone, which shows a slightly longer dimension (Balini *et al.* 2010).

Generally the sediments of the Late Triassic are dominated by diverse Tethyan ammonoid assemblages, which can simply be distinguished from the less diverse, endemic Boreal ammonoid assemblage. Sirenitinae, Ussuritidae, Arcestidae and Gymnitidae are the representatives of the Boreal ammonoids, which show an order of magnitude poorer record than the Tethyan assemblage (Dagys 1988; Balini *et al.* 2010).

More detailed investigations of the ammonoid fauna from Aşağiyaylabel will help to decipher the biostratigraphical background around the Julian – Tuvalian boundary within the Taurus Mountains of southern Turkey. Lower Carnian faunal elements, exclusively detected at Aşağiyaylabel and characterized by *Kasimlarceltites krystyni* gen. et sp. nov., *Klipsteinia disciformis* sp. nov. and *Anasirenites crassicrenulatus* sp. nov., show a type of isolated but still connective palaeoceanographic position of the intrashelf area on the western end of the Cimmerian System. The main aim of the present work is, besides describing new faunal elements, a review of the Late Triassic ammonoid fauna. This is accompanied by a global stratigraphic and palaeogeographic comparison.

4.2. Geological Setting

The outcrop at Aşağiyaylabel is situated at steep limestone walls (50 degrees towards NE) within the Taurus Mountains of southern Turkey (Anatolia), about 90 km north–north-east from Antalya, between the lakes Eğirdir and Beyşehir (Fig. 4.1). The section crops out near the little village Aşağiyaylabel (WGS84 coordinates N 37.551389°, E 31.304444°), at approximately 1050–1100 m above sea level. Tectonically, the area around the locality is part of the Taurus Platform Units (Dumont and Kerey 1975; Dumont 1976; Lukeneder *et al.* 2012). Within the latter units, the outcrop is located on the Anamas Dag or Anamas Autochthon (Dumont 1976; Gallet *et al.* 2007; Lukeneder *et al.* 2012). The deposits of this section belong to two formations, the stratigraphically older Kartoz Formation (lowermost Carnian) and the younger Kasimlar Formation (Carbonate, Marlstone and Shale members; Lukeneder *et al.* 2012), which reaches from Lower to Upper Carnian age (Julian 2 – Tuvalian 1). The fossil fauna reported within this work derives from the Kasimlar Formation with Lower Carnian to Upper Carnian sediments (Julian 2 – Tuvalian 1; Fig. 4.2).

Fig. 4.1. Position of the Aşağiyaylabel section in the Taurus Mountains (Anatolia, Turkey). **A**, geography and **B**, geology of the investigated area. Modified after Lukeneder *et al.* (2012).

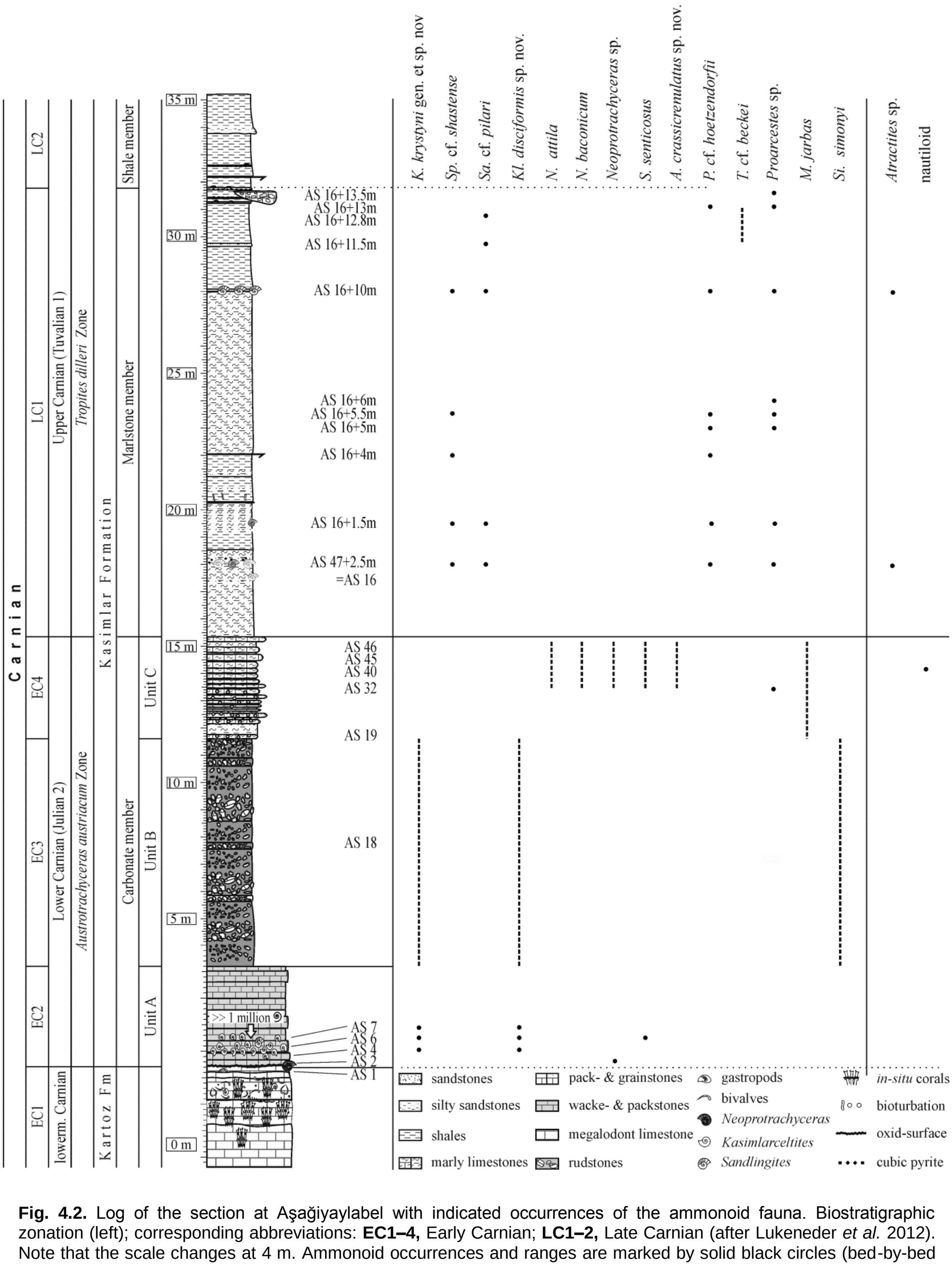

Fig. 4.2. Log of the section at Aşağiyaylabel with indicated occurrences of the ammonoid fauna. Biostratigraphic zonation (left); corresponding abbreviations: **EC1–4,** Early Carnian; **LC1–2,** Late Carnian (after Lukeneder *et al.* 2012). Note that the scale changes at 4 m. Ammonoid occurrences and ranges are marked by solid black circles (bed-by-bed sampling). Bold horizontal line indicates substage and zonal boundary, dashed vertical lines indicate ammonoid sampling from sequences or from reworked rock samples.

4.3. Materials and Methods

All specimens described within this study were extensively collected from the Kasimlar Formation at the section Aşağiyaylabel (Taurus Mountains, Turkey). The material was collected (1995–2012) by the authors, by Mathias Harzhauser and Franz Topka (Natural History Museum Vienna), and on earlier field excursions (1980–1997) by Leopold Krystyn, Andreas Gindl and Philip Strauss (excursions organized by the University of Vienna). Two sections are compiled on to one log as AS, and material from the earlier field excursions by Leopold Krystyn was correlated with the new log. Therefore, new numbers are combined with old ones, for example, AS 47 + 2.5 m = AS 16 (Fig. 4.2). Unfortunately, the exact bed location of some ammonoid examples could not be identified. Such examples are indicated as dashed vertical lines on Figure 4.2 (e.g. between beds AS 19 and AS 46).

The ammonoids are well preserved, mostly with secondary calcite shells. Only few specimens of the genera *Kasimlarceltites* gen. nov., *Klipsteinia*, *Anasirenites* and *Megaphyllites* show suture lines. A total of 479 ammonoid specimens, two nautiloid specimens and four coleoid specimens have been collected and, whenever possible, determined to species level. The ammonoid assemblages consist of 12 ammonoid genera (*Kasimlarceltites* gen. nov., *Spirogmoceras*, *Sandlingites*, *Klipsteinia*, *Neoprotrachyceras*, *Sirenites*, *Anasirenites*, *Paratropites*, *Trachysagenites*, *Proarcestes*, *Megaphyllites* and *Simonyceras*) containing 13 species and a single coleoid genus *Atractites*. The nautiloid specimen could not be determined at generic level. Conch parameters from specimens presented herein and compared taxa from literature, given in the remarks below, are shown in Tables 4.1–3 as well as in Lukeneder and Lukeneder (2013). Measurements were taken by using a vernier micrometer. For measuring smaller specimens or details (e.g. suture lines), SEM pictures were used and details measured with a digital scale. Thin sections were made to investigate different ammonoid growth stages, septa and body chamber length. Suture lines were also investigated using SEM (JEOL JSM-6400). Photographed specimens were coated with ammonium chloride. Additional facies investigations were conducted under a dissecting microscope (Zeiss Discovery V20) with attached digital camera (AxioCam MRc5). Sectioning and photographing were performed at the Natural History Museum in Vienna.

The collected material is stored within the systematic type collection of the Geological Palaeontological Department of the Natural History Museum, Vienna (NHMW), and the compared type material at the collection of the Geological Survey of Austria, Vienna (GBA).

4.3.1. Statistical methods

In addition to conventional methods, we conducted principal component analyses (PCAs), bivariate plots and coefficients of determination with respect to the conch parameters. This visualizes the diagnosis of the conch parameters of *Kasimlarceltites* gen. nov. It also tests for similarities or differences between *Kasimlarceltites* gen. nov. and related genera, as well as between *Kl. disciformis* sp. nov. and related species. The measured conch parameters D, H, W, U and ah (Fig. 4.3) are the controlling variables of the PCAs. Bivariate diagrams and coefficients of determination were carried out with the software package SPSS (IBM Corp. 2012). For the principal components analyses, the software package PAST (Hammer *et al.* 2001) was used.

4.3.2. Abbreviations

ah, aperture height; D, maximum diameter; d, diameter exclusive of last whorl; H, whorl height; H/D, proportional height; H/U, degree of involution; H/W, whorl compression; mOF, measured original figure; NCA, Northern Calcareous Alps; r^2, coefficient of determination; rOP, reported from original paper; SA, Southern Alps; sd, siphuncle diameter; sm, self-measured; st, shell thickness; swt, siphuncle wall thickness; U, umbilical width; U/D, proportional umbilical width; W, whorl breadth; W/D, proportional whorl breadth; WER, whorl expansion rate = $[D/(D - ah)]^2$, adapted after formula WER = $[dm/(dm - ah)]^2$ of Korn (2000) for subdivision in ammonoid coiling (Klug 2001; Monnet *et al.* 2012). WER standard: l, low < 1.60; m, moderate 1.61–2.0; mh, moderately high 2.01–2.40; h, high 2.41–2.80; and vh, very high > 2.80 (Korn 2000).

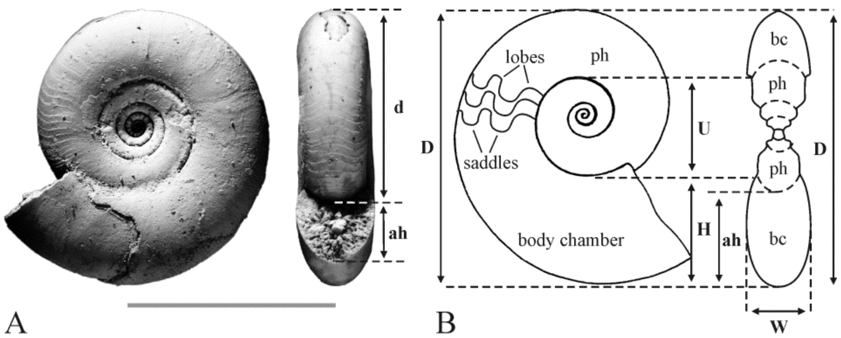

Fig. 4.3. Explanation of dimensions and conch parameters used. **A,** *Kasimlarceltites krystyni* gen. et sp. nov. (see also Fig. 4.5I–J; 2012z0133/0262). **B,** schematic ammonoid sketch with indicated conch parameters. Abbreviations: ah, aperture height; bc, body chamber; D, diameter; d, diameter exclusive of last whorl; H, whorl height; ph, phragmocone; U, umbilical width; W, whorl breadth. Scale bar represents 1 cm.

4.4. Systematic Palaeontology

This published work and the nomenclatural acts it contains, have been registered in Zoobank: http://zoobank.org/urn: lsid:zoobank.org:pub:A5D0B92D-913D-4A80-819A-7D03 C3EF5248

Order CERATITIDA Hyatt, 1884
Suborder CERATITINA Hyatt, 1884
Superfamily CERATITACEAE Mojsisovics, 1879
Family CELTITIDAE Mojsisovics, 1893
Genus *KASIMLARCELTITES* gen. nov.
Figures 4.3A, 4.4A–P, 4.5A–AH

2000 *Orthoceltites* n. sp. 1 Gindl, p. 36–52, pl. 1, figs 1–4.
2012 *Orthoceltites* Lukeneder *et al.*, p. 280, 282, 284, 285, 289–290, fig. 5.

LSID. urn:lsid:zoobank.org:act: E74134E3-B84B-420C-8F15D3E213327FB0

Derivation of name. After the Upper Triassic Kasimlar Formation in Anatolia, Turkey.

Type species. *Kasimlarceltites krystyni* gen. et sp. nov. from the Upper Triassic Kasimlar Formation in Aşağiyaylabel (Anatolia, Turkey).

Type locality. Kasimlar Formation at Asagiyaylabel, Carbonate member Unit A, beds AS 4 and AS 6 (Fig. 4.2), N 37.551389°, E 31.304444°, Upper Triassic (Lower Carnian, Julian 2).

Diagnosis. Evolute, medium-sized (up to 33 mm, Table 4.1). *Kasimlarceltites* gen. nov. occurs with four recognizable, distinct and different ontogenetic stages of shell ornamentation. The ontogeny starts with smooth ammonitellae (Fig. 4.4A–C), followed by widely spaced and distinctly ribbed juvenile morphologies. Strong ribs cross flanks, but weaken on venter, occasionally cross venter or disappear (Fig. 4.4D–F). Fine to weak, striate ribbing evolves at the mid-aged to preadult phase (Fig. 4.4G–H), finally ending with strongly ribbed adult shell morphologies (Fig. 4.5AC–AD). Whorl sections strongly depressed in juveniles (Fig. 4.4N), becoming increasingly compressed towards adult stages (Fig. 4.4O–P) with narrow, rounded venter. A clear positive correlation of the conch parameters H, W, U and ah with respect to D is evident, with coefficients of determination (r^2) being 0.93, 0.90, 0.94 and 0.88, respectively (Fig. 4.6A–D). With increasing diameters, the conch parameters H, W, U and ah as well as the ratio H/W increase gradually (quadratic, Fig. 4.6A, C; cubic, Fig. 4.6B, D–E). The increasing ratio of H/W with D (Fig. 4.6E–F) confirms the already described change from a more depressed (juvenile) to compressed (adult) conch morphology (Fig. 4.6F); the ratio H/W has been tested at different ontogenetic stages of three specimens of *Kasimlarceltites* gen. nov. (for more details see Discussion). The goniatitic to weakly ceratitic suture, with smooth lobes and a ventral saddle, is shallow in juveniles and more prominent in adults (Fig. 4.4I–J).

Composition of genus. Monospecific.

Remarks. *Kasimlarceltites* gen. nov., incorrectly assigned to the genus *Orthoceltites* by Lukeneder *et al.* (2012), differs from other similar Upper Triassic (Carnian) ammonoids by the combination of its ontogenetic change in the ribbing and by numerous morphological conch parameters. The following discussion of the relationships between similar genera is based on the examination of data from the literature as well as of material from different Carnian type localities such as Glamoca (Bosnia and Herzegovina), St. Cassian (northern Italy), as well as from the Feuerkogel and Röthelstein (Austria).

A principal component analysis (PCA, Fig. 4.7A) as well as bivariate plots with respect to D (Fig. 4.7B–G), for testing similarities of conch parameters, was conducted for *Kasimlarceltites* gen. nov. and its related genera. The first two axes of the PCA explain a total of 99.20 per cent of the variance (PC1 explains 97.82 per cent; PC2 explains 1.38 per cent), which clearly separate the genus *Cycloceltites*, as well as most specimens of the species *Dinarites avisianus* and *Lecanites vogdesi*, from *Kasimlarceltites* gen. nov. (Fig. 4.7A). The related genus *Cycloceltites* Mojsisovics, 1893 appears in the Carnian and Norian with the type species *Cycloceltites arduini* differing from *Kasimlarceltites* gen. nov. by strong, radially flared ribbing throughout the shell and by its general conch morphology (Fig. 4.7A). This difference is also present in the more evolute Carnian genus *Coeloceltites* Spath, 1951 with its type *Coeloceltites rectangularis* (Hauer, 1860), which plots randomly to *Kasimlarceltites* gen. nov. (Fig. 4.7A).

In contrast to this, the genus *Orthoceltites* Spath, 1951, and most species of the genera *Celtites* Mojsisovics, 1882 and *Lecanites* Mojsisovics, 1882 plot close to *Kasimlarceltites* gen. nov., possessing similar conch parameters. The conch parameters of ‘*Goniatites*’ *buchi* (Klipstein 1843), representing the type species of *Orthoceltites*, as well as the parameters of

O. belcheri (Tozer 1994) and *O. klipsteinianus* (= '*Ammonites*' *klipsteinianus*; Laube 1870), are characteristic for the genus *Orthoceltites*. Nonetheless, *Kasimlarceltites* gen. nov. exhibits weaker or no ribbing throughout, compared with the genus *Orthoceltites*. *Orthoceltites buchii* and *O. klipsteinianus* additionally show a different suture line (pointed ventral lobes), and *O. belcheri* shows wrinkled lobes and saddles (Tozer 1994).

The Late Anisian genus *Aplococeras*, defined by Hyatt (1900) based on the type species *'Dinarites' avisianus* Mojsisovics, 1882, is morphologically closely related to *Kasimlarceltites* gen. nov. However, nearly all specimens of *Dinarites* plot clearly separated from *Kasimlarceltites* gen. nov., except for one example which plots randomly. '*Dinarites' avisianus* differs by almost every conch parameter from *Kasimlarceltites* gen. nov., including a higher H (10–14 mm), W (7.5–10 mm) and ah (8.57–11.51 mm; Fig. 4.7B–D), but similar values of U (12.5–16.5 mm; Fig. 4.7E) and H/W (1.33–1.4; Fig. 4.7F). *Aplococeras transiens* Manfrin *et al.*, 2005 (figs 5, 10–18), seems to be very close to *Kasimlarceltites* gen. nov. Nevertheless, *Aplococeras* shows an almost flat venter, and the main ribbing is stronger throughout; moreover, *Aplococeras* has been described so far only from Anisian beds (Assereto 1969; Manfrin *et al.* 2005).

Further analytical measurements were taken on numerous species of the genus *Celtites*, including *C. conifer*, *C. edithae* (Mojsisovics 1893), *C. laevior* (Diener 1917) and *C. neumayri* (Mojsisovics 1893; Fig. 4.7A). Species such as *C. conifer*, *C. laevior* and *C. edithae*, which plot close to *Kasimlarceltites* gen. nov. (Fig. 4.7A), show high similarities with *Kasimlarceltites* gen. nov. in the conch parameters H, ah and U (Fig. 4.7B, D–E). Only within the conch parameter W, *C. edithae* plot randomly (6.0 mm) compared with *Kasimlarceltites* gen. nov., with W of 0.43–6.8 (mean 3.6 mm; Fig. 4.7C). In contrast to all other species of *Celtites*, *Celtites neumayri* plots randomly to *Kasimlarceltites* gen. nov. (Fig. 4.7A), due to the higher values of the whorl breadth (Fig. 4.7C). The major difference between the genus *Celtites* and *Kasimlarceltites* gen. nov. appears to be the more evolute coiling of *Celtites*, indicated by mean U/D values of 0.52 vs 0.40 (Table 4.1 and Lukeneder and Lukeneder 2013). *Celtites laevior* and *C. conifer* show a similar suture, but differ from *Kasimlarceltites* gen. nov. in strong, tuberculate ribbing throughout the shell.

Assereto (1969), Balini *et al.* (2000) and Manfrin *et al.* (2005) described different species of the Ladinian to Lower Carnian genus *Lecanites* Mojsisovics, 1882, closely related to *Kasimlarceltites* gen. nov. The smooth shell, with weak sigmoidal ribs (Mojsisovics 1882; Arkell *et al.* 1957), is quite similar. In contrast to the specimens of *L. vogdesi*, which generally plot separated, respectively, randomly from *Kasimlarceltites* gen. nov., *L. glaucus* and *L.*

misanii plot close and are therefore quite similar in their conch morphology (Fig. 4.7A). However, both species (*L. glaucus* and *L. misanii*) show a higher ratio of H/W (2.0 and 1.69; Fig. 4.7F), what represents a more compressed conch than *Kasimlarceltites* gen. nov. (mean 1.19; Fig. 4.7F). The notable differences in *L. vogdesi* compared with *Kasimlarceltites* gen. nov. are due to a higher W (mean 9.34 mm vs mean 3.6 mm; Fig. 4.7C) and with mostly wider diameters (mean 32.84 mm vs mean 13.2 mm; Fig. 4.7G). The type species of *Lecanites*, *'Ammonites'* (*Ceratites*) *glaucus* Münster, 1834, differs from *Kasimlarceltites* gen. nov. by lacking the distinct ribbing, a feature characteristic for juvenile stages in *Kasimlarceltites* gen. nov.

Although some genera mentioned above generally show certain similar conch parameters (Fig. 4.7A), most of them differ at least in one parameter from *Kasimlarceltites* gen. nov. (Fig. 4.7B–G), but also by stronger ribbing throughout ontogeny and by more evolute whorls. Based on shell morphology and suture line, we follow Arkell *et al.* (1957) and include *Kasimlarceltites* gen. nov. into the family Celtitidae Mojsisovics, 1893.

Stratigraphic distribution and age. The co-occurrence of *Kasimlarceltites* gen. nov. together with *Klipsteinia* (beds AS 4, AS 6 and AS 7) and *Sirenites* (bed AS 6) suggests at least Julian age. Due to the presence of *Neoprotrachyceras* sp. within bed AS 2, and therefore below the occurrence of *Kasimlarceltites* gen. nov., the stratigraphic distribution of *Kasimlarceltites* gen. nov. can be defined as not older than Julian 2/Ib.

Fig. 4.4. Ontogenetic stages, morphology and suture of *Kasimlarceltites krystyni* gen. et sp. nov. **A–G,** early whorls, scale bars represent 100 µm. **A,** lateral view of the ammonitella, paratype, 2012z0133/0266. **B,** ventral view of the ammonitella, 2012z0133/0267. **C,** lateral view of the ammonitella, 2012z0133/0268. **D,** juvenile stage of specimen, paratype, 2012z0133/0269. **E,** detailed photograph of juvenile whorls, 2012z0133/0270. **F,** ventral view of juvenile stage, paratype, 2012z0133/0271. **G,** detailed photograph of inner whorls, 2012z0133/0272. **H,** detailed photograph of the striae, paratype, 2012z0133/0273; scale bar represents 1000 µm (1 mm). **I–K,** scale bars represent 100 lm. **I,** suture, paratype, 2012z0133/0274. **J.** drawing of the suture line from specimen 2012z0133/0274. **K,** detailed photograph of the siphuncle, 2012z0133/0275. **L–P,** scale bars represent 1000 µm (1 mm). **L.** median thin section, paratype, 2012z0133/0276. **M,** thin section of the body chamber, paratype, 2012z0133/0277 with emphasis (arrow) on the siphuncle. **N,** transversal thin section of a juvenile specimen, paratype, 2012z0133/0278, note corresponding H/W values for compression/depression. **O.** transversal thin section of an intermediate stage, paratype, 2012z0133/0279, with indicated H/W values. **P,** adult stage, paratype, 2012z0133/0280, with indicated H/W values. **A–K,** figured specimens and paratypes from bed AS 6. **L–P,** paratypes from bed AS 4. Abbreviations: a, ammonitella; bc, body chamber; ll, lateral lobe; ls, lateral saddle; s, siphuncle; ul, umbilical lobe; vl, ventral lobe; vls, ventrolateral saddle; vs, ventral saddle. →

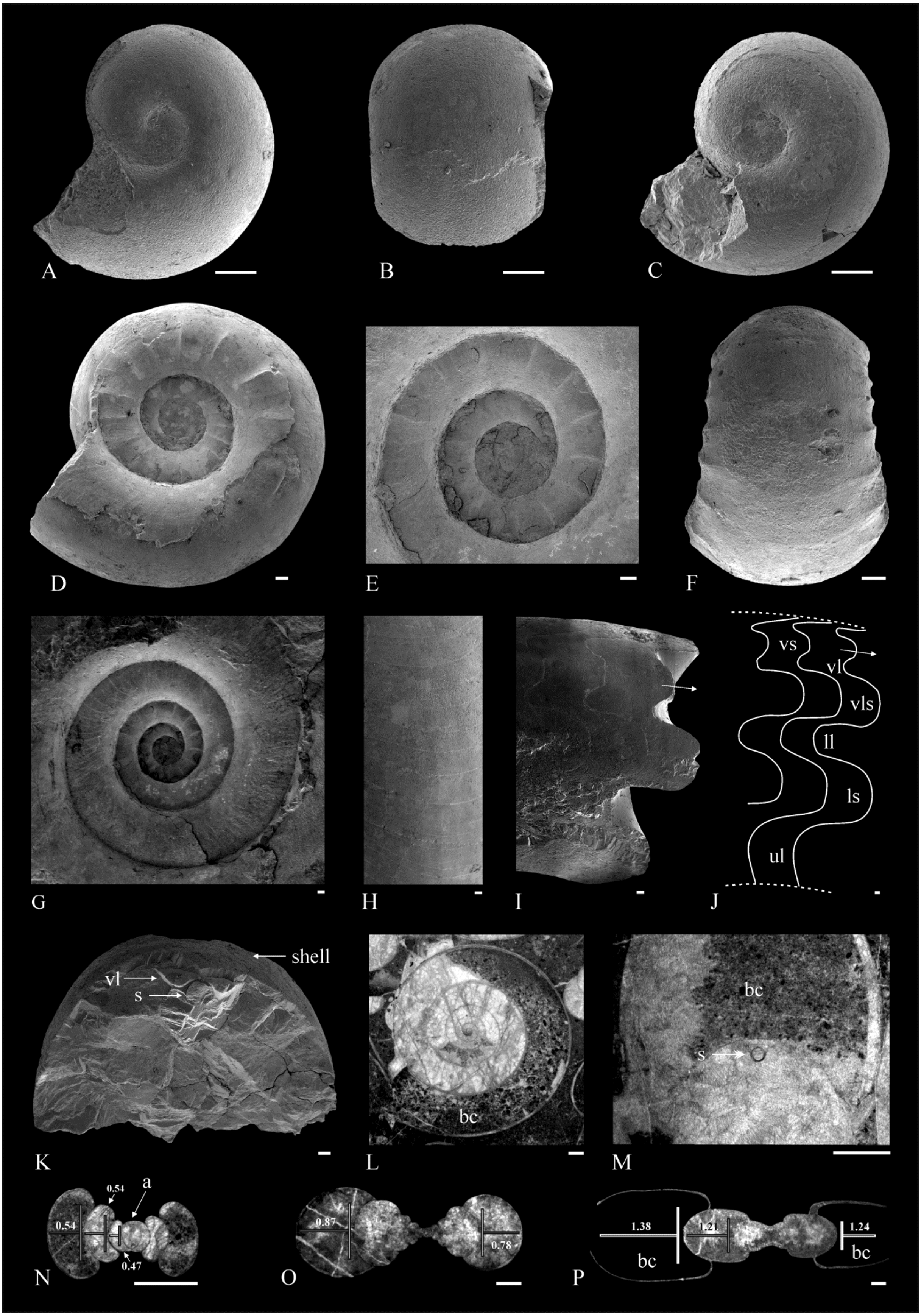
A
B
C
D
E
F
G
H
I
J
vs
vl
vls
ll
ls
ul
K
shell
vl
s
L
bc
M
bc
s
N
0.54
0.54
a
0.47
O
0.87
0.78
P
1.38
1.21
1.24
bc
bc

Kasimlarceltites krystyni sp. nov.

Figures 4.3A, 4.4A–P, 4.5A–AH

2000 *Orthoceltites* n. sp. 1 Gindl, p. 36–52, pl. 1, figs 1–4.
2012 *Orthoceltites* sp. Lukeneder *et al.*, pp. 280, 282, 284,
285, 289–290, fig. 5.

LSID. urn:lsid:zoobank.org:act: 820A9EAF-9564-4A0A-877E0418E039B317.

Derivation of name. Named after Leopold Krystyn (Vienna, Austria) in honour of his inspiring work on Triassic ammonoids.

Holotype. Natural History Museum, Vienna, NHMW2012z0133/0014 (Fig. 4.5AE–AF).

Paratypes. Sixteen paratypes have been defined: NHMW2012z0133/0266 (Fig. 4.4A), NHMW-2012z0133/0269 (Fig. 4.4D), NHMW-2012z0133/0271 (Fig. 4.4F), NHMW-2012z0133/0273–0274 (Fig. 4.4H–I), NHMW-2012z0133/0276–0277 (Fig. 4.4L–M), NHMW-2012z0133/278–280 (Fig. 4.4N–P), NHMW-2012z0133/0001 (Fig. 4.5A–B), NHMW-2012z0133/0002 (Fig. 4.5C–D), NHMW-2012z0133/0003 (Fig. 4.5E–F), NHMW-2012z0133/0004 (Fig. 4.5G–H), NHMW-2012z0133/0005 (Fig. 4.5K–L), NHMW-2012z0133/0013 (Fig. 4.5AC–AD).

Type locality and horizon. Aşağiyaylabel, Anatolia, Turkey, Kasimlar Formation, Carbonate member Unit A, bed AS 6 (holotype NHMW-2012z0133/0014) and paratypes (NHMW-2012z0133/0266, 0269, 0271, 0273–0274, 0001–0005, 0013), bed AS 4 (paratypes NHMW-2012z0133/0276–0280; Fig. 4.2) (WGS84: N 37.551389°, E 31.304444°), Upper Triassic (Lower Carnian, Julian 2).

Material. About 280 specimens from the Carbonate member, Units A–B (NHMW-2012z0133/0001–0280).

Measurements. See Table 4.1 and Lukeneder and Lukeneder (2013).

Diagnosis. Evolute shell, up to 33 mm D (Fig. 4.7G), with mesolongidome body chamber. Four different ontogenetic stages of shell morphology are characterized by different ribbing (smooth ammonitellae at the early stage of juvenile shells, followed by strongly ribbed juvenile morphologies, evolving a fine-ribbed mid-aged to preadult phase and finally a strongly ribbed adult stage), different whorl shape (from depressed to compressed, see Fig. 4.6E–F) and different umbilical wall (from shallow arched to steep; Fig. 4.4N–P). The lack of an adventive lobe classifies the initially goniatitic suture as ceratitic (Gindl 2000). Lobe size and saddle size generally decrease in ventral direction.

Description. *Kasimlarceltites krystyni* gen. et sp. nov. generally shows an evolute shell with U/D = 0.23–0.50 (Table 4.1). The parameters H and U show a positive quadratic correlation with D (r^2= 0.93, 0.94), whilst W, ah and H/W show positive cubic correlations with D (r^2 = 0.90, 0.88, 0.70; Fig. 4.6A–E). Whorl shape changes from highly depressed to compressed in ontogeny (Figs 4.4N–P, 4.6E–F). Juvenile whorl sections are depressed, with H/W 0.35–0.60 (paratype, Figs 4.4N, 4.6F), whereas preadult stages show H/W values of 0.58–0.91 (paratype, Figs 4.4O, 4.6F), and adult whorl stages are compressed (paratype, Fig. 4.4P), with maxima of H/W 2.15 (Fig. 4.6E–F). The meso- to longidome body chamber comprises almost the entire whorl (270–360 degrees; paratype, Fig. 4.4L). Ribbing differs in the various growth stages (Fig. 4.4A–H). Juveniles have a shallow, arched umbilical wall, whereas adults have a steep umbilical wall (paratype, Fig. 4.4N–P).

Juvenile, smooth shells (e.g. ammonitellae) have a maximum D of 0.6 mm (paratype, Fig. 4.4A; see also Fig. 4.4B–C). Whorl shape is globular to depressed; tube-like whorl sections with H/W 0.75 are present (Fig. 4.6F). At a D of 0.7 mm, the H is 0.3 mm and W 0.4 mm (Fig. 4.4A). A smooth embryonic protoconch at the juvenile stage (ammonitella until first whorl) is followed by strong ribbing. One whorl bears 16 prominent, very well and widely spaced strong ribs (paratype, Fig. 4.4D; see also Fig. 4.4E). Ribbing appears sharp, distinct and prominent on flanks. Single ribs start at upper umbilical edge and cross the flanks. Ribs are weaker (hardly visible) on venter (paratype, Fig. 4.4F). Strongly ribbed stage ends at a D of approximately 2–4 mm. The juvenile phase with strong ribbing is replaced by two to four whorls exhibiting fine, slightly sigmoidal ribbing (crossing the venter in a proverse adoral bow; paratype, Fig. 4.4H) to almost smooth whorls at the end of the juvenile stage up to the mid-aged (preadult) stage (holotype, Fig. 4.5AE–AF; see also Figs 4.4G, 4.5S–W). Ribbing, somewhat variable in strength, ranges from very fine ribs over striae (narrow-spaced striae; paratypes, Figs 4.4H, 4.5K–L) to stronger ribs (holotype Fig. 4.5AE–AF). A final strong ribbing near the aperture is visible only in large adult specimens (paratype, Fig. 4.5AC–AD;

see also Fig. 4.5W–Z). This rib type starts at the mid-flank, crossing the venter in a proverse adoral bow (paratype, Fig. 4.5AC–AD).

Width and depth of lobes and saddles generally decrease in ventral direction (Fig. 4.4I–J). The umbilical lobe is five times wider than the ventral lobe. A wide and deep umbilical lobe and a subsequent smooth and rounded lateral saddle are followed by a deep and narrow lateral lobe and again by a wide smooth and rounded ventrolateral saddle. The ventrolateral saddle is again followed by a shallow and narrow ventral lobe, ending in a smooth and rounded, but flattened ventral saddle (paratype, Fig. 4.4I–J). The lack of an adventive lobe classifies the initially pseudo-goniatitic suture as a primitive, ceratitic suture (Gindl 2000).

Siphuncle structures of *K. krystyni* gen. et sp. nov. (Fig. 4.4L–M) are preserved in numerous (n = 6) thin sections from AS 4c (Fig. 4.4L). Siphuncle walls appear as black rings within the transparent, secondary calcite filling of the phragmocone. The shell is also replaced by secondary calcite crystals (Fig. 4.4L–P). The siphuncle is described from thin section AS 4c (paratype, Fig. 4.4M). At an H of 4 mm, a W of 3 mm and a st of 0.01 mm, the sd is 0.21 mm. Swt in that specimen is 0.010 mm. A second specimen on the same thin section shows values of H 5 mm, W 3 mm, st 0.09, sd 0.22 mm and swt 0.013 mm. Additionally, siphuncle structures on one specimen (Fig. 4.4K) could be measured after taking SEM photographs.

Remarks. The herein described *K. krystyni* gen. et sp. nov. differs from all other known members of the family Celtitidae Mojsisovics, 1893 by its distinctive morphological conch parameters (Fig. 4.7A–G).

Stratigraphic range. Upper Triassic, Lower Carnian, Julian 2.

Regions. Aşağiyaylabel, Taurus Mountains, Turkey.

Fig. 4.5. Fauna of Aşağiyaylabel, Kasimlar Fm., Carbonate member Unit A, *Austrotrachyceras austriacum* Zone (Julian 2), bed AS 6. **A–Z.** and **AA–AH.** ontogenetic stages of *Kasimlarceltites krystyni* gen. et sp. nov., **AI–AJ.** *Sirenites senticosus*. **A.** lateral view, paratype, 2012z0133/0001. **B.** ventral view, paratype, 2012z0133/0001. **C.** lateral view, paratype, 2012z0133/0002. **D.** ventral view, paratype, 2012z0133/0002. **E.** lateral view, paratype, 2012z0133/0003. **F.** ventral view, paratype, 2012z0133/0003. **G.** lateral view, paratype, 2012z0133/0004. **H.** ventral view, paratype, 2012z0133/0004. **I.** lateral view, 2012z0133/0262. **J.** ventral view, 2012z0133/0262. **K.** lateral view, paratype, 2012z0133/0005. **L.** ventral view, paratype, 2012z0133/0005. **M.** lateral view, 2012z0133/0006. **N.** ventral view, 2012z0133/0006. **O.** lateral view, 2012z0133/0007. **P.** ventral view, 2012z0133/0007. **Q.** lateral view, 2012z0133/0008. **R.** ventral view, 2012z0133/0008. **S.** lateral view, 2012z0133/0009. **T.** ventral view, 2012z0133/0009. **U.** lateral view, 2012z0133/0010. **V.** ventral view, 2012z0133/0010. **W.** lateral view, 2012z0133/0011. **X.** ventral view, 2012z0133/0011. **Y.** lateral view, 2012z0133/0012. **Z.** ventral view, 2012z0133/0012. **AA.** lateral view, 2012z0133/0264. **AB.** ventral view, 2012z0133/0264. **AC.** lateral view, paratype, 2012z0133/0013. **AD.** ventral view, paratype, 2012z0133/0013. **AE.** lateral view, holotype, 2012z0133/0014, note corresponding H/W value. **AF.** ventral view, holotype, 2012z0133/0014. **AG.** lateral view, 2012z0133/0015. **AH.** ventral view, 2012z0133/0015. **AI.** lateral view, 2012z0133/0281. **AJ.** ventral view, 2012z0133/0281. Scale bars represent 1 cm. →

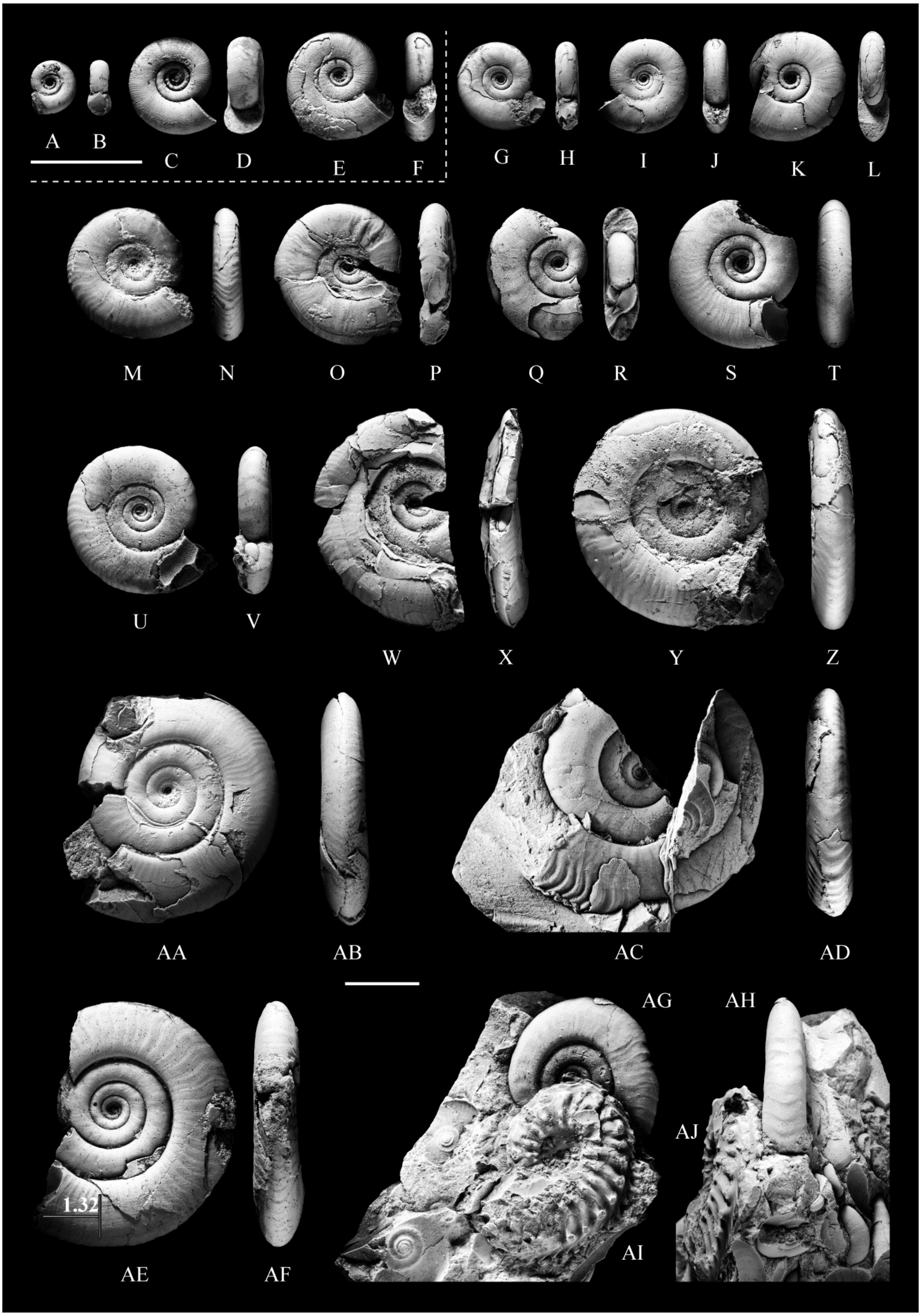
A B C D E F G H I J K L
M N O P Q R S T
U V W X Y Z
AA AB AC AD
AE AF AG AH AI AJ
1.32

Type / Inv. Nr.	Fig.	D	H	W in mm	U	ah	H/W	H/D	H/U	U/D	W/D	WER
Kasimlarceltites krystyni **gen. et sp. nov.**												
HT / NHMW-2012z0133/0014, data source: sm	4.5AE–AF	33.0	9.0	6.8	16.5	7.5	1.32	0.27	0.55	0.50	0.21	1.675 (m)
PT / NHMW-2012z0133/0266, data source: sm	4.4A	0.6	0.3	-	0.2	0.3	-	0.45	1.91	0.23	-	4.000 (vh)
PT / NHMW-2012z0133/0269, data source: sm	4.4D	2.5	0.9	-	1.0	0.7	-	0.36	0.95	0.38	-	1.999 (m)
PT / NHMW-2012z0133/0278, data source: sm	4.4N	2.4	0.8	1.4	1.0	0.6	0.53	0.32	0.80	0.40	0.60	1.747 (m)
PT / NHMW-2012z0133/0279, data source: sm	4.4O	9.0	3.2	3.6	3.4	2.4	0.89	0.35	0.92	0.38	0.40	1.828 (m)
PT / NHMW-2012z0133/0280, data source: sm	4.4P	21.7	8.4	6.7	6.7	6.5	1.35	0.39	1.25	0.31	0.29	2.046 (mh)
PT / NHMW-2012z0133/0013, data source: sm	4.5AC–AD	31.4	8.3	5.9	13.3	7.8	1.41	0.26	0.62	0.42	0.19	1.770 (m)
PT / NHMW-2012z0133/0001, data source: sm	4.5A–B	5.0	1.6	2.0	2.0	1.9	0.8	0.32	0.8	0.40	0.40	2.601 (h)
PT / NHMW-2012z0133/0002, data source: sm	4.5C–D	7.5	2.3	3.0	3.4	2	0.77	0.31	0.68	0.45	0.40	1.860 (m)
PT / NHMW-2012z0133/0003, data source: sm	4.5E–F	10.0	3.0	3.0	4.0	3.2	1.00	0.30	0.75	0.40	0.30	2.163 (mh)
PT / NHMW-2012z0133/0004, data source: sm	4.5G–H	12.3	3.9	3.4	4.9	4.3	1.15	0.32	0.80	0.40	0.28	2.364 (mh)
PT / NHMW-2012z0133/0005, data source: sm	4.5K–L	16	5.6	4.1	6.1	4.8	1.37	0.35	0.92	0.38	0.26	2.041 (mh)

Table 4.1. Measurements of the holotype and 11 paratypes of *Kasimlarceltites krystyni* gen. et sp. nov. from Aşağiyaylabel (Taurus Mountains, Turkey). **ah**, aperture height; **D,** maximum diameter; **H,** whorl height; **H/D,** proportional height; **H/U,** degree of involution; **H/W,** whorl compression; **sm,** self-measured; **U,** umbilical width; **U/D,** proportional umbilical width; **W,** whorl breadth; **W/D,** proportional whorl breadth; **WER,** whorl expansion rate; WER standard: **m,** moderate 1.61–2.0; **mh,** moderately high 2.01–2.40; **h,** high 2.41–2.80 and **vh,** very high > 2.80.

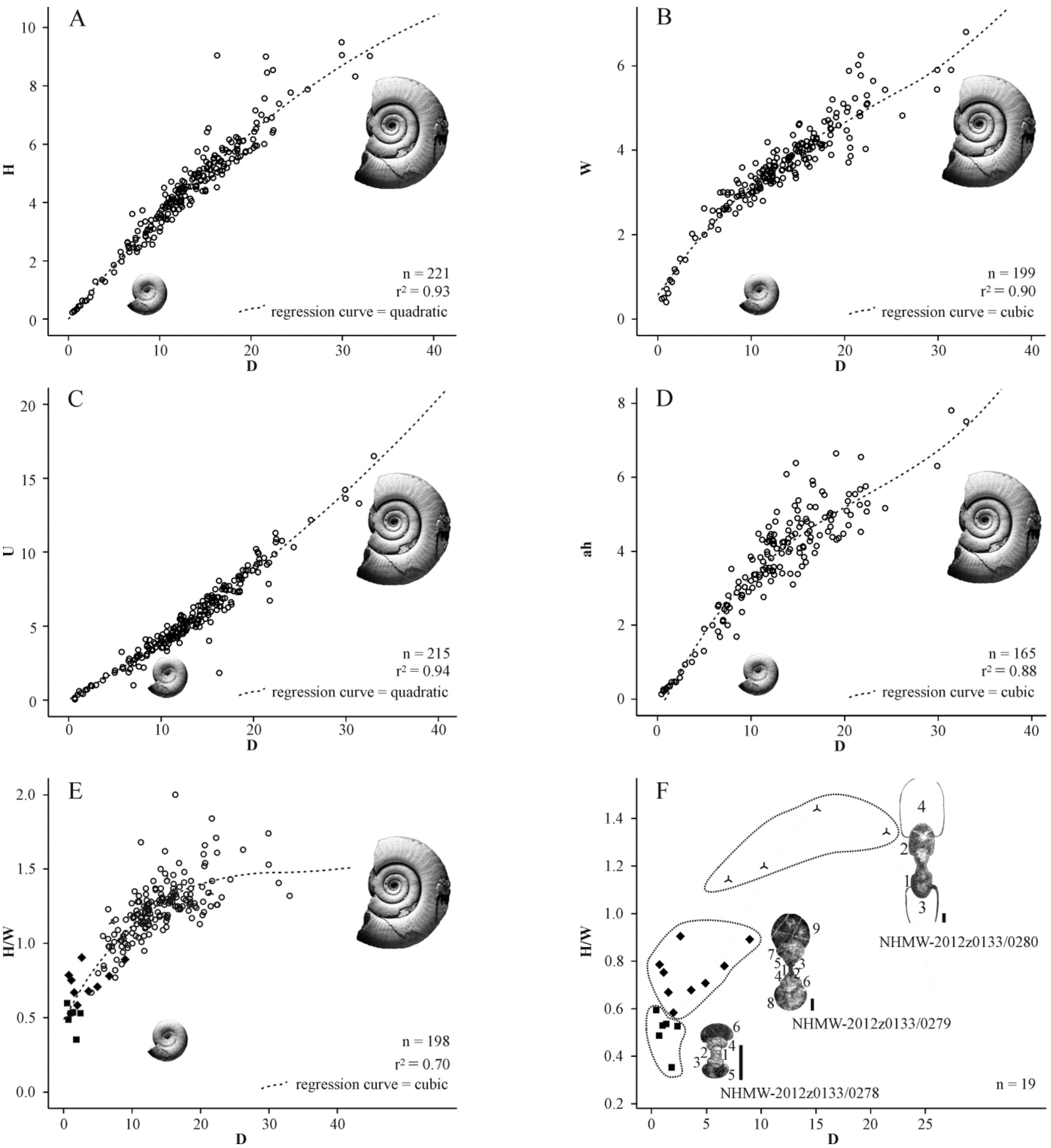

Fig. 4.6. Bivariate diagrams of conch parameters of *Kasimlarceltites krystyni* gen. et sp. nov. with indicated coefficient of determination (r^2). **A–D,** variability in the conch parameters H, W, U and ah related to D. **E,** variability in the H/W ratios related to D. **F,** variability of the H/W ratios related to D measured from three different ontogenetic stages of the paratypes NHMW-2012z0133/0278–0280. All scale bars represent 1 mm.

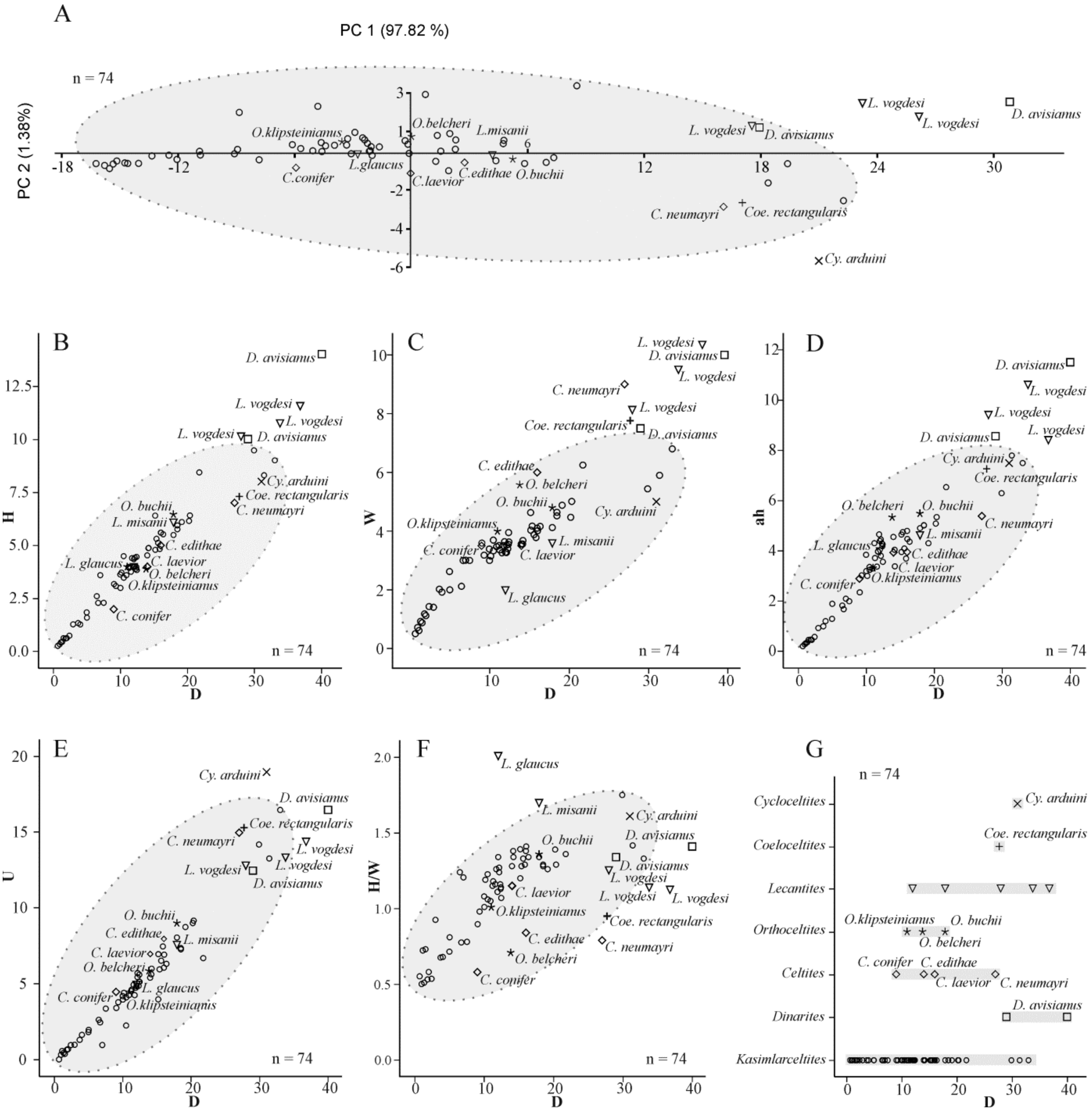

Fig. 4.7. Statistical analyses for testing the differences between conch parameters of *Kasimlarceltites* gen. nov. and its related genera. **A,** principal component analysis, comparing *Kasimlarceltites* gen. nov. and related genera; included variables: D, H, W, U and ah. **B–F,** bivariate diagrams showing differences and similarities of conch parameters (H, W, ah, U and H/W) related to D of *Kasimlarceltites* gen. nov. compared with related genera. **G,** range of D related to each genus. Grey-shaded ellipses mark the area at which the values of *Kasimlarceltites* gen. nov. plot.

Superfamily CLYDONITACEAE Mojsisovics, 1879

Family TRACHYCERATIDAE Haug, 1894

Subfamily PROTRACHYCERATINAE Tozer, 1971

Genus SPIROGMOCERAS Silberling, 1956

1956 *Spirogmoceras* Silberling, p. 1147.

1981 *Spirogmoceras* Tozer, p. 95.

2002 *Spirogmoceras* Sepkoski, p. 131.

2012 *Spirogmoceras* Lukeneder *et al.*, p. 284.

Type species. *Trachyceras* (*Protrachyceras*) *shastense* Smith, 1904, from the *Tropites subbullatus* Zone of Shasta County, California, Brock Mountain, on the trail from Squaw Creek to Pitt River, 6 miles north-east of the Bully Hill Mine (Smith 1904).

Remarks. Silberling (1956) established the genus *Spirogmoceras* for the type species *Protrachyceras shastense* (Smith, 1904). He defined *Spirogmoceras* as differing from *Protrachyceras* Mojsisovics, 1893 by: (1) more involute and more compressed shells bearing, in contrast to *Protrachyceras*, more numerous tubercles; (2) distinct longitudinal ridges forming the major ornamentation; and (3) a poorly developed ventral furrow, with less prominent spiral tubercles, bordering the ventral furrow, and more complex ammonitic septa (Silberling 1956).

Stratigraphic range. Upper Triassic, Upper Carnian, *Tropites dilleri* Zone (Tuvalian 1).

Spirogmoceras cf. *shastense* (Smith, 1904)

Figure 4.8A

cf. *1904 *Trachyceras* (*Protrachyceras*) *shastense* Smith, p. 391, pl. 46, fig. 9–9a, pl. 48, figs 3–4.

2012 *Spirogmoceras* Lukeneder *et al.*, p. 284.

Material from Aşağiyaylabel. Eight specimens from the Marlstone member, from sequence AS 16 – AS 16 + 10 m (Fig. 4.2): NHMW-2012z0133/0467–0474.

Measurements. See Lukeneder and Lukeneder (2013).

Description. The pictured specimen (Fig. 4.8A) of *Spirogmoceras* cf. *shastense*, which is only partly preserved, bears dichotomous falcoid ribs. The shell shows a fine sculpture comprising 8–10, spirally arranged, well-defined rows of longitudinal ridges (Fig. 4.8A), which form the dominant ornamentation. *Spirogmoceras* additionally shows complex septa (Smith 1927), a feature not observable in the material from Aşağiyaylabel.

Discussion. Poorly preserved fragments of the flanks, without any remains of the venter or the umbilicus, have been collected. No suture line could be observed. Nevertheless, the specimens show characteristic spiral sculptures as described for *Sp*. *shastense*, but due to taxonomic uncertainties of this species, we decided to assign the material in open nomenclature. It closely resembles *Sp. shastense* from the Lower Carnian of north-western Nevada figured by Silberling (1961). Further similarities are evident with specimens described and figured by Tozer (1967, 1994) from the Upper Carnian of Canada. As noted by Silberling (1956, 1961), numerous forms such as *Trachyceras* (*Protrachyceras*) *lecontei* Hyatt and Smith, 1905, *Trachyceras* (*Protrachyceras*) *beckeri* Smith, 1927, *Trachyceras* (*Protrachyceras*) *californicum* Smith, 1927, *Trachyceras* (*Protrachyceras*) *lindgreni* Smith, 1927, and *Trachyceras* (*Protrachyceras*) *madisonense* Smith, 1927 should be placed in one species designated as *Sp. Shastense* (Smith, 1904). This opinion was shared by Tozer (1994) and is followed herein.

Stratigraphic range. Upper Triassic, Upper Carnian, *Tropites dilleri Zone* (Tuvalian 1).

Regions. British Columbia (Tozer 1994); Shasta County, California (Smith 1904, 1927; Silberling 1956); Sonora, Mexico (Lucas and Estep 1999); north-west Nevada (Silberling 1961); Aşağiyaylabel, Taurus Mountains, Turkey.

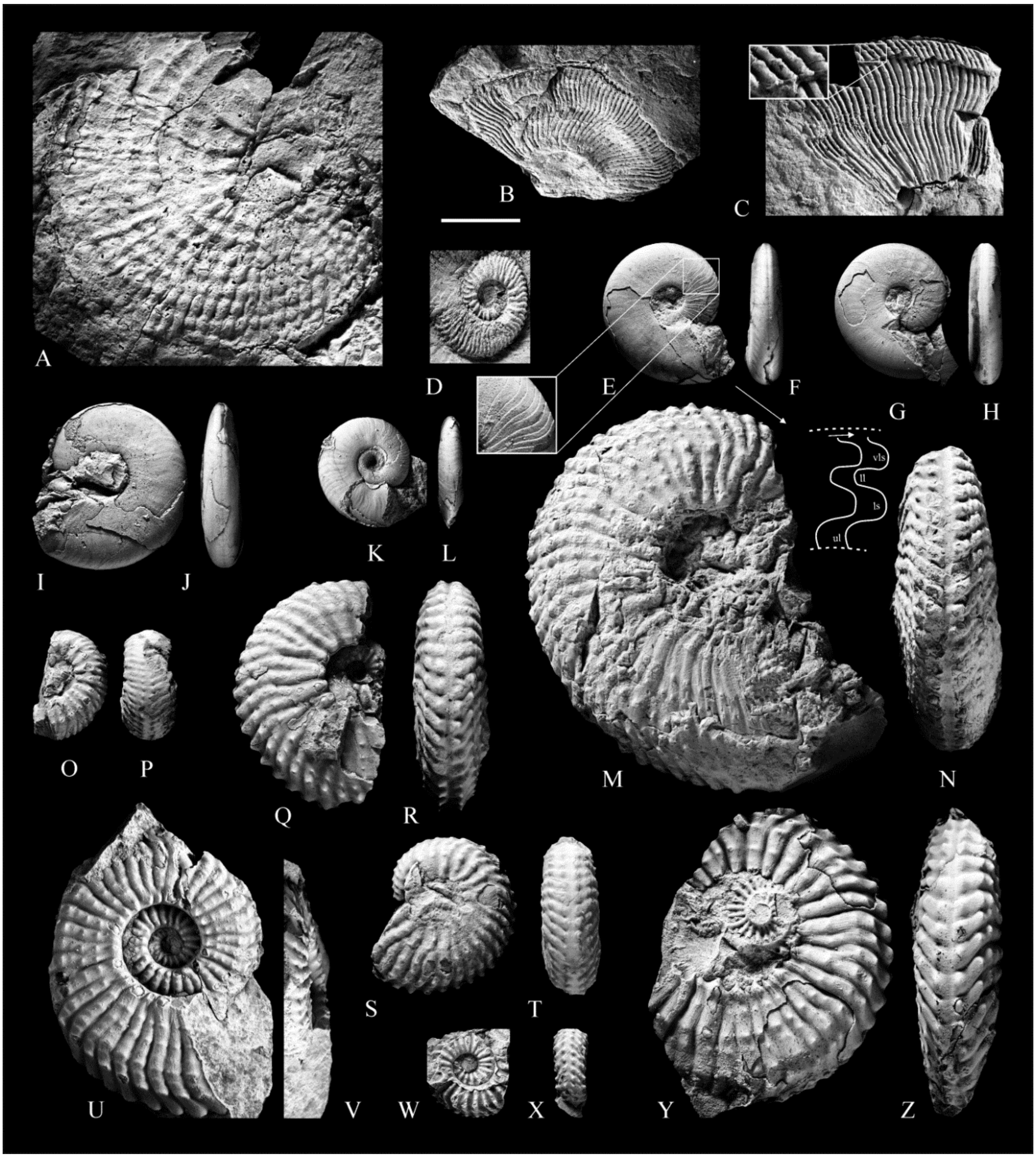

Fig. 4.8. Fauna of Aşağiyaylabel, Kasimlar Fm. **A–D,** Marlstone member, *Tropites dilleri* Zone (Tuvalian 1). **E–L,** Carbonate member Unit A, **M–Z,** Carbonate member Unit C, *Austrotrachyceras austriacum* Zone (Julian 2). **A,** *Spirogmoceras* cf. *shastense*, 2012z0133/0467, from bed AS 16 + 5.5 m. **B–D,** *Sandlingites* cf. *pilari*. B. lateral view, 2012z0133/0335, from bed AS 47 + 2.5 m. **C.** lateral view, with enlarged ventrolateral part, 2012z0133/0336, from bed AS 47 + 2.5 m. **D,** lateral view, 2012z0133/0475, from sequence AS 16 – AS 16 + 12.8 m. **E–L,** *Klipsteinia disciformis* sp. nov, from bed AS 6. **E,** lateral view, paratype, 2012z0133/0291, with detailed picture of ribbing and arrow to corresponding suture. **F,** ventral view, paratype, 2012z0133/0291. **G.** lateral view, paratype, 2012z0133/0292. **H,** ventral view, paratype, 2012z0133/0292. **I,** lateral view, holotype, 2012z0133/0290. **J,** ventral view, holotype, 2012z0133/0290. **K,** lateral view, paratype, 2012z0133/0293. **L,** ventral view, paratype, 2012z0133/0293. **M–N,** *Neoprotrachyceras attila*, 2012z0133/0331, from sequence AS 32 – AS 46. **M,** lateral view. **N,** ventral view. **O–Z**, *Neoprotrachyceras baconicum*, from sequence AS 32–AS 46. **O,.** lateral view, 2012z0133/0314. **P,** ventral view, 2012z0133/0314. **Q,** lateral view, 2012z0133/0316. **R,** ventral view, 2012z0133/0316. **S,** lateral view, 2012z0133/0315. **T,** ventral view, 2012z0133/0315. **U,** lateral view, 2012z0133/0319. **V,** ventral view, 2012z0133/0319. **W,** lateral view, 2012z0133/0317. **X,** ventral view, 2012z0133/0317. **Y,** lateral view, 2012z0133/0320. **Z,** ventral view, 2012z0133/0320. Scale bar represents 1 cm. Abbreviations: ll, lateral lobe; ls, lateral saddle; ul, umbilical lobe; vls, ventrolateral saddle

Family SANDLINGITIDAE Tozer, 1971
Genus SANDLINGITES Mojsisovics, 1893

1893 *Sandlingites* Mojsisovics, p. 706.
1981 *Sandlingites* Tozer, p. 97.
2002 *Sandlingites* Sepkoski, p. 131.

Type species. *Ammonites oribasus* Dittmar, 1866 (p. 384, pl. 18, figs 8–10), from the ‘Vorderer Sandling’ near Goisern, Austria.

Remarks. Mojsisovics (1893) described three different ontogenetic stages: Whilst the inner whorls show a typical *Tirolites*-like smooth venter, an abrupt change to a *Protrachyceras*-like stage takes place. The body chamber shows the final sculpture stage, on which no further spines or tubercles are present. The increasing H shows smooth falcoid, branching ribs. The initially narrow median furrow vanishes, and lateral ribs cross the venter. *Sandlingites* shows a goniatitic to ceratitic suture. Entirely rounded saddles and entirely, or at most, slightly lobulate lobes are present (Mojsisovics 1893).

Stratigraphic range. Upper Triassic, Upper Carnian – Norian stage. According to Krystyn (1973) and Tatzreiter (1980), the genus *Sandlingites* is characteristic for the Upper Carnian.

Sandlingites cf. *pilari* Diener, 1917
Figure 4.8B–D

cf.*1917 *Sandlingites Pilari* Diener, p. 379, pl. 3, figs 4–6.

Material from Aşağiyaylabel. Fifteen specimens from the Marlstone member, from beds AS 16 – AS 16 + 12.8 m (Fig. 4.2): NHMW-2012z0133/0335–0349, NHMW-2012z0133/0475.

Measurements. See Lukeneder and Lukeneder (2013).

Description. All specimens from Aşağiyaylabel are poorly preserved and laterally compressed, obscuring the venter. A ventral furrow is present and detected on the figured specimen (Fig. 4.8C). Shell involute, with wide umbilicus and rounded umbilical walls. Ribs coarse and straight on inner whorls. At a D of about 9 mm, ribs start to bifurcate near mid-flanks. At a D of about 28 mm, ribs become finer and exhibit falcoid curvation. At this stage, sculpture occurs with at least 14 spirally arranged tubercle lines (Fig. 4.8B–D). Ribs generally start at the umbilicus. They are stronger near the umbilicus, starting from prominent elongated, clavate ridges, especially in juvenile forms. Most ribs bifurcate, intercalated by ribs starting from umbilical wall or on mid-flank.

Discussion. We compared our material from Aşağiyaylabel with the type material of *Sandlingites pilari* Diener, 1917 from Carnian deposits of Bosnia. The specimen from Diener (1917, pl. 3, fig. 4a,b) is designated herein as lectotype and Diener's (1917, pl. 3, fig. 5) specimen as paratype. The species *Sa. pilari* Diener, 1917 was assigned by Krystyn (1973) and Breda *et al.* (2009) as *Shastites pilari* (Diener, 1917). The genus *Shastites* was primarily described by Hyatt and Smith (1905) as subgenus of *Clionites* Mojsisovics 1893. Tozer (1994) described '*Sandlingites*' *pilari* as '…probably related species to *Shastites compressus*, differing in having more falcoid ribbing'. There is no official taxonomic redesignation of *Sa. pilari* to *Sh. pilari* in the literature. Hence, we assigned our material, by the comparison of Diener's material 1917, to *Sa.* cf. *pilari* Diener, 1917. Distinct, very fine, spirally arranged tubercle lines are visible in Diener's material: these are not mentioned in Diener's description and cannot be seen on his plates. Nonetheless, tuberculation on spiral lines occurs at the same diameters as in the material from Aşağiyaylabel. Therefore, we classify the specimens from Aşağiyaylabel as *Sa*. cf. *pilari*. '*Sandlingites*' *reyeri* (Mojsisovics, 1893) from the 'Vorderer Sandling' (=Millibrunnkogel, Upper Austria), which is in juvenile stages quite similar to *Sa. pilari* Diener, 1917, does not show tuberculation on flanks and is younger in age (Norian). Besides other species of *Sandlingites*, Tatzreiter (1980) included *S. reyeri* into the genus *Leislingites*. *Sandlingites tuckeri* (Diener, 1923) differs from *Sa.* cf. *pilari* from Aşağiyaylabel by having only marginal and external tubercle rows, in contrast to numerous very fine tubercle rows as described for *Sa. pilari*.

Stratigraphic range. Upper Triassic, Upper Carnian, *Tropites dilleri* Zone (Tuvalian 1) – *Tropites subbullatus* Zone (Tuvalian 2).

Regions. Glamoča, Bosnia and Herzegovina (Diener 1917), Aşağiyaylabel, Taurus Mountains, Turkey.

Family ARPADITIDAE Hyatt, 1900

Genus KLIPSTEINIA Mojsisovics, 1882

1882 *Klipsteinia* Mojsisovics, p. 47.

1981 *Klipsteinia* Tozer, p. 96.

2002 *Klipsteinia* Sepkoski, p. 130.

Type species. *Ammonites (Ceratites) achelous* Münster, 1834, from marly beds at the Stuores Wiesen near St. Cassian. Whilst the genus *Klipsteinia* was defined by Mojsisovics (1882), its type species *'Ammonites achelous'* was subsequently selected by Diener (1915).

Remarks. *'Ammonites' achelous* resembles *Dinarites eduardi*, but at about 12 mm D, the initially flat furrow at the venter becomes deeper. At approximately 20–24 mm, ribs become more prominent and end in nodes, which border the ventral furrow (Mojsisovics 1882). Similar to *Dinarites* and *Tirolites*, *Klipsteinia* shows a primitive suture line with only one lateral lobe. As shown by the relationship of *D. eduardi* with *'A.' achelous*, *Klipsteinia* evolves a deepening of the median furrow on venter, bordered by accompanying spines and nodes or sometimes by granulated keels (e.g. *Klipsteinia nataliae* Mojsisovics, 1882). The lateral tubercles can be present or absent (Arkell *et al.* 1957).

Stratigraphic range. Upper Triassic, Lower Carnian (Krystyn 1978, Tozer 1981, Urlichs 1994).

Klipsteinia disciformis sp. nov.

Figure 4.8E–L

LSID. urn:lsid:zoobank.org:act: 96310FF2-1D3C-4DE2-B202FE8FE0974A0E.

Derivation of name. From the Latin term discus and disciformis for discus shaped.

Holotype. NHMW-2012z0133/0290 (Fig. 4.8I–J).

Paratypes. Three paratypes have been defined: NHMW2012z0133/0293 (Fig. 4.8K–L), NHMW-2012z0133/0291 (Fig. 4.8E–F) and NHMW-2012z0133/0292 (Fig. 4.8G–H).

Type locality and horizon. Aşağiyaylabel (WGS84: N 37.551389°, E 31.304444°), Anatolia, Turkey, from the Carbonate member Unit A, bed AS 6, of the Kasimlar Formation, Upper Triassic (Lower Carnian, Julian 2) (Fig. 4.2).

Material. Nineteen specimens (NHMW-2012z0133/0290–0308).

Measurements. See Table 4.2.

Description. The description is based on the holotype (Fig. 4.8I–J). Shell exhibits discoidal whorls, slightly rounded flanks, a steep umbilical wall and an involute coiling, opening in adults. The rounded venter bears a distinct, sharp, but smooth furrow. The venter is more rounded in juveniles, with almost straight mid-part in adults (Fig. 4.8E–L). Flanks are straight, but bend at the upper third with subrounded shape to venter. At a D of around 10 mm, a sculpture element with sigmoidal incisions, accompanied by the 'overlapping' segments in between the latter, occurs. This 'segmented' part appears step-like in lateral view (Fig. 4.8E). The generally smooth shell, upon more detailed examination, bears a weak, dense, sigmoidally curved ribbing. Ribs start at a steep umbilical wall, pass the flanks sigmoidally and cross the venter (hardly visible), from a D of 20 mm, in a proverse bow towards the aperture. Ribs can end at the distinct ventral furrow. Rib interspace at the umbilicus is about 0.7 mm, and rib interspace increases at the venter to 2.2 mm. At a D of about 12 mm, ribs are distinctly developed and then become weaker and broader with increasing D. The ventral furrow is most prominent at a D of 12 mm. No swellings of ribs at the shoulder. The suture is characterized by smooth lobes and saddles. A wide and rounded ventrolateral saddle is followed by a narrow and deep lateral lobe and again by a wide and rounded lateral saddle and a smooth deep and rounded umbilical lobe (Fig. 4.8E).

Discussion. *Klipsteinia disciformis* sp. nov. and related species of *Klipsteinia* were compared by performing a PCA and different bivariate plots on conch parameters (Fig. 4.9A–G). The respective data sources from specimens are indicated in Table 4.2 and Lukeneder and Lukeneder (2013). The first two axes of the PCA explain a total of 96.16 per cent of the variance (PC1 85.87 per cent; PC2 10.29 per cent). They clearly separate *Klipsteinia boetus* (Münster, 1834), *Klipsteinia irregularis* (Münster, 1841) and *Kl. nataliae* Mojsisovics, 1882 from *Kl. disciformis* sp. nov. (Fig. 4.9A). The species *Klipsteinia achelous* (Münster, 1834) and *Klipsteinia hirschi* (Laube, 1870) plot closer to *Kl. disciformis* sp. nov., resembling *Kl. disciformis* sp. nov. in H, U and ah, but having higher W (4.88 and 5.0 vs mean 4.5 mm) and therefore a lower ratio of H/W (1.16 and 1.12 vs mean 1.77; Fig. 4.9B–F). Hence, these species show a more depressed whorl section (lower H/W values; Fig. 4.9F). *Klipsteinia karreri* Mojsisovics, 1882 plots similar to *Kl. disciformis* sp. nov. within the PCA due to its similar parameters H, U and ah (Fig. 4.9B, D–E). However, *Kl. karreri* clearly differs from *Kl. disciformis* sp. nov. in a higher W with 6.5 vs mean 4.5 (Fig. 4.9C), and therefore, like the other species of *Klipsteinia*, in a lower ratio of H/W (1.23 vs 1.77; Fig. 4.9F), due to a more depressed conch morphology. *Kl. disciformis* sp. nov., therefore, has a more compressed whorl section (Fig. 4.9F) than the measured species of *Klipsteinia*, for example the type material from Münster (1834, 1841; Lukeneder and Lukeneder 2013). The generally narrow and discoidal (more compressed) character of *Kl. disciformis* sp. nov. slightly resembles *Kl. nataliae* (Fig. 4.9F; Lukeneder and Lukeneder 2013), but differs in a much weaker and smoother ventral furrow. *Kl. nataliae* furthermore exhibits stronger ribbing and granulated external ridges, which run parallel to the deep, ventral furrow. Specimens of *Kl. disciformis* with D< 20 mm closely resemble *Kl. achelous* (Münster, 1834). Finally, *Kl. achelous* has a more rectangular whorl section.

In contrast to all other species, in which lateral lobes are serrate (trifid), the lobes and saddles in *Kl. disciformis* sp. nov. are smooth (Fig. 4.8E). *Kl. disciformis* sp. nov. additionally differs from *Kl. achelous*, *Kl. boetus*, *Kl. hirschi* and *Kl. karreri* in lacking nodular swellings or external nodes. *Kl. irregularis* further differs from *Kl. disciformis* sp. nov. in a smooth venter (no furrow) at the inner whorls, as well as in bearing a furrow on the last whorl, bordered by a keel on each side. WER in *Kl. disciformis* sp. nov. measures 2–2.5 (mh–h) and is smaller than the very high values in *Kl. achelous* (3.1) and *Kl. hirschi* (2.9; Fig. 4.9G; Table 4.2; Lukeneder and Lukeneder 2013; see Discussion).

Stratigraphic range. Upper Triassic, Lower Carnian, *Austrotrachyceras austriacum* Zone (Julian 2).

Regions. Aşağiyaylabel, Taurus Mountains, Turkey.

Type / Inv. Nr.	Fig.	D	H	W in mm	U	ah	H/W	H/D	H/U	U/D	W/D	WER
***Klipsteinia disciformis* sp. nov.**												
HT (NHMW-2012z0133/0290), data source: sm	4.8I–J	20.5	9.0	5.0	5.0	6.0	1.80	0.44	1.80	0.24	0.24	1.999 (m)
PT (NHMW-2012z0133/0293), data source: sm	4.8K–L	14.0	5.5	3.0	4.0	5.2	1.83	0.39	1.38	0.29	0.21	2.531 (h)
PT (NHMW-2012z0133/0291), data source: sm	4.8E–F	19.0	8.0	4.8	5.0	6.7	1.67	0.42	1.60	0.26	0.25	2.386 (mh)
PT (NHMW-2012z0133/0292), data source: sm	4.8G–H	18.1	8.60	4.4	4.0	5.90	1.95	0.48	2.15	0.22	0.24	2.201 (mh)

Table 4.2. Measurements of the holotype and three paratypes of *Klipsteinia disciformis* sp. nov. from Aşağiyaylabel (Taurus Mountains, Turkey). **ah,** aperture height; **D,** maximum diameter; **H,** whorl height; **H/D,** proportional height; **H/U,** degree of involution; **H/W,** whorl compression; **sm,** self-measured; **U,** umbilical width; **U/D,** proportional umbilical width; **W,** whorl breadth; **W/D,** proportional whorl breadth; **WER,** whorl expansion rate; WER standard: **m,** moderate 1.61–2.0; **mh,** moderately high 2.01–2.40; **h,** high 2.41–2.80.

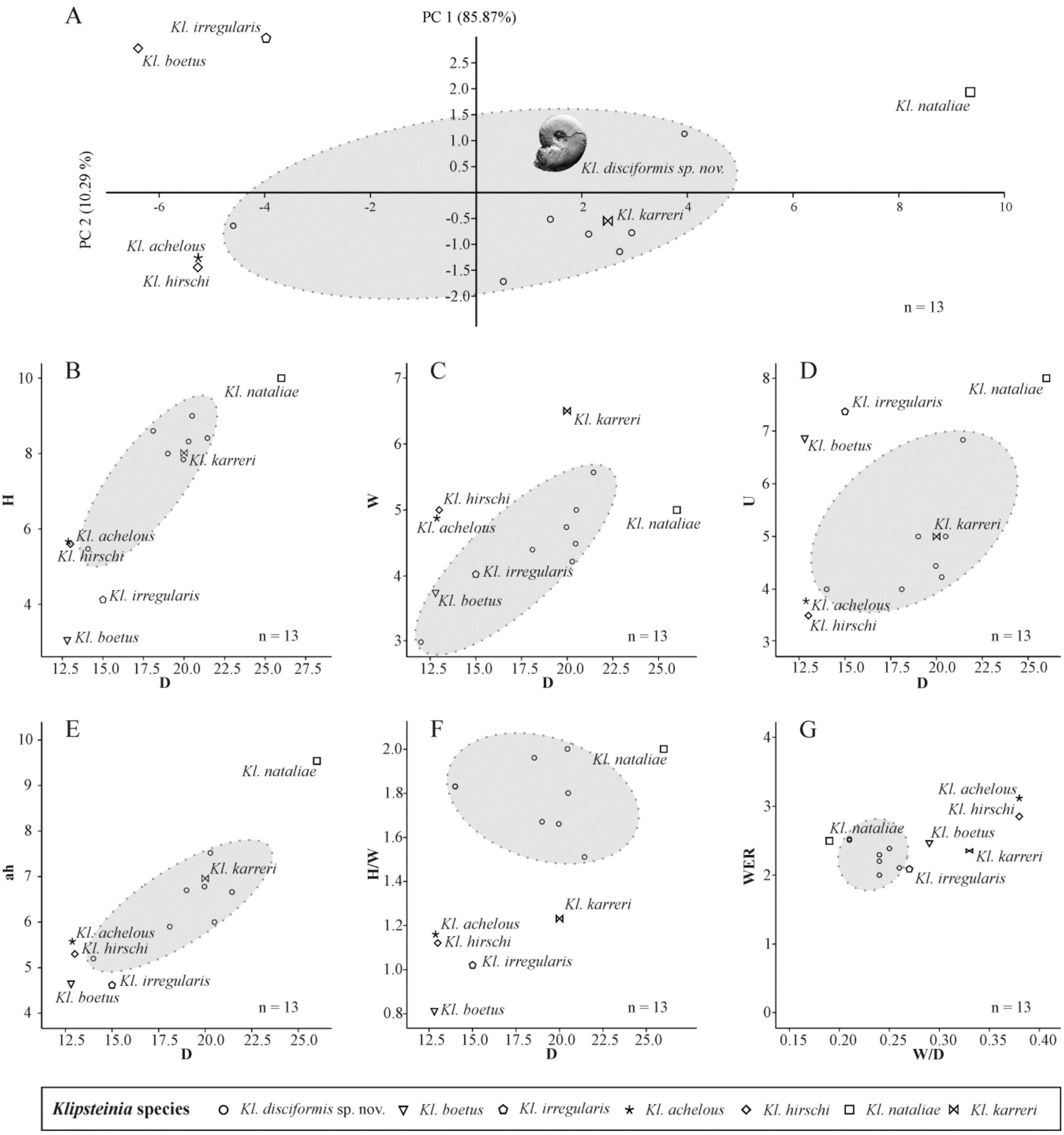

Fig.4.9. Statistical analyses for the variability in different shell parameters of *Klipsteinia disciformis* sp. nov. and its related species. **A,** principal component analysis; included variables: D, H, W, U and ah. **B–G,** bivariate plots showing differences and similarities in shell parameters and ratios (H, W, U, ah, H/W and WER) related to D, respectively, to W/D. Grey-shaded ellipses mark the area at which the values of *Kasimlarceltites* gen. nov. plot.

Suborder TRACHYCERATINA Krystyn, 1978

Superfamily TRACHYCERATACEAE Haug, 1894

Family TRACHYCERATITIDAE Haug, 1894

Subfamily TRACHYCERATINAE Haug, 1894

Genus NEOPROTRACHYCERAS Krystyn, 1978

1978 *Neoprotrachyceras* Krystyn, p. 69.
1981 *Neoprotrachyceras* Tozer, p. 95.
2002 *Neoprotrachyceras* Sepkoski, p. 130.
2012 *Neoprotrachyceras* Lukeneder *et al.*, p. 282, 284.

Type species. *Trachyceras attila* Mojsisovics, 1870, from Veszprém, Bakony Mountains, Hungary.

Remarks. The genus *Neoprotrachyceras* is characterized by a *Trachyceras*-like form (involute to moderately evolute coiling) bearing nodular ribs. The venter is externally interrupted by a furrow. In contrast to *Trachyceras*, lateral nodes might be absent in *Neoprotrachyceras*. Whilst in *Neoprotrachyceras* the ventral furrow is bordered on each side by a row of single nodes (with a trend to reduplication at the adult stage), *Trachyceras* shows a row of double-pointed nodes on both sides of the venter (Krystyn 1978).

Stratigraphic range. Upper Triassic, Lower Carnian – Upper Carnian, Julian 2 – Tuvalian 1.

Neoprotrachyceras attila (Mojsisovics, 1893)

Figure 4.8M–N

*1870 *Trachyceras Attila* Mojsisovics, p. 105–106, pl. 5, figs 2–4.
1893 *Trachyceras (Protrachyceras) attila* E. v. Mojsisovics; Mojsisovics, p. 633–634, pl. 169, figs 6–9, pl. 170, figs 1–2.

Material from Aşağiyaylabel. One specimen from the Carbonate member Unit C, from sequence AS 32 – 46 (Fig. 4.2): NHMW2012z0133/0331.

Measurements. See Lukeneder and Lukeneder (2013).

Description. Whorls are generally involute, with a narrow umbilicus. The venter bears a broad and deep furrow, which is bordered by two coarse, spirally arranged external tubercle rows. Ribs are slightly curved on flanks, but appear with a sharp adapical bow (proverse towards aperture) at the upper third of the flanks (Fig. 4.8M). Up to a D of approximately 15–19 mm, ribs are coarse and strong. Branching is irregular, and bifurcation occurs at the umbilical shoulder, on tubercles or from lateral tubercles at mid-flank, occurring mainly at the fourth tubercle row from umbilicus. Ribs start to become more distinct and finer and seem to be more crowded from a D of 19 mm. The specimen in Figure 4.8M exhibits a different arrangement of the spiral tubercle lines on both flanks. The furrow on one shell side is bordered by three external tubercle lines (lateral view Fig. 4.8M and right side on Fig. 4.8N), whereas at the corresponding opposite side, the external flank is bordered by only a single external tubercle line (Fig. 4.8N). All other spiral tubercle lines, towards the umbilicus (from the marginal, mid-flank), are equally arranged. Overall, 12 spiral tubercle lines are visible on the right side, but only ten on the left side: two umbilical – lateral tubercle lines, six lateral tubercle lines, one marginal tubercle line and one external line (left), respectively, three lines (right).

Discussion. The specimens from Aşağiyaylabel resemble mostly the type material from the Bakony Mountains from Hungary described by Mojsisovics (1870) as *Neoprotrachyceras attila*. A comparable specimen was also figured by Diener (1925) as *Trachyceras* (*Protrachyceras) attila* (Mojsisovics, 1870) from the Carnian of Feuerkogel (Styria). *Neoprotrachyceras attila* from Aşağiyaylabel differs from *Neoprotrachyceras thous* (Dittmar, 1866) in having more distinct spiral tubercle rows, numbering 12 versus 3–4 in *N. thous* of Dittmars' material (Röthelstein, Styria). This difference, marked by an almost tuberculate ribbing style in *N. thous*, is also visible on specimens from Mojsisovics′ (1893, pl. 168, figs 2–11) material from the Röthelstein, near Bad Aussee (Styria). *Neoprotrachyceras attila* from Aşağiyaylabel (Fig. 4.8M–N) furthermore resembles *Neoprotrachyceras baconicum* (Mojsisovics, 1870), with the contrast that the latter has only 8–9 rows of tubercle spirals and differs in a broader umbilicus (Mojsisovics 1893). The external furrow is less prominent in *N. attila*. Differences in whorl proportions from our specimen (Fig. 4.8M–N) were measured and compared with material from *N. attila* (Mojsisovics, 1893) and *N. baconicum* (Mojsisovics, 1870; see measurements and remarks for *N. baconicum*). The respective data sources from specimens are indicated in Lukeneder and Lukeneder (2013). *N. attila* from Aşağiyaylabel (Fig. 4.8M–N) shows nearly similar whorl proportions to *N. baconicum*, but with the difference that *N. attila* shows lower values of U/D (≤0.2) compared with *N. baconicum* with U/D values ≥0.2, what reflects the more narrow umbilicus of *N. attila* (see Lukeneder and Lukeneder 2013).

Stratigraphic range. Upper Triassic, Lower Carnian (Julian 2).

Regions. Bakony Mountains, Hungary (Mojsisovics 1870; Diener 1925); Feuerkogel, NCA, Austria (Mojsisovics 1873–1902; Krystyn 1978; Kittl 1903; Geyer 1915); Aşağiyaylabel, Taurus Mountains, Turkey.

Neoprotrachyceras baconicum (Mojsisovics, 1870)

Figure 4.8O–Z

1869 *Ammonites (Trachyceras)* sp.; Mojsisovics, p. 93.

*1870 *Trachyceras Baconicum* Mojsisovics, p. 106, pl. 5, fig. 5.

2000 *Neoprotrachyceras* cf. *thous* (DITTMAR), 1866; Gindl, p. 54–56, pl. 2, fig. 1a–c.

Material from Aşağiyaylabel. Eleven specimens from the Carbonate member Unit C, from sequence AS 32 – AS 46; Fig. 4.2): NHMW-2012z0133/0314–0317, NHMW-2012z0133/0319–0325.

Measurements. See Lukeneder and Lukeneder (2013).

Description**.** Medium-sized (up to D 38.5 mm), moderately involute shells with open umbilicus, steep umbilical wall and strong ornamentation. Sculpture consists of strong, straight ribs in juveniles to weakly sigmoidal curved ribs in adults. Juvenile specimens (Fig. 4.8O–P, S–T, W–X) bear a rounded venter with a shallow median furrow. The almost smooth median area at the venter is bordered by the typical *Neoprotrachyceras*-like single and distinct external tubercle rows. In juveniles, that is, smaller specimens up to 15 mm (Fig. 4.8O–P, W–X), whorls are more compressed with H/W values of 0.86 and 0.96. In the figured 20-mm specimen (Fig. 4.8S–T), the H is more depressed, with an H/W value of 1.38. In adult specimens (Fig. 4.8U–V, Y–Z), whorl shape is, at diameters of approximately 40 mm, more depressed, with H/W values of 1.52–1.68 (see Lukeneder and Lukeneder 2013). Juvenile specimens (Fig. 4.8O–P, S–T and W–X) exhibit strong, bifurcate ribbing. Ribs start at a strong umbilical tubercle. Umbilical wall smooth. Ribs are almost radial, up to the round mid-flank, where they bifurcate at a big lateral tubercle, in slightly proverse direction. Ribs end at pointed tubercles on each side of the smooth ventral area. On the single main ribs, between the umbilical and the larger lateral tubercles (Fig. 4.8O–P, S–T), two to three weaker spiral tubercle lines are visible. The prominent lateral spiral tubercle line is again followed by two closely running marginal spiral lines, followed by the external tubercles. Ribs can also bifurcate on umbilical tubercles, and one branches a second time at the lateral shoulder (Fig. 4.8S–T). The same specimen already has eight spiral tubercle lines. Ribbing is broader in adults than in juveniles, up to 2–3 mm thick. The maximum thickness of the ribs occurs on a proverse spatulate end, between external and last lateral ridge-like tubercles. Eight rows of tubercles run up to the end of the body chamber, becoming more longitudinal, ridge-like, on adult forms (Fig. 4.8U–V, Y–Z). Umbilical tubercles and external tubercles are spine-like. The external furrow is deep and prominently edged. In most cases, spines are present as tubercles because they have been broken during preparation. Fine striae, or growth lines, occur on body chambers of adult specimens (Fig. 4.8U–V, Y–Z). The finer lines run subparallel to the ribbing, but cross the venter in an adapical bow. Lines are visible only on the outer surface of shell, not on internal moulds (Fig. 4.8Y–Z).

Discussion. *Neoprotrachyceras baconicum* closely resembles *N. attila*. Both species are furthermore quite similar to *Neoprotrachyceras archelaus* (Laube, 1868), with the difference that they show a much denser ribbing as well as finer ribs and nodes in contrast to *N. archelaus* (Mojsisovics 1870). Alongside the broader umbilicus of *N. baconicum*, and the different number of tubercle spirals, already mentioned, the external furrow is more prominent in *N. baconicum* observed from Aşağiyaylabel (Fig. 4.8R, Z) compared with *N. attila* (Mojsisovics 1870, 1893). The finer and denser ribbing, compared with *N. archelaus*, as well as the broader umbilicus and the more prominent furrow, and the fewer count of tubercle lines compared with *N. attila*, clearly identifies most specimens from Aşağiyaylabel as *N. baconicum.*

Stratigraphic range. Upper Triassic, Lower Carnian – Upper Carnian (Julian 2–Tuvalian 1).

Regions. NCA, Austria (Mojsisovics 1873–1902; Kittl 1903; Geyer 1915; Krystyn 1978); Bakony Mountains, Hungary (Mojsisovics 1870); Aşağiyaylabel, Taurus Mountains, Turkey.

Subfamily SIRENITINAE Tozer, 1971

Genus SIRENITES Mojsisovics, 1893

1893 *Sirenites* Mojsisovics, p. 725.

1981 *Sirenites* Tozer, p. 96.

2002 *Sirenites* Sepkoski, p. 131.

2012 *Sirenites* Lukeneder *et al.*, p. 284.

Type species. *Ammonites senticosus* Dittmar, 1866, p. 375, pl. 17, figs 8–9, from red limestones of the Feuerkogel, Röthelstein, near Bad Aussee, Styria, Austria. Subsequent designation by Hyatt and Smith (1905, p. 198).

Remarks. Mojsisovics (1893) introduced the name *Sirenites* for *Trachyceras*-like species bearing sigmoidal external ribs, closely prelocating the external nodes. Whereas both genera (*Sirenites* and *Trachyceras*) show a tendency to reduplicate their external tubercles, the ribs of *Trachyceras* still branch longitudinally, whilst the ribs of *Sirenites* exhibit a radial bifurcation (Mojsisovics 1893). *Sirenites* represents a compressed form with a distinct furrow on venter and flattened convex whorl flanks, bearing two rows of lateral tubercles (Arkell *et al.* 1957). Its sigmoidal, sharply adorally projecting ribs bifurcate on a tubercle near the ventrolateral edge. Two rows of tubercles on flanks and tubercles on the umbilical edge are arranged in spiral lines (Arkell *et al.* 1957). *Sirenites* is described with ceratitic (Diener 1925) as well as with ammonitic suture (Arkell *et al.* 1957).

Stratigraphic range. Upper Triassic, Carnian.

Sirenites senticosus (Dittmar, 1866)

Figures 4.5AI–AJ, 4.10A–B

1866 *Ammonites senticosus* Dittmar, p. 375, pl. 17, figs 8–9.

1893 *Sirenites senticosus* (A. v. Dittmar); Mojsisovics, p. 727–728, pl. 161, figs 8–12, 14–15.

1893 *Sirenites* cf. ind. ex aff. *S. senticosi*; Mojsisovics, p. 731, pl. 161, fig. 17.

1905 *Ammonites senticosus* Dittmar; Hyatt and Smith, p. 198.

1923 *Sirenites senticosi* Mojs.; Diener, p. 246, 248, 250.

1925 *Sirenites senticosus* Dittm.; Diener, p. 95, pl. 18, figs 6a–b.

1927 *Ammonites senticosus* Dittmar; Smith, p. 81.

1957 *S. (S.) senticosus* (Dittmar); Arkell *et al.*, p. L158, fig. 190, 9a–b
(refigured type specimen of Mojsisovics 1893, pl. 161, fig. 8).

1976 *Sirenites senticosus* (Dittmar); Hahn, p. 155–169.

1978 *Sirenites senticosus* (Dittmar, 1866); Krystyn, p. 70, pl. 4, fig. 3.

1982 *Sirenites (Sirenites) senticosus* (v. Dittmar); Hahn, p. 1049.

1982 *Sirenites senticosus* (Dittmar, 1866); Tatzreiter, p. 139.

1994 *Sirenites senticosus* (Dittmar); Tozer, p. 170.

2000 *Sirenites* n. sp. 1; Gindl, p. 53–54, pl. 1, figs 7a–8b.

2000 *Sirenites multicostatus* Mojsisovics, 1893; Gindl, p. 56–57, pl. 2, fig. 2a–c.

2009 *Sirenites senticosus* (Dittmar); Breda *et al.*, p. 82.

2012 *Sirenites* sp.; Lukeneder *et al.*, p. 284.

Holotype. *Ammonites senticosus* Dittmar, 1866 (p. 375, pl. 8–9; GBA-1893/001/0646) from the *Trachyceras austriacum* beds at the Feuerkogel at Röthelstein, near Bad Aussee, Styria, Austria.

Material from Aşağiyaylabel**.** One specimen from the Carbonate member Unit A, bed AS 6: NHMW-2012z0133/0281, and four specimens from Unit C, from sequence AS 32 – AS 46 (Fig. 4.2): NHMW-2012z0133/0282, NHMW-2012z0133/0284–0285 and NHMW-2012z0133/0289.

Measurements. See Lukeneder and Lukeneder (2013).

Description**.** Both figured specimens (Figs 4.5AI–AJ, 4.10A–B) show a medium-sized, strongly ornamented shell and a half involute, compressed whorl section with H/W values of 1.57 (Fig. 4.10A–B; Lukeneder and Lukeneder 2013) and 1.85 (Fig. 4.5AI–AJ; Lukeneder and Lukeneder 2013). The wide umbilicus bears a steep umbilical wall. H increases rapidly, with a high WER between 2.65 (NHMWz0133/0285; Lukeneder and Lukeneder 2013) and 2.70 (Figs 4.5AI–AJ, 4.10A–B; Lukeneder and Lukeneder 2013). All specimens show typical *Sirenites*-like single ribs as well as bifurcating ribs. Ribs are broad (2–3 mm; Fig. 4.10A–B) and bifurcate on the umbilical edge or laterally. Ribs show tuberculation with four tubercle rows, including umbilical and external flank tubercles. Single ribs cross the steep umbilical wall; they start from strong umbilical tubercles and sigmoidally cross the straight flanks, ending at tubercles on the external flank. These tubercles give rise to falcoid, pointed, adapically directed (80–90 degrees) short ribs. The latter ribs end at a distinct and prominent tubercle row, which consists mainly of spines, string-like arranged. Two of these ‘spine rows’ border a deep, sharp and smooth ventral furrow. Outer shell may bear fine striae on the body chamber, running parallel to the sigmoidal ribs. No suture line visible.

***Discussion*.** Specimens resemble the type *‘Ammonites’ senticosus* Dittmar, 1866. Whilst specimens from Aşağiyaylabel show similar values of H/W (1.57–1.85), they show a slightly higher WER (mean 2.683) than the holotype of Dittmar (1866; 2.535; Lukeneder and Lukeneder 2013). Specimens figured as *S. senticosus* by Mojsisovics (1893) seem almost identical in sculpture and shape. The typical shape is shown by Diener (1925), when he refigured the specimen of Mojsisovics (1893). Both authors figured the type specimen, even though they show prominent differences, probably due to the illustration of the opposite side of the type specimen by Mojsisovics (1893), Diener (1925) and Arkell *et al.* (1957).

Stratigraphic range. Upper Triassic, Lower Carnian, *Trachyceras aonoides* Zone (Julian 1) – *Austrotrachyceras austriacum* Zone (Julian 2).

Regions. NCA, Austria (Dittmar 1866; Mojsisovics 1893; Krystyn 1978; Tatzreiter 1982); Cortina Area, SA (Breda *et al.* 2009); Mersin Melange and Aşağiyaylabel, Taurus Mountains, Turkey (Kozur *et al.* 2009; Moix *et al.* 2011); California (Smith 1896); Guanling Area, south west China (Xiaofeng *et al.* 2008); northern Thailand (Hahn 1976, 1982). Bihati, Timor (Diener 1923).

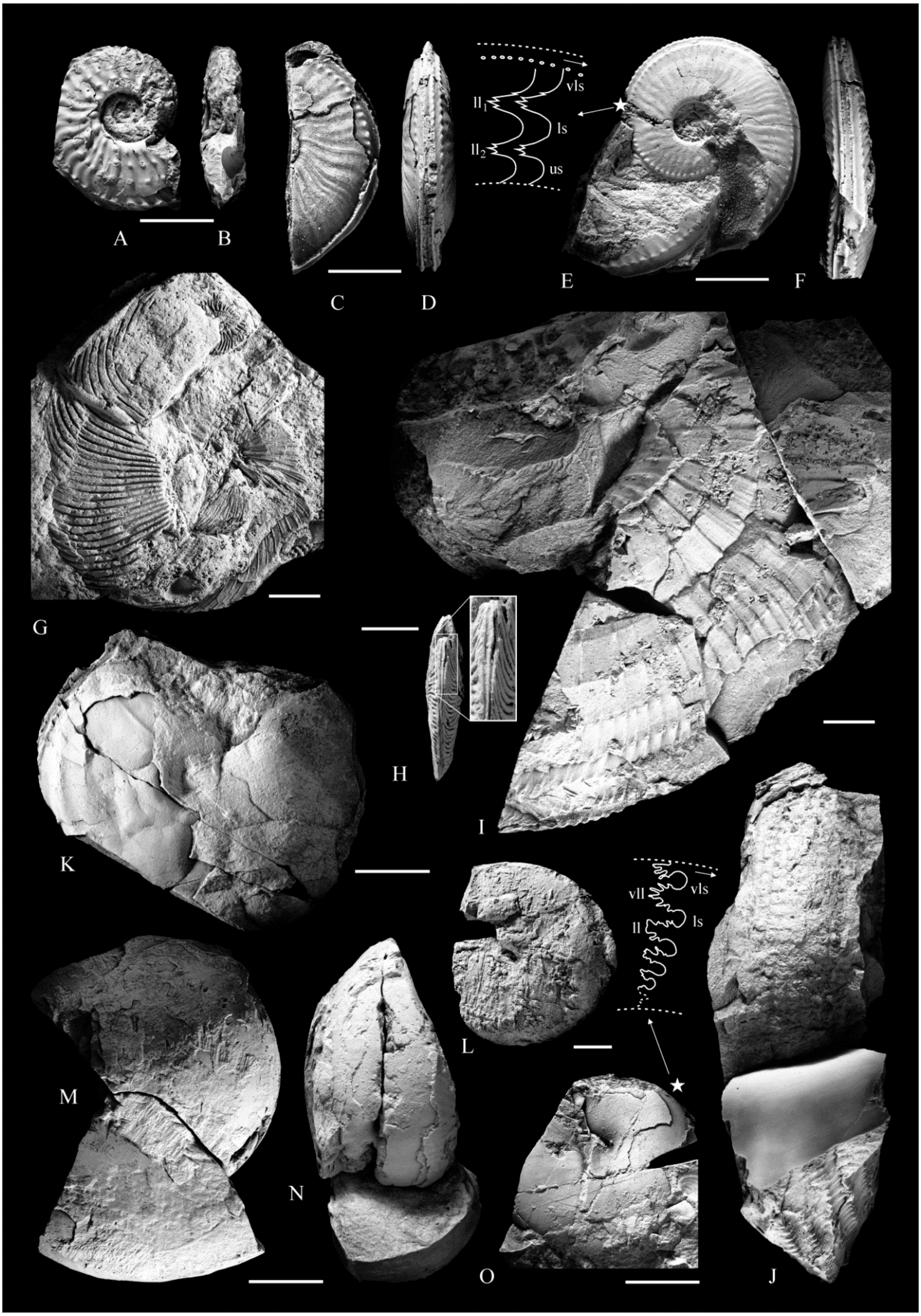
A
B
C
D
ll1
ll2
vls
ls
us
E
F
G
H
I
K
L
vll
ll
vls
ls
M
N
O
J

← **Fig. 4.10.** Fauna of Aşağiyaylabel, Kasimlar Fm., **A–F,** and **O,** Carbonate member Unit C, *Austrotrachyceras austriacum* Zone (Julian 2), **G–N,** Marlstone member, *Tropites dilleri* Zone (Tuvalian 1). **A–B,** *Sirenites senticosus*, from sequence AS 32–AS 46 (2012z0133/0289). **A,** lateral view. **B,** ventral view. **C–F,** *Anasirenites crassicrenulatus* sp. nov, from sequence AS 32 – AS 46. **C,** lateral view, paratype, 2012z0133/0309. **D,** ventral view, paratype, 2012z0133/0309. **E.** lateral view, holotype, 2012z0133/0310, with arrow to corresponding suture line. **F,** ventral view, holotype, 2012z0133/0310. **G–H,** *Paratropites* cf. *hoetzendorfii*. **G,** adult, lateral view, 2012z0133/0352, from bed AS 16 + 5 m. **H,** juvenile, ventral view, 2012z0133/0368, with enlarged ventral part, from bed AS 16 + 13 m. **I–J,** *Trachysagenites* cf. *beckei* 2012z0133/0350, from sequence AS 16 + 11.5 m – AS 16 + 13 m. **I,** lateral view. **J,** ventral view. **K–N,** *Proarcestes* sp. **K,** lateral view, 2012z0133/0443, from bed AS 16 + 5 m. **L,** lateral view, 2012z0133/0444, from bed AS 32. **M–N,** 2012z0133/0445, from bed AS 16 + 13 m. **M,** lateral view. **N,** ventral view. **O,** lateral view of *Megaphyllites jarbas*, 2012z0133/0479, from sequence AS 19 – AS 46, white star marks the position of last septum. All scale bars represent 1 cm. Abbreviations: ll, lateral lobe; ls, lateral saddle; us, umbilical saddle; vll, ventrolateral lobe; vls, ventrolateral saddle.

Genus ANASIRENITES Mojsisovics, 1893

1893 *Anasirenites* Mojsisovics, p. 773.

1981 *Anasirenites* Tozer, p. 96.

2002 *Anasirenites* Sepkoski, p. 128.

2012 *Anasirenites* Lukeneder *et al.*, p. 284.

Type species. *Sirenites (Anasirenites) ekkehardi* Mojsisovics, 1893 (p. 773, pl. 159, fig. 5), from the Carnian stage of the 'Vorderer Sandling' near Goisern, Austria. Subsequent designation by Diener (1915).

Remarks. The ventral furrow with the pair of continuous keels at the external side, which developed from the external nodes of the protrachyceratid ancestors, is the main characteristic of the genus *Anasirenites*. Mojsisovics (1893) defined *Anasirenites* as a subgenus of the genus *Sirenites*, characterized by its smooth external keel (Mojsisovics 1893). Arkell *et al.* (1957) followed the idea of a subgenus *Sirenites* (*Anasirenites*). Tozer (1971, 1981) increased the hierarchic level of the former subgenera to the level of genus in his general reviews of Triassic ammonoids (Tozer 1971, 1981).

Stratigraphic range. Upper Triassic, Carnian to Norian.

Anasirenites crassicrenulatus sp. nov.

Figure 4.10C–F

2000 *Anasirenites* sp. Gindl, p. 57–58, pl. 2, fig. 3a–c.

2000 *Anasirenites* cf. *tripunctatus* (Mojsisovics, 1893); Gindl, p. 58–59.

2012 *Anasirenites* Lukeneder *et al.*, p. 284.

LSID. urn:lsid:zoobank.org:act: 2F53CAE1-4D81-4E9B-A28E0B10AD9E58FB.

Derivation of name. From the Latin terms '*crassi'*, which means '*dense'*, and '*crena'*, which means '*serration'*; characterized by the presence of two densely granulated external keels.

Holotype. NHMW-2012z0133/0310 (Fig. 4.10E–F). Steinkern with partial shell preservation. Paratype. One paratype: NHMW-2012z0133/0309 (Fig. 4.10C–D).

Type locality and horizon. Aşağiyaylabel (WGS 84: N 37.551389°, E 31.304444°), Anatolia, Turkey, from the Carbonate member Unit C, from sequence AS 32 – AS 46 (Fig. 4.2), which belongs to the Upper Carnian *Austrotrachyceras austriacum* Zone (Julian 2).

Material from Aşağiyaylabel. Four specimens from the Carbonate member Unit C (from sequence AS 32 – AS 46): NHMW2012z0133/0309–0312.

Measurements. See Table 4.3.

Diagnosis. Involute, small-sized and depressed shell, bearing a steep and narrow, but smooth and rounded umbilical edge. *Anasirenites crassicrenulatus* sp. nov. is characterized by strong and multituberculate (3–4 tubercles) ribbing at the inner whorls. *A. crassicrenulatus* sp. nov. bears a weak ribbing on adult whorls and on body chamber, a more pointed ventrolateral tubercle line as well as granulated keels, which become more and more smooth until the end of the last whorl.

Description. Small- to medium-sized (up to 30.7 mm), involute forms with narrow umbilicus. Whorls are depressed with high whorls having H/W values of 1.56 (paratype, Fig. 4.10C–D) to 2.1 (holotype, Fig. 4.10E–F). Whorl expansion rate is high with a WER of 2.5 in the holotype (Fig. 4.10E–F; Table 4.3) and a WER of 2.6 in the paratype (Fig. 4.10C–D). The following description is of the holotype (Fig. 4.10E–F). Umbilicus is narrow, and the umbilical edge is smooth, steep, but rounded. Flanks are straight, rounded only on their upper half to venter. Ribbing starts on the umbilical edge. Ribbing on inner whorls, up to a D of 10 mm, is strong and radially directed with single ribs or sometimes with bifurcating ribs from umbilicus. The latter ribs are tuberculate with four tubercles per rib. Strong ribbing and prominent tuberculation disappear after that phase. From H = 4 mm, ribs tend to start proversly and bifurcate on mid-flank. The branches end at small, pointed tubercles on the ventrolateral edge, resembling a ‘pearl necklace’. This spiral line of tubercles is followed by a smooth, furrow-like area, edged on the venter by one of the external granulated keels. The granulation of the keels appears to be due to the fading of most ventral ribbing, rising from the lower ventrolateral tubercle line. A ventral median deep smooth furrow is bordered by those granulated external keels. At the phragmocone, keels seem to be smooth on steinkerns, but clearly strongly granulated in the case of shell preservation (Fig. 4.10E–F). Keels become smooth until the end of the last whorl. From H 8 mm onward, ribs become weaker and falcoid, branching on mid-flank and ending at tiny, but elongated proversly directed crests. Two to three very shallow, but present, tubercle rows are spirally arranged throughout the shell, accompanied by fine, striate spiral lines. The suture line appears ceratitic (trifid). The body chamber has a length of three-quarters of the last whorl (mesodome).

Discussion. *Anasirenites crassicrenulatus* sp. nov. and the above-described *Sirenites senticosus* (Dittmar, 1866) show similarities in juvenile ribbing, in tuberculation and in the arrangement of external tubercles and furrows. Mojsisovics (1893) already noted the close relation of the subgenus *Anasirenites* Mojsisovics, 1893 and certain species of *Sirenites* Mojsisovics, 1893, now confirmed by the comparison of faunal elements from Aşağiyaylabel. The species *Anasirenites* (Mojsisovics 1893) is clearly characterized by smooth external keels. These typical keels are also detected in *A. crassicrenulatus* sp. nov. and are therefore the reasons for attributing this species to *Anasirenites*. Anyhow, the keels of *A. crassicrenulatus* sp. nov. are not generally constantly smooth, but, and this is the important fact, become smooth at the end of the last whorl. This is similar to Mojsisovic′s description of *Anasirenites marthae* as well as of *Anasirenites tripunctatus*. Both forms bear tiny nodes at their keels and show the typical smoothness of the characteristic keels not before the end of the last whorl. Although *A. crassicrenulatus* sp. nov. resembles *A. tripunctatus* Mojsisovics, 1893, *A. briseis* Mojsisovics, 1893, *Anasirenites friederici* Mojsisovics, 1893 and *A. marthae* Mojsisovics, 1893 from Carnian faunas (*Austrotrachyceras austriacum* Zone) from the Feuerkogel (Styria, Austria; Mojsisovics 1893), they differ in sculpture.

A. crassicrenulatus sp. nov. exhibits very strong and multituberculated (3–4 tubercles) ribbing in inner whorls, but in contrast much weaker ribbing on adult whorls and on the body chamber than in all other species within *Anasirenites*. The weaker ribbing, the more pointed ventrolateral tubercle line and the more granulated keels, except for the end of the last whorl, are the motivation for establishing the new species *A. crassicrenulatus* sp. nov.

Stratigraphic range. Upper Carnian, *Austrotrachyceras austriacum* Zone (Julian 2).

Regions. Aşağiyaylabel, Taurus Mountains, Turkey.

Type / Inv. Nr.	**Fig.**	**D**	**H**	**W** in mm	**U**	**ah**	**H/W**	**H/D**	**H/U**	**U/D**	**W/D**	**WER**
***Anasirenites crassicrenulatus* sp. nov.**												
HT / NHMW-2012z0133/0310, data source: sm	4.10E–F	27.0	11.5	5.5	5.5	10.0	2.09	0.43	2.09	0.20	0.20	2.522 (h)
PT / NHMW-2012z0133/0309, Data source: sm	4.10C–D	30.7	11.4	7.3	–	11.7	1.56	0.37	–	–	0.24	2.611 (h)

Table 4.3. Measurements of the holotype and the paratype of *Anasirenites crassicrenulatus* sp. nov. from Aşağiyaylabel (Taurus Mountains,Turkey). **ah,** aperture height; **D,** maximum diameter; **H,** whorl height; **H/D,** proportional height; **H/U,** degree of involution; **H/W,** whorl compression; **sm,** self-measured; **U,** umbilical width; **U/D,** proportional umbilical width; **W,** whorl breadth; **W/D,** proportional whorl breadth; **WER,** whorl expansion rate; WER standard: **h,** high 2.41–2.80.

Superfamily TROPITACEAE Mojsisovics, 1875

Family TROPITIDAE Mojsisovics, 1875

Genus PARATROPITES Mojsisovics, 1893

1893 *Paratropites* Mojsisovics, p. 234.

1927 *Paratropites* Smith, p. 43.

1981 *Paratropites* Tozer, p. 98.

1994 *Paratropites* Tozer, p. 215.

2002 *Paratropites* Sepkoski, p. 131.

2012 *Pleurotropites* Lukeneder *et al.*, p. 284, 292.

Type species. *Ammonites saturnus* Dittmar, 1866 (p. 367, pl. 16, figs 1–8) from the yellowish-grey limestones, together with *Tropites subbullatus*, of the 'Vorderer Sandling' near Goisern, Austria. Subsequent designation by Diener (1915).

Remarks. Slowly growing, quite involute and discoid shells, which enclose a narrow umbilicus. The distinct umbilical margin is adorned with umbilical tubercles, what excludes the genus *Pleurotropites*, which lacks in umbilical tubercles (Tozer 1994). Ribs project beyond the umbilical margin and end as angular, forward-facing nodes within the external furrows. The narrow furrows border a thick external keel (Dittmar 1866; Mojsisovics 1893), in contrast to the genus *Discotropites* (Hyatt and Smith, 1905), which lacks these furrows, bordering the keel (Arkell *et al.* 1957). Additionally, the ribs do not show that conspicuous sigmoidal character observed in *Discotropites* (Diener 1917) and its spiral ornamentation, which might be represented only by weak striae (Krystyn 1982). Tubercles give rise to rounded, distinct, sinuous ribs, separated by narrow intercostal 'furrows'. Ribs are simple or branched; intercalary ribs may occur on flanks. Whilst juvenile stages mostly show dichotomous ribbing, adult stages dominantly bear tripartite ribbing. At the body chamber, additional quadripartite ribs are developed. Mojsisovics (1893) reported a ratio of 1:3 of umbilical nodes versus external ribs.

Stratigraphic range. Upper Triassic, Upper Carnian, *Tropites dilleri* Zone (Tuvalian 1) – *Tropites subbullatus* Zone (Tuvalian 2).

Regions. NCA, Austria (Mojsisovics 1893; Tozer 1971; Krystyn 1973); north-east British Columbia (Tozer 1994); Aşağiyaylabel, Taurus Mountains, Turkey.

Paratropites cf. *hoetzendorfii* Diener, 1917

Figure 4.10G–H

cf. *1917 *Paratropites Hoetzendorfii* Diener, p. 369, pl. 1, figs 1–4.
2012 *Pleurotropites* Lukeneder *et al.*, p. 284, 292.

Material from Aşağiyaylabel. Sixty-five specimens from sequence AS 16–AS 16+ 13 m of the Marlstone Member (Fig. 4.2): NHMW-2012z0133/0351–0368, NHMW-2012z0133/0371–0393, NHMW-2012z0133/0396–0399, NHMW-2012z0133/0402–0403, NHMW-2012z0133/0405, NHMW-2012z0133/0407–0408, NHMW2012z0133/0410–0417, NHMW-2012z0133/0420–0424, NHMW2012z0133/0426–0427.

Measurements. See Lukeneder and Lukeneder (2013).

Description. The existing material, especially the juvenile examples, are poorly preserved and are laterally compacted. The whorl shape can be studied only in few, undeformed specimens. In specimen NHMW-2012z0133/0352 (Fig. 4.10G), whorl thickness decreases from the umbilical edge towards the venter. The juvenile specimen (Fig. 4.10H) shows a more evolute shell morphology, in contrast to the involute whorls in adults (Fig. 4.10G; Lukeneder and Lukeneder 2013). Ribbing in juveniles appears from the umbilical edge as thick main ribs, bifurcating at the mid-flank (Fig. 4.10H). The latter specimen shows badly preserved suture lines, resembling those in specimens shown by Diener (1917) for his type material from Bosnia and Herzegovina. The strong and smooth external keel is bordered by two furrows (Fig. 4.10H), at which the dense, flat, but rounded ribs are interrupted. From a D of approximately 20 mm onward, typical *Paratropites* ribbing occurs. Ribs, distinct on inner whorls, bifurcate at the umbilicus and/or on mid-flank. Bifurcation is irregular, and the point of bifurcation is shifted towards the umbilicus in adult stages. Ribs are generally slightly proverse and straight, bending adapically, near the ventrolateral shoulder, with a slightly sigmoidal character. Umbilical tubercles are present, whilst spiral lines are absent, as characteristic for *Paratropites*.

Discussion. Diener (1917) described similarities between medium-sized forms of *P. hoetzendorfii* Diener, 1917 and *Pleurotropites anakreontis* Mojsisovics, 1893. Note that the specimen shown by Mojsisovics (1893) as *P. anakreontis* from the Upper Carnian (Tuvalian) from the Raschberg (Upper Austria) bears a prominent ventral keel, but lacks ventral furrows. Therefore, the presence of the typical furrows, which border the keel, the bifurcate ribbing, as well as the absence of spiral lines within material from Aşağiyaylabel, proves the close relationship with *P. hoetzendorfii*. Due to the strong deformation of our material, we operate with an open nomenclature in *Paratropites* cf. *hoetzendorfii*. Morphological details such as the strong keel bordered by two furrows and the characteristic bifurcation of ribbing are detected. Umbilical tubercles are present, but there is no evidence for spiral lines. Adult specimens from Aşağiyaylabel are similar to those described by Diener (1917) from Bosnia and Herzegovina. Specimens show the typical characteristics of *P. hoetzendorfii* with dense, straight ribbing on flanks, exhibiting a strong adapical bow on outer flanks. In particular, the maximum thickness of the shell at the umbilical margin described by Diener (1917) for his type material can be observed in the material from Aşağiyaylabel.

Stratigraphic range. Upper Triassic, Upper Carnian, *Tropites dilleri* Zone (Tuvalian 1) – *Tropites subbullatus* Zone (Tuvalian 2).

Regions. Glamoča, Bosnia and Herzegovina (Diener 1917, Ćorić 1999); Aşağiyaylabel, Taurus Mountains, Turkey.

Family HALORITIDAE Mojsisovics, 1893

Subfamily SAGENITINAE Spath, 1951

Genus TRACHYSAGENITES Mojsisovics, 1893

1893 *Trachysagenites* Mojsisovics, p. 156.

1981 *Trachysagenites* Tozer, p. 96.

2002 *Trachysagenites* Sepkoski, p. 132.

Type species. *Ammonites erinaceus* Dittmar, 1866 (p. 380, pl. 17, figs 15–17), from the yellowish-grey limestone of the 'Vorderer Sandling', Carnian, Upper Triassic. Subsequent designation by Hyatt and Smith (1905).

Remarks. Strongly involute, subglobose whorls, broader than high, bearing a long body chamber (Mojsisovics 1893; Hyatt and Smith 1905). Flanks and venter are rounded. The narrow umbilicus shows a rounded but steep umbilical margin (Mojsisovics 1893; Hyatt and Smith 1905). Radial dichotomous ribs, almost straight on flanks, cross the venter. Ribs bear rows of regularly arranged blunt spines. Based on those spines, Mojsisovics (1893, p. 179) defined the subgenus *Trachysagenites* for the group *Sagenites spinosi*.

Stratigraphic range. Upper Triassic, Upper Carnian, *Tropites dilleri* Zone (Tuvalian 1) – *Tropites welleri* (equals *Tropites subbullatus* Zone, Tuvalian 2).

Regions. NCA, Austria (Mojsisovics 1893); Glamoča, Bosnia and Herzegovina (Diener 1917); Shasta County, California (Hyatt and Smith 1905; Smith 1927; Spath 1951); Canada (Tozer 1994); Toeboe Lopo, Timor (Spath 1951); Himalaya, India and Nepal (Diener 1908; Krystyn 1982); Aşağiyaylabel, Taurus Mountains, Turkey.

Trachysagenites cf. *beckei* Diener, 1921

Figure 4.10I–J

cf.*1921 *Trachysagenites Beckei* Diener, p. 501 (37), pl. 5, fig. 1a–b.

Material from Aşağiyaylabel. One specimen from the Marlstone member, from sequence AS 16 + 11.5 m – AS 16 + 13 m (Fig. 4.2), NHMW-2012z0133/0350.

Measurements. See Lukeneder and Lukeneder (2013).

Description. The observed specimen (Fig. 4.10I–J) shows a large D, up to 100 mm (see Lukeneder and Lukeneder 2013). Regular arrangement of blunt spines in rows (or broken base) on subglobose inner whorls with rounded venter. No ventral furrow. Adult stage and body chamber are deformed. The ribbing is more distinct on body chamber, with 8–10 tubercles or spine rows. Rib spacing and strength vary on body chamber, up to 10 mm apart. Stronger ribs are intercalated by finer ribs, also bearing tubercles. The first tubercle row occurs on umbilical edge. The steep umbilical whorl is crossed by fine ribs that end in the latter umbilical tubercles.

Discussion. Diener's (1917) figured *Trachysagenites glamocensis* Diener, 1917 (NHMW-1998z0056/0025 and 0027, syntypes) from Carnian beds of Bosnia and Herzegovina also shows similarities in juvenile to mid-aged whorls. The involute coiling of the specimen *T.* cf. *beckei* additionally resembles *Trachysagenites herbichi* Mojsisovics, 1893 and figured Carnian specimens of *'Sagenites' herbichi* Mojsisovics, 1893 by Hyatt and Smith (1905) from Shasta County (California, North America). Similarities are also observable with figured specimens of *Sag.* (*Trachysagenites*) *herbichi* Mojsisovics, 1893 by Smith (1904), from the same locality (Tuvalian 2, Upper Carnian). Due to the poor preservation, we choose an open taxonomy with *T.* cf. *beckei* Diener, 1921. The figured *Trachysagenites* cf. *beckei* (Fig. 4.10I–J) from the Kasimlar Fm. of Aşağiyaylabel is similar, especially the adult size and sculpture, to the Upper Carnian (Tuvalian) *T. beckei* Diener, 1921 from the Feuerkogel (Styria, Austria). The holotype (NHMW-1926/0002/0688) of Diener (1921) exhibits a fine, spiral striation. Only few shown in Diener (1921). Due to preparation, most of the spines were broken, yielding the typical verrucous sculpture. Rows of tubercles are crowded at the shoulder and on the venter, with up to 10 rows in 30 mm width. The same can be observed in the specimen from Aşağiyaylabel (Fig. 4.10I–J), with 10 rows within 20 mm width. Number of ventrolateral tubercle rows is apparently constant in ontogeny. The holotype shows a typical weakening of sculpture at the steinkerns, where shell is removed. The venter seems to be less rounded and straighter in the adult stage of the holotype.

Stratigraphic range. Upper Triassic, Upper Carnian*, T. dilleri* Zone (Tuvalian 1) – *Tropites subbullatus* Zone (Tuvalian 2).

Regions. NCA, Austria (Diener 1921); Glamoča, Bosnia and Herzegovina (Diener 1917); Aşağiyaylabel, Taurus Mountains, Turkey.

Superfamily ARCESTACEAE Mojsisovics, 1875

Family ARCESTIDAE Mojsisovics, 1875

Genus PROARCESTES Mojsisovics, 1893

1893 *Proarcestes* Mojsisovics, p. 785.
1981 *Proarcestes* Tozer, p. 95.
2002 *Proarcestes* Sepkoski, p. 131.

Type species. *Arcestes bramantei* Mojsisovics, 1869 (p. 18), from limestone beds of Hallstatt, near Bad Aussee, Austria. Subsequent designation by Mojsisovics (1893).

Remarks**.** Ribs and constrictions on phragmocone appear similar to that on body chamber (Arkell *et al.* 1957). Mojsisovics (1893) defined the genus *Proarcestes* for a group of Arcestidae in which the body chamber shows structural elements similar to those in the phragmocone.

Stratigraphic range. Middle Triassic – Upper Triassic, Anisian – Carnian (Arkell *et al.* 1957).

Proarcestes sp.

Figure 4.10K–N

Material from Aşağiyaylabel. One specimen from the Carbonate member Unit C, bed AS 32: NHMW-2012z0133/0444, as well as 23 specimens from the Marlstone member, from beds AS 16 – AS 16 + 13.5 m (Fig. 4.2): NHMW-2012z0133/0443, 0445–0466.

Measurements. See Lukeneder and Lukeneder (2013).

***Description*.** The preservation of the specimens from Aşağiyaylabel (Fig. 4.10K–N) is generally too bad (deformed and crushed) for a classification at species level. Specimens are smooth and subglobular, with very involute shells. Constrictions occur on the body chamber (Fig. 4.10K–M), and in one specimen (Fig. 4.10K), the adult aperture shows an aberrant form. We therefore use open nomenclature for this material.

***Stratigraphic range*.** Middle Triassic – Upper Triassic (Anisian – Carnian; Arkell *et al.* 1957). At Aşağiyaylabel, *Proarcestes* sp. was found at the Carbonate member Unit C, Lower Carnian (Julian 2), as well as at the Marlstone member, which belongs to the Upper Carnian *Tropites dilleri* Zone (Tuvalian 1).

Superfamily MEGAPHYLLITACEAE Mojsisovics, 1882

Family MEGAPHYLLITIDAE Mojsisovics, 1896

Genus MEGAPHYLLITES Mojsisovics, 1879

1879 *Megaphyllites* Mojsisovics, p. 135.

1981 *Megaphyllites* Tozer, p. 92.

1994 *Megaphyllites* Tozer, p. 91.

2002 *Megaphyllites* Sepkoski, p. 130.

Type species. *Ceratites jarbas* Münster, 1841 (p. 135, pl. 15, fig. 25), from the beds of St. Cassian, South Tyrol.

Remarks. Small-sized, discoidal, compressed, involute and smooth shell. Generally without any sculpture, except for weak sigmoidal growth lines and regular constrictions on body chamber (Münster 1841; Hauer 1846; Arkell *et al.* 1957; Tozer 1994). The genus *Megaphyllites* shows a specific ceratitic suture. Lobes are rather similar to that of *Monophyllites*, but do not show that phylloid tops of the main lateral branches, as well as do not have an alternating occurrence of bigger versus smaller lateral branches and of serrated lobes (Fig. 4.10O). Saddles are nearly circular. Lobes are separated into three to four sharp and acute beaks. The external lobus is divided by a median depression, as known from Palaeozoic forms. Lateral lobes of Triassic forms are divided into two 'lobes' (Mojsisovics 1882).

Stratigraphic range. Middle Triassic – Upper Triassic, Anisian – Rhaetian stage (Diener 1916), Ladinian – Carnian (Arkell *et al.* 1957).

Megaphyllites jarbas (Münster, 1841)
Figure 4.10O

*1841 *Ceratites jarbas* Münster, p.135, pl. 15, fig. 25 a–c.
1843 *Ammonites umbilicatus*; Klipstein, p. 117, pl. 6, fig. 5.
1846 *Ammonites Jarbas* Münster; Hauer, p. 26, pl. 1, fig. 15.
1847 *Ammonites Jarbas* sp. Münster; Hauer, p. 15.
1849 *Ammonites Jarbas* Münst.; Hauer, p. 16, 26.
1846–1849 *Ammonites Jarbas* Münst.; Quenstedt, p. 240, pl. 18, fig. 12.
1855 *Ammonites Jarbas* sp. Münst.; Hauer, p. 26.
1864 *Ammonites Jarbas* Münst sp.; Laube, p. 412.
1870 *Phylloceras Jarbas* Münster sp.; Laube, p. 85, pl. 41, fig. 12.
1873 *Pinacoceras* cf. *jarbas* Münster; Mojsisovics, p. 47, pl. 19, figs 9, 10, 16.
1880 *Megaphyllites Jarbas* v. Mstr. sp.; Branco, p. 62 pl. 10, fig. 5.
1882 *Megaphyllites Jarbas* Münst.; Bittner, p. 318.
1882 *Megaphyllites Jarbas* (Graf Münster); Mojsisovics, p. 193, pl. 53, figs 7a–b, 8.
1896 *Megaphyllites Jarbas*; Mojsisovics, p. 94.
1906 *Megaphyllites Jarbas* Mstr. sp.; Arthaber, pl. 44, fig. 3a–c.
1906 *Megaphyllites Jarbas*,Münst.; Diener, p. 39, pl. 5, fig. 1.
1907 *Megaphyllites Jarbas* Münst.; Frech, p. 19, pl. 4, fig. 1a–d.
1907 *Megaphyllites Jarbas* Mnstr.; Renz, p. 79.

1908 *Megaphyllites jarbas* Münst.; Diener, p. 39, pl. 5, fig. 1.

1908 *Megaphyllites jarbas* Mstr.; Kittl, p. 53.

1909 *Megaphyllites jarbas* Münster; Renz, p. 263, 265, 270, 272, pl. 10, fig. 2.

1910 *Megaphyllites jarbas* Münster; Renz, p. 521, 523, pl. 22, fig. 5.

1911 *Megaphyllites jarbas* Münster; Renz, p. 3, 5, 15, 66–67, 95.

1915 *Megaphyllites Jarbas* Mstr. sp.; Arthaber, p. 163.

1915 *Megaphyllites Jarbas* Gf. Muenster; Arthaber, p. 199.

1916 *Megaphyllites Jarbas* Münst.; Diener, p. 465.

1925 *Megaphyllites Jarbas* Mstr.; Diener, p. 75, pl. 17, fig. 2.

1927 *Megaphyllites Jarbas* Muenstr; Arthaber, p. 113.

1927 *Megaphyllites Jarbas* Muenst.; Kutassy, p. 137, pl. 2, fig. 11.

1932 *Megaphyllites jarbas* Muenstr. 1841; Kutassy, p. 587.

1966 *Megaphyllites jarbas* Münster; Masutomi and Hamada, p. 82, pl. 41, fig. 2a–b.

1957 *Megaphyllites jarbas* (Münster); Arkell *et al.*, p. L179, fig. 210, 4a–c (refig. holotype).

1973 *Megaphyllites jarbas*; Kollárová-Andrusovová and Kochanová, p. 102.

1973 *Megaphyllites jarbas* Münster; Yurttas Özdemir, p. 64–65, 79–80, pl. 5, figs 3–6.

1994 *Ammonites jarbas* Münster; Tozer, p. 91.

1994 *Megaphyllites jarbas* (Münster); Urlichs, p. 36.

2004 *Megaphyllites jarbas* (Münster); Urlichs, p. 1, 18, 20–21, 24, 29, fig. 9.

2007 *Megaphyllites jarbas*; Hornung *et al.*, p. 271, 279, fig. 6e.

2009 *Megaphyllites jarbas* (Münster 1841); Kozur *et al.*, p. 26.

2011 *Megaphyllites jarbas* (Münster); Moix *et al.*, p. 70.

Type material. Holotype from Münster (1841), from Carnian beds of St. Cassian, South Tyrol, northern Italy.

Material from Aşağiyaylabel. One specimen from the Carbonate member Unit C, from sequence AS 19 – AS 46 (Fig. 4.2): NHMW2012z0133/0479 (Fig. 4.10O).

Measurements. See Lukeneder and Lukeneder (2013).

***Description*.** The specimen from Aşağiyaylabel (Fig. 4.10O) is small (D 33 mm; Lukeneder and Lukeneder 2013), discoidal, with slightly flattened flanks and a rounded venter. Whorls are compressed and very involute, bearing a narrow and deep umbilicus with rounded umbilical walls. The shell is smooth, bearing growth striae only where shell is preserved. Where shell is removed, parts of the clearly phylloceratid, nearly circular ventrolateral and lateral saddles are visible, as typical for that form (see Arkell *et al.* 1957). The last suture line is visible and reveals that the body chamber embraces the last half whorl. Furthermore, one very shallow, poorly visible constriction occurs on the body chamber.

***Discussion*.** Generally, specimens of this species lack strong sculpture, except for weak sigmoidal growth lines and regular constrictions on the body chamber (Münster 1841; Hauer 1846; Diener 1925; Arkell *et al.* 1957; Tozer 1994). The discoid and completely involute shell, the narrow, deep umbilicus as well as details of the ventrolateral suture (Arkell *et al.* 1957) are most similar to those forms shown in the articles provided in the synonymy list. The described specimen resembles specimens shown by Mojsisovics (1893) from the Carnian beds of the Röthelstein (Styria, Austria) and the Raschberg (Upper Austria, Austria). Very similar examples of *M. jarbas* (Münster, 1841) are given and figured in the early literature from Carnian faunas of Epidaurus (Greece) by Frech (1907), from Carnian beds of St. Cassian (South Tyrol, northern Italy) by Diener (1925) and Urlichs (2004) and from Carnian beds of Tepeköy (north-west Turkey) by Yurttaş-Özdemir (1973).

Stratigraphic range. Middle Triassic – Upper Triassic, Ladinian – Carnian (up to *Tropites subbullatus* Zone, Tuvalian 2).

***Regions*.** NCA, Austria (Hauer 1847; Mojsisovics 1873, 1882; Bittner 1882; Wöhrmann 1893; Arthaber 1906; Frech 1907); southern Germany (Wöhrmann 1893; Hornung *et al.* 2007); Bosnia and Herzegovina (Bittner 1880; Mojsisovics 1882; Hoernes 1903; Kittl 1903); St. Cassian, South Tyrol (Münster 1841; Klipstein 1843; Laube 1870; Neumayr and Uhlig 1880–1881; Mojsisovics 1882; Wöhrmann 1893; Frech 1907; Urlichs 1994); Greece (Frech and Renz 1906; Frech 1907; Renz 1907, 1909, 1910, 1911, 1922; Diener 1925); Dobrudscha, south-east Romania to north-east Bulgaria (Anastasiu 1897; Kittl 1908; Diener 1925); Himalaya (Diener 1915, 1925); Western Pontian Mountains, Mersin and Aşağiyaylabel, Taurus Mountains, Turkey (Arthaber 1914, 1915; Yurttaş-Özdemir 1973; Kozur *et al.* 2009).

Order PHYLLOCERATITIDA Zittel, 1884

Suborder PHYLLOCERATINA Arkell, 1950

Superfamily USSURITACEAE Hyatt, 1900

Family USSURITIDAE Hyatt, 1900

Subfamily MONOPHYLLITINAE Smith, 1913

Genus SIMONYCERAS Wiedmann, 1970

1970 *Simonyceras* Wiedmann, p. 970.
1981 *Simonyceras* Tozer, p. 99.
2002 *Simonyceras* Sepkoski, p. 132.

Type species. *Ammonites simonyi* Hauer, 1847 (p. 14, pl. 9, figs 4–6), from the red limestones of Bad Aussee, Austria.

***Remarks*.** Medium- to large-sized, evolute shells with subrounded whorl section. *Simonyceras* exhibits a distinct biconcave striation, passing the round venter without interruption. Wiedmann (1970) established the new genus *Simonyceras* based on the coexistence of sculptural characteristics of the real *Monophyllites* and the suture characteristics of *Eopsiloceras* (Spath, 1930). Arkell *et al.* (1957) included the genus *Monophyllites* into the family Ussuritidae Hyatt, 1900, which is a synonym of the family Monophyllitidae Smith, 1913. See Wiedmann (1970) and Rakús (1993) for a more detailed discussion on the genus *Simonyceras* Wiedmann, 1970.

Stratigraphic range. Upper Triassic, Lower Carnian.

Simonyceras simonyi (Hauer, 1847)

Figure 11A

*1847 *Ammonites simonyi* Hauer, p. 270, pl. 9, figs 4–6.
1873 *Lytoceras simonyi* Hauer; Mojsisovics, p. 32, pl.17, fig. 1–6, pl. 18, fig. 1.
1902 *Monophyllites simonyi* (Fr. v. Hauer); Mojsisovics, p.316.
1934 *Monophyllites simonyi* (Hauer); Spath, p.291, textfig. 101.
1970 *Simonyceras simonyi* (Hauer); Wiedmann, p. 970, pl. 2, figs 1, 2, pl. 3, text-fig. 4b, 30B (cum syn.).

Material from Aşağiyaylabel. One specimen from a reworked rock sample of the Carbonate member Unit B (Fig. 2): NHMW-2012z0133/0477.

Measurements. See Lukeneder and Lukeneder (2013).

Description. Only a large part of the body chamber (length 165 mm; Lukeneder and Lukeneder 2013) was found at Aşağiyaylabel (Fig. 11A). Although only partly preserved, the sculpture is unique and characterizes *Simonyceras simonyi* (Hauer, 1847) unequivocally. The specimen bears the typical, distinct sigmoidal biconcave ribbing of *Si. simonyi* (Wiedmann 1970). A strong, adapical bow of ribbing is present on the rounded venter. Rib thickness and rib interspace are equal.

Discussion. The typical, distinctly sigmoidal biconcave sculpture of the specimen from Aşağiyaylabel (Fig. 11A) is unique and closely resembles the specimens figured by Rakús (1993) as *Si. simonyi* (Hauer, 1847). Rakús reinvestigated the figured material of Mojsisovics (1873). The specimens figured by Rakús (1993) are the originals of Mojsisovics (1873, GBA 1873/5/48) along with one additional specimen (GBA 1993/3/1) from the same locality from the Lower Carnian of the Feuerkogel (Styria, Austria). The specimen from Aşağiyaylabel is similar in ribbing to *Si. simonyi* figured by Wiedmann (1970).

Stratigraphic range. Upper Triassic, Lower Carnian.

Regions**.** NCA, Austria (Hauer 1847; Dittmar 1866; Mojsisovics 1873–1902; Neumayr 1879; Wähner 1882–1898; Arthaber 1906; Kutassy 1932; Spath 1934); St. Cassian, SA (Quenstedt 1846–1849); Western Carpathians (Kollárová-Andrusovová and Kochanová 1973); Romania (Shevyrev 1990); Greece (Renz 1909, 1910, 1911; Kutassy 1932); Lombardy (Allasinaz 1968); Aşağiyaylabel, Taurus Mountains, Turkey; Himalaya and Timor (Diener 1908, 1909; Welter 1915; Arthaber 1927; Wiedmann 1970; Kutassy 1932).

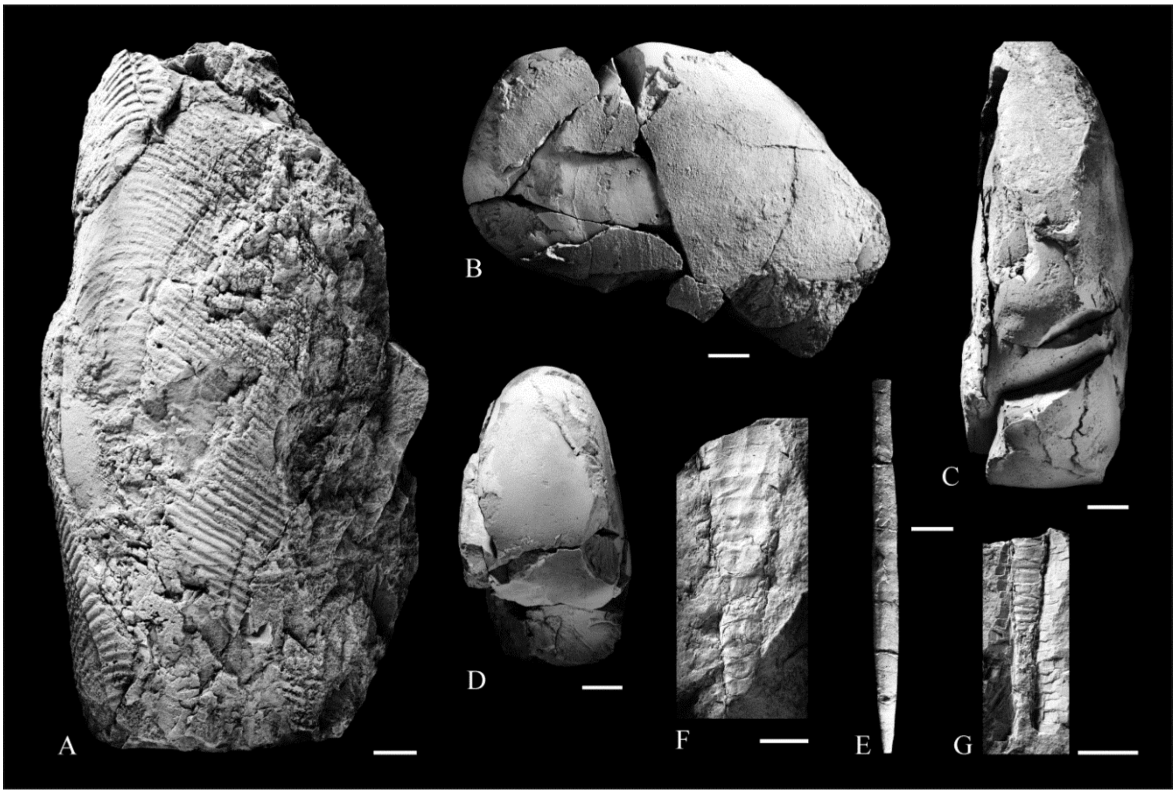

Fig. 4.11. Fauna of Aşağiyaylabel, Kasimlar Fm.; **A,** Carbonate member Unit B, from a reworked rock sample; **B–D,** Carbonate member Unit C**.** *Austrotrachyceras austriacum* Zone (Julian 2), bed AS 40; **E–G,** Marlstone member, *Tropites dilleri* Zone (Tuvalian 1), bed AS 47 + 2.5 m and AS 16 + 10 m. **A,** *Simonyceras simonyi*, 2012z0133/0477. **B–D,** nautiloid cephalopod, 2012z0133/0478. **B,** lateral view. **C,** ventral view. **D,** septal view. **E–G,** *Atractites* sp. **E,** 2012z0133/0439. **F,** 2012z0133/0440. **G,** 2012z0133/0441. All scale bars represent 1 cm.

4.5. Biostratigraphy

The Kasimlar Formation of Aşağiyaylabel (Taurus Mountains, Turkey) consists of two ammonoid assemblages, representing the Lower Carnian *Austrotrachyceras austriacum* Zone (Carbonate member Unit A; Julian 2) and the Upper Carnian *Tropites dilleri* Zone (Marlstone member; Figs 4.2, 4.12).

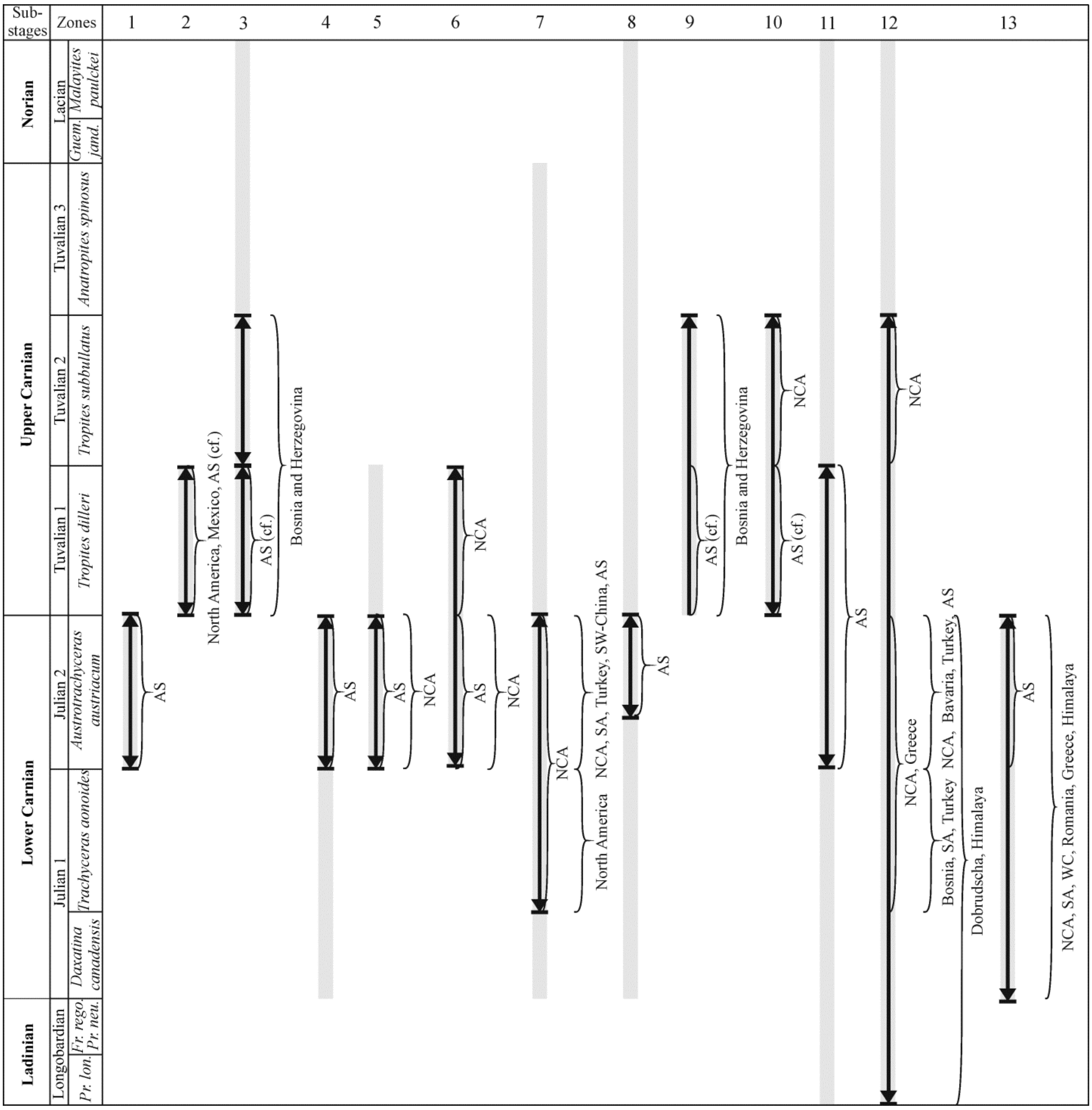

Fig. 4.12. Chronostratigraphic scale with indicated range and general geographic occurrences of recognized species (black arrows) and genera (grey bars) found at Aşağiyaylabel. Localities that bear species with open nomenclature are indicated with cf. in brackets. Numerical code: **1,** *Kasimlarceltites krystyni* gen. et sp. nov. **2,** *Spirogmoceras shastense* and *Spirogmoceras* sp. **3,** *Sandlingites pilari* and *Sandlingites* sp. **4,** *Klipsteinia disciformis* sp. nov. and *Klipsteinia* sp. **5,** *Neoprotrachyceras attila* and *Neoprotrachyceras* sp. **6,** *Neoprotrachyceras baconicum* and *Neoprotrachyceras* sp. **7,** *Sirenites senticosus* and *Sirenites* sp. **8,** *Anasirenites crassicrenulatus* sp. nov. and *Anasirenites* sp. **9,** *Paratropites hoetzendorfii* and *Paratropites* sp. **10,** *Trachysagenites beckei* and *Trachysagenites* sp. **11,** *Proarcestes* sp. at AS and *Proarcestes* sp. **12,** *Megaphyllites jarbas* and *Megaphyllites* sp. **13,** *Simonyceras simonyi* and *Simonyceras* sp. Abbreviations: AS, Aşağiyaylabel; *Fr. rego*., *Frankites regoledanus*; *Guem. jand*., *Guembelites jandianus*; NCA, Northern Calcareous Alps; *Pr. lon*., *Protrachyceras longobardicum*; *Pr. neu*., *Protrachyceras neumayri*; SA, Southern Alps; WC, Western Carpathians.

Carbonate member Unit A.

It should be noted that the specimen of *Neoprotrachyceras* sp., wrongly assigned previously to bed AS 1 (top) at the top of the Kartoz Formation (Lukeneder *et al.* 2012), actually derived from the bottom of bed AS 2, and therefore from the bottom of the Carbonate member of the Kasimlar Formation (Fig. 4.2). Nevertheless, the Carbonate member Unit A of the Kasimlar Formation has therefore to be dated, due to this occurrence of *Neoprotrachyceras* sp., as Julian 2 (*Austrotrachyceras austriacum* Zone; Fig. 4.12), but not older than Julian 2/Ib. The occurrence of *K. krystyni* sp. nov. together with *Kl. disciformis* sp. nov. and *Sirenites senticosus* within the layers of the Carbonate member Unit A strengthens the biostratigraphical assignment of Julian age (Fig. 4.12).

Carbonate member Unit B.

The species found within the reworked material from the Carbonate member Unit B (*K. krystyni* gen. et sp. nov., *Kl. disciformis* sp. nov., *Simonyceras simonyi*) all together represent Julian age (Fig. 4.12). Due to the deposition above the Carbonate member Unit A, which indicates at least Julian 2/Ib, the sediments of the Carbonate member Unit B can be dated as not older than Julian 2/Ib (Figs 4.2, 4.12).

Carbonate member Unit C.

Significant ammonoids found within Carbonate member Unit C are *N. attila*, *N. baconicum*, *S. senticosus*, *A. crassicrenulatus* sp. nov., *Proarcestes* sp. and *M. jarbas* (Fig. 4.2). Whilst *M. jarbas* and *Proarcestes* sp. are known within a long time interval, *S. senticosus* in contrast is limited to Julian age (Fig. 4.12). The occurrence of *N. attila* and *N. baconicum* would reflect at least Julian 2/Ib. The co-occurrence of *S. senticosus* and *Neoprotrachyceras* therefore dates Unit C as Julian 2. Moreover, *A. crassicrenulatus* sp. nov. at the top of the Carbonate member (Unit C) allows a more detailed classification of Unit C to Julian 2 /II (Figs 4.2, 4.12). This classification (latest Early Carnian) has already been investigated from conodonts (*Gladigondolella tethydis* and *Metapolygnathus* sp.) and stratigraphically important ammonoids (*Neoprotrachyceras* sp. and *Anasirenites* sp.) by Lukeneder *et al.* (2012).

Marlstone member.

The second and stratigraphically younger assemblage from the Kasimlar Formation of Aşağiyaylabel was detected within the Marlstone member (Fig. 4.2). All ammonoid species found within the Marlstone member suggests a late Carnian age (Tuvalian). Whilst *Sa. pilari*, *P. hoetzendorfii* and *Trachysagenites beckei* are characteristic elements for Tuvalian 1 – 2, *Sp. shastense* would indicate Tuvalian 1 (Fig. 4.12). Due to the fact that *Sp*. cf. *shastense* was found within the same beds as the species characteristic for Tuvalian 1–2 (Fig. 4.2), the sediment can be placed as Tuvalian 1. The stratigraphic age of the Marlstone member is therefore dated as Tuvalian 1, *Tropites dilleri* Zone (Fig. 4.2). Previously, Lukeneder *et al.* (2012) dated the Marlstone member, based on the occurrence of the ammonoid genera *Pleurotropites* sp. and *Spirogmoceras* sp. as earliest Late Carnian (Tuvalian). It has to be noted that Lukeneder *et al.* (2012) misinterpreted *P.* cf. *hoetzendorfii* as *Pleurotropites* sp. Although there are still biostratigraphical inconsistencies (i.e. condensation, possible hiatus) at the top of the Kartoz Formation, the Lower Carnian – Upper Carnian (Julian – Tuvalian) boundary can be identified precisely at Aşağiyaylabel, between the Carbonate and the Marlstone members (Figs 4.2, 4.12).

4.6. Taphonomy of the ammonoid fauna

The ammonoid fauna of Aşağiyaylabel is variable in the quantity of taxonomic groups, and the quality of preservation through the section. *Kasimlarceltites krystyni* gen. et sp. nov. forms a mass occurrence (≫1 million specimens; Fig. 4.2) within the Carbonate member Unit A, as well as being present within reworked ‘Cipit-like’ boulders of Unit B (i.e. bed 18). The quantity *of K. krystyni* gen. et sp. nov. has been extrapolated from an 150 x 45 x 140 mm block of bed AS 6 and calculated from the known distribution of the mass occurrence at Asagiyaylabel within a 112-m^3 bed. 2D and 3D reconstructions were made from this reference block, which yielded more than 3000 ammonoids.

Even within Unit A, different beds show different kinds of preservation of *K. krystyni* gen. et sp. nov. Layers with ‘normal’ sedimentation, in which *K. krystyni* gen. et sp. nov. occurs on and off, alternate with ‘event beds’ (e.g. AS 6) in which *K. krystyni* gen. et sp. nov. occurs in masses and seems to be transported and orientated by currents (turbidity or water currents). The genesis of this mass occurrence as well as a detailed description and interpretation is beyond the field of this article, but is the topic of future publications in preparation.

In most beds within Unit A, *K. krystyni* gen. et sp. nov. occurs together with rare *Kl. disciformis* sp. nov. (AS 4, AS 6 and AS 7) and *Sirenites senticosus* (AS 6). All ammonoids show shell preservation, in which shell is secondary replaced by calcite.

Within the reworked material of Carbonate member Unit B, *K. krystyni* gen. et sp. nov and *Kl. disciformis* sp. nov. occur within reworked blocks (i.e. ‘Cipit’ blocks). The ammonoid material (*Kl. disciformis* sp. nov., *S. senticosus*) seems to be redeposited from shallower areas down to deeper environments on the ramp, along with shallow-water organisms (e.g. gastropods, sponges). Due to the erosive process and weathering over thousands of years at the surface, ammonoids can be easily removed from the mother rock. Nevertheless, the ammonoids are generally well preserved (e.g. body chamber, siphuncle structure) with shell preservation, not compacted, not fragmented, without borings, but replaced by secondary calcite. A large specimen of *Si. simonyi*, found in Unit B, is preserved only as fragment of the body chamber.

Ammonoids from the Carbonate member Unit C (*Kl. disciformis* sp. nov., *N. attila*, *N. baconicum*, *S. senticosus* and *A. crassicrenulatus* sp. nov.) stem from bedded limestones and are well preserved, mostly with shell preservation, but replaced by secondary calcite and without any compaction.

Ammonoid specimens from the Marlstone member (*Sp*. cf. *shastense*, *Sa*. cf. *pilari*, *P*. cf. *hoetzendorfii*, *Trachysagenites* cf. *beckei* and *Proarcestes* sp.) are generally compacted, sometimes with shell preservation (i.e. secondary calcite). Due to compaction, specimens are often fragmented.

4.7. Discussion

4.7.1. Faunal composition, stratigraphy and facies change within the section at Aşağiyaylabel

The section at Aşağiyaylabel, located within the Taurus Mountains (southern Turkey), consists of the older Kartoz Formation (lowermost Carnian) and the younger Kasimlar Formation (Lower Carnian, Julian 2 – Upper Carnian, Tuvalian 1), Lukeneder *et al.* (2012, figs 1–3). New data led to a revised log concerning the different thicknesses of the members (Fig. 4.2), redefined after Lukeneder *et al.* (2012).

Kartoz Formation

The lowermost 1.7 m of the log contains only rare ammonoids (n= 1). Only one specimen of *Neoprotrachyceras* sp. was wrongly assigned to bed AS 1 (at the top of the Kartoz Formation) by Lukeneder *et al.* (2012), but actually belongs to bed AS 2 (at the bottom of the Kasimlar Formation; Fig. 4.2). The rare ammonoid occurrence in the Kartoz Formation is due to the shallow palaeowater depth, indicated by in situ reefs, megalodont bivalves, gastropods and sponges (Lukeneder *et al.* 2012).

Kasimlar Formation

The lower 28 m bears two ammonoid assemblages. The stratigraphically older one belongs to the *Austrotrachyceras austriacum* Zone (Julian 2; Fig. 4.2), whereas the younger is characteristic for the *Tropites dilleri* Zone (Tuvalian 1). The Kasimlar Formation (1.7 m up to about 35 m) has been subdivided by Lukeneder *et al.* (2012) into the Carbonate member comprising Units A, B and C (1.7–15.35 m), into the Marlstone member (15.4–31.7 m) and into the Shale member (31.8 m up to about 35 m; Fig. 4.2). The Lower – Upper Carnian boundary (i.e. Julian – Tuvalian boundary) is marked by a lithological change between the Carbonate member (Unit C) and the Marlstone member (Lukeneder *et al.* 2012).

The lowermost part of the Carbonate member (1.7–3.6 m; Fig. 4.2) is characterized by well-bedded dark limestones. They bear a microfacies of bioclastic pelagic wackestones, deposited within a deep shelf margin or mid-ramp position (Lukeneder *et al.* 2012). The ammonoid assemblage of the lowermost Unit A (Fig. 4.2) is extremely monotonous. The ceratitid ammonoid *K. krystyni* gen. et sp. nov. occurs as mass occurrence within Unit A, bed AS 4–7, and therefore dominates (> 99 per cent) the cephalopod assemblage (Carbonate member Unit A). Rare specimens of *Kl. disciformis* sp. nov., *Sirenites senticosus* and *Sirenites* sp. co-occur. The abundance of the genus *Kasmilarceltites* gen. nov. reflects its accumulations in mass occurrences within single layers (beds AS 4–AS 7; Fig. 4.2). These event beds alternate between 'normal' sedimentation, bearing sporadically deposited ammonoids, and almost monospecific layers crowded with *Kasimlarceltites* gen. nov. The entire sequence reflects a tectonic deepening, hence a manifestation of deeper water sedimentation, leading to the deposition of ammonoid beds over shallow-water reefal limestone, which clearly lack cephalopods.

Carbonate member Unit B (3.6–11.6 m; Fig. 4.2) consists of mass flow deposits – 'Cipit'-like blocks (Lukeneder *et al.* 2012) – which contain almost the same ammonoid fauna as described in Unit A with *K. krystyni* gen. et. sp. nov., *Kl. disciformis* sp. nov. and one, most probably drifted, specimen of *Si. simonyi* (Fig. 4.11A). Due to the faunal similarities between Carbonate member Units A and B, the transported blocks of Unit B are interpreted as being derived from an isochronously deposited site as proximal mid-ramp, comprising corals, sponges and gastropods (Lukeneder *et al.* 2012). The Turkish specimen of *Si. simonyi* described herein is most probably drifted based on its fragmentation and rareness (n= 1), hence interpreted as an allochthonous element.

Carbonate member Unit C (11.7–15.2 m; Fig. 4.2) appears again with dark grey, well-bedded limestone layers. Ammonoids here include *Kl. disciformis* sp. nov., *N. attila*, *N. baconicum*, *Neoprotrachyceras* sp., *S. senticosus*, *Sirenites* sp., *Austrotrachyceras crassicrenulatus* sp. nov., and *Megaphyllites jarbas*, accompanied by a single nautiloid cephalopod (Fig. 4.11B–D). The occurrence of *Neoprotrachyceras* and *S. senticosus* dates the whole Carbonate member to the *Austrotrachyeras austriacum* Zone (Julian 2; Krystyn 1978; Lukeneder *et al.* 2012). The occurrence of *A. crassicrenulatus* sp. nov. within Unit C allows a more detailed classification into the upper part of the *A. austriacum* Zone (Julian 2/II; Krystyn 1978; Lukeneder *et al.* 2012). Unit C bears the first occurrence of *Proarcestes* at Aşağiyaylabel. It inhabited greater depths between 180 and 450 m, as assumed by Hewitt (1996) and Westermann (1996), calculated on shell strength data (e.g. septa and shell).

The composition of the whole Carbonate member (Units A–C) is dominated to 88 per cent by the newly established *K. krystyni* gen. et sp. nov. (Fig. 4.13). This is followed by *Kl. disciformis* sp. nov. (6 per cent), *N. baconicum* (3 per cent), *Sirenites senticosus* (2 per cent) and *A. crassicrenulatus* sp. nov. (1 per cent). The residual species (*N. attila*, *M. jarbas*, and

Si. simonyi) show a maximum of 1 per cent, each occurring with only one specimen (Fig. 4.13).

The Marlstone member (15.3–31.7 m; Fig. 4.2) of the Kasimlar Formation at Aşağiyaylabel consists of calcareous marls and marlstones (Lukeneder *et al.* 2012). The ammonoid fauna is dominated by *P.* cf. *hoetzendorfii*, which constitutes 58 per cent of the whole ammonoid fauna, within this assemblage (Fig. 4.13). Further ammonoids, which belong to this assemblage, are *Proarcestes* sp. (21 per cent), *Sa.* cf. *pilari* (13 per cent), *Sp*. cf. *shastense* (7 per cent), *T*. cf. *beckei* (1 per cent) as well as coleoids represented by some specimens of *Atractites* sp. (Figs 4.11E–G, 4.13). The entire cephalopod assemblage and the occurrence of *Sp*. cf. *shastense* indicate a Tuvalian age (Tuvalian 1, *Tropites dilleri* Zone) for the Marlstone member. The Julian – Tuvalian boundary is marked by a lithological change and by the occurrence of *A*. *crassicrenulatus* sp. nov. immediately below (Carbonate member Unit C) and *Sp*. cf. *shastense* above that boundary (Marlstone member; Lukeneder *et al.* 2012). The deep-water inhabitant *Proarcestes* occurs throughout the Marlstone member and reflects the general drowning trend from the Carbonate member Unit C onward, as also shown by facies analyses (Lukeneder *et al.* 2012).

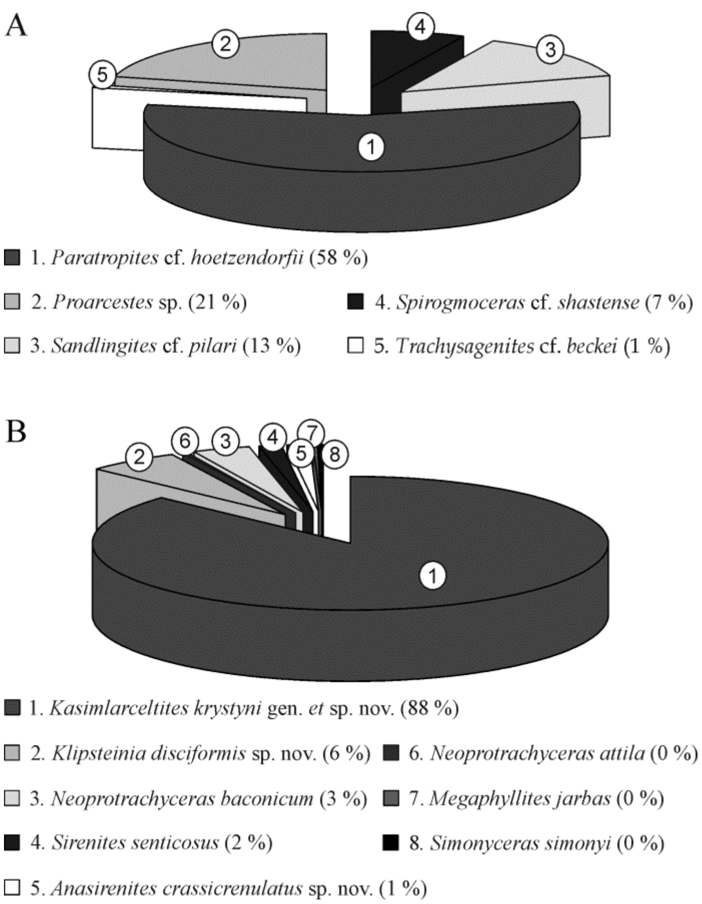

Fig. 4.13. Ammonoid composition from the Carbonate and the Marlstone members of the Kasimlar Formation at Aşağiyaylabel, represented by two pie charts. **A,** Marlstone member, *Tropites dilleri* Zone (Tuvalian 1). **B,** Carbonate member, *Austrotrachyceras austriacum* Zone (Julian 2).

4.7.2. The ammonoid fauna from Aşağiyaylabel in the Tethyan Realm

The ammonoid fauna from Aşağiyaylabel embraces a time interval around the Lower – Upper Carnian boundary within the Upper Triassic. The locality offers one of the few opportunities to investigate ammonoid faunas across the Lower – Upper Carnian boundary. Hence, the section at Aşağiyaylabel represents a key section for a detailed investigation of an ammonoid fauna affected by an environmental turnover. It is one of the few sections in the world that bears a record of lower Upper Carnian to upper Lower Carnian ammonoids (Marco Balini, pers. comm. 2013), a further reason which makes this section highly important. Most of the figured and reported sections are composite stratigraphic sections (Breda *et al.* 2009). Although there are some records of Julian as well as of Tuvalian ammonoids, for example, at the Heiligenkreuz Formation (Dolomites, SA; Keim *et al.* 2006; Breda *et al.* 2009), the majority of Lower – Upper Carnian sections are dated by conodonts (e.g. Lagonegro Basin, Rigo *et al.* 2007). Furthermore, the famous type localities within the Northern Calcareous Alps generally bear well preserved ammonoids, but are usually strongly condensed.

The Carnian is characterized within the Tethys by an intense facies replacement (e.g. carbonate platform and reef demise), the so-called Carnian pluvial episode or Carnian crisis (Simms and Ruffell 1989; Breda *et al.* 2009; Lukeneder *et al.* 2012). At Aşağiyaylabel, this crisis occurred, with a delay of about one ammonoid zone, exactly at the Lower – Upper Carnian substage boundary, time equivalent to the Julian – Tuvalian zone boundary. The mentioned facies alteration is reflected by a turnover from an open-platform margin, to a deeper shelf margin setting, to open, marine-influenced basinal conditions (Lukeneder *et al.* 2012). New Carnian ammonoids detected at Aşağiyaylabel are *K. krystyni* gen. et. sp. nov., *Kl. disciformis* sp. nov., and *A. crassicrenulatus* sp. nov. The new taxa appear at an isolated, but generally connective palaeoceanographic position on the western end of the Cimmerian System.

The almost worldwide distribution of Triassic pelagic to hemipelagic ammonoids during that time makes these cephalopods suitable for biostratigraphic correlations within the Tethyan Realm. Ammonoids are therefore a valuable tool to test palaeoceanographic hypotheses and intercontinental biostratigraphic correlations. The zonation of stages and substages assumed by Mojsisovics (1869, 1870, 1873–1902, 1879, 1882, 1896), Diener (1906, 1917, 1921, 1923), Spath (1934) and Tozer (1967, 1971, 1981, 1984, 1994) is still in use, even though adapted to modern taxonomy (Krystyn 1973, 1978; Mietto *et al.* 2008; Balini *et al.* 2010; Lucas 2010). Detailed work on comparable Upper Triassic ammonoid faunas from the Tethyan Realm was, for example, conducted by Krystyn and Schlager (1971), Tozer (1971, 1981, 1984, 1994), Krystyn (1973, 1978, 1980, 1982), Tatzreiter (1980, 1982), Balini and Jenks (2007) and Balini *et al.* (2007).

4.7.3. Implications for the marine Upper Triassic Mediterranean–Himalayan–Andean Realm

The general Tethyan-wide drastic change within the ammonoid fauna from Lower – Upper Carnian (Julian 2 to Tuvalian 1) is clearly reflected at Aşağiyaylabel. The Julian – Tuvalian boundary, and therefore the Lower – Upper Carnian boundary, is located between the Carbonate and Marlstone members at Aşağiyaylabel (Figs 4.2, 4.12). The locality yields two distinct ammonoid assemblages, the Lower Carnian assemblage from the *Austrotrachyceras austriacum* Zone (Julian 2) and the Upper Carnian assemblage from the *Tropites dilleri* Zone (Tuvalian 1; Fig. 4.12). The stratigraphy and palaeogeography of each species from Aşağiyaylabel are given in Figure 4.12 and Table 4.4.

The Tethyan-wide crisis within the Trachyceratinae affected genera such as *Trachyceras*, *Austrotrachyceras* and *Neoprotrachyceras*. *Trachysagenites* cf. *beckei* is the last representative at the Marlstone member (Tuvalian) of Aşağiyaylabel. During the Lower Carnian (Julian), Trachyceratinae generally flourished within the whole Tethys, as also observable at Aşağiyaylabel (Carbonate member, Julian 2). Characteristic faunal elements of the Carbonate member at Asagiyaylabel are *Sirenites senticosus* and *A. crassicrenulatus* sp. nov., Tethyan-wide known only from the Lower Carnian. The initiation of *P*. cf. *hoetzendorfii* at the Marlstone member (Tuvalian) clearly reflects the radiation of Tropitidae within the whole Tethyan area (Balini *et al.* 2010) from the Tuvalian onward.

The ammonoid fauna from Aşağiyaylabel mirrors the connective palaeoceanographic position of the intrashelf area on the western end of the Cimmerian System. *Spirogmoceras*, *Sandlingites*, *Klipsteinia*, *Neoprotrachyceras*, *Sirenites*, *Anasirenites*, *Paratropites*, *Trachysagenites*, *Proarcestes*, *Megaphyllites* and *Simonyceras* appear with worldwide distribution or at least Tethyan-wide (Fig. 4.12; Table 4.4). These genera are characteristic cephalopods for the Carnian of Tethyan and Andean realms (Balini *et al.* 2010; Lucas 2010). Typical and frequent ammonoids for the Upper Triassic Mediterranean–Himalayan–Andean Realm are *Sandlingites*, *Klipsteinia*, *Neoprotrachyceras*, *Sirenites*, *Anasirenites*, *Paratropites*, *Trachysagenites* and *Simonyceras*. The ammonoid assemblage of Aşağiyaylabel resembles Lower Carnian assemblages of Austria (NCA) and Germany (e.g. Rappoltstein), based on the co-occurrence of *Megaphyllites jarbas*, *Neoprotrachyceras*, *Sirenites* and *Anasirenites*. Clear analogies, strengthening the concept of a Mediterranean–Himalayan–Andean Realm, are detected by comparison and correlation with European, Asian and American faunas. Well-known and comparable sections are in the southern Alps (near St. Cassian, Stuores Wiesen in South Tyrol, northern Italy; Münster 1841; Klipstein 1843; Laube 1870; Neumayr and Uhlig 1880–1881; Mojsisovics 1882; Wöhrmann 1893; Frech 1907; Urlichs 1994), in the Bakony Mountains (Veszprém, Hungary; Mojsisovics 1870, 1893), in the Dinarides (Glamoča, Dragolac, Bosnia and Herzegovina; Bittner 1880; Mojsisovics 1882; Hoernes 1903; Kittl 1903; Diener 1917), and in India (Himalaya) and Timor (Diener 1915, 1921). *Spirogmoceras* cf. *shastense* appears to be a North America–Andean faunal element, typically found in Canada (British Columbia; Tozer 1994) and in the USA (Shasta County, California; Smith 1904, 1927; Hyatt and Smith 1905; Silberling 1956; Tozer 1994).

Further conclusions on the palaeogeography or on migration paths, based on the ammonoid fauna from Aşağiyaylabel, would be highly speculative, and more material from Triassic cephalopod faunas from the Taurus Mountains is needed.

Genus/ species name	Ladinian	Lower Carnian		Upper Carnian	
		Julian 1	Julian 2	Tuvalian 1	Tuvalian 2
Kasimlarceltites krystyni gen. et sp. nov.			AS		
Klipsteinia housiformis sp. nov.			AS		
Neoprotrachyceras attila			NCA, AS		
Neoprotrachyceras baconicum			NCA, AS	NCA	
Sirenites senticosus		NCA, California	NCA, SA, MM, SW-China, AS		
Anasirenites crassicrenulatus sp. nov.			AS		
Megaphyllites jarbas	Dobrudscha, Himalaya	NCA, SA, Greece, B & H, Dobrudscha, WPM (Turkey), Himalaya	NCA, Bavaria, Dobrudscha, Greece, MM (Turkey), AS Himalaya		NCA
Simonyceras simonyi		NCA, SA, WC, Romania, Greece	AS		
Spirogmoceras shastense				AS (cf.), Canada, USA, Mexico	Nevada
Sandlingites pilari				AS (cf.)	B & H
Paratropites hoetzendorfii				AS (cf.)	B & H
Trachysagenites beckei				AS (cf.)	NCA

Table 4.4. Compendium of stratigraphic and palaeogeographic occurrences of all species found at Aşağiyaylabel. **AS,** Aşağiyaylabel; **B & H,** Bosnia and Herzegovina; **MM,** Mersin Melange; **NCA,** Northern Calcareous Alps; **SA,** Southern Alps; **WC,** Western Carpathians; **WPM,** Western Pontian Mountains. Localities that yield species with open nomenclature are indicated with cf. in brackets.

4.8. Conclusions

The macrofauna of the Kasimlar Formation at the Aşağiyaylabel section (Taurus Mountains, Turkey) is mainly represented by ammonoids. A total of 479 ammonoid specimens, two nautiloid specimens and four coleoid specimens were collected and investigated. Material from former excursions and collection type material was correlated with the more recent material (bed-by-bed sampling). The biostratigraphic ammonoid zonation is based on the presence of single ammonoids, assemblage data and composition of the corresponding ammonoid fauna.

The locality offers one of the few opportunities to investigate ammonoid faunas across the Lower – Upper Carnian boundary. Hence, the deposits at Aşağiyaylabel represent a key section for a detailed investigation of an ammonoid fauna affected by an environmental turnover. It is one of the few sections in the world that bears a record of upper Lower Carnian to lower Upper Carnian ammonoids.

The Lower Carnian (*Austrotrachyceras austriacum* Zone) and the Upper Carnian (*Tropites dilleri* Zone) were confirmed by the ammonoid biostratigraphy. The assemblages consist of 12 ammonoid genera with *Kasimlarceltites* gen. nov., *Spirogmoceras*, *Sandlingites*, *Klipsteinia*, *Neoprotrachyceras*, *Sirenites*, *Anasirenites*, *Paratropites*, *Trachysagenites*, *Proarcestes*, *Megaphyllites* and *Simonyceras* bearing 13 species, accompanied by a single coleoid genus with *Atractites*.

The cephalopod fauna drastically changed from the Lower to Upper Carnian (Julian 2 to Tuvalian 1) at Aşağiyaylabel, a change also reflected throughout the Tethyan Realm. The stratigraphically older assemblage, which is dominated by *K. krystyni* gen. et sp. nov. (88 per cent), belongs to the Carbonate member (Units A–C) and is dated as Lower Carnian (Julian 2; *A. austriacum* Zone). The occurrence of *A. crassicrenulatus* sp. nov. at the top of the Carbonate member (Unit C) allows a more detailed classification of Unit C to Julian 2/II.
The second and younger assemblage, which is dominated by *P*. cf. *hoetzendorfii* (58 per cent), belongs to the overlying Marlstone member. The co-occurrence of *P*. cf. *hoetzendorfii* and *Sp*. cf. *shastense* within this member is indicative of Upper Carnian (Tuvalian 1, *T. dilleri* Zone). The occurrence of *Paratropites* confirms a Tuvalian age because the family Tropitidae flourished from the Tuvalian (Upper Carnian) onward, and *Paratropites* is not detected from the Lower Carnian.

Ammonoid assemblages clearly indicate a Mediterranean–Tethyan–Andean affinity, as reported from numerous comparable Upper Triassic (Carnian) localities in East Central Europe (Austria, Germany, Hungary, Italy), Eastern Europe (Bosnia and Herzegovina, Bulgaria, Rumania), Asia (India, Timor, Turkey), Central America (Mexico) as well as North America (Canada, USA).

The ammonoid fauna and facies are correlatable, both indicating a general deepening from open-platform margins, over deeper shelf settings down to an open marine influenced basinal environment reflecting water depths between 180 and 450 m.

The main faunal differences between Aşağiyaylabel and all other known Carnian ammonoid faunas are the newly described *K. krystyni* gen. et. sp. nov., *Kl. disciformis* sp. nov. and *A. crassicrenulatus* sp. nov. Biometric data on shell parameters and ratios (D, H, W, ah, U, H/W, W/D and WER), and comparison of PCAs, support the taxonomic conclusions on the newly established genus and species.

The ammonoid data collection is the first step in producing a detailed biostratigraphic scheme for the Aşağiyaylabel key section, part of the Cimmerian System between the European, African and Asian continents. The main focus of further studies will be to define the mechanisms behind the genesis of ammonoid mass occurrences of *K. krystyni* gen. et sp. nov. Forthcoming analyses will include palaeomagnetic, isotope and geochemical analyses.

4.9. Acknowledgements

This study benefited from grants from the Austrian Science Fund (FWF) within the project P 22109-B17. The authors highly appreciate the help and support from the General Directorate of Mineral Research and Exploration (MTA, Turkey) and are thankful for the digging permission within the investigated area. Special thanks go to Yeşim Íşlamoğlu (MTA, Ankara) for organization and guiding two field trips. The authors thank Leopold Krystyn and Andreas Gindl (University of Vienna), Mathias Harzhauser and Franz Topka (Natural History Museum Vienna) and Philipp Strauss (Austrian Oil Exploration Company OMV, Vienna), who provided material from previous field trips. We are thankful to Martin Maslo (University of Vienna), who supplied an unpublished name revision of the ammonoid holotypes of Mojsisovics' collection. Oleg Mandic (Natural History Museum Vienna) helped with some translation of Croatian and Bosnian literature. Simon Schneider (CASP, Cambridge, United Kingdom) and Thomas Hofmann (Geological Survey of Austria, Vienna) are acknowledged for their support in collecting literature. Photographs of ammonoid specimens were taken by Alice Schumacher (Natural History Museum Vienna). We kindly acknowledge Marco Balini (State University of Milan), Christian Klug (UZH, Zurich) as well as an anonymous reviewer for their comments, which greatly improved the quality of this manuscript. We are grateful to the editor in chief Andrew Smith (Natural History Museum, London) and to the former editor in chief Svend Stouge (Geological Museum, Copenhagen), as well as to the managing editor Julia Sigwart (Queen′s University, Belfast) for their encouragement and helpful comments.

4.10. Data archiving statement

Data for this study are available in the Dryad Digital Repository:
http://dx.doi.org/10.5061/dryad.s0rp6
Editor. Julia Sigwart

4.11. References

AIGNER T. and BACHMANN G.H. 1992. Sequence stratigraphic framework of the German Triassic. *Sedimentary Geology*, **80**, 115–135.

ALLASINAZ A. 1968. Trias in Lombardia. Cephalopodi e Gastropodi dello Julico in Lombardia. *Rivista Italiana di Palaeontologica*, **74**, 327–374.

ANASTASIU V. 1897. Le Trias de la dobrogea. *Bulletin de la Societe Geologique de la France*, *Troisiéme Serie*, **25**, 890–894.

ARKELL W.J. 1950. A classification of the Jurassic ammonites. *Journal of Palaeontology*, **24**, 354–364.

ARKELL W., FURNISH W.M., KUMMEL B., MILLER A.K., MOORE R.C., SCHINDEWOLF O.H., SYLVESTERBRADLEY P.C. and WRIGHT C.W. 1957. Mesozoic Ammonoidea. *In:* MOORE R.C. (ed.). Treatise on invertebrate palaeontology, part L, Mollusca 4. Geological Society of America and the University of Kansas Press, Lawrence, 1–490.

ARTHABER G. 1906. Die alpine Trias des Mediterran Gebietes. Schweizerbart′sche Verlagshandlung (E. Nägerle), Stuttgart, pp. 475.

ARTHABER G. 1914. Die Trias von Bithynien (Anatolien). *Beiträge zur Paläontologie und Geologie Österreich-Ungarns und des Orients*, **27**, 87–206.

ARTHABER G. 1915. Die Entwicklung der Trias in Anatolien. *Mitteilungen der Geologischen Gesellschaft in Wien*, **8**, 47–61.

ARTHABER G. 1927. Ammonoidea Leiostraca aus der oberen Trias von Timor. *Jaarboek van het Mijnwezwn in Nederlandsch Oost-Indie, Verhandelingen*, **1926**,1–174.

ASSERETO R. 1969. Sul significato stratigrafico della ‘Zona ad Avisianus’ del trias medio delle Alpi. *Bolletin Societe Geologic Italia*, **88**, 123–145.

BALINI M. and JENKS J.F. 2007. The Trachyceratidae from South Canyon (Central Nevada): record, taxonomic problems and stratigraphic sequence for the definition of the Ladinian–Carnian boundary. *In*: LUCAS S.G. and SPIELMANN J.A. (eds). The Global Triassic. *New Mexico Museum of Natural History and Science Bulletin*, **41**, 14–22.

BALINI M., GERMANI D., NICORA A. and RIZZI E. 2000. Ladinian/Carnian ammonoids and conodonts from the classic Schilpario-Pizzo Camino area (Lombardy): revaluation of the biostratigraphic support to chronostratigraphy and paleogeography. *Rivista Italiana di Paleontologia e Stratigrafia,* **106**, 19–58.

BALINI M., JENKS J.F., MCROBERTS C.A. and ORCHARD M.J. 2007. The Ladinian–Carnian Boundary succession at South Canyon (New Pass Range, Central Nevada). *In*: LUCAS, S.G. and SPIELMANN J.A. (eds). Triassic of the American West. *New Mexico Museum of Natural History and Science Bulletin*, **40**, 127–138.

BALINI M., LUCAS S.G., JENKS J.F. and SPIELMANN J.A. 2010. Triassic ammonoid biostratigraphy: an overview. *In*: LUCAS S.G. (ed.). The Triassic timescale. *Geological Society of London, Special Publication*, **334**, 221–262.

BITTNER A. 1880. Die Hercegovina und die südöstlichsten Theile von Bosnien. *Jahrbuch der Kaiserlich-Königlichen Geologischen Reichsanstalt*, **30**, 353–438.

BITTNER A. 1882. Neue Petrefactenfundorte im Lias und in der Trias der Salzburger Alpen. *Verhandlungen der Kaiserlich-Königlichen Geologischen Reichsanstalt*, **16**, 317–319.

BRANCO W. 1880. Beiträge zur Entwicklungsgeschichte der fossilen Cephalopoden. Palaeontographica. *Beiträge zur Naturgeschichte der Vorzeit*, **27**,12–81.

BREDA A., PRETO N., ROGHI G., FURIN S., MENEGUOLO R., RAGAZZI E., FEDELE P. and GIANOLLA F. 2009. The Carnian Pluvial Event in the Tofane area (Cortina d’Ampezzo, Dolomites, Italy). *GeoAlp*, **6**, 80–115.

ĆORIĆ S. 1999. Die geologische Erforschung von Bosnien und der Herzegowina und der Grundlegende Beitrag der Österreichischen Geologen. *Abhandlungen der Geologischen Bundesanstalt*, **56/1**, 117–152.

DAGYS A.S. 1988. Major features of the geographic differentiation of Triassic ammonoids. *In*: WIEDMANN J. and KULLMANN J. (eds). Cephalopods present and past. E. Schweizerbart'sche Verlagshandlung, Stuttgart, 341–349.

DIENER K. 1906. Fauna of the Tropites-limestone of Byans. *Palaeontologia Indica*, *15th Series*, **5**, 1–201.

DIENER K. 1908. Ladinic, Carnic and Noric Fauna of Spiti. Memoirs of the Geological Survey of India, *Palaeontologia Indica*, **15**, 1–157.

DIENER K. 1909. Fauna of the *Traumatocrinus* limestone of Painkhanda. *Palaeontologia Indica*, **15**, 1–39.

DIENER K. 1915. Part 8, Cephalopoda Triadica. *In*: *Frech* F. (ed.). Fossilium Catalogus I, Animalia. W. Junk, Berlin, 1–369.

DIENER K. 1916. Die marinen Reiche der Triasperiode. *Denkschriften der Kaiserlichen Akademie der Wissenschaften*, **92**, 405–549.

DIENER K. 1917. Gornjotriadićka fauna cefalopoda iz Bosne. *Glasnik Zemaljskog muzeja u Bosni i Hercegovini*, **28 (1916)**, 359–396.

DIENER K. 1921. Neue Tropitoidea aus den Hallstätter Kalken des Salzkammergutes. *Denkschriften der Akademie der Wissenschaften in Wien, Mathematisch-Naturwissenschaftliche Klasse*, **97**, 465–519.

DIENER K. 1923. Ammonoidea Trachyostraca aus der Mittleren und Oberen Trias von Timor. *Jaarboek van het Mijnwezen in Nederlandsch Oost-Indie, Verhandelingen*, **1920.4**, 75–276.

DIENER K. 1925. Leitfossilien der Trias. Gebrüder Bornträger, Berlin, pp. 118.

DITTMAR A.V. 1866. Zur Fauna der Hallstädter Kalke. *Geognostisch-Palaeontologische Beiträge*, **2**, 319–398.

DUMONT J.F. 1976. Etudes géologiques dans les Taurides Occidentales: Les formations paléozoiques et mésozoiques de la coupole de Karacahisar (Province d'Isparta, Turquie). Unpublished PhD thesis, University of South Paris, pp. 213.

DUMONT J.F. and KEREY E. 1975. The Kirkavak Fault. *Bulletin of the Geological Society of Turkey*, **18**, 59–62.

FRECH F. 1907. Die Hallstätter Kalke bei Epidauros (Argolis) und ihre Cephalopoden. *Neues Jahrbuch für Mineralogie, Geologie und Palaeontologie, Festband*, **1907**, 1–32.

FRECH F. and RENZ C. 1906. Sur la repartition du Trias à facies océanique en Grèce. *Comptes Rendus Hebdomadaires des Séances de l' Academie des Sciences*, **143**, 523–525.

GALLET Y., KRYSTYN L., MARCOUX J. and BESSE J. 2007. New constraints on the End-Triassic (Upper Norian–Rhaetian) magnetostratigraphy. *Earth and Planetary Science Letters*, **255**, 458–470.

GEYER G. 1915. Aus den Umgebungen von Mitterndorf und Grundlsee. *Jahrbuch der Kaiserlich-Königlichen Geologischen Reichsanstalt*, **65**, 177–238.

GINDL A. 2000. Paläoökologie triassischer Ammonitenfaunen des Taurusgebirges (Türkei). Unpublished Diploma thesis, University of Vienna, pp. 80.

GUTNIC M., MONOD O., POISSON A. and DUMONT J.F. 1979. Géologie des Taurides Occidentales (Turquie). *Mémoire de la Société Géologique de France*, **137**, 1–112.

HAHN L. 1976. Stratigraphie und Palaeogeographie des kontinentalen Mesozoikums in Nord Thailand. *Geologisches Jahrbuch Reihe B*, **21**, 155–169.

HAHN L. 1982. The Triassic in Thailand. *Geologische Rundschau*, **71**, 1041–1056.

HAMMER Ø., HARPER D.A.T. and RYAN P.D. 2001. PAST: Paleontological statistics software package for education and data analysis. *Palaeontologia Electronica*, **4 (1)**, pp. 9.

HAUER F.R. 1846. Über die Cephalopoden des Muschelmarmors von Bleiberg. *Haidinger's Naturwissenschaftliche Abhandlungen*, **1**, 22–25.

HAUER F.R. 1847. Neue Cephalopoden von Aussee. *Haidinger's Naturwissenschaftliche Abhandlungen*, **1**, 257–277.

HAUER F.R. 1849. Über neue Cephalopoden aus den Marmorschichten von Hallstatt und Aussee. *Haidinger´s Naturwissenschaftliche Abhandlungen*, **3**, 1–26.

HAUER F.R. 1855. Beiträge zur Cephalopoden-Fauna der Hallstätter Schichten. *Denkschriften der Mathematisch-Naturwissenschaftlichen Klasse der Kaiserlichen Akademie der Wissenschaften*, **9**, 141–166.

HAUER F.R. 1860. Nachträge zur Kenntnis der Caphalopoden-Fauna der Hallstätter Schichten. *Sitzungsberichte der Akademie der Wissenschaften*, **41**, 113–150.

HAUG E. 1894. Les ammonites du Permien et du Trias. *Bulletin de la Société Géologique de France*, **33 (22)**, 1–411.

HEWITT R.A. 1996. Architecture and strength of the ammonoid shell. *In*: LANDMAN, N.H., TANABE K. and DAVIS R.A. (eds). Ammonoid paleobiology. Topics in geobiology, Vol. 13, Plenum Press, New York, 297–339.

HOERNES R. 1903. Zur Ontogenie und Phylogenie der Cephalopoden. *Jahrbuch der Kaiserlich-Königlichen Reichsanstalt*, **53**, 1–32.

HORNUNG T. and BRANDNER R. 2005. Biochronostratigraphy of the Reingraben Turnover (Hallstatt Facies Belt): local black shale events controlled by regional tectonics, climatic change and plate tectonics. *Facies*, **51**, 475–494.

HORNUNG T., SPATZENEGGER A. and JOACHIMSKI M.M. 2007. Multistratigraphy of condensed ammonoid beds of the Rappolstein (Berchtesgaden, southern Germany): unravelling palaeoenvironmental conditions on ‘Hallstatt deep swells’ during the Reingraben Event (Late Lower Carnian). *Facies*, **53**, 267–292.

HYATT A. 1884. Genera of fossil cephalopods. *Proceedings of Boston Society of Natural History*, **22**, 253–338.

HYATT A. 1900. Cephalopods. *In*: EASTMAN C.R. (ed.). Text-Book of Palaeontology, First English edition. MacMillan and Co., London, 502–604.

HYATT A. and SMITH J.P. 1905. The Triassic cephalopod genera of America. *United States Geological Survey Professional Paper*, **40**, 1–394.

IBM CORP. 2012. IBM SPSS statistics for Windows, version 21.0. IBM Corporation, Armonk, NY.

KEIM L., SPÖTL C. and BRANDNER R. 2006. The aftermath of the Carnian carbonate platform demise: a basinal perspective (Dolomites, Southern Alps). *Sedimentology*, **53**, 361–386.

KITTL E. 1903. Salzkammergut. Geologische Exkursionen unter der Führung von E. Kittl. *Führer für die Exkursion des 9. Internationalen Geologischen Kongress*, Wien, pp. 118.

KITTL E. 1908. Kenntnis der Triasbildungen der nordöstlichen Dobrudscha. *Denkschriften der Mathematisch-Naturwissenschaftlichen Klasse der Kaiserlichen Akademie der Wissenschaften*, **81**, 447–532.

KLIPSTEIN A.V. 1843. Beiträge zur Geologischen Kenntnis der östlichen Alpen. Georg Friedrich Heyer´s Verlag, Giessen, pp. 312.

KLUG C. 2001. Life-cycles of some Devonian ammonoids. *Lethaia*, **34**, 215–233.

KOLLÁROVÁ-ANDRUSOVOVÁ V. and KOCHANOVÁ M. 1973. Molluskenfauna des Bleskový pramen bei Drnava (Nor, Westkarpaten). Slowakische Akademie der Wissenschaften, Bratislava, pp. 115.

KORN, D. 2000. Morphospace occupation of ammonoids at the Devonian–Carboniferous Boundary. *Paläontologische Zeitschrift*, **74**, 247–259.

KOZUR H.W., MOIX P. and OZSVÁRT P. 2009. New Spumellaria (Radiolaria) from the Early Tuvalian *Spongotortilispinus moixi* Zone of southeastern Turkey, with some remarks on the age of this fauna. *Jahrbuch der Geologischen Bundesanstalt*, **149**, 25–59.

KRYSTYN L. 1973. Zur Ammoniten- und Conodonten-Stratigraphie der Hallstätter Obertrias (Salzkammergut, Österreich). *Verhandlungen der Geologischen Bundesanstalt*, **1973/1**, 113–115.

KRYSTYN L. 1978. Eine neue Zonengliederung im alpin-mediterranen Unterkarn. Schriftenreihe der Erdwissenschaftlichen Kommissionen. *Österreichische Akademie der Wissenschaften*, **4**, 37–75.

KRYSTYN L. 1980. Stratigraphy of the Hallstatt region. *Abhandlungen der Geologischen Bundesanstalt in Wien*, **35**, 69–98.

KRYSTYN L. 1982. Obertriassische Ammonoideen aus dem zentralnepalesischen Himalaya (Gebiet von Jomsom). *Abhandlungen der Geologischen Bundesanstalt in Wien*, **36**, 1–63.

KRYSTYN L. and SCHLAGER W. 1971. Der Stratotypus des Tuval. *Annales Instituti Geologici Publici Hungarici*, **54**, 591–605.

KUTASSY A. 1927. Beiträge zur Stratigraphie und Paläontologie der Alpinen Triasschichten in der Umgebung von Budapest. *Jahrbuch der Königlichen Ungarischen Geologischen Anstalt*, **27**, 105–175.

KUTASSY A. 1932. Cephalopoda triadica 2. *Fossilium Catalogus*, **56**, 372–832.

LAUBE G.C. 1864. Bemerkungen über die Münster´schen Arten von St. Cassian in der Münchner paläontologischen Sammlung. *Jahrbuch der Kaiserlich-Königlichen Geologischen Reichsanstalt*, **14**, 402–412.

LAUBE G.C. 1868. Cephalopoden von St. Cassian. *Sitzungsberichte der Kaiserlichen Akademie der Wissenschaften*, **1868**, pp. 539.

LAUBE G.C. 1870. Die Fauna der Schichten von St. Cassian. *Denkschriften der Akademie der Wissenschaften, Wien*, **30**, 1–106.

LUCAS S.G. 2010. The Triassic chronostratigraphic scale: history and status. *In*: LUCAS S.G. (ed.). The Triassic timescale. *Geological Society, Special Publication*, **334**, 17–39.

LUCAS S.G. and ESTEP J.W. 1999. Permian, Triassic and Jurassic stratigraphy, biostratigraphy, and sequence stratigraphy in the Sierra del Alamo Muerto, Sonora, Mexico. *Geological Society of America Special Paper*, **340**, 271–286.

LUKENEDER S. and LUKENEDER A. 2013. *Data from*: A new ammonoid fauna from the Carnian (Upper Triassic) Kasimlar Formation of the Taurus Mountains (Anatolia, Turkey). Dryad Digital Repository. http://dx.doi.org/10.5061/ dryad.s0rp6

LUKENEDER S., LUKENEDER A., HARZHAUSER M., İSLAMOĞLU Y., KRYSTYN L. and LEIN R. 2012. A delayed carbonate factory breakdown during the Tethyan-wide Carnian Pluvial Episode along the Cimmerian terranes (Taurus, Turkey). *Facies*, **58**, 279–296.

MANFRIN S., MIETTO P. and PRETO N. 2005. Ammonoid biostratigraphy of the Middle Triassic Latemar platform (Dolomites, Italy) and its correlation with Nevada and Canada. *Geobios*, **38**, 477–504.

MASUTOMI K. and HAMADA T. 1966. Fossils in colour. Hoikusha Publishing Co., Osaka, pp. 268.

MIETTO P., BURATTI N., CIRILLI S., DE ZANCHE V., GIANOLLA P., MANFRIN S., NICORA A., PRETO N., RIGO M. and ROGHI G. 2007a. New constraints for the Ladinian–Carnian boundary in the southern Alps: suggestions for global correlation. *In:* LUCAS S.G. and SPIELMANN J.A. (eds). The global Triassic. *New Mexico Museum of Natural History and Science Bulletin*, **41**, 275–281.

MIETTO P., ANDREETTA R., BROGLIO LORIGA C., BURATTI N., CIRILLI S., DE ZANCHE V., FURIN S., GIANOLLA P., MANFRIN S., MUTTONI G., NERI C., NICORA A., POSENATO R., PRETO N., RIGO M., ROGHI G. and SPÖTL C. 2007b. A candidate of the global stratotype section and point for the base of the Carnian Stage (FAD of Daxatina) in the Prati di Stuores/Stuores Wiesen section (Southern Alps, NE Italy). *Albertiana*, **36**, 78–97.

MIETTO P., MANFRIN S., PRETO N. and GIANOLLA P. 2008. Selected ammonoid fauna from Prati di Stuores/Stuores Wiesen and related sections across the Ladinian–Carnian boundary (Southern Alps, Italy). *Rivista Italiana di Paleontologia e Stratigrafia*, **114**, 377–429.

MOIX P., BECCALETTO L., MASSET O., KOZUR H.W., DUMITRIĆA P., VACHARD D., MARTINI R. and STAMPFLI G.M. 2011. Geology and Correlation of the Mersin Mélanges, Southern Turkey. *Turkish Journal of Earth Sciences*, **20**, 57–98.

MOJSISOVICS E. 1869. Über die Gliederung der oberen Triasbildungen der östlichen Alpen. *Jahrbuch der Kaiserlich-Königlichen Geologischen Reichsanstalt*, **19**, 91–149.

MOJSISOVICS E. 1870. Beiträge zur Kenntnis der Cephalopoden-Fauna der oenischen Gruppe. *Jahrbuch der Kaiserlich-Königlichen Reichsanstalt*, **20**, 93–112.

MOJSISOVICS E. 1873–1902. Das Gebirge um Hallstatt, erste Abtheilung. Die Cephalopoden der Hallstätter Kalke, erster Band. *Abhandlungen der Kaiserlich-Königlichen Geologischen Reichsanstalt*, **6/1**, 1–82, 83–174, 175–356.

MOJSISOVICS E. 1879. Vorläufige kurze Übersicht der Ammoniten-Gattungen der Mediterranen und Juvavischen Trias. *Verhandlungen der Kaiserlich-Königlichen Geologischen Reichsanstalt*, **7**, 133–143.

MOJSISOVICS E. 1882. Die Cephalopoden der Mediterranen Triasprovinz. *Abhandlungen der Kaiserlich-Königlichen Geologischen Reichsanstalt*, **10**, 1–322.

MOJSISOVICS E. 1893. Das Gebirge um Hallstatt, erste Abtheilung. Die Cephalopoden der Hallstätter Kalke, zweiter Band. *Abhandlungen der Kaiserlich-Königlichen Geologischen Reichsanstalt, Wien*, **6/2**, 1–835.

MOJSISOVICS E. 1896. Beiträge zur Kenntnis der Obertriadischen Cephalopoden-Fauna des Himalaya. *Denkschriften der Mathematisch-Naturwissenschaftlichen Klasse der Kaiserlichen Akademie der Wissenschaften*, **63**, 1–120.

MONNET C., BUCHER H., GUEX J. and WASMER M. 2012. Large-scale evolutionary trends of Acrochordiceratidae Arthaber, 1911 (Ammonoidea, Middle Triassic) and Cope's rule. *Palaeontology*, **55**, 87–107.

MONOD O. 1977. Recherches géologiques dans le Taurus Occidental au sud de Beyşehir (Turquie). University of South Paris, unpublished Dissertation, pp. 442.

MÜNSTER G.V. 1834. Über das Kalkmergellager von St. Cassian in Süd-Tirol und die darin vorkommenden Ceratiten. Leonhard und Bronn's Neues Jahrbuch für Mineralogie, Geologie und Petrefaktenkunde. E. Schweizerbart'sche Verlagshandlung, Stuttgart, pp. 15.

MÜNSTER G.V. 1841. Beschreibung und Abbildung der in den Kalkmergelschichten von St. Cassian gefundenen Versteinerungen. *Beiträge zur Petrefacten-Kunde*, **4**, 25–152.

NEUMAYR M. 1879. Zur Kenntnis der Fauna des untersten Lias in den Nordalpen. *Abhandlungen der Kaiserlich-Königlichen Geologischen Reichsanstalt*, **7**, 1–46.

NEUMAYR M. and UHLIG V. 1880–1881. Über Ammonitiden aus den Hilsbildungen Norddeutschlands. Palaeontographica. *Beiträge zur Naturgeschichte der Vorzeit*, **27**, 129–203.

ÖZGÜL N. and ARPAT E. 1973. Structural units of Taurus orogenic belt and their continuation in the neighbouring regions. *Bulletin of the Geological Society of Greece*, **10**, 156–164.

POISSON A. 1977. Recherches géologiques dans les Taurides occidentals (Turquie). University of South Paris, Dissertation, pp. 759.

QUENSTEDT F.A. 1846–1849. Cephalopoden. *Petrefactenkunde Deutschlands*, **1**, 1–580.

RAKÚS M. 1993. Late Triassic and Early Jurassic Phylloceratids from the Salzkammergut (Northern Calcareous Alps). *Jahrbuch der Geologischen Bundesanstalt*, **136**, 933–963.

RENZ C. 1907. Zur Geologie Griechenlands. A. Trias in der Argolis und auf Hydra. *Verhandlungen der Österreichischen Geologischen Reichsanstalt*, **41**, 11–98.

RENZ C. 1909. Etudes Stratigraphiques et Paleontologiques sur le Lias et le Trias en Gréce. *Bulletin de la Société Géologique de France, Quatriéme Série*, **9**, 249–273.

RENZ C. 1910. Stratigraphische Untersuchungen im griechischen Mesozoikum und Paläozoikum. *Jahrbuch der Kaiserlich-Königlichen Geologischen Reichsanstalt*, **60**, 421–636.

RENZ C. 1911. Die mesozoischen Faunen Griechenlands. Palaeontographica. *Beiträge zur Naturgeschichte der Vorzeit*, **58**, 1–104.

RENZ C. 1922. Neue griechische Trias Ammoniten. *Verhandlungen der Naturforschenden Gesellschaft in Basel*, **33**, 218–255.

RIGO M., PRETO N., ROGHI G., TATEO F. and MIETTO P. 2007. A rise in the Carbonate Compensation Depth of the western Tethys in the Carnian (Late Triassic): deep-water evidence for the Carnian Pluvial Event. *Palaeogeography, Palaeoclimatology, Palaeoecology*, **246**, 188–205.

ROBERTSON A.H.F. 1993. Mesozoic–Tertiary sedimentary and tectonic evolution of Neotethyan carbonate platforms, margins and small ocean basins in the Antalya Complex, southwest Turkey. *Special Publications of International Association of Sedimentologists*, **20**, 415–465.

ROBERTSON A.H.F. 2000. Mesozoic–Tertiary tectonic-sedimentary evolution of a south Tethyan Oceanic Basin and its margins in southern Turkey. *Geological Society, London, Special Publications*, **173**, 97–138.

ROBERTSON A.H.F., POISSON A. and AKINCI Ö. 2003. Developments in research concerning Mesozoic–Tertiary Tethys and neotectonics in the Isparta Angle, SW Turkey. *Geological Journal*, **38**, 195–234.

SENEL M. 1997. Geological map of Turkey. Nr. 4, Isparta Paftasi, Department of Geology, Ankara, pp. 23.

SEPKOSKI J.J.Jr 2002. A Compendium of Fossil Marine Animal Genera. *Bulletin of American Palaeontology*, **363**, 1–560.

SHEVYREV A.A. 1990. Ammonoids and chronostratigraphy of the Triassic. Nauka, Moskow, pp. 179.

SILBERLING N.J. 1956. '*Trachyceras* Zone' in the Upper Triassic of the western United States. *Journal of Paleontology*, **30**, 1147–1153.

SILBERLING N.J. 1961. Upper Triassic marine Mollusks from the Natchez pass formation in northwestern Nevada. *Journal of Paleontology*, **35**, 535–542.

SIMMS M.J. and RUFFELL A. 1989. Synchroneity of climatic change and extinctions in the Late Triassic. *Geology*, **17**, 265–268.

SMITH J.P. 1896. Classification of marine Trias. *The Journal of Geology*, **4**, 385–398.

SMITH J.P. 1904. The comparative stratigraphy of the marine Trias of Western America. *Proceedings of the California Academy of Sciences, Third Series*, **1**, 323–430.

SMITH J.P. 1913. Ammonoidea. *In*: EASTMAN, C. R. (ed.). Text-Book of Paleontology. Second English edition, Vol. 1. Macmillan and Co., London, 617–677.

SMITH J.P. 1927. Upper Triassic marine invertebrate faunas of North America. *United States Geological Survey, Professional Paper*, **141**, 1–261.

SPATH L.F. 1930. Eotriassic invertebrate fauna of East Greenland. *Meddelelser om Groenland*, **83**, 1–90.

SPATH L.F. 1934. The Ammonoidea of the Trias. *Catalogue of the Fossil Cephalopoda in the British Museum (Natural History)*, **4**, 1–521.

SPATH L.F. 1951. The Ammonoidea of the Trias (II). *Catalogue of the Fossil Cephalopoda in the British Museum (Natural History)*, **5**, 1–228.

STAMPFLI G.M. and BOREL G.D. 2002. A plate tectonic model for the Paleozoic and Mesozoic constrained by dynamic plate boundaries and restored synthetic oceanic isochrons. *Earth and Planetary Science Letters*, **196**, 17–33.

TATZREITER F. 1980. Neue trachyostrake Ammonoideen aus dem Nor (Alaun 2) der Tethys. New Upper Triassic (Columbianus Zone, Norian) ammonoids from the Tethys. *Verhandlungen der Geologischen Bundesanstalt*, **2**, 123–159.

TATZREITER F. 1982. Katalog der Typen und Abbildungsoriginale der Geologischen Bundesanstalt. Dritter Teil: Typen, Abbildungsoriginale und Belegstücke zu Mojsisovics, E. v. (1893): Die Cephalopoden der Hallstätter Kalke. *Verhandlungen der Geologischen Bundesanstalt*, **2**, 123–147.

TOLLMANN A. 1976. Analyse des klassischen nordalpinen Mesozoikums: Stratigraphie, Fauna und Fazies der Nördlichen Kalkalpen. Monographie der Nördlichen Kalkalpen 2. Franz Deuticke, Wien, pp. 580.

TOZER E.T. 1967. A standard of Triassic time. *Geological Survey of Canada, Bulletin*, **156**, 1–103.

TOZER E.T. 1971. Triassic time and ammonoids. Problems and proposals. *Canadian Journal of Earth Sciences*, **8**, 989–1031.

TOZER E.T. 1981. Triassic Ammonoidea: geographic and Stratigraphic Distribution. *In*: HOUSE, M.R. and SENIOR, J.R. (eds). The Ammonoidea. The Systematic Association Special Volume, 18, Academic Press, London, 397–432.

TOZER E.T. 1984. The Trias and its ammonoids: the evolution of a time scale. *Geological Survey of Canada Miscellaneous Report*, **35**, 1–171.

TOZER E.T. 1994. Canadian Triassic Ammonoid Faunas. *Geological Survey of Canada, Bulletin*, **467**, 1–663.

URLICHS M. 1994. *Trachyceras laube* 1869 (Ammonoidea) aus dem Unterkarn (Obertrias) der Dolomiten (Italien). *Stuttgarter Beiträge zur Naturkunde Serie B (Geologie und Palaeontologie)*, **217**, 1–55.

URLICHS M. 2004. Kümmerwuchs bei *Lobites* Mojsisovics, 1902 (Ammonoidea) aus dem Unter-Karnium der Dolomiten (Ober-Trias, Italien) mit Revision der unterkarnischen Arten. Stunting in *Lobites* MOJSISOVICS, 1902 (Ammonoidea) from the Lower Karnian of the Dolomites (Upper Triassic, Italy) with revision of the Lower Carnian species. *Stuttgarter Beiträge zur Naturkunde Serie B (Geologie und Palaeontologie)*, **344**, 1–37.

WÄHNER F. 1882–1898. Beiträge zur Kenntnis der tieferen Zonen des Unteren Lias in den nordöstlichen Alpen 1–8. *Beiträge zur Geologie und Paläontologie Österreich und Ungarns*, **2–11**, 1–291.

WELTER O. 1915. Die Ammoniten und Nautiliden der ladinischen und anisischen Trias von Timor. *Palaeontologie von Timor*, **5**, 71–136.

WESTERMANN G.E.G. 1996. Ammonoid Life and Habitat. 607–707. *In*: LANDMAN N.H., TANABE K. and DAVIS R.A. (eds). Ammonoid Paleobiology. Topics in Geobiology, Vol. 13, Plenum, New York, pp. 857.

WIEDMANN J. 1970. Über den Ursprung der Neoammonoideen. Das Problem einer Typogenese. *Eclogae Geologicae Helvetiae*, **63**, 923–1020.

WÖHRMANN S. FRH. 1893. Die Raibler Schichten. *Jahrbuch der Kaiserlich-Königlichen Geologischen Bundesanstalt*, **43**, 617–768.

XIAOFENG W., BACHMANN G.H., HAGDORN H., SANDER P.M., CUNY G., XIAOHONG C., CHUANSHANG W., LIDE C., LONG C., FANSONG M. and GUANGHONG X. 2008. The Late Triassic Black Shales of the Guanling Area, Guizhou Province, South-West China: a unique marine Reptile and pelagic Crinoid fossil Lagerstätte. *Palaeontology*, **51**, 27–61.

YURTTAS-ÖZDEMIR Ü. 1973. Kocaeli yarımadası Tepeköy Triyasının biyostratigraf ve makrofaunası (Biostratigraphy and Macrofauna of the Tepeköy Triassic, Kocaeli Peninsula, in Turkish). *Maden Tetkik ve Arama Dergisi*, **77**, 57–98.

ZITTEL K.A. v. 1884. Paläozoologie. II. Handbuch der Palaeontologie 1, Oldvenbourg, München and Leipzig, pp. 983.

CHAPTER V,

PUBLISHED 2014 IN COMPUTERS AND GEOSCIENCES 64: 104–114.

COMPUTED RECONSTRUCTION OF SPATIAL AMMONOID-SHELL ORIENTATION CAPTURED FROM DIGITIZED GRINDING AND LANDMARK DATA

Susanne Lukeneder[a], AlexanderLukeneder[a], Gerhard W. Weber[b]

[a] Natural History Museum Vienna, Geological-Paleontological Department, Burgring7, A-1010 Vienna, Austria

[b] Department of Anthropology, University of Vienna, Althanstraße 14, A-1090 Vienna, Austria

Abstract

The internal orientation of fossil mass occurrences can be exploited as useful source of information about their primary depositional conditions. A series of studies, using different kinds of fossils, especially those with elongated shape (e.g., elongated gastropods), deal with their orientation and the subsequent reconstruction of the depositional conditions (e.g., paleocurrents and transport mechanisms). However, disk-shaped fossils like planispiral cephalopods or gastropods were used, up to now, with caution for interpreting paleocurrents. Moreover, most studies just deal with the topmost surface of such mass occurrences, due to the easier accessibility. Within this study, a new method for three-dimensional reconstruction of the internal structure of a fossil mass occurrence and the subsequent calculation of its spatial shell orientation is established. A 234 million-years-old (Carnian, Triassic) monospecific mass occurrence of the ammonoid *Kasimlarceltites krystyni* from the Taurus Mountains in Turkey, embedded in limestone, is used for this pilot study. Therefore, a 150 x 45 x 140 mm^3 block of the ammonoid bearing limestone bed has been grinded to 70 slices, with a distance of 2 mm between each slice. By using a semi-automatic region growing algorithm of the 3D-visualization software Amira, ammonoids of a part of this mass occurrence were segmented and a 3D-model reconstructed. Landmarks, trigonometric and vector-based calculations were used to compute the diameters and the spatial orientation of each ammonoid. The spatial shell orientation was characterized by dip and dip-direction and aperture direction of the longitudinal axis, as well as by dip and azimuth of an imaginary sagittal-plane through each ammonoid. The exact spatial shell orientation was determined for a sample of 675 ammonoids, and their statistical orientation analyzed (i.e., NW/SE). The

study combines classical orientation analysis with modern 3D-visualization techniques, and establishes a novel spatial orientation analyzing method, which can be adapted to any kind of abundant solid matter.

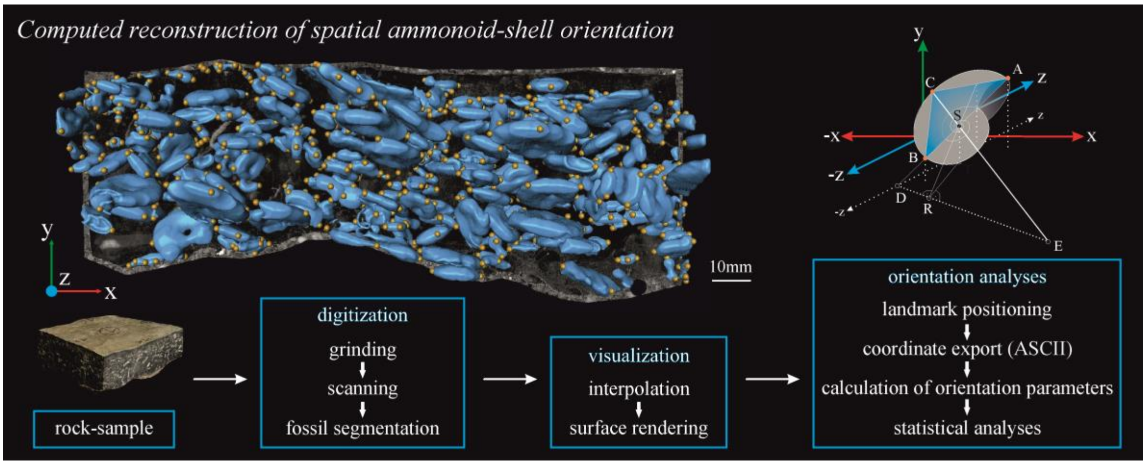

Graphical Abstract. Steps for computed reconstruction of spatial ammonoid-shell orientation.

Keywords: Spatial shell orientation, Destructive 3D-visualization, Amira 3D-software, Triassic ammonoids, Mass occurrences, Stereographic analyses.

5.1. Introduction

5.1.1. Mass occurrences and their internal orientation as key to paleoenvironments

Abundant marine fossils, especially with elongated shapes (e.g., belemnites), are useful indicators to draw conclusions about influencing factors (e.g., sea floor paleocurrents and transport mechanisms) of paleoenvironments. Since Hall (1843) regarded the orientation of brachiopod valves as current induced, a series of studies have been conducted concerning fossil orientation measurements (Potter and Pettijohn 1977). Orthocone cephalopods (e.g., nautiloids like *Orthoceras*; Wendt *et al.* 1984; Wendt 1995), gastropods (e.g., Seilacher 1959, 1960; Wendt 1995; Cataldo *et al.* 2013), bivalves (Kelling and Moshrif 1977), foraminifers (King 1948), tentaculite shells (Hladil *et al.* 1996), trilobites (Seilacher 1959, 1960) and vertebrate bones (e.g. Vasiļkova *et al*. 2012) have been used so far in field-based spatial orientation studies (Flügel 2004). Kidwell *et al.* (1986) analyzed two-dimensional geometries of skeletal accumulations with focus on their preferred orientation. However, the indication of current patterns is not only restricted to fossils with elongated basic shape and their nature to be reoriented by any kind of current. Planispirally coiled (disk-shaped) forms like gastropods, but also cephalopods such as ammonoids can also provide such depositional information (e.g., Futterer 1982; Wendt 1995; Lukeneder 2005; Olivero 2007; Seilacher 1971; Wani 2006, 2007).

The main aim of this study is to present a novel method for analyzing spatial orientation, which can be adapted to all kinds of abundant solid matter such as fossils and particles or to geological features such as faults, folds or rock core analyses.

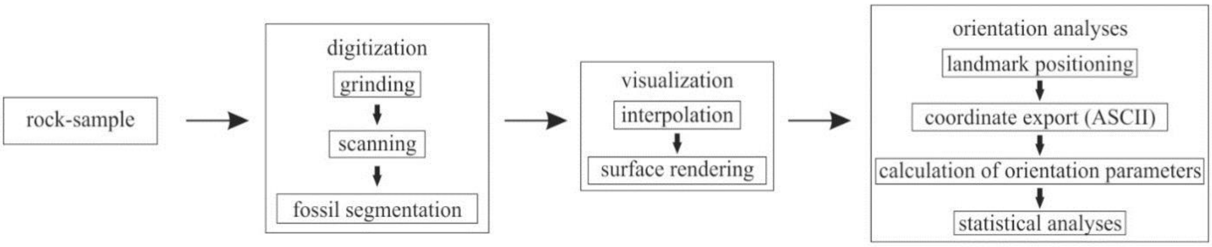

Fig. 5.1. Steps used for digitization and visualization of the ammonoids as well as for subsequent calculation and evaluation of their spatial shell-orientation.

5.1.2. Serial-grinding as possible alternative to computed tomography

The application of 3D-visualization on different kinds of objects and in different scientific fields has increased enormously. Since Sollas (1903) introduced the method of serial sectioning within his work on Therapsida and Lysorophia (Camp and Hanna 1937), 3D-visualization has been adapted for a wide field of paleontological studies (e.g., VanderHoof 1931; Simpson 1933; Koslowski 1932; Stensiö 1927; Fourie 1974; Conroy and Vannier 1984; Ketcham and Carlson 2001; Marschallinger 2001, 2011; Dockner 2006; Sutton 2008; Garwood *et al.* 2010; Briguglio *et al*. 2011; Kruta *et al.* 2011; Lukeneder 2012). The most obvious method used for digitization today is computed tomography (CT) with all its derivatives (e.g., macro-CT, µ-CT, nano-CT, etc.). However, CT is not always successful, particularly when the density contrast of the involved materials is too low. This is exactly the case for the herein presented ammonoid mass occurrence, caused by the almost equal density of the ammonoid shells (i.e., secondary calcite shells, 2.6–2.8 g/cm^3) and the embedding source rock (limestone, 2.8 g/cm^3). Therefore, we applied the classic method of serial-grinding, despite its invasive and (partially or entirely) destructive character. If samples are large enough to sacrifice fractions of it, serial grinding represents a good alternative in cases when digital recording methods fail, because in addition to a good resolution, color information (not available in CT-scans) can be obtained as well.

In our approach, we focus on the three-dimensional reconstructions of the ammonoids from the entire bed, instead of focusing on the fossil orientation on the surface of a sedimentary horizon. This and the spatial analysis of their orientation within a stereographic projection plot are the main innovations of this study compared to other conventional fossil-orientation-studies. An overview over the entire approach, from fossil collection to orientation analyses, can be gleaned from Fig. 5.1.

5.2. Paleontological material

The directional data are derived from a monospecific (>99%) ammonoid mass occurrence of *Kasimlarceltites krystyni* (Lukeneder and Lukeneder, in press). The mass occurrence is situated within the Taurus Mountains of Turkey, at the Kasimlar Formation of the section Aşağiyaylabel, about 90 km northeast of Antalya and 70 km southeast of Isparta (WGS 84, N 37.551389° E 31.304444°; Fig. 5.2A). It is part of a limestone bed (Fig. 5.2 A and B), deposited during the Late Triassic (234 mya) within an intrashelf-basin at the western end of the “Cimmerian terranes” (western Tethys Ocean; Şengör *et al.* 1984; Dercourt *et al*. 1993, 2000; Gindl 2000; Scotese *et al*. 1989; Scotese 1998, 2001; Stampfli and Borel 2002; Stampfli *et al*. 2002; Lukeneder *et al.* 2012). The deposition of this mass occurrence during an important time-slice makes them suitable for investigations related to conclusions about its paleoenvironment. The reference material of this limestone bed has been collected during a field trip in 2007. The resulting raw-data-slices as well as the extant material are stored at the Natural History Museum of Vienna (NHMW-2012/0133/0480-550).

5.3. Methods

5.3.1. Serial grinding and digitization

A 150 x 45 x 140 mm^3 block was cut from the ammonoid-bearing limestone bed of Aşağiyaylabel, and for stabilization, set into concrete (Fig. 5.2B). For designation and the subsequent exact digital stacking of the resulting slices, two cores of 4.4 mm diameter were drilled on the lower right and the upper left edge of the block and a 1mm iron rod inserted. By using a stone saw, the block was grinded longitudinally (from slice 1A to 1C; Fig. 5.2B) into 70 slices with a spacing of 2mm (Fig. 5.2C). All slices were scanned using the commercial scanning system Epson Perfection 4990 Photo. They were digitized with a resolution of 1200 dpi, and stored as 8 bit gray-scale TIFF image (Fig. 5.2C and D).

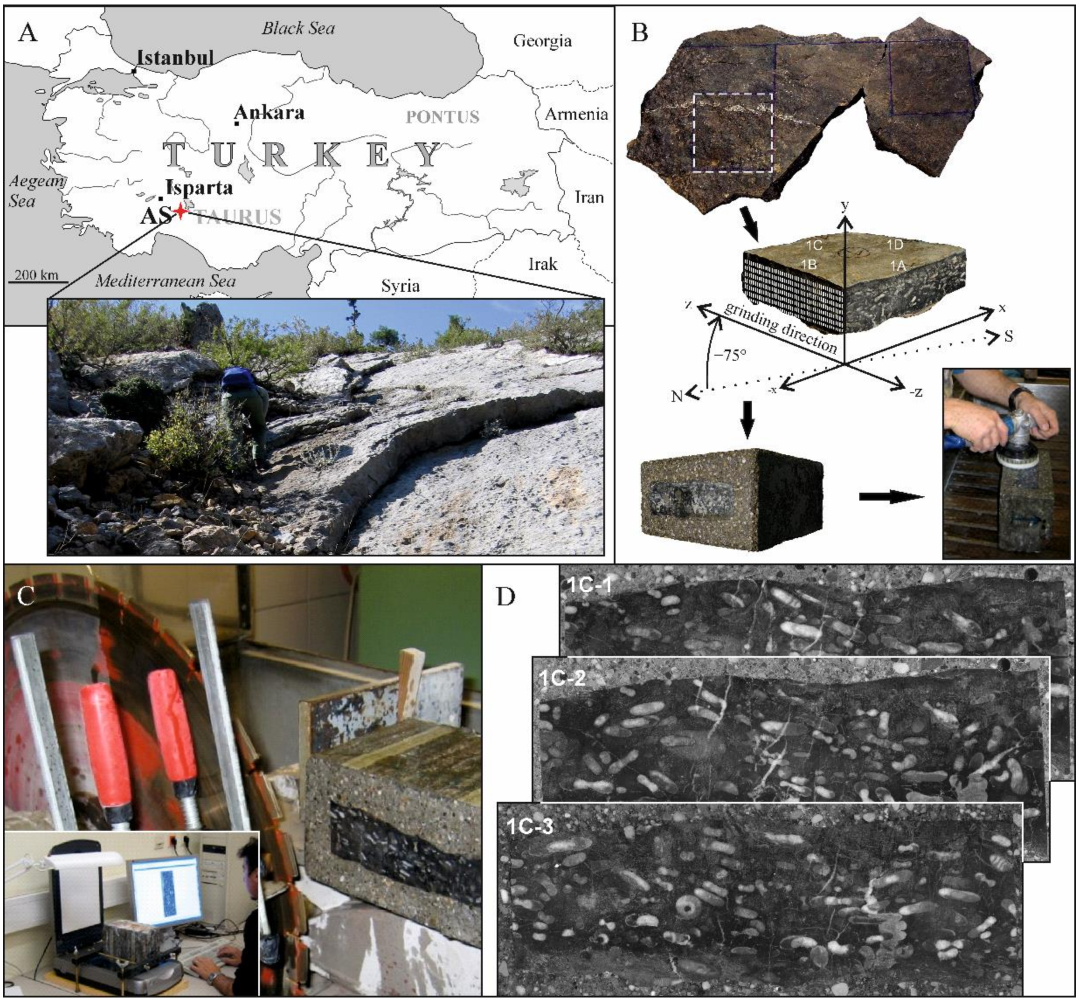

Fig. 5.2. Explanation of the grinding and digitizing method of the ammonoid mass occurrence from Aşağiyaylabel. **A,** Geographic location of the limestone bed. **B,** The recovered limestone bed and the 150 x 45 x 140 mm^3 limestone sample, which was geographically adjusted and set into concrete. **C,** Grinding, polishing and scanning of the slices. **D,** Three examples of the 70 scanned slices, with a distance of 2 mm.

5.3.2. 3D-visualization

For the visualization of the ammonoids, two different methods of computer facilities have been tested. Manual digitization with Corel-DRAW X4 and Gocad (Mayrhofer and Lukeneder 2011; Lukeneder and Lukeneder 2011; see Supplementary Fig. 1) has been declined after testing a more appropriate method, the semi-automatic region growing algorithm of the 3D-visualization software Amira.

Amira

The software package Amira is a 3D-Software for Life Sciences & Biomedical Data. 3D-volume objects can be segmented relatively fast and easily from 2D-slices using sophisticated segmentation algorithms.

1*. Alignment of slices* – For uploading the slices into Amira, consistent physical dimensions of the pictures are needed for registration. Therefore, a template was created to standardize the pixel size and scope of all slices, after correcting the alignment of their designation-cores, using the software Corel DRAW. Each slice was aligned to the subsequent and copied onto a black rectangular template (Fig. 5.3A), which guarantees constant physical dimensions. The stack of scanned slices with consistent pixel size (0.254) and dimensions (1377 x 669 pixels) were loaded into Amira, and placed at the correct distance of grinding (2 mm) by using the bounding box tool.

2. Ammonoid segmentation – While ammonoids cannot successfully be distinguished from their surrounding matrix in CT- applications, they show different gray values (Fig. 5.3A) in the photographed slices. Therefore, the semi-automatic region growing algorithm of Amira allowed a quite fast segmentation. This algorithm is based on a particular threshold gray-value, defined by the user. After setting a seed point at a suitable spot, the neighboring pixels respectively voxels will be added to an entity called label-field as long as they correspond to the defined parameters, i.e., gray-value range (Weber and Bookstein 2011). To prevent the region growing algorithm from escaping into unwanted areas (where gray values of the matrix are too similar), limits had to be set manually at some locations (therefore we call the method “semi-automatic” instead of “automatic”). The number of these interventions was kept as minimal as possible to proceed with the segmentation. For detailed information about different segmentation techniques see Malcom and Jones (2001), Spinsby *et al.* (2008) as well as Weber and Bookstein (2011).

3. Surface rendering – The 2 mm space between the segmented ammonoid slices (segmented label-fields; Fig. 5.3B) was interpolated (interpolated label-fields; Fig. 5.3C). Subsequently, 3D ammonoid surfaces (triangulated isosurfaces) were rendered from the interpolated label-fields (Fig. 5.3D). Each ammonoid could be assigned to its own triangulated isosurface and color (Fig. 5.3D and E).

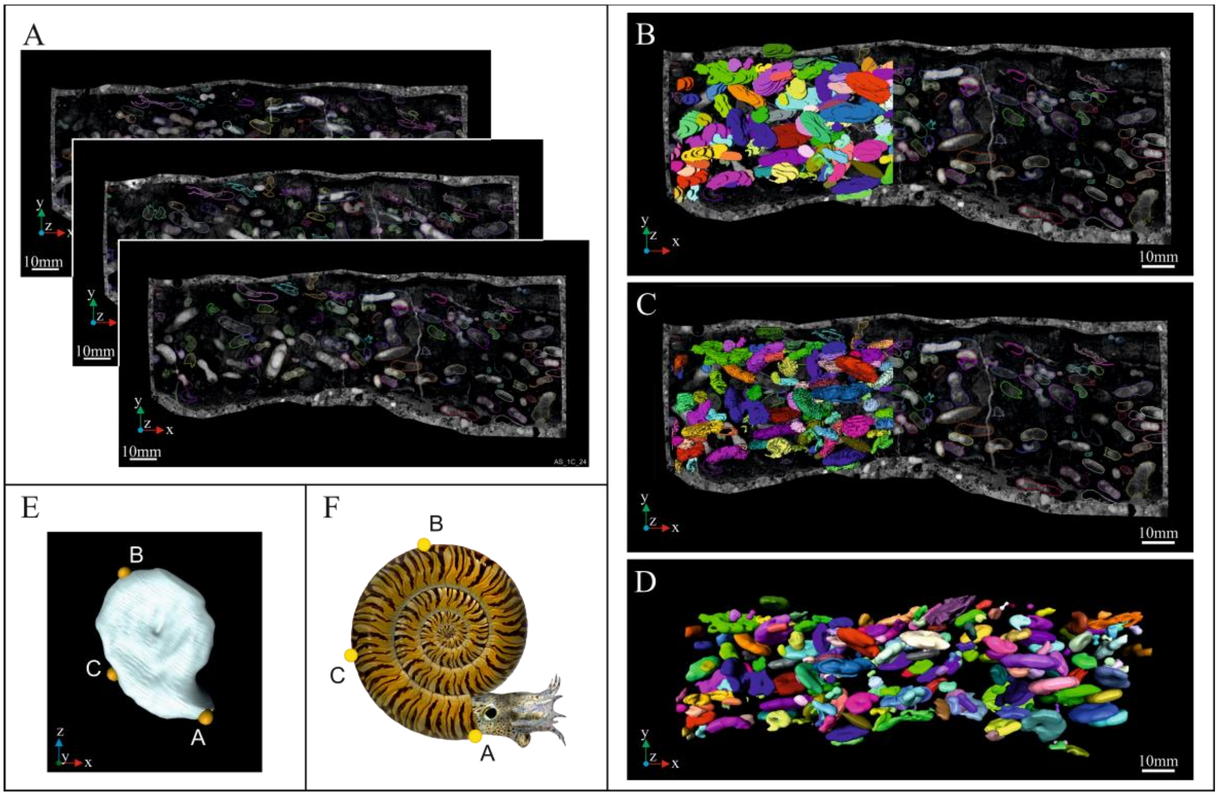

Fig. 5.3. Steps of the segmentation-procedure applied to the ammonoids from the scanned slices via Amira. **A,** Indicated segmentation of ammonoids via semi-automatic region growing technique. **B,** Lablefields and **C,** interpolated lablefields of the segmented ammonoids. **D,** Rendered ammonoid surfaces from interpolated lablefields. **E,** Positions of the landmarks, set on every ammonoid-surface. **F,** Landmark positions shown at a virtual ammonoid model, designed by 7 Reasons.

5.3.3. Orientation measurements

The basic data for computing orientation values of the ammonoids were also produced in Amira using landmarks set at each segmented ammonoid (Fig. 5.3E and F).

Landmark positioning

The first landmark (A) was set at the aperture (end of body chamber) of the ammonoid (Fig. 5.3E). The body chamber is the final part of the shell that protects the soft parts of the ammonoid (see reconstruction in Fig. 5.3F). The second landmark (B) was set opposite of the aperture in a way to obtain the longest distance (longitudinal axis, Fig. 5.4A–C). In cases where the aperture could not be identified, mostly due to bad preservation, points A and B were never the less set but carry less information, i.e., they indicate length but correspond only randomly to the position of the aperture. Data from those latter ammonoids were excluded from analyses at which the aperture direction would be important. The third landmark, needed for defining the orientation of an imaginary sagittal-plane through the ammonoid (Fig. 5.4D–F), was set at the venter (external position) of the ammonoid, lateral and between points A and B (Fig. 5.3E and F). The Cartesian coordinates were exported as ASCII-file and imported to Microsoft Excel to calculate the spatial orientation of each ammonoid specimen.

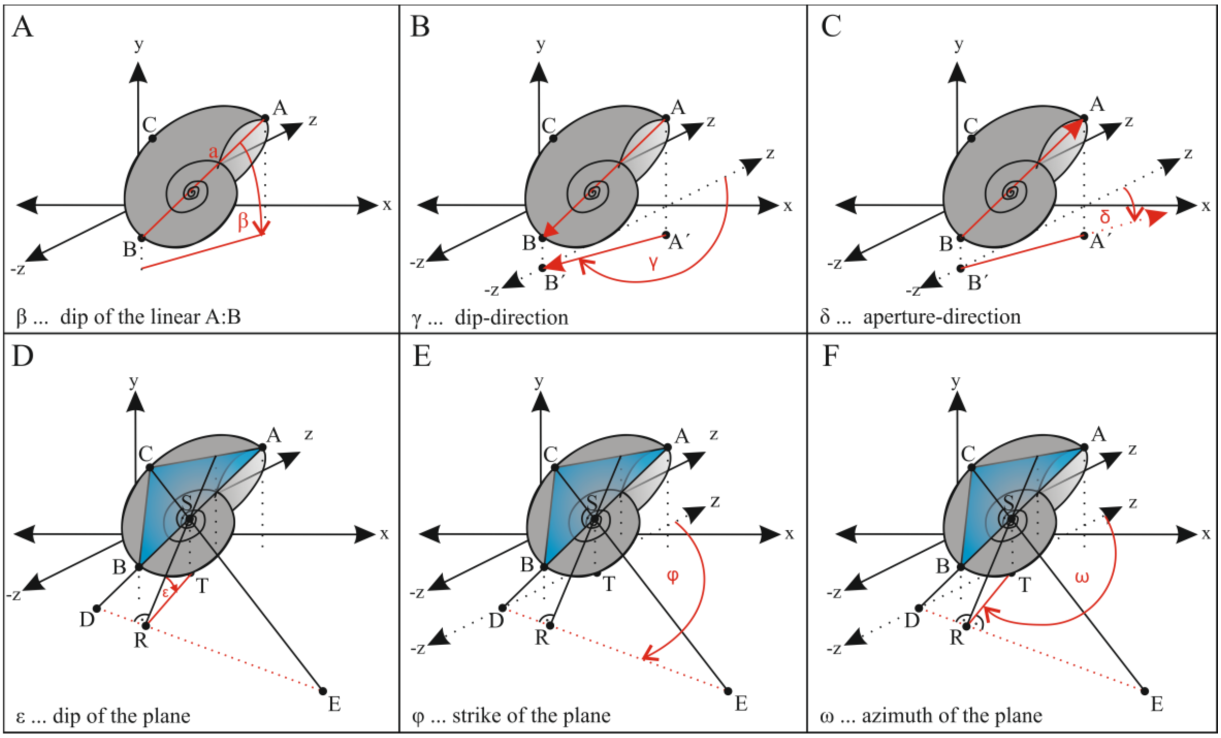

Fig. 5.4. Explanation of the orientation parameters used for subsequent investigation of the spatial orientation of each ammonoid. **A,** Maximum diameter and dip of the linear A:B. **B,** Dip-direction. **C,** Aperture direction. **D,** Dip of the plane (A–B–C). **E,** Strike of the plane. **F,** Azimuth of the plane.

Table 5.1. Formulae used for calculating orientation parameters of each ammonoid.

Parameter	Calculation	Calc. no.	Figures
Computing diameter and dip of the linear A:B (β):			
Diameter (distance A:B)	$= \text{square root } [(A_x - B_x)^2 + (A_y - B_y)^2 + (A_z - B_z)^2]$	1	5.4A, SF2[1]
Dip A:B (β)	$= \sin^{-1} [\text{abs } (A_y - B_y) / \text{distance A:B}]\ 180 / \pi$	2	5.4A, SF2
Calculation of dip direction (γ) and Aperture direction (δ):			
Inner product (0,0,1)	$= A_z - B_z$	3	
Absolute value	$= (A_z - B_z) / \text{square root } [(A_x - B_x)^2 + (A_y - B_y)^2 + (A_z - B_z)^2]$	4	
ρ	$= \cos^{-1} [(A_z - B_z) / \text{square root } [(A_x - B_x)^2 + (A_y - B_y)^2 + (A_z - B_z)^2)]\ 180 / \pi$	5	5.4B, SF2
Dip direction (γ)	$= \text{If } A_x > B_x \rightarrow \rho$; $\text{if } A_x < B_x \rightarrow 360 - \rho$	6	SF3
Aperture direction (δ)	$= \text{if } A_y < B_y \rightarrow$ aperture direction (δ) = dip direction (γ) = $\text{if } A_y > B_y \rightarrow \delta = 180 + \gamma$	7	5.4C
Computing coordinates of point S (S_x, S_y, S_z), needed for subsequent calculation of the dip of the plane (ε):			
Vector AB	$= (x_1, y_1, z_1)$; $\mathbf{x_1} = A_x - B_x$; $\mathbf{y_1} = A_y - B_y$; $\mathbf{z_1} = A_z - B_z$	8	SF2
Plane	$= x_1\, x + y_1\, y + z_1\, z = x_1\, C_x + y_1\, C_y + z_1\, C_z$	9	SF2
Straight line	$(x,y,z) = (A_x, A_y, A_z) + \Lambda\, (x_1, y_1, z_1)$	10	SF2
Straight line inserted in plane	$= x_1\, (A_x + \Lambda\, x_1) + y_1\, (A_y + \Lambda\, y_1) + z_1\, (A_z + \Lambda\, z_1) =$ $= x_1\, C_x + y_1\, C_y + z_1\, C_z$	11	SF2
Solving the equation based on Λ	$\Lambda\, (x_1^2 + y_1^2 + z_1^2) = x_1\, (C_x - A_x) +$ $+ y_1\, (C_y - A_y) + z_1\, (C_z - A_z)$ $\mathbf{x_2} = C_x - A_x$; $\mathbf{y_2} = C_y - A_y$; $\mathbf{z_2} = C_z - A_z$ $\Lambda = (x_1\, x_2 + y_1\, y_2 + z_1\, z_2) / (x_1^2 + y_1^2 + z_1^2)$ $\Lambda = [(A_x - B_x)\, (C_x - A_x) + (A_y - B_y)\, (C_y - A_y) + (A_z - B_z)$ $(C_z - A_z)] / [(A_x - B_x)^2 + (A_y - B_y)^2 + (A_z - B_z)^2]$	12	SF2
Initiation of Λ into the linear equation	$\mathbf{S_x} = A_x + \Lambda\, (A_x - B_x)$ $\mathbf{S_y} = A_y + \Lambda\, (A_y - B_y)$ $\mathbf{S_z} = A_z + \Lambda\, (A_z - B_z)$	13	SF2
Computing coordinates of points D (D_x, D_y, D_z), E (E_x, E_y, E_z) and T (T_x, T_y, T_z) needed for subsequent calculation of the dip of the plane (ε):			
D_x	$= A_x + [(-1\, A_y) / (A_y - B_y)]\, (A_x - B_x)$	14	SF2
D_y	$= 0$		SF2
D_z	$= A_z + [(-1\, A_y) / (A_y - B_y)]\, (A_z - B_z)$	15	SF2
E_x	$= C_x + [(-1\, C_y) / C_y - S_y)]\, (C_x - S_x)$	16	SF2
E_y	$= 0$		SF2
E_z	$= C_z + [(-1\, C_y) / C_y - S_y)]\, (C_z - S_z)$	17	SF2

1. SF = Supplementary Figure, see Appendix p. 346–347

Table 5.1. Continued.

Parameter	Calculation	Calc. no.	Figures
Computing distances needed for subsequent calculation of the dip of the plane (ε):			
T_x	$= S_x$	18	5.4D, SF2
T_y	= 0	19	5.4D, SF2
T_z	$= S_z$	20	5.4D, SF2
Distance D:E	= square root $[(D_x - E_x)^2 + (D_z - E_z)^2]$	21	5.4D, SF2
Distance D:T	= square root $[(D_x - T_x)^2 + (D_z - T_z)^2]$	22	
Distance E:T	= square root $[(E_x - T_x)^2 + (E_z - T_z)^2]$	23	
Distance S:T	= Sy		
Distance S:D	= square root $[(D{:}T)^2 + (S{:}T)^2]$	24	
Distance S:E	= square root $[(E{:}T)^2 + (S{:}T)^2]$	25	
Height R:S (triangle D,E,S)	= (S:D) (S:E) / (D:E)	26	
Dip of the plane (ε)	$= \sin^{-1}$ [(S:T) / (height R:S)]	27	
Calculation of the Strike (φ) of the plane:			
ρ	$= \cos^{-1} [(D_z - E_z)$ / square root $[(D_x - E_x)^2 + (D_y - E_y)^2 + (D_z - E_z)^2)] \, 180 / \pi$	28	
Strike (φ)	= if $D_x > E_x \rightarrow \rho$; if $D_x < E_x \rightarrow 360 - \rho$	29	5.4E, SF3
Computing coordinates of points R (R_x, R_y, R_z), needed for subsequent calculation the Azimuth (ώ):			
Vector DE	$= (x_1, y_1, z_1)$; $x_1 = D_x - E_x$, $y_1 = D_y - E_y$, $z_1 = D_z - E_z$	30	SF2
Plane	$= x_1 x + y_1 y + z_1 z = x_1 T_x + y_1 T_y + z_1 T_z$	31	
Straight line	$(x, y, z) = (D_x, D_y, D_z) + \Lambda (x_1, y_1, z_1)$	32	
Straight line inserted in plane	$= x_1 (D_x + \Lambda x_1) + y_1 (D_y + \Lambda y_1) + z_1 (D_z + \Lambda z_1) =$ $= x_1 T_x + y_1 T_y + z_1 T_z$	33	
Solving the equation based on Λ	$\Lambda (x_1^2 + y_1^2 + z_1^2) = x_1(T_x - D_x) + y_1(T_y - D_y) + z_1 (T_z - D_z)$ $x_2 = T_x - D_x$; $y_2 = T_y - D_y$; $z_2 = T_z - D_z$ $\Lambda = (x_1 x_2 + y_1 y_2 + z_1 z_2) / (x_1^2 + y_1^2 + z_1^2)$ $\Lambda = [(A_x - B_x)(C_x - A_x) + (A_y - B_y)(C_y - A_y) + (A_z - B_z)(C_z - A_z)] / [(D_x - E_x)^2 + (D_y - E_y)^2 + (D_z - E_z)^2]$	34	
Initiation of Λ into the linear equation	$R_x = D_x + \Lambda (D_x - E_x)$ $R_y = D_y + \Lambda (D_y - E_y)$ $R_z = D_z + \Lambda (D_z - E_z)$	35	
Azimuth (ώ)	If $E_x < D_x$, $E_z > D_z$, $T_x > R_x$ → Strike – 90° If $E_x < D_x$, $E_z > D_z$, $T_x < R_x$ → Strike + 90° If $E_x > D_x$, $E_z > D_z$, $T_x < R_x$ → Strike + 90° If $E_x > D_x$, $E_z > D_z$, $T_x > R_x$ → Strike – 90° If $E_x < D_x$, $E_z < D_z$, $T_x > R_x$ → Strike + 90° If $E_x < D_x$, $E_z < D_z$, $T_x < R_x$ → Strike – 90° If $E_x > D_x$, $E_z < D_z$, $T_x < R_x$ → Strike – 90° If $E_x > D_x$, $E_z < D_z$, $T_x > R_x$ → Strike – 90°	36	5.4F

Spatial orientation parameters computed from landmark coordinates

Trigonometric and vector-based calculations were used to compute the orientation of the diameter (linear between points A and B = α; Fig. 5.4A–C) as well as of an imaginary sagittal-plane through each ammonoid (triangles in blue, Fig. 5.4D–F). Therefore the following parameters, comparable to geological features (e.g., Wallbrecher 1978, 1979, 1986; Adler *et al.* 1982), were calculated from the segmented ammonoids using Microsoft Excel, (Fig. 5.4A–F and Table 5.1):

(1) Orientation of the linear:

- α – maximum diameter (Fig. 5.4A).
- β – dip of the linear A:B (Fig. 5.4A).
- γ – dip direction (Fig. 5.4B).
- δ – aperture direction (Fig. 5.4C).

(2) Orientation of the imaginary sagittal-plane:

- ε – dip of the plane (Fig. 5.4D).
- φ – strike (Fig. 5.4E).
- ώ – azimuth (Fig. 5.4F).

The associated equations to each parameter can be gleaned from the corresponding calculation number (Calc.no.) of Table 5.1. The orientations of the ammonoids were calculated in relation to the grinding sections, thus the z-axis (Fig. 5.2B). The plane spanned by the x- and the z- axes indicates the ground plane. The direction of the positive y-axis represents the height from the ground plane (Fig. 5.2B). For calculating the orientation of the ammonoids as they were deposited in the field, it is necessary to know the deviation of the z-axis from true north, and to add this geographic angle to the calculated geographic parameters (i.e., dip direction, azimuth respectively strike). As dip and azimuth values of the whole bed are 50/075 we add 75° to the calculated aperture direction, dip direction as well as to the calculated azimuth (Fig. 5.2B).

(1) Orientation of the linear A:B (α)

Maximum diameter of each ammonoid (a)

Definition: The maximum diameter (a) of each ammonoid is represented by the spatial distance between the points A and B (Table 5.1, Calc.no.1; Fig. 5.4A). Associated variables are shown within Supplementary Fig. 2.

Dip of the linear (β)

Definition: The dip (β), or also called the “angle of fall” from the linear (a) represents the angle between the diameter (linear of the landmarks A:B) and the ground plane, spanned by the x- and z-axes (Table 5.1, Calc.no. 2; Fig. 5.4A, Supplementary Fig. 2).

Dip direction (γ)

Definition: The dip direction is the geographic orientation towards that the linear A:B is inclined. It is represented by the angle between north (positive z-axis -75°; see Fig. 5.2B), and the projected linear A:B vectored to A or B respectively, on the ground plane (spanned by the x- and the z-axes). If point B shows a lower y-value (Fig. 5.4B), the linear A:B is inclined to B and therefore the vector A´:B´ is directed to point

B´. If point A shows a lower y-value, the linear A:B is inclined to A and the vector A´:B´ is directed to point A´ (Table 5.1, Calc. nos. 3–6; Supplementary Figs. 2 and 5.3).

Aperture direction (δ)

Definition: The aperture direction is defined as the geographic orientation in which the aperture of the ammonoid is directed (Fig. 5.4C). It is represented by the angle between north (z-axis -75°; Fig. 5.2B), and the projected linear A:B vectored always to A on the ground plane (Table 5.1, Calc.no.7; Fig. 5.4C).

(2) Orientation of the imaginary sagittal-plane (A–B–C) through the ammonoid

As already described by Wallbrecher (1986), the orientation of a plane can be defined exactly by two angles. The dip represents the degree of inclination of the plane from the horizontal earth surface. The second angle needed is the azimuth, which is the angular deviation of this declination (dip) from the north (Fig. 5.4D and F).

Dip of the plane A–B–C (ε)

Definition: The dip of the plane, represented by the inclination of the plane from the earth surface, can be defined more precisely as the linear representing the steepest possible angle between the plane (A–B–C) and the ground-plane (spanned by the x- and z-axes) (Fig. 5.4D). To investigate this linear, the intersection line at which the extended plane (A–B–C to A–C–D–E; see Fig. 5.4D–F) crosses the ground plane, was constructed and calculated (linear D:E; Fig. 5.4D). The height (R:S) of the triangle S:D, S:E and D:E, perpendicular to the linear D:E represents the steepest possible linear. Its inclination to the ground floor represents the sought dip of the plane (ε; Table 5.1; Calc.nos. 8–27; Fig. 5.4D, Supplementary Fig. 2).

Strike (φ).

Definition: The “strike” represents the geographic angular deviation from north (z -75°; Fig. 5.2B) of the linear at which the extended plane A–B–C intersects with the ground-plane (D:E; Table 5.1, Calc.no. 29; Fig. 5.4E; Supplementary Figs. 2 and 3).

Azimuth (ώ).

Definition: The azimuth is the geographical direction in which the dip of the plane is inclined. It is the angle between north (z-axis -75°) and the projected linear of the steepest possible linear of the plane (R:S) to the ground plane (Fig. 5.4F). The azimuth represents the strike +/- 90° (Table 5.1, Calc. nos. 30–36; Fig. 5.4F, Supplementary Fig. 2).

5.4. Spatial orientation as key to the paleoenvironment

The geographic orientations (cardinal directions) of the ammonoids were analyzed in rose diagrams. The Schmidt net analyses (stereographic projections) were used for combined analyses of geographic orientation and inclination of the ammonoids. These statistical analyses have become standard methods for analyzing spatial orientation of geological features in geoscience and are therefore not explained in detail. Detailed information about these methods can be found in a series of geological literature (e.g., Wallbrecher 1986; Adler *et al.* 1982), but also in Mardia and Jupp (2000) which focuses on directional statistics. All analyses and their concluding assumptions were based on the results obtained by the statistical software Fabric8.

5.4.1. Geographical alignment of the aperture

To investigate the statistical aperture orientation (i.e., direction in the coordinate system), only data from ammonoids with known apertural position (n = 193) were analyzed. By plotting the aperture direction within a rose diagram a bimodal distribution with 66% preferred orientation, bearing a dominant mean SSE vector (155°), was found (Fig. 5.5A). With a class-size of 20°, the maximum volume lies within the 160–180° class and represents 18.2%. However, there are two more dominating classes (320–340° and 340–360°) exactly opposite the most dominant class (160–180°), each represented by a volume of 14.9%. Due to this dubious result (almost precise NNW–SSE orientation of the apertures, showing a low skewness (-0.37), but a relatively high kurtosis (-42.52; Fig. 5.5A)), we had to exclude a possible error. For identifying, quantifying and correcting the possible error source, the following test series was carried out (Fig. 5.5B).

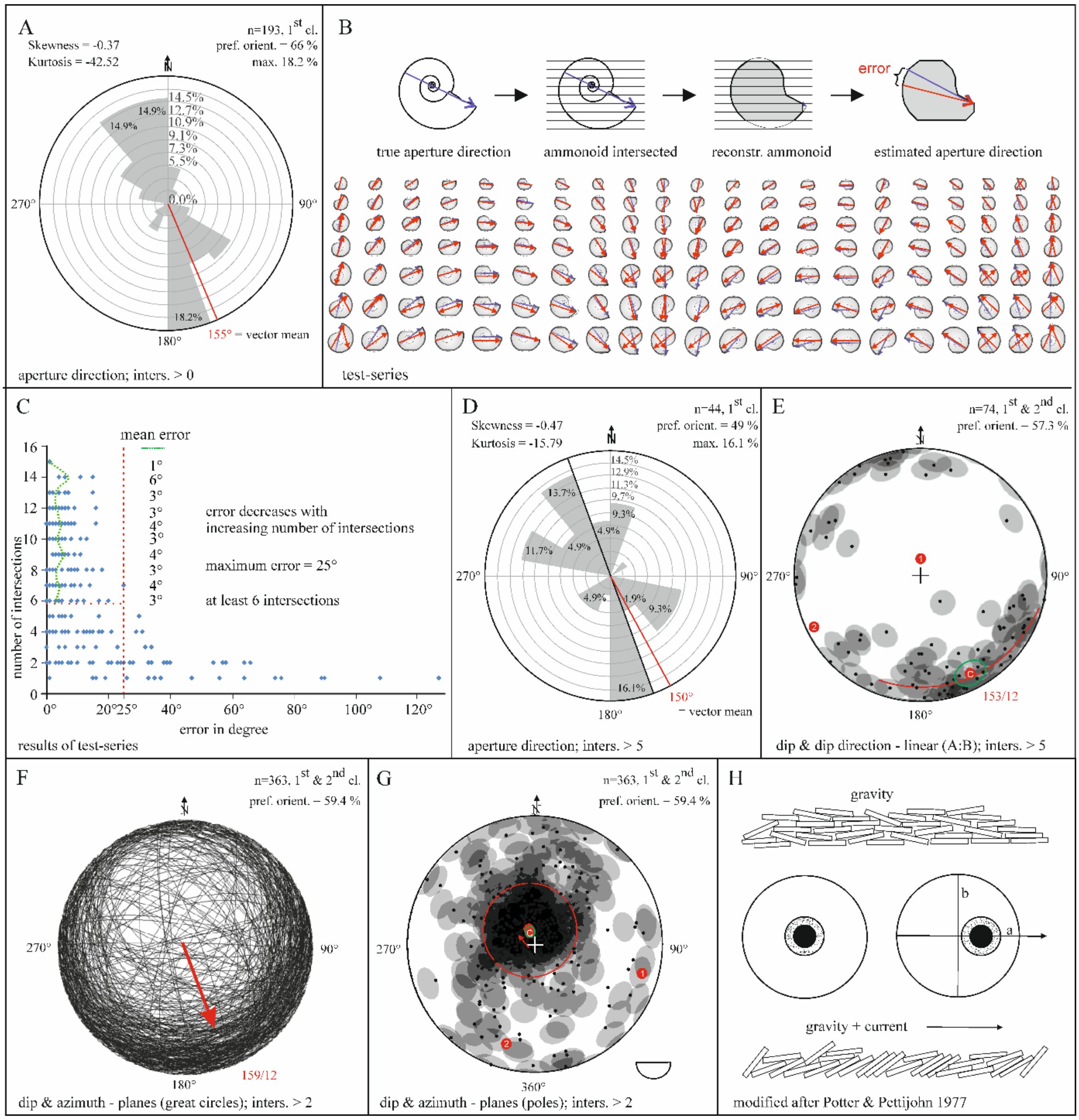

Fig. 5.5. Results of analyzed spatial shell orientation. **A,** Rose diagram showing nearly exact NNW/SSE aperture orientation of all ammonoids at which the aperture could be identified. **B,** Example of the test series for calculating the error between estimated and true aperture direction. **C,** Analysis of test series. **D,** Rose diagram showing revised orientation of the aperture direction, only from ammonoids intersected at least 6 times (NW/SE). **E,** Results of dip and dip direction of the linear (A:B) analyzed within a Schmidt net plot. **F–G,** Results of dip and azimuth of the planes (A–B–C) respectively ammonoids analyzed within a Schmidt net plot. **F,** Plot of great circles. **G,** Plot of plane–poles. **H,** Comparison of the orientation of disks due to gravity respectively gravity plus current action, modified after Potter and Pettijohn (1977).

Test series

The aperture of a hypothetical ammonoid, with indicated true aperture direction (blue arrow) was orientated to 21 different directions (0–360°) with periodic displacements of 17° (Fig. 5.5B). This series of differently orientated ammonoids was copied 12 times and each of them assigned to an artificial ammonoid diameter (1 mm, 3.5 mm, 6 mm, 8.5 mm, 11 mm, 13.5 mm, 16 mm, 18.5 mm, 21 mm, 23.5 mm, 26 mm and 28.5 mm). The resulting sample of 252 ammonoid specimens featuring different diameters and orientations were intersected every 2 mm (Fig. 5.5B).

This setting simulates our grinding approach that in fact eliminates the whole material of the fossilized block while only preserving one snapshot at 2 mm each. Thus, the position of landmarks A–C can, within limits, be wrongly assessed. To learn more about this effect, we studied the possible error between the true- and the estimated aperture-direction (red/ blue arrows; Fig. 5.5B). A simple bivariate plot shows that the error (maximum = 127°) decreases with increasing diameter, respectively with increasing number of intersection lines (Fig. 5.5C). The non-linear distribution suggests a reasonable cut-off point at 25° (red pointed lines), which means that each ammonoid should be intersected at least six times (Fig. 5.5C). Hence, for analyzing parameters of the linears (A:B), we used only those ammonoids which were intersected at least six times. For analyzing the orientation of the plane (A–B–C), three intersections were enough because it is reconstructed from three points and therefore the error is significantly lower.

It has to be noted, that the orientation of the intersected 2D ammonoids describes the worst case, a position at which the aperture can hardly be identified. If the ammonoid would be intersected sagittally (perpendicular to the tested direction of intersection) the error would become much lower.

5.4.2. Revised aperture direction

The geographic distribution of the aperture direction shows a higher variation (kurtosis = -15.79) by using only ammonoids intersected at least six times (n = 44). The distribution is unchanged bimodal with an almost similar vector mean at 150°. The maximum class volume (16.1% at 160–180°) still plots closely to the south (Fig. 5.5D). The preferred orientation declines to 49% and changes from NNW–SSE to NW–SE. Furthermore, the opposite dominant class-volume is constricted to the class 320–340°, bearing 13.7%, what results in the already mentioned shift from NNW–SSE to NW–SE. Although the skewness changed slightly (-0.47 vs. -0.37), the kurtosis changed from -42.52 to -15.79, due to the higher variation (Fig. 5.5A, D).

5.4.3. Dip and dip direction of the linear A:B

Dip and dip direction of the linear (A:B) were analyzed in combination, by using a Schmidt net plot (Fig. 5.5E). Data from all reconstructed ammonoids intersected at least six times (n = 74) were included. Identification of the aperture direction is, in this case, of no importance. Each data point represents one dip in combination with its dip direction. Most points are plotted at the outer edge of the circle, which indicates a relatively slight dip. Points close to the center would reflect a steep dip. The geographic distribution can be gleaned from this plot in the same way as from rose diagrams. Points near the top (N) indicated a northern direction, etc. The plot shows a preferred orientation of 57.3% of the linears (length of vector sum; 100% = parallel orientation), which are slightly inclined (12°) toward SE (153°). The true center of gravity (comparable to the mean within the linear statistics) plots with a significance of 0.05 within the cone of confidence (8.6°; Fig. 5.5E green circle) around the center of gravity (153/12).

5.4.4. Dip and azimuth of the plane A–B–C

Dip and azimuth of the plane (A–B–C) were analyzed in the same way as dip and dip direction of the linear (A:B), with the difference that the data were taken from ammonoids intersected at least three times (n = 363). The identification of the aperture direction is of no importance here as well. Fig. 5.5F shows a stereographic projection of great circles. Each great circle represents the geographic orientation (dip and azimuth) of one plane (respectively ammonoid). Like for the data points of the linears, great circles plotting close to the center indicate a steep inclination, whilst great circles near the periphery indicate a slight inclination. The data plot (Fig. 5.5F) therefore shows that 59.4% (preferred orientation, length of vector sum) are slightly inclined (12°) toward SE (159°). Another possibility for analyzing planes within a stereographic graph is by plotting their plane–poles (orthogonal axis through the center of gravity of the triangles; Fig. 5.5G). In the case of analyzing the poles, data points indicate the projection of the orthogonal axis of the planes. Points plotting close to the center indicate only a slight inclination of the planes respectively of the ammonoids. The geographic distribution can be interpreted in the same way as from the plots of the linears. While the planes are inclined toward SE (see great circles, Fig. 5.5F), their plane poles plot toward NW due to the fact that the plane poles are orthogonal to the planes (Fig. 5.5G). The preferred orientation of the plane–poles (vector sum = 59.4%) plot near to, but not in the center (white cross), toward NW. The true center of gravity of the planes (comparable to the true mean within the linear statistics) plots with a significance of 0.05 within the cone of confidence (3.71) around the center of gravity (159/12; Fig. 5.5G). This indicates a slight inclination of the planes (respectively ammonoids) toward SE (Fig. 5.5F and G). Potter and Pettijohn (1977), for comparison, described the orientation of disks for gravity as well as for gravity plus current actions by the use of stereographic projections (Fig. 5.5H). The imbrication of such disks would result in a shift of the center of gravity from the center of the Schmidt net plot in the down-current direction, as a result of tangential transport (Sander 1930; Potter and Pettijohn 1977). By comparing these conclusions to the slightly NW shifted maximum concentration of the plane poles herein, the latter can be interpreted as a smooth but significant movement of the ammonoids, or respectively as a current direction, oriented toward NW (Fig. 5.6).

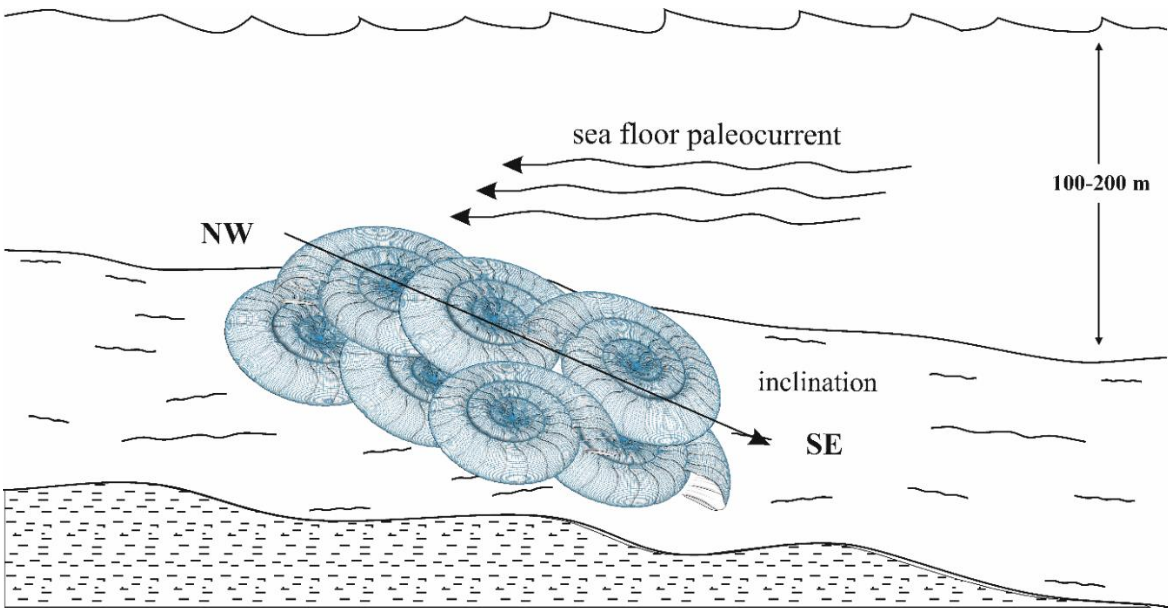

Fig. 5.6. Reconstructed current- and environmental conditions of the primary ammonoid-deposition on the sea floor. Ammonoid-grids were modeled by Michael Klein (7 Reasons Media Corporation).

5.5. Discussion

As mentioned in Section 5.1.2, the investigation of fossil orientation from bedding planes for estimating ancient paleocurrents has been conducted in numerous studies (e.g., Hall 1843; King 1948; Kidwell *et al.* 1986). However, the majority of these studies deal with elongated fossils (e.g., belemnites, cephalopods with orthoconic shells and gastropods, etc.), excluding planispirally coiled (flat to disk-shaped) morphologies (e.g., shells of ectocochleate cephalopods such as ammonoids). Brenner (1976), and more recently Wani (2006), claimed that the body chambers of empty ammonoid shells can be used as current indicators, orientated with their aperture downstream. Futterer (1982) reported that planispiral gastropod shells (e.g., *Planorbina* sp.) manifested their stable position with the aperture downstream. Lukeneder (2005) interpreted planispiral and elongated ammonoids, orientated on the sea floor of an Early Cretaceous section in Upper Austria, as bottom current induced. Moreover, Wendt (1995) compared the orientation of goniatitic (planispiral-coiled) cephalopods and orthoconic cephalopods (elongated shells). He reported that the orientations of goniatites (disk-shaped shells) in some cases appear nearly randomly. Therefore, he suggested caution for interpreting paleocurrents from the aperture direction of coiled cephalopods. However, none of these studies interpreted planispiral-coiled cephalopods with respect to the orientation of their disk-like morphologies. As shown in this study, the orientation of these forms can simply be interpreted like the orientation of disks, compared to Sander's approach (1930) (Fig. 5.5H) on the alignment-behavior of disk-like particles (Potter and Pettijohn, 1977).

Additionally, conventional studies of fossil-orientation-measurements, predominantly deal with the two-dimensional geographic orientation of a certain axis of the fossil, analyzed within rose diagrams. Azimuth directions of fossils have been measured for tentaculite shells of Bohemia (Hladil *et al.*, 1996), or for nerineoid shell beds (Cataldo *et al.* 2013), though disregarding stereographic plots for a combined interpretation of dip and azimuth. Numerous studies on sedimentology dealt with the imbrication of pebbles as proxies for determination of paleocurrents (e.g., Sengupta 1966; Trendell *et al.* 2013; Karátson *et al.* 2002). White (1952) investigated the flow direction of a depositing stream from the Houghton conglomerate with respect to the initial imbrication of pebbles. Even more than a decade earlier, Krumbein (1940) used imbricated pebbles to determine the transport direction of California flood gravels. More recent studies automated the analysis of imbrication and flow direction by using Laser-Scan data (Millane *et al*. 2006). We applied Sander's (1930) approach of the orientation of disk-like particles to the disk-shaped ammonoids (i.e., *Kasimlarceltites*). Both results, the orientation of the aperture, as well as the orientation of the estimated sagittal-plane through the ammonoids (dip and azimuth), indicate a movement of the ammonoids or respectively a current direction toward NW (Fig. 5.6). It shows that the combined interpretation of dip and azimuth of disk-shaped fossils represents a significant approach for interpreting sea floor paleocurrents.

Hitherto, the investigation of fossil-orientation was only used for the topmost surface of fossil mass occurrences, deposited directly on the sea floor. Due to the fast development of virtual methods (e.g., macro-CT, µ-CT, nano-CT, etc.) it became possible, to investigate the interior orientation of such fossil mass occurrences in three-dimensional detail. Although, a series of paleontological studies deal with 3D-visualization of fossil-elements, no mass occurrence has previously been reconstructed three dimensionally for investigating their interior orientation. This study illustrates an interdisciplinary approach of virtual reconstruction, analyses and interpretation of the interior orientation of an ammonoid mass occurrence. The method established herein produces clear and consistent results using planispirally coiled ammonoid shells – fossils, that so far would have been used only with caution for depositional interpretations. This method can be applied to any kind of fossil mass occurrence, or even other abundant organic elements and particles, to examine their orientation and depositional conditions to conclude on their paleoenvironment, particularly on paleocurrents.

5.6. Conclusions

In our study, we introduce a new method, which combines digital fossil-segmentation, subsequent 3D-reconstruction and calculation of spatial ammonoid-orientation, performed on a Triassic ammonoid mass occurrence, deposited within a limestone layer, at Aşağiyaylabel (Taurus Mountains, Southern Turkey). Since computed tomography could not be used for digitization because of insufficient density contrast, the classic method of serial grinding was applied. A block, 150 x 45 x 140 mm^3, of the limestone layer was ground and 70 slices with a distance of 2 mm were scanned in longitudinal direction (from 1A to 1C; Fig. 5.2B). The semi-automatic region growing tool of Amira was applied for segmentation and 3D-reconstruction of the ammonoids. Six orientation parameters, already known from geological features, were calculated from these ammonoids. The use of the Cartesian coordinates of three different landmarks, placed on three particular points of each ammonoid, made it possible to calculate the orientation parameters and therefore the spatial orientation of 675 segmented ammonoids from a 26 mm part of the whole block. The analyses, via rose diagrams and Schmidt net plots, show a general NW/SE orientation of the aperture direction of the ammonoids, as well as a slightly SE inclination of the whole ammonoids, indicating a slight but significant sediment movement or even possible a current direction toward NW.

Using this method in an ongoing study, the orientation of all ammonoids from the whole block will be investigated. The statistical orientation of all ammonoids from the mass occurrence, combined with additional 2D-reconstructions and facies-analyses of the limestone-layer, should lead to more detailed conclusions about the depositional conditions of the ammonoid mass occurrence. The newly established method can be used as template for measuring spatial orientations on all kinds of fossil mass occurrences or other geological objects. A new animation clip (see Supplementary material) explains all steps, from segmentation, over surface-reconstruction to landmark-positioning, within the software package Amira, hence helping to apply this method to comparable material and scientific fields. Video1[2]

2. See supplementary material p. 221.

5.7. Acknowledgments

This study was funded by the Austrian Science Fund (FWF, P 22109-B17). The authors thank Yeşim Islamoğlu (Ankara) and the General Directorate of Mineral Research and Exploration (Ankara) for the digging permission and the organization of two field trips. We are grateful to Mathias Harzhauser (Vienna), Philipp Strauss (Vienna) and Leopold Krystyn (Vienna) for providing material from previous field trips. Special thanks go to Franz Topka (Vienna) for his help during field trips and for grinding the reference-block. The authors thank Robert Marschallinger (Salzburg) and Christian Klug (Zurich) for constructive reviews of the manuscript. We thank Michael Schwaiger (Linz) and Martin Mayrhofer (Waldegg) for fruitful discussions concerning mathematical questions as well as Ulrike Exner (Vienna) for the possibility of using the software package Amira on her high-capacity PC. Andreas Kroh (Vienna) helped with useful advices concerning the digitization of the slices. Eckart Wallbrecher (Graz) is thanked for advice on statistical questions concerning the stereographic projection. Additionally, we acknowledge Simon Schneider (Cambridge) for his support in collecting hardly obtainable literature. The authors thank Maarten Voorn (Vienna) for the introduction to the software package Avizo as well as Martin Dockner (Vienna) for hardware-advices. Michael Klein (Vienna) from 7 reasons Media Corporation is thanked for the help with the final animation clip-rendering.

5.8. Appendix. Supplementary material

Supplementary data associated with this article can be found in the online version at http://dx.doi.org/10.1016/j.cageo.2013.11.008.

5.9. References

ADLER R., FENCHEL W. and PILGER A. 1982. Statistische Methoden in der Tektonik II. *Clausthaler Tektonische Hefte,* **4**, 1–89.

BRENNER K. 1976. Ammoniten-Gehäuse als Anzeiger von Palaeo-Strömungen. *Neues Jahrbuch für Geologie und Paläontologie, Abhandlungen*, **151**, 101–118.

BRIGUGLIO A., METCHER B. and HOHENEGGER J. 2011. Growth rate biometric quantification by x-ray microtomography on larger benthic foraminifera: three-dimensional measurements push nummulitids onto the fourth dimension. *Turkish Journal of Earth Sciences*, **20**, 683–699.

CAMP C.L. and HANNA G.D. 1937. Methods in Paleontology. University of California Press, Berkley, 53–55.

CATALDO C.S., LAZO D.G., TUNIK M.A. and AGUIRRE-URRETA M.B. 2013. Taphonomy and palaeoecology of Hauterivian-Barremian nerineoid shell beds from the Neuquén Basin, west-central Argentina. *Lethaia,* **46**, 114–126.

CONROY G.C. and VANNIER M.W. 1984. Noninvasive three-dimensional computer imaging of matrix-filled fossil skulls by high-resolution computed tomography. *Science,* **226**, 456–458.

DERCOURT J., RICOU L.E. and VRIELYNCK B. 1993. Atlas Tethys Palaeoenvironmental Maps. Gaulthier-Villars, Paris, pp. 307.

DERCOURT J., GAETANI M., VRIELYNCK B., BARRIER E., BIJU-DUVAL B., BRUNET M.F., CADET J.P., CRASQUIN S. and SANDULESCU M. (eds). 2000. Atlas Peri-Tethys – Palaeogeographical Maps. Commission of the Geological Map of the World, Paris.

DOCKNER M. 2006. Comparison of *Crocuta crocuta* and *Crocuta crocuta spelaea* through computer tomography (Unpublished Diploma thesis). University of Vienna, Vienna, pp. 68.

FLÜGEL E. 2004. Microfacies of Carbonate Rocks. Analysis, Interpretation and Application. Springer, Berlin Heidelberg New York, pp. 182.

FOURIE S. 1974. The cranial morphology of *Thrinaxodon liorhinus* Seeley. *Annals of the South African Museum*, **65**, 337–400.

FUTTERER E. 1982. Experiments on the distinction of wave and current influenced shell accumulations. *In*: EINSELE G. and SEILACHER A. (eds). Cyclic and Event Stratification, 175–179.

GARWOOD R.G., IMRAN A.R. and SUTTON M.D. 2010. From clergymen to computers – the advent of virtual palaeontology. *Geology Today*, **26 (3)**, 96–100.

GINDL A. 2000. Paläoökologie Triassischer Ammonitenfaunen des Taurusgebirges (Türkei) (Unpublished Diplomathesis). University of Vienna, pp. 80.

HALL J. 1843. Geology of New York, Part IV. Carrolland Cook, Albany, pp. 683.

HLADIL J., ČEJCHAN P., GABAŠOVÁ A., TDĚÁBORSKÝ Z. and HLADÍKOVÁ J. 1996. Sedimentology and orientation of tentaculite shells in turbidite lime mudstone to packstone: Lower Devonian, Barrandian, Bohemia. *Journal of Sedimentary Research*, **66**, 888–899.

KARÁTSON D., SZTANÓ O. and TELBISZ T. 2002. Preferred clast orientation in vulcaniclastic mass-flow deposits: Application of a new photo-statistical method. *Journal of Sedimentary Research*, **72 (6)**, 823–835.

KELLING G. and MOSHRIF M.A. 1977. The orientation of fossil bivalves in a pene-littoral sequence (the Rhaetian of South Wales). *Journal of Sedimentary Petrology*, **47 (3)**, 1342–1346.

KETCHAM R.A. and CARLSON W.D. 2001. Acquisition, optimization and interpretation of X-ray computed tomographic imagery: applications to the geosciences. *Computers and Geosciences*, **27**, 381–400.

KIDWELL S.M., FÜRSICH F.T. and AIGNER T. 1986. Conceptual framework for the analysis and classification of fossil concentrations. *Palaios,* **1**, 228–238.

KING P.B. 1948. Geology of the Southern Guadaloupe Mountains, Texas. *United States Geological Survey Professional Paper*, **215**, 1–183.

KOSLOWSKI R., 1932. Sur un procédé simple et précis d´effectuer les coupes sérielles des fossiles. *Paläontologische Zeitschrift*, **13**, 316–318.

KRUMBEIN W.C. 1940. Flood gravels of San Gabriel Canyon. *Geological Society of American Bulletin*, **51**, 639–676.

KRUTA I., LANDMAN N., ROUGET I., CECCA F. and TAFFOREAU P. 2011. The role of ammonites in the Mesozoic Marine Food Web revealed by Jaw Preservation. *Science*, **331/ 6013**, 70–72.

LUKENEDER A. 2005. Taphonomy and Stratigraphy of Early Cretaceous ammonoid mass occurrences (Late Valanginian; Northern Calcareous Alps; Upper Austria). *Austrian Journal of Earth Sciences*, **98**, 34–51.

LUKENEDER A. 2012. Computed 3D visualization of an extinct cephalopod using computer tomographs. *Computers and Geosciences*, **45**, 68–74.

LUKENEDER S. and LUKENEDER A. 2011. Methods in 3D modelling of Triassic ammonites from Turkey (Taurus, FWF P22109-B17). *In*: MARSCHALLINGER R., ZOBL F. (eds). Mathematical Geosciences at the Cross roads of Theory and Practice. Proceedings IAMG 2011 Conference, 497–507.

LUKENEDER S., LUKENEDER A., HARZHAUSER M., ISLAMOGLU Y., KRYSTYN L. and LEIN R. 2012. A delayed carbonate factory breakdown during the Tethyan-wide Carnian Pluvial Episode along the Cimmerian terranes (Taurus, Turkey). *Facies*, **58**, 279–296.

LUKENEDER S. and LUKENEDER A. 2014. A new ammonoid fauna from the Carnian (Upper Triassic) Kasimlar Formation of the Taurus Mountains (Anatolia, Turkey). *Palaeontology*, **57 (2)**, 357–396.

MALCOM J.H. and JONES B.J. 2001. Contour correspondence for serial section reconstruction: complex scenarios in palaeontology. *Computers and Geosciences*, **27**, 427–440.

MARDIA K.V. and JUPP P.E. 2000. Directional Statistics. Wiley, Chister, NewYork, Weinheim, Brisbane, Singapore, Toronto, pp. 430.

MARSCHALLINGER R. 2001. Three-dimensional reconstruction and visualization of geological materials with IDL – examples and source code. *Computers and Geosciences*, **27**, 419–426.

MARSCHALLINGER R., HOFMANN P., DAXNER-HÖCK G. and KETCHAM R.A. 2011. Solid modeling of fossil small mammal teeth. *Computers and Geosciences*, **37**, 1364–1371.

MAYRHOFER S. and LUKENEDER A. 2011. 3D modelling in palaeontology – a case study on the Triassic ammonite *Orthoceltites* (Carnian, Taurus, Turkey). *Geophysical Research Abstracts*, **13**, (EGU2011–1833).

MILLANE R.P., WEIR M.I. and SMART G.M. 2006. Automated analysis of imbrication and flow direction in alluvial sediments using laser-scan data. *Journal of Sedimentary Research*, **76**, 1049–1055.

OLIVERO E.B., 2007. Taphonomy of ammonites from the Santonian - Lower Campanian Santa Marta Formation, Antarctica: Sedimentological controls on vertically embedded ammonites. *Palaios*, **22**, 586–597.

POTTER P.E. and PETTIJOHN F.J. 1977. Paleocurrents and Basin Analysis, 2nd ed. Springer-Verlag, Berlin, Heidelberg, New York, pp. 425.

SANDER B. 1930. Gefügekunde der Gesteine. Springer-Verlag, Wien, pp. 352.

SCOTESE C.R. 1998. Quick time Computer Animations. PALEOMAP Project. Department of Geology, University of Texas at Arlington.

SCOTESE C.R. 2001. Paleomap Project. http://www.scotese.com/ (accessed July 2001).

SCOTESE C.R., GAHAGAN L.M. and LARSON R.L. 1989. Plate tectonic reconstructions of the Cretaceous and Cenozoic ocean basins. *In*: SCOTESE C.R. and SAGER W.W. (eds). Mesozoic and Cenozoic plate reconstructions. Elsevier, Amsterdam, 27–48.

SEILACHER A. 1959. Fossilien als Strömungs-Anzeiger. *Aus der Heimat*, **67**, 170–177.

SEILACHER A. 1960. Strömungsanzeichen im Hunsrückschiefer. *Notizblatt des Hessischen Landesamtes für Bodenforschung*, **88**, 88–106.

SEILACHER A. 1971. Preservational history of ceratite shells. *Palaeontology*, **14 (1)**, 16–21.

ŞENGÖR A.M.C., YILMAZ Y. and SUNGURLU O. 1984. Tectonics of the Mediterranean Cimmerids: Nature and Evolution of the Western Termination of Paleo-Tethys. *Geological Society of London Special Publications*, **17**, 77–112.

SENGUPTA S. 1966. Studies on orientation and imbrication of pebbles with respect to cross-stratification. *Journal of Sedimentary Petrology*, **36 (2)**, 362–369.

SIMPSON G.G. 1933. A simplified serial sectioning technique for the study of fossils. *American Museum Novitates*, **634**, 1–6.

SOLLAS W.J. 1903. A method for investigation of fossils by serial sections. *Philosophical Transactions of the Royal Society*, **B196**, 259–265.

SPINSBY J., FRIEDRICH H. and BUSECK P.R. 2008. Volume and surface-area measurements using tomography, with an example from the Brenham pallasite meteorite. *Computers and Geosciences*, **34**, 1–7.

STAMPFLI G.M. and BOREL G.D. 2002. A plate tectonic model for the Paleozoic and Mesozoic constrained by dynamic plate boundaries and restored synthetic oceanic isochrons. *Earth and Planetary Science Letters*, **196**, 17–33.

STAMPFLI G.M., BOREL G.D., MARCHANT R. and MOSAR J. 2002. Western Alps geological constraints on western Tethyan reconstructions. *Journal of the Virtual Explorer*, **8**, 77–106.

STENSIÖ E.A. 1927. The Downtonian and Devonian Vertebrates of Spitsbergen, Pt. I. Familiy Cephalaspidae. *Skrifter Om Svalbard Og Nordishavet*, **12**, 1–391.

SUTTON M.D. 2008. Tomographic techniques for the study of exceptionally preserved fossils. *Proceedings of the Royal Society*, **B275**, 1587–1593.

TRENDELL A.M., ATCHLEY S.C. and NORDT L.C. 2013. Facies analysis of a probable large-fluvial-fan depositional system: The Upper Triassic Chinle Formation at Petrified Forest National Park, Arizona. U.S.A. *Journal of Sedimentary Research*, **83**, 873–895.

VANDERHOOF V.L. 1931. *Borophagus littoralis* from the marine Tertiary of California. *University of California Publications, Bulletin Department of Geological Science*, **21**, 15–24.

VASIĻKOVA J., LUKŠEVIČS E., STINKULIS Ģ. and ZUPIŅŠ I. 2012. Taphonomy of the vertebrate bone beds from the Klūnas fossil site, Upper Devonian Tērvete Formation of Latvia. *Estonian Journal of Earth Sciences*, **61**, 105–119.

WALLBRECHER E. 1978. Ein Cluster-Verfahren zur richtungsstatistischen Analyse tektonischer Daten. *Geologische Rundschau*, **67**, 840–857.

WALLBRECHER E. 1979. Methods for a quantitative comparison of orientation data using vectorstatistics and eigenvalue analysis with special reference to degrees of preferred orientation and distribution shapes. *Neues Jahrbuch für Geologie und Paläontologie, Abhandlungen*, **159**, 113–149.

WALLBRECHER E. 1986. Tektonische und gefügeanalytische Arbeitsweisen. Ferdinand Enke Verlag, Stuttgart, pp. 244.

WANI R. 2006. Planispiral Cephalopod Shells as a sensitive indicator of modern and ancient bottom currents: new data from flow experiments with modern *Nautilus pompilius*. *Palaios*, **21**, 289–297.

WANI R. 2007. How to recognize insitu fossil cephalopods: evidence from experiments with modern *Nautilus*. *Lethaia*, **40**, 305–311.

WEBER G.W. and BOOKSTEIN F.L. 2011. Virtual Anthropology – A Guide to a New Interdisciplinary Field. Springer Verlag, Wien, New York, pp. 423.

WENDT J. 1995. Shell directions as a tool in palaeocurrent analysis. *Sedimentary Geology*, **95**, 161–186.

WENDT J., AIGNER T. and NEUGEBAUER J. 1984. Cephalopod limestone deposition on a shallow pelagic ridge: the Tafilalt Platform (upper Devonian, eastern Anti-Atlas, Morocco). *Sedimentology*, **31**, 601–625.

WHITE W.S. 1952. Imbrication and initial dip in a Keweenawan conglomerate bed. *Journal of Sedimentary Petrology*, **22**, 189–199.

CHAPTER VI,

ACCEPTED 2016 FOR PUBLICATION IN LETHAIA

TAPHONOMY AND PALAEOECOLOGY OF LATE TRIASSIC (CARNIAN) AMMONOID CONCENTRATIONS FROM THE TAURUS MOUNTAINS, TURKEY

Susanne Mayrhofer[a]*, Alexander Lukeneder[b], Leopold Krystyn[c]

[a] Natural History Museum Vienna, Department for Exhibition & Education, Burgring 7, A-1010 Vienna, Austria

[b] Natural History Museum Vienna, Geological-Paleontological Department, Burgring 7, A-1010 Vienna, Austria

[c] Department of Palaeontology, University of Vienna, Vienna, Austria

Abstract

The deposits of the Carnian Kasımlar Formation within the Taurus Platform Units of south-western Turkey represent an important archive of a Late Triassic ecosystem. New palaeontological information was obtained by analysing the *Kasimlarceltites* mass occurrence, located within the Kasımlar Formation and named after the Lower Carnian (Julian) ammonoid genus *Kasimlarceltites*. This is the dominant taxon (> 94%) within the mass occurrence: nearly 775 million ammonoids and 50 million gastropods were extrapolated for the whole extension (at least 5 km^2) of the *Kasimlarceltites* beds. This calculation is one of the main findings within this study, as it is the first time that such a fossil mass occurrence was quantified. Additionally, orientation measurements of the planispiral ammonoids and the helical gastropods enabled reconstructing the history of the mass occurrence and interpreting the underlying transport mechanisms. Further taphonomic aspects (e.g. biofabric, preservation, bioerosion or genetic classification) as well as comparisons with samples of the same acme zone from different localities near Aşağiyaylabel (AS IV, KA I, II & IV) point to a two-phased genetic history. Accordingly, local mass mortality within the *Kasimlarceltites* fauna due to oxygen fluctuations or methane degassing may have initially led to a primary accumulation. These deposits were then reworked and redeposited basinward by gravity flows to create the present-day secondary allochthonous concentrations.

Keywords: Spatial shell orientation, Taphonomy, Ammonoids, *Kasimlarceltites*, Late Triassic, Carnian Crisis, Turkey, Taurus Mountains.

6.1. Introduction

The interpretation of depositional conditions of ammonoid mass occurrences based on combined taphonomic and palaeoecological information has become an increasingly hot topic during the last few decades (e.g. Seilacher 1960, 1968, 1971, 1990; Maeda and Seilacher 1996; Keupp 1997; Maeda 1999; Lukeneder 2003, 2004, 2005; Fernández-López 2007; Olivero 2007; Wani 2007; Reyment 2008; Tomašových and Schlögl 2008; Maeda and Shigeta 2009; Lukeneder and Mayrhofer 2014). The mass occurrence investigated here consists to 94–99% of the single species *Kasimlarceltites krystyni*, which is presently known only from the area around Aşağiyaylabel. The *Kasimlarceltites* mass occurrence was deposited during Carnian time (Late Triassic) within an intra-shelf basin of the western Cimmerian terranes. The Carnian is best known for a Tethyan-wide carbonate platform demise (Carnian Crisis = Carnian Pluvial Event; Simms and Ruffell 1989; Lukeneder *et al.* 2012). The deposition of these ammonoids at an equatorial position (for Turkey about 9° according to Stampfli *et al.* 2002 and Moix *et al.* 2008) makes them suitable for taphonomic investigations on the genesis of this huge shell deposit, but also yields new insights into the Carnian Crisis at equatorial regions. We therefore investigated and analysed parameters related to the orientation of the ammonoid shells. We adopted a new study-approach on such planispirally coiled ammonoids, already tested by Lukeneder *et al.* (2014).

The study was performed to test the number and orientation of the ammonoids within the known extension of the *Kasimlarceltites* mass occurrence, and therefore represents a quantification of an ammonoid mass occurrence done for the first time. The quantitative data were interpreted in combination with qualitative information about the depositional conditions from different slices and thin-sections taken from various parts of the mass occurrence. The main aim of this study was to solve the following research questions: Are these ammonoids orientated in the same way as already tested within the smaller reference block (done by Lukeneder *et al.* 2014), and what does this result mean for the depositional conditions? Does the orientation of the ammonoids fit with the taphonomic interpretation of this shell bed? How might the life habitat of *Kasimlarceltites* and the environmental conditions, which occurred throughout the deposition of this mass occurrence, looked like?

The answers to these questions shed light into the genesis of this mass occurrence and consequently into the environmental conditions which occurred throughout its deposition during the time of the Carnian Crisis.

6.2. Geographical and geological setting

The outcrop with the investigated bed AS 6 is situated near the village Aşağiyaylabel (Anatolia; N 37.551389° and E 31.304444°) in the western Taurus Mountains of Turkey (Fig. 6.1A–B). The sedimentary record at Aşağiyaylabel belongs to the top of the Kartoz and the base of the Kasımlar Formation and is therefore of late Early Carnian (Julian 2) to early Late Carnian age (Tuvalian 1). The Kasımlar Formation at Aşağiyaylabel represents one of the rare complete successions with a Lower to Upper Carnian ammonoid fauna (see Lukeneder and Lukeneder 2014).

Fig. 6.1. A, Map of Turkey indicating the outcrop position of Aşağiyaylabel. **B**, Detailed map of the area around Aşağiyaylabel and Karapinar.

The ammonoid coquinas (mass occurrence), on which this study focuses, belong to the Carbonate member (Unit A), near the bottom of the Kasımlar Formation. The *Kasimlarceltites* shell beds are composed of at least eight layers (1.8 m at AS I) to a maximum of 113 layers (16.5 m at KA II), with an extension over an area of at least 5 km^2. Single beds are 2–40 cm thick. Detailed investigations were conducted in bed AS 6 of the section AS I, and compared with further samples from the *Kasimlarceltites* acme zone of the sections AS IV, KA I and KA II (Fig. 6.2). The layers of section AS IV are preserved in an overturned position. This is proven by geopetal fills, exhibiting their calcitic crystallisation (i.e. filling of voids, sediment free) at the "bottom" of the ammonoids, as well as by the inverse gradation of the sediment. In addition, in the field, at section AS IV and sections KA I and KA II, the *Kasimlarceltites* beds were found above the rudstone layers and below the shallow-water limestones in a stratigraphically overturned position. For a better comparison of the four localities, the stratigraphic overturn was corrected in the figured logs (Fig. 6.2).

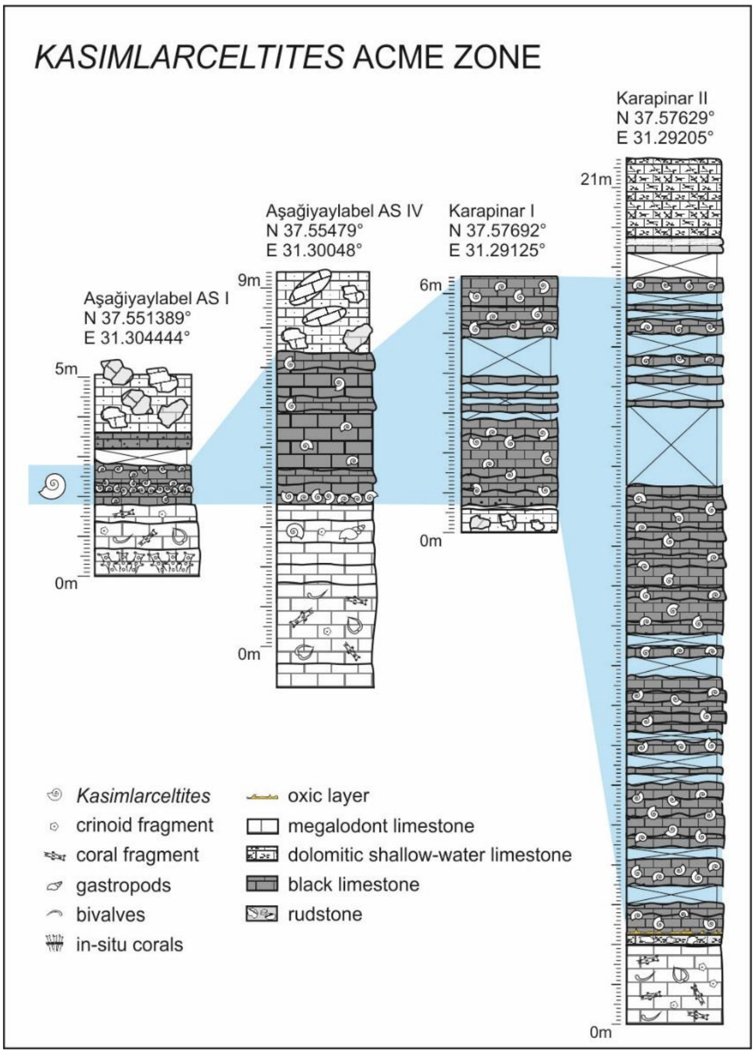

Fig. 6.2. Logs of Aşağiyaylabel (AS I, AS IV) and Karapinar (KA I, KA II) with indicated position of the *Kasimlarceltites* acme zone (blue area).

6.3. Material and methods

The number and orientation of the ammonoids was tested based on a 150 × 45 × 140 mm reference block taken at the locality AS I from bed AS 6 (Fig. 6.3A). The block was cut from the limestone bed, ground and scanned at 2 mm intervals to produce 70 slices (Fig. 6.3A–C). From there the ammonoids were virtually segmented and a 3D-surface rendered (Fig. 6.4A–E). The destructive method of grinding (Lukeneder *et al.* 2014; Naglik *et al.* 2015a, 2015b; Tajika *et al.* 2015) was used because the non-destructive method of computed tomography did not work due to similar density of the ammonoids (i.e. secondary calcite shells, about 2.6–2.8 g/cm^3) and the host rock (limestone matrix, about 2.8 g/cm^3).

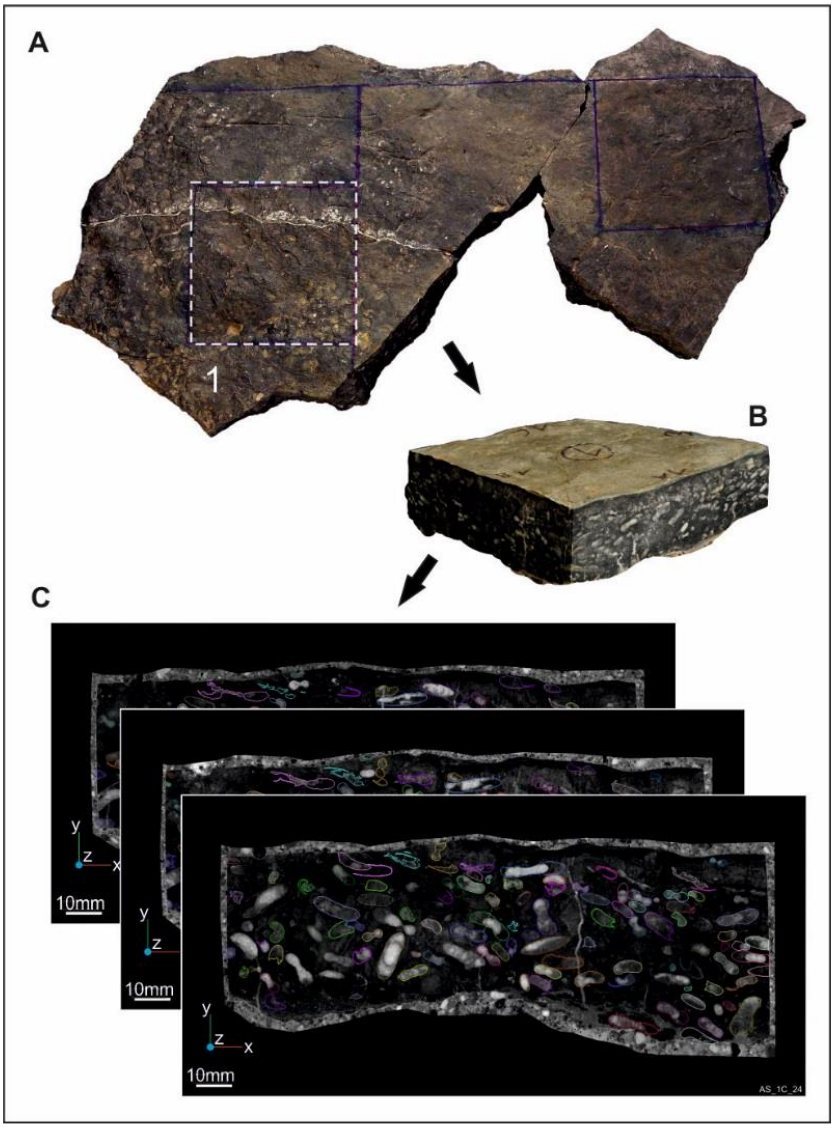

Fig. 6.3. Steps from bed to ammonoid segmentation. **A**, Ammonoid bed taken from the field (AS I, bed 6) with indicated position of the reference block. **B**, Segmented reference block (150 × 45 × 140 mm). **C**, Scanned slices of the reference block.

The 3D-visualisation-method described by Lukeneder *et al.* (2014) was used to analyse a possible spatial orientation of the ammonoids within the shell bed AS 6. The whole ammonoids, but also the gastropods (Fig. 6.4F–G), from the reference block were virtually segmented (Fig. 6.4A–G), counted and, if possible, their orientation analysed. By using landmark data (each segmented ammonoid was equipped with three and each segmented gastropod with two specified landmarks; Fig. 6.4E, G) the statistical orientation of each ammonoid and gastropod was investigated. Orientation parameters (maximum diameter, dip, dip direction and aperture direction of the lineation A:B through the gastropods and ammonoids, as well as dip and azimuth of an imaginary sagittal-plane A-B-C through the ammonoids), already known from geological orientation measurements, were calculated (Fig. 6.5A).

Following Lukeneder *et al.* (2014) we used only those ammonoids for orientation analyses that were reconstructed from at least six slices when analysing the lineation A:B. At least three slices were required when analysing the imaginary sagittal-plane (Fig. 6.5A). We furthermore adapted the method described by Lukeneder *et al.* (2014) for the segmented gastropods. Here, the orientation of the lineation A:B was analysed for 20 gastropods (intersected at least twice). For a detailed description of the method used see Lukeneder *et al.* (2014).

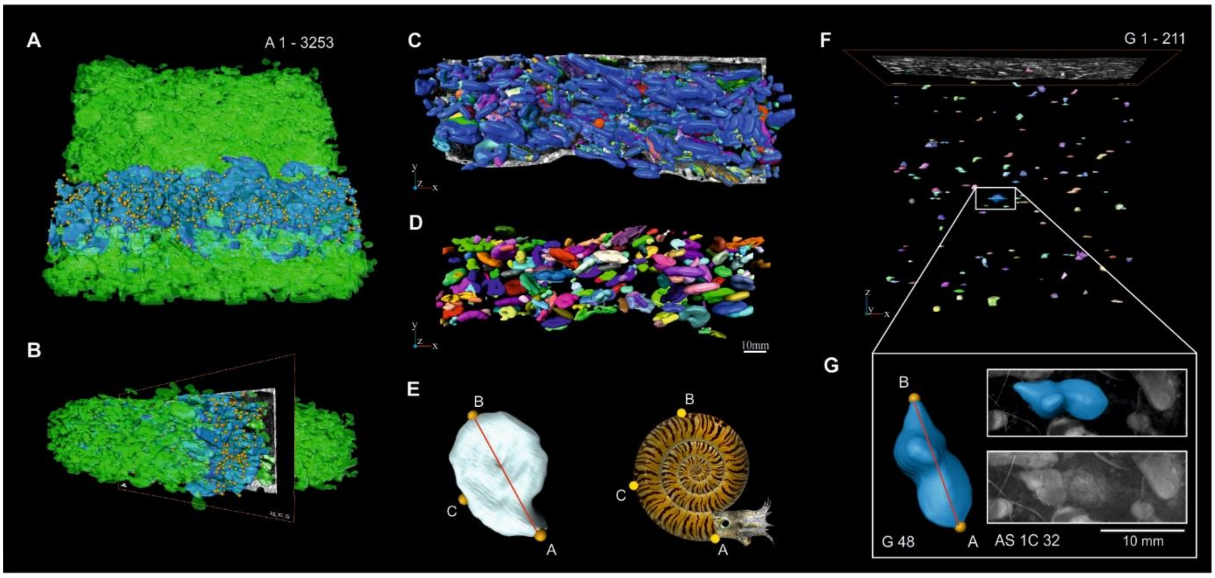

Fig. 6.4. Ammonoid segmentation pictures (made with Amira). Virtual reconstruction and land-mark-setting of the ammonoids and gastropods from the reference block. **A–B**, 3,253 segmented ammonoids (blue and green ammonoids). Blue ammonoids (n = 675) already investigated in Lukeneder *et al*. (2014). **A**, View from top. **B**, Side view. **C–D**, Frontal view of segmented ammonoids. **E**, Landmark positions (A–C), placed on every ammonoid surface and shown at a virtual ammonoid model designed by 7Reasons. **F**, Segmented gastropods from the whole reference block. **G**, Segmented gastropod with indicated landmarks (A–B) that were placed on every segmented gastropod.

6.3.1. Statistical methods for analysing the orientation

The spatial orientation of the segmented ammonoids and gastropods was statistically analysed with the software package Fabric8, usually used for the graphical display and analysis of tectonic data. The orientations of the aperture directions, as well as of the strike data were analysed within rose diagrams (Fig. 6.5B). Dip and dip direction of the lineations (A:B) as well as dip and azimuth of the planes (A-B-C) were analysed by plotting them stereographically (Fig. 6.5C–F). The orientation of 675 specimens of these ammonoids have already been published by Lukeneder *et al.* (2014).

6.3.2. Rose diagrams

Rose diagrams (Figs 6.5B, 6.6A, E) are circular histograms used for graphical analyses of pure directional data in a two-dimensional way, without dip, dip direction, or strike. Raw data of directions were classified according to defined intervals. These intervals are drawn as sectors into a circle with a radius defined such that the most frequent percentage of the raw data directions plots at the circumference. Charting the percentages of the intervals into the diagram yields a graphical interpretation (Figs 6.5B, 6.6A, E). The software Fabric8 enabled statistical analyses of the directional data, complementing the graphical method. For more details about rose diagrams see Wallbrecher (1986).

6.3.3. Stereographic plots

Stereographic plots (Figs 6.5C–F, 6.6B–D, F) were used to analyse spatial directional data in a three-dimensional way. Pure directions were analysed in combination with their angle of dip (e.g. dip + dip direction of a lineation, resp. dip + azimuth of a plane). The stereographic projection (Fig. 6.5D, F) represents the equatorial plane of the so-called “sphere diagram” (Fig. 6.5C, E). When placing a projected lineation “L” (Fig. 6.5C) within this sphere diagram, the intersection-point of the elongation of this lineation “L” with the lower hemisphere represents the sphere projection point “S”. When projecting a lineation from point “S” to the zenith of this sphere diagram, the intersection point “I” at the equatorial plane represents the data point “I” of the lineation “L” at the stereographic plot (Fig. 6.5C–D). The same procedure can be performed with single planes. When projecting a plane within this sphere diagram (Fig. 6.5E), the intersection point “I” of the sphere projection point “S” of an imaginary orthogonal lineation from the plane “p” towards the sphere represents the data-point “I” of the plane “p” on the stereographic plot (Fig. 6.5E–F). The stereographic projection plane bears a net of curves of constant latitudes and longitudes (Mardia and Jupp 2000). A more detailed description of stereographic plots and sphere diagrams is given by Wallbrecher (1978, 1979, 1986). Compared to other statistical methods of analysing directional data, the advantage of stereographic plots is the spatial approach. The possibility of representing planes and lineations in the stereographic plot with a single point allows dealing with large data-sets (Adler *et al.* 1982; Wallbrecher 1986). The strike and azimuth of single points nevertheless can be precisely quantified. Complex statistical analyses are replaced by investigating maxima and fields of similar population density (Adler *et al.* 1982). The stereographic plot is mostly used for tectonic, but also for sedimentological analyses. For example, Potter and Pettijohn (1977) used stereographic plots to analyse disk-shaped particles in respect to current versus gravity transport. Within our study, Potter and Pettijohn´s method is adapted for orientation analyses of planispiral cephalopods. Azimuth and azimuth direction of the ammonoids should be analysed in the same way as the disk-shaped particles described by Potter and Pettijohn (1977).

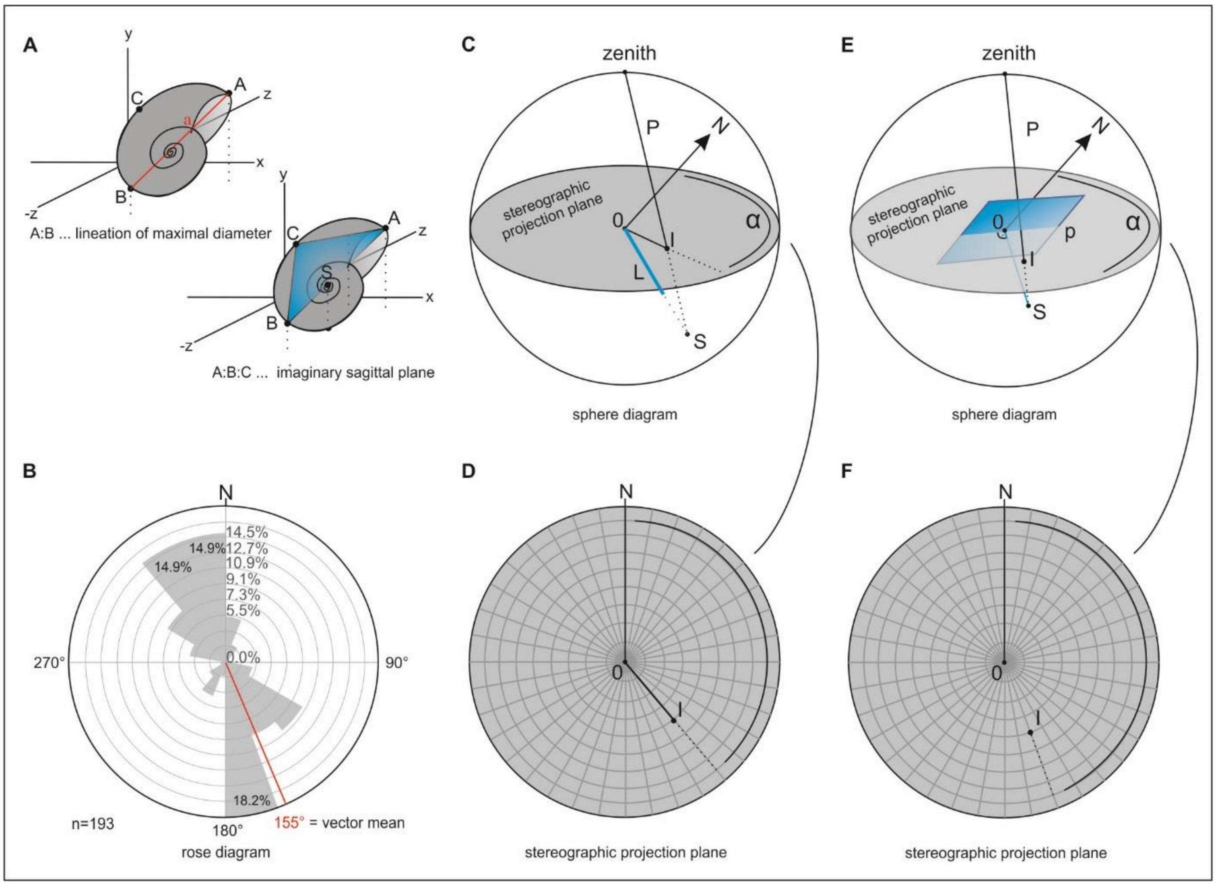

Fig. 6.5. **A**, Explanation of the orientation parameters used for subsequent investigation of the spatial orientation of each ammonoid. **B**, Example of a rose diagram. **C**, Sphere diagram with an intended lineation “L” and its projection point “I” at the stereographic projection plane. **D**, Stereographic projection plane of the sphere diagram (**C**) at which the projection point “I” of the lineation “L” plots. **E**, Sphere diagram with intended plane “p” and its projection point “I” at the stereographic projection plane. **F**, Stereographic projection plane of the stereographic plot (**E**) with indicated projection point “I” from the intended plane “p”.

6.4. Results

As described by Kidwell *et al.* (1986), shell concentrations can be classified using a descriptive nomenclature (taxonomic composition, biofabric, geometry and internal structure) as well as a genetic classification (lithological-, biological- or diagenetic genesis; see Martin 1999). To analyse the *Kasimlarceltites* mass occurrence from Aşağiyaylabel, we used Kidwell´s approaches. We also applied terminological terms of Seilacher (1990) to estimate the ancient environment of the depositional area and the mechanisms that led to the genesis of these fossil ammonoid concentrations.

6.4.1. Geometry and internal structure

Following Kidwell *et al.* (1986) the mass occurrence has to be interpreted as a "bed" instead of clump, pod, lens or wedge. The lateral distribution of the *Kasimlarceltites* layers differs at each section between 20 m and 50 m: more than 30 m at AS I and 50 m at AS II and AS IV, as well as over 20 m at KA I and KA III and 50 m at KA II. Due to the known distribution, we assume that it represents a more or less consistent three-dimensional structure over an area of about 5 km^2 (Fig. 6.1). The whole acme zone, which consists of several beds (e.g. bed AS 6), is 1.8 m (at AS I) to 16.5 m thick (at KA II; Lukeneder and Mayrhofer 2014), and alternates between beds full of ammonoids and beds yielding only scattered ammonoid shell remains (Fig. 6.2). The accumulation beds generally show the same thickness and shell density along the whole extension. The internal structure of the *Kasimlarceltites* mass occurrence is not uniform, but shows an upward fining trend in bioclasts. The lower part of the mass occurrence at bed AS 6 consists of almost entire ammonoid shells, whereas the topmost third of the bed shows partly fragmented ammonoid shells which are topped by densely packed halobiid bivalve shell remains, and therefore represent a graded sediment structure.

6.4.2. Lithology and microfacies of the host sediment

The background sediment of bed AS 6 represents a bioclastic pelagic wackestone (Fig. 6.7A), deposited within a deep shelf or mid-ramp (sensu Flügel 2004). The thin-shelled halobiid bivalves, deposited in masses at the top of the bed, generally occur in deep-water, oxygen-deficient settings or in ''pelagic'' or ''filamentous'' limestones, which represent fully oxygenated marine settings (McRoberts *et al.* 2008; McRoberts 2000, 2010; Lukeneder *et al.* 2012). Lagenid Foraminifera, *Omphaloptycha*-like gastropods and some thick-shelled bivalves, which also occur in bed AS 6 and within under- and overlying beds, represent allochthonous biogens, transported from the fore slope or shallow-marine ramp (Lukeneder *et al.* 2012). Geopetal fills show different directions, pointing to a phase of reworking following pre-lithification of the ammonoids (Fig. 6.7A–B). Compared to bed 6 of section AS I, the background sediment at the localities AS IV and KA I is more grain-supported, hence representing a bioclastic packstone (Fig. 6.7B–E). This is in contrast to wackestone, which occurs both at section AS I (Fig. 6.7A) and section KA II (Fig. 6.7F). Anyhow, due to the high density of allochthonous biogens, at both localities, the fabric of the accumulation layers represent floatstones.

6.4.3. Taxonomic composition

Ninety-four to 99% of the shells found within the mass occurrence of bed AS 6 at the section Aşağiyaylabel I (AS I) are identified as the ammonoid species *Kasimlarceltites krystyni*. The rest consists of the ammonoids *Sirenites senticosus* and *Klipsteinia disciformis* along with *Omphaloptycha*-like gastropods (Fig. 6.8A–B). Furthermore, the ammonoid coquina is covered by halobiid bivalves (for taxonomic details see Lukeneder and Lukeneder 2014). The fact that nearly 99% of the shells belong to *K. krystyni* and the rare additional ammonoid and gastropod species document a paucispecific assemblage (Kidwell *et al*. 1986). The macrofauna of the ammonoid mass occurrence of the sections AS IV, KA I and KA II shows nearly the same composition as found at AS I. Besides the dominance of *Kasimlarceltites*, some *Omphaloptycha*-like gastropods and thin-shelled halobiid bivalves, fragments of corals and sponges are also present. AS IV additionally contains siliceous sponge spicules (Fig. 6.7B). Different from AS I, AS IV and KA II, *Kasimlarceltites krystyni* is less dominant in section KA I, where it represents only 50% of the ammonoid specimens (Fig. 6.7E).

6.4.4. Number of ammonoids and gastropods

An extrapolation of the counted ammonoids (3,253) and gastropods (211) from the reference block (section AS I, bed AS 6) for the whole extension of the *Kasimlarceltites* bed detected to date (AS I, AS IV, KA I, KA II; 5 km^2) gives nearly 775 million ammonoids and 50 million gastropods. These values were extrapolated using the following calculation:

$$x = \frac{\text{no. of specimens of one group from the reference block}}{\text{square footage of the reference block}} \cdot \text{ square footage of whole extenion}$$

6.4.5. 3D-arrangement of ammonoid shells

The orientation of the ammonoids was analysed to determine their distribution (random or uniform). For this purpose we analysed the significant orientation of the aperture as well as the orientation of an imaginary lineation and plane through each ammonoid of the reference block from bed AS 6 of section AS I (Fig. 6.5A).

Aperture orientation (Fig. 6.6A) shows a bimodal NNW/SSE distribution with a preferred orientation of 47%. Although the vector mean of 156° is SSE directed, the maximum class volume (15.1%) is located within the interval 320°–340° and is therefore NNW directed. Analysing the dip in combination with the dip direction of the imaginary lineation (Fig. 6.5A, C–D) within a stereographic plot (Fig. 6.6B) revealed a preferred (46.8%) SE orientation of the lineations (100% would indicate a perfect parallel orientation). The lineations (Fig. 6.6B) show a slight inclination of 18° toward SE (= 144°).

Analysing ammonoid orientation with respect to the dip and azimuth of the imaginary sagittal-plane through each ammonoid (Fig. 6.5A, E–F), we found that 66.2% (preferred orientation) are inclined with 14° toward 155° (SSE; Fig. 6.6C–D). The true center of gravity (cone of confidence; green circle), comparable within the mean of the linear statistic, plots with a significance of 0.05 at 155°/14° (Fig. 6.6D).

6.4.6. 3D-arrangement of gastropod shells

Analysing the aperture direction of the gastropods within a rose diagram (Fig. 6.6E) showed a bimodal SSE/NNW distribution with a preferred orientation of 88%. The maximum class volume (30.5%) lies at the interval 140°–160°, at which the vector mean plots SSE-directed at 156°. Dip and dip direction of the lineations (A:B) of the gastropods furthermore show a preferred SSE orientation (72.4%), with an inclination of 24° toward 153° (Fig. 6.6F).

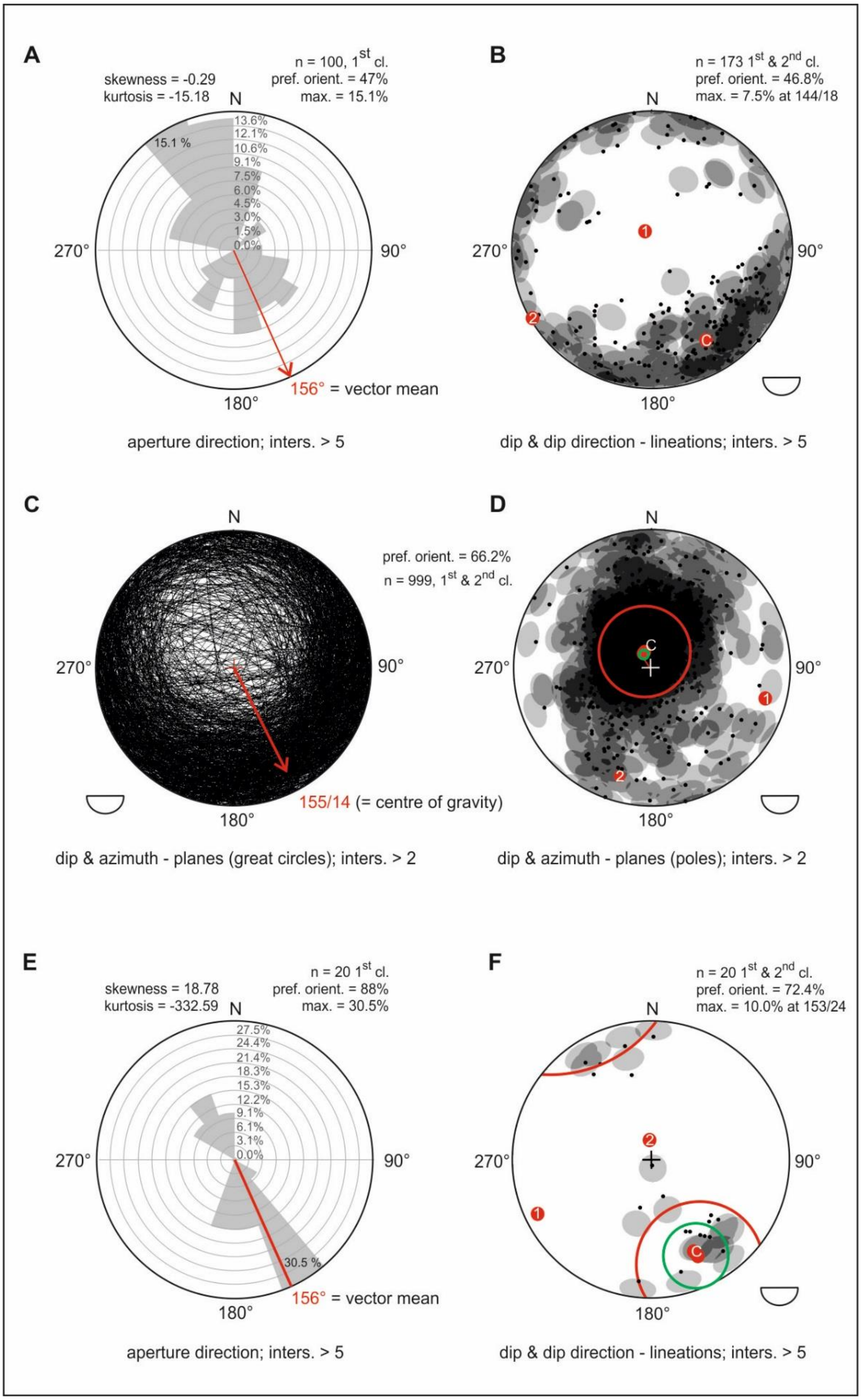

Fig. 6.6. Results of analysed spatial shell orientation. **A**, Rose diagram, indicating a bimodal SSE/NNW aperture orientation of the tested ammonoids with indicated aperture. **B**, Dip and dip direction of the lineation (A:B) of the ammonoids), plotted on a stereographic projection plane. **C–D**, Dip and azimuth of the planes (A-B-C), respectively ammonoids analysed within a sphere diagram. **C**, Plot of great circles. **D**, Plot of plane poles. **E**, Rose diagram, indicating a bimodal SSE/NNW aperture orientation of the tested gastropods with indicated aperture. **F**, Dip and dip direction of the lineation (A:B) of the gastropods, plotted on a stereographic projection plane.

6.4.7. Shell morphology

The genus *Kasimlarceltites* is morphologically (i.e. serpenticone, highly evolute; see Lukeneder and Lukeneder 2014) similar with, and in this case taxonomically closely related to other celtitid ammonoids such as *Aplococeras*, *Lecanites* and *Celtites*. The *Kasimlarceltites* shell morphology shows a trend from spherical (embryonic stage) via strongly depressed (juvenile phase) to compressed forms (adult to pre-adult stages; Fig. 6.8C). This is also reflected in WER (whorl expansion rate) and W/D (whorl width/diameter) measurements (Lukeneder and Lukeneder 2014). Whilst most WER values (Korn 2000) of *K. krystyni* range between moderate (1.61–2.0) and moderately high (2.01–2.4), some of them show even high WER values (e.g., 2.6).

6.4.8. Size, shape and sorting

The size of the virtually segmented planispiral ammonoids (Fig. 6.4) from the block of bed AS 6 ranges from 1.5–27.7 mm. This is quite similar to the size variation of the physically segmented specimens of *Kasimlarceltites krystyni* from bed AS 6 at section AS I, where ammonoid size is 0.6–33.0 mm (Lukeneder and Lukeneder 2014). Within block AS 6, ammonoids are abundant, but rare gastropods were also found (Fig. 6.8A). The virtually segmented gastropods are helical and their size ranges from 2.8–11.3 mm (Fig. 6.8A). The size of *Kasimlarceltites* at AS IV ranges from 4.4–25.9 mm, at KA I from 1.6–20.2 mm and at KA II from 3.0–26.8 mm. Not only at section AS I bed 6, but also at the other localities, small ammonoid shells (ammonitellae, juveniles or microconchs) are mixed with large shells (adult forms or macroconchs; Fig. 6.7A–F).

6.4.9. Biofabric

The biofabric differs between beds (Fig. 6.7A–F). In some places it is matrix-supported (Fig. 6.7A, F), which yields scattered ammonoid shell remains. In others it is shell-supported (Figs 6.7B–E, 6.8D), which represents an ammonoid concentration. Interfacial contact zones and areas between the ammonoid shells range from single point-contacts (Fig. 6.8Da, yellow circle) to concave/convex contacts (Fig. 6.8Db, Ec, yellow circles). At all the investigated sections where the *Kasimlarceltites* acme zone was found (AS I, AS IV, KA I and KA II), the sediment alternates between beds bearing *Kasimlarceltites* in masses (shell-supported structure, as seen at section AS I within bed AS 6; Fig. 6.9A–H), and beds containing only rare ammonoids with a scattered distribution (matrix-supported). Even the shell-supported beds, however, still contain parts, for example at KA II (Fig. 6.7F) or at AS I (Fig. 6.7A) that are matrix-supported.

6.4.10. Sedimentary infilling

Most ammonoid body chambers are filled with matrix accompanied by shell fragments (Figs 6.8F–Gb, 6.9A). Phragmocones are typically filled by sparry calcite (Fig. 6.8Ga), except for fragmented ones, which also contain matrix (Fig. 6.8Fa). Most geopetal structures show a similar arrangement in bed AS 6 (Fig. 6.8H–L, indicated by the base line of the sparry calcite and white arrows normal to them). Nonetheless, a number of ammonoid shells have inverse geopetal fills (Fig. 6.8Ha–Ia, yellow circles), and some intraclasts yield shells with inclined geopetal structures (Fig. 6.8La). Inverse geopetal structures are recognisable by sparry calcite at the bottom, in contrast to “normal” calcitic tops, and therefore point to reworking of the ammonoid shells after initial deposition (Fig. 6.8H–L). Ammonoids in AS IV, KA I and KA II show the same patterns. Most body chambers are filled by background sediment, and phragmocones are crystallised by sparry calcite (Fig. 6.7B–F). Especially within sections AS IV and KA I (Fig. 6.7B–E) the calcite filling of the phragmocones preserves the fine structures of the shells, the chambers or of the siphonal tubes (Fig. 6.7C, yellow circles) and enables them to be measured. The geopetal structures within the mass occurrence at sections AS IV, KA I and KA II reflect almost the same depositional conditions as in AS I (Fig. 6.8H–L). The inverse geopetal structures in AS IV (Fig. 6.7C) confirm the overturned nature of the whole succession.

6.4.11. Encrustation, abrasion and bioerosion

Lukeneder and Mayrhofer (2014) found no traces of encrustation, abrasion or bioerosion in the *Kasimlarceltites* mass occurrence (Fig. 6.8A–L). This indicates a relatively short exposure time on the sea floor. Precipitation of framboidal pyrite took place after burial. This pyrite growth is visible in Figure 6.8I (small yellow circles) and 6.9B–F (small yellow circles). Additionally, Figure 6.9F shows pressure solution in the form of stylolithic dissolution seams on many ammonoid shells; such shells, however, are recorded only in some areas of the reference block (AS 6). Framboidal pyrite is common at sections AS IV, KA I and KA II too, where it commonly occur within the background sediment and within the sediment-filled body chambers of the ammonoids (Fig. 6.7B–F).

6.4.12. Mode of preservation and fragmentation

Within the thin- and polished sections, but also within the 3D-reconstructions, most ammonoids within the lowermost two-thirds of bed AS 6 are well preserved; the topmost third of the layer, in contrast, yields mainly crushed shells and shell fragments (Fig. 6.9H). Most of the ammonoids exhibit the body chamber and lack marks of bioerosion and infestation (e.g., borings). Unfortunately, the ammonoids were hardly separable from the limestone matrix and, specifically, the body chambers could not be saved during physical extraction from the embedding limestone. The same holds true for the gastropods, for which only virtual segmentation could be performed. Nonetheless, due to the great abundance, enough specimens could be extracted for the taxonomic investigation (Lukeneder *et al.* 2014). In almost all ammonoids the shell is preserved as recrystallised calcite. Most phragmocones are filled with this secondary calcite too (Fig. 6.8Eb, Ga), whereas body chambers are filled with sediment (Fig. 6.8Ea, Gb). Chamber walls and a series of siphuncle tubes are well preserved (Figs 6.7C, 6.8G).

6.4.13. Genetic classification

Comparing the *Kasimlarceltites* mass occurrence with the three possible end-members of the ternary diagram of genetic types of skeletal accumulations (Kidwell *et al.* 1986), a sedimentological genesis is most plausible (Fig. 6.10). A mixture between a sedimentological end-member (type 2) and a mixed concentration (type 5; Kidwell *et al.* 1986) is assumed due to the stylolithic structures (e.g., Fig. 6.9F) and the ammonoid shell alteration from primary aragonite into secondary calcite.

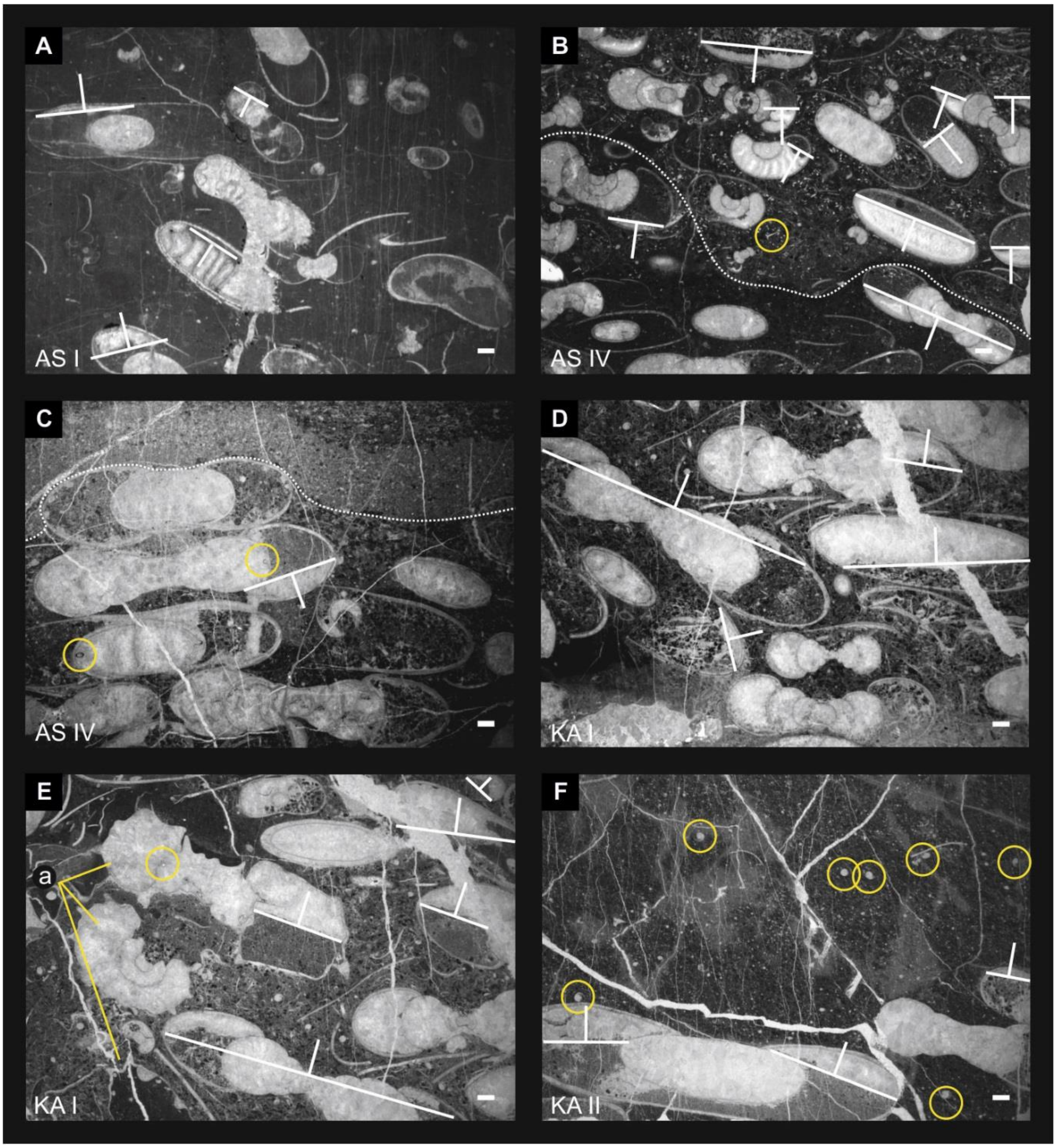

Fig. 6.7. Thin-sections of the *Kasimlarceltites* beds from different localities of the *Kasimlarceltites* acme zone. **A**, AS I, bed 6 – bioclastic pelagic floatstone. **B–C**, AS IV bed C – bioclastic packstone resp. floatstone with well-preserved sponge spicules (**B**, yellow circle); note the geopetal fills, which indicates an inverse position of this layer/section, and the fine-developed calcitic preservation of the phragmocones with their single chambers (**B**) as well as the siphonal tubes (**C**, yellow circle). **C**, NHMW 2014/0091/0008. **D–E**, KA I - NHMW 2014/0092/0003 – bioclastic packstone resp. floatstone; in addition to the dominant *Kasimlarceltites* (**D**), additional ammonoid genera (**E**) are well preserved at the mass occurrence of KA I. **F**, KA II – NHMW2014/0092/0004 – pelagic bioclastic wackestone, small ammonoid shells (ammonitellae, juveniles or microconchs = yellow circles) are mixed with large shells (adult forms or macroconchs. All scale bars: 1 mm.

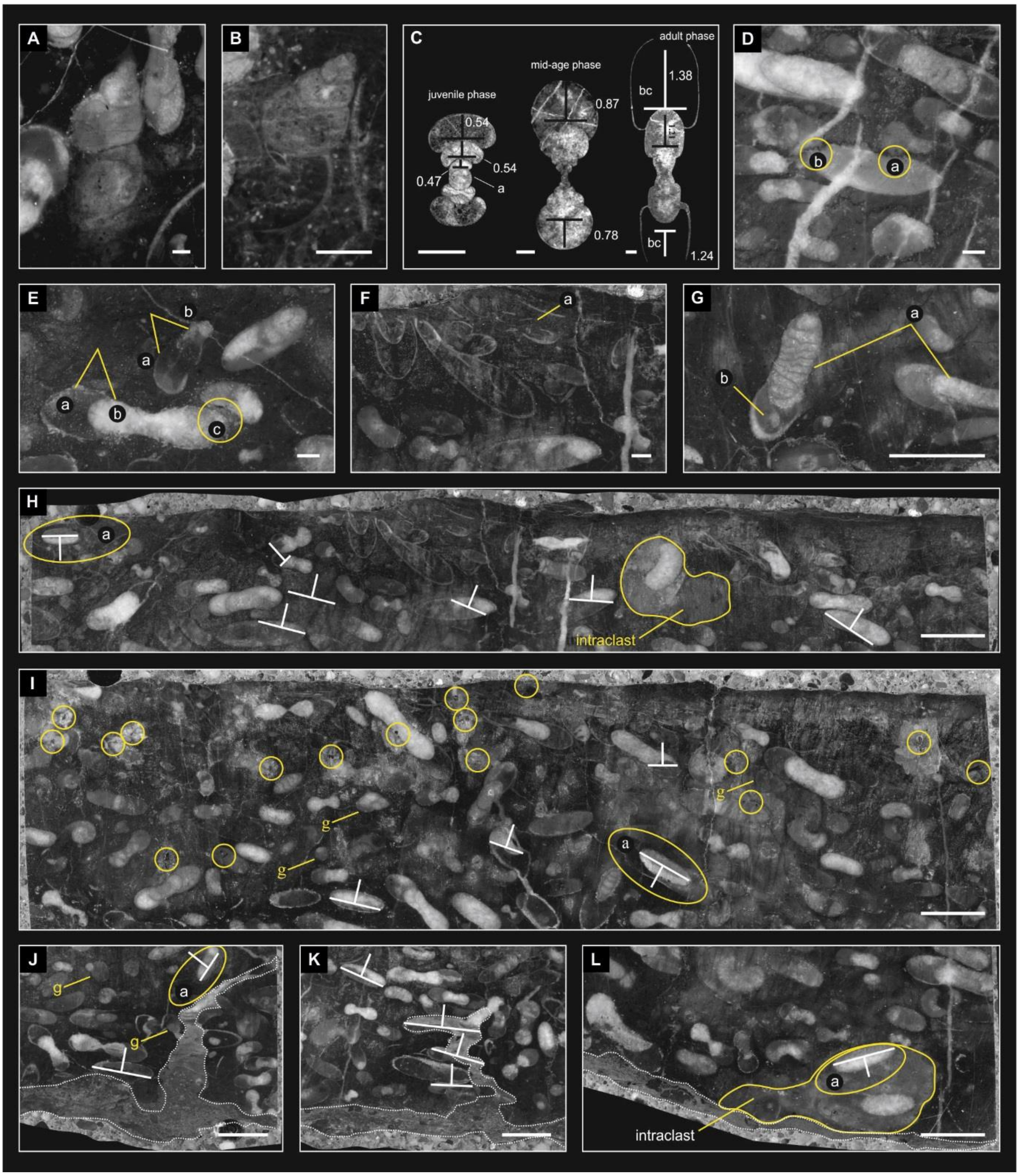

Fig. 6.8. A–B, Gastropods within the reference block from section AS I bed AS 6, at slice AS 1C 32 (**A**) and section AS IV bed C (**B**). **C**, Transversal thin-sections of three different ontogenetic phases of *Kasimlarceltites krystyni* with indicated H/W values (juvenile, mid-age, and adult phase; 2012z0133/0278-0290). **D–E**, Detailed pictures from the polished slice of bed AS 6/12 representing different textures. **D**, Grain- and shell-supported texture within some parts of AS 6/12, yellow circles point to stylolithic point contact (**a**) and stylolithic concave-convex contact (**b**), respectively. **E**, Matrix-supported part of AS6/12 with some concave-convex-contact (yellow circle). **F**, Fragmented ammonoid shells from the topmost part of slice AS 1C 21. **G**, Ammonoid shells with secondary calcite filling at the phragmocones, and matrix filling the body chamber at slice AS 1C 27. **H–I**, Geopetal fills of ammonoid shells, two specimens (yellow circles) show inverse positions and therefore indicate redeposition after lithification. **I**, Pyrite crystals resp. framboids (precipitation; small yellow circles). **H**, AS 1C 21. **I**, AS 1C 44. **J–K**, Synsedimentary dike fissure, filled with laminated sediment; most geopetal structures show similar orientation. **J**, Slice AS 1C 14. **K**, Slice AS 1C 11. **L**, Slice AS 1C 46 – erosional surface at the bottom; intraclast yielding ammonoids with inverse geopetal fills. White lineations indicate orientation of geopetal fills. Scale bars: **A–F**, 1mm, **G–I**, 10 mm.

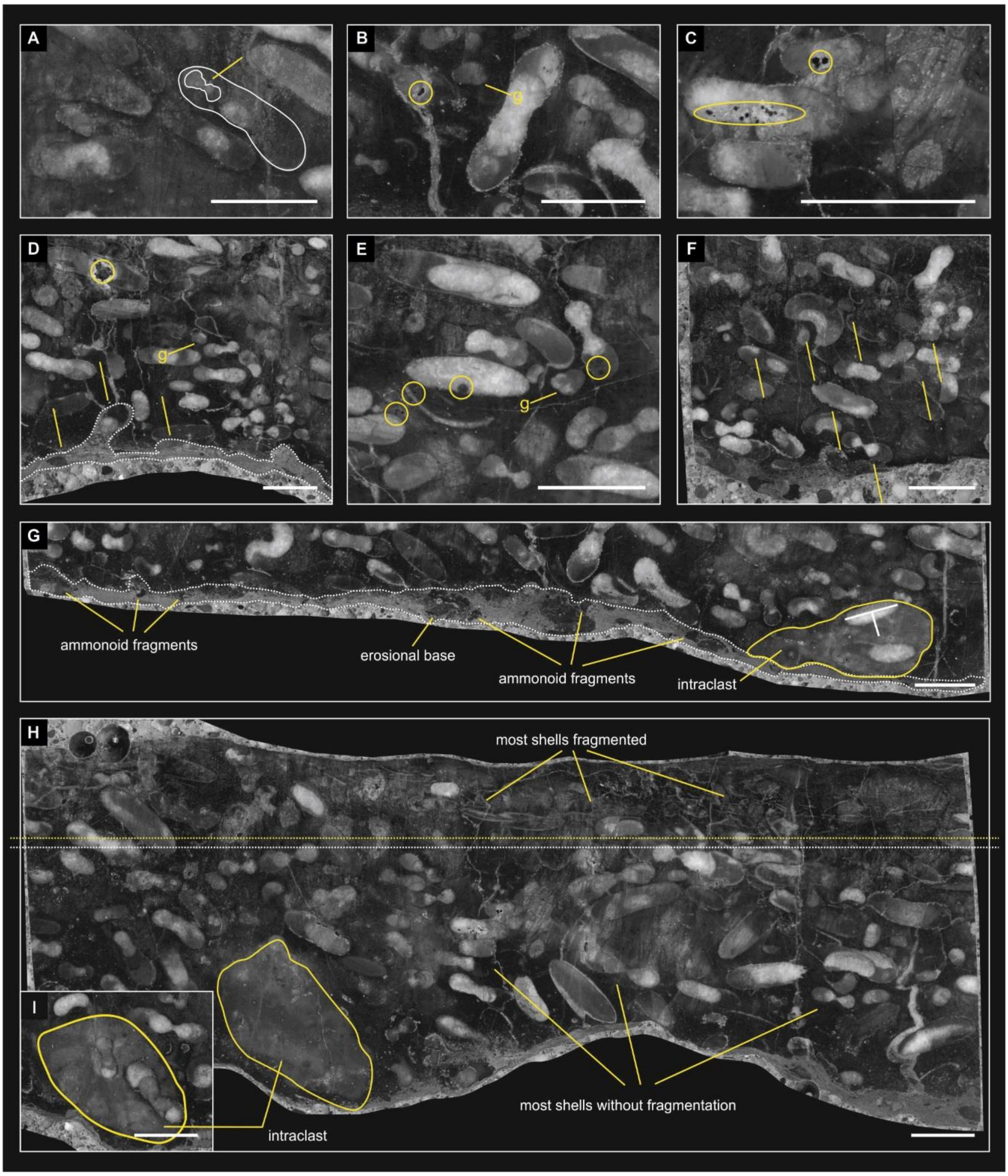

Fig. 6.9. Different slices of the reference block of bed AS 6. **A**, Ammonoid shell containing another ammonoid shell fragment within its body-chamber (slice AS 1C 37). **B–G**, Pyrite crystals resp. framboids (precipitation; **B–E**; AS 1C 47, AS 1C 56, AS 1 C 51, AS 1C 33), dissolution patterns such as stylolithic structures (**F**; AS 1C 39), and an erosional base (**D**, AS 1C 51; **G**, AS 1C 46). **H**, AS 1C 56 – lowermost two-thirds of the slice shows mostly complete ammonoids, whereas the topmost third is dominated by mostly fragmented ammonoid shells. **H–I**, Intraclast yielding ammonoid shells. **I**, AS 1C 54. All scale bars: 10 mm.

6.5. Discussion

Within this study a quantification of the specimens forming a fossil mass occurrence was done for the first time, which is furthermore one of the most important findings within this study. Besides this quantitative finding, taphonomical and sedimentological interpretations shed light into the genesis of this mass occurrence. Different hypotheses for the origin of such shell concentrations have been proposed in the last decades, from “primary biogenic concentrations” (Fürsich and Oschmann 1993), over “catastrophic mass mortality accumulations” and “post-spawning mortality accumulations” (Doyle and MacDonald 1993) to “winnowed, condensed or resedimented accumulations” (Doyle and MacDonald 1993; Fürsich and Oschmann 1993).

In studying the genesis of such mass occurrences, Fürsich and Oschmann (1993) defined nine types of skeletal concentrations: “fair-weather wave concentrations”, “storm wave concentrations”, “proximal tempestites”, “distal tempestites”, “current concentrations”, “primary biogenic concentrations”, “winnowed concentrations”, “transgressive lags” and “condensed concentrations”. Those authors furthermore described how the genesis can be identified based on taphonomic studies.

Due to the lack of cross-bedding within the *Kasimlarceltites* mass occurrence, lack of abrasion and only minimal shell breakage, a genesis of the ammonoid mass occurrences by “fair weather waves” or generally by “current actions” seems highly unlikely. The above mentioned features in combination with the well-sorted components (*Kasimlarceltites* shells – *Kasimlarceltites* shell fragments – halobiid bivalves) along with minimal bioerosion or encrustation at the *Kasimlarceltites* beds does not indicate a genesis by “primary biogenic concentrations”, “transgressive lags” as well as “condensed“ or ”winnowed concentrations”. The up to 70% well preserved *Kasimlarceltites* shells do not hint to “winnowed concentrations” or “transgressive lags”. “Winnowed concentrations” do not play a role as the fine material is not removed and the shell pavements are much thicker than 1 cm (Fürsich and Oschmann 1993). A mixture of different age fossils or the alteration of intensively burrowed beds, which also would be a hint to “winnowed concentrations” (Brett and Baird 1986; Flügel 2004), are furthermore not observed at the *Kasimlarceltites* shell beds. Additionally, the amount of encrustation, trace fossils or partly dissolved shells is too low (Flügel 2004). The paucispecific character of the *Kasimlarceltites* mass occurrence additionally excludes it from being “current“, or “condensed concentrations”. Following Fürsich and Oschmann (1993), the paucispecific character points to a genesis of the shell accumulation beds by “storm waves” or “tempestites”. Additional hints in the same direction are the good preservation of the ammonoids (scarce shell fragmentation, little to no bioerosion, abrasion or encrustation), the close packing, as well as the sharp erosional base of the bed.

The fabric of the *Kasimlarceltites* beds at sections AS I and KA II represents a bioclastic pelagic floatstone which Fürsich and Oschmann (1993) interpret as deposited by low-energy transport. The more grain-supported bioclastic packstone beds at sections AS IV and KA I are, after Fürsich and Oschmann (1993), short-term higher energy transport deposits.

6.5.1. Transport mechanisms deduced from spatial fossil orientation

Although most results between the segmented ammonoids from the entire block (n ≥ 3,000) and those done on fewer ammonoids (n = 675; Lukeneder *et al.* 2014) are quite similar (e.g. bimodal NNW/SSE orientation, slightly different vector mean of 156° instead of 150°, Fig. 6.6A), the preferred orientation (47%) tested within this study is slightly lower. Furthermore, the maximal class volume plots with 15.1% (vs. 16.1%) at 320°–340° and therefore exactly opposite to the maximum class volume tested within the smaller ammonoid sample of Lukeneder *et al.* 2014 (tested aperture directions in Lukeneder *et al.* 2014: n = 44).

In contrast to these differences, similar results as in the earlier study were obtained for the dip and dip direction of the lineations A:B (18°/144°, 46.8% preferred orientation; Fig. 6.6B) and for the dip and azimuth of the planes A-B-C and their plane poles (14°/155°, 66.2% preferred orientation; Fig. 6.6C–D). Lukeneder *et al.* (2014) reported 12°/153° as dip and dip direction of the lineation with a preferred orientation of 57.3% (n = 74); tested dip and azimuth of the plane was 12°/159° with 59.4% preferred orientation (n = 363).

These differences show that a certain sample size is required for stable results. The large difference in the maximum class volume of the gastropods can be explained by the fact that the tested gastropods (only those intersected at least twice) had a much smaller sample size (n = 20) which apparently did not reach the sample size required for significant results. Interestingly, the general bimodal orientation is the same (SSE/NNW) as for the ammonoids, but the maximum class volume plots at the 140°–160° class (Fig. 6.6E–F), i.e. exactly opposite to the maximum class volume of the ammonoids (320°–340°). Accordingly, a different (aperture) orientation behavior of gastropods and ammonoids can be assumed. Despite the small sample size (20 gastropods), we believe the results to be reliable.

Interestingly, the aperture direction of the ammonoids in Lukeneder *et al.* (2014; n = 44) is the same as that tested for the gastropods (n = 20) within the present study.

In summary, all tested apertures show a general bimodal SSE/NNW resp. NNW/SSE orientation. The different orientations of geopetal fills within the ammonoid mass occurrence and the presence of intraclasts containing ammonoids and inverse geopetal structures (Figs 6.8L, 6.9H–I) hint to a reworking of the fossils after primary deposition. At the same time, the absence of encrustation, abrasion or bioerosion argues against a lengthy exposure time of the shells on the seafloor. A possible explanation for the readjustment of the geopetal structures is quick burial, reworking shortly after lithification, and transport with the still unconsolidated surrounding sediment to final deposition. The general SSE imbrication of the ammonoids within the stereographic analyses also hints to a slight but significant sediment movement or current direction toward NNW (see Lukeneder *et al.* 2014). As the carbonate platform of the Dipoyraz Dag is located E of Aşağiyaylabel, and the Kartoz Fm. generally shows a N–S striking orientation, a westerly transport would have been more logical. As the wider Isparta Angle area (an area around Isparta bearing a prominent tectonic feature, the Isparta Angle; Altuncu *et al.* 2007) shows a strong post-sedimentary tectonic compressional overprint (Robertson 2000), local rotations could have contributed to the present NNW orientation. Anyhow, an additional possibility might be represented by currents which ran parallel to the slope resp. the platform edge.

Already Krumbein (1939), Potter and Pettijohn (1977), Rust (1972) and, more recently, Millane *et al.* (2006) argued that pebble orientation in alluvial sediments might indicate the flow direction. Nagle (1967) and Brenchley and Newall (1970) reported that freely moving conical shells generally are orientated parallel to unidirectional currents (apex up-current). Potter and Pettijohn (1977) analysed the orientation of disks by gravity and by gravity-plus-current action. They concluded that a shifted maximum concentration within a stereographic plot points to down-current transport of these disks (see also Lukeneder *et al*. 2014). The orientation data of the planispiral cephalopod shells thus substantiate the supposed transport.

Although we found no internal size sorting of the ammonoid-shells itself, we discovered that the sediment within the accumulation beds is graded from well preserved ammonoid shells at the bottom of the bed (lower two-thirds of the bed), over fragmented ammonoid shells at the upper third of the bed, to thin-shelled halobiids which cover the beds. This represents a size grading of the components within the *Kasimlarceltites* beds. This kind of grading, in combination with the fact that the *Kasimlarceltites* acme zone exists of several shell beds resp. event beds, intercalated with the autochthonous background sediment, hints to a genesis by gravity flows (Flügel 2014). The gravity flows were most probably triggered by earth quakes, as we already know that during this time the Isparta Angle area was tectonically active. As the accumulation beds show more or less the same thickness and packing density along the whole extension, the same history of development can be assumed. In contrast to this, different thicknesses of the whole acme zone, which ranges between 1.8 m at AS I and 16.5 m at KA II, would argue for different conditions concerning its preservation.

6.5.2. Genetic classification of the *Kasimlarceltites* mass occurrence

According to Kidwell *et al.* (1986), fossil concentrations are generally not solely formed as biogenic concentrations, sedimentological concentrations or diagenetic concentrations. They are typically a mixture of two or perhaps of all three concentration types (Fig. 6.10). In the *Kasimlarceltites* mass occurrence, the sedimentological genesis dominates. A late diagenetic influence is evident from pressure solution remnants along stylolithic structures. Classifying the *Kasimlarceltites* mass occurrence in the ternary diagrams of Kidwell *et al.* (1986) yields type 2, influenced by type 5 (Fig. 6.10). This would mean deposition between a beach or an inner shelf environment (Fig. 6.10; Kidwell *et al.* 1986). Concerning the studied microfacies, the inner shelf environment would be more probable. Sedimentological concentrations refer to ancient hydraulic processes (i.e. hardpart concentration), whereas diagenetic concentrations refer to physical and chemical processes (e.g. compaction, selective pressure solution, destruction of hard parts in adjacent beds; Johnson 1960). This also points to primary hydraulic processes in combination with subordinate physical and/or chemical processes (stylolites) for the genesis of the *Kasimlarceltites* mass occurrence.

The most plausible scenario for the genesis of the shell-supported *Kasimlarceltites krystyni* mass occurrence is short-term high-energy events such as gravity flows (proximal tempestites or maybe turbidites).

6.5.3. The *Kasimlarceltites* mass accumulation as a fossil-Lagerstätte

Seilacher (1990) classified fossil-Lagerstätten into two major groups: conservation and concentration deposits. Since fossils within the concentration type are preserved in high quantity, one might tend to interpret the *Kasimlarceltites* case as a concentration-Lagerstätte, possibly in form of a condensation deposit (Seilacher 1990). The ammonoids, however, are preserved not only in high quantity, but also in good quality. Besides adult apertures, delicate shell structures such as ribs and growth lines, chamber- and suture details, and even the siphuncle tubes are well preserved. The presence of all shell size classes from juvenile to adult specimens is also remarkable. A possible explanation for the genesis of the primary accumulation deposit is oxygen fluctuations (Hemleben 1976; Wendt 1976, 1995; Seilacher 1990) with short-term anoxic conditions in the water column, which should have led to mass mortality of the ammonoids. The pyrite concentration and dark colour of the limestone beds argue for recurrent short-term anaerobic conditions. As the ammonoids are nektonic organisms and therefore they should have been able to escape anoxic bottom water conditions, the anoxic conditions are interpreted to have been extended throughout the water column, at least for short time. Enhanced tectonism and volcanism, which led to an increase in temperature and with them to an increase in nutrient supply, are plausible reasons for widespread anoxic conditions (Arthur and Sageman 1994; Leckie *et al.* 2002; Meyer and Kump 2008). Another potential explanation is methane degassing triggered by tectonic instabilities. This is planed to be tested by stable isotopes within future research. Either scenario would have led to recurrent ammonoid mass mortality by intensified ecological changes during the Carnian Pluvial Episode. We therefore interpret that the primary mass accumulation was most probably triggered by oxygen fluctuations. Minimal encrustation or bioerosion indicate lack of bottom dwellers and/or rapid burial. Reworking and transport by gravity or turbidity flows led in a second step to the present concentration-Lagerstätte type sensu Seilacher (1990).

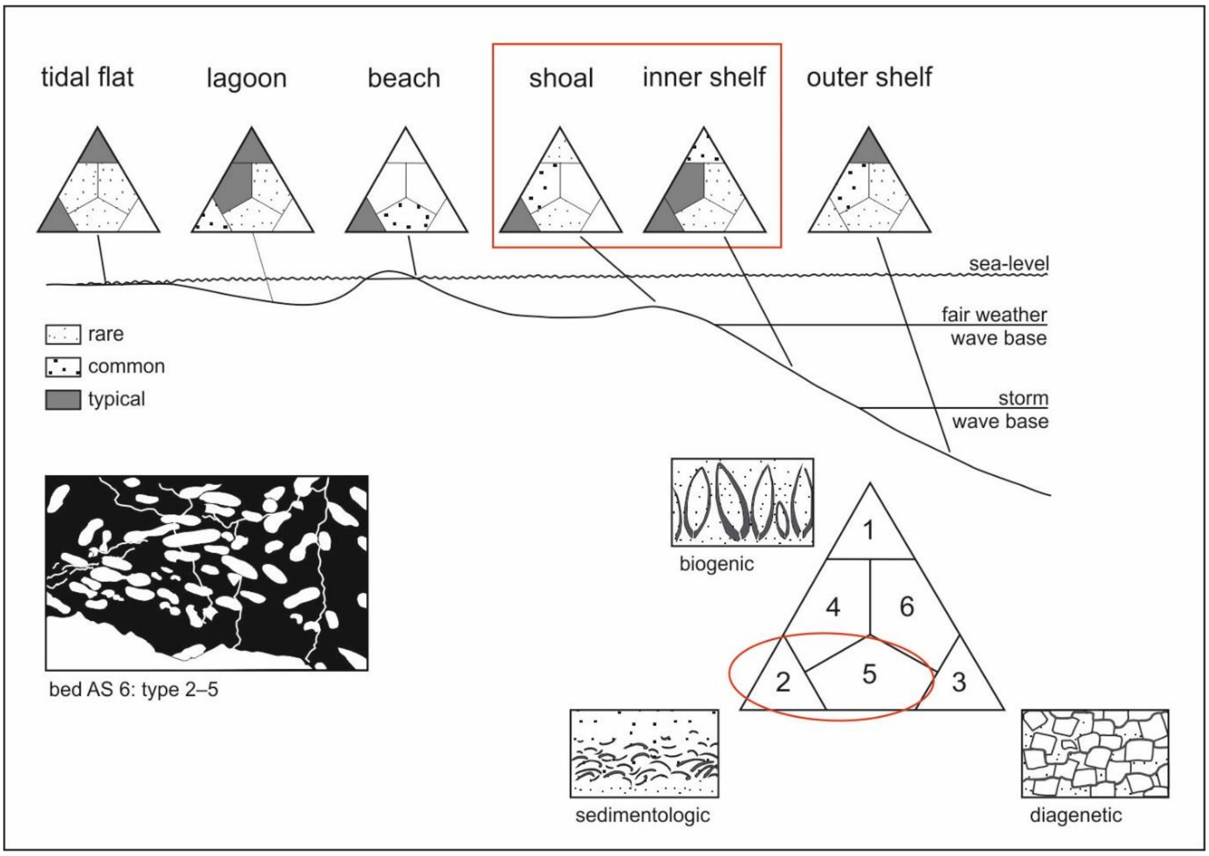

Fig. 6.10. Ternary diagram, adapted from Kidwell *et al.* (1986), of genetic types of skeletal accumulations, with indicated "genetic" position of the *Kasimlarceltites* mass occurrence.

6.5.4. Ecology and primary habitat of *Kasimlarceltites*

As the *Kasimlarceltites krystyni* mass accumulations subsequently experienced transport and therefore are allochthonous, the habitat and mode of life of *Kasimlarceltites* cannot be deduced from surrounding sediments. Since *K. krystyni* is currently known only from Aşağiyaylabel, any interpretations of its mode of life can only be made based on related taxa whose habitat has already been established within an autochthonous context.

Numerous studies deal with the relationship between ammonoid shell morphology and habitat (e.g., Ziegler 1963, 1967; Kauffmann 1977; Donovan 1985; Batt 1989, 1993; Jacobs *et al.* 1994; Westermann 1996; Neige *et al.* 1997; Navarro *et al.* 2005). For example, conch parameters such as shell morphology or siphuncle strength can be indicators for specific primary habitat conditions (e.g. depth, temperature; Westermann 1996; Klug 2002; Ritterbush and Bottjer 2012; Ritterbush *et al.* 2014).

Therefore the reconstructed modes of life of the genera *Aplococeras*, *Lecanites* and *Celtites* (celtitid ammonoids; i.e. serpenticone, highly evolute, “primitive” ceratitid suture) can yield an approximation for the mode of life and habitat of *Kasimlarceltites*. The above-mentioned genera have been interpreted by Assereto (1969) from the Latemar or Marmolada carbonate platforms (Dolomites, Italy) as shallow “platform faunal associations”. Vörös (2002) in contrast described *Aplococeras* as related to peri-platform environments. According to Assereto (1969), celtitids are rare to absent in deeper basinal environments. The facies dependency was interpreted to be controlled by ecological factors (Brack and Rieber 1993, 1996). These assumptions on a facies or depth gradient dependency of celtitids, hence also of *K. krystyni*, would fit well the interpretation of the Carbonate member Unit A at Aşağiyaylabel. The base of the Carbonate member is, based on its microfacies (e.g. bioclastic wackestones resp. floatstones) and faunal components (e.g. transported ammonoids, sponges, gastropods), interpreted as deposited within a shelf or deeper ramp (Lukeneder *et al.* 2012). For information on facies dependency of Mesozoic ammonoids see Westermann (1996) and Lukeneder (2015). Manfrin *et al.* (2005) also found celtitid ammonoids in adjacent basinal series surrounding the Latemar platform but reported a faunal mixing with benthic gastropods, and therefore interpreted these findings as clearly transported via storm processes. This fits well with the *Kasimlarceltites* mass occurrence at Aşağiyaylabel. The use of celtitid-dominated ammonoid assemblages as primary habitat indicators for platform or shallow ramp environments is arguable but needs confirmation through additional shallow-water ammonoid studies.

The hypothesis that similar shell morphologies can be related to similar habitats or life-styles prompted us to use the habitat knowledge of forms closely resembling the serpenticone morphotype of *Kasimlarceltites* (e.g. *Paraceltites*, *Psilorceras* and *Celtites*) to help determine the habitat and life-style of *Kasimlarceltites*. The interpreted habitats of the mentioned genera – *Paraceltites* (Permian; Spinosa *et al.* 1975), *Psiloceras* (Jurassic; Westermann 1996), and *Celtites* (Triassic; Rieber 1973, 1975) – are summarised in Westermann (1996) and evaluated in Lukeneder (2015). Spinosa *et al.* (1975), for example, proposed a “tropical platform limestone depositional area” for the Permian genus *Paraceltites*.

A planktonic life-style was assumed for costate, celtitid morphotypes (Rieber 1973, 1975; Westermann 1996). As postulated by Korn and Klug (2007), ontogenetic changes in morphology reflect, at least in early ammonoid taxa, a change in the mode of life. Nevertheless, the quality of the swimming capability in ammonoids is somewhat speculative and requires more data. Within *K. krystyni* the early ontogenetic changes from spherical to compressed shell morphologies probably represent a change from a planktonic to a nektonic or active swimming form.

6.6. Conclusions

Comparing the palaeontology, taphonomy, sedimentology and palaeoecology of bed AS 6 (section AS I) with shell beds of the *Kasimlarceltites* acme zone from surrounding sections (AS IV, KA I–II) yields the following conclusions about the genesis of the *Kasimlarceltites krystyni* mass occurrence within the Taurus Mountains of Turkey:

- More than 3,000 ammonoids and 200 gastropods were counted within the 150 × 45 × 140 mm reference block. This yielded an extrapolated number of nearly 775 million ammonoids and 50 million gastropods within the known extension of the *Kasimlarceltites* mass occurrence of 5 km^2.

- The ammonoid concentrations are paucispecific; 94–99% of the fossils belong to the ammonoid species *Kasimlarceltites krystyni* in co-occurrence with rare *Sirenites senticosus* and *Anasirenites crassicrenulatus*. Anyhow, section KA I shows, in contrast to sections AS I, AS IV and KA II, a lower dominance (about 50%) of the genus *Kasimlarceltites.*

- Orientation measurements performed on the ammonoids prove, as already indicated by Lukeneder *et al.* (2014), that they were transported toward NNW.

- Sedimentological structures and orientation measurements of the shell-supported beds of the *Kasimlarceltites* mass occurrence support their interpretation as event beds caused by gravity flows (e.g. debris flows, turbidites or tempestites). Interbedded matrix-supported sediments contain *Kasimlarceltites* only as scattered elements. Distinct taphonomic features such as preferred alignment and tilted geopetal fills corroborate this interpretation.

- Supposing a life habitat for *Kasimlarceltites* similar to that of the morphologically and/or taxonomically related genera *Aplococeras*, *Lecanites* and *Celtites* (celtitid ammonoids; i.e. serpenticone, highly evolute), *K. krystyni* may have lived in a shallow platform environment or a peri-platform environment. A tropical carbonate platform environment can also be inferred when considering the morphological similarities of *K. krystyni* with other serpenticone morphotypes such as the Permian *Paraceltites*, the Triassic *Celtites* and the Jurassic *Psiloceras*.

- If *K. krystyni* changed its mode of life from planktonic to nektonic, it might also have changed its habitat during ontogeny.

By testing taphonomic, sedimentological, lithological as well as palaeoecological features, we conclude that the present ammonoid mass concentrations at Aşağiyaylabel were initially formed by short anoxic events and secondarily transported by gravity flows (e.g. debris flows, turbidites or tempestites) to their present position. Their primary life habitat might have been a shallow platform environment (Assereto 1969), a peri-platform environment (Vörös 2002) or a tropical carbonate environment (Spinosa *et al.* 1975). The postulated approximately 9° palaeolatitude for the area around Aşağiyaylabel (Lukeneder *et al.* 2012) also suggests a tropical carbonate-rich environment for *Kasimlarceltites*.

The *Kasimlarceltites* mass occurrence was deposited during the Carnian Crisis = Carnian Pluvial Episode, which is known for an at least Tethyan-wide carbonate platform demise caused by changing climate conditions. A warmer and more humid climate paired with hydrodynamic (storms) or seismic events (e.g. earthquakes) may also be seen as a trigger of the ammonoid event beds (through gravity flows such as turbidites, debris flows or tempestites). We underline the dependency between such events and ammonoid mass accumulations.

6.7. Acknowledgements

The study has been financially supported by the Austrian Science Fund (FWF, P 22109-B17). We thank Yeşim İslamoğlu (Ankara) and the General Directorate of Mineral Research and Exploration (Ankara) for the working permission and for organising two field trips. The authors furthermore thank Mathias Harzhauser (Vienna) and Philipp Strauss (Vienna) for providing material from previous field trips. Franz Topka (Vienna) is acknowledged for grinding the reference block and for help during the field trips, and Anton Englert (Vienna) for preparation of the thin-sections. The authors furthermore thank Christian Klug (Zurich) and Franz Fürsich (Erlangen) for constructive comments which improved the quality of this manuscript. Andrzej Kaim (Warsaw) determined some gastropods. We further thank Ulrike Exner (Vienna), Andreas Kroh (Vienna), Martin Dockner (Vienna) and Martin Voorn (Vienna) for introduction to diverse software packages, technical help, as well as for hardware advice. Eckart Wallbrecher (Graz) and Ulrike Exner (Vienna) helped with the analyses of the stereographic projections. We are grateful to Michael Schwaiger (Linz), Gerhard W. Weber (Vienna), Martin Mayrhofer (Vienna) and Martin Maslo (Vienna) for fruitful mathematical discussions. Further thanks go to Simon Schneider (Cambridge) for providing hardly obtainable literature. Julia Wöger (Vienna) is acknowledged for additional hints and ideas concerning the use of the software package Amira.

6.8. References

ARTHUR M.A. and SAGEMAN B.B. 1994. Marine black shales: depositional mechanisms and environments of ancient deposits. *Annual Review of Earth and Planetary Sciences*, **22**, 499–551.

ALTUNCU S., YILMAZER M., PINAR A. and KALAFAT D. 2007. A present day evidence for the active tectonics in the inner part of Isparta Angle in SW Turkey. *International Earthquake Symposium Kocaeli*, **2007**, 131–135.

ADLER R., FENCHEL W. and PILGER A. 1982. Statistische Methoden in der Tektonik II. *Clausthaler Tektonische Hefte,* **4**, 1–89.

ASSERETO R. 1969. Sul significato stratigrafico della 'Zona ad Avisianus' del Trias medio delle Alpi. *Bolletino Società Geologica Italiana,* **88**, 123–145.

BATT R.J. 1989. Ammonite shell morphotype distributions in the Western Interior Greenhorn Sea and some paleoecological implications. *Palaios,* **4**, 32–42.

BATT R.J. 1993. Ammonite shell morphotypes as indicators of oxygenation in ancient epicontinental seas: Example from Late Cretaceous Greenhorn Cyclothem (U.S.A.). *Lethaia,* **26**, 49–64.

BRACK P. and RIEBER H. 1993. Towards a better definition of the Anisian/ Ladinian boundary: New biostratigraphic data and correlations of boundary sections from the Southern Alps. *Eclogae Geologicae Helvetiae,* **86**, 415–527.

BRACK P. and RIEBER H. 1996. The "High resolution Middle Triassic ammonoid standard scale" proposed by Triassic researchers from Padova – a discussion of the Anisian/ Ladinian boundary interval. *Albertiana,* **17**, 42–50.

BRENCHLEY P.J. and NEWALL G. 1970. Flume experiments on the orientation and transport of models and shell valves. *Palaeogeography, Palaeoclimatology, Palaeoecology,* **7**, 185–220.

BRETT C.E. and BAIRD G.C. 1986. Comparative Taphonomy: A key to paleoenvironmental interpretation based on fossil preservation. *Palaios,* **1**, 207–227.

DOYLE P. and MACDONALD D.I.M. 1993. Belemnite battlefields. *Lethaia,* **26**, 65–80.

DONOVAN D.T. 1985. Ammonite shell form and transgression in the British Lower Jurassic. *In:* BAYER U. and SEILACHER A. (eds). Sedimentary and Evolutionary Cycles*,* Springer-Verlag, Berlin, Heidelberg, New York, Toronto, 48–57.

FERNÁNDEZ-LÓPEZ S.R. 2007. Ammonoid taphonomy, palaeoenvironments and sequence stratigraphy at the Bajocian/Bathonian boundary on the Bas Auran area (Subalpine Basin, south-eastern France). *Lethaia,* **40**, 377–391.

FLÜGEL E. 2004. Microfacies of Carbonate Rocks: Analysis, Interpretation and Application, Springer-Verlag, Berlin-Heidelberg, pp. 976.

FÜRSICH F.T. and OSCHMANN W. 1993. Shell beds as tools in basin analysis: the Jurassic of Kachchh, western India. *Journal of the Geological Society, London,* **150**, 169–185.

HEMLEBEN CH. 1976. 1. Fossil-Lagerstätten in plattigen Kalken. *Zentralblatt für Geologie und Paläontologie II*, **1976**, 214–222.

JACOBS D.K., LANDMAN N.H. and CHAMBERLAIN J.A. JR. 1994. Ammonite shell shape covaries with facies and hydrodynamics: Iterative evolution as a response to changes in basinal environment. *Geology,* **22**, 905–908.

JOHNSON R.G. 1960. Models and methods for analysis of the mode of formation of fossil assemblages. *Geological Society of American Bulletin,* **71**, 1075–1086.

KIDWELL S.M., FÜRSICH F.T. and AIGNER T. 1986. Conceptual framework for the analysis and classification of fossil concentrations. *Palaios,* **1**, 228–238.

KAUFFMANN E.G. 1977. Evolutionary rates and biostratigraphy. *In:* KAUFFMANN E.G. and HAZEL J.E. (eds). Concepts and methods of biostratigraphy, Hutchinson and Ross, Dowden, 109–141.

KEUPP H. 1997. Paläopathologische Analyse einer “Population” von *Dactylioceras athleticum* (SIMPSON) aus dem Unter-Toarcium von Schlaifhausen/Oberfranken. *Berliner geowissenschaftliche Abhandlungen,* **25**, 243–267.

KLUG C. 2002. Conch parameters and habitats of Emsian and Eifelian ammonoids from the Tafilalt (Morocco) and their relation to global events. *Abhandlungen der Geologischen Bundesanstalt*, **57**, 523–538.

KORN D. 2000. Morphospace occupation of ammonoids at the Devonian–Carboniferous boundary. *Paläontologische Zeitschrift,* **74**, 247–259.

KORN D. and KLUG C. 2007. Conch form analysis, variability, and morphological disparity of a Frasnian (Late Devonian) ammonoid assemblage from Coumiac (Montagne Noire, France). *In:* LANDMAN N.H., DAVIS R.A., MANGER W. and MAPES R.H. (eds). Cephalopods Present and Past. Springer, New York*,* 57–86.

KRUMBEIN W.C. 1939. Preferred orientation of pebbles in sedimentary deposits. *Journal of Geology,* **47**, 673–706.

LECKIE R.M., BRALOWER T.J. and CASHMAN R. 2002. Oceanic anoxic events and plankton evolution: biotic response to tectonic forcing during the mid-Cretaceous. *Paleoceanography*, **17 (3)**, 1041.

LUKENEDER A. 2003. The *Karsteniceras* Level: Dysoxic ammonoid beds within the Early Cretaceous (Barremian, Northern Calcareous Alps, Austria). *Facies,* **49**, 87–100.

LUKENEDER A. 2004. The *Olcostephanus* Level: An Upper Valanginian ammonoid mass-occurrence (Lower Cretaceous, Northern Calcareous Alps, Austria). *Acta Geologica Polonica,* **54/1**, 23–33.

LUKENEDER A. 2005. Taphonomy and stratigraphy of Early Cretaceous ammonoid mass occurrences (Late Valanginian, Northern Calcareous Alps; Upper Austria). *Austrian Journal of Earth Sciences,* **98**, 34–51.

LUKENEDER A. 2015. Ammonoid habitats and life history. *In:* KLUG C., KORN D., KRUTA I., DE BAETS K., MAPES R.H. (eds). Ammonoid Paleobiology: From anatomy to ecology. *Topics in Geobiology,* **43**, Springer, Dordrecht, 689–791.

LUKENEDER A. and MAYRHOFER S. 2014. Taphonomical implications from Upper Triassic mass flow deposits: 2–dimensional reconstructions of an ammonoid mass occurrence (Carnian, Taurus Mountains, Turkey). *Geologica Carpathica,* **65/5**, 339–364.

LUKENEDER S., LUKENEDER A., HARZHAUSER M., İSLAMOĞLU Y., KRYSTYN L. and LEIN R. 2012. A delayed carbonate factory breakdown during the Tethyan-wide Carnian Pluvial Episode along the Cimmerian terranes (Taurus, Turkey). *Facies,* **58**, 386–390.

LUKENEDER S. and LUKENEDER A. 2014. A new ammonoid fauna from the Carnian (Upper Triassic) Kasımlar Formation of the Taurus Mountains (Anatolia, Turkey). *Palaeontology,* **57/2**, 357–396. Open Access. DOI: 10.1111/pala. 12070

LUKENEDER S., LUKENEDER A. and WEBER G.W. 2014. Computed reconstruction of spatial ammonoid-shell orientation captured from digitized grinding and landmark data. *Computers & Geosciences,* **64**, 104–114.

MAEDA H. 1999. Did ammonoid carcasses surface or sink? *Memoirs of the Geological Society of Japan,* **54**, 131–140.

MAEDA H. and SEILACHER A. 1996. Ammonoid taphonomy. *In:* Landman N.H., TANABE K. and DAVIS R.A. (eds). Ammonoid paleobiology. *Topics in Geobiology,* **13,** Plenum Press, New York, 543–578.

MAEDA H. and SHIGETA Y. 2009. Ammonoid mode of occurrence. *In:* SHIGETA Y., ZAKHAROV Y.D., MAEDA H. and POPOV A.M. (eds). The Lower Triassic system in the Abrek Bay area, South Primorye, Russia. *National Museum of Nature and Science Monographs,* **38**, 36–38.

MANFRIN S., MIETTO P. and PRETO N. 2005. Ammonoid biostratigraphy of the Middle Triassic Latemar platform (Dolomites, Italy) and its correlation with Nevada and Canada. *Geobios,* **38**, 477–504.

MARDIA K.V. and JUPP P.E. 2000. Directional Statistics. Wiley, Chister, New York, Weinheim, Brisbane, Singapore, Toronto, pp. 430.

MARTIN R.E. 1999. 1 Introduction: the science of taphonomy. *In*: BRIGGS D.E.G., Dodson P., Macfadden B.J., Sepkoski J.J. and Spicer R.A. (eds). Taphonomy. A Process Approach. Cambridge University Press, Cambridge, 1–26.

MCROBERTS C.A. 2000. A primitive *Halobia* (Bivalvia: Halobioidea) from the Triassic of northeast British Columbia. *Journal of Paleontology*, **74**, 599–603.

MCROBERTS C.A. 2010. Biochronology of Triassic bivalves. *In*: LUCAS S.G. (ed.). The Triassic timescale. *Geological Society of London Special Publications*, **334**, 201–219

MCROBERTS C.A., KRYSTYN L. and SHEA A. 2008. Rhaetian (Late Triassic) *Monotis* (Bivalvia: Pectinoida) from the eastern Northern Calcareous Alps (Austria) and the end-Norian crisis in pelagic faunas. *Palaeontology*, **51**, 721–735.

MEYER K.M. and KUMP L.R. 2008. Oceanic Euxinia in Earth History: Causes and Consequences. *Annual Review of Earth and Planetary Sciences*, **36**, 251–288.

MILLANE R.P., WEIR M.I. and SMART G.M. 2006. Automated analysis of imbrication and flow direction in alluvial sediments using laser-scan data. *Journal of Sedimentary Research,* **76**, 1049–1055.

MOIX P., BECCALETTO L., KOZUR H.W., HOCHARD C., ROSSELET F. and STAMPFLI G. 2008. A new classification of the Turkish terranes and sutures and its implication for the paleotectonic history of the region. *Tectonophysics,* **451**, 7–39.

NAGLE J.S. 1967. Wave and current orientation of shells. *Journal of Sedimentary Petrology,* **37/4**, 1124–1138.

NAGLIK C., RIKHTEGAR F.N. and KLUG C. 2015a (online). Buoyancy in Palaeozoic ammonoids from empirical 3D-models and their place in a theoretical morphospace. *Lethaia*, pp. 10, Oslo. DOI: 10.1111/let.12125

NAGLIK C., MONNET C., GÖTZ S., KOLB C., DE BAETS K. and KLUG C. 2015b. Growth trajectories in chamber and septum volumes in major subclades of Paleozoic ammonoids. *Lethaia*, **48**, 29–46.

NAVARRO N., NEIGE P. and MARCHAND D. 2005. Faunal invasions as a source of morphological constraints and innovations? The diversification of the early Cardioceratidae (Ammonoidea; Middle Jurassic). *Paleobiology,* **31**, 98–116.

NEIGE P., MARCHAND D. and BONNOT A. 1997. Ammonoid morphological signal versus sea-level changes. *Geological Magazine,* **134 (2)**, 261–264.

OLIVERO E.B. 2007. Taphonomy of ammonites from the Santonian–Lower Campanian Santa Marta Formation, Antarctica: Sedimentological controls on vertically embedded ammonites. *Palaios,* **22**, 586–597.

POTTER P.E. and PETTIJOHN F.J. 1977. *Paleocurrents and basin analysis*, 2nd edn. Springer-Verlag, Berlin, Heidelberg, New York, pp. 425.

REYMENT R.A. 2008. A review of the post-mortem dispersal of cephalopod-shells. *Palaeontologia Electronica,* **11 (3)**, 1–13.

RIEBER H. 1973. Ergebnisse paläontologisch-stratigraphischer Untersuchungen in der Grenzbitumenzone (Mittel Trias) des Monte San Giorgio. *Eclogae Geologicae Helvetiae,* **66**, 667–685.

RIEBER H. 1975. Der Posidonienschiefer (Ober Lias) von Holzmaden und die Grenzbitumenzone (Mittel Trias) des Monte San Giorgio (Kt. Tessin, Schweiz). *Jahreshefte der Gesellschaft für Naturkunde in Württemberg,* **130**, 163–190.

RITTERBUSH K.A. and BOTTJER D.J. 2012. Westermann Morphospace displays ammonoid shell shape and hypothetical paleoecology. *Paleobiology,* **38 (3)**, 424–446.

RITTERBUSH K.A., HOFFMANN R., LUKENEDER A. and DE BAETS K. 2014. Pelagic palaeoecology: the importance of recent constraints on ammonoid palaeobiology and life history. *Journal of Zoology,* **292**, 229–241.

ROBERTSON A.H.F. 2000. Mesozoic–Tertiary tectonic-sedimentary evolution of a south Tethyan oceanic basin and its margin in southern Turkey. *In:* BOZKURT E., WINCHESTER J.A. and PIPER J.D.A. (eds). Tectonics and magmatism in Turkey and the surrounding area. *Geological Society of London, Special Publication,* **173**, 43–82.

RUST B.R. 1972. Pebble orientation in fluvial sediments. *Journal of Sedimentary Petrology,* **42**, 384–388.

SEILACHER A. 1960. Strömungsanzeichen im Hunsrückschiefer. *Notizblatt hessisches Landesamt für Bodenforschung,* **88**, 88–106.

SEILACHER A. 1968. Sedimentationsprozesse in Ammoniten-Gehäusen. *Akademie der Wissenschaften und der Literatur zu Mainz, Abhandlungen der Mathematisch-Naturwissenschaftlichen Klasse,* **9**, 191–203.

SEILACHER A. 1971. Preservational history of ceratite shells. *Palaeontology,* **14**, 16–21.

SEILACHER A. 1990. Taphonomy of Fossil-Lagerstätten: Overview. *In*: BRIGGS D.E.G. and CROWTHER P.R. (eds). Paleobiology: a synthesis. Blackwell Scientific, Oxford, 266–270.

SIMMS M.J. and RUFFELL A.H. 1989. Synchronicity of climate change and extinctions in the Late Triassic. *Geology,* **17**, 265–268.

SPINOSA P.L., FURNISH W.M. and GLENISTER G.F. 1975. The Xenodiscidae, Permian ceratitoid ammonoids. *Journal of Paleontology,* **49**, 239–283.

STAMPFLI G.M., BOREL G.D., MARCHANT R. and MOSAR J. 2002. Western Alps geological constraints on western Tethyan reconstructions. *Journal of the Virtual Explorer,* **8**, 77–106.

TAJIKA A., NAGLIK C., MORIMOTO N., PASCUAL-CEBRIAN E., HENNHÖFER D.K. and KLUG C. 2015. Empirical 3D-model of the conch of the Middle Jurassic ammonite microconch *Normannites*, its buoyancy, the physical effects of its mature modifications and speculations on their function. *Historical Biology*, **27/2**, 181–191.

TOMAŠOVÝCH A. and SCHLÖGL J. 2008. Analyzing variations in cephalopod abundances in shell concentrations: The combined effects of production and density-dependent cementation rates. *Palaios,* **23**, 648–666.

VÖRÖS A. 2002. Paleoenvironmental distribution of some Middle Triassic ammonoid genera in the Balaton Highland (Hungary). *Abhandlungen der Geologischen Bundesanstalt,* **57**, 479–490.

WALLBRECHER E. 1978. Ein Cluster-Verfahren zur richtungsstatistischen Analyse tektonischer Daten. *Geologische Rundschau,* **67**, 840–857.

WALLBRECHER E. 1979. Methods for a quantitative comparison of orientation data using vectorstatistics and eigenvalue analysis with special reference to degrees of preferred orientation and distribution shapes. *Neues Jahrbuch für Geologie und Paläontologie Abhandlungen,* **159**, 113–149.

WALLBRECHER E. 1986. Tektonische und gefügeanalytische Arbeitsweisen. Ferdinand Enke Verlag, Stuttgart, pp. 244.

WANI R. 2007. How to recognize in situ fossil cephalopods: evidence from experiments with modern *Nautilus*. *Lethaia,* **40**, 305–311.

WENDT J. 1976. Projektbereich B "Fossil-Lagerstätten". *Zentralblatt für Geologie und Paläontologie II,* **1976**, 211–213.

WENDT J. 1995. Shell directions as a tool in palaeocurrent analysis. *Sedimentary Geology*, **95/3–4**, 161–186.

WESTERMANN G.E.G. 1996. Ammonoid life and habitat. *In:* LANDMAN N.H., TANABE K. and DAVIS R.A. (eds). *Ammonoid paleobiology. Topics in Geobiology,* **13**, Plenum, New York, pp. 857.

ZIEGLER B. 1963. Ammoniten als Faziesfossilien. *Paläontologische Zeitschrift,* **37**, 96–102.

ZIEGLER B. 1967. Ammonitenökologie am Beispiel des Oberjura. *Geologische Rundschau,* **56**, 439–446.

CHAPTER VII,

PUBLISHED 2014 IN GEOLOGICA CARPATHICA 65: 339–364.

TAPHONOMIC IMPLICATIONS FROM UPPER TRIASSIC MASS FLOW DEPOSITS: 2-DIMENSIONAL RECONSTRUCTIONS OF AN AMMONOID MASS OCCURRENCE (CARNIAN, TAURUS MOUNTAINS, TURKEY)

Alexander Lukeneder [a], Susanne Mayrhofer [a]

[a] Natural History Museum, Geological-Palaeontological Department, Burgring 7, A-1010 Wien, Austria

Abstract

Ammonoid mass occurrences of Late Triassic age were investigated in sections from Aşağıyaylabel and Yukarıyaylabel, which are located in the Taurus Platform-Units of eastern Turkey. The cephalopod beds are almost monospecific, with >99.9 % of individuals from the ceratitic genus *Kasimlarceltites*, which comprises more than hundreds of millions of ammonoid specimens. The ontogenetic composition of the event fauna varies from bed to bed, suggesting that these redeposited shell-rich sediments had different source areas. The geographical extent of the mass occurrence can be traced over large areas up to 10 km^2. Each of the Early Carnian (Julian 2) ammonoid mass occurrences signifies a single storm (e.g. storm-wave action) or tectonic event (e.g. earthquake) that caused gravity flows and turbidity currents. Three types of ammonoid accumulation deposits are distinguished by their genesis: 1) matrix-supported floatstones, produced by low density debris flows, 2) mixed floatstones and packstones formed by high density debris flows, and 3) densely ammonoid shell-supported packstones which result from turbidity currents. Two-dimensional calculations on the mass occurrences, based on sectioning, reveal aligned ammonoid shells, implying transport in a diluted sediment. The ammonoid shells are predominantely redeposited, preserved as mixed autochthonous/ parautochthonous/ allochthonous communities based on biogenic and sedimentological concentration mechanisms (= in-situ or post-mortem deposited). This taphonomic evaluation of the *Kasimlarceltites* beds thus reveals new insights into the environment of deposition of the Carnian section, namely that it had a proximal position along a carbonate platform edge that was influenced by a nearby

shallow water regime. The *Kasimlarceltites*-abundance zone is a marker-zone in the study area, developed during the drowning of a shallow water platform, which can be traceable over long distances.

Keywords: *Kasimlarceltites*, ammonoid mass occurrence, taphonomy, Triassic, Taurus Mountains, Turkey.

7.1. Introduction

Upper Triassic sediments, especially of the Carnian age, form the major element within the Taurus Mountains. The area around Aşağıyaylabel has already been investigated by Özgül and Arpat (1973), Dumont and Kerey (1975), Monod (1977), Poisson (1977), Gutnic *et al.* (1979), Robertson (1993, 2000), Şenel (1997), Gindl (2000), Robertson *et al.* (2003), Lukeneder *et al.* (2012) and Lukeneder and Lukeneder (2014).

The Carnian section at Aşağıyaylabel displays a lithological change from pure carbonatic to more siliciclastic sedimentation (Lukeneder *et al.* 2012). The facies change occurs exactly at the Lower–Upper Carnian boundary (= Julian–Tuvalian boundary), and represents the beginning of the so-called Carnian Pluvial Event in the section at Aşağıyaylabel. Facies interpretations change from open platform margin conditions, through deeper shelf margin conditions, to finally open marine-influenced basinal conditions (Lukeneder *et al.* 2012).

During the Carnian time, the sediments around the area of Aşağıyaylabel were deposited within an intrashelf area on the western end of the Cimmerian System (Gindl 2000; Stampfli and Borel 2002; Lukeneder *et al.* 2012). Sedimentological and paleontological investigations show a delayed carbonate factory collapse during that time.

Lower Carnian faunal elements, exclusively detected at Aşağıyaylabel and characterized as *Kasimlarceltites krystyni*, *Klipsteinia disciformis* and *Anasirenites crassicrenulatus* (Lukeneder and Lukeneder 2014) indicate a rather isolated but still connective paleoceanographic position of the intrashelf area on the western end of the Cimmerian System.

The present study examines deposits representing an acme zone, registered within the Upper Triassic (Carnian) Kartoz and Kaslımlar formations, which crop out at Aşağıyaylabel (= Kartoz) and Yukarıyaylabel (= Karapınar). This acme zone is characterized by several beds yielding ammonoid mass occurrences of the Carnian ammonoid-genus *Kasimlarceltites*. The aim of the present work is to detail the distribution and taphonomy of the *Kasimlarceltites* mass occurrence at the lowermost part of the Kasımlar Formation within the Julian 2. Results on taphonomy and environmental processes, obtained by the two dimensional analyses of sections, thin sections, as well as by conclusions from outcrop logs and block data, are presented. This leads to a more detailed picture of the sedimentological dynamics, hence to a better understanding of the taphonomy and sedimentology of such Upper Triassic shell beds (e.g. ammonoids). Dynamic processes for specific mass flow deposits (e.g. debris flows, grain flows or turbidity currents; Middleton and Hampton 1973, 1976; Flügel 1978, 2004; Lowe 1982; Brown and Loucks 1993; Stow and Mayall 2000; Mulder and Alexander 2001; Kawakami and Kawamura 2002; Potter *et al.* 2005; Nichols 2009; SEPM 2014), also termed gravity flows or density currents, will be discussed in respect to resedimentation of sediments and biogenic components. The determination of specific mechanisms in terms of the genesis concerning event bed deposition, storm deposition, shell accumulation and the consequences for the facies and bioclastic fabric were reported and discussed in Aigner (1982a, 1985), Einsele and Seilacher (1982), Kreisa and Bambach (1982), Brett and Baird (1986), Kidwell (1986, 1991a,b, 1993a,b), Kidwell *et al.* (1986), Tucker and Wright (1990), Brett and Seilacher (1991), Chuanmao *et al*. (1993), Einsele *et al.* (1991a,b), Seilacher and Aigner (1991), Soja *et al.* (1996), Hips (1998), Fürsich and Pandey (1999), Martin (1999), Storms (2001), Lukeneder (2003a,b; 2004a,b), Fernández-López (2007), Montiel-Boehringer *et al.* (2011), and Pérez-Lopéz and Pérez-Valera (2012).

The result is a detailed succession of abundance or accumulation layers (i.e. distinct layers with ammonoid mass occurrences) within an acme zone in the Upper Triassic of the Aşağıyaylabel section. Such 'ammonoid-beds' are the result of bio-events, which are often manifested by the abundance or mass occurrence of ammonoids (Lukeneder 2001, 2003b). The presented paper is a first step and the initial point for the lateral correlation of such ammonoid mass occurrences and establishment of ammonoid abundance zones within the Taurus Mountains. Trigger mechanisms and potential scenarios, causing the accumulation of such ammonoid shell beds, are discussed.

7.2. Geographical setting

The Aşağıyaylabel (AS) sections (i.e. AS I–AS IV) are located in southwest Turkey, about 90 km northeast of Antalya and approximately 70 km southeast of Isparta (Figs. 7.1–7.3). Aşağıyaylabel is accessible from the two major cities of the region, Eğirdir and Beyşehir, located 50 km and 40 km away, respectively. The locality adjoins the small village Aşağıyaylabel (1000 m above sea level) on the northern slope of an east-west trending ridge, between 1050 m to 1100 m at N 37.551389° and E 31.304444°. The former name of Aşağıyaylabel was Kartoz, after which the Kartoz Formation was named (Dumont 1976; Gindl 2000; Lukeneder *et al.* 2012; Lukeneder and Lukeneder 2014). A particular depositional situation is marked by the small, Triassic (Late Carnian – Julian 2) blocks containing ammonoid mass occurrences, which are included within a Cenozoic conglomerate fan (Deynoux *et al.* 2005), mainly formed by Triassic sediments from the nearby area at AS III (Figs. 7.1, 7.3). The Yukarıyaylabel (= Karapınar, KA) sections (i.e. KA I–KA III) are located 5 km to the north of the Aşağıyaylabel (AS) sections (Figs. 7.1, 7.2, 7.4) near a small road through the village. The village is situated at 1328 m to 1340 m above sea level with N 37.5769° and E 31.2912°.

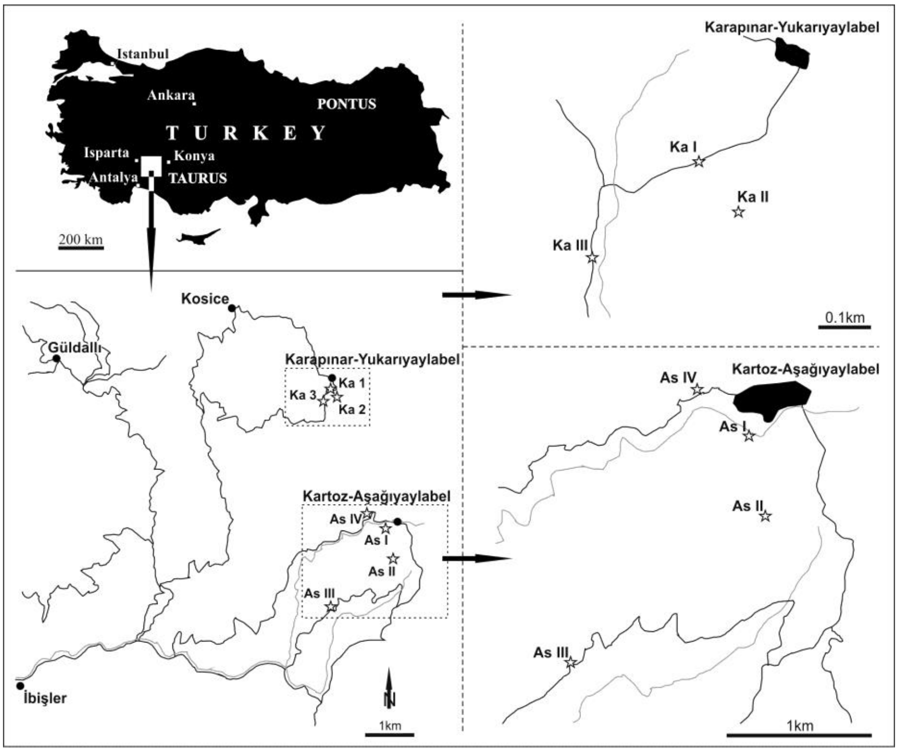

Fig. 7.1. Locality map of the investigated area showing the outcrops of Upper Triassic sediments around the area of Aşağıyaylabel (= Kartoz) and Yukarıyaylabel (= Karapınar) within the Anamas Dağ carbonate platform in the Taurus Mountains (southwest Turkey). Investigated sections are indicated as AS I, II, III and IV and KA I, II and III.

7.3. Geological setting

Geologically the area is located on the Anamas Dağ carbonate platform or Anamas-Akseki Autochthonous. The Anamas Dağ is part of the so-called Taurus-Platform-Units between the Antalya Suture in the South and the Izmir-Ankara Suture in the North, south of the Isparta Angle (Robertson 1993; Şenel 1997; Andrews and Robertson 2002; Robertson *et al.* 2003). The Anamas-Akseki Autochthonous (= Karacahisar-Autochthonous) includes Middle to Upper Triassic limestones, marlstones and shales of up to 500 m thickness (Gindl 2000). The geology of southwestern Turkey and the Anamas Dağ carbonate platform has been extensively investigated by Özgül and Arpat (1973), Dumont and Kerey (1975), Monod (1977), Poisson (1977), Gutnic *et al.* (1979), Robertson (1993, 2000), Şenel (1997), and Robertson *et al.* (2003).

The deposits of this area belong to two formations, the stratigraphically older Kartoz Formation (earliest Carnian), and the younger Kasımlar Formation (Carbonate, Marlstone and Shale member; Lukeneder *et al.* 2012), which reaches from Early to Late Carnian age (Julian 2 – Tuvalian 1). The fossil fauna (Lukeneder and Lukeneder 2014) reported within this work derives from the Kasımlar Formation with Lower Carnian to Upper Carnian sediments (Julian 2 – Tuvalian 1; Fig. 7.2).

The paleogeographic domain of the Anatolian System (Taurus Mts, Turkey) was characterized during Triassic times by microplates located in the middle of the western Tethys Ocean. The investigated succession was deposited in an intra-shelf basin of equatorial paleolatitude at the western end of the 'Cimmerian terranes' or 'Cimmerian blocks' (Şengör *et al.* 1984; Scotese *et al.* 1989; Dercourt *et al.* 1993, 2000; Scotese 1998, 2001; Gindl 2000; Stampfli and Borel 2002; Stampfli *et al.* 2002; Lukeneder *et al.* 2012; Lukeneder and Lukeneder 2014). This area was located between the 'old' Paleotethys in the North and the Neotethys in the South during the Late Triassic (Carnian, 228–216 Ma – Gindl 2000; Gradstein *et al.* 2012). While the Paleotethys Ocean underwent subduction along the southern margin of Eurasia, the young Neotethys Ocean (southern branch of Neotethys, sensu Şengör and Yılmaz 1981) was widened between the African continent and the Cimmerian terranes, which consisted of Turkey, Iran, Afghanistan, Tibet, and Malaysia (Golonka 2004). In the North of these Cimmerian terranes the Izmir-Ankara Ocean (northern branch of the Neotethys, sensu Şengör and Yılmaz 1981) and the 'old' Paleotethys were still open to the East (Tekin *et al.* 2002; Golonka 2004; Tekin and Göncüoğlu 2007; Göncüoğlu *et al.* 2010).

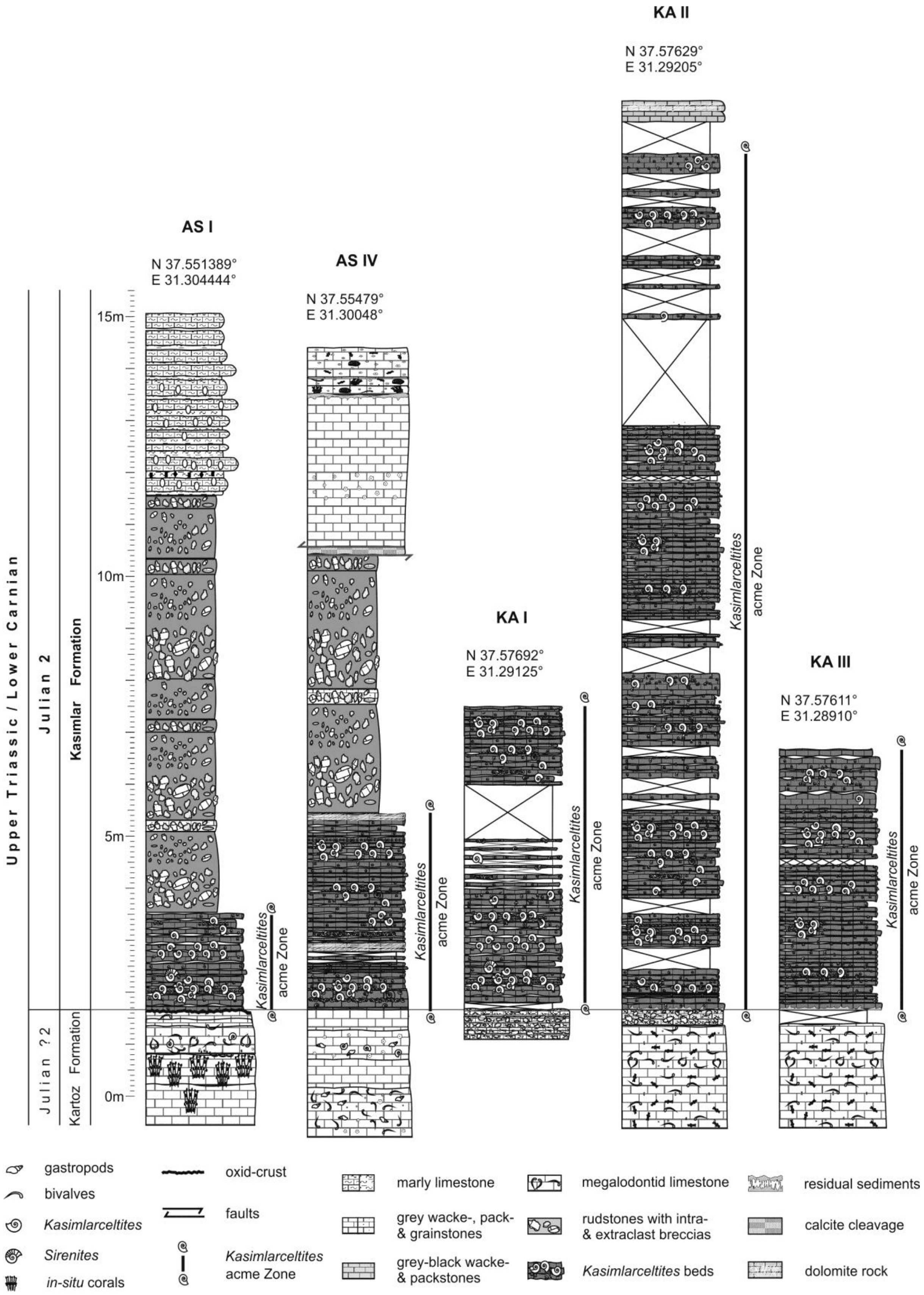

Fig. 7.2. Lithology and biostratigraphy (left) of the section investigated at Aşağıyaylabel and Yukarıyaylabel with indicated occurrences and ranges of the *Kasilmarceltites* acme zone.

7.4. Lithology and facies

The Triassic succession of Aşağıyaylabel starts with an angular unconformity above Carboniferous rocks (Dumont 1976; Gindl 2000). The main formations are the Middle to Upper Triassic Kartoz Formation (Late Carnian) and the Kasımlar Formation (uppermost Lower Carnian to Upper Carnian). The Kartoz Formation consists of shallow-water platform carbonates with thick-shelled bivalves (megalodonts) and corals. In contrast, the overlying Kasımlar Formation starts disconformably (i.e. hiatus) with an 8-m-thick pile of deeper-water limestones; this precedes 12 m marlstone-part into shales (Fig. 7.2). The section is dated based on conodonts, ammonoids, and halobiids (Lukeneder *et al.* 2012; Lukeneder and Lukeneder 2014). A detailed age assignment follows Krystyn *et al.* (2002) and Gallet *et al.* (2007). The strata dip approximmately 50° towards the Northeast.

The studied successions at Aşağıyaylabel (= Kartoz) and Yukarıyaylabel (= Karapınar) start with shallow-water limestones of the Kartoz Formation, with thick-shelled bivalves and corals (Lukeneder *et al.* 2012; Lukeneder and Lukeneder 2014; Fig. 7.2). This phase ends with a corroded and iron oxide-stained dissolution surface (without any traces of boring), pointing probably to subaerial exposure or sedimentological omission. The Kartoz Formation represents a drowned carbonate platform and is disconformably overlain by deeper-water, hemipelagic, black limestones of the Kasımlar Formation, which includes, at its base (i.e. 1.8–16.0 m) levels of thin ammonoid floatstone- and packstone layers (*Kasimlarceltites* beds = acme range zone – Fig. 7.2). This lower part is followed by a thick slump breccia (e.g. preserved at AS I and AS IV), containing up to meter-sized patch reef blocks (interpreted as Cipit-boulders by Lukeneder *et al.* 2012) together with comparably small ammonoid coquinas and filament limestone components. The Lower to Upper Carnian boundary is marked by a change to grey limy marlstones, with rare ammonoid- and pelagic-bivalve-bearing layers, passing upwards into a thick pile of sterile dark shale with thin silty and rare siliciclastic interbeds. Microfacies analyses identify the Carnian depositional system around Aşağıyaylabel and Yukarıyaylabel as an intrashelf platform environment grading upwards into deeper zones, influenced by pelagic conditions (Lukeneder *et al.* 2012).

All sections where the ammonoid mass occurrence of *Kasimlarceltites* exists start with shallow water carbonates of the Kartoz Formation (Figs. 7.2, 7.3). Coral-bafflestones, megalodontid limestones and shallow water breccias predominate. This facies is characterized by a dense abundance of in-situ corals and megalodontid shells (Lukeneder *et al.* 2012), trapped by a cortoid grainstone matrix representing an open platform environment.

Directly above an unconformity, the younger Kasımlar Formation is divided into the Carbonate member (units A, B, and C), the Marlstone member, and the Shale member. The lowermost Carbonate member appears at the base with the *Kasimlarceltites* beds (acme zone). The *Kasimlarceltites* beds are bioclastic pelagic wackestones, which were deposited in a deep shelf margin or mid ramp position (Lukeneder *et al.* 2012; see Flügel 1978, 2004 for facies types). The faunal spectrum mirrors two different source areas of the bioclastic input: thin-shelled bivalves (halobiids), which are most common, represent the autochthonous component (deeper shelf margin), whereas the original habitat of the benthic foraminifera (lagenids), the thick-shelled bivalves (megalodontiids), and the large, low-spired gastropods was situated on a fore slope or on a shallow marine ramp. Tilted geopetal fills of gastropods and ammonoids (e.g. *Kasimlarceltites*), together with clasts of eroded semilithified sedimentary layers ('plasticlasts'), prove episodic erosion, downward transport, and resedimentation. Bioturbation has mostly obliterated the original arrangement of autochthonous fine grained sediments (together with thin-shelled bivalves and radiolaria) alternating with coarser-grained 'tempestitic' or 'turbiditic' layers. When the original layering is preserved, bedding planes are strongly affected by stylolites. Common authigenic pyrite (mostly well-developed as cubic crystals) in different levels of the section is probably of synsedimentary origin. As indicated by the high abundance of halobiid bivalves and the dark-coloured sediment, it could point to temporary dysaerobic conditions of the bottom waters and/ or the pore-fluids of the unconsolidated sediments (Flügel 1978, 2004; McRoberts 2010).

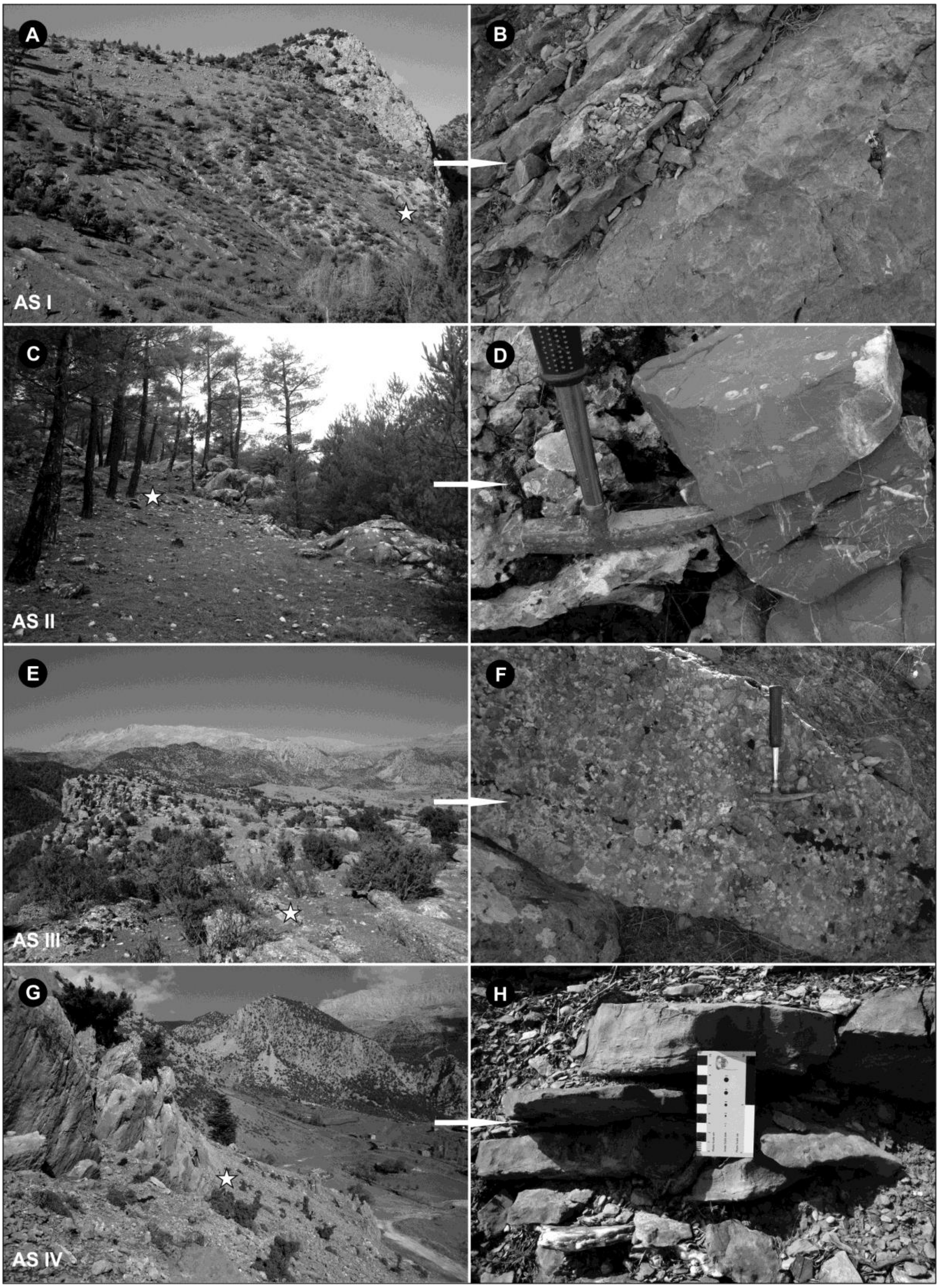

Fig. 7.3. Localities and detailed views on the *Kasimlarceltites* layers within shallow water carbonates from the Kasımlar Formation of the sections around Aşağıyaylabel (AS I, AS II, AS III, AS IV). **A,** The locality Aşağıyaylabel 1 (AS I); **B,** Detail of the *Kasimlarceltites* acme zone at AS I, base of the Kasımlar Formation; **C,** The locality Aşağıyaylabel 2 (AS II); **D,** Detail of the *Kasimlarceltites* acme zone at AS II; **E,** The locality Aşağıyaylabel 3 (AS III) within Cenozoic (middle Miocene) conglomerates of the Köprüçay Formation; **F,** Detail of the conglomerates comprising Triassic blocks with *Kasimlarceltites* accumulations; **G,** The locality Aşağıyaylabel 4 (AS IV); **H,** Detail of the *Kasimlarceltites* acme zone at AS IV, base of the Kasımlar Formation.

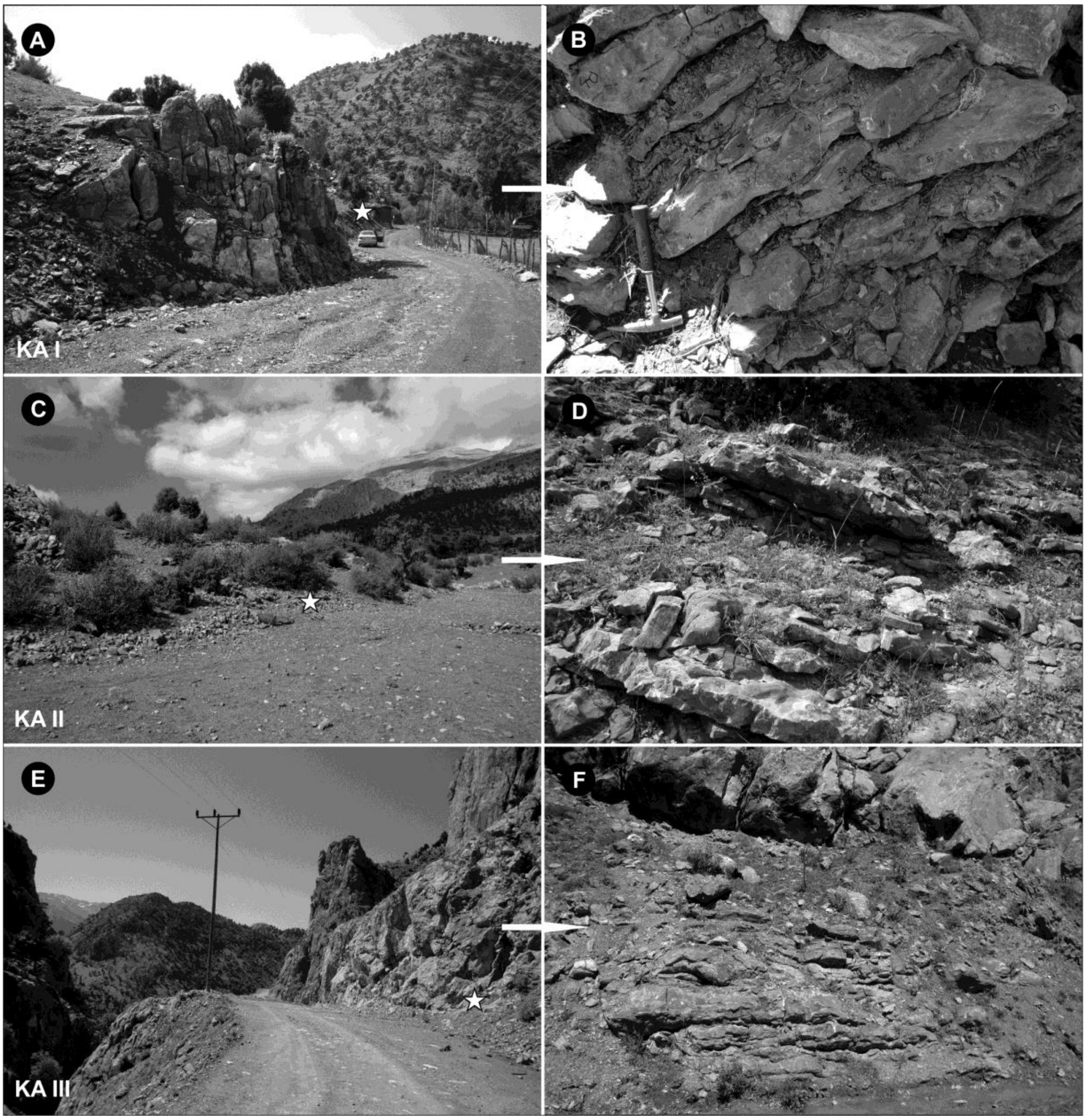

Fig. 7.4. Localities and detailed views of the *Kasimlarceltites* layers within shallow water carbonates from the Kasımlar Formation of the sections around Karapınar (KA I, KA II, KA III). **A,** The locality Karapınar 1 (KA I); **B,** Detail of the *Kasimlarceltites* acme zone at KA I, base of the Kasımlar Formation; **C,** The locality Karapınar 2 (KA II); **D,** Detail of the *Kasimlarceltites* acme zone at KA II, middle part of the Kasımlar Formation; **E,** The locality Karapınar 3 (KA III); **F,** Detail of the *Kasimlarceltites* acme zone at KA III, base of the Kasımlar Formation.

7.5. Material and fossil assemblage

The fossil material was collected by the authors (1995–2011), by Mathias Harzhauser and Franz Topka (both Natural History Museum Vienna), and on earlier field excursions (1980–1997) by Leopold Krystyn, Andreas Gindl and Philip Strauss (excursion organized by the University of Vienna). All specimens described within this study have been extensively collected from the Kasımlar Formation at the sections Aşağıyaylabel and Yukarıyaylabel, which consists of a Lower Carnian (*Austrotrachyceras austriacum* Zone) ammonoid fauna (Lukeneder and Lukeneder 2014). The ammonoid fauna contains ammonoids of all ontogenetic stages.

The ammonoids are well preserved, phragmocones are mostly filled with secondary calcite and the shell is neomorphically replaced by secondary calcite. Due to the fact that draught filling (= draft filling; Seilacher 1968; Maeda and Seilacher 1996; Olivero 2007) is absent, which led to a preserved primary phosphatic siphuncle, a fast deposition and sedimentation after death can be assumed. Only a few specimens of the genera *Kasimlarceltites*, *Klipsteinia*, *Anasirenites* and *Megaphyllites* show suture lines. A total of 479 ammonoid specimens, two nautiloid specimens and four coleoid specimens have been collected (Lukeneder and Lukeneder 2014). The ammonoid assemblages consist of 12 ammonoid genera with *Kasimlarceltites*, *Spirogmoceras*, *Sandlingites*, *Klipsteinia*, *Neoprotrachyceras*, *Sirenites*, *Anasirenites*, *Paratropites*, *Trachysagenites*, *Proarcestes*, *Megaphyllites*, *Joannites*, *Simonyceras*, containing 13 species, a single coleoid genus (*Atractites*), and a single nautiloid species.

The ammonoids are clearly dominated by the genus *Kasimlarceltites* with more than 100 million specimens (counting method: see Mayrhofer and Lukeneder, in prep.), due to the fact that it is the main faunal element of the mass occurrences, followed by *Sirenites* with 56 specimens.

The matrix contains mainly juvenile to adult halobiid bivalves (i.e. *Halobia rugosa*), megalodontid shells, gastropods (i.e. *Omphaloptycha* type), chaetitids, corals, calcareous sponges, sponge spicules, foraminifera, radiolaria, dasycladaceaes, cyanobacteria, peloids, and planktic crinoids (e.g. *Osteocrinus*). Lower Carnian conodonts are present with *Gladigondolella* and *Metapolygnathus*.

Detailed stratigraphic sections of the Lower to Upper Carnian interval were measured and described from Aşağıyaylabel (= Kartoz, AS) and Yukarıyaylabel (= Karapınar, KA). 325 thin-sections of 200 layers, collected in 2007 and 2012, were made and used for petrographic studies. Additional sectioning and polishing was performed on block samples in longitudinal, horizontal and tangential (90°) directions for reconstructions of the orientation and alignment of the ammonoids (see Potter and Pettijohn 1977; Futterer 1982; Olivero 2007) within the mass occurrence. The corresponding bed numbers are indicated by the abbreviation AS (for Aşağıyaylabel) and KA (for Yukarıyaylabel = Karapınar), by the corresponding succession number (as there are several successions at each locality AS I–AS IV resp. KA I–KA III) and the corresponding bed number (e.g. AS I/1= sample from Aşağıyaylabel, succession I, bed 1). Additional facies investigations were conducted under a dissecting microscope (Zeiss Discovery V20) with attached digital camera (AxioCam MRc5). Sectioning and photographing were done at the Natural History Museum in Vienna (NHMV = NHMW).

Detailed petrographic analyses were done using a petrographic polarization microscope from Leica (Leica DDM4500P) and a digital camera (Leica DFC4420). Sectioning and photographing were done at the Natural History Museum Vienna and at the University of Vienna (Department of Petrography).

The material is stored within the collection of the Geological-Paleontological Department of the NHMV. The inventory numbers of blocks are: for AS I NHMW 2012/0133/0551–0561, for NHMW AS II 2014/0094/0001, for AS III NHMW 2014/0095/0001, for AS IV NHMW 2014/0091/0001–0007, for KA I NHMW 2014/0092/0001–0003, for KA II NHMW 2014/0093/0001–0004, and for KA III 2014/0096/0001.

7.6. Biostratigraphy

The sections at Aşağıyaylabel (AS I–AS IV) and the biochrono-stratigraphically equivalent sections at Karapınar (KA I–KA IV) comprise about 50 m of essentially calcareous beds passing into marlstones (in part marly limestones) and shaly beds with considerable siliciclastic input at the top. The lowermost part is represented by the Kartoz Formation, an Upper Triassic (earliest Carnian; Fig. 7.2) light-grey, shallow-water carbonate succession. It comprises corals and thick-shelled bivalves. *Neoprotrachyceras* sp., found in the lower part of bed AS I/2, dates at least the top of the Kartoz Formation as Julian 2 (*Austrotrachyceras austriacum* Zone). A hiatus between this top and the overlying Kasımlar Formation cannot be excluded for all sections.

The overlying Kasımlar Formation can be divided into three 'members': a carbonate member, a marlstone member, and a shale member (Lukeneder *et al.* 2012). The carbonate member starts with dark-grey to black, thin-bedded limestones containing ammonoid-rich beds with a nearly monospecific assemblage of *Kasimlarceltites* and very rare *Sirenites*, represented by floatstones of latest Early Carnian age (Julian 2/II; Fig. 7.2). Towards the top thick slump breccias follow; they contain up to meter-sized patch-reef blocks together with small ammonoid coquinas and filament-limestone components. The overlying well-bedded (cm–dm thick) peloidal filament-wackestone with Lower Carnian conodonts (e.g. *Gladigondolella tethydis* and *Metapolygnathus*) and an ammonoid fauna dominated by the genera *Neoprotrachyceras* and *Anasirenites* are of latest Early Carnian age (*Anasirenites* level of Julian 2/IIb). The bioturbated matrix contains juvenile halobiid bivalves, sponge spicules, radiolaria, peloids, and planktic crinoids (= *Osteocrinus* sp.). The interval with the comprising *Kasimlarceltites* acme zone (lowermost Carbonate member) represents the latest Early Carnian (Julian 2 – Lukeneder and Lukeneder 2014; Fig. 7.2).

7.7. The *Kasimlarceltites* mass occurrence

The *Kasimlarceltites* mass-occurrence resp. acme zone is quite common in the area around Aşağıyaylabel and Karapınar. For a detailed data set of the Aşağıyaylabel area (AS Ia, AS Ib, AS II, AS III) and the Karapınar area (KA I, KA II, KA III) on lithology, microfacies, geochemistry, geophysics, fossil content and environment see Table 7.1. The standard Microfacies zones (i.e. SMF zones) are in accordance with Flügel (1978, 2004; see also Carrillat and Martini 2009) and Lukeneder *et al.* (2012).

7.7.1. The Aşağıyaylabel (Kartoz) area

Locality: Aşağıyaylabel Ia, AS Ia (Figs. 7.1, 7.2, 7.3A–B; Table 7.1)

Lithology: Dark grey to black limestone

Interpretation: Debris flow, event bed

Locality: Aşağıyaylabel Ib, AS Ib (Figs. 7.1, 7.2, 7.3A; Table 7.1)

Lithology: Dark grey to black limestone

Interpretation: Debris flow

Locality: Aşağıyaylabel II, AS II (Figs. 7.1, 7.2, 7.3C–D; Table 7.1)

Lithology: Dark grey to black limestone

Interpretation: Debris flow, event bed

Locality: Aşağıyaylabel III, AS III (Figs. 7.1, 7.3E–F; Table 7.1)

Lithology: Dark grey to black limestone

Interpretation: Primary debris flow, secondary fan-delta conglomerates

Locality: Aşağıyaylabel IV, AS IV (Figs. 7.1, 7.2, .3G–H; Table 7.1)

Lithology: Dark grey to black limestone

Interpretation: Turbidite, event bed

7.7.2. The Karapınar (Yukarıyalabel) area

Locality: Karapınar I, KA I (Figs. 7.1, 7.2, 7.4A–B; Table 7.1)

Lithology: Dark grey to black limestone

Interpretation: Debris flow, event bed

Locality: Karapınar II, KA II (Figs. 7.1, 7.2, 7.4C–D; Table 7.1)

Lithology: Dark grey to black limestone

Interpretation: Debris flow, event bed

Locality: Karapınar III, KA III (Figs. 7.1, 7.2, 7.4E–F; Table 7.1)

Lithology: Dark grey to black limestones

Interpretation: Debris flow, event bed.

Parameters	*Kasimlarceltites* abundance zones at different localities in the Aşağıyaylabel and Karapınar area							
	AS Ia	**AS Ib**	**AS II**	**AS III**	**AS IV**	**KA I**	**KA II**	**KA III**
GEOGRAPHY, GEOLOGY AND STRATIGRAPHY								
Locality	Aşağıyaylabel N 37.551389° E 31.304444°	Aşağıyaylabel N 37.551389° E 31.304444°	Aşağıyaylabel N 37.546389° E 31.306389°	Aşağıyaylabel N 37.536944° E 31.292222°	Aşağıyaylabel N 37.55479° E 31.30048°	Karapınar N 37.57692° E 31.29125°	Karapınar N 37.57629° E 31.29205°	Karapınar N 37.57611° E 31.28910°
Dipping (°/°)	50/075	single blocks			70/340	70/075	20/010	50/280
Thickness of acme (m)	≈ 1.8	≈ 8.0	single blocks	single blocks in Cenozoic (Miocene) conglomerates	≈ 4.0	≈ 6.0	≈ 16.5	≈ 5.0
Lateral distribution (m)	ammonite layers detected over 30 m	ammonite boulders detected over 30 m	ammonite boulders detected over 50 m	boulder field, 500 m	ammonite layers detected over 50 m	ammonite layers detected over 20 m	ammonite layers detected over 50 m	ammonite layers detected over 20 m
Biostratigraphy	early Carnian, Julian 2, *Austrotrachyceras austriacum* Zone							
Age (Ma)	≈ 234			15 Ma (boulder ≈234)	≈ 234			
Lithological unit	Kasımlar Formation, Carbonate member, Unit A	Kasımlar Formation, Carbonate member, Unit B		Cenozoic Köprüçay Formation	Kasımlar Formation, Carbonate member, Unit A			
SEDIMENTOLOGY								
Sediment classification of accumulation bed	bioclastic pack- to floatstone	bicolastic rudstones with intra- and extraclast breccias	bioclastic pack- to floatstone, rudstone		bioclastic packstone	ammonoid-bivalve-bioclastic pack- to floatstone	bioclastic (radiolarian) floatstone	bioclastic floatstone
Standard microfacies types, SMF zone	SMF 12	SMF 6	SMF 12/6	SMF 12/6	SMF 12	SMF 12	SMF 12	SMF 12
Sediment structure/ fabrics	vertical neptunian dikes	no orientation of bioclasts	orientation/ no orientation	no orientation of bioclasts	orientation of bioclasts		≈ horizontal weakly oblique orientation	slightly oblique
Base of bed	erosional wavy	Cipit boulders	boulder		straight	styliolitic base	straight	
Top of bed	erosional wavy	Cipit boulders	boulder		straight			
Bioturbation	yes, frequent		yes, distinct	present	distinct to frequently	frequent		present
Sediment classification below the accumulation bed	bioclastic packstone (AS 3)	bioclastic floatstone to packstone (AS 7)	boulder		bioclastic floatstones (AS 7)	peloidal pack- to floatstone, silt to fine sand (KA I 9)	peloidal pack- to floatstone, silt (KAII ZBb)	peloidal pack- to floatstone, silt (KA III)
Sediment classification above the accumulation bed	bioclastic floatstone to packstone (AS 7)	bioclastic floatstone to packstone (AS 19)	boulder		bioclastic floatstones AS (9)	peloidal pack- to floatstone, silt to fine sand (KA I 11)	peloidal pack- to floatstone, silt (KA II)	peloidal pack- to floatstone, silt (KA III)
GEOCHEMISTRY AND GEOPHYSICS								
Grey scale (0–255)	130.5	98.5	124	113	105.5	93	96.5	112
$CaCO_3$ (%)	91.8	89.8	90.6	88.9	91.4	91.7	90.9	89.7
Colour	dark grey to black							
TOC (%)	0.132	0.203	–	–	–	–	–	–
S (%)	0.03	0.11	–	–	–	–	–	–
Pyrite	frequent, framboidal							and cubes
Gamma ray (cps)	27	15	21	26	28	135	19	23
Suscecptibility (SI 10^{-6})	55	52	49	57	20	66	43	47
$\delta^{13}C$ (‰)	2.10	1.70	–	–	1.94	2.09	2.07	–
$\delta^{18}O$ (‰)	-8.80	-8.80	–	–	-6.65	-7.16	-7.17	–

Table 7.1. Parameters of the *Kasimlarceltites* Abundance Zone and measured blocks at different localities in the Aşağıyaylabel and Karapınar area. Data are measured within this study for the first time.

Parameters	*Kasimlarceltites* abundance zones at different localities in the Aşağıyaylabel and Karapınar area							
	AS Ia	**AS Ib**	**AS II**	**AS III**	**AS IV**	**KA I**	**KA II**	**KA III**
TAPHONOMY								
Shell infill	matrix in body chamber within numerous specimens	matrix in body chamber, peloids	matrix in body chamber, frequent pelloids to silts, secondary calcite in phragmocone		matrix in body chamber, frequent pelloids, silts to very fine sand, secondary calcite in phragmocone		matrix in body chamber, frequent pelloids, silts, secondary calcite in phragmocone	
	shallow water fragments in body chamber, secondary calcite in phragmocone					juvenile ammonites		
Shell orientation alignment	inhomogenous and heterogenous within bed, present in parts of layer, horizontal to oblique	absent, oblique	present to absent, horizontal to oblique	absent, oblique, nesting	present, weakly oblique			
Fabric/ packing	dense, partly disorientated, partly aligned	dense		loosely to dense	dense		dense only at base of layer	dense in the mid of layer
Sorting of shells	present	absent			good	absent	bad	absent
Geopetal structures	slightly divergent; in top of body chambers	dislocated against each other, in body chambers			slightly divergent, in top of body chambers	oblique, dislocated against each other, in body chambers	dislocated against each other, in body chambers	slightly dislocated against each other
Biodegradation	no soft parts or aptychi, septal necks visible in thin sections							
Incrustation	absent							
Bioerosion	absent							
Transport	no abrasion, but frequent breakage due to transport	strong transport, redeposition, mixed shallow water faunas (patch reefs), deeper ramp facies and pelagic basin elements, no abrasion, but frequent breakage in ammonites			strong transport, redeposition, coquina on top of laminated silt layers	strong transport, redeposition, frequent breakage in ammonites	strong transport, redeposition, rare breakage in ammonites	
Dissolution of shell	stylolites and pressure seems frequent	pressure seems frequent	absent		stylolites and pressure seems frequent	rare stylolites	stylolites, pressure seems	stylolites
Diagentical deformation and compaction	on top of beds	present	absent to strong	strong	absent to strong	present	rare	rare
Depositional area	mid–outer ramp, slope to basin	outer ramp to slope		primary: outer ramp to slope; secondary: conglomerate field	mid–outer ramp, slope to basin			
Interpretation	debris flow, event bed	debris flow			turbidity, event bed,	debris flow, event bed		
FAUNAL ASSEMBLAGE								
Genus	*Kasimlarceltites*							
Quantity	> 95%	≈ 40–90%	≈ 50–90%	> 50–90%	> 95%	50 %	> 95%	> 95%
Ratio in fauna	> 95%	40–90%	50–90%	> 50–90%	> 95%	50%	> 95%	> 95%
Acme zone (m)	1.8	≈ 8.0	boulders	blocks and boulders	≈ 4.0	≈ 6.0	≈ 16.5	≈ 5.0
Accumulation layers	AS Ia 4, 6	AS Ib 18	AS Ia 18 boulders	blocks and boulders	AS IV 8	KA I /10 (12)	KA II 2, 11, 16	KA III 8
Event bed thickness (m)	≈ 0.1	≈ 8.0	boulders	blocks and boulders	0.1–0.15, in the middle part 0.05, shell coquina	0.03–0.05	0.03–0.05	0.05–0.1
Ontogenetical stages	juvenile & adult	ammonitellae, juvenile & adult			juvenile & adult	ammonitellae, juvenile & adult		
Size range (cm) min–max	0.5–3.3	0.01–3.3	0.01–3.3	0.001–3.3	0.001–2	0.001–2.2	0.001–2.5	0.001–2.2
Shell material	secondary calcite							
Accompanying macro-fauna	ammonites (*Sirenites* sp.), gastropods (omphaloptychids) bivalves (halobiids),				rare bivalves	50% *Sirenites* sp., bivalves, rare gastropods, rare sponges	bivalves, rare gastropods	
	sponges	(chaetitids), corals, echinoids, crinoids						
Accompanying micro-fauna	ostracods, foraminifera, radiolarian, conodonts							
						radiolarian-bloom		

Table. 7.1. continued.

7.8. The *Kasimlarceltites* mass occurrence as an abundance zone

An abundance zone or acme zone is a stratum or body in which the abundance of a particular taxon or specified group of taxa is significantly greater than is usual in the adjacent parts of the section (Salvador 1994; Murphy and Salvador 1999). Its boundaries are made of biohorizons and the name is given by the abundant taxon or taxa (Lukeneder 2003b). Biohorizons are, for example, characterized by a sharp and significant biostratigraphic change within the fossil assemblage and/ or the change of frequency of its members (see Salvador 1994; Steininger and Piller 1999). The latter authors recommended the term biohorizon to be used instead of the terms 'surface', 'level', 'marker' and 'datum planes'. Such biohorizons are of great importance for lateral correlation over wide distances. Densely fossiliferous layers were also termed as 'shell beds', 'coquinas', 'concentration-Lagerstätten', 'lumachelles', 'bioclastic limestones' and 'bioclastic beds' (Brett and Seilacher 1991; Kidwell 1991a,b; Martin 1999).

Patterns which lead to beds with a notable abundance of ammonoid shells have been called 'inter-regional mass occurrences' or 'stray occurrences' (Kemper *et al.* 1981). Such abundance zones are of exceptional value for intra-regional correlation in the Triassic.

An Upper Triassic monotonous ammonoid assemblage representing a thickness of at least one single bed up to a few meters, were reported and taxonomically described by Lukeneder *et al.* (2012 – 'ammonite floatstones with *Orthoceltites'*; *Orthoceltites* = old synonym of *Kasimlarceltites*) and Lukeneder and Lukeneder (2014 – '*Kasimlarceltites* mass occurrence').

At the investigated Aşağıyaylabel (AS I–IV) and Kasımlar (KA I–III) sections the *Kasimlarceltites* ammonoid abundance zone (characterized by abundance or mass occurrence of ammonoids) could be detected for the first time. The names of the separated beds were given following the dominating genus *Kasimlarceltites*.

The *Kasimlarceltites* acme zone starts at every section from Aşağıyaylabel and Karapınar directly above the shallow water carbonates of the Kartoz Formation (Fig. 7.2). At AS Ia and AS IV, the *Kasimlarceltites* acme zone is capped by an interval of debris flow deposits comprising Cipit boulders (Lukeneder *et al.* 2012). At the Karapınar sections, the upper edge of the sections is not visible, hence ending within the *Kasimlarceltites* beds. The acme zone appears with deviant ranges or thickness in distinct localities (Fig. 7.2; Table 7.1). It occurs at the sections AS Ia with 1.8 m, at AS Ib with 8.0 m, at AS II in single blocks, at AS III within Cenozoic conglomerates (Deynoux *et al.* 2005) as reworked blocks, and at AS IV with 4.0 m.

The acme zone sections at Karapınar appear at KA I with 6.0 m, at KA II with 16.5 m and at KA III with 5.0 m. The most undisturbed and entire section occurs at KA II. Other sections (e.g. AS Ia, AS IV, KA I, KA III) are characterized by tectonics or seem to be affected by more or less strong shearing mechanisms.

7.9. Biostratinomy and taphonomy

The biostratinomy is defined as the sum of environmental factors that affect organic remains between death and the final burial or embedding (Müller 1963; Brett and Baird 1986; Martin 1999). Biostratinomy is thus a very important part of work in taphonomy, the study of the entire post mortem history of organic remains resulting in fossil material (Fernández-López and Fernández-Jalvo 2002; Fernández-López 2007).

The taphonomic investigations of fossil cephalopod assemblages provide insight, not only into the autecology of these organisms, but also into their paleoenvironment and paleocommunity structure (Brett and Baird 1986; Allison and Briggs 1991; Brett and Seilacher 1991; Bottjer *et al.* 1995).

Sediments of the lower Upper Triassic (Carnian) of the Kasımlar Formation appear in the lower part with well preserved and mostly entire (> 95%) ammonoid specimens (Fig. 7.5). The distinct ammonoid shell concentration beds within single logs and different localities (i.e. Aşağıyaylabel and Karapınar) differ in lateral distribution, thickness, sedimentological features, packing of shells, diversity of organisms, alignment and taphonomic processes (Figs. 7.6, 7.7, 7.9, 7.10; Tables 7.1, 7.2, 7.3; see also Fürsich and Pandey 1999).

The ammonoids are tiny with a maximum diameter of 33 mm. They show an involute more spheroidal shape and are accumulated in the beds AS Ia – beds 4, 6; AS IV – bed 8; KA I – beds 10, 12; KA II – beds 2, 11, 122; KA III – bed 8. Less than 5% of those accumulated ammonoids are preserved only with fragmentation. Small accumulated ammonoids of all ontogenetic stages (i.e. *Kasimlarceltites*) as well as shell fragments in body chambers of adjacent large ammonoids can be found within the above mentioned beds, which might hint at the effect of agglomeration and comminution by dense sediment flows with a laminar internal flow. Both, straight shells (e.g. *Atractites*) and also planispiral coiled shells (e.g. *Kasimlarceltites*, *Sirenites*, *Neoprotrachyceras*) are present within the *Kasimlarceltites* acme zone. Erosional features, as described by Fernández-López (2007) and encrustation of ammonoids are absent. Whilst in some thin and distinct layers ammonoids are accumulated in masses with an almost horizontal alignment (Figs. 7.8–7.10), ammonoids are less abundant in the limestone beds between the ammonoid mass occurrence beds (Figs. 7.5, 7.6, 7.9).

In accumulated mixed assemblages (i.e. autochthonous, parautochthonous and allochthonous; Martin 1999), detected at the Aşağıyaylabel outcrops AS Ia (Lukeneder *et al.* 2012), AS II–IV and the Karapınar KA I–III sections, females (= macroconchs) and

corresponding males (= microconchs) are found together. In most cases even ammonitellae, juvenile and adult stages are detected in the same layers. Some ammonoid specimens show different sediment-infillings within the body chamber (coarser material) compared to the surrounding finer limestone chamber ('normal' sedimentation = ambient sediment). All of these facts might point to post-mortem, biostratinomic mixing of ecologically age-separated populations as discussed by Olóriz (2000) and Olóriz and Villaseñor (2010). Due to the long body chamber (i.e. mesodome–longidome) in *Kasimlarceltites*, geopetal structures (i.e. sparry calcite on top) are also observable in numerous body chambers (see Olivero 2007; cf. Seilacher 1968), hence body chambers were not entirely filled. Geopetal structures are generally aligned in almost identical directions. No serious mixture and dislocation of geopetal alignments occurs (Figs. 7.7, 7.9). Furthermore, the mixed assemblages comprise a considerable amount of bivalves, gastropods, sponges and corals from shallower environments from a nearby platform or upper ramp (Lukeneder *et al.* 2012).

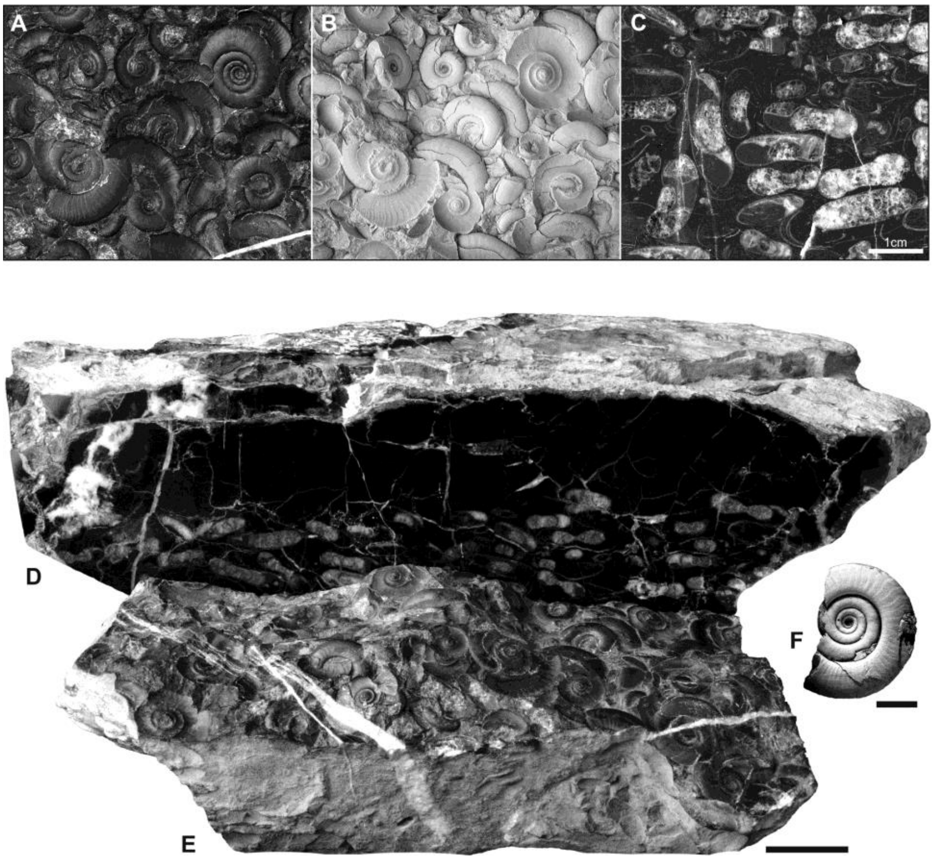

Fig. 7.5. A, Surface of an accumulation layer of *Kasimlarceltites*, uncoated, NHMW 2012/0133/0558; **B,** Same specimen coated with ammonium chloride, NHMW 2012/0133/0558; **C,** Top-to-bottom thin section of the same layer with densely packed ammonoid shells, NHMW 2012/0133/0559; **D,** Polished slice of an ammonoid accumulation layer at section AS IV – block 1 slice C (89 mm, frontal view), NHMW 2014/0091/0001; **E,** Ammonoid accumulation surface from section AS IV, NHMW 2012/0133/0558; **F,** *Kasimlarceltites krystyni*, lateral view, holotype, NHMW 2012/0133/0014. Kasımlar Formation, Carbonate member Unit A, *Austrotrachyceras austriacum* Zone (Julian 2). Each scale bar represents 1 cm.

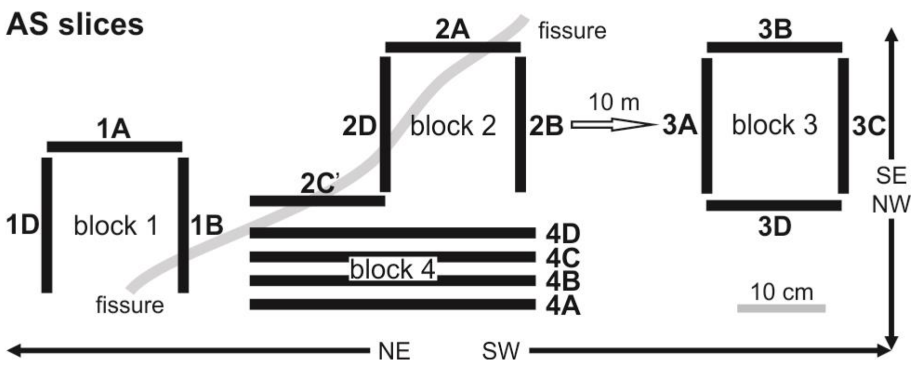

Fig. 7.6. Terminology and orientation of frontal and orthogonal sections measured from the locality Aşağıyaylabel I, with indicated present-days cardinal directions for blocks AS I, AS II, AS III and AS IV.

Fig. 7.7. Thin-section photographs of accumulation layers and facies from the Kasımlar Formation at Aşağıyaylabel → and Karapınar. **A–H,** Note the well preserved shell geometry indicating very early cementation (i.e. early selective lithification): **A,** Bioclastic floatstone with the abundant ammonoid *Kasimlarceltites* and halobiids, accompanied by rare gastropods. The ammonoids and gastropods are filled with coarse sparry calcite floating in micritic matrix, base of *Kasimlarceltites* Formation, AS I – bed 6, NHMW 2012/0133/0560; **B–C,** Very irregular packing = "injection" of heterometric bioclasts (**B**), and the same but with larger heterometric range (**C**); **B,** Bioclastic floatstone-packstone, characteristic sponge-accentuated Cipit facies dominated by *Kasimlarceltites* and sponges, accompanied by *Sirenites*, gastropods and corals, Kasımlar Formation, AS I – bed18, NHMW 2012/0133/0561; **C,** Bioclastic floatstone-packstone, sponge-accentuated Cipit facies dominated by *Kasimlarceltites* and sponges, accompanied by gastropods and corals, peloidal matrix, Kasımlar Formation, AS II, NHMW 2014/0094/0001; **D,** Allochthonous block with mixed packstone (left) and floatstone (right) areas, dominated by *Kasimlarceltites* and sponges, accompanied by *Sirenites*, gastropods and corals; found within the Cenozoic (middle Miocene) conglomerates, Köprüçay Formation, AS III, NHMW 2014/0095/0001; shelter effects favouring very dense packing; **E,** Bioclastic packstones with the abundant ammonoid *Kasimlarceltites* above laminated, peloidal packstone layers, base of Kasımlar Formation AS IV – bed 8, NHMW 2014/0091/0008; sheltering by fragmented body chamber infilled by a very fine comminute matrix; **F,** Bioclastic packstones with the abundant ammonoids *Kasimlarceltites* and *Sirenites*, peloidal matrix, base of Kasımlar Formation, KA I, NHMW 2014/0092/0003; comminute, bioclastic matrix and reworked ammonoids; **G,** Bioclastic wackestone with a redeposited, floated *Kasimlarceltites* shell (note dislocated geopetal structure, different infilling and colour) at the base, matrix contains radiolarian, ammonitellae and juvenile ammonoids, middle Kasımlar Formation, KA II, NHMW 2014/0093/0004; very fine matrix with diagenetic patches; **H,** Bioclastic wackestone with floated *Kasimlarceltites* shells in the middle, and peloidal packstone at the base, peloidal matrix contains radiolarian, ammonitellae and juvenile ammonoids, base of Kasımlar Formation, KA III, NHMW 2014/0096/0001; geopetals indicate ammonoid reworking. Thin-sections are orientated in upright position. Each scale bars represent 1 mm.

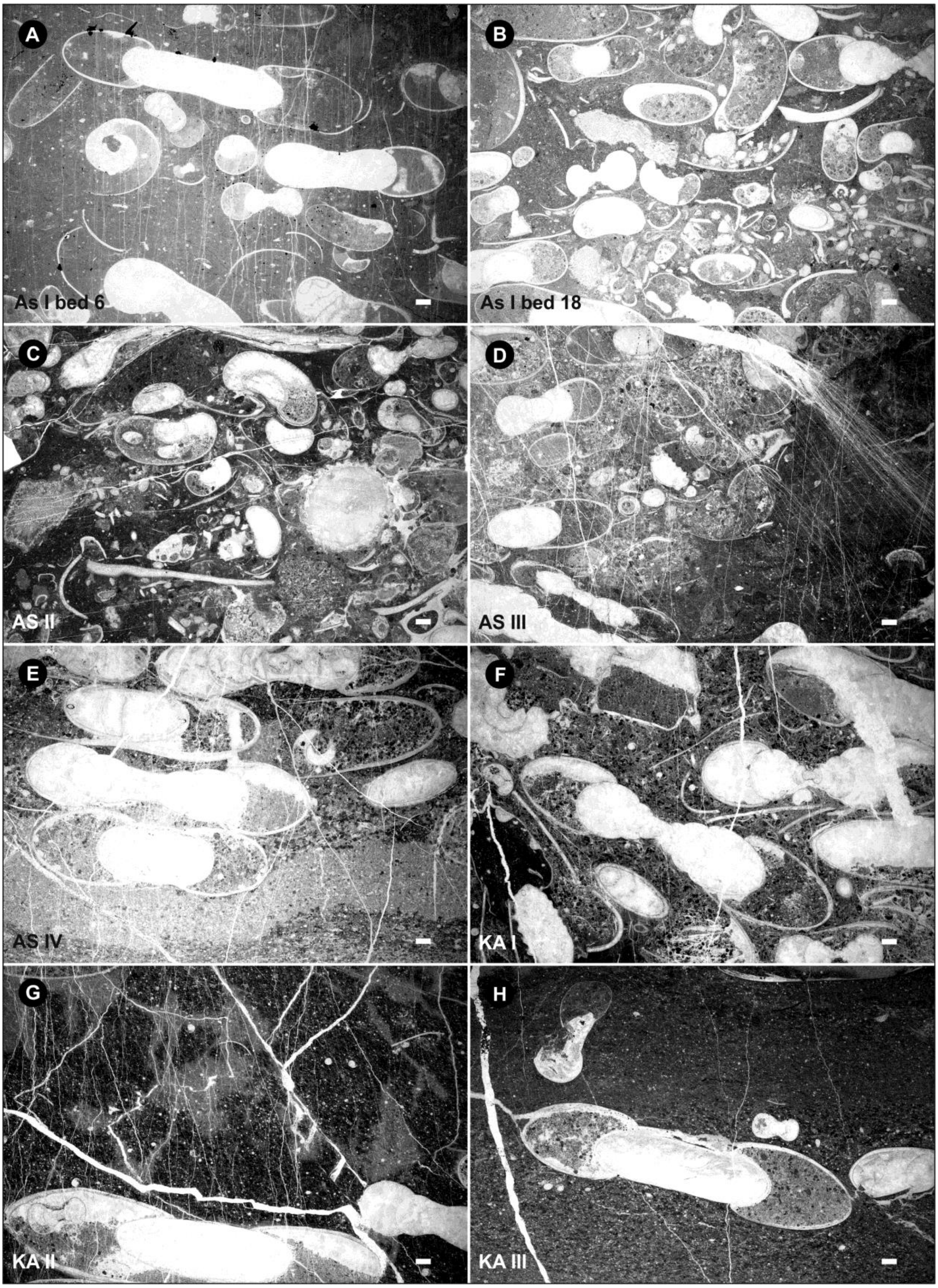
A
As I bed 6
B
As I bed 18
C
AS II
D
AS III
E
AS IV
F
KA I
G
KA II
H
KA III

7.9.1. Ammonoid shell alignment

Angles and orientation of shells and body chambers (both in respect to the horizontal block surface) from 20 blocks with 34 polished slices from 4 different sites (i.e. AS Ia,b, AS IV, KA I, KA II) were measured in addition with maximal visible diameters on the slices and thin sections. Additional measurements were made on visible geopetal structures. 2,367 ammonoid specimens were analysed on slices and sections. Ammonoid shell directions and alignment were not measured in chaotic, transported 'Cipit' boulders from debris flow deposits at AS Ib – bed 18 and within Triassic boulders and blocks incorporated in Cenozoic gravels (Deynoux *et al.* 2005) of AS III, because they do not mirror the primary mechanism of orientation and transport of ammonoid shells, due to their repeated transport and reorientation.

The most reliable data were obtained from AS I where blocks could be taken orientated (Fig. 7.6). The front section of the AS I blocks (as taken in the field) is orientated with a direction from NE to SW (NE is left on the block, orientated toward the valley). On a horizontal line, marking the base and surface of the layers and blocks, 0° is located at the right (SW), 90° at the top, 180° at the left (NE) and 270° at the base (Figs. 7.9, 7.10). In addition, where possible, slices at 90° (= orthogonal) to the frontal view were performed to get ideas on the three dimensional orientation of the ammonoids in the blocks. To gain the true dip direction (Nichols 2009) of the ammonoid shell 'plane' the calculation needs two different apparent dip measurements (i.e. ammonoid shell axes; Fig. 7.11). This implies a direction (i.e. only AS I blocks) of the later slices rotated by 90° to a direction of NW (front) to SE (back).

A clear orientation and alignment (Potter and Pettijohn 1977) can be detected in the accumulation layers.

The predominant orientation of shell axes (only AS Ia with cardinal direction) versus the layer base/ surface of blocks in frontal and orthogonal slices was analysed at Aşağıyaylabel (Figs. 7.6, 7.10, 7.11, Tables 7.2, 7.3).

Frontal

AS Ia, AS IV

Orthogonal

AS Ia, AS IV

Within accumulation layers from the Karapınar area the orientation of shell axes (not in cardinal direction) appears in frontal and orthogonal slices (Fig. 7.10, Tables 7.2, 7.3). Layers in KA I can be separated in two parts (accumulation = event layer and above with normal sedimentation), KA II (geopetal axe in body chambers varies in angle section).

Frontal

KA I, KA II

Orthogonal

KA I, KA II

The internal fabric of the accumulation layers (i.e. ammonoid shells) ranges from densely packed, ammonoid shell supported packstones (e.g. AS IV – bed 8; KA I – bed 10) to ammonoid-floatstones (AS Ia – beds 4, 6; Figs. 7.7). The event layers are heterogeneous, with cases of shell imbrication in parts (see imbrication in turbidite Bouma interval Ta, Bouma *et al.* 1982; Eberli 1991) and cases of loosely packed or floating specimens in different parts. Even in single blocks, the density diverges from the base, mid part and top of beds (Fig. 7.9). The matrix infills the body chambers and the space between shells. The imbricated shells show a horizontal or at least low-angle deposition. Vertical or perpendicular ammonoid specimens are extremely rare in accumulation layers of Aşağıyaylabel and Karapınar. An alignment of the biogenic particles (i.e. ammonoid shells) was observed in the majority of the accumulation layers (AS I – beds 4, 6; most beds at KA I, KA II). Although the alignment within most accumulation layers (AS I – beds 4, 6; most beds at KA I, KA II) took place within the sediment, in blocks 1 and 2 (corresponding to the same layer) in AS IV and KA II (e.g. blocks 1, 2) the aligned ammonoids are accumulated in a shell coquina on the top of laminated, peloidal ‘silts’.

The body chambers are filled with the same matrix, which is formed by peloids from a shallower environment, representing the primary depositional area. The shells are densely packed, well sorted and in contact with numerous other shells. The densely packed accumulation layer marks an ammonoid packstone. Siphonal structures are preserved, hindering sediment to fill the phragmocones (see Olivero 2007), hence rapidly buried after death exhibiting the final, hollow 'particles' embedded in the peloidal layers. The matrix above and below this event layer differs distinctly as it consists of fine mud with only rare and smaller ammonoid specimens, deposited under 'normal' conditions. An additional block from AS IV (i.e. block 3) marks a 'normal' calm deposition at, or near the habitat of the ammonoids, appearing with rare, entire ammonoid shells with almost undisturbed and horizontal alignment (Fig. 7.9, Table 7.1). The shell axis in block AS IV – block 3 shows a clear picture with dominant intervals at 160–180°/340–360° with 75.0% and even more expressed in the interval 160–200°/340–020° with 97.2%.

The acme zone of the genus *Kasimlarceltites* ranges due to tectonics from 1.8 m at AS Ia to 16.5 m at KA II, and is intercalated by accumulation event beds (Figs. 7.2, 7.3, 7.4, 7.7). On the basis of the geological time scale of Gradstein *et al.* (2012) a stratigraphical range from one third to one half of the *Austrotrachyceras austriacum* Zone can be assumed, which approximately equals a duration of 200 ky (at AS I, AS IV) - 500 ky (at KA II) for the *Kasimlarceltites* abundance zones. This time span is calculated without consideration of any hiatus or time-averaging, which might occur. The overall quantity of more than 100 million ammonoid specimens is estimated by the data gained from numerous localities from Aşağıyaylabel and Karapınar (e.g. layer thickness, number of mass occurrence layers and specimens etc.) and the geographical distribution (over 10 km^2) of the *Kasimlarceltites* abundance zone. Single blocks from both localities (Aşağıyaylabel and Karapınar) with 15 × 15 × 8 cm contain up to 3500 specimens (Mayrhofer and Lukeneder in prep.).

The calculated mean angle of all combined sections and specimen axes (n 1696) in frontal view is almost horizontal with 172°/352° (Fig. 7.10) indicating a shallow orientation (low angle) of ammonoid shells throughout the various localities (Tables 7.1, 7.2, 7.3). Within the polyspecific KA II – block 4 an increased angle with 164°/344° was observed, as well as an increased number of steeper orientations in body chambers. In contrast the mean angle of shell axes in KA II – block 3 is shallow (low angle – almost planar) with 178°/358°. The measured angle is influenced by the ontogenetic stage and the morphological differences in whorl height. Adult specimens show an angle of 2° whereas juveniles appear with 3° owing to the different whorl expansion rates.

The same situation can be observed in the combined orthogonal data (Fig. 7.10, Table 7.3). The mean angle of all specimen axes (n 1696) in orthogonal view is 177°/357° (172°/352° frontal), depicting a very shallow orientation of ammonoid shells throughout the various localities. Anyhow, an increased angle of 15°/195° in KA II – block 4, where *Kasimlarceltites* occurs together with some specimens of *Sirenites*, was detected. As already observed in frontal view, the orthogonal data strengthen the contrasting picture with an almost horizontal, very shallow mean angle of shell axes in KA II – block 3 by 179°/359° (Fig. 7.10, Table 7.3). The lower accumulation layer in KA I – block 1a (Fig. 7.10) shows mean angles of 004°/184° whereas the 'normal' sedimentation part above (KA I – block 1n; Fig. 7.10) appears with an increased angle of 018°/198°.

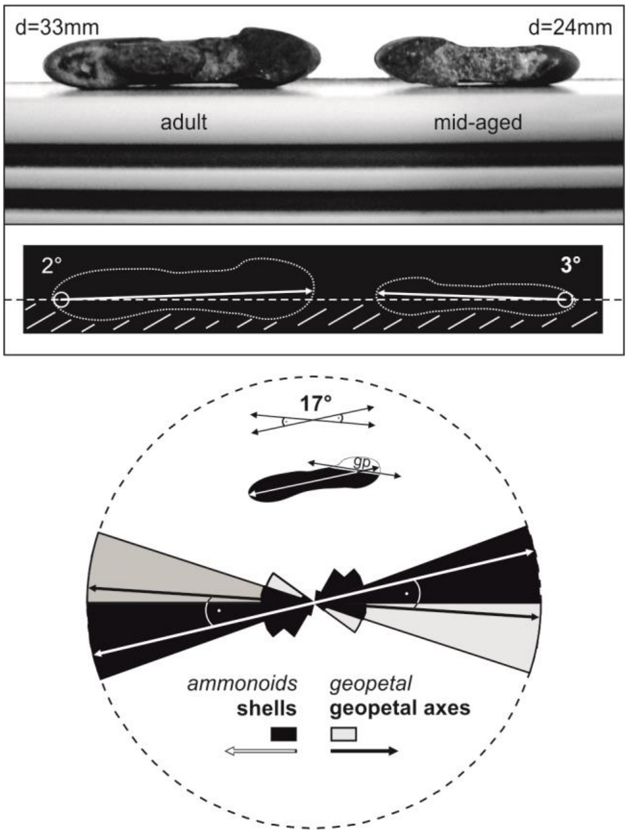

Fig. 7.8. A, Primary angles in shell axes (i.e. 2–3°) caused by the ontogenetic variation of whorl breadth in mid-aged and adult *Kasimlarceltites* (adult = holotype, NHMW 2012/0133/0014); **B,** Shell axes (black pies, white arrow) and geopetal axes (grey pies, black arrow) of *Kasimlarceltites* and *Sirenites* within a sample KA II – block 4 (sections D–E–F).

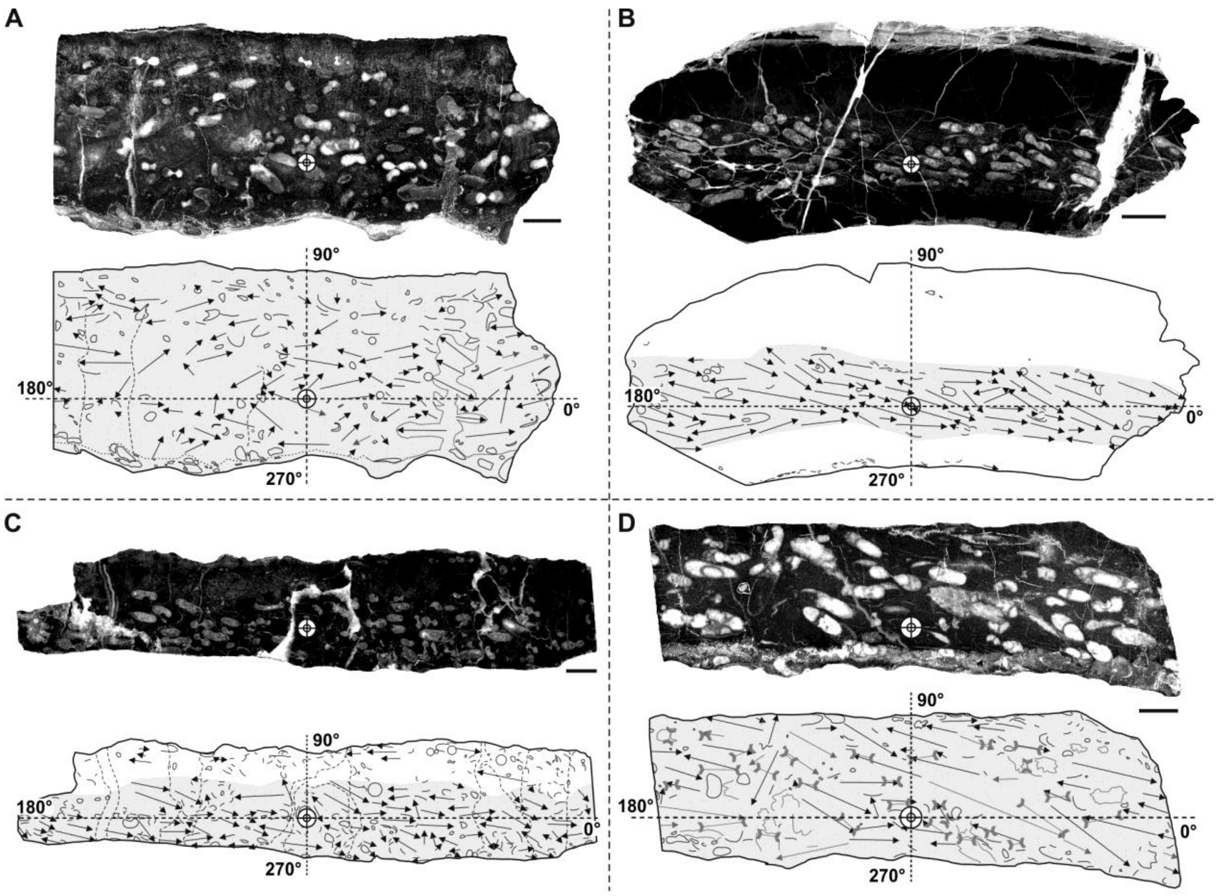

Fig. 7.9. Ammonoid shell alignment in Carnian blocks from Aşağıyaylabel and Karapınar, with indicated accumulation layers and measurements. **A,** AS I – block 1, slice B (orthogonal view), NHMW 2012/0133/0554; **B,** AS IV – block 1, slice C (89 mm, frontal view), NHMW 2014/0091/0003; **C,** KA I – block 1, slice A (frontal view), NHMW 2014/0092/0001; **D,** KA II – block 4, slice A,B,C (0 degree, frontal view), NHMW 2014/0093/0003. Primary angles in shell axes indicated by arrows, arrowheads directed to the body chamber (= maximum whorl breadth). Sketches (below sections) of the corresponding shell axes (black arrows) of each ammonoid specimen within the event layer (grey shading). Scale bar represents 1 cm.

7.9.2. Size groups in *Kasimlarceltites*

In general the ceratitid genus *Kasimlarceltites* Lukeneder and Lukeneder (2014) is a small sized, 1.0 to 3.3 cm, almost smooth ammonoid. The abundance of different ontogenetic stages within the occurring size classes (Fig. 7.10, Tables 7.2, 7.3) varies from locality to locality, even from layer to layer in the same locality. Densely spaced sutures at the phragmocone/ body chamber boundary of some specimens mark the adult stage in numerous ammonoids. For more detailed description see Lukeneder and Lukeneder (2014, fig. 7.4–7.5). At different localities minimum and maximum range size values of *Kasimlarceltites* differs markedly (Fig. 7.10, Tables 7.2, 7.3). Size ranges and dominant diameters (in mm) are given for all accumulation layers, in frontal and orthogonal direction for comparison of potential spatial alignments (Fig. 7.10, Tables 7.2, 7.3).

Aşağıyaylabel

Frontal (Fig. 7.10, Table 7.2)

AS Ia, AS IV

Orthogonal (Fig. 7.10, Table 7.3)

AS Ia, AS IV

Karapınar

Frontal (Fig. 7.10, Table 7.2)

KA I, KA II

Orthogonal (Fig. 7.10, Table 7.3)

KA I, KA II

The overall impression fixed by the data (i.e. angles and diameters) of all specimens measured (n 1696) in frontal views shows a unimodal positively skewed distribution of size classes. For better comparison of distribution, curve shapes and visualization of size classes, distribution curves were set to 100% (Fig. 7.10). A clear dominance of small forms from 2.1–12.5 mm is evident (Fig. 7.10). The maximum size class appears at 4.2–6.2 mm. Maximal size classes from 25.2–29.3 mm are rare to absent in most localities. From the taxonomical work by Lukeneder and Lukeneder (2014) on prepared specimens from the same localities, a maximal diameter of *Kasimlarceltites* is known with 33 mm. The difference in maximal diameters of about 37 mm shows the uncertainty and imprecision in numerical measurements in slices and sections, since the majority of excavated ammonoids from the sections miss the aperture area and therefore fail to reflect the maximum size.

Specimens from AS Ia – block 4, AS Ia – block 3 and KA I – block 1 show their maximum size in frontal view with unimodal curves (positively skewed) at 2.1–10.4 mm. Somewhat shifted curves, increasing in mean size, are present in KA II – block 2 (bimodal) and KA II – block 3 with positively skewed, unimodal curves around a maximum of 4.2–14.6 mm. Exceptional, broad distribution curves occur in AS IV – block 3 with 2.1–23.0 mm and KA I – block 1 with 2.1–20.9 mm.

Analogously, the picture of all specimens measured (n 675) in orthogonal views show a unimodal positively skewed distribution of size classes. The abundance peak also lies within the class 4.2–6.2 mm as seen in the frontal view (Fig. 7.10). A clear dominance of small forms from 2.1–10.4 mm is established (Fig. 7.10). The maximum size class appears at 4.2–6.2 mm. Maximal size classes from 25.2–27.2 mm are rare to absent in some localities.

Specimens from AS Ia – blocks 1, 2, 3 and KA II – block 2 show the maximum size in frontal view with unimodal curves (positively skewed) at 2.1–10.4 mm. Somewhat shifted curves, increasing in mean size, with a slightly bimodal mode are present in AS IV – block 3 and KA I – block 1a (accumulation layer) with positively skewed curves around a maximum of 4.2–14.6 mm. Exceptional, broad distribution curves occur in KA II – block 3 with a wide range of 2.1–18.8 mm.

Variation in diameters and size classes, as reported above for angles, is also present within single layers, as seen in KA I – block 1 (a – accumulation, n – normal). The lower accumulation layer (KA I – block 1a; Fig. 7.10, Tables 7.2, 7.3) shows an abundance of the mean size class 4.2–12.6 mm, whereas the normal sedimentation part above (KA I – block 1n) appears with a decreased diameter class of 0.0–6.2 mm. Both distribution curves are positively skewed but KA I – block 1a shows weak bimodal distribution. Hence the latter ammonoid assemblage comprises juvenile and adult specimens. While juvenile specimens are compressed in shape, adult specimens are much more depressed. This might be interpreted as mating community, environmental forcing or transport mechanism (e.g. current or drift selection of different size or morphology classes).

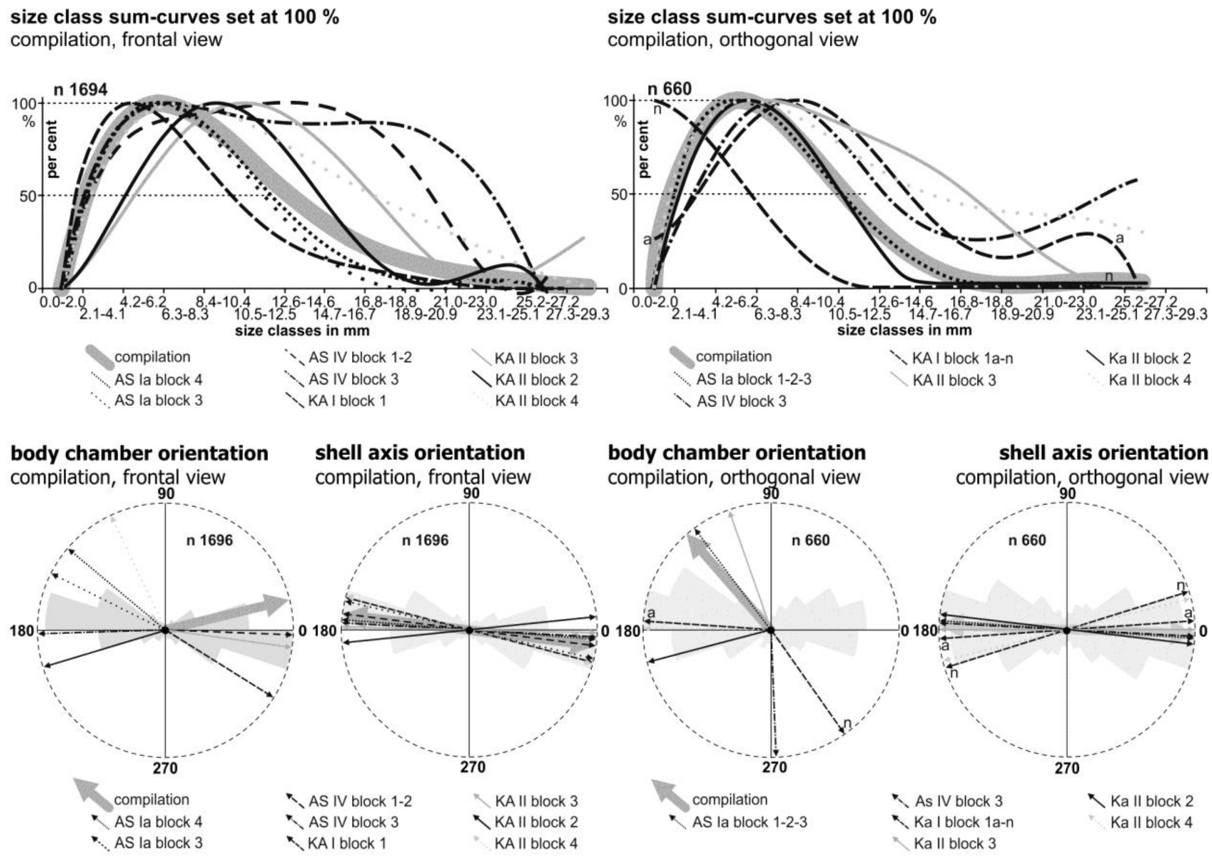

Fig. 7.10. Compilation of size classes, shell axes and body chamber orientations from *Kasimlarceltites* in frontal and orthogonal view of all measured blocks of Aşağıyaylabel (AS I, AS II, AS III, AS IV) and Karapınar (KA I, KA II), Kasımlar Formation, *Kasimlarceltites* acme zone, Lower Carnian, Upper Triassic. See text for description and details.

Shell parameters ammonid shells	Orientation and size of *Kasimlarceltites* at different localities in the Aşağıyaylabel and Karapınar area, frontal view							
	AS Ia	AS Ia	AS IV	AS IV	KA I	KA II	KA II	KA II
BIOFABRICS OF AMMONOID SHELLS								
Block/ bed	long block 4	block 3	blocks 1, 2	block 3	block 1	block 3	block 2	block 4
Orientation in field, front view	left NE, SW right		-	-	-	-	-	-
Slices	1A, 1B, 1C, 1D	3B, 3D	1A 0 mm, 1B 81 mm, 1B thin 85 mm, 1C 89 mm, 2B 100 mm, 2C 240 mm	3A 0 mm, 3B 2 mm, 3C 100 mm, 3D 102 mm	1A 0 mm, 1C 84 mm, 1D 86 mm	3A	2B	4A, B, C 0°
Quantity of angles (n)	853	114	373	36	225	25	27	43
Dominant shell axis	160–180°/ 340–360° **35.4%**	140–160°/ 320–340° **28.75%**	160–180°/ 340–360° **43.1%**	160–180°/ 340–360° **75.0%**	160–180°/ 340–360° **38.7%**	160–180°/ 340–360° **32.0%**	180–200°/ 000–020° **29.6%**	160–180°/ 340–360° **58.1**
Dominant angle interval	160–200°/ 340–020° **59.1%**	140-200°/ 320–020° **37.0%**	160-200°/ 340-020° **68.1%**	160–200°/ 340–020° **97.2%**	160–200°/ 340–020° **55.6%**	160–200°/ 340–020° **82.0%**	160–200°/ 340–020° **34.4%**	160–200°/ 340–020° **67.4%**
Comments on axis angle	weakly oblique unimodal	more oblique bimodal	weakly oblique unimodal				more oblique broad unimodal	weakly oblique, unimodal
Dominant body chamber, up	160–180° **20.2%**	140–160° **23.1%**	160–180° **14.2%**	160–180° **50.0%**	160–180° **16.0%**	000–020° **28%**	140–160° **14.8%**	160–180° **39.5%**
Dominant body chamber, down	340°–360° **15.2%**	no dominant range	340°–360° **29.0%**	340°–360° **25.0%**	340°–360° **22.7%**	180–200° **20.0%**	180–200° **22.2%**	340°–360° **18.6%**
Comments on body chamber angles	weakly oblique, bimodal	more oblique unimodal	weakly oblique, unimodal					
SIZE CLASSES AND DIAMETERS								
Quantity of diameters (n)	853	114	373	36	225	25	27	41
Dominant size class (mm)	4.2–6.2 **24.7%**	4.2–6.2 **26.3%**	12.6–14.6 **13.7%**	8.4–10.4 **16.7%**	4.2–6.2 **24.4%**	6.2–8.2, 10.4–12.4 both **20%**	8.4–10.4 **40.7%**	8.2–10.2 **22.0%**
Dominant size range (mm)	4.2–10.4 **62.6%**	4.2–10.4 **65.8%**	2.1–18.8 **89.0%**	2.1–23.0 **100%**	2.1–10.4 **74.7%**	6.2–20.2 **80%**	4.2–12.2 **74.1%**	2.2–18.2 **87.1%**
Dispersal curve	unimodal, positively skewed		broad unimodal–bimodal		unimodal, positively skewed	bimodal	unimodal, positively skewed	
Mean size (mm)	8.3	7.6	11.7	12.4	7.2	12.6	9.8	11.2
Comment on size	small	small	larger	larger	small	larger	small	larger
Miniumum size (mm)	1.7	1.9	1.1	2.5	1.4	2.4	3.8	2.3
Maximum size (mm)	26.0	18.1	26.2	22.3	18.6	29.0	18.5	26.0
Size range (mm)	24.3	16.2	25.1	19.8	17.2	26.6	14.7	23.7

Table. 7.2. Results on the biofabric, orientation and size classes of *Kasimlarceltites krystyni* at different localities in the Aşağıyaylabel and Karapınar area, frontal view.

Shell parameters of ammonid shells	Orientation and size of *Kasimlarceltites* at different localities in the Aşağıyaylabel and Karapınar area, orthogonal view							
	AS Ia	**AS IV**	**KA Ia**	**KAIb**	**KA II**	**KA II**	**KA II**	**KA II**
BIOFABRICS OF AMMONOID SHELLS								
Block/ bed	blocks 1, 2, 3	block 3	block 1	block 1	block 3	block 2	block 4	block 4
Orientation in field, orthogonal	front NW, SE back	-	-	-	-	-	-	-
Slices	1B, 1D, 2B, 2D, 3A, 3C	3A 210 mm, 3B 0 mm	1B accumulation	1B normal	3B	2C	4def 110°	4def 110°
Quantity of angles (n)	563	16	21	9	16	11	24	15
Dominant shell axis	160–180°/ 340–360° **23.1%**	160–180°/ 340–360° **68.8%**	180–200°/ 000–020° **52.4%**	220–240°/ 040–060° **33.3%**	160–180°/ 340–360° **31.3%**	160–180°/ 340–360° **36.4%**	180–200°/ 000–020° **50.0%**	geopetal axis 180–200° **29.4%**
Dominant angle interval	160–200°/ 340–020° **45.2%**	160–200°/ 340–020° **93.8%**	160–200°/ 340–020° **81.0%**	no dominant angle interval	160–200°/ 340–020° **43.9%**	160–200°/ 340–020° **63.7%**	160–200°/ 340–020° **70.8%**	geopetal axis 340–360° **52.9%**
Comments on axis angle	bimodal	weakly oblique, unimodal		polymodal		weakly oblique, unimodal		shifted to ammonoid axes, polymodal
Dominant body chamber, up	160–180° **14.4%**	160–180° **31.3%**	000–020°, 160–180° both **14.3%**	000–020°, 40–60°, 140–160° all **14.3%**	160–180° **25.0%**	000–020°, 140–160°, 160–180°, all **18.2%**	000–020° **20.8%**	-
Dominant body chamber, down	180–200° **10.1%**	340–360° **37.5%**	180–200° **38.1%**	220–240°, 340–360° both **22.2%**	180–200°, 340–360° **6.3%**	340–360° **18.2%**	180–200° **29.2%**	-
Comments on body chamber angles	weakly oblique, unimodal	bimodal		bimodal to polymodal		weakly oblique, unimodal	bimodal	-
SIZE CLASSES AND DIAMETERS								
Quantity of diameters (n)	562	16	21	9	15	11	21	-
Dominant size class (mm)	4.2–6.2 **26.6%**	4.2–8.2 **37.6%**	8.4–10.4 **38.1%**	0.0–4.2 **66.6%**	6.3–10.4 **40.0%**	6.3–8.3 **45.5%**	10.5–12.5 **23.8%**	-
Dominant size range (mm)	2.2–10.2 **80.0%**	4.2–12.2 **56.3%**	2.1–10.4 **66.7%**	0.0–6.2 **88.9%**	4.2–16.7 **80.0%**	4.2–10.4 **100%**	2.1–12.5 **61.9%**	-
Dispersal curve	unimodal, positively skewed	broad unimodal to bimodal		unimodal, positively skewed	bimodal	unimodal, positively skewed	broad bimodal	-
Mean size (mm)	7.2	12.9	9.9	3.5	10.7	6.9	12.1	-
Comment on size	small	larger	small	very small	larger	small	larger	-
Miniumum size (mm)	1.0	4.4	1.9	1.6	3.5	5.3	2.0	-
Maximum size (mm)	20.2	25.9	20.2	8.8	19.0	10.3	26.8	-
Size range (mm)	19.2	21.5	18.3	7.2	15.5	5.0	24.8	-

Table. 7.3. Results on the biofabric, orientation and size of *Kasimlarceltites krystyni* at different localities in the Aşağıyaylabel and Karapınar area, orthogonal view.

7.10. Discussion

7.10.1. The *Kasimlarceltites* mass occurrence as an abundance zone

The trigger mechanisms and possible processes, which cause the abundance and accumulation of ammonoids and the formation of such widespread ammonoid mass occurrences or ‘event’ layers, are discussed. Current induced alignment, winnowing and earth quakes or storm events (Aigner 1985; Brett and Baird 1986; Seilacher and Aigner 1991; Hips 1998; Radley and Barker 1998; Storms 2001; Pérez-Lopéz and Pérez-Valera 2012) are discussed as trigger factors for such gravity forced ‘event beds’. The described examples are thus autocyclic (Einsele *et al.* 1991b), formed by nonperiodic mass flows and/ or turbidites endemic to the tectonic setting (Bouma *et al.* 1982; Cook *et al.* 1982; Howell and Normark 1982; Tucker and Wright 1990; Potter *et al.* 2005; Hornung 2008). Final deposition took place on tectonically unstable slope areas, shown by the presence of frequent neptunian dykes (see Flügel 2004; Črne *et al.* 2007) within the *Kasimlarceltites* acme zone.

In the majority of such fossil accumulation beds, several reasons amplify the primary signal (Kidwell 1986; Kidwell *et al.* 1986). Pérez-Lopéz and Pérez-Valera (2012) presented a tripartite model for storm influenced beds and near platform carbonate environments with the pot/gutter casts, the tempestite beds and the storm winnowed deposits. According to Aigner (1985) storm processes can be distinguished in three distinct physical categories with barometric effects, wind effects, and wave effects. The causes and features of such rapidly deposited ‘event’ sediments are extensively reviewed by Einsele and Seilacher (1982) and Einsele *et al.* (1991a), and the depositional environment of sandy turbidites and other mass flows deposits are summarized by Einsele (1991).

As noted by Aigner (1985), storm-generated tempestites show a clear gradation with fine sediments that is extremely subtle or lacking in distal tempestite fronts (difficult to separate from distal turbidites), which is not seen in the Carnian layers at Aşağıyaylabel and Karapınar. Specifically, he noted that proximal storm-event layers contain more mixed faunas, with allochthonous specimens, in contrast to distal layers, where autochthonous and parautochthonous assemblages predominate, having been reworked in-situ (see also Golebiowski 1991).

Progressing gravity, debris flows show typical transition to turbidity currents, due to changes in different transportation phases when variable degrees of debris dilution occur. Therefore the transportation of debris might indicate net reworking (pers. comm. Olóriz 2014).

The dynamic history and the influence of sediment transport to that area during the Carnian can also be traced by the frequent Cipit boulders (directly above the *Kasimlarceltites* acme zone), derived from the shallow-platform edge and transported by gravity down across the slope, as well as by the frequently silty, turbidite layers in the Kasımlar shales in the Tuvalian.

Geochemical and geophysical data (Lukeneder *et al.* in prep.) will confirm or contradict the idea of drastic changes in ecological factors (e.g. anoxic events, methane eruptions, for toxic events see also Noe-Nygaard *et al.* 1987) during the sedimentation of the *Kasimlarceltites* acme zone. Such ecological factors can act as trigger mechanisms for potentially catastrophic ammonoid mass mortality of the ammonoid deposits from Turkey. Such traces are not observed in the redeposited layers (episodic deposits in Brett and Baird 1986) and in the 'normal', background sedimentation beds (= 'host' beds) where *Kasimlarceltites* rarely occurs. In contrast to this, Adamíkova *et al.* (1983) discussed mass natality as a possible trigger for a lower Barremian (Cretaceous) mass occurrence of ammonoids (Adamíkova *et al.* 1983).

The presence of ammonoid abundance zones ('ammonoid-beds'; characterized by abundance or mass-occurrence of ammonoids) seems to be related to sea-level rises or falls (Kidwell 1988, 1991a,b, 1993a,b; Martin 1999; Lukeneder 2001, 2003b). Most probably ammonoid mass occurrences reflect transgressive phases (see also Hoedemaeker 1994; Aguirre-Urreta and Rawson 1998, 1999). Anyhow, Fernández-López *et al.* (2002) argued that ammonoid mass occurrences deposited within shallow water environments reflect regressive phases, whilst ammonoid mass occurrences deposited within deeper water environments reflect transgressive trends (Fernández-López *et al.* 2002). The observation of different preservational features (e.g. sedimentary infilling, encrustation, abrasion, bioerosion, reorientation and dispersal) might hint to the right interpretation (a shallow or deeperwater environment – Fernández-López *et al.* 2002).

7.10.2. Biostratinomy and taphonomy

The nearly entire (> 95 %) well preserved ammonoid specimens of the lower Upper Triassic (Carnian) of the Kasımlar Formation, suggest no-to-moderate, non-destructive transport mechanisms and therefore favour a more autochthonous to parautochthonous nature of the specimens. Judging from internal structures of the limestone beds and the alignment of the fossil content (Potter and Pettijohn 1977), water saturated gravity flows (= liquified flows – Mulder and Alexander 2001; SEPM 2014) are induced at a medial position between a proximal (near-source) and a distal depositional development (see Aigner 1985). Hence, moderate transportation of at least some intraclasts, plasticlasts and bioclasts such as gastropods and in parts ammonoids, is presumed.

The fragmentation (e.g. broken body chamber) of less than 5 % of the ammonoids provides evidence for no, gentle or very weak post mortem transport, without breakage on the sea floor through current effects, and/or consequences of predation (Lukeneder 2004a,b). Anyway, the tiny shells (max. 33 mm) of *Kasimlarceltites* were probably resistant against breakage by impact of shells with other bioclasts transported by the currents. Ruptures reflecting post mortem histories, caused by current-induced transport before embedding, are absent. It may also reflect the enhanced stability of ammonoid shells with smaller size, more 'spheroidal' shape and suggests that involute morphologies are more resistant to damage compared to other ammonoid shell morphologies (e.g. broken body chamber of *Simonyceras*; specimen figured on Fig. 7.11A in Lukeneder and Lukeneder 2014). Furthermore, buccal masses with preserved beak apparatus (e.g. aptychi like jaws) are completely missing in the Turkish material, hinting at more parautochthonous than autochthonous depositional conditions.

Accumulated small ammonoids (i.e. *Kasimlarceltites*) of all ontogenetic stages (e.g. ammonitellae, juveniles to adults) and shell fragments in body chambers of adjacent large ammonoids, in combination with cephalopod alignment in several single layers (e.g. AS Ia – beds 4, 6; AS IV – bed 8; KA I – beds 10, 12; KA II – beds 2, 11, 122; KA III – bed 8) also suggest transport-effects on deposition (e.g. mass flow, bottom currents, winnowing – Potter and Pettijohn 1977; Flügel 2004; Potter *et al.* 2005; Fernández-López 2007; Nichols 2009). The accumulation of the shells which show almost horizontal alignment (Figs. 7.8, 7.9, 7.10) in thin and distinct layers, is probably due to episodes of reworking and current-induced removal of sediment (i.e. winnowing). Horizontally aligned specimens were most probably secondarily re-orientated and aligned during a first gravity flow sedimentation phase.

The absence of any erosional feature (i.e. mechanical- or bio-erosion; see Fernández-López 2007) or encrustation on any side of the ammonoids suggest calm environments with relatively fast burial processes. The shell transport took place during single events or phases of slow gravity sediment flows, as is reflected by the occurrence in several separated ammonoid layers up to 10 cm in thickness (Figs. 7.3, 7.4, 7.5, 7.7).

The 'normal' occurrence range, with rare specimens of *Kasimlarceltites*, clearly shows the inhabitation of that paleogeographical area during the Carnian (Late Triassic) over a hundred thousand years (Lukeneder and Lukeneder 2014; for numerical age see Gradstein *et al.* 2012). In contrast, accumulation in masses occurs only within single event beds, caused by huge storms or tectonically induced earthquakes (= seismic activity in Einsele 1991; see slope failures in Potter *et al.* 2005).

Mixed assemblages are defined in Lukeneder (2004a,b) as comprising allochthonous elements (e.g. gastropods, sponges, corals) transported from the shallower shelf to upper slope and autochthonous benthic and parautochthonous pelagic elements (e.g. ceratitid ammonoid *Kasimlarceltites*) from deeper marine environments. See also the discussions by Olóriz and Villaseñor (2010) on post-mortem and possible biostratinomic mixing of ecologically age-separated populations. Assuming an analogous situation for the Aşağıyaylabel sections as for the Karapınar sections, this would mean that the presence of undamaged macroconchs accompanied by intact microconchs within the same bed points to a similar derivation of the ammonoids from the same source, in this case the pelagic fauna of the water column above, without assuming any depth. This points to a huge problem in the understanding of ammonoids life and habitats. The question, if ammonoids in general, and *Kasimlarceltites* or *Sirenites* from Turkey in detail, were planktonic drifters, nektic swimmers or nektobenthic swimmers is beyond the field of the study here. Nonetheless, the answer to this question would make a serious difference to the study of biostratinomic features in chambered cephalopods, both fossil (e.g. ammonoids, nautiloids) and recent (e.g. *Nautilus*, *Spirula*).

The post mortem history, hence the subsequently complicated drifting mechanisms (i.e. waterlogging and sinking versus surfacing and floating; see Seilacher 1968; Olivero 2007) in ammonoid shells depends mostly on the water depth and hydrostatic pressure (Maeda and Seilacher 1996) when the animal dies. This interpretation is contrasted to the occurrence of some specimens showing different sediment infillings of the body chambers as compared to the surrounding and embedding finer limestone. Reasons for these differences in sediment infilling reflect the difference in sediment and shell transportation history. Specimens filled with coarser material (i.e. shallower water relicts) are redeposited from shallower areas. Shells are preserved without fragmentation (i.e. body chamber present), mostly with almost similar alignment and rare infilling of phragmocones by sediment (see Olivero 2007). Observed geopetal structures, aligned in almost identical directions, within the accumulated ammonoids give evidence for a fast burial history of almost the entire contingent of ammonoids. Ammonoid specimens shown by Olivero (2007) from the Santonian—Lower Campanian mass flow deposits of Antarctica also exhibit preserved siphuncle tubes preventing the infill of phragmocones with sediment.

The cephalopods of the Aşağıyaylabel and Karapınar sections thus constitute a mixed autochthonous/parautochthonous/allochthonous (Martin 1999) fauna. This effect is enhanced by the fact that gravity currents, submarine mass-flows (mud supported and water saturated) may already contain a mixed shelf and slope assemblage by picking up bioclasts from different bathymetric zones along their way (Einsele and Seilacher 1991). The Carnian mixed assemblages comprise a considerable amount of bivalves, gastropods, sponges and corals from shallower environments from a nearby located platform or upper ramp (Lukeneder *et al.* 2012; see Eberli 1991). The term 'mixed' assemblage is used in the sense of Kidwell and Bosence (1991). The latter authors described a mixed assemblage as the addition of shells of one assemblage to the members of another assemblage. For classification and reviews on taphonomic processes of marine shelly faunas see also Norris (1986), Kidwell *et al.* (1986), Brett and Seilacher (1991), Kidwell (1991a,b), Kidwell and Bosence (1991), and Speyer and Brett (1991).

7.10.3. Ammonoid shell alignment

The ammonoid shell orientation (i.e. rose diagrams of shell axes, body chamber orientation; Figs. 7.9, 7.10, 7.11) within the accumulation layers was measured to gain information on the prevailing conditions and mechanisms (e.g. bottom water currents, debris flows, turbidites, storms etc.; Goldring 1991) at the time of deposition (Early Carnian, *Austrotrachyceras austriacum* Zone).

A more detailed picture of the three-dimensional alignment of specimens from AS I-block 1 (i.e. 150×45×140 mm block, 70 slices with 2 mm distance) is presented in Lukeneder *et al.* (2014). Lukeneder *et al.* (2014) show that the internal, dominant orientation of specimens in fossil mass occurrences can be exploited as a useful source of information about the flow type and direction determining the precise conditions for their transportation and accumulation. A series of studies, using different kind of fossils, especially those with elongated shape (e.g. elongated gastropods), deal with their orientation and the subsequent reconstruction of the depositional conditions (e.g. paleocurrents, transport mechanisms). However, disk-shaped fossils like planispiral cephalopods or gastropods were used, up to now, with caution for interpreting paleocurrents. Moreover, most studies just deal with the topmost surface of such mass occurrences, due to its easier accessibility. Within Lukeneder *et al.* (2014) the exact spatial shell orientation was determined for a sample of 675 ammonoids, and the statistical orientation analysed with a NW/SE-orientation. The study of Lukeneder *et al.* (2014) from the Aşağıyaylabel mass occurrence combines classical orientation analysis with modern 3D-visualization techniques, and establishes a novel spatial orientation analysing method, which can be adapted to any kind of abundant identifiable object. Such a spatial alignment with imbrication in a gravity flow was detected by Hladil *et al.* (1996) for Lower Devonian tentaculite shells from the Czech Republic. There, the analysed fossils show a similar oblique orientation (i.e. upward and downward) due to gravity transport (Hladil *et al.* 1996), caused by a rapid consolidation of the host sediment. It should be noted that the natural, post mortem orientation angle of a particular ammonoid shell (i.e. *Kasimlarceltites*) after sinking onto the sea floor, is almost horizontal with approximately 2-3° (Fig. 7.8), depending on the ontogenetic stage. This phenomenon is caused by the maximal whorl breath at the body chamber near the aperture. The horizontal shell orientation dominates over oblique alignment in layers formed during undisturbed background sedimentation.

The Triassic assemblages differ significantly from a Middle Devonian example of nautiloid mass occurrences (= concentrates in Soja *et al.* 1996), which was interpreted as being a combination of mass spawning and mass mortality events (biological process; see Lukeneder, in print) with storm-related accumulations (physical process). In contrast to the Triassic accumulation layers from Turkey, the densely packed Devonian cephalopod mass occurrence (i.e. nautiloid grainstone) shows no orientation, alignment or imbrication of the shells (Soja *et al.* 1996). *Goniatites* beds from Upper Devonian of Poland (Niechwedowicz and Trammer 2007) were described as post mortem shell accumulation, not transported very far, deposited within the habitat realm and interpreted as the result of condensation, which has often been noted for cephalopod limestones. Niechwedowicz and Trammer (2007) interpreted the shell alignment due to wave or current transport in shallower environments.

At least some of the abundant ammonoid specimens seem to have been redeposited from shallower shelf regions into a slope environment. Similar occurrences were reported from low density gravity flows (e.g. slump deposits and turbidites) from Lower Triassic redeposited ammonoid accumulations of East Russia (Maeda and Shigeta 2009). The authors note sporadically intercalated ammonoid beds (with nearly horizontal alignment of ammonoid shells) within otherwise 'normal' mudstone sedimentation. Maeda and Shigeta (2009) identified an allochthonous source (i.e. primary shelf edge biotope) for ammonoids deposited and transported in such fossiliferous, turbidite layers. Taxonomical related findings of celtitids were presented by Manfrin *et al.* (2005) from adjacent basinal series, surrounding the Middle Triassic Latermar Platform (N Italy). The faunas from these ammonoid layers were interpreted by Manfrin *et al.* (2005) as storm deposits, due to the mixture of pelagic and platform derived fossils and the partly perpendicular (= non-equilibrium in Manfrin *et al.* 2005) alignment of ammonoids within the coquinas. It is evident that such layers consist of transported, mixed faunal elements (i.e. pelagic ammonoids and benthic gastropods – Manfrin *et al.* 2005), deposited by distinct and short events. This is almost identical to the assemblages found at Aşağıyaylabel, but with the remarkable difference of chaotic shell-alignment, enhanced shell-fracturing and variation of sedimentological features.

Mass flow transport is evident from the orientation of shells within the layers (Middleton and Hampton 1973, 1976; Brown and Loucks 1993; Potter *et al.* 2005; Nichols 2009), not only at the top of beds as is the case when water current causes mass occurrence or turbidite accumulation. A somehow mixed or transitional mechanism of debris flow (i.e. laminar flow) and turbidity current (i.e. turbulent flow) deposition is assumed for floatstones of AS Ia and AS II. A low density, less concentrated and water saturated debris flow (= liquefied debris flow) with transitional features into a turbidite transport (pers. comm. Michael Wagreich 2013;

see Lowe 1982; Einsele 1991; Hladil *et al.* 1996; Mulder and Alexander 2001; Olivero 2007) is highly presumable. A horizontal or at least low-angle deposition of imbricated shells is caused by low-density transports (Hladil *et al.* 1996). A positive enhancement of an existing inclination can be forced by slipping or sliding processes of the not consolidated sediment layers, down the slope or ramp.

The mostly erosive base of the accumulation layers, furthermore undulated with fragmented ammonoid shells, reflects sudden and punctual reworking phases at the base of the sediment flow to some extent (see Sepkoski *et al.* 1991).

The majority of the accumulation layers (AS I – beds 4, 6; most beds at KA I, KA II) were formed by water saturated debris flow deposition which caused the alignment of the biological particles (i.e. ammonoid shells) within the sediment. A contrasting exception can be observed in section AS IV (e.g. bed 8; Figs. 7.10, 7.11, Tables 7.1, 7.2, 7.3) and KA II within the blocks 1 and 4. In blocks 1 and 2 (corresponding to the same layer) in AS IV and KA II (e.g. blocks 1, 2) a clear short-term turbidite transport took place. Ammonoid shells seem to float on the peloidal-silt level, most probably due to hydrodynamic sorting. Hence, low density, empty ammonoid shells (1.1–1.2 g/cm^3 – Maeda 1999; Maeda and Shigeta 2009), subsequently filled by calcite, remain suspended in the water column during or shortly after the transport event.

All of the distinct ammonoid event layers represent only episodic (i.e. formed during days to weeks), punctual thin horizons (see Brandner *et al.* 2012) which interrupt the ‘normal’ background sedimentation phase, consisting of limestone beds with only rare occurrences of ammonoids (e.g. *Kasimlarceltites*, *Klipsteinia*, *Sirenites*). Brett and Baird (1986) distinguished two kind of deposition, characterized by the mode of sedimentation rate with the long-lasting background deposition (1–10 cm/10^3 yr) and the punctual episodic sedimentation (1–50 cm/10^{-2} yr).

The almost horizontal alignment of the shells from the ammonoid-rich horizons reflects the normal long-term sedimentation and no-to-weak transport of shells before embedding. The observed angle is similar to angles detected when single specimens are lain on a horizontal ground (Fig. 7.8). Contrastingly, the increased angle in the polyspecific KA II – block 4 with 164°/344° (frontal data) resp. 15°/195° (orthogonal data) is interpreted as caused by a more turbulent transport and the mixture with specimens of the bigger *Sirenites* (strong ribs and spines), on which *Kasimlarceltites* (almost smooth) specimens often ‘lean’. The increased obliqueness in axes is also caused by the increased number of steeper orientations in body chambers with a mean direction of 111° in KA II – block 4 (Fig. 7.10).

The increased angle seems to reflect bioturbation and secondary dislocation of the small objects (i.e. 0.5–8.0 mm). Such small sized skeletal objects are easily orientated by common depositional processes (e.g. bottom currents, turbidites, storms, mass flows) but not obliged to be aligned related to their shell axes, owing to the almost globular morphology of small objects.

A more indistinct and imprecise picture is seen when interpreting the body chamber orientation in both, frontal and orthogonal two-dimensional slices (Fig. 7.10, Tables 7.2, 7.3). As the body chamber length in *Kasimlarceltites* varies from three-fourths to an entire whorl (i.e. mesodome to longidome; see Westermann 1996), measurements and data can only show the direction of the biggest part of the outer whorl, not assuming to show the definite, final apertural direction. This problem should be solved with 3D sectioning and reconstruction (Lukeneder *et al.* 2014). Hence the data show unimodal (only one direction of body chambers) to bimodal (two opposite directions) distribution roses (Fig. 7.10). As shown above, the data on axes orientations, hence the transport induced directions and alignments are more reliable within our two-dimensional based work.

7.10.4. Size groups in *Kasimlarceltites*

The intraspecific variation of size classes and the difference within layers and localities is the expression of either different sources (i.e. environments, depth range) of the transported sediment (i.e. including ammonoids shells), or the result of sexual (i.e. females = macroconchs – M, males = microconchs – m) or ontogenetic (i.e. ammonitellae, juveniles and adults) separation of ammonoids habitats during life.

The difference in abundance and resulting distribution curves from frontal and orthogonal size classes in several blocks of different localities, once again strengthens the concept of an alignment of ammonoid shells after intense and detectable transport. This important issue can be noticed in KA II – block 2 with frontal values of 8.4–10.4 mm versus smaller orthogonal values between 4.2–6.2 mm, KA I – block 1 smaller frontal values (4.2–6.2 mm) versus orthogonal values (8.4–10.4 mm), and AS IV – block 3 with a frontal wide range (6.3–18.8 mm) versus a narrow orthogonal range of 6.3–8.3 mm and a second peak at 25.2–27.2 mm. Frontal and orthogonal size class distribution is almost identical in AS Ia – blocks 1, 2, 3 (Fig. 7.10).

7.11. Conclusions

The Upper Triassic macrofauna of Aşağıyaylabel and Karapınar (Taurus Mountains, Turkey) is represented especially by ammonoids (i.e. ceratitids) and bivalves (i.e. halobiids). The whole section yielded over 2,300 ammonoids, extracted and prepared as well as embedded in blocks and sections. The fauna can be assigned to the Lower Carnian *Austrotrachyceras austriacum* Zone (Lukeneder and Lukeneder 2014) and contains ammonoids of all ontogenetic stages, from ammonitallae to adults (for more detail see Lukeneder and Lukeneder 2014).

The invertebrate fauna (e.g. ammonoids, bivalves, gastropods, sponges, corals) is accumulated in isolated and distinct single-event layers. The cephalopod shells are aligned and concentrated in particular levels and some show, to some extent, current-induced orientation. Alignment of shells into diverse orientations suggests mass flow currents or other turbulent bottom-water currents.

The ammonoid fauna at Aşağıyaylabel and Karapınar were deposited together with sediments formed by gravity induced flows and turbidites under the influence of winnowing and bottom currents. The sediments were partly reworked and transported in suspension for some distance, from shallower areas at the platform edge to the upper slope onto the deeper parts of the slope and basin. The sediments were initially deposited on the platform shelf close to the slope edge (shelf break area), which is also near the final embedding place of the ammonoid remains. In this area, unstable marine sediment accumulations create the prerequisite conditions for remobilization by gravity flows and/or turbidity currents (Einsele 1991; Potter *et al.* 2005). Those flows and currents then built up the floatstones and packstones comprising the ammonoid mass occurrences. The final deposition of the floatstones to packstones from Aşağıyaylabel and Karapınar took place on tectonically unstable slope areas during conditions of relatively high sedimentation rates. Successions with abundant or accumulated ammonoid-layers are widespread over a 15 km^2 area.

Debris flows and turbidity current, or a combination of both, were triggered either by storm wave activity or by forcing other physical events such as earthquakes, tsunamis and less probably sediment overloading, which led to the formation of event beds and ammonoid accumulation layers on the upper slope to basin of the Carnian (*Austrotrachyceras austriacum* Zone) from the Taurus Mountains. The ammonoid accumulation layers (and therefore the lower part of the Kasımlar Formation) are almost monospecific, dominated by the ceratitid genus *Kasimlarceltites* with up to 99.9 %. The thickness of the *Kasimlarceltites* acme zone ranges from 1.8 m at Aşağıyaylabel (section AS I) and 16.5 m at Karapınar II (section KA II). The position, and hence the exact geographical cardinal direction of the source area, is unknown.

The orientation measurements (e.g. angles of axes and body chambers) of the ammonoids also point to origination by water-saturated, liquefied debris flows, resulting in biogenic floatstones or packstones (i.e. matrix supported and ammonoid shell supported; see Flügel 1978, 2004). The two-fold picture clearly points to various transport mechanisms, hence a change of source areas or transport history during the Julian–Tuvalian in Carnian times (Late Triassic). An increasing water depth, either due to a sea level rise or a tectonic drop of the carbonate platform is also evident for that Anatolian area, clearly detectable in the sedimentological and paleontological record. Subsequently, current systems changed during that time of paleo-oceanographic modification and restructuring, resulting in unstable conditions and thus redeposited accumulation layers.

The *Kasimlarceltites* event layers are intercalated with ‘normal’ sedimentation beds, which are represented by wackestones with only rare, floating *Kasimlarceltites* specimens. Small ammonoids (i.e. juvenile *Kasimlarceltites*) and shell fragments in the body chambers of somewhat larger ammonoids also support the assumed effect of agglomeration and comminution by dense sediment flows with a laminar internal flow. The accumulation of ammonoid layers indicates either on-site deposition at short, favourable ‘timeintervals’, or reworked accumulation-layers after gravity flow transport (slow debris flow). Most ammonoid specimens are not fragmented and do not show bioerosion (i.e. boring, encrustation). This suggests a short transport history of the sediment masses and rapid incorporated shells (e.g. ammonoids, bivalves, gastropods) as well as relatively fast burial. Moreover, because most body chambers of the ammonoid specimens are filled with debris, they were already dead at the time when they were transported. These are thus true, redeposited accumulations, and their initial accumulation in shallow water must have also been characterized by fairly rapid burial, to avoid postmortem bioerosion. The presence of ammonoids bearing intraclasts (i.e. different colour due to different source areas), of sponges associated with corals and gastropods, of slightly dislocated shell angles in ammonoids, of dislocated geopetal structures (i.e. in ammonoid shells) and in cases of a cover of broken ammonoid shells and bivalve coquinas (Kidwell 1991a,b) signify a turbulent transport and redeposition of sediments and fossils.

The assemblages within the described accumulation layers depict an indefinite mixture of autochthonous (= indigenous in Kidwell 1991b), parauthochthonous, and allochthonous (= exotic in Kidwell 1991b) sedimentological and biogenic elements. Concentrations of ammonoid shells are mainly based on primary biogenic (sensu Kidwell *et al.* 1986) and sedimentological concentration mechanisms (see Kidwell *et al.* 1986; Meldahl 1993). The combination of both (biogenic and sedimentological skeletal concentrations) suggest inner shelf and inner ramp environments (Kidwell *et al.* 1986).

The enormous quantity of ammonoid shells in these thin beds also suggests a possible gregarious life style of the ceratitid *Kasimlarceltites*, at least during times of mating and spawning (see also Soja *et al.* 1996; Lukeneder, in print). Buccal masses with preserved beak apparatus (e.g. aptychi like jaws) are completely missing in the Turkish material. Isolation took place, either through transport, due to different behaviour within the water column, or through current-induced grain differentiation during accumulation. The latter scenario leads to different, and unknown, places of deposition for these two cephalopod elements of the same animal.

A highly variable sea floor morphology is induced by the lithological and sedimentological deviations within the adjacent sections. Bottom physiography produced different accumulation models and ammonoid shell bed types.

This leads consequently to the question of the time during which *Kasimlarceltites* dominated the fauna in this Late Triassic (i.e. Carnian – Julian 2) area. A stratigraphical range (Gradstein *et al.* 2012) from one third to one half of the *Austrotrachyceras austriacum* Zone (approximately 200 ky at AS I and AS IV – 500 ky at KA II) is calculated for the *Kasimlarceltites* acme zone, not considering any hiati or time averaging, which might have occurred. A possible geographical differentiation into habitats from sexual dimorphic pairs (i.e. females, males and juveniles), and hence the original water depths inhabited by different size and morphogroups, bears the potential to change the picture of the formation mechanisms and habitats in ceratitid ammonoids and to produce such mass occurrences or event beds in particular. The obtained information encourages future research focused on the preservation history and processes causing ammonoid accumulations.

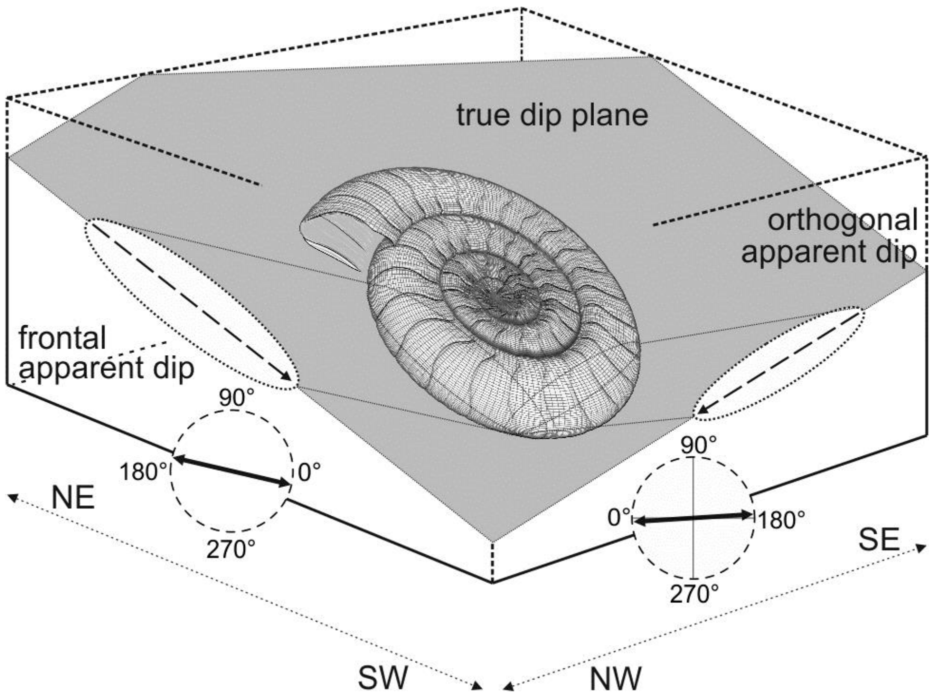

Fig. 7.11. Calculation scheme for true dip direction in ammonoid shells from Aşağıyaylabel (AS I, AS I – blocks 1, 2, 3, 4). True dip direction of the ammonoid shell 'plane' needs two different (frontal and orthogonal) apparent dip measurements of ammonoid shell axes. For more details on this method and three dimensional calculations see Lukeneder *et al.* (2014).

7.12. Acknowledgments

This study benefited from Grants from the Austrian Science Fund (FWF) within the Project P 22109-B17. The authors highly appreciate the help and support from the General Directorate of Mineral Research and Exploration (MTA, Turkey) and are thankful for the digging permission within the investigated area. Special thanks go to Yeşim Islamoğlu (MTA, Ankara) for organizing and guiding two field trips. The authors thank Leopold Krystyn and Andreas Gindl (both University of Vienna), Mathias Harzhauser and Franz Topka (both Natural History Museum Vienna) and Philipp Strauss (Austrian Oil Exploration Company OMV, Vienna), who provided material from previous field trips. Simon Schneider (CASP, Cambridge, United Kingdom) and Thomas Hofmann (Geological Survey of Austria, Vienna) are acknowledged for their support in collecting literature. We thank Simon Schneider (CASP, Cambridge, United Kingdom) for explanations of some details concerning the new established method. Photographs of ammonoid specimens were taken by Alice Schumacher (Natural History Museum Vienna). We kindly acknowledge Susan Kidwell (University of Chicago), Federico Olóriz (Universidad de Granada) as well as Jozef Michalík (Slovak Academy of Science) for their comments, which greatly improved the quality of this manuscript. We are grateful to Michael Wagreich (University Vienna, Vienna) for discussions and helpful comments. We, the authors, dedicate the paper to Eva Chorvátová (Bratislava) who passed away much too early in 2014. She supervised the first steps of our submission to Geologica Carpathica.

7.13. References

ADAMÍKOVA G., MICHALÍK J. and VAŠÍČEK Z. 1983. Composition and ecology of the "*Pseudothurmannia*-Fauna", Lower Barremian of the Krížna-Nappe in the Strážovské Vrchy Mts. *Geologica Carpathica,* **34/5**, 591–615.

AGUIRRE-URRETA M.B. and RAWSON P.F. 1998. The early Cretaceous (Valanginian) ammonite *Chacantuceras* gen. nov. – a link between the Neuquén and Austral basins. *Revista de la Asociación Geológica Argentina*, **53**, 354–364.

AGUIRRE-URRETA M.B. and RAWSON P.F. 1999. Lower Cretaceous ammonites from the Neuquén Basin, Argentina: Viluceras, a new Valanginian subgenus of *Olcostephanus*. *Cretaceous Research*, **20**, 343–357.

AIGNER T. 1982a. Calcareous tempestites: storm-dominated stratification in Upper Muschelkalk Limestones (Middle Trias, SW-Germany). *In*: EINSELE G. and SEILACHER A. (eds). Cyclic and event and stratification. Springer-Verlag, Berlin–Heidelberg, 181–198.

AIGNER T. 1982b. Proximiality trends in modern storm sands from the Helgoland Bight (North Sea) and their implications for basin analysis. *Senckenbergiana maritima*, **14**, 183–215.

AIGNER T. 1985: Storms depositional systems. *In*: FRIEDMAN G.M., NEUGEBAUER H.J. and SEILACHER A. (eds). *Lecture notes in Earth Sciences*, **3**, Springer-Verlag, Berlin–Heidelberg, 1–174.

ALLISON P.A. and BRIGGS D.E.G. (eds) 1991. Taphonomy. Releasing the data locked in the fossil record. *Topics in Geobiology*, **9**, Plenum Press, New York–London, 1–560.

ANDREWS T. and ROBERTSON A. 2002. The Beysehir-Hoyran-Hadim nappes: genesis and emplacement of Mesozoic marginal and oceanic units of the northern Neotethys in southern Turkey. *Journal of the Geological Society, London*, **159**, 529–543.

BOTTJER D.J., CAMPBELL K.A., SCHUBERT J.K. and DROSER M.L. 1995. Palaeoecological models, non-uniformitarism, and tracking the changing ecology of the past. *In*: BOSENCE D.W.J. and ALLISON P.A. (eds). Marine palaeoenvironmental analysis from fossils. *Geological Society of London, Special Publications*, **83**, 7–26.

BOUMA A.H., BERRYHILL H.L., KNEBEL H.J. and BRENNER R.L. 1982. Continental shelf. *In*: SCHOLLE P.A. and SPEARING D. (eds). Sandstone depositional environments. *American Association of Petroleum Geologists, Memoir*, **31**, 281–327.

BRANDNER R., HORACEK M. and KEIM L. 2012. Permian-Triassic boundary and Lower Triassic in the Dolomites, southern Alps (Italy). *Journal of Alpine Geology*, **54**, 379–404.

BRETT C.E. and BAIRD G.C. 1986. Comparative taphonomy: a key to palaeoenvironmental interpretation based on fossil preservation. *Palaios,* **1**, 207–227.

BRETT C.E. and SEILACHER A. 1991. Fossil Lagerstätten: a taphonomic consequence of event sedimentation. *In*: EINSELE G., RICKEN W. and SEILACHER A. (eds). Cycles and events in stratigraphy. Springer-Verlag, Berlin–Heidelberg, 283–297.

BROWN A.A. and LOUCKS R.G. 1993. Toe of slope. *In*: BEBOUT D.G. and KERANS C. (eds). Guide to the Permian reef geology trail, McKittrick Canyon, Guadalupe Mountains National Park, West Texas. *The University of Texas at Austin, Bureau of Economic Geology Guidebook*, **26**, 5–13.

CARRILLAT A. and MARTINI R. 2009. Palaeoenvironmental reconstruction of the Mufara Formation (Upper Triassic, Sicily): High resolution sedimentology, biostratigraphy and sea-level changes. *Palaeogeography, Palaeoclimatology, Palaeoecology*, **283**, 60–76.

CHUANMAO L., FRIEDMAN G.M. and ZHAOCHANG Z. 1993: Carbonate storm deposits (tempestites) of Middle to Upper Carnian age in the Helan Mountains, northwest China. *Carbonates and Evaporites*, **8**, 181–190.

COOK H.E., FIELD M.E. and GARDNER J.V. 1982. Characteristics of sediments on modern and ancient continental slopes. *In*: SCHOLLE P.A. and SPEARING D. (eds). Sandstone depositional environments. *American Association of Petroleum Geologists, Memoir*, **31**, 329–364.

ČRNE A.E., ŠMUC A. and SKABERNE D. 2007. Jurassic neptunian dikes at Mt Mangart (Julian Alps, NW Slovenia). *Facies*, **53**, 249–265.

DERCOURT J., RICOU L.E. and VRIELYNCK B. 1993. Atlas Tethys palaeoenvironmental maps. Gaulthier-Villars, Paris, 1–307.

DERCOURT J., GAETANI M., VRIELYNCK B., BARRIER E., BIJU-DUVAL B., BRUNET M.F., CADET J.P., CRASQUIN S. and SANDULESCU M. (eds) 2000. Atlas Peri-Tethys-Palaeogeographical maps. Commission of the Geological Map of the World, Paris, 1–269.

DEYNOUX M., ÇINAR A., MONOD O., KARABIYIKOGLU M. and MANATSCHAL TUZCU S. 2005. Facies architecture and depositional evolution of alluvial fan to fan-delta complexes in the tectonically active Miocene Köprüçayc Basin, Isparta Angle, Turkey. *Sedimentary Geology*, **173**, 315–343.

DUMONT J.F. 1976. Etudes géologiques dans les Taurides Occidentales: Les formations paléozoiques et mésozoiques de la coupole de Karacahisar (Province d'Isparta, Turquie). Dissertation, University of South Paris, 213.

DUMONT J. F. and KEREY E. 1975. The Kirkavak Fault. *Bulletin of the Geological Society of Turkey*, **18**, 59–62.

EBERLI G.P. 1991. Calcareous turbidites and their relationship to sealevel fluctuations and tectonism. *In*: EINSELE G., RICKEN W. and SEILACHER A. (eds). Cycles and events in stratigraphy. Springer-Verlag, Berlin–Heidelberg, 341–359.

EINSELE G. P. 1991. Submarine mass flow deposits and turbidites. *In*: EINSELE G., RICKEN W. and SEILACHER A. (eds). Cycles and events in stratigraphy. Springer-Verlag, Berlin–Heidelberg, 313–339.

EINSELE G. and SEILACHER A. (eds) 1982. Cyclic and event stratification. Springer-Verlag, Berlin–Heidelberg, 1–536.

EINSELE G. and SEILACHER A. 1991. Distinction of tempestites and turbidites. *In*: EINSELE G., RICKEN W. and SEILACHER A. (eds). Cycles and events in stratigraphy. Springer-Verlag, Berlin–Heidelberg, 377–382.

EINSELE G., RICKEN W. and SEILACHER A. (eds) 1991a. Cycles and events in stratigraphy. Springer-Verlag, Berlin–Heidelberg, 1–955.

EINSELE G., RICKEN W. and SEILACHER A. 1991b. Cycles and events in stratigraphy – Basic concepts and terms. *In*: EINSELE G., RICKEN W. and SEILACHER A. (eds). Cycles and events in stratigraphy. Springer-Verlag, Berlin–Heidelberg, 1–19.

FERNÁNDEZ-LÓPEZ S.R. 2007. Ammonoid taphonomy, palaeoenvironments and sequence stratigraphy at the Bajocian/Bathonian boundary on the Bas Auran area (Subalpine Vasin, south-eastern France). *Lethaia*, **40**, 377–391.

FERNÁNDEZ-LÓPEZ S. and FERNÁNDEZ-JALVO Y. 2002. The limit between biostratinomy and fossil diagenesis. *In*: DE RENZI M., PARDO ALONSO M.V., BELINCHÓN M., PEÑALVER E., MONTOYA P. and MÁRQUEZ-ALIAGA A. (eds). Current topics on taphonomy and fossilization. International Conference on Taphonomy and Fossilization, Valencia, 27–36.

FERNÁNDEZ-LÓPEZ S.R., HENRIQUES M.H. and DUARTE L.V. 2002. Taphonomy of Ammonite Condensed Associations – Jurassic examples from Carbonate Platforms of Iberia. *Abhandlungen der Geologischen Bundesanstalt*, **57**, 423–430.

FLÜGEL E. 1978. Mikrofazielle Untersuchungsmethoden von Kalken. Springer-Verlag, Berlin–Heidelberg–New York, 1–454.

FLÜGEL E. 2004. Microfacies of carbonate rocks. Analysis, interpretation and application. Springer-Verlag, Berlin–Heidelberg, 1–976.

FUTTERER E. 1982. Experiments on the distinction of wave and current influenced shell accumulation. *In*: EINSELE G. and SEILACHER A. (eds). Cyclic and event stratification. Springer-Verlag, Berlin–Heidelberg, 175–179.

FÜRSICH F.T. and PANDEY D.K. 1999. Genesis and environmental significance of Upper Cretaceous shell concentrations from the Cauvery Basin, southern India. *Palaeogeography, Palaeoclimatology, Palaeoecology*, **145**, 119–139.

GALLET Y., KRYSTYN L., MARCOUX J. and BESSE J. 2007. New constraints on the end-Triassic (Upper Norian–Rhaetian) magnetostratigraphy. *Earth and Planetary Science Letters*, **255**, 458–470.

GINDL A. 2000. Paläoökologie triassischer Ammonitenfaunen des Taurusgebirges (Türkei). Unpublished Diploma Thesis, University of Vienna, 1–80.

GOLDRING R. 1991. Fossils in the field. Information potential and analysis. Longman Scientific & Technical, pp. 218.

GOLEBIOWSKI R. 1991. Becken und Riffe der alpinen Obetrias. Lithostratigraphie und Biofazies der Kössener Formation. *In*: NAGEL D. and RABEDER G. (eds). Exkursionen im Jungpaläozoikum und Mesozoikum. Österreichische Paläontologische Gesellschaft, Wien, 79–119.

GOLONKA J. 2004. Plate tectonic evolution of the southern margin of Eurasia in the Mesozoic and Cenozoic. *Tectonophysics*, **381**, 235–273.

GÖNCÜOĞLU C.M., SAYIT K. and TEKIN U.K. 2010. Oceanization of the northern Neotethys: geochemical evidence from ophiolitic mélange basalts within the Izmir-Ankara suture belt, NW Turkey. *Lithos*, **116**, 175–187.

GRADSTEIN F.M., OGG J.G., SCHMITZ M.D. and OGG G.M. 2012. The Geologic Time Scale 2012. Volume 2. Elsevier, Boston, 437–1144.

GUTNIC M., MONOD O., POISSON A. and DUMONT J.F. 1979. Géologie des Taurides Occidentales (Turquie). *Mémoires de la Société géologique de France*, **137**, 1–112.

HIPS K. 1998. Lower Triassic storm-dominated ramp sequence in northern Hungary: an example of evolution from homoclinal through distally steepened ramp to Middle Triassic flat-topped platform. *In*: WRIGHT V.P. and BURCHETTE T.P. (eds). Carbonate ramps. *Geological Society London, Special Publications*, **149**, 315–338.

HLADIL J., ČEJCHAN P., GABAŠOVÁ A., TÁBORSKÝ Z. and HLADÍKOVÁ J. 1996. Sedimentology and orientation of tentaculite shells in turbidite lime mudstone to packstone: Lower Devonian, Barrandian, Bohemia. *Journal of Sedimentary Research*, **66**, 888–899.

HOEDEMAEKER P.J. 1994. Ammonite distribution around the Hauterivian-Barremian boundary along the Río Argos (Caravaca, SE Spain). *Géologie Alpine*, **20**, 219–277.

HORNUNG T. 2008. The Carnian Crisis in the Tethys Realm. Verlag Dr. Müller, Saarbrücken, 1–235.

HOWELL D.G. and NORMARK W.R. 1982. Sedimentology of submarine fans. *In*: SCHOLLE P.A. and SPEARING D. (eds). Sandstone depositional environments. *American Association of Petroleum Geologists, Memoir,* **31**, 365–404.

KAWAKAMI G. and KAWAMURA M. 2002. Sediment flow and deformation (SFD) layers: evidence for intrastratal flow in laminated muddy sediments of the Triassic Osawa Formation, northeast Japan. *Journal of Sedimentary Research*, **72**, 171–181.

KEMPER E., RAWSON P.F. and THIEULOY J.P. 1981. Ammonites of Tethyan ancestry in the early lower Cretaceous of northwest Europe. *Palaeontology*, **24/2**, 251–311.

KIDWELL S.M. 1986. Models for fossil concentrations: paleobiologic implications. *Paleobiology*, **12**, 6–24.

KIDWELL S.M. 1988. Taphonomic comparison of passive and active continental margins: Neogene shell beds of the Atlantic coastal plain and northern Gulf of California. *Palaeogeography, Palaeoclimatology, Palaeoecology*, **63**, 201–224.

KIDWELL S.M. 1991a. The stratigraphy of shell concentrations. *In*: ALLISON P.A. and BRIGGS D.E.G. (eds). Taphonomy: Releasing the data locked in the fossil record. *Topics in Geobiology*, **9**, Plenum Press, New York, 211–290.

KIDWELL S.M. 1991b. Taphonomic feedback (Live/ dead interactions) in the genesis of bioclastic beds: Keys to reconstruction sedimentary dynamics. *In*: EINSELE G., RICKEN W. and SEILACHER A. (eds). Cycles and events in stratigraphy. Springer-Verlag, Berlin–Heidelberg, 268–282.

KIDWELL S.M. 1993a. Patterns of time-averaging in shallow marine fossil assemblages. *In*: KIDWELL S.M. and BEHRENSMEYER A.K. (eds). Taphonomic approaches to time resolution in fossil assemblage. *Paleontological Society Short Course,* **6**, 275–300.

KIDWELL S.M. 1993b. Taphonomic expressions of sedimentary hiatus: field observations on bioclastic concentrations and sequence anatomy in low, moderate and high subsidence settings. *Geologische Rundschau*, **82**, 189–202.

KIDWELL S.M. and BOSENCE D.W.J. 1991. Taphonomy and time-averaging of marine shelly faunas. *In*: Allison P.A. and Briggs D.E.G. (eds). Taphonomy: Releasing the data locked in the fossil record. *Topics in Geobiology*, **9**, Plenum Press, New York, 115–209.

KIDWELL S.M., FÜRSICH F.T. and AIGNER T. 1986. Conceptual framework for the analysis and classification of fossil concentrations. *Palaios*, **1**, 228–238.

KREISA R.D. and BAMBACH R.K. 1982. The role of storm processes in generating shell beds in Palaeozoic shelf environments. *In*: EINSELE G. and SEILACHER A. (eds). Cyclic and event stratification. Springer-Verlag, Berlin–Heidelberg, 200–207.

KRYSTYN L., GALLET Y., BESSE J. and MARCOUX J. 2002. Integrated Upper Carnian to Lower Norian biochronology and implications for the Upper Triassic magnetic polarity time scale. *Earth and Planetary Science Letters*, **203**, 343–351.

LOWE D.R. 1982. Sediment gravity flows. II. Depositional models with special reference to the deposits of high-density turbidity currents. *Journal of Sedimentary Petrology*, **52**, 279–297.

LUKENEDER A. 2001. Palaeoecological and palaeooceanographical significance of two ammonite mass-occurrences in the Alpine Lower Cretaceous. PhD. Thesis, University of Vienna, 1–316.

LUKENEDER A. 2003a. The *Karsteniceras* Level: Dysoxic ammonoid beds within the Early Cretaceous (Barremian, Northern Calcareous Alps, Austria). *Facies,* **49**, 87–100.

LUKENEDER A. 2003b. Ammonoid stratigraphy of Lower Cretaceous successions within the Vienna Woods (Kaltenleutgeben section, Lunz Nappe, Northern Calcareous Alps, Lower Austria). *In*: PILLER W.E. (ed.). *Stratigraphia Austriaca, Schriftenreihe der Erdwissenschaftlichen Kommissionen der Österreichischen Akademie der Wissenschaften*, **16**, 165–191.

LUKENEDER A. 2004a. Late Valanginian ammonoids: Mediterranean and Boreal elements – implications on sea-level controlled migration (Ebenforst Syncline; Northern Calcareous Alps; Upper Austria). *Austrian Journal of Earth Sciences*, **95/96**, 46–59.

LUKENEDER A. 2004b. The *Olcostephanus* Level: An Upper Valanginian ammonoid mass-occurrence (Lower Cretaceous, Northern Calcareous Alps, Austria). *Acta Geologica Polonica*, **54**, 1, 23–33.

LUKENEDER A. (in print) 2014: Ammonoid habitats and life history. *In*: KLUG C. and KORN D. (eds). *Cephalopods present and past*, **9**, Ammonoid paleobiology. Springer, Dordrecht.[3]

LUKENEDER S. and LUKENEDER A. 2014. A new Ammonoid Fauna from the Carnian (Upper Triassic) Kasımlar Formation of the Taurus Mountains (Anatolia, Turkey). *Palaeontology*, **57/2**, 357–396. Open Access. Doi: 10.1111/pala.12070

LUKENEDER S., LUKENEDER A. and WEBER G.W. 2014. Computed reconstruction of spatial ammonoid-shell orientation captured from digitized grinding and landmark data. *Computers & Geosciences*, **64**, 104–114.

LUKENEDER S., LUKENEDER A., HARZHAUSER M., ISLAMOGLU Y., KRYSTYN L. and LEIN R. 2012. A delayed carbonate factory breakdown during the Tethyan-wide Carnian pluvial episode along the Cimmerian terranes (Taurus, Turkey). *Facies*, **58**, 279–296.

MAEDA H. 1999. Did ammonoid carcasses surface or sink? *Memoirs of the Geological Society of Japan*, **54**, 131–140.

MAEDA H. and SEILACHER A. 1996. Ammonoid taphonomy. *In*: LANDMAN N.H., TANABE K. and DAVIS R.A. (eds). Ammonoid paleobiology. *Topics in Geobiology*, **13**, Plenum Press, New York, 543–578.

MAEDA H. and SHIGETA Y. 2009. Ammonoid mode of occurrence. *In*: SHIGETA Y., ZAKHAROV Y.D., MAEDA H. and POPOV A.M. (eds). The Lower Triassic system in the Abrek Bay area, South Primorye, Russia. *National Museum of Nature and Science Monographs*, **38**, 36–38.

MANFRIN S., MIETTO P. and PRETO N. 2005. Ammonoid biostratigraphy of the Middle Triassic Latemar platform (Dolomites, Italy) and its correlation with Nevada and Canada. *Geobios*, **38**, 477–504.

MARTIN R.E. 1999. Taphonomy. A process approach. *In*: BRIGGS D.E.G., DODSON P., MACFADDEN B.J., SEPKOSKI J.J. and SPICER R.A. (eds). *Cambridge paleobiology*, **4**, Cambridge University Press, 1–508.

---

3. Since the paper has been published, this reference has changed and its updated form is: LUKENEDER A. 2015. Ammonoid habitats and life history. *In:* KLUG C., KORN D., KRUTA I., DE BAETS K., MAPES R.H. (eds). Ammonoid Paleobiology: From anatomy to ecology. *Topics in Geobiology,* **43**, Springer, Dordrecht, 689–791.

MAYRHOFER S. and LUKENEDER A. (in prep). Taphonomy and palaeoecology of Carnian (Upper Triassic) ammonoid shell beds from the Taurus Mountain, South Turkey. Fossil ammonoid mass occurrence (*Kasimlarceltites krystyni*) as key to a Carnian environment (Taurus Mountains, Turkey). *Lethaia*.[4]

MCROBERTS C.A. 2010. Biochronology of Triassic bivalves. *In*: Lucas S.G. (ed.). The Triassic timescale. *Geological Society of London, Special Publication*, **334**, 201–219.

MELDAHL K.H. 1993. Geographic gradients in the formation of shell concentration: Plio-Pleistocene marine deposits, Gulf of California. *Palaeogeography, Palaeoclimatology, Palaeoecology*, **101**, 1–25.

MIDDLETON G.V. and HAMPTON M.A. 1973. Sediment gravity flows: mechanics of flow and deposition. *In*: MIDDLETON G.V. and BOUMA A.H. (eds). Turbidites and deep water sedimentation. Short course notes. Society of Economic Paleontologists and Mineralogists, Special Publication, Anaheim, 1–23.

MIDDLETON G.V. and HAMPTON M.A. 1976. Subaqueous sediment transport and deposition by sediment gravity flows. *In*: STANLEY D.J. and SWIFT D.J.P. (eds). Marine sediment transport and environmental management. Wiley, New York, 197–218.

MONOD O. 1977. Recherches géologiques dans le Taurus Occidental au sud de Beyşehir (Turquie). PhD. Thesis, University of South Paris, 1–442.

MONTIEL-BOEHRINGER A.Y., LEDESMA-VÁSQUEZ J. and AVILA-SERRANO G.E. 2011. Fossil beds, gravity flows, and sand waves during the Pliocene: Gulf of California. *Journal of Coastal Research*, ***27***, 549–554.

MULDER T. and ALEXANDER J. 2001. The physical character of subaqueous sedimentary density flows and their deposits. *Sedimentology*, **48**, 269–299.

MURPHY M.A. and SALVADOR A. (eds) 1999. International stratigraphic guide – An abridged version. *Episodes*, **22/4**, 255–271.

---

4. This reference has changed and its updated form is: MAYRHOFER S., LUKENEDER A. and KRYSTYN L. accepted 2016. Taphonomy and palaeoecology of Late Triassic (Carnian) ammonoid concentrations from the Taurus Mountains, Turkey. *Lethaia*.

MÜLLER A.H. 1963. Lehrbuch der Paläozoologie. 1. Allgemeine Grundlagen. C. Die Fossilisationslehre. Fischer, Jena, 17–134.

NICHOLS G. 2009. Sedimentology and stratigraphy. Wiley-Blackwell, Pondicherry, 419.

NIECHWEDOWICZ M. and TRAMMER J. 2007. Hydrodynamically controlled anagenetic evolution of Famenian goniatites from Poland. *Acta Palaeontologica Polonica*, **52**, 63–75.

NOE-NYGAARD N., SURLYK F. and PIASECKI S. 1987. Bivalve mass mortality caused by toxic dinoflagellate blooms in a Berriasian–Valanginian lagoon, Bornholm, Denmark. *Palaios*, **2**, 263–273.

NORRIS R.D. 1986. Taphonomic gradients in shelf fossil assemblages: Pliocene Purisma Formation, California. *Palaios*, **1**, 256–270.

OLIVERO E.B. 2007. Taphonomy of ammonites from the Santonian–Lower Campanian Santa Marta Formation, Antarctica: Sedimentological controls on vertically embedded ammonites. *Palaios*, **22**, 586–597.

OLÓRIZ F. 2000. Time averaging and long term palaeoecology in macroinvertebrate fossil assemblages with ammonites (Upper Jurassic). *Revue de Paléobiology, Special Volume*, **8**, 123–140.

OLÓRIZ F. and VILLASEÑOR A.B. 2010. Ammonite biogeography: From descriptive to dynamic, ecological interpretations. *In*: TANABE K., SHIGETA Y., SASAKI T. and HIRANO H. (eds). Cephalopods – Present and past. Tokai University Press, Tokyo, 253–265.

ÖZGÜL N. and ARPAT E. 1973. Structural units of Taurus orogenic belt and their continuation in the neighbouring regions. *Bulletin of the Geological Society of Greece*, **XLIII. 10**, 156–164.

PÉREZ-LOPÉZ A. and PÉREZ-VALERA F. 2012. Tempestite facies models for the epicontinental Triassic carbonates of the Betic Cordillera (southern Spain). *Sedimentology*, **59**, 646–678.

POISSON A. 1977. Recherches géologiques dans les Taurides occidentals (Turquie). PhD. Thesis, University of South Paris, 1–759.

POTTER P.E. and PETTIJOHN F.J. 1977. Paleocurrents and basin analysis. 2nd corrected and updated edition. Springer–Verlag, Berlin–Göttingen–Heidelberg, 1–425.

POTTER P.E., MAYNARD J.B. and DEPETRIS P.J. 2005. Mud & mudstones. Springer, Berlin–Heidelberg, 1–297.

RADLEY J.D. and BARKER M.J. 1998. Palaeoenvironmental analysis of shell beds in the Waelden Group (Lower Cretaceous) of the Isle of Wight, southern England: an initial account. *Cretaceous Research*, **19**, 489–504.

ROBERTSON A.H.F. 1993. Mesozoic-Tertiary sedimentary and tectonic evolution of Neotethyan carbonate platforms, margins and small ocean basins in the Antalya Complex, southwest Turkey. *International Association of Sedimentologists, Special Publications,* **20**, 415–465.

ROBERTSON A.H.F. 2000. Mesozoic-Tertiary tectonic-sedimentary evolution of a south Tethyan Oceanic Basin and its margins in southern Turkey. *Geological Society of London, Special Publication*, **173**, 97–138.

ROBERTSON A.H.F., POISSON A. and AKINCI Ö. 2003. Developments in research concerning Mesozoic-Tertiary Tethys and neotectonics in the Isparta Angle, SW Turkey. *Geological Journal*, **38**, 195–234.

SALVADOR A. 1994. International stratigraphic guide (A guide to stratigraphic classification, terminology and procedure). 2^{nd} ed., XIX + 214 International Union of Geological Science and Geological Society of America, pp. 214.

SCOTESE C.R. 1998. Quicktime computer animations. PALEOMAP Project, Department of Geology. University of Texas at Arlington, Arlington.

SCOTESE C.R. 2001. Paleomap Project. http://www.scotese.com/ (July 2001).

SCOTESE C.R., GAHAGAN L.M. and LARSON R.L. 1989. Plate tectonic reconstructions of the Cretaceous and Cenozoic ocean basins. *In*: SCOTESE C.R. and SAGER W.W. (eds). Mesozoic and Cenozoic plate reconstructions. Elsevier, Amsterdam, 27–48.

SEILACHER A. 1968. Sedimentationsprozesse in Ammoniten-Gehäusen. *Akademie der Wissenschaften und der Literatur, Abhandlungen der Mathematisch-Naturwissenschaftlichen Klasse*, **9**, 191–203.

SEILACHER A. and AIGNER T. 1991. Storm deposition at the bed, facies, and basin scale: the geological perspective. *In*: EINSELE G., RICKEN W. and SEILACHER A. (eds). Cycles and events in stratigraphy. Springer-Verlag, Berlin–Heidelberg, 249–267.

SEPKOSKI J.J. JR., BAMBACH R.K. and DROSER M.L. 1991. Secular changes in Phanerozoic event bedding and the biological overprint. *In*: EINSELE G., RICKEN W. and SEILACHER A. (eds). Cycles and events in stratigraphy. Springer-Verlag, Berlin–Heidelberg, 298–312.

SEPM STRATA (2014). Deepwater processes & sediment. SEPM stratigraphy. Web – http://sepmstrata.org (accessed 11 January 2014).

SOJA C.M., GOBETZ K.E., THIBEAU J., ZAVALA E. and WHITE B. 1996. Taphonomy and paleobiological implications of Middle Devonian (Eifelian) nautiloid concentrations, Alaska. *Palaios*, **11**, 422–436.

SPEYER S.E. and BRETT C.E. 1991. Taphofacies controls. Backround and episodic processes in fossil assemblage preservation. *In*: ALLISON P.A. and BRIGGS D.E.G. (eds). Taphonomy. Releasing the data locked in the fossil record. *Topics in Geobiology,* **9**, Plenum Press, New York & London, 501–545.

STAMPFLI G.M. and BOREL G.D. 2002. A plate tectonic model for the Paleozoic and Mesozoic constrained by dynamic plate boundaries and restored synthetic oceanic isochrons. *Earth and Planetary Science Letters*, **196**, 17–33.

STAMPFLI G.M., BOREL G.D., MARCHANT R. and MOSAR J. 2002. Western Alps geological constraints on western Tethyan reconstructions. *Journal of the Virtual Explorer*, **8**, 77–106.

STEININGER F.F. and PILLER W.E. 1999. Empfehlungen (Richtlinien) zur Handhabung der stratigraphischen Nomenklatur. *Courier Forschungsinstitut Senckenberg*, **209**, 1–19.

STORMS J.E.A. 2001. Simulating event deposition: effects of storms on the shallow marine stratigraphic record. IAMG extended abstract, September 2001, Cancun, 1–19.

STOW D.A.V. and MAYALL M. 2000. Deep-water sedimentary systems: New models for the 21st century. *Marine and Petroleum Geology*, **17**, 125–135.

ŞENEL M. 1997. 1:250,000 scaled Turkey Geological map, Isparta section. 4. [Türkiye Jeoloji Haritalari. Nr. 4. Isparta Paftasi.] Mineral Research and Exploration General Directorate, Geological Department, Ankara, 1–47 (in Turkish).

ŞENGÖR A.M.C. and YLLMAZ Y. 1981. Tethyan evolution of Turkey: A plate tectonic approach. *Tectonophysics*, **75**, 181–241.

ŞENGÖR A.M.C., YLLMAZ Y. and SUNGURLU O. 1984. Tectonics of the Mediterranean Cimmerids: Nature and evolution of the western termination of Paleo-Tethys. *Geological Society of London, Special Publication*, **17**, 77–112.

TEKIN U.K. and GÖNCÜOĞLU C. 2007. Discovery of the oldest (Upper Ladinian to Middle Carnian) radiolarian assemblages from the Bornova Flysch Zone in Western Turkey: implications for the evolution of the Neotethyan Izmir–Ankara Ocean. *Ofioliti*, **32**, 131–150.

TEKIN U.K., GÖNCÜOĞLU C. and TURHAN N. 2002. First evidence of Late Carnian radiolarians from the Izmir-Ankara suture complex, central Sakarya, Turkey: implications for the opening age of the Izmir-Ankara branch of Neo-Tethys. *Geobios*, **35**, 127–135.

TUCKER M.E. and WRIGHT V.P. 1990. Carbonate sedimentology. Blackwell Scientific Publications, Oxford, London, Edinburgh, 1–482.

WESTERMANN G.E.G. 1996. Ammonoid life and habitat. *In*: LANDMAN N.H., TANABE K. and DAVIS R.A. (eds). Ammonoid paleobiology. *Topics in Geobiology*, **13**, Plenum Press, New York 857, 607–707.

CHAPTER VIII,

SYNOPSIS – STRATIGRAPHIC AND PALAEOENVIRONMENTAL CONCLUSIONS ABOUT THE CARNIAN SEDIMENTS AROUND AŞAĞIYAYLABEL AND KARAPINAR (TAURUS MOUNTAINS, TURKEY) IN A TETHYAN WIDE CONTEXT

In this thesis, selected Carnian sections (Aşağiyaylabel I–IV, Karapinar I–IV) from the area of Aşağiyaylabel (Taurus Mountains, Turkey) were investigated by means of facies analysis (Chapter II), geophysical measurements (Chapter III), faunistic composition (Chapter IV), as well as by means of orientational and taphonomical fossil analyses (Chapter V–VII). The overall goal was to interpret the environmental setting of this area during the Carnian time in comparison with time-equivalent deposits of the western Tethyan realm.

Lower- to Upper Carnian sediments, deposited within the Tethyan realm, represent a window to a time at which a major climatic crisis occurred. This crisis, which is generally known as the Carnian Crisis, is reflected by a sedimentary change from carbonate- to argillaceous-dominated deposits, in combination with a major decrease in marine and epicontinental faunas (Hallam 1996, Hornung 2008). Although the most effected group were marine shallow-water inhabitants, the effect could be also detected in terrestrial groups as for example tetrapods (Hallam 1996). The reason for this climatic crisis is still under discussion. Therefore a series of different names were chosen by different authors for one and the same "event" respectively "episode". Schlager and Schöllnberger (1974) originally introduced the "Reingraben turning point", whereas Simms and Ruffell (1989) created the term "Carnian Pluvial Episode (CPE). Hornung and Brandner (2005) named it the "Middle Carnian Pluvial Event", whilst Kozur and Bachmann (2010) described it as the "Middle Carnian Wet Intermezzo". Due to the fact that most studies point to a longer multi-phased process, instead to a single event, the term "Carnian Pluvial Episode" was preferred within this thesis.

The real mechanisms behind this Early Carnian climatic turnover are still under discussion. An enhanced humidification due to global warming (induced by the rifting of Pangea), combined with increased freshwater runoff, was originally supposed (Simms and Ruffell 1989; Hornung *et al*. 2007a, b). Later on, Dal Corso *et al.* (2012) linked this event with the eruption of the Wrangellia flood basalt province. The humidification was most probably triggered by monsoonal phases and furthermore led to a nutrification of shelf-areas in the

Tethyan Ocean (Hornung *et al.* 2006, 2007a, b; Hornung 2008). A further result of the multistratigraphic studies argued that this climatic turnover occurred synchronously throughout the whole Tethys within Early Carnian time (Hornung 2008).

8.1. A delayed climatic facies change in the Taurus Mountains of Turkey

A timely comparable facies change from a carbonate platform through marly dominated limestones to shaley sediments has been investigated around the area of Aşağiyaylabel (Chapter II), about 70 km southeast of the town Isparta. Whilst the Kartoz Formation represents a shallow water carbonate platform, the Kasımlar Formation starts at its base (Carbonate member unit A) with well bedded dark limestone-layers (pelagic wackestones). Although the carbonate platform, which is restricted to the Kartoz Formation, was replaced by deeper water limestones at the base of the Kasımlar Formation, the sedimentation remains carbonatic throughout the late Early Carnian time (Carbonate member unit A–C) and starts to become terrigenous only from the base of the Marlstone member (= Upper Carnian) onward. As the boundary between the Carbonate- and the Marlstone member corresponds to the Julian / Tuvalian resp. the Lower- / Upper Carnian boundary, the interpreted climatic turnover in the area of Aşağiyaylabel took place about 2 Ma later than in the western Tethys.

Other classical Early Carnian Tethyan terrigenous sequences, such as the Alpine Reingraben Shales (Hornung and Brandner 2005), the *Halobia Shales* of northern Turkey (Yurttas-Özdemir 1973) or the Rama Formation of the Indian Himalaya (Hornung *et al*. 2006, 2007 a, b) are all together older than the Kasımlar Formation of Aşağiyaylabel. Only in the Lagonegro Basin (southern Apennines, Italy), a succession of green shales and radiolarites, represents a time equivalent turnover to that of the Taurus Mountains (Rigo *et al.* 2007). In contrast to Rigo *et al.* (2007), who set the later turnover in the Lagonegro Basin in context with a shallowing of the carbonate compensation depth, we conclude that the higher palaeolatitudes of the Taurus Mountains (about 7° N) and the Lagonegro Basin (8–9° N) might have been the reason for a diachronic turnover to the South- and Austroalpine (17° N) and to the Himalaya (about 30 °S). Nevertheless, it might have been a combination of different factors, why the turnover occurred 2 Ma later in equatorial palaeolatitudes.

8.2. Facies change supported by geophysical measurements (MS- and radiometry data)

The described lithological change from the Carbonate- to the Marlstone member is additionally supported by the first geophysical measurements (Magnetic Susceptibility- and radiometry data) taken from Lower- to Upper Carnian carbonate sequences (Chapter III). They reflect a distinct MS- and radiometry increase at the Lower- to Upper Carnian boundary at the sections AS I. A comparable increase in MS- and radiometric data could be investigated at the section Karapinar IV, at which the boundary from well bedded dark grey limestones to marlstones could be observed as well (Chapter III). But not only the Julian / Tuvalian boundary could be found again within the surroundings of Aşağiyaylabel. Equivalent shallow water limestones (Kartoz Fm., AS I) and well bedded *Kasimlarceltites* beds (Kasımlar Fm., Carbonate member Unit A, AS I) could be detected at the surrounding sequences AS IV and KA I–II. These sediments are not only equivalent concerning their lithology resp. facies, but also concerning their geophysical values. Within all sections, the values start with low MS rates at the shallow-water carbonates (-11–71 x 10^{-6} SI; Kartoz Fm.), become higher at the well bedded *Kasimlarceltites* limestones (3–108 x 10^{-6} SI; Carbonate member, Kasımlar Fm.) and show their highest values at the calcareous marls and marlstones (62–458 x 10^{-6} SI; Marlstone member, Kasımlar Fm.). This fits well to the additionally investigated decrease of the $CaCo_3$ content from the Carbonate to the Marlstone member (Chapter III).

The abrupt increase of the MS- but also of the radiometry measurements (Chapter III) at the Julian / Tuvalian boundary perfectly reflect the already estimated increased influx of detrital materials resp. siliciclastic minerals into the system, due to the enhanced river run-off, triggered by the rising humidification (Tollmann 1976; Aigner and Bachmann 1992; Hornung and Brandner 2005). The MS- values of the carbonate platforms or shallow-water limestones are very low to negative. This is what is expected for such sediments high in diamagnetic minerals as for example calcite (Algeo *et al.* 2007a, b). The trend of such geophysical hand held instruments can be used for stratigraphic correlation, were no macrofossils are found, as it is the case for the section Karapinar IV. Geophysical measurements can therefore be used, with caution, as additional preliminary tool for correlation of characteristic features in the field, as for example sequence boundaries or marker horizons.

8.3. The Lower- to Upper Carnian ammonoid fauna at Aşağiyaylabel

The climatic turnover at Aşağiyaylabel coincides with an extinction event at the Julian / Tuvalian boundary, which effected a series of pelagic ammonoid and conodont taxa (Krystyn 1983, 1991; Rigo *et al.* 2007; Hornung *et al.* 2007 a, b). The stratigraphic correlation of the sediments at Aşağiyaylabel was done by ammonoid biostratigraphy. The characteristic faunal change, which is Tethyan wide detected at the Julian (Lower Carnian) / Tuvalian (Upper Carnian) boundary could additionally be proven at the section AS I. While the Carbonate member represents ammonoids corresponding to the *Austrotrachyceras austriacum* Zone, and therefore represents Julian 2, the Marlstone member mostly yields ammonoids representing the *Tropites dilleri* Zone which corresponds with Tuvalian I. Some characteristic Lower Carnian taxa found within the Carbonate member are two species of *Neoprotrachyceras (N. attila* and *N. baconimum)* as well as *Sirenites senticosus. Neoprotrachyceras* belongs to the Trachyceratinae, which flourished Tethyan wide during the Early Carnian but were mostly replaced within the Late Carnian by the Tropitidae. The Tropitidae are represented within the Marlstone member by the species *Paratropites hoetzendorfii*. Furthermore, the occurrence of *Spirogmoceras* cf. *shastense* indicate a Tuvalian 1 age for the Marlstone member. Consequently the Julian / Tuvalian boundary is biostratigraphically proven by the occurrence of *Anasirenites crassicrenulatus* immediately below and *Sp.* cf. *shastense* above the boundary.

Section AS I represents one of the rare opportunities for the investigation of the Lower- to Upper Carnian ammonoid fauna. Tethyan wide, most sections are dated by conodont biostratigraphy (e.g. Lagonegro Basin, Rigo *et al.* 2007). Those rare sections, which comprises Julian to Tuvalian ammonoid faunas are composite stratigraphic sections (Breda *et al.* 2009) or condensed horizons, as for example the well preserved ammonoids of the type localities within the Northern Calcareous Alps.

The deep-water inhabitant *Proarcestes* sp., which is found at Aşağiyaylabel I from the Marlstone member onward, proves the general drowning of this section, which was already shown by the facies analysis (Chapter II) and the geophysical data (Chapter III). The newly described species from the Lower Carnian beds, *Kasimlarceltites krystyni, Klipsteinia disciformis* and *Anasirenites crassicrenulatus* reflect an isolated, but generally connective palaeoceanographic position of this area on the western end of the Cimmerian system. A comparison of the ammonoid fauna from Aşağiyaylabel with European, Asian and American faunas reflects a Mediterranean-Himalayan-Andean ammonoid assemblage, with the exception of *Spirogmoceras* cf. *shastense*, which shows a North American-Andean faunal affinity.

8.4. The *Kasimlarceltites* mass occurrence used as proxy for the environmental conditions during Early Carnian Time

The occurrence of the newly described genus and species *Kasimlarceltites krystyni* in a huge mass occurrence (Carbonate member unit A), which is widespread over an area of at least 5 km^2 makes it suitable for taphonomic investigations, which allow new insights into the environmental conditions at a time when the Carnian Pluvial Episode took place. The accumulation beds reflect only short event-layers within the *Kasimlarceltites* acme zone, as they alternate with limestone beds yielding isolated *Kasimlarceltites* remains. The scattered occurrence of *Kasimlarceltites krystyni* over 16.5 metres of rocks, shows that during several hundred thousand years *K. krystyni* must have lived within this area and therefore formed an autochthonous element within the background sediment (Chapter VII).

Calculating a number of ammonoids and gastropods for an estimated extension of at least 5 km^2 of the mass occurrence within the area around Aşağiyaylabel, nearly 775 million ammonoids and more than 50 million gastropods were extrapolated (Chapter VI). Comparing the mass occurrence with the nine types of skeletal concentrations defined by Fürsich and Oschmann (1993), a genesis by “storm waves” or “tempestites” would be assumed. According to Kidwell (1986) the *Kasimlarceltites* mass occurrence might have been deposited within a beach or an inner shelf environment, whereat an inner shelf environment would be more probable (Chapter VI).

Two-dimensional orientation measurements (Chapter VII) taken from different reference blocks from the *Kasimlarceltites* acme zone of the sections AS I–IV and KA I–III, as well as three-dimensional orientation analyses conducted from a reference block (150 x 45 x 140 mm) of section AS I bed 6 (Chapter V–VI) prove a general alignment of the ammonoids which hint to an at least slight transport, most probably caused by gravity flows resp. turbidity currents.

Whilst planispiral fossils (e.g. cephalopods) were so far only used with caution for orientation analyses (most studies uses only elongated fossils) and furthermore fossil orientations are conducted only by two-dimensional geographic orientation methods, the studies done within this thesis use “disk shaped” planispiral coiled ammonoid shells (Chapter V–VII) as well as additional three-dimensional orientation measurements (Chapter V–VI) for yielding more detailed information about the fossils orientation.

The orientation of more than 3.000 ammonoids and 200 gastropods, virtually segmented from the reference block of bed AS I/6 (Chapter V–VI), show a SSE/NNW resp. NNW/SSE alignment of the ammonoids (Chapter V–VI). The alignment of the ammonoids as well as the orientation of the geopetal structures observed at some ammonoid shells (Chapter VI) in combination with the intraclasts, which also bear ammonoids with geopetal structures, hint to a re-transport of the ammonoid shells after their primary deposition. The allochthonous character of this mass occurrence is furthermore indicated by the absence of any bioerosion or encrustation. We therefore assume that the ammonoids were primary accumulated due to short anoxic conditions or maybe due to tectonical methane-degassing periods and buried quickly. In a second step they were reworked, and again transported in combination with the unconsolidated surrounding material of their primary deposition. Regarding the fossil-Lagerstätten concept of Seilacher (1990), we interpret, that parts of the primary *Kasimlarceltites* mass accumulation deposits have been, in a second step, reworked and transported downslope to the basin where they now form a concentration-Lagerstätte sensu Seilacher.

Anyhow, the fact that less than 5% of the ammonoid shells are fragmented would much more lead to an autochthonous occurrence. This contradiction was explained by the relatively small (maximum diameter = 31mm) and therefore relatively robust shells and furthermore by a relatively slight and short transport. The missing buccal masses resp. preserved beak apparatus much more hint to an at least par- or allochthonous, but not to an autochthonous deposition. As most ammonoids within the accumulation layers are imbricated toward SSE within the stereographic analyses, we assume a slight but significant sediment movement toward NNW most probably triggered by gravity flows.

8.5. Summary

This thesis combines different kind of classical palaeontological methods (facies analysis, taxonomic and taphonomic investigations) in combination with modern techniques (geophysical methods, virtual segmentation methods and three-dimensional orientation analyses) carried out at an interval of sediments of the Taurus Mountains in Turkey with important information on the Lower- to Upper Carnian boundary.

The taxonomical investigation of the ammonoid fauna led to the description of one new genus and three new species from the Lower Carnian beds at Aşağiyaylabel. It further allowed the exact recognition of the Lower- to Upper Carnian boundary and the proof of a distinct ammonoid turnover at this boundary. The facies analysis in combination with the geophysical measurements demonstrates that the characteristic climatic turnover of the so called "Carnian Pluvial Event" is Tethyan-wide not time-correlative as previously assumed, but may vary within a time interval of 2 Ma. Although this enigma is not finally solved, it is an important fact that should be followed up within future studies dealing with this topic. This thesis furthermore shows that geophysical measurements, conducted from hand held instruments, just used with caution as trend data, can be used as preliminary tool for detecting sequence boundaries or marker horizons in the field and therefor can be used for correlating single logs. Last but not least, the newly established method of three-dimensional orientation analyses tested at the *Kasimlarceltites* mass occurrence, can easily be adapted for different kind of fossil mass occurrences in which the fossil orientation is of special interest.

Using facies analysis (Chapter II), geophysical measurements (Chapter III), faunistic composition (Chapter IV), as well as orientational and taphonomical fossil analyses (Chapter V–VII) in combination, the environmental setting of the area around Aşağiyaylabel during the Lower- to Upper Carnian time could be interpreted as follows:

The sediments generally reflect a late Triassic drowning succession with a facies change from carbonates (Lower Carnian) to argillaceous sediments (Upper Carnian). A sudden drowning of the Kartoz Formation (due to synsedimentary tectonics) during the Lower Carnian, led to a new basin geometry with a low energy bottom environment at which the deeper water limestones were deposited. Periodical anoxic conditions, probably in combination with tectonically induced methane degassing, led to the primary accumulation of *Kasimlarceltites*. In that aftermath, episodically deposition of the *Kasimlarceltites* event beds

(*Kasimlarceltites* mass occurrence) took place. The original habitat of *Kasimlarceltites krystyni* was interpreted as a shallow tropical peri-platform carbonate environment (Chapter VI).

Due to unstable conditions, the event beds of the *Kasimlarceltites* mass occurrence were formed most probably by gravity flows from the surrounding carbonate platforms. Reef-favourable conditions seems to have occurred until the end of the Early Carnian. At the base of the Late Carnian the actual major sedimentary change from a carbonatic to siliciclastic-dominated sedimentation, known as the Carnian Pluvial Episode occurred. This change is most probably due to the already postulated humidification of the climate during the Early Late Carnian time.

8.6. References

AIGNER T. and BACHMANN G.H. 1992. Sequence stratigraphic framework of the German Triassic. *Sedimentary Geology*, **80**, 115–135.

ALGEO T.J., ELLWOOD B., NGUYEN T.K.T., ROWE H. and MAYNARD J.B. 2007a. The Permian-Triassic boundary at Nhi Tao, Vietnam: Evidence for recurrent influx of sulfidic watermasses to a shallow-marine carbonate platform. *Palaeogeography, Palaeoclimatology, Palaeoecology*, **252**, 304–327.

ALGEO T.J., HANNIGAN R., ROWE H., BROOKFIELD M., BAUD A., KRYSTYN L. and ELLWOOD B.B. 2007b. Sequencing events across the Permian-Triassic boundary, Guryul Ravine (Kashmir, India). *Palaeogeography, Palaeoclimatology, Palaeoecology*, **252**, 328–346.

BREDA A., PRETO N., ROGHI G., FURIN S., MENEGUOLO R., RAGAZZI E., FEDELE P. and GIANOLLA F. 2009. The Carnian Pluvial Event in the Tofane area (Cortina d'Ampezzo, Dolomites, Italy). *Geo.Alp*, **6**, 80–115.

DAL CORSO J., MIETTO P., NEWTON R.J., PANCOST R.D., PRETO N., ROGHI G., WIGNALL P.B. 2012. Discovery of a major negative $d^{13}C$ spike in the Carnian (Late Triassic) linked to the eruption of Wrangellia flood basalts. *Geology,* **40**, 79–82.

FÜRSICH F.T. and OSCHMANN W. 1993. Shell beds as tools in basin analysis: the Jurassic of Kachchh, western India. *Journal of the Geological Society London,* **150**, 169–185.

HALLAM A. 1996. Major bio-events in the Triassic and Jurassic. *In*: WALLISER O.H. (ed). Global events and event-stratigraphy. Springer, Berlin Heidelberg New York, 265–283.

HORNUNG T. 2008. A Tethys-wide mid-Carnian (Upper Triassic) carbonate productivity crisis: evidence for the Alpine Reingraben Event from Spiti (Indian Himalaya ?). *In*: Hornung T. (ed). The Carnian Crisis in the Tethys Realm. Multistratigraphic studies and palaeoclimate constraints. VDM Verlag Dr. Müller, Saarbrücken, pp. 237.

HORNUNG T. and BRANDNER R. 2005. Biochronostratigraphy of the Reingraben Turnover (Hallstatt Facies Belt): local black shale events controlled by regional tectonics, climatic change and plate tectonics. *Facies,* **51**, 475–494.

HORNUNG T., KRYSTYN L. and BRANDNER R. 2006. A Tethys-wide mid-Carnian (Upper Triassic) carbonate productivity decline: Evidence for the Alpine Reingraben Event from Spiti (Indian Himalaya). *Journal of Asian Earth Sciences,* **30**, 285–302.

HORNUNG T., SPATZENBERGER A. and JOACHIMSKY M.M. 2007a. Multistratigraphy of condensed ammonite beds of the Rappoltstein (Berchtesgaden, Southern Germany): unravelling palaeo-environmental conditions on 'Hallstatt deep swells' during the Reingraben Event (late Lower Carnian). *Facies*, **53**, 267–292.

HORNUNG T., BRANDNER R., KRYSTYN L., JOACHIMSKY M.M. and KEIM L. 2007b. Multistratigraphic constraints on the NW Tethyan ''Carnian Crisis''. *New Museum of Natural History and Science Bulletins*, **4**, 59–67.

KIDWELL S.M., FÜRSICH F.T. and AIGNER T. 1986. Conceptual framework for the analysis and classification of fossil concentrations. *Palaios*, **1**, 228–238.

KOZUR H.W. and BACHMANN G.H. 2010. The middle Carnian Wet Intermezzo of the Stuttgart Formation (Schilfsandstein), Germanic Basin. *Palaeogeography, Palaeoclimatology, Palaeoecology*, **290**, 107–119.

KRYSTYN L. 1983. Das Epidaurus-Profil (Griechenland): ein Beitrag zur Conodonten-Standardzonierung des tethyalen Ladin und Unterkarn. *Schriftenreihe der Erdwissenschftlichen Kommision der Österreichischen Akademie der Wissenschaften*, **5**, 231–258.

KRYSTYN L. 1991. Die Fossillagerstätten der alpinen Trias. Exkursionsführer, 23–78.

RIGO M., PRETO N., ROGHI G. and TATEO F. 2007. A rise in the carbonate compensation depth of western Tethys in the Carnian (Late Triassic): Deep-water evidence for the Carnian Pluvial Event. *Palaeogeography, Palaeoclimatology, Palaeoecology,* **246**, 188–205.

SCHLAGER W. and SCHÖLLNBERGER W. 1974. Das Prinzip stratigraphischer Wenden in der Schichtfolge der Nördlichen Kalkalpen. *Mitteilungen der Geologischen Gesellschaften in Wien*, **66/67**, 165–193.

SEILACHER A. 1990. *Taphonomy of Fossil-Lagerstätten: Overview*. *In*: BRIGGS D.E.G. and CROWTHER P.R (eds). Paleobiology: a synthesis. Blackwell Scientific, Oxford, 266–270.

SIMMS M.J. and RUFFELL A.H. 1989. Synchronicity of climate change and extinctions in the Late Triassic. *Geology*, **17**, 265–268.

TOLLMANN A. 1976. Analyse des klassischen nordalpinen Mesozoikums: Stratigraphie, Fauna und Fazies der Nördlichen Kalkalpen. Monographie der Nördlichen Kalkalpen 2. Franz Deuticke, Wien, pp. 580.

YURTTAŞ-ÖZDEMIR Ü. 1973. Über den Schieferton mit Halobia der Halbinsel Kocaeli*. Bulletin of the Mineral Research and Exploration Institute of Turkey (Foreign Edition)*, **80**, 43–49.

Appendix I - Supplementary Tables for Chapter IV

Measurements of the holotypes, paratypes and related genera from Aşağiyaylabel (Taurus Mountains, Turkey):

Type / Inv. Nr.	Fig.	D	H	W	U	ah	H/W	H/D	H/U	U/D	W/D
		in mm									
Kasimlarceltites krystyni **gen. et sp. nov. and related genera**											
NHMW-2012z0133/0268, data source: sm	4.4C	0.6	0.3	–	0.1	0.2	–	0.42	1.93	0.22	–
NHMW-2012z0133/0006, data source: sm	4.5M–N	18.5	5.8	4.5	7.4	5.0	1.27	0.31	0.78	0.4	0.24
NHMW-2012z0133/0007, data source: sm	4.5O–P	18.5	5.9	4.6	7.3	5.0	1.28	0.32	0.81	0.40	0.25
NHMW-2012z0133/0008, data source: sm	4.5Q–R	19.1	6.1	4.9	8.8	4.3	1.25	0.32	0.69	0.46	0.25
NHMW-2012z0133/0009, data source: sm	4.5S–T	20.4	6.4	5.0	9.2	5.4	1.28	0.32	0.70	0.45	0.25
NHMW-2012z0133/0010, data source: sm	4.5U–V	20.2	6.2	4.5	9.0	5.1	1.38	0.30	0.68	0.45	0.22
NHMW-2012z0133/0011, data source: sm	4.5W–X	29.9	9.5	5.4	14.2	6.3	1.74	0.32	0.67	0.48	0.18
Dinarites avisianus in Mojsisovics 1882 (p. 13, pl. 27, fig. 17), data source: rOP	–	40	14	10	16.5	11.5	1.40	0.35	0.85	0.41	0.25
D. avisianus in Mojsisovics 1882 (p. 13, pl. 27, fig. 19), data source: rOP	–	29	10	7.5	12.5	8.57	1.33	0.34	0.80	0.43	0.26
HT of *Aploceras transiens* in Manfrin *et al*. 2005 (fig. 5, 10–11), data source: mOF	–	24.6	7.24	5.7	10.6	–	1.27	0.29	0.69	0.43	0.23

Type / Inv. Nr.	Fig.	D	H	W	U	ah	H/W	H/D	H/U	U/D	W/D
		in mm									
Kasimlarceltites krystyni **gen. et sp. nov. and related genera**											
A. laczkoi in Manfrin *et al*. 2005 (fig. 5, 1–2), data source: mOF	–	21.4	7.6	5.4	9.1	–	1.42	0.36	0.83	0.43	0.25
HT of *Celtites neumayri* Mojsisovics 1893 (p. 348, pl. 200, figs. 5a–b), data source: rOP	–	27	7	9	15	5.4	0.78	0.26	0.47	0.56	0.33
HT of *C. edithae* Mojsisovics 1893 (p. 349, pl. 200, fig. 7), data source: rOP	–	16	5	6	8	3.96	0.83	0.31	0.63	0.50	0.38
HT of *C. epolensis* Mojsisovics 1882 (p. 149, pl.38, fig. 13), data source: rOP	–	26	6	–	15	–	–	0.23	0.40	0.58	–
HT of *C. laevior* Diener 1917 (p. 390, pl. 3, fig. 9), data source: sm	–	14.0	4.0	3.5	7.0	3.9	1.14	0.29	0.57	0.5	0.25
HT of *C. ottiliae* Diener 1921 (p. 512, pl. 8, figs. 8a–b), data source: sm	–	12.5	3.5	3.0	6.0	–	1.17	0.28	0.58	0.48	0.24
HT of *C. laevissimus* Diener 1921 (p. 512, pl. 8, figs. 7a–b), data source: sm	–	11.0	3.0	3.0	5.5	–	1.00	0.27	0.55	0.50	0.27
HT of *C. conifer* Diener 1917, (p. 390–391, pl. 3, fig. 10), data source: sm	–	9.0	2.0	3.5	4.5	2.9	0.57	0.22	0.44	0.50	0.39
HT of *O. belcheri* Tozer 1994, (p. 125, pl. 103, figs 1a–b), data source: mOF	–	13.8	3.9	5.6	5.9	5.4	0.70	0.28	0.66	0.43	0.4
Type of *“Goniatites” buchi* Klipstein 1843 (p. 137, pl. 8, figs 11a–c), data source: mOF	–	17.9	6.47	4.8	9.1	5.5	1.35	0.36	0.71	0.51	0.27

Type / Inv. Nr.	Fig.	D	H	W	U	ah	H/W	H/D	H/U	U/D	W/D
				in mm							
Kasimlarceltites krystyni **gen. et sp. nov. and related genera**											
Type of *"Ammonites" klipsteinianus* Laube 1870 (p. 83, p. 37, fig. 8), data source: rOP	–	11	4	4	4.5	3.3	1.00	0.36	0.89	0.41	0.36
Type of *Lecanites glaucus* Mojsisovics 1882 (p. 200, pl. 30, fig. 4), data source: rOP	–	12	4	2	5	4	2.00	0.33	0.80	0.42	0.17
L. vogdesi in Assereto 1969 (p. 2, fig. 2), data source: mOF	–	50.9	13.9	–	26.1	12.9	–	0.27	0.53	0.51	–
L. vogdesi in Assereto1969 (p. 1, figs 6a–c), data source: mOF	–	36.8	11.6	10.4	14.4	8.4	1.12	0.32	0.80	0.39	0.28
L. vogdesi in Assereto 1969 (p. 2, figs 7a–c), data source: mOF	–	28.0	10.1	8.1	12.9	9.4	1.25	0.36	0.79	0.46	0.29
L. vogdesi in Assereto 1969 (p. 2, figs 10a–c), data source: mOF	–	33.8	10.8	9.5	13.4	10.6	1.13	0.32	0.80	0.40	0.28
L. misanii in Manfrin *et al*. 2005 (p. 484, fig. 5, 21–22), data source: mOF	–	17.9	6.1	3.6	7.6	4.6	1.69	0.34	0.80	0.43	0.20
Type of *Coeloceltites rectangularis* (Hauer, 1860, p. 351), data source: rOP	–	27.7	7.3	7.8	15.3	7.3	0.94	0.26	0.48	0.55	0.28
Type of *Cycloceltites arduini* (Mojsisovics 1893, p. 360, pl. 122, fig. 6), data source: rOP	–	31	8	5.0	19	7.5	1.60	0.26	0.42	0.61	0.16

Type / Inv. Nr.	Fig.	D	H	W	U	ah	H/W	H/D	H/U	U/D	W/D
				in mm							
Spirogmoceras* cf. *shastense* and type material of *Sp. shastense											
NHMW-2012z0133/0467	4.8A	46	24	–	–	–	–	0.52	–	–	–
HT of *Sp. lecontei* (Hyatt & Smith 1905), data source: rOP	–	141	83	41	14	60	2.02	0.59	5.93	0.10	0.29
HT of *Sp. californicum* (Smith 1927), data source: rOP	–	170	90	63	26	–	1.43	0.53	3.46	0.15	0.37
NHMW-2012z0133/0335, data source: sm	4.8B	–	12.1	–	–	–	–	–	–	–	–
NHMW-2012z0133/0338, data source: sm	–	16.0	6.41	–	6.0	–	–	0.40	1.07	0.38	–
NHMW-2012z0133/0475, data source: sm	4.8D	13.3	5.2	2.0	5.3	4.5	2.60	0.39	0.98	0.40	0.15
LT of *Sa. pilari* Diener 1917, NHMW-1998z0056/0007, data source: rOP	–	30.0	12.0	8.0	11.0	12.1	1.50	0.40	1.09	0.37	0.27
PT of *Sa. pilari* Diener 1917 NHMW-1998z0056/0019, data source: sm	–	22.3	9.4	7.6	8.0	9.4	1.24	0.42	1.18	0.36	0.34

Type / Inv. Nr.	Fig.	D	H	W in mm	U	ah	H/W	H/D	H/U	U/D	W/D	WER
Klipsteinia disciformis **sp. nov. and related species**												
"Ammonites" hirschi in Laube (1870, pl.41, fig. 9), data source: rOP, mOF (ah)	–	13	5.6	5	3.5	5.30	1.12	0.43	1.6	0.27	0.38	2.850 (vh)
"Ceratites" achelous in Münster (1841, p. 134, pl. 15, figs. 23a–c), data source: mOF	–	12.87	5.67	4.88	3.78	5.58	1.16	0.44	1.50	0.29	0.38	3.117 (vh)
"Ceratites" boetus in Münster (1841, p. 129, pl. 14, figs 14a–d), data source: mOF	–	12.8	3.04	3.74	6.85	4.64	0.81	0.24	0.44	0.54	0.29	2.461 (h)
„Ceratites" irregularis in Münster (1841, p. 135, pl. 15, fig. 26a–c), data source: mOF	–	15.0	4.13	4.03	7.37	4.62	1.02	0.28	0.56	0.49	0.27	2.088 (mh)
Kl. karreri in Mojsisovics (1882, pl.25, fig. 27), data source: rOP, mOF (ah)	–	20	8	6.5	5	6.96	1.23	0.40	1.60	0.25	0.33	2.352 (mh)
Kl. nataliae in Mojsisovics (1882, pl. 25, fig. 17), data source: rOP, sm (ah)	–	26	10	5	8	9.5	2.0	0.38	1.25	0.31	0.19	2.495 (h)
Neoprotrachyceras attila **and type material**												
NHMW-2012z0133/0331, data source: sm	4.8M–N	52.2	27.5	14.5	10.5	–	1.90	0.53	2.62	0.20	0.28	–
Mojs. measured syntype (1870, pl. 5, fig. 2), data source: rOP	–	58	26	–	10	–	–	0.45	2.60	0.17	–	–
"Protr. (Trach.)" attila Mojs. (1893, p. 634, pl. 170, figs. 2a–b), data source: rOP, mOF (ah)	–	63	32	19	10.5	23.5	1.68	0.51	3.05	0.17	0.30	2.544 (h)

Type / Inv. Nr.	Fig.	D	H	W	U	ah	H/W	H/D	H/U	U/D	W/D	WER
				in mm								
***Neoprotrachyceras baconicum* and type material**												
NHMW-2012z0133/0317, data source: sm	4.8W–X	14.1	5.4	5.6	6.5	–	0.96	0.38	0.83	0.46	0.40	–
NHMW-2012z0133/0314, data source: sm	4.8O–P	14.5	6.0	7.0	4.0	5.4	0.86	0.41	1.50	0.28	0.48	2.539 (h)
NHMW-2012z0133/0315, data source: sm	4.8S–T	20.0	11.0	8.0	4.0	9.0	1.38	0.55	2.75	0.20	0.40	3.306 (vh)
NHMW-2012z0133/0316, data source: sm	4.8Q–R	30.3	13.9	9.7	8.4	11	1.43	0.46	1.65	0.28	0.32	2.465 (h)
NHMW-2012z0133/0319, data source: sm	4.8U–V	38	16.43	12	12.5	12.97	1.52	0.43	1.31	0.33	0.28	2.305 (mh)
NHMW-2012z0133/0320, data source: sm	4.8Y–Z	38.5	16.8	10	12.8	13.1	1.68	0.44	1.31	0.33	0.26	2.297 (mh)
“Trachyceras“ baconicum (Mojs. 1870), pl. 5, fig. 5, data source: rOP, mOF (ah)	–	90	45	25	20	35.0	1.80	0.50	2.25	0.22	0.28	2.678 (h)
“*Protr. Trach.” baconicum* in (Mojs. 1893, p. 635, pl. 170, fig. 7), data source: rOP, mOF (ah)	–	54	24	14	14	19.95	1.71	0.44	1.71	0.26	0.26	2.515 (h)

Type / Inv. Nr.	Fig.	D	H	W in mm	U	ah	H/W	H/D	H/U	U/D	W/D	WER
***Sirenites senticosus* and type material**												
NHMW-2012z0133/0281, data source: sm	4.5AI–AJ	23	9	5	6.32	9	1.85	0.39	1.42	0.27	0.22	2.699 (h)
NHMW-2012z0133/0289, data source: sm	4.10A–B	22.76	9.21	5.87	6.94	8.9	1.57	0.40	1.33	0.30	0.26	2.697 (h)
NHMW-2012z0133/0285, data source: sm	–	29.0	12.5	7.5	10.0	11.2	1.67	0.43	1.25	0.34	0.26	2.654 (h)
NHMW-2012z0133/0284, data source: sm	–	–	12.0	6.5	–	–	1.85	–	–	–	–	–
HT from Dittmar (1866, p. 375, pl. 17, figs 9–10), data source: rOP	–	26	12.1	7.25	6.65	9.67	1.67	0.47	1.82	0.26	0.28	2.535 (h)
Sirenites senticosus in Mojs. (1893, p. 727, pl. 161, fig. 12), data source: rOP	–	26	12	7	6	–	1.71	0.46	2.00	0.23	0.27	–
***Anasirenites crassicrenulatus* and related species**												
HT of *Anasirenites tripunctatus* Mojsisovics, 1893 (p. 777, pl. 161, fig. 1; GBA 1893/001/0706), data source: rOP, mOF (ah)	–	43	21	11	9	4.5	1.91	0.49	2.33	0.21	0.26	1.247 (l)
HT of *Anasirenites briseis* Mojsisovics, 1893 (p. 776, pl. 160, fig. 15; GBA 1893/001/0705), data source: rOP, mOF (ah)	–	30	16	7.5	3.5	10.0	2.13	0.53	4.57	0.12	0.25	2.250 (mh)
HT of *Anasirenites friederici* Mojsisovics, 1893 (p. 777, pl. 161, fig. 2; GBA 1893/001/0708), data source: rOP, mOF (ah)	–	43	21	11	9	16.0	1.91	0.49	2.33	0.21	0.26	2.536 (h)
HT of *Anasirenites marthae* Mojsisovics, 1893 (p. 777, pl. 161, fig. 3; GBA 1893/001/0707), data source: rOP, mOF (ah)	–	40	17	12	12	11.0	1.42	0.43	1.42	0.30	0.30	1.902 (m)

Type / Inv. Nr.	Fig.	D	H	W	U	ah	H/W	H/D	H/U	U/D	W/D	WER
		in mm										
Paratropites* cf. *hoetzendorfii* and type material of *P. hoetzendorfii												
NHMW-2012z0133/0352, data source: sm	4.10G ad	73	37	–	6	–	–	0.51	6.17	0.08	–	–
NHMW-2012z0133/0368, data source: sm	4.10H juv	29.82	15.33	7.5	–	–	2.04	0.51	–	–	0.25	–
Syntype of Diener´s *P. hoetzendorfii* 1917 (p. 369, pl. 1, fig. 1; NHMW-1998z0056/0021; ad), data source: rOP, sm (ah)	–	95	54	30	6	32.7	1.80	0.57	9.00	0.09	0.32	2.325 (mh)
Syntype of Diener´s *P. hoetzendorfii,* 1917 (p. 369, pl. 1, fig. 2a–c; NHMW-1998z0056/0026; juv); data source: sm	–	43.0	24.3	21.48	7.15	15.1	1.13	0.57	3.40	0.17	0.50	2.380 (mh)
Trachysagenites* cf. *beckei* and type material of *T. beckei												
Inner whorl of NHMW-2012z0133/0350, data source: sm	4.10I–J	*65*	*33*	*24*	*9*	–	*1.38*	*0.51*	*3.67*	*0.14*	*0.37*	–
HT of *Trachysagenites beckei* Diener 1921 (p. 501, pl. 5, figs 1a–b), NHMW-1926z0002/0688) data source: rOP, sm (ah)	–	150	79	63	29	66	1.25	0.53	2.72	0.19	0.42	3.189 (vh)
Syntype of *Trachysagenites glamocensis* Diener, 1917, (p. 362, pl. 2, fig. 1; NHMW-1998z0056/0025), data source: rOP, sm (W, ah)	–	81	46	32	13	36	1.44	0.57	3.54	0.16	0.40	3.240 (vh)
***Proarcestes* sp.**												
NHMW-2012z0133/0443, data source: sm	4.10K	52	27	26	2.9	14	1.04	0.52	9.31	0.06	0.50	*1*.873 *(m)*
NHMW-2012z0133/0445, data source: sm	4.10M–N	50	26	26	2.0	11	1.00	0.52	13.0	0.04	0.52	1.664 (m)

Type / Inv. Nr.	Fig.	D	H	W in mm	U	ah	H/W	H/D	H/U	U/D	W/D	WER
***Megaphyllites jarbas* and type material**												
NHMW-2012z0133/0479, data source: sm	4.10O	33.0	16.5	9.5	0.5	10.0	1.74	0.50	33.00	0.02	0.29	2.059 (mh)
HT of „*Ceratites jarbas*“ (Münster 1841), p. 135, pl. 15, fig. 25 data source: mOF	–	18.5	9.9	–	1.9	8.0	–	0.54	5.21	0.10	–	3.104 (vh)
***Simonyceras simonyi* and type material**												
NHMW-2012z0133/0477 max. length: 165 mm, data source: sm	4.11A	–	80.0	82.0	–	–	–	–	–	–	–	–
Syntype of Mojsisovics (1873, pl. 17, fig. 1; GBA 1873/5/48), data source: rOP	–	248	111	55	82	72.5	2.02	0.45	1.35	0.33	0.22	1.997 (m)

Abbreviations: ah, aperture height; **D,** maximum diameter; **H,** whorl height; **H/D,** proportional height; **H/U,** degree of involution; **H/W,** whorl compression; **sm,** self-measured; **U,** umbilical width; **U/D,** proportional umbilical width; **W,** whorl breadth; **W/D,** proportional whorl breadth; **WER,** whorl expansion rate; WER standard: **m,** moderate 1.61–2.0; **mh,** moderately high 2.01–2.40; **h,** high 2.41–2.80 and **vh,** very high > 2.80.

Appendix II - Supplementary Figures (SF) for Chapter V

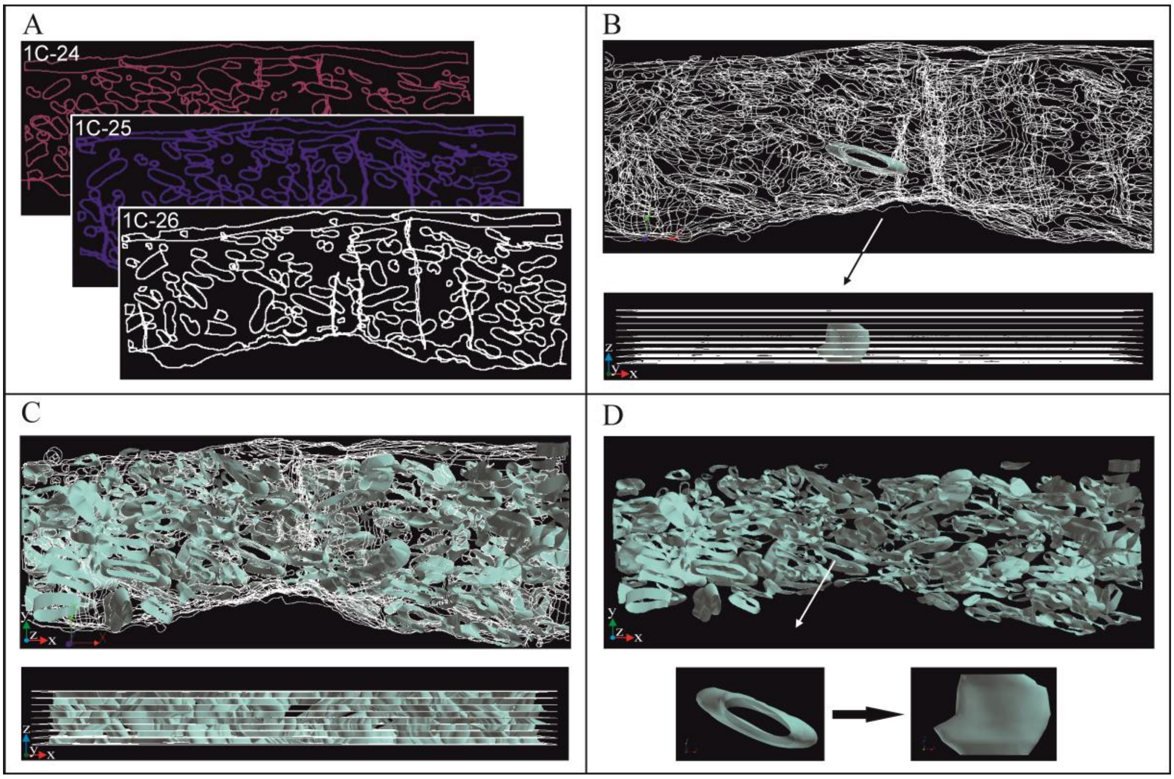

Suppl. Fig. 1. Steps for segmentation of the ammonoids from the scanned slices via Gocad. **A,** Polylines drawn via CorelDRAW. **B,** Polylines uploaded into Gocad, with created surface of one ammonoid. **C–D,** Reconstructed ammonoid surfaces from polylines with and without polylines.

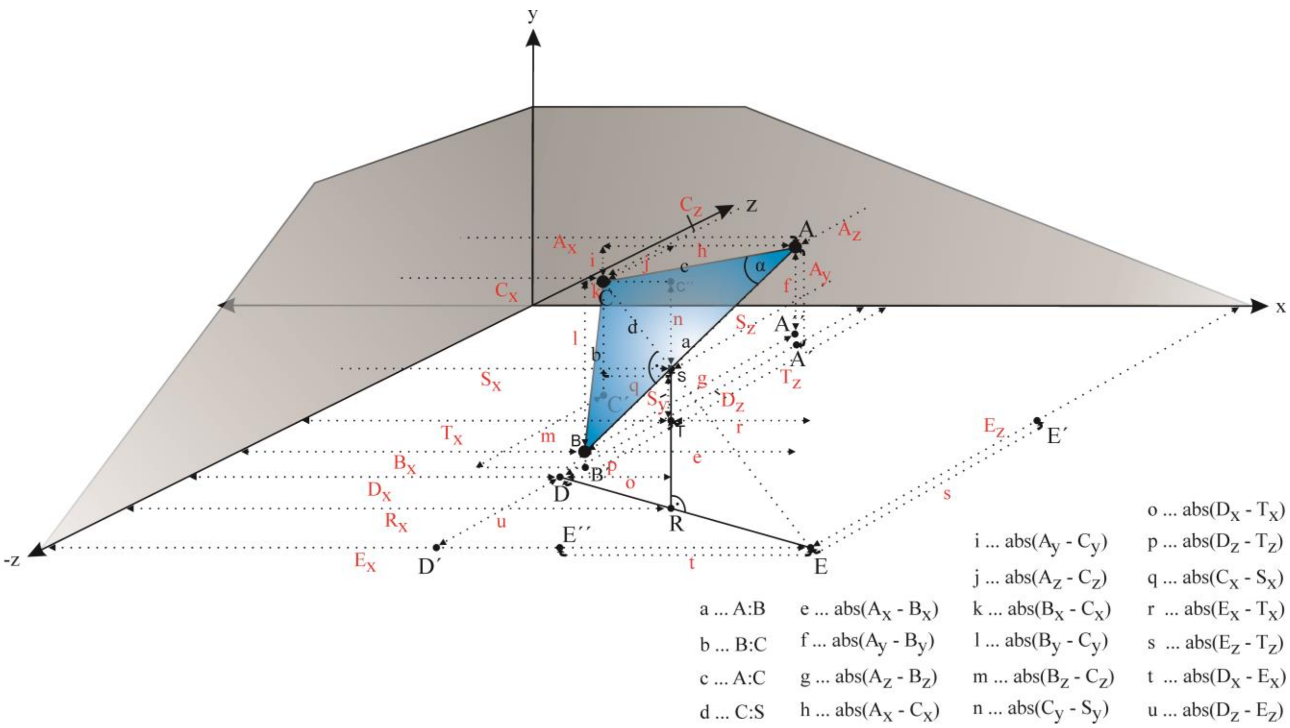

Suppl. Fig. 2. Description of variables used for calculations of ammonoid orientations.

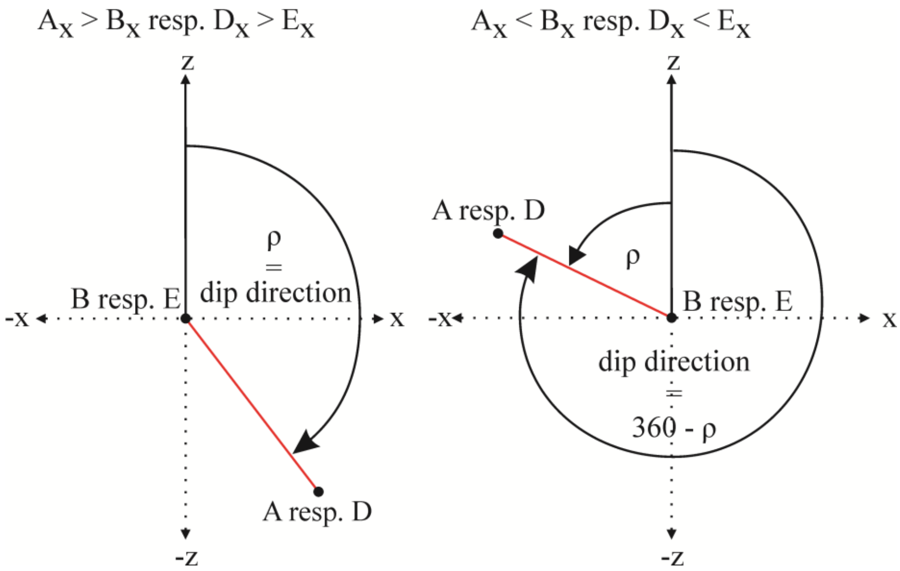

Suppl. Fig. 3. Graphical explanation for calculating dip direction respectively azimuth from ρ.